Content

POSTER SESSION 1: ROADSIDE AND TUNNEL STUDIES

POSTER SESSION 1: EMISSION MEASUREMENT

POSTER SESSION 1: ELECTRO AND HYBRID VEHICLES

POSTER SESSION 1: NON ROAD TRAFFIC EMISSIONS

POSTER SESSION 1: AIR QUALITY MEASUREMENT AND MODELLING

EMPA

Materials Science & Technology

Preface

Ladies and Gentlemen, Dear Participants,

Traffic emissions and air quality have been topics for several decades already. Many improvements were achieved by a better control of combustion and appropriate aftertreatment systems. These achievements however were beaten out to a certain extent by the grow of traffic and of vehicle size and weight, such that in many “hot spots” local air quality is not satisfactory and mostly these hot spots are close to urban areas, where people live and work.

In parallel the global warming became a central environmental problem and traffic as a major contributor of CO_2 and other greenhouse gases is in focus in this discussion. On the side of impact this means that air quality research today shows two dimensions, the global one dealing with global warming, and the local one of polluting humans, animals, plants and soil. On the side of technology the researchers and car manufacturers are challenged by a variety of technologies and fuels all promising reduced greenhouse gas potential, for which engines and aftertreatment systems need to be developed to improve or at least keep the low unit emissions of the actual models.

All these open questions ask for new tools in measurement and simulation for two aspects: to understand the mechanisms that are not well known yet, as well as to develop the necessary technology on time. Thus, this field of traffic related air pollution will keep its actuality for the future.

The Transport and Air Pollution symposium provides a forum for a broad interdisciplinary research community for knowledge exchange at a scientific level. The French National Institute for Transport and Safety Research (INRETS), the Institute of Internal Combustion Engines and Thermodynamics at the University of Technology of Graz and formerly the National Centre of Air Pollution (NCAR) jointly organized the TAP conferences. Newly from this year on also Empa the Swiss research institute for Material Science & Technology and the EU Joint Research Centre (JRC) of Ispra are in this team of organisers.

This conference is the 18th in this Transport and Air Pollution series and we hope you will enjoy your visit to Zurich and Duebendorf. We hope that the conference will meet your expectations in promoting the scientific exchange, extending and strengthening of contacts.

The work of all contributing authors and the scientific committee is gratefully acknowledged. We also want to express special thanks to the staff organising this conference.

Christian Bach Martin Weilenmann

Dübendorf, May 2010

PM10 emission factors for non-exhaust particles generated by road traffic in Switzerland

N. Bukowiecki[*1, now at 2], *P. Lienemann*[1, now at 3], *M. Hill*[1], *M. Furger*[2], *A. Richard*[2], *A. S.H. Prévôt*[2], *U. Baltensperger*[2], *B. Buchmann*[1] *and R. Gehrig*[1]

[1]Empa, Swiss Federal Laboratories for Materials Testing and Research, 8600 Duebendorf, Switzerland, nicolas.bukowiecki@psi.ch
[2]Paul Scherrer Institut, Laboratory of Atmospheric Chemistry, 5232 Villigen PSI, Switzerland
[3]Zurich University of Applied Sciences ZHAW, CH-8820 Wädenswil, Switzerland

Introduction

Recent research identified a clear contribution of non-exhaust emissions to the traffic related PM10 load of the ambient air. These emissions consist of particles produced by abrasion from brakes, road wear, tire wear, as well as vehicle induced resuspension of deposited road dust. For many urban environments, quantitative information about the contributions of the individual abrasion processes is still scarce. For effective PM10 reduction scenarios it is of particular interest to know whether road wear, resuspension or fresh abrasion from vehicles dominates the non-exhaust PM10 emissions. The main scope of this work was to identify and quantify the non-exhaust fraction of traffic related PM10 for several road-side locations with characteristic traffic regimes. The selection of the investigated locations was based a) on their traffic and roadside characteristics being typical also for other real-world situations and b) on their experimental and conceptual applicability. To separate traffic related emissions from the total ambient PM10 load, representative background measurements were performed either upwind of the selected measuring location, or at a suitable background site. The identification of individual traffic related sources was based on specific elemental fingerprint signatures for the various sources. These fingerprints were obtained by hourly elemental mass concentration measurements in three size classes (2.5-10, 1-2.5 and 0.1-1 micrometers). A rotating drum impactor (RDI) was used as sampling device for this purpose. The collected samples were analyzed by synchrotron radiation X-ray fluorescence spectrometry (SR-XRF). The elemental fingerprint measurements were accompanied by additional aerosol, gas phase and meteorological measurements, and by traffic counting for light and heavy duty vehicles. The mathematical identification of the abrasion sources from the experimental data was performed by positive matrix factorization (PMF), a statistical method widely used for this purpose. The atmospheric dilution of the emissions from their point of emission to the point of sampling (10-20 m) was obtained by background corrected NOx measurements and known NOx emissions at the considered site. This dilution, along with the traffic counts, allowed for the calculation of vehicle specific emission factors for the measured tracer species and for the identified abrasion sources with help of a statistical model. To ensure a statistically significant calculation of emission factors, only time periods with distinctively high background corrected NOx concentrations (ΔNOx > 20 µg m^{-3}) were considered for analysis. The presented emission factors are independent of the exact measurement position along the road.

Measurements in an urban street canyon (Zürich Weststrasse/Kaserne, February and March 2007)

The Zürich-Weststrasse site represented an urban street canyon with the following traffic characteristics:

- 'Stop-and-go traffic': Urban main road with traffic lights, strong disturbances (Category 'IO_HVS3' according to *Handbook of Emission Factors* (INFRAS, 2007), http://www.hbefa.net). Closed for transit traffic from 22:00 to 06:00.
- Pavement: Asphalt concrete (AB12), year of application: 1995/98.
- Vehicle counting: <6m; (Light duty vehicles including 9% delivery vans), >6m (Heavy duty vehicles including motor coaches).
- Weekdays: 22000 vehicles per day (heavy duty vehicle fraction 12%); Saturdays: 21000 vehicles per day (heavy duty vehicle fraction 5%); Sundays: 19000 vehicles per day (heavy duty vehicle fraction 4%).

To quantify the local PM10 contributions at Zürich-Weststrasse, simultaneous measurements of the urban background were performed at Zürich-Kaserne (urban courtyard, approximately 600 m distance from Zürich-Weststrasse). During the considered time periods, PM10 at Zürich-Kaserne was shown to also represent the urban background at Zürich-Weststrasse. It consisted of the accumulated contributions of all urban PM10 sources (both traffic and non-traffic related sources).

Measurements along an interurban freeway (Reiden, July – November 2007)

Measurements were performed in Reiden (Canton Lucerne), along the national freeway A2 with the following traffic characteristics:

- Motorway with free-flowing traffic at 120 km h^{-1} (Category 'AB_120' according to *Handbook of Emission Factors* (INFRAS, 2007), http://www.hbefa.net).
- Pavement: Splitt-mastix asphalt (compact pavement comparable to asphalt concrete); direction Luzern SMA 11 B 80/100+NAF; direction Basel SMA 11 B55/70+NAF, year of application: 1999.
- Vehicle counting: Light duty vehicles (including 15% delivery vans) versus heavy duty vehicles (including motor coaches).
- Weekdays: 49000 vehicles per day (heavy duty vehicle fraction 16%); Saturdays: 45000 vehicles per day (heavy duty vehicle fraction 7%); Sundays: 41000 vehicles per day (heavy duty vehicle fraction 2%, including coaches).

Measuring stations were placed at both sides of the freeway. For time periods with perpendicular wind, the upwind station measured the local background PM10 load, while the downwind station detected the background plus the local traffic PM10 emissions.

Results (adopted from Bukowiecki et al., 2009a,b, 2010)

Traffic related PM10 emissions in the urban street canyon

For Zürich-Weststrasse, the following mass relevant traffic related PM10 sources were identified from the hourly measurements by the applied statistical method (positive matrix factorization):

- Brake wear. Brake wear was characterized by a specific pattern of Fe, Cu, Zn, Zr, Mo, Sn, Sb and Ba. These elements are widely used constituents of brake linings and are likely to be oxidized during the brake abrasion process.
- Exhaust emissions: Exhaust emissions predominantly consisted of organic and inorganic carbon species, expressed as total traffic related carbon. Trace elements originating from fuel additives were not specifically identified from the road side measurements, indicating that these contributions are low on a mass base and other emission sources of these elements are more relevant.
- Vehicle induced resuspension of road dust: Besides the large abundance of mineral elements in deposited and resuspended road dust, characteristic contributions of brake wear and exhaust particles (carbon) were clearly identified.

Road wear and tire wear were not identified as separate sources from the measurements at Zürich-Weststrasse, due to the absence of unique tracer species. With the applied approach of analysis, any unidentified contributions from road wear and tire wear were added to the other sources. However, the presented source apportionment is only minimally biased by undetermined contributions from these sources:

- Road wear versus road dust resuspension: Additional controlled experiments with a mobile load simulator showed that direct abrasion wear from the road surface is of minor importance for pavements in good condition (Gehrig, 2010). However, damaged pavement surfaces can cause quite significant PM10 emissions.
- Tire wear: Reliable information for PM10 emissions from tire wear can hardly be found in literature. Some older works report contributions up to 10% to urban PM10 concentrations. However, none of the applied methods was specific enough to be convincing. A new, still unpublished study at two urban traffic sites in Wiesbaden (Germany) for the first time uses a

method that seems to be really specific (analysis of pyrolysis products of tire rubber) and find a mean contribution of tire wear of 0.5% to PM10. The same work shows that the earlier assumed contribution of up to 10% tire wear assumed earlier really exists, but in particle fractions >10 µm and not in PM10. This was also qualitatively confirmed by microscopic evidence. In agreement with these findings, PM10 tire wear emissions for the simulator experiments performed during this study were found to be negligible.

Table 1 shows emission factors for the traffic related PM10 sources, with separate values for light and heavy duty vehicles, and for the average vehicle fleet. Emission factors were calculated from the hourly mass concentrations of the individual traffic sources. For the calculations, the atmospheric dilution of the emissions was taken into account, which was obtained from background corrected NOx measurements and known NOx emissions at the considered site. The applied calculation models also considered individual vehicle counts for light and heavy duty vehicles, which allowed for the calculation of separate emission factors for light and heavy duty vehicles. Table 1 shows that considerable uncertainties were introduced by splitting the fleet emission factors into vehicle type specific emission factors.

Table 1: Emission factors for the individual sources contributing to traffic related PM10, valid for Zürich-Weststrasse (urban street canyon). LDV: Light duty vehicles (including 9% delivery vans), HDV: Heavy duty vehicles (including motor coaches). Brake wear was quantified assuming a brake dust antimony content of 1% and a copper content of 5%. Total traffic related carbon was estimated from black carbon measurements, using an experimentally determined ratio of 1.45 for traffic related carbon to emitted black carbon. Values are based on 12 days of measurements in February an March 2007, ΔNOx > 20 µg m^{-3}, dry time periods only) and are based on NOx emission factors estimated for Zürich-Weststrasse (Year: 2007, EF NOx(LDV) = 286.8 mg km^{-1}, EF NOx(HDV) = 10559 mg km^{-1}, NOx calculated as NO2, Handbook of Emission Factors, http://www.hbefa.net, INFRAS (2007). For comparison, emission factors for road wear and resuspension from mobile load simulator experiments are shown.

Source	**Source quantification**	**Emission factor calculation**	**Zürich-Weststrasse**		
			Fleet 10% HDV[*1] mg/km/veh	**LDV [*2] mg/km/veh**	**HDV[*2] mg/km/veh**
Traffic related PM10	Measured (PM10-Difference: Street canyon - background	Estimated from mass balance	**71**	**24 ± 8**	**498 ± 86**
Brake wear	Statistical modelling[*3]	Multilinear regression	**15**	**8 ± 4**	**81 ± 39**
Exhaust (Total traffic related carbon species)	Statistical modelling[*3]	Multilinear regression	**29**	**15 ± 6**	**155 ± 67**
Road dust resuspension	Statistical modelling[*3]	Estimated from mass balance	**27**	**1 ± 11**	**262 ± 115**
Road Wear	Mobile load simulator experiments		-	(<3)[*a,d]	(7)[*a] (80[*b])
Resuspension[*d]			-	(5)[*d] (76)[*a]	(110)[*c] (660[*b])

[*1] Average heavy duty vehicle fraction during the entire field campaign in February and March 2007 (varies strongly within a day)
[*2] Multilinear model with individual consideration of hourly traffic composition
[*3] PMF (positive matrix factorization)
[*a] new asphalt concrete
[*b] asphalt concrete in poor condition
[*c] asphalt concrete in good condition
[*d] new porous asphalt

The calculated PM10 emission factors for Zürich-Weststrasse show the following characteristics:

- Vehicle Fleet : The average PM10 emission factor, related to a HDV fraction of 10%, was mainly caused by exhaust emissions (41%) and vehicle induced resuspension of road dust (38%), followed by brake wear (21%).
- Light and heavy duty vehicles: Exhaust (63%) and brake wear (33%) were the dominant PM10 emissions for light duty vehicles. In contrast, emissions from resuspension of road dust were estimated to be totally less than 5 % for light duty vehicles. Compared to light duty vehicles, the absolute emission factors for heavy duty vehicles were 15 times higher for total PM10 and 10 times higher for brake wear and the exhaust emissions. For heavy duty vehicles, the road dust resuspension capability of an individual heavy duty vehicle was estimated to be substantial. 53% of the PM10 emissions of an individual heavy duty vehicle were attributed to road dust resuspension. Exhaust emissions (31%) and brake wear (16%) are additional important contributions. In the heavily trafficked street canyon at Zürich-Weststrasse, the emissions from resuspension are likely to be limited by the amount of resuspendable dust. The available dust on the surface was resuspended and kept in suspended state mainly by the turbulence induced by the heavy duty vehicles, leaving only small amounts of dust to be resuspended by the light duty vehicles. From this finding at Weststrasse, however, it can not be concluded, that resuspension is generally not induced by LDV. In the case of little or no heavy duty vehicle traffic, the resuspension would also be induced by the light duty vehicle fleet.

While a strong correlation of brake wear and exhaust emissions with the hourly traffic frequencies was found, the diurnal pattern of vehicle induced resuspension was less correlated and characterized by a larger statistical variation. Therefore emission factors expressed as mg/km/vehicle are not appropriate for road dust resuspension. As a consequence, vehicle specific emission factors could not be calculated using the multilinear regression model, but could only be indirectly estimated with accordingly high absolute uncertainties. Since resuspension was found to be a relevant contributor to total traffic related PM10, the same applies to PM10.

Traffic related PM10 emissions along the interurban freeway

For Reiden, the following mass relevant traffic related PM10 sources were identified from the hourly measurements by the applied statistical method (positive matrix factorization):

- Brake wear: Brake wear was characterized by a specific pattern of Fe, Cu, Zn, Zr, Mo, Sn, Sb and Ba. The pattern was very similar to the one found at Zürich-Weststrasse.
- Exhaust emissions: The exhaust emissions were predominantly formed by organic and inorganic carbon species, expressed as total traffic related carbon. Like at Zürich-Weststrasse, trace elements originating from fuel additives were not specifically identified from the road side measurements, indicating that the contributions are low and other emission sources of these elements were more relevant on a mass base.

Contributions of mineral dust elements to traffic emissions were identified, pointing to vehicle induced road dust resuspension. A specific quantification for resuspension based on these contributions was however not possible, because no reliable composition profile was available for road dust deposited on the freeway.

Table 2 shows emission factors for the traffic related PM10 sources, with separate values for light and heavy duty vehicles, and for the average vehicle fleet. The calculated PM10 emission factors for Reiden show the following characteristics:

- Vehicle fleet: The average PM10 emission factor for Reiden (15% HDV fraction during the entire campaign) was caused by exhaust emissions (41%) and very low contributions from brake wear emissions (3.2%). The remaining 56% of the traffic emissions were not directly identified, but probably represented contributions from road dust resuspension (and minor contributions from tire wear and road wear).
- LDV and HDV emission factors: The PM10 emission factor for HDV was 5.8 times higher than for LDV. Because the mass contributions of both brake wear and traffic related carbon were extrapolated from the same traffic source identified by PMF, the resulting LDV and HDV emission factors showed virtually identical source contributions. An alternative calculation of LDV and HDV emission factors for brake wear and exhaust directly from

measured concentration differences of specific marker species (Sb, BC) did not lead to statistically significant results. In contrast to Zürich-Weststrasse, the resuspended dust was removed laterally due to the perpendicular winds (upwind/downwind concept), rather than being kept in suspended state by the turbulence induced by heavy duty vehicles. Therefore a part of the resuspended road dust was also attributed to light duty vehicles.

Table 2: Emission factors for the individual sources contributing to traffic related PM10, valid for Reiden LU (interurban freeway). LDV: Light duty vehicles (including 15% delivery vans), HDV: Heavy duty vehicles (including motor coaches). Brake wear was quantified assuming a brake dust antimony content of 1% and a copper content of 5%. Total traffic related carbon was estimated from black carbon using the same empirical conversion factor of 1.45 as for Zürich-Weststrasse, due to the lack of a specific factor for Reiden. Values are based on 4 days of measurements in October and November 2007, dry time periods only) and are based on NOx emission factors estimated for Reiden LU (Year: 2007, EF NOx(LDV) = 448 mg km^{-1}, EF NOx(HDV) = 5421 mg km^{-1}, NOx calculated as NO2, Handbook of Emission Factors, http://www.hbefa.net, INFRAS (2007). The table shows that considerable uncertainties were introduced by splitting the fleet emission factors into vehicle type specific emission factors.

Source	**Source quantification**	**Emission factor calculation**	**Reiden (LU) A2**		
			Fleet 15% HDV[*1] mg/km/veh	**LDV[*2] mg/km/veh**	**HDV[*2] mg/km/veh**
Traffic related PM10	Measured (PM10-Difference: Downwind - Upwind	Multilinear regression	**86**	**50.0 ± 13**	**288 ± 72**
Brake Wear	Statistical modelling[*3]	Multilinear regression	**3**	**1.6 ± 1.1**	**9 ± 7**
Exhaust (Total traffic related carbon species)	Statistical modelling[*3]	Multilinear regression	**35**	**20.4 ± 7**	**119 ± 38**
Rest (Resuspension and minor sources[*4])	Estimated from mass balance		**48**	**28 ± 14**	**160 ± 82**

[*1] Average heavy duty vehicle fraction in October and November 2007 (varies strongly within a day)

[*2] Multilinear model with individual consideration of hourly traffic composition

[*3] PMF (positive matrix factorization)

[*4] Tire wear and road wear

Conclusions and Outlook

The following statements are made based on the performed investigations and provide indications for future pollution abatement strategies:

Mass contribution of non-exhaust sources: During the time periods considered for the measurements in the urban street canyon at Zürich-Weststrasse (February and March 2007) and along the national freeway A2 in Reiden (October and November 2007), the sum of direct abrasion sources and vehicle induced road dust resuspension made up 60% of the total traffic related PM10 emissions.

Brake wear: Brake wear was characterized by a characteristic pattern of Fe, Cu, Zn, Mo, Zr, Sn, Sb and Ba, which is similar to real-world fleet emissions for brake wear reported in other studies. In contrast, the pattern of these elements in individual brake linings is extremely inhomogeneous. Compared to older studies, the measured emission factors for brake wear related lead (Pb) were considerably lower, indicating that lead has in the mean time largely been replaced in brake linings. At Zürich-Weststrasse, the heavily disturbed traffic flow resulted in brake wear emissions that made up 20% (15 mg/km/vehicle) of the total PM10 emissions from traffic. In contrast, brake wear emissions contributed less along the freeway in Reiden (3%, 3 mg/km/vehicle), due to the free-flowing traffic regime. For both locations the brake wear emissions from heavy duty vehicles were approximately 10 times higher than from light duty vehicles.

Traffic induced resuspension of road dust: Generally, road dust resuspension is strongly influenced by available road dust and thus by the pollution of the road surface. In the street canyon at Zürich-Weststrasse, up to 40% of the traffic related PM10 emissions were assigned to resuspended road dust during the period of measurements in February and March 2007. Along the freeway in Reiden, the contribution of resuspended road dust to traffic related PM10 emissions was estimated to be higher than 50% in October and November 2007. In the heavily trafficked street canyon at Zürich-Weststrasse, the available dust on the surface was resuspended and kept in suspended state mainly by the turbulence induced by the heavy duty vehicles, leaving only small amounts of dust to be resuspended by the light duty vehicles.

Road wear and tire wear: PM10 contributions from road wear and tire wear were not directly identified from the measurements at Zürich-Weststrasse and Reiden. Controlled experiments with a mobile load simulator showed that for intact pavements road wear is negligible compared to resuspension of deposited road dust, which shows a similar composition. Damaged pavements however led to significantly higher road wear emissions. Quantitative information for road wear under real-world traffic conditions has to be gained by further investigations. While not specifically investigated in this study, tire wear has been found by other investigations to be only relevant in the size range above 10 µm. Recent work indicates that certain pyrolytic products of rubber might be suitable tracers for tire wear.

Emission factors: The presented emission factors are independent of the exact measurement position along the road, because the emissions were corrected for their atmospheric dilution. However, for road dust resuspension at Zürich-Weststrasse emissions were only insufficiently described in terms of mg/km/vehicle, because there was no strictly linear relation with hourly traffic counts due to the complex mechanisms of these emissions. As a consequence, vehicle specific emission factors could only be indirectly estimated with high absolute uncertainties. Since resuspension of road dust was found to be a relevant contributor to total traffic related PM10, the same applied to PM10. Future work will have to address this problem and define refined models for emission inventories.

Particle size of non-exhaust emissions: The investigated particle size ranged from 0.1 to 10 µm. Mass relevant contributions from abrasion related particles and resuspended road dust to traffic related PM10 were mainly found for particles larger than 1 µm.

Exhaust: Although not in the main scope of this work, exhaust emissions were estimated from black carbon measurements to complete the mass balance for traffic related PM10. These emissions were assigned to the particle size range below 1 µm. Trace elements originating from fuel additives (Zn, Ca, S, P) were not specifically identified from the road side measurements, indicating that other emission sources of these elements are more relevant on a mass base. Zn and P show a relative enrichment in the submicron particle fraction which was however not attributed to traffic.

References

Bukowiecki, N., Lienemann, P., Hill, R., Richard, A., Furger, M., Prévôt, A.S.H., Baltensperger, U, Buchmann, B. and Gehrig, R. (2010). PM10 emission factors for non-exhaust particles generated by road traffic in an urban street canyon and along a freeway in Switzerland. *Atmos. Environ.*, in press.

Bukowiecki, N., Lienemann, P., Hill, M., Figi, R., Richard, A., Furger, M., Rickers, K., Falkenberg, G., Zhao, Y., Cliff, S.S., Prévôt, A.S.H., Baltensperger, U, Buchmann, B. and Gehrig, R. (2009a). Real-world emission factors for antimony and other brake wear related trace elements: Size-segregated values for light and heavy duty vehicles. *Env. Sci. Technol.* 43 (21), 8072–8078.

Bukowiecki, N., Gehrig, R. and the APART team (2009b). PM10 emission factors of abrasion particles from road traffic, Forschungsauftrag ASTRA 2005/2007, VSS-Report No. 1268, available from http://partnershop.vss.ch, Bern, Switzerland.

Gehrig, R., Zeyer, K., Bukowiecki, N., Lienemann, P., Poulikakos, L., (2010). Mobile load simulators – a tool to distinguish between abrasion and resuspension of PM10 from road surfaces. *Atmos. Environ.*, submitted.

INFRAS. (2007). Handbook of Emission Factors, http://www.hbefa.net . Zürich.

The assessment of green house gases emissions from road transport along proposed bus rapid transit corridor in Lagos, Nigeria

*A.F. Oluwole *[1], O. Joshua[1],O. Oyediran[1] S.Gutttikunda[2],O.I. Asubiojo[3] , I.I. Omoniyi[4],O.O. Taiwo[4]*

1. SEEMS Nig. Ltd., 23b, Ixora Drive, M.K.O.Abiola Gardens, Lagos.
2. Desert Research Institute, Reno, USA
3. Department of Chemistry, Obafemi Awolowo University, Ile-Ife, Nigeria.
4. Lagos Metropolitan Area Transport Authority (LAMATA), Ikeja, Lagos

Abstract

An emissions inventory of Green House Gases (GHG) and other atmospheric pollutants along a proposed Rapid Bus Transit route in Lagos metropolis in Nigeria is reported. The study involved three components – traffic count, vehicular emission measurements, and emission inventory calculations by Simple Interactive Model (SIM)-Air (Guttikunda) for the various atmospheric pollutants (CO_2, CO, HC, and NO_x).

CO, CO_2, HC, NO_x Emission Factors (EF) for both new and used vehicles were made using the automotive 5-Gas Analysers. The EF for new vehicles were close to EURO-2 Standards while the EF for CO in used vehicles is 3 to 4 times that of the European values.

Calculated emissions of the GHG along the corridor for the cars are CO (3620.59kg/day), CO2 (11.64tonnes/day), HC (111.10kg/day), NO_x (37.26kg/day) while buses are CO (4639.49kg/day), CO2(40.19tonnes/day), HC(64.14kg/day), NO_x (56.09kg/day). Some scenarios were explored for the reduction of GHG concentrations. A change in emission standards from Euro 2 to Euro 4 was found to be most promising.

Introduction

Environmental pollution issues have been receiving considerable attention in Nigeria in recent times. Most of the earlier studies on air pollution by transport systems were based on trace element characterization of Suspended Particulate Matter [Osibanjo 1980].

A country wide inventory of air pollutants in Nigeria was published in 1988 (Obioh et al 1988). The group also carried out an inventory and emission of various transport modes in Nigeria (Obioh et al 1994). Their results showed that the transport sector contributed over 10% of the greenhouse gases nationally and is responsible for about 30% of total fossil fuel consumption annually. This report has since been updated (Obioh 2000). More recent studies have estimated the contribution of transport sector to air pollution to be around 30-45% (MDS 2008, Asubiojo et al 2009, SEEMS 2009).

Lagos, the erstwhile administrative capital and still the commercial capital of Nigeria, with an estimated population of 15 million inhabitants is of particular interest from pollution considerations because of its high population density, commercial and industrial activities. Previous studies of the Lagos environment have implicated vehicular traffic as a major contributor to pollution of the environment of the city. For example, an Environmental Impact Assessment (EIA) study carried out by Mechelec Construction Company (1996) for Lagos Urban Transport contained estimates of air emission from three principal sources (Stationary, Mobile and Industrial) in Lagos with transport sector contributing about 50% of VOC, 90% of CO and 60% of NOx. While emission factor measurements have been made for stationary sources, none exists for mobile sources in the country. This makes greenhouse gases inventory from vehicular sources inaccurate. Hence there is need for accurate emission factor measurements from which emission standards can be deduced and emission regulations set.

This study was designed to carry out an emission inventory of greenhouse gases from vehicles currently plying one of the proposed mass transit routes in the city. The study encompasses vehicular traffic count, greenhouse gas emissions, and vehicular emission factor measurements and exploring various scenarios for the reduction of GHG emission.

Materials and Methods

Sampling

Nine sampling locations were identified along the proposed route and their coordinates were determined using an Explorist 400 handheld GPS receiver.

Equipped with survey plan and layout of the study site, Global Positioning System (GPS), a GIS map was used for the modeling. Sampling and observations were made of vehicular counting and vehicular emission testing.

Field assistants were employed as enumerators and supplied with manual traffic counters. Five enumerators were stationed on each side of the road to count the different types of vehicles, viz: passenger cars including SUVs, light commercial vehicles, heavy duty trucks, urban buses, motorcycles and tricycles. Hourly counts for each type were carried out every day at each of the nine identified monitoring sites along the corridor for 2 weeks.

Vehicular Emission & Emission Factor (EF) Measurements

About 10 vehicles from each of the categories (cars, buses, trucks, motorcycles, SUVs) were randomly selected at each of the sampling sites along the corridor.

Two vehicular exhaust analyzers - the UEI – Automotive 5 gas fuel efficiency analyzers and Infrared Company Inc – DC 5 gas analyzers were used for the vehicular emission measurements both of which are capable of measuring the following gases in the stated ranges:

HC (0-10,000 ppm); CO (0-10%); CO2 (0-20%); NOx; O2 (0 – 10%)
TACH Tachometer (0-30,000 ppm); Air/Fuel(A/F) ratio (0-50), LAMBDA (λ) 0-5 where λ = (A/F)/14.17 ; Engine Temp (0-150^{o}); Emission factor (Gram per km)

FGA 4000XDS Gas Analysers (Infra Red Industries) were used to measure five gases in the automotive exhaust of the selected vehicles. The analyser has capability for determining volume concentration of HC (as Non Hexane), CO, CO2, O2 and NOx.

To measure the Emission factors (EF), the analyzer was put in the Grams per Kilometers (GPK) mode and implements an approximate IM240 tests. This was done for the different vehicle mix (cars, buses, trucks and motorcycles) and different ages (new, 0-5years, 5-10years, 10-15 years, >15years) to obtain average Emission Factors (gm/km).

Results and Discussion

Vehicular Emission Measurements

The results of the vehicular emission measurements for the various vehicle types at idling state are summarized in Table 1 below.

Table 1: Average Mean of Vehicular Emission (Idle State) for Vehicular Mix of Age 0-10 Yrs

Age		**CO**	**HC**	**CO2**	**O2**	**NOX**	**NO**	**Lamda**
Years		**%**	**ppm**	**%**	**%**	**ppm**	**ppm**	**constant**
Cars (0-10)		0.44	200.43	12.71	3.29	141.36	138.36	1.10
Buses (0-10)		3.90	175.50	12.30	7.06	80.50	76.00	0.93
SUVs (0-10)		0.20	38.00	15.03	0.52	211.33	220.33	1.01
Trucks (0-10)		0.60	560.67	6.50	12.33	399.33	434.00	1.28
Motorcycle (0-10)		2.13	244.00	3.10	14.28	4.00	1.00	4.18
Molue (10 above)		1.99	2818.50	2.88	10.88	89.75	68.50	4.93
BRT Buses Marcopolo		0.02	70.00	2.50	18.83	90.00	87.00	2.40
Ashok leyland		0.01	85.00	4.50	18.40	55.00	53.00	2.30
Ideal values		0.50	100.00	15.00	1.00	500.00		1.00
US Health & Safety code		1.5	150.00			350.00		
Egyptian Exhaust Pollutant Concentration	A	1.2	200					
	B	2.0	400					
	C	4.5	900					

A=Cars; B=Trucks; C= Motorcycles

It can be seen that SUVs and passengers cars under 10 years comply with these other standards. This is especially true for the SUVs, a lot of which are under 5 years old.

The HC, O_2, NO_x levels are too high while the CO_2 levels are too low for the other vehicular types – buses, Trucks and Motorcycles.

The emission factors for each vehicle were obtained directly from the gas analyzer described above. They were then combined with the average age and fuel mix of the different vehicle types to obtain the effective emission factors. These are presented in Table 2 below, alongside European standards for comparison. The results show that the emission factors for the Nigerian vehicles are close to the Euro 2 standards.

Table 2: European Emission Standards and Measured Emission Factors

Gasoline (Standard)	**As From***	**CO**	**HC**	**NOx**	
Euro 1	1992	4.05	0.66	0.49	
Euro 2	1996	3.28	0.34	0.25	
Euro 3	2000	2.3	0.2	0.15	
Euro 4	2005	1.00	0.10	0.08	
Gasoline					

Measured(Lagos)		CO	HC	NOx	CO2
Cars:					
New		3	0.006	1.2	165.9
> 15yrs		7.1	0.219	0.07	22.92
< 5yrs		14.96	0.22	0.19	121.2
SUVS:					
New		11.37	0.01	0.40	300.75
Used		4.84	0.04	0.37	198.3
Buses:					
New		8.07	0.006	0.36	229.2
used		12.45	0.17	0.15	107.9

Inventory of Green House Gases Emissions along the Corridor for the Year 2008

Pollutant emissions (kg/day) at each sampling point along the corridor were calculated using the traffic count, Emission Factor and Kilometer travelled using the following equation

Emission = Vehicle count * Distance * Emission Factor (EF)

The SIMS – Air model was used for the GHG Emission Inventory along the corridor. This required the following inputs:

Traffic count for the base year

Vehicle mix by age

Vehicle mix by fuel mix

Since our measured EF for gasoline vehicles is close to EURO 2 Standards and equipment for measuring EF is only good for vehicles with spark plugs (not diesel fuelled), the emissions are calculated based on the EURO 2 Standards and the results are presented in Table 4 below.

The traffic count data was then projected to future years using the follow equation:

New count = Base Count * (1 + growth rate) $^{\text{(Projection year – Base Year)}}$

The vehicle growthrate is conducted up to year 2025 (Table 3). The emissions calculated on the basis for the base year (2008) as well as year 2020 under Business As Usual scenario given in table table 4.

Table 3: Vehicles Growth rates through 2025

	Growth Rate
4WD	2.0%
Cars	5.0%
Molue	0.0%
Trucks	1.5%
Buses	1.5%
3W/2W	1.0%

Table 4: Summary of Emissions for the projected Year 2020 under BAU

		Summary for the Projected Year					2020	
		4WD	Cars	Molue	Trucks	Buses	3W/2W	Total
Total Traffic Count	2008	80,190	296,918	6,176	82,000	197,474	222,490	885,248
	2020	101,700	533,222	6,176	98,041	236,104	250,707	1,225,950
	% change	26.8%	79.6%	0.0%	19.6%	19.6%	12.7%	38.5%
CO2 (tons/day)	Petrol	52.9	401.6	0.3	12.9	977.2	112.3	1,557
	Diesel	14.2	22.6	31.0	446.2	32.4	-	546
	CNG	-	-	-	-	-	-	-
	Total	67.1	424.2	31.3	459.0	1,009.6	112.3	2,104
CO (kg/day)	Petrol	722.7	5,484.8	4.3	189.7	14,383.7	1,860.0	22,645
	Diesel	82.1	131.2	514.8	7,397.5	536.6	-	8,662
	CNG	-	-	-	-	-	-	-
	Total	804.8	5,616.0	519.1	7,587.2	14,920.3	1,860.0	31,307
SO2 (kg/day)	Petrol	23.0	174.5	0.2	8.0	606.7	18.6	831
	Diesel	11.5	18.4	36.0	517.4	37.5	-	621
	CNG	-	-	-	-	-	-	-
	Total	34.5	192.9	36.2	525.4	644.3	18.6	1,452
NOx (kg/day)	Petrol	82.1	623.3	7.5	331.9	25,171.4	139.5	26,356
	Diesel	49.3	78.7	900.9	12,945.6	939.1	-	14,914
	CNG	-	-	-	-	-	-	-
	Total	131.4	702.0	908.4	13,277.5	26,110.5	139.5	41,269

GHG Emission Reduction

The following scenarios were examined for possible emission reduction:

Scenario1: Change in vehicle fuel mix

Scenario 2: Banning molues and buses with 15+yrs age

Scenario 3: Increasing the number of buses

Scenario 4: Non-motorized transport (NMT)

Scenario 5: Introducing EURO IV Standard

Scenario 6: All buses to CNG

Table 4: GHG Reduction Scenario through Year 2020

Pollutant Conc.	**Baseline**	**Scenario 1**	**Scenario 2**	**Scenario 3**	**Scenario 4**	**Scenario 5**	**Scenario 6**
		Reduction in (%)					
CO (kg/day)	24,756	-8.8	-9.8	-4.1	-7.6	-65.0	-14.5
CO2 (tons/day)	1,648	-7.6	-9.6	-4.5	-7.9	-24.7	-13.6

HC (kg/day)	5,897	0.2	-11.6	-1.1	-7.2	-57.7	-0.3
NOx (kg/day)	34,470	-0.1	-13.0	1.0	-6.9	-59.9	-0.4

The results are presented in table 4. It does appear that introducing a stricter standard (say EURO 4), conversion of engines from gasoline or diesel to CNG and of vehicular older than 15 years appear most effective.

Conclusion

The Emission Factors for most vehicles plying Lagos Roads are close to EURO 2. Also, the EF for CO, in particular is 3 to 4 times of the European values, while EFs for NO_X and HC are comparable to European values. Also, idling emission concentrations of the gases from the cars SUVs are generally in compliance with United States Health and Safety standards. However, the emission concentrations of HC, O2 and NOx are too high and CO2 levels too low for the buses, trucks and motorcycles/tricycles. This study establishes the need for Emission Standards and limits for mobile vehicular sources.

REFERENCES

1. Baumbach, G., Vogt, U., Hein, K.R.G., Oluwole, A.F., Ogunsola, O.J. Olaniyi, H.B and Akeredolu, F.A. (1995): Air pollution in a large tropical city with high traffic density – results of measurements in Lagos, Nigeria. Science of Total Environment

2. EPA (1992) Automobile Emissions: An Overview U.S. Environmental Protection Agency. EPA 400-F-92-007, Emission Factors (AP – 42).

3. Guttikunda S., www.sim-air.org

4. Orubu, C.O (2004) Using Transportation Control Measures and Economic Instruments to Reduce Air Pollution Due to Automobile Emissions. J. Soc. Sci., 8(3):227-236 (2004).

5. Obioh I. B., A.F. Oluwole and F. A. Akeredolu (1993): The Methodology and Status of the National GHG Inventory in Nigeria: Proceedings of the IPCC/OECD Workshop in National \Green House Gases (GHG) Inventories Hadley Centre, Bracknell 20 Sept. – 2 Oct. 1992.

6. Environmental Resources Management Legal And Technical Review Report 139.

7. Obioh, I.B., Ogunsola, O.J., Oluwole, A.F. and Akeredolu, F.A. (1994a): "Inventory and emissions of various transport modes in Nigeria" Poster Proceedings Third International Symposium on 'Transport and Air Pollution' Avignon, France, 6-10 June, 1994, pp. 236-241.

8. Obioh, I.B. Oluwole, A.F., Akeredolu, F.A. and Asubiojo, O.I. (1994b): "National inventory of greenhouse gases and toxic air pollutants in Nigeria: for year 1988" 388pp. Monograph, Ilupeju Press Ltd. Benin City, ISBN 978-2012-60-2.

9. Osibanjo O.and Ajayi, S.O. (1980): "Trace metal levels in tree barks as indicators of atmospheric pollution" Environment International 4, 239-244.

10. SEEMS NIG LTD: "Acid Rain Studies – Inventory of Air Pollutants and GHG, Ambient Air Measurements in Relation to Rainwater Acidity around Utorogu Power Plant" 140pp. Report submitted SPDC (1994).

11. Transpoconsult (1976) "Lagos Metropolitan Transportation Study". Prepared for The Federal Military Government and The Ministry of Works. Final Report (Chapter 2).

12. LAMATA, 2007. Lagos State Air Quality Management study report

13. Lagos State Licensing Office and Lagos State Central Office of Statistics [MEPB] Ikeja

14. NNPC, Corporate Planning and Development Division, 2009

Determination of road transport primary NO_2 (f-NO_2) from measurements in a road tunnel

W. Simmons[1] and P. Seakins[1]*

[1] School of Chemistry, University of Leeds, LS2 9JT Leeds, UK, chm2was@leeds.ac.uk

Introduction

All combustion processes in air generate nitric oxide (NO) and nitrogen dioxide (NO_2), collectively known as NO_x. Exposure to NO_2 is linked to negative cardiovascular and respiratory health effects (Latza et al., 2009, Sunyer et al., 2006), particularly in those with pre-existing conditions such as asthma (Chauhan et al., 2003, English et al., 1999), and in the young and elderly (Barnett Adrian et al., 2006, Larrieu et al., 2007). In order to protect health NO_2 is subject to European legislation (Directive 2008/50/EC) in the form of annual (40 µg m^{-3}) and hourly mean (200 µg m^{-3} not to be exceeded more than 18 times per year) limit values. European member states are required to measure NO_2 and are responsible for ensuring that the target values are met. At present throughout the UK and Europe exceedences of the target limits are widespread (EEA, 2010) and there is evidence that exceedences are increasing in prevalence (EEA, 2010, UK-AQA, 2010).

Across Europe, road transport is the largest contributor of NO_x, accounting for 40% of total European NO_x (EEA, 2010). Total European and UK NO_x emissions have been in decline from the early 1990s, largely due to the introduction of EURO standards to reduce NO_x and other pollutants from road transport. However, total NO_2 emissions have been decreasing at a lower rate than NO_x and roadside measurements have reported increases in NO_2 concentrations (AQEG, 2007), mirroring increases in exceedences of limit values. It is thought that increasing f-NO_2, the fraction of NO_x as NO_2 emitted from road transport, is responsible for the roadside observations of NO_2. This effect is significant for the continued difficulties in meeting European limit values (AQEG, 2007). Historically it was believed that f-NO_2 was 0.05 (AQEG, 2004, Lenner et al., 1983) but this appears to be a significant underestimate. An increasing fraction in London was suggested by (Carslaw et al., 2005) who noted a markedly increased mean of about 5–6 vol% in 1997 to about 17 vol% in 2003 from statistical analysis of roadside NO_x and NO_2 concentrations. It is now widely accepted that the fraction is significantly greater than 0.05 and is continuing to increase (AQEG, 2007, Grice et al., 2009).

Production of NO_x and a vehicle's f-NO_2 is a factor of the combustion and exhaust after-treatment technology (AQEG, 2004, Heywood, 1988, Miller and Bowman, 1989). Current compression ignition (CI - diesel) vehicle technology leads to greater production of total NO_x and a greater f-NO_2 than spark ignition (SI - petrol) (AQEG, 2007). This is reflected by EURO standards where CI vehicles are permitted to produce greater quantities of NO_x than spark ignition. Whereas the total amount of NO_x that can be produced is regulated, the fraction, or amount, that is as NO or NO_2 (f-NO_2) is not. In order to meet EURO standards for PM10 some CI vehicles employ exhaust after-treatment devices or combustion modification which further increases f-NO_2. The combination of these factors leads to estimations of 0.05 – 0.7 for CI f-NO_2 (COPERTIV, 2010) which is considerably greater than SI f-NO_2 of 0.02 – 0.04. Within the UK the current penetration of CI into the car fleet is 30% (NAEI, 2010), but 42% of new cars sales are expected to be CI in 2010 (AQEG, 2007). This increasing penetration is likely to cause a rise in typical on-road f-NO_2. In order to accurately predict future air quality it is important that a typical on-road f-NO_2 is quantified, yet it is still relatively poorly defined due to uncertainty in vehicle f-NO_2 and the limited number of on-road measurements. The inherent difficulty in measuring primary NO and NO_2 is its reactivity with ambient O_3 and sunlight:

$$NO + O_3 \rightarrow NO_2 + O_2$$ Typical rate in region of seconds (Boule et al., 1999)

$$NO_2 + h\nu \rightarrow NO + O(+O_2 \rightarrow O_3)$$ Typical rate in region of minutes (Boule et al., 1999)

The rate of reactivity means that roadside or kerbside measurements cannot be used to directly measure f-NO_2 as chemistry will have occurred to change NO_x composition between the tailpipe and measurement site. In this case f-NO_2 can only be derived by the application of models or statistical analyses (Carslaw and Beevers, 2005, Carslaw et al., 2007, Carslaw et al., 2005, Grice

et al., 2009, Jenkin, 2004). f-NO_2 can be measured from lab based chassis dynamometer studies of vehicles to give detailed information about the vehicle pool being tested. However there is some question over how representative of the fleet a sample pool can be, particularly as f-NO_2 appears to vary widely dependent upon vehicle even within the same EURO class or manufacturer (AQEG, 2007, COPERTIV, 2010). Therefore it is desirable to measure real-world on-road f-NO_2 and compare with calculated and chassis-dynamometer measured f-NO_2.

A road tunnel provides a real-world experiment chamber where primary NO and NO_2 can be measured. Dispersion and dilution are limited raising vehicle emission concentrations considerably greater than in normal ambient air, which acts to minimise, or prevent, secondary NO_2 formation from NO + O_3. Similarly the absence of sunlight prevents photolytic NO_2 degradation. Despite their suitability for f-NO_2 measurements there have been relatively few studies conducted, particularly with reference to the European vehicle fleet. The notable exception is a UK based study measuring f-NO_2 in the Hatfield and Bell Common tunnels which produced values of 0.16 – 0.25 for light duty vehicles and 0.09 – 0.11 and 0.06 for HGVs (TRL, 2007). Road tunnels are recognised as a valuable source of real-world f-NO_2 and can provide validation of road transport emissions factors (AQEG, 2007).

Aims

We are conducting a long term (October 2008 to October 2010) measurement campaign in a road tunnel to investigate f-NO_2. We aim to:

- Characterise the tunnel environment
- Investigate different methodologies to measure f-NO_2
- Quantify f-NO_2 as a function of traffic, speed, engine loading (gradient) and season

Experimental

The road tunnel (**Figure 1**) is located on the A58 (M), a busy city inner ring road used by 80,000 vehicles daily and has several features which make it suitable for investigating f-NO_2:

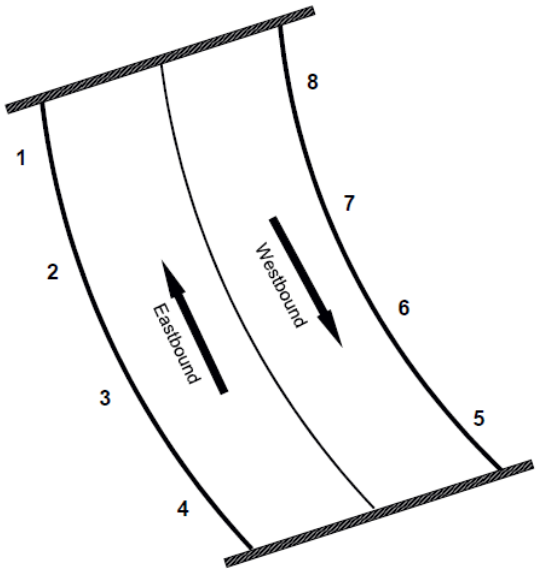

Figure 1. Schematic of tunnel and sampling positions (numbered)

- Individual 380 m long two-lane bores for each direction of travel with a significant 5% road grade (positive eastbound) - permits investigation of engine loading
- No ventilation system – transport of air reliant upon “piston effect” of traffic flow
- Four spaced sampling positions throughout the length of each bore that can be accessed from a single access point – straightforward to sample from different positions
- CCTV – traffic counting
- 40 mph (64 kph) limit – equivalent speed for all vehicle types unlike a typical motorway where heavier duty vehicles such as HGVs are subject to lower speed restrictions than other traffic

Both mobile and static monitoring techniques have been employed to investigate NO_x emissions in the tunnel. Mobile measurements were performed with an instrumented vehicle, the Mobile

Atmospheric Chemistry Unit (MACU), which contained a fast response (< 10 s) ECO Physics CLD 88 Y NO_x chemiluminescence analyser. Static measurements have been performed by a combination of the ECO Physics analyser and an additional chemilumescence analyser, a Teledyne-API M200A.

The road that the tunnel is located on is situated in a street canyon like environment, with walls of approximately 10 m height on either side of the road. The effect of a street canyon is that dispersion of pollutants is restricted leading to higher concentrations to that compared of an 'open-air' road (Hoy and Larssen, 1984), similar in principle to a tunnel. Mobile measurements of journeys through the tunnel revealed that this effect is present on the tunnel road canyon (**Figure 2**), where there is an appreciable concentration (>200 ppb) of NO_x at the entrances of each tunnel bore. Therefore a single sample position from within the tunnel cannot be used to measure f-NO_2 directly. NO_x measured at each sample position (SP) would contain a significant component of the street canyon air drawn in by the piston effect, with increasing significance by proximity to the entrance. The street canyon air would likely have experienced secondary chemistry, altering the fraction of NO_x as NO_2 and hence effect our perceived tunnel f-NO_2.

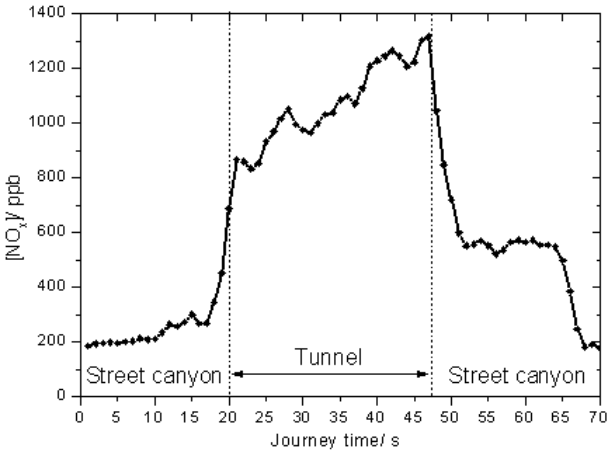

Figure 2. Eastbound journey through tunnel in MACU (measurement rate = s^{-1})

In order to negate this effect we have used two 'deductive' techniques, a long-term deduction and a real-time deduction, to measure the difference between sample positions within a bore. This allows us remove the effect of air drawn into the tunnel from emissions made solely in the tunnel alone and hence measure f-NO_2. The long term deduction is based upon the database of measurements collected by each instrument at SP2 and SP3 throughout the measurement campaign (75 weeks to date). The real-time deduction is based upon 8 weeks of simultaneous measurement, and deduction, at different sampling positions by the ECO Physics (SP2) and Teledyne-API (SP3) instruments.

Tunnel air is pumped by a BOC-Edwards XDS-10 scroll pump to an adjoining room housing the instrumentation via 3/8" tubing connected to each of the sample positions. The residence time within the tubing is < 60 s for all positions, and is sufficiently short to prevent greater than negligent (< 1 ppb) termolecular conversion via the $2NO + O_2 \rightarrow 2NO_2$ pathway observed in other tunnels (Indrehus and Vassbotn, 2001). Data is collected as a minute average, providing a high resolution for a long term experiment. Each instrument is calibrated twice a week and has undergone inter-comparison experiments within the tunnel that demonstrate a high level of agreement.

Results

To date measurements have been focused on the eastbound (uphill) bore, with sample positions SP2 and SP3 used for both the real-time and long-term deduction experiments. Analysis of our measurement database has yielded a high level of reproducibility within the tunnel under 'normal' conditions. On 'normal' days traffic counting has shown that half hourly composition, volume and flow are consistent on the weekdays Monday to Thursday (**Figure 3**). Events such as public holidays provide different traffic to 'normal' days and are not part of our long-term and real-time f-NO_2 comparison databases. Normal weekday NO_x concentrations within the tunnel rise during the morning rush hour as the number of vehicles increases towards a morning peak, traffic and NO_x fluctuate during the course of the day before rising towards an evening rush hour peak, and then decline towards the night as traffic levels decrease. Owing to the high level of reproducibility displayed by weekdays Monday to Thursday, measurements have been amalgamated as a 'weekday'.

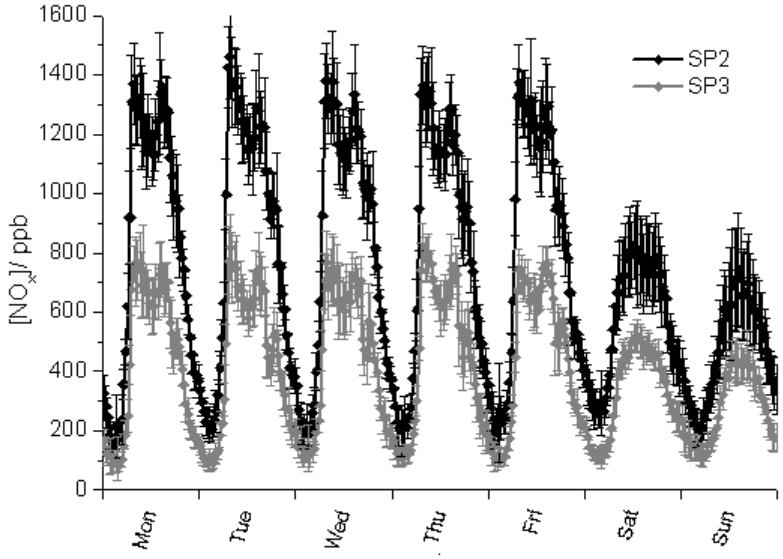

Figure 3. 30 minute average normal diurnal profile of NO_x at SP2 and SP3 throughout measurement campaign (error bars = 1σ of data)

As displayed by the mobile measurements (**Figure 1**) and diurnal profiles of SP2 and SP3 (**Figure 3**) concentration increases with distance into the tunnel. This provides a difference in concentration between SP3 and SP2 which we treat as emissions made solely in the tunnel alone and without the influence of street canyon air. The long-term and real-time f-NO_2s from SP2-SP3 deductions for weekdays between 08:00 and 18:00, where traffic volume is high and consistent, are compared with a modelled f-NO_2 in **Figure 4**. The model f-NO_2 is constructed from the typical daytime tunnel traffic composition from traffic counting and UK fleet weighted f-NO_2 for different vehicle types in **Table 1** (NAEI, 2010).

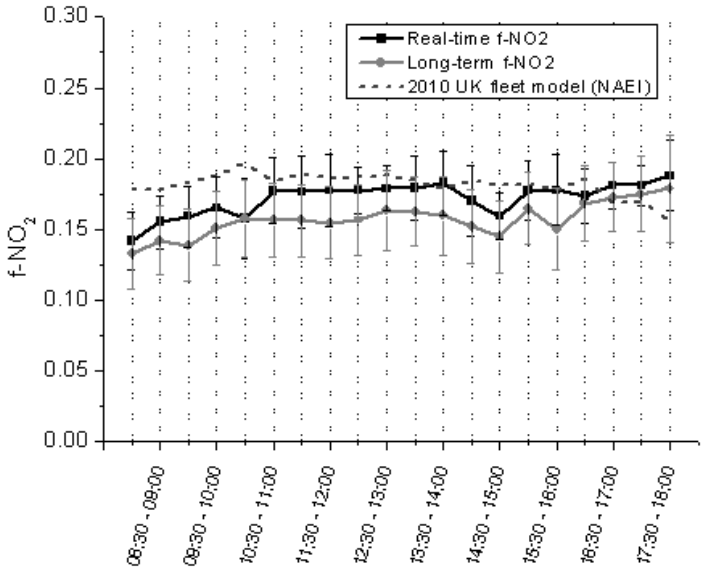

Figure 4. Graph of weekday long-term and real-time f-NO_2 from tunnel studies to date and comparison with 2010 UK fleet projections (error bars = 1σ of data)

Vehicle type	f-NO_2	% veh
Cars & Taxis	0.15	80
LGVs	0.362	15
Rigid HGVs	0.125	5
Artic HGVs	0.127	
Buses	0.125	
Motorcycles	0.04	<1

Table 1. UK fleet f-NO_2 by vehicle type (NAEI – outside of London) used in model (Figure 4) and typical weekday daytime tunnel traffic composition

Both approaches to date have provided an f-NO_2 of significantly greater than the previously thought 0.05 with weekday daytime mean real-time f-NO_2 of 0.17 ± 0.021(1σ), and mean long-term calculated f-NO_2 of 0.16 ± 0.027(1σ). There is a good level of agreement between 2010 NAEI fleet projected f-NO_2 and real-time f-NO_2 between 10:30 – 11:00 and 13:30 – 14:00, and 15:00 – 15:30

and 16:30 – 17:00. The lower morning f-NO_2, afternoon dip at 14:30 – 15:00 and increase beyond 17:00 are not explained by the traffic model. While the long-term f-NO_2 displays similar trend like behaviour to real-time it provides a lower fraction and does not agree as closely with the traffic model. As mentioned previously in this paper the penetration of higher f-NO_2 CI vehicles into the fleet is ever increasing, suggesting that on-road f-NO_2 may be subject to continual gradual increase. Long-term f-NO_2 is calculated from comparison of measurements made by both instruments throughout the measurement campaign and includes data that has been collected from October 2008 onwards. It is therefore possible that the f-NO_2 reported by real-time measurements in 2010 is greater than long-term due to long-term being influenced by older, lower f-NO_2, conditions. The greater variability (1σ) of the long-term data may further suggest that this effect is taking place. This hypothesis draws into question the validity of the long-term approach in a potentially continually changing f-NO_2 environment and will be given consideration during the final analysis of data at the end of the measurement campaign.

Discussion

Our measurements to date have provided two f-NO_2s that are significantly greater than historically thought 0.05 and support the statistical analyses of roadside data suggesting f-NO_2 is increasing (Carslaw et al., 2005, Grice et al., 2009). Application of the f-NO_2 values derived in the Hatfield and Bell Common tunnel study (TRL, 2007) to the traffic composition in the tunnel provides an f-NO_2 range of 0.172 – 0.247 in comparison to 0.17 ± 0.021(1σ) and 0.16 ± 0.027(1σ) provided by our real-time and long-term approaches. However care must be taken with direct comparison due to the proximity of the Hatfield and Bell Common tunnels to London, which is distinguished from other UK areas in the NAEI f-NO_2 projections due to an alternate fleet composition. Good agreement however has been found during periods of the normal weekday for real-time f-NO_2 with 2010 NAEI f-NO_2 projections for the UK fleet. This suggests that the tunnel traffic is representative of the UK vehicle fleet and that the NAEI projections may be used elsewhere in the UK when trying to predict on road f-NO_2 from traffic counting.

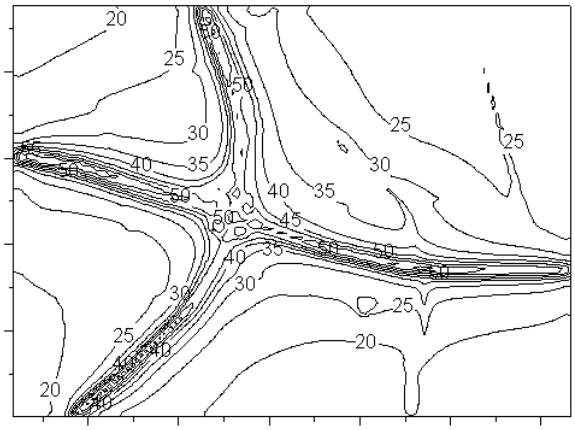

Figure 5. Airviro dispersion model of annual mean NO_2 with f-NO_2 = 0.05 (2x2.5 km grid)

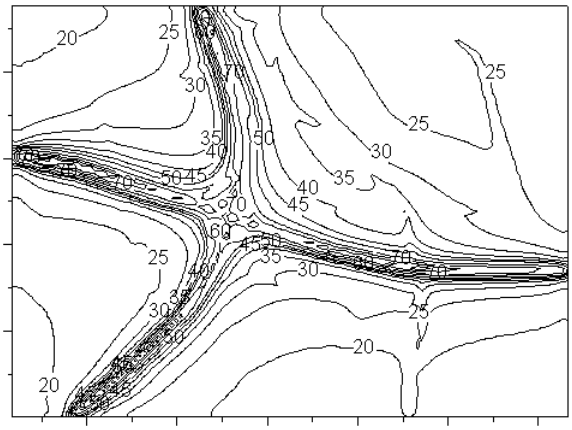

Figure 6. Airviro dispersion model of annual mean NO_2 with f-NO_2 = 0.17 (2x2.5 km grid)

f-NO_2 is a required input for a number of air quality models used to predict ambient NO_2 with regard to European target limits. The current uncertainty in on-road f-NO_2 makes construction of an accurate and closely representative model difficult. **Figure 5** and **Figure 6** display the difference in predicted annual mean NO_2 with f-NO_2 of 0.05 and 0.17 from a motorway intersection NO_x source. Dependent upon the f-NO_2 used the distance from the road where the annual limit (40 μg m^{-3}) is breached varies considerably; reinforcing the requirement for an accurate determination of f-NO_2 in order to predict air quality and design strategies to meet the European target limits.

References

AQEG (2004) Nitrogen Dioxide in the United Kingdom. Air Quality Expert Group.

AQEG (2007) Trends in Primary Nitrogen Dioxide in the UK. Air Quality Expert Group.

BARNETT ADRIAN, G., WILLIAMS GAIL, M., SCHWARTZ, J., BEST TRUDI, L., NELLER ANNE, H., PETROESCHEVSKY ANNA, L. & SIMPSON ROD, W. (2006) The effects of air pollution on hospitalizations for cardiovascular disease in elderly people in Australian and New Zealand cities. *Environ Health Perspect FIELD Full Journal Title:Environmental health perspectives,* 114**,** 1018-23.

BOULE, P., HUTZINGER, O. & BAHNEMANN, D. (1999) *Environmental Photochemistry*, Springer.

CARSLAW, D. C. & BEEVERS, S. D. (2005) Estimations of road vehicle primary NO2 exhaust emission fractions using monitoring data in London. *Atmospheric Environment,* 39**,** 167-177.

CARSLAW, D. C., BEEVERS, S. D. & BELL, M. C. (2005) Evidence of an increasing NO2/NOX emissions ratio from road traffic emissions. *Atmospheric Environment,* 39**,** 4793-4802.

CARSLAW, D. C., BEEVERS, S. D. & BELL, M. C. (2007) Risks of exceeding the hourly EU limit value for nitrogen dioxide resulting from increased road transport emissions of primary nitrogen dioxide. *Atmospheric Environment,* 41**,** 2073-2082.

CHAUHAN, A. J., INSKIP, H. M., LINAKER, C. H., SMITH, S., SCHREIBER, J., JOHNSTON, S. L. & HOLGATE, S. T. (2003) Personal exposure to nitrogen dioxide (NO2) and the severity of virus-induced asthma in children. *Lancet,* 361**,** 1939-1944.

COPERTIV (2010), Laboratory of Applied Thermodynamics, Aristotle University of Thessaloniki.

EEA (2010), European Environment Agency.

ENGLISH, P., NEUTRA, R., SCALF, R., SULLIVAN, M., WALLER, L. & ZHU, L. (1999) Examining associations between childhood asthma and traffic flow using a geographic information system. *Environ Health Perspect FIELD Full Journal Title:Environmental health perspectives,* 107**,** 761-7.

GRICE, S., STEDMAN, J., KENT, A., HOBSON, M., NORRIS, J., ABBOTT, J. & COOKE, S. (2009) Recent trends and projections of primary NO2 emissions in Europe. *Atmospheric Environment,* 43**,** 2154-2167.

HEYWOOD, J. B. (1988) *Internal Combustion Engine Fundamentals*, McGraw-Hill.

HOY, O. & LARSSEN, S. (1984) Street canyon concentrations of nitrogen dioxide in Oslo. Measurements and model calculations. *Environ. Sci. Technol. FIELD Full Journal Title:Environmental Science and Technology,* 18**,** 82-7.

INDREHUS, O. & VASSBOTN, P. (2001) CO and NO2 pollution in a long two-way traffic road tunnel: investigation of NO2/NOx ratio and modelling of NO2 concentration. *Journal of Environmental Monitoring,* 3**,** 220-225.

JENKIN, M. E. (2004) Analysis of sources and partitioning of oxidant in the UK--Part 2: contributions of nitrogen dioxide emissions and background ozone at a kerbside location in London. *Atmospheric Environment,* 38**,** 5131-5138.

LARRIEU, S., JUSOT, J.-F., BLANCHARD, M., PROUVOST, H., DECLERCQ, C., FABRE, P., PASCAL, L., LE TERTRE, A., WAGNER, V., RIVIERE, S., CHARDON, B., BORRELLI, D., CASSADOU, S., EILSTEIN, D. & LEFRANC, A. (2007) Short term effects of air pollution on hospitalizations for cardiovascular diseases in eight French cities: The PSAS program. *Science of the Total Environment,* 387**,** 105-112.

LATZA, U., GERDES, S. & BAUR, X. (2009) Effects of nitrogen dioxide on human health: Systematic review of experimental and epidemiological studies conducted between 2002 and 2006. *International Journal of Hygiene and Environmental Health,* 212**,** 271-287.

LENNER, M., LINDQVIST, O. & ROSEN, A. (1983) The nitrogen dioxide/nitrogen oxides ratio in emissions from gasoline-powered cars: high nitrogen dioxide percentage in idle engine measurements. *Atmospheric Environment (1967-1989),* 17**,** 1395-8.

MILLER, J. A. & BOWMAN, C. T. (1989) Mechanism and modeling of nitrogen chemistry in combustion. *Progress in Energy and Combustion Science,* 15**,** 287-338.

NAEI (2010) National Atmospheric Emissions Inventory

SUNYER, J., JARVIS, D., GOTSCHI, T., GARCIA-ESTEBAN, R., JACQUEMIN, B., AGUILERA, I., ACKERMAN, U., DE MARCO, R., FORSBERG, B., GISLASON, T., HEINRICH, J., NORBACK, D., VILLANI, S. & KUNZLI, N. (2006) Chronic bronchitis and urban air pollution in an international study. *Occup. Environ. Med. FIELD Full Journal Title:Occupational and Environmental Medicine,* 63**,** 836-843.

TRL (2007) Primary NO2 emissions from road vehicles in the Hatfield and Bell Common tunnels. IN P. BOULTER, I. M. A. J. G. (Ed.).

UK-AQA (2010) UK Air Quality Archive.

Air Quality in the Ile de France road tunnels (AIRTURIF project) : presentation , methodology and preliminary results

A.Guilloteau[1], *B. Vidal*[2], *L.Paillat*[3], *G.Thiaut*[3], *D. Preterre*[4], *V. Dunez*[5].

[1] Centre d'Etudes Techniques de l'Equipement *Ile de France*, 12 rue Teisserenc de Bort 78 Trappes en Yvelines angelique.guilloteau@developpement-durable.gouv.fr
[2] Centre d'Etudes des Tunnels, 25 avenue François Mitterrand 69674 Bron
[3] Laboratoire Central de la Préfecture de Police, 39bis, rue Dantzig 75015 Paris
[4] Centre d'Etude et de Recherche Technologique en Aérothermique et Moteur, 1 rue Joseph Fourier 76800 St-Etienne du Rouvray
[5] Centre d'Etudes Techniques de l'Equipement *Nord Picardie*, 2 rue de Bruxelles 59019 Lille

CONTEXT AND OBJECTIVES

Despite reductions in emissions due to road traffic in the last ten years, epidemiological studies show the negative impact of pollution in urban areas on breathing and cardiovascular systems, or even on mortality (Institut de veille sanitaire, June 2008). The pollutants emitted by road traffic therefore remain a health concern with many uncertainties.

In Ile de France, studies performed by AIRPARIF and INSERM on the exposure of drivers to air pollution related to traffic showed that pollutant concentrations could reach significant values at rush hours, notably in some urban road tunnels (Morin and al, 2006), (Airparif, 2009). This leads to the question about the possible impact of road tunnels on the health of their regular users and local residents living very close to their portals.

The choice of implementing a road urban tunnel presents obvious advantages for the quality of life by removing congestion of vehicles on the surface (improvement of the outdoor air quality, noise levels, town plannings). However emissions (particulates, NO_2, benzene…) of vehicles using these structures are not, for that matter, removed. By their confined nature, the exhaust fumes accumulate, especially in congestion situations, with a possible negative impact on the users' health (World Health Organization, 2005). On the other hand the portals or exhaust stack releases must be carefully controlled under pain of having the nearby residents health affected. Finally the question of observing the standards concerning air quality in and around the road tunnels is a particularly sensitive subject.

The current international recommendations on air quality in road tunnels today concern carbon monoxide (CO), nitrogen dioxide (NO_2) and opacity (PIARC, 2008). In France, circular 99.329 of June 8, 1999 regulates, for averages along the structure, the concentrations of CO (90 ppm over 15 minutes) and NO_2 (400 ppb over 15 minutes) (Conseil Supérieur d'Hygiène Publique de France, 1998). Besides, the World Health Organization (WHO) recommends the measurement of many other pollutants not regulated at present, for both ambient air and vehicle emissions (World Health Organization, 2005).

On the other hand, several ways exist to reduce the concentrations of pollutants in and at the interfaces of tunnels. They can be classified in two families according to their action: devices allowing the dilution of pollutants by the supply of fresh air or treatment of pollutants. After a bibliographic study, certainly not exhaustive, about thirty treatment structures have been listed. In France, tunnels usually have dispersion devices – usually referred to as health ventilation – generally driven by levels of CO and opacity. Since these pollutants are no longer very relevant indicators of traffic pollution, NO_2 detectors are beginning to be used; on the other hand, no structure is equipped with a device for air cleaning.

With 22 underground structures, the national road network of Ile de France alone totals 45 km of tunnels. Trips often long, combined with high traffic density, force users to an increased risk of exposure to pollutants emitted by road traffic. Recognizing this, the state services initiated the AIRTURIF (Air Quality in the Road Tunnels of Ile de France) study with the following objectives :

- characterization of air pollution in and around the Ile de France tunnels ;
- estimating the impact of this pollution on the drivers and residents near the road tunnel emission releases ;

- evaluation of mechanical ventilation systems and pollution clearing devices.

This article present the general methodology adopted for this project and the preliminary results of the first measurement campaign conducted in 2009.

GENERAL METHODOLOGY OF THE STUDY

To achieve the objectives mentioned, the following lines are identified :

- performance of field measurements as comprehensive as possible ;
- assessing the impact on drivers by measures on board a vehicle included in the traffic and especially in all the tunnels ;
- estimate of the impact of health ventilation on a wide range of compounds ;
- testing of the major solutions of on site air pollution removal available on the market.

Pollution related to road tunnels in Ile de France

With lengths of 300 to 2200 meters, the typology of the 22 tunnels of Ile de France also varies greatly depending on their traffic and their health ventilation system. The measurement campaigns have focused on the tunnels most sensitive to pollution and the sites to be studied were chosen according to high instrumentation constraints (access to a space under traffic, availability of a suitable location) in the hostile environment (soot, corrosion,…) of tunnels for equipment. The goal is to install two measurement points per structure :

- a site outside the structure, around the portal, representative of the areas frequented by the public ;
- a site within the structure, preferably near the exit.

The choice of the pollutants selected for measurement is very wide. In tunnels, it is a question of deepening knowledge of conventionally monitored pollutants (NO_2, CO, opacity) as well as acquiring knowledge of others – Volatile Organic Compounds (VOCs), particles (PM_{10}, $PM_{2,5}$), metals – less documented from the prior bibliographic study. In the field of metrology, various techniques are used :

- continuous measurements of NO_X, CO, BTEX, PM_{10} and $PM_{2,5}$;
- measurements of particle mass concentration with an impactor or with a tapered element oscillating microbalance ;
- continuous measurement of particle number concentrations ;
- sampling on activated charcoal or by canister then deferred analysis for MAH (Monocyclic Aromatic Hydrocarbon), PAH (Polycyclic Aromatic Hydrocarbon) and aldehydes ;
- detection of metals and platinoids by chemical analysis of the particles.

In addition to the two main measurement sites, the average pollution is assessed using passive diffusion tubes for NO_2 and HAMs for mapping the pollution inside the structure (longitudinally) and throughout the area potentially subject to polluted air release. To take into account possible seasonal variability, several measurement campaigns of two weeks are planned and will be extended by recording for several weeks with automatic analyzers of both main tracers of vehicle pollution: the NO_X and the particles matter PM_{10} and $PM_{2.5.}$

Exposure of drivers in Ile de France

The on-road measurements, at one second intervals and coupled with GPS location, are conducted by a commercial vehicle equipped by the CERTAM. The sampling is done at the central air intakes of the cabin and supplies :

- a Topaze 32M (Environnement SA) NO_X double chamber dynamic analyzer ;
- a CO dynamic analyzer 12M (Environnement SA) ;
- an ELPI (Dekati) particle size meter and a Ptrak (TSI) condensation particle counter.

To be as representative as possible of the actual pollution in these tunnels, the experimental sampling must be sufficiently variable to represent all traffic conditions (flow and composition). Thus, five weeks of measures have been planned ; the measuring vehicle journeys on the urban motorways have been made to obtain 15 crossings per structure and per direction with departure time between 6 am and 2 pm.

Analysis of the results

The recordings, completed by the data of traffic, ventilation, weather and the pollution levels of the urban background, will allow :

- statistical treatment for comparison with the Toxicological Reference Values ;
- to establish daily patterns of the pollution in tunnels ;
- to look for correlations to try to assess the impact of the structure discharges on its immediate environment.

The on-road measurements will show the levels and the exposure times of the drivers depending on the type of roads (tunnels, motorways…) and whether the flow of traffic is fluid or not. They can also help to highlight the specificities of each structure (observable levels and the average longitudinal profile) and will be compared with those collected at the same time on the tunnel instrumented sites.

Improving air quality in road tunnels and their immediate surroundings

The first objective is to confirm the effectiveness of the pollutant dilution measures, functioning by the injection of fresh air, by conducting tests on the occasion of the field measurements. On the other hand, the AIRTURIF program provides the inter-comparison of different systems of air cleaning in the same traffic conditions and levels of concentration. This study will allow for example to assess some operation parameters (flow, time of use, energy consumption…) in order to develop a doctrine for the design of the future structures. The efficiency of these devices will be controlled by a continuous analysis of the particles, nitrogen oxides upstream and downstream from the treatment units. The possible impact on other compounds such as the VOC will also be studied. Four solutions for the air cleaning could be tested :

- filtration of the particles by electrostatic precipitation, followed by denitrification ;
- biofiltration using plants selected for their purifying ability ;
- the technique of “cold plasma” which uses the reactivity of the plasma to convert the toxic effluents into harmless gases ;
- photocatalysis which destroys nitrogen oxides (NO_X) by converting them into acid solutions (HNO_3).

The pollution removal device models will be established close to an exhaust duct which control the air outflow of a tunnel where traffic can offer a high potential in terms of pollution. The air sample collected (about 6 m^3/sec) will then be dispatched to various pilot units for air cleaning.

MEASUREMENT CAMPAIGNS IN 2009

The first measurement campaign was conducted for two weeks from March 23 to April 5 2009 and has allowed the instrumentation of two tunnels of different types :

- *The Landy Tunnel:* 1357m, unidirectional reversible semi-transversal ventilation, 103,000 vehicles/day in the direction in which the measurements were performed, little gradient *;*
- *The Saint-Cloud Tunnel :* 832m, longitudinal ventilation, unidirectional, 78,000 vehicles/day in the direction that the measurements were performed, average gradient 1.2%.

The health ventilation has never worked in these structures during the measurement campaign. Only the air stream created by the piston effect of the traffic caused longitudinal ventilation. During this campaign, three sites were instrumented with automatic analysers :

- A measurement point on the outside, near the the Landy tunnel exit, about 50 meters from the South portal ;
- Two measuring points in tunnel, the first 1207m from the Landy tunnel entrance and the second at 400m from the Saint-Cloud tunnel entrance.

In addition, mapping was carried out around the portal and inside the two tunnels, and the vehicle dedicated to the on-road measurements covered, from 5 to 12 times, 17 of the 22 tunnels.

The measurements were carried out with the collaboration of the Laboratoire Central de la Préfecture de Police de Paris for the fixed measurements inside the tunnel, the CETE Nord

Picardie for the fixed measurements outside the Landy tunnel, and the CERTAM for the on board measurements.

PRELIMINARY RESULTS AND DISCUSSION

Overall results of the main pollutants

The concentrations of NO_2, CO and (PM_{10} and $PM_{2.5}$) particles are measured continuously and averaged every 5 minutes throughout the campaign. Table 1 presents the averages for the entire campaign for the 3 instrumented sites.

Table 1: Averages of the concentration levels of the measured pollutants

	Landy-inside	Landy-outside	Saint-Cloud-inside
NO_2 (µg/m^3)	542	68	360
CO (mg/m^3)	4.5	0.5	4
PM_{10} (µg/m^3)	232	42	-
$PM_{2.5}$ (µg/m^3)	128	-	-

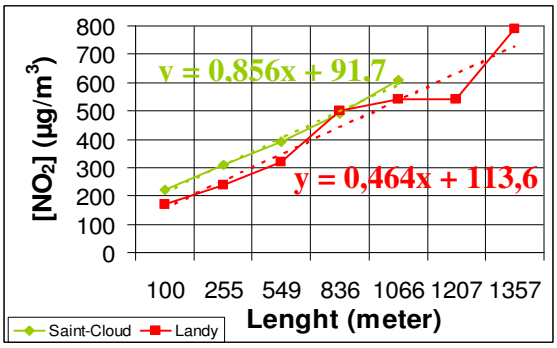

Figure 1 : Average longitudinal profiles of NO_2

Figure 1 shows the average longitudinal profiles of the NO_2 levels for the 2 tunnels (averages over 14 days with diffusion tubes). These profiles are linear (or near linear for Landy). Regression straight lines are used to extrapolate the averages in space. These linear longitudinal profiles confirm that tunnels are usually longitudinally ventilated by the traffic piston effect (excluding congestion) and show far from negligible average levels at the entrance of about 100 µg/m^3.

Retaining the assumption of a linear longitudinal profile for the pollutant levels in tunnel throughout the measurement campaign, the levels of the extrapolated spatial averages of NO_2 would be slightly higher in the tunnel of Saint-Cloud (448 µg/m^3) than those of Landy (428 µg/m^3). The extrapolated values of the average levels of discharges would be 743 µg/m^3 and 804 µg/m^3 respectively for Landy and Saint-Cloud.

Concerning the concentration levels around the Landy tunnel, they are considerably lower than at the portal, demonstrating a rapid dispersion of release.

Results obtained for the Landy tunnel

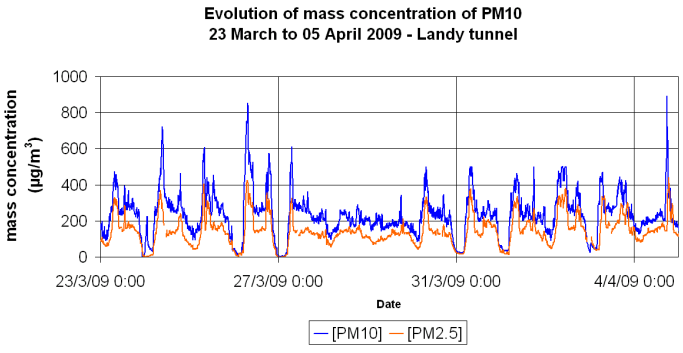

Figure 2 : Average concentrations of $PM_{2.5}$ (orange) and PM_{10} (blue)

- inside the tunnel

Changes in pollutant concentrations vary in the same manner (figure 2) and are explained by the variation of traffic in the tunnel (figure 3) with a large daily peak every morning of working days. Table 2 presents the statistic data of concentrations measured on working days between 6 am and 9 pm.

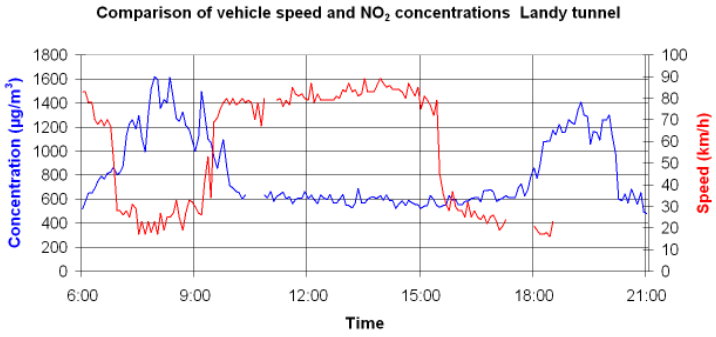

Figure 3 Comparison of the change of NO_2 (blue) and vehicles speed (red)

Table 2 : Statistical data at the measuring point in the Landy tunnel

Concentrations over 5 minutes in µg/m^3, working days, from 6am to 9pm	NO_2 (µg/m^3)	PM_{10} (µg/m^3)	$PM_{2.5}$ (µg/m^3)
Daily average	762	314	196
Daily maximum	1970	854	426
Daily minimum	470	165	109
P25	580	245	144
P50	628	278	167
P75	893	363	244
P90,4	1215	462	310
P98	1545	585	358

Since the traffic in the Landy tunnel is much more often fluid (or quasi-fluid) than congested, we could extrapolate the average measurements of NO_2 over the 6am-9pm period on weekdays, according to two assumptions. Either considering that NO_2 levels are low at night (closing of the tunnel for repairs), we could then estimate the average by only shifting the ordinate at the origin of the regression line (+89µg/m^3) ; or by using a medium level of 375µg/m^3 in the tunnel entrance according to the on-road measurements, we estimate the NO_2 average with a lower gradient linear profile. The average levels of NO_2 (daytime spatial average on weekdays) thus estimated in the Landy tunnel would be in the range from 517 to 592 µg/m^3 and the average levels of discharge in the range from 809 to 832 µg/m^3.

- *On-road measurements*

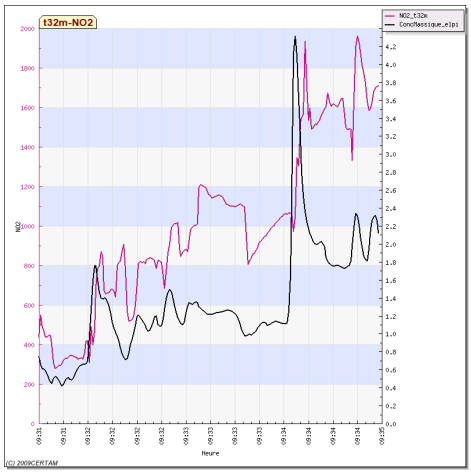

Figure 4 represents the concentration changes of NO_2 and PM_{10} measured in the vehicle passenger compartments as it travels through the tunnel. This example shows a situation of congestion : the vehicle crosses the tunnel in 4 minutes. Major fluctuations in these two curves are often related to emissions from vehicles preceding the measurement vehicle. In this example, the driver is exposed to concentrations ranging from 279 to 1962 µg/m^3 for NO_2 and 422 to 4318 µg/m^3 for PM_{10}, with average levels of 1002 µg/m^3 for NO_2 and 1348 µg/m^3 for PM_{10} during this passage.

Figure 4 Changes of the average concentrations of NO_2 (pink) and PM_{10} (black) measured in the vehicle passenger compartment during its passage in the Landy tunnel.

For the NO_2, the Conseil Supérieur d'Hygiène Publique de France recommends not to exceed 800 µg/m^3 on an average over the length of the tunnel over a period of 15 minutes. But this average in space is difficult to estimate, particularly in situations of congestion, unless the whole structure is instrumented with automatic analyzers. For the Saint Cloud tunnel, the traffic is

always fluid (or quasi fluid). Since the measuring station is located at the middle of the structure, it can be more easily estimated that the value registered at this point also represents the average in space and conclude that the regulation for NO_2 is observed during 99.6% of the time during the 6am-9pm period.

For the example illustrated by figure 4, the concentration of NO_2, in the vehicle passenger compartment is, on an average 1002 µg/m^3 during the 4 minutes of the Landy tunnel crossing. The value measured at the same moment on the analyzer in the tunnel is 1250 µg/m^3, which is globally consistent with the on-road measurement. Since it is a case of traffic congestion and in view of the average level of NO_2 observed in the vehicle, the occurrence of a crossing of the regulatory threshold is quite plausible but cannot be confirmed by the measurement of the automatic station alone without knowing the longitudinal profile of the pollution.

Outside the tunnel, the regulatory values for NO_2, are 200 µg/m^3 on an average over one hour and 40 µg/m^3 as an annual average. During the measuring campaign, 100% of the values are in compliance with the hourly recommendation for the site around the tunnel, while the average measured over the two weeks is 68.2 µg/m^3.

CONCLUSIONS

AIRTURIF is an ambitious programme whose purpose is to better understand the exposure of drivers and neighbourhood residents to the specific pollution of road tunnels in Ile de France and to evaluate the means to reduce it (health ventilation or treatment of the exhaust air). Study of this pollution began during a preliminary campaign with fixed station monitoring of a wide range of pollutants (NO_X, CO, particles, MAH, PAH, aldehydes, metals). This overall view is completed by on road measurements on NO_X, CO and particles and later by the measurement of VOC.

The first conclusions of the preliminary measuring campaign (March 2009) show that :

- *For the exposure of the drivers* : besides the significant levels measured in the passenger compartment on urban motorways, the crossing of tunnel represented non-negligible pollution peaks but over short times. The most sensitive situations which are also the most complex to analyse are congestions with higher concentration of pollutants for extended transit times. However, the durations of the exposure time remain rather short and, in these cases, the health ventilation could give considerable improvements. On the other hand, the exposure of drivers must be understood over the whole trip.
- *For the exposure of neighbouring residents* : no exceeding of the regulatory levels is noted on the hourly averages for NO_2 in the course of the two weeks of measurement on the measuring site outside, very close to the discharge. This analysis remains to be developed for the whole of the neighbourhood around, for other pollutants and according to various weather conditions.
- *For the regulatory thresholds in the tunnels* : they are well observed for CO and exceeding of the 800 µg/m^3 threshold is observed for the NO_2. On-board measurements showed the tunnels which were most sensitive to pollution.

This vast project will be continued in 2010 by new measuring campaigns including tests with health ventilation. Three additional weeks of measurements will allow drawing up the longitudinal profiles of pollution in the tunnels, particularly in cases of congestion. Besides, it is foreseen in 2011 to launch an inter-comparison of the various air cleaning systems which will be covered by specific measurements from 2010 for NO_X, particles and benzene.

BIBLIOGRAPHY

Agence Française de Sécurité Sanitaire de l'Environnement et du Travail, Recommandations pour la qualité de l'air dans les parcs de stationnement couverts, April 2007.

AIRPARIF, Exposition des automobilistes franciliens à la pollution atmosphérique liée au trafic routier, October 2009.

Conseil Supérieur d'Hygiène Publique de France, Qualité de l'air dans les ouvrages souterrains ou couverts , 1998, p.19-26.

Institut de Veille Sanitaire, Programme de Surveillance air et santé, Analyse des liens à court terme entre pollution atmosphérique urbaine et mortalité dans neuf villes françaises, June 2008.

Morin J-P., Dionnet F., Delmas V., Caractérisation des expositions professionnelles et des usagers des transports routiers : Mesures dynamiques en habitacles de véhicule inséré dans le trafic, *Institut National de la Santé et de la Recherche Médical*, 2006.

PIARC, Road tunnels: a guide to optimising the air quality impact upon the environment, *Technical Committee C3.3 Road Tunnel Operations*, 2008.

World Health Organization , Air Quality Guidelines, global update, 2005.

Passive and Active regeneration modes and their characteristics on a modern Diesel Particulate Filter System

A. Karpf[1], D. Schreiber[2], P. Dimopoulos Eggenschwiler[3] and R. Wachter[4]

[1] ETH Zurich, Aerothermochemistry and Combustion Systems Laboratory and Institute for Dynamic Systems and Control, CH-8092 Zurich, Switzerland, akarpf@ethz.ch or Alessandro.Karpf@empa.ch
[2] Empa, Swiss Federeal Laboratories for Materials Testing and Research, Laboratory for Internal Combustion Engines (Lab137), CH-8600 Dübendorf, Switzerland, Daniel.Schreiber@empa.ch
[3] Empa, Swiss Federeal Laboratories for Materials Testing and Research, Laboratory for Internal Combustion Engines (Lab137), CH-8600 Dübendorf, Switzerland, Panayotis.Dimopoulos@empa.ch
[4] Fiat Powertrain Technologies, Iveco Motorenforschung AG, Ralph.Wachter@fptpowertrain.com

Abstract

Diesel particulate matter (soot) can easily be removed from the exhaust gas streams by means of mechanical filtration using Diesel Particulate Filters (DPF). The filtered soot has to be periodically removed from the filter during a process commonly known as 'regeneration' in order to avoid a series of implications deteriorating engine operation characteristics. Regeneration of the filtered soot mainly occurs via oxidation processes. Conditions typical for diesel exhaust gas are not very favourable for oxidation. Although there is no lack of oxygen, the low temperatures prevailing, mainly attributed to the high energy conversion efficiency of diesel engines, impose a critical impediment.

In order to regenerate particulate filters, the loaded soot can be oxidized by the exhaust gas components O_2 and NO_2. The filter regeneration only with O_2 requires high temperatures, above 600ºC, in order to oxidize the stored soot within acceptable times. Due to the high O_2 concentration, the resulting reaction rates can be much higher than those obtained by NO_2, which, on the other hand, can be used for soot oxidation at lower temperatures, above 200ºC. Since engines emit mainly NO, the oxidation catalyst has, apart from abating other emissions, also to oxidize engine-out NO to NO_2. The NO_2 production in the oxidation catalyst on the other hand is limited by the thermodynamic equilibrium. In summary the above described modes of regeneration are called passive. In most cases passive regeneration does not suffice. From time to time active regeneration processes are triggered. During active regeneration engine combustion is retarded and several other means are used in order to increase exhaust gas temperature as much as possible. During these periods fuel consumption increases, while emissions are altered.

In order to analyse and understand the coupled physical and chemical processes was built a dedicated exhaust gas after treatment system on a state-of-art heavy duty light truck where exhaust gas analysis was performed upstream and downstream the diesel oxidation catalyst (DOC) as well as downstream the particulate filter (DPF). Particulate emissions quantification was performed in terms of particle number, photo acoustic soot measurement, as well as classic gravimetric measurement.

The DOC shows very good oxidation performance. The few 100 ppm of carbon monoxide (CO) and unburned hydrocarbon (THC) coming from the engine are almost completely oxidized from the DOC. The average nitrogen oxide (NO_X) produced from the combustion shows a composition of 81-93% of NO and the rest NO_2, where high engine load reduces the relative NO_2 ratio. The DOC oxidation behaviour changed the NO_X composition ratio, reducing the NO to 57-82% of NO_X and increasing the NO_2/NO_x. As expected, the NO_2 level increases before the DPF with higher engine out temperatures and loads, where higher NO_X are emitted. DOC reduces the soot particles number from 3-4%. The DPF shows soot and PM number filtration efficiency higher than 99.9%. During active regeneration higher fuel consumption was observed and few mg of emitted soot were detected.

Introduction

Diesel engines became very popular in the last years for trucks and passenger cars due to their lower fuel consumption respect to the gasoline engines. There are several reasons which justify the lower fuel consumption and the most important are the higher compression ratios, the possibility of a lean mixture combustion (where higher efficiencies can be reached) and also the lower fresh air pumping losses; respect to the gasoline engines. Nevertheless diesel engine needs more sophisticated exhaust gas after treatment systems to reduce nitrogen oxides (NO_x) and particulate matter (PM). The process of NO_x formation take place during the combustion, nevertheless the excess of oxygen doesn't permit a NO_x reduction with the typical three-way catalyst used for the gasoline cars. The PM originates on the core of the injected fuel via cracking process. Summarizing, the main harmful species emitted from diesel engine are: carbon monoxide (CO), unburned hydrocarbon (THC), nitrogen oxides (NO_x) and particulate matter (PM). In order to accomplish the emission restriction proposed by the European emissions regulations for heavy-duty diesel trucks, the exhaust gas must be treated after the combustion. Tab. 1 reports the European emissions regulations standards for heavy-duty diesel trucks under steady state engine conditions (ESC, European Stationary Cycle).

Grade	Since date	CO	THC	NO_x	PM
EURO 3	10/2000	2.1	0.66	5.0	0.10
EURO 4	10/2005	1.5	0.46	3.5	0.02
EURO 5	10/2008	1.5	0.46	2.0	0.02
EURO 6	01/2013	1.5	0.13	0.4	0.01

Tab. 1: European emissions regulations for heavy-duty diesel truck under steady state conditions (ESC) in g/kWh (Dieselnet, 2010).

In compress ignited (diesel) engine it is not possible to efficiently reduce NO_x and PM at the same time. The exhaust gas after treatment system analyzed in this work proposes a diesel oxidation catalyst and downstream a diesel particulate filter.

The diesel particulate filter utilized in this work is a wall-flow monolith filter, consisting of several honey-comb structures (segments) cemented together, without catalyst coating and composes from silicon carbide. Has a volume of 6.5l, a cells density of 200cpsi and a dry weight of 5346.5g at new conditions. The passive regeneration is a continuous regeneration that occurs during normal engine conditions. The stored soot in the DPF reacts primarily with NO_2 (enhanced by the presence of O_2 and H_2O, (Setiabudi et al., 2003; Jacqot et al., 2002)) at low exhaust gas temperature conditions and for the higher temperature range the soot oxidation is dominated from the reductant O_2. The temperature range of the soot oxidation with NO_2 is between 200-500°C limited by the NO_2 thermodynamic equilibrium (Després et al., 2004). The products of the regeneration are CO, CO_2 and NO. Despite passive regeneration, all the soot in the DPF cannot be completely removed (except when the engine load is very high so that the exhaust gas becomes very hot), therefore the active regeneration is trigged by the ECU. The consequence is higher exhaust gas temperatures which enhance soot oxidation by O_2 at higher rates.

In this paper is analyzed the behavior of the exhaust gas after treatment system by driving at constant speed, first by varying the delivered force at the wheels under steady state conditions and therefore investigating the passive regeneration modes; and second analyzing the exhaust gas compositions at the end of the tile pipe during an active regeneration.

Experimental setup

The experiments were conduced with a new diesel particulate filter (DPF), installed in a modified exhaust gas after treatment case, consenting exhaust gas composition analysis. Upstream is positioned a diesel oxidation catalyst (DOC) which is a honeycomb monolith with catalyst coating surface, composed from cordierite. The modified case allows measurements up- and downstream the DOC and DPF; with eccentric inlet manifold before DOC (Fig.1).

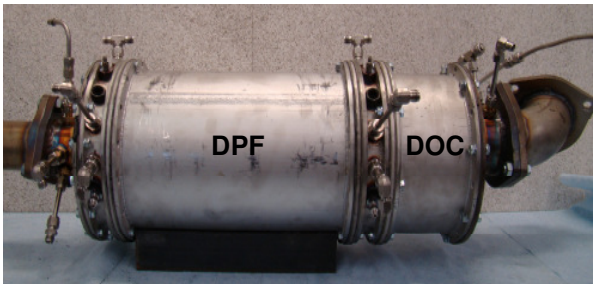

Fig. 1: Modified exhaust gas after treatment system

The utilized vehicle was installed on a test bench (chassis dynamometer), where different analyzers are connected to the exhaust gas after treatment system. The vehicle is a light truck, 2.3-litre 4 cylinders common rail diesel with turbocharger producing 110 ps. The test bench delivers the measured force at the wheels and allows for constant speed experiments. With these outputs it is possible to calculate the specific emitted mass of every exhaust species related to the energy delivered at the wheels as g/kWh.
The analyzers used in this work calculates the volume concentration of the exhaust gas species; dry CO with NDIR (Non-Dispersive Infrared), dry NO_x with CLD (Chemi-Luminescence Detection), dry CO_2 with NDIR (Non-Dispersive Infrared), wet THC with FID (Flame Ionization Detection) and dry O_2 with EGC (Electro-Galvanic Cell). The analyzers are: Horiba Mexa-7400H and CVS-9400T, Horiba Portable Multi-Gas analyzer PG-250, J.U.M Engineering HFID Model 3-200, Eco Physics CLD-700 EL ht and Leybold Hereaus Binos 1 analyzer. The additional soot mass and particulate matter number were investigated via a MSS (Micro Soot Sensor, AVL 483) with Photo Acoustic Soot Sensor and condensation particle counters CPC (Model 3022A) with optical counter detector.

The first result refers to the passive regeneration mode, where the vehicle was driven with constant speed (70 km/h) and fifth gear, varying the delivered force at the wheels between 670 and 2317N. Every step of force was driven for 20 min, in order to obtain steady state results (Fig. 2).

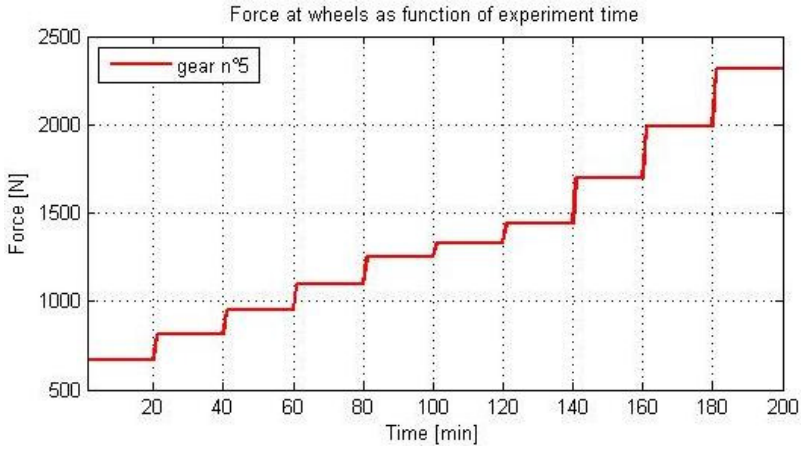

Fig. 2: force at the wheels varied during the time for passive regeneration experiments

For the active regeneration mode, the vehicle was driven with the fifth gear, a constant speed of 70 km/h and a measured delivered force at the wheels of 650±10N.

Results and discussion

Passive regeneration. The DOC has the role to oxidize the exhaust gas species emitted from the engine. The DOC conversion efficiency is defined as the ratio of the converted to the inlet exhaust species. The conversion efficiency of CO is between 93.9% and 98.8%, THC is between 92% and 95.7% and up to 35% for NO (Fig. 3).

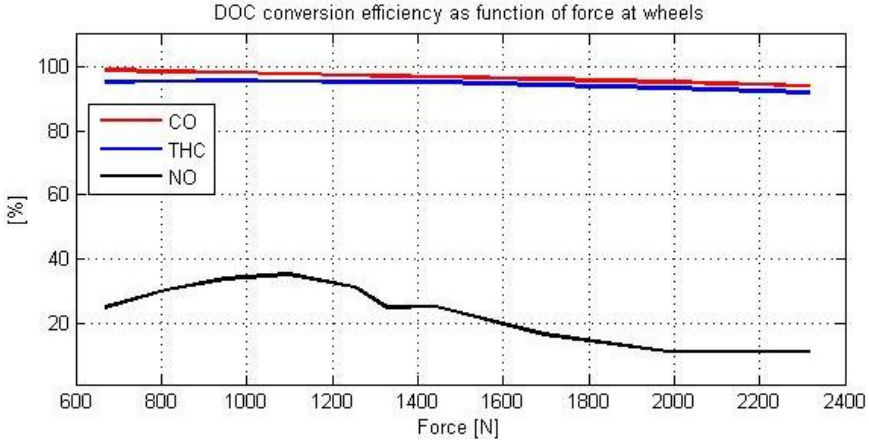

Fig. 3: DOC conversion efficiency for CO, THC and NO

For CO and THC the concentration in the exhaust and conversion efficiency decreases at higher measured force at the wheels. The measured force at the wheels is proportional to the engine load, which is also proportional to the engine out exhaust gas temperature. The conversion efficiency of NO first increases and then decreases at higher engine load, where the exhaust temperature increases, therefore reducing the NO_2 amount coming from the NO oxidation. The thermodynamic equilibrium of NO_2/NO_x ratio reveals that NO_2 is more stable respect to NO at low temperatures and vice versa NO is more stable at higher temperatures (Després et al., 2004), which is at least 10 to 30% higher respect to the NO_2/NO_x ratio measured after DOC. The NO/NO_X ratio before DOC increases by increasing the engine load from 81 to 93%. Successive the NO/NO_X ratio reduces from 57 to 82% after the oxidation reactions in the DOC. Then the NO/NO_X ratio increases due to the soot oxidation via NO_2 in the DPF with value of 83 to 97%, higher than before DOC.

The specific mass emitted in g/kWh after DPF as a function of the delivered force at the wheels is: CO increases from 0.043 and 0.104, CO_2 decreases from 960 to 749, THC decreases from 0.021 to 0.003, NO increases from 0.78 to 2.16, NO_2 between 0.055 and 0.241, and NO_X increases from 1.02 to 2.32 (Fig. 4).

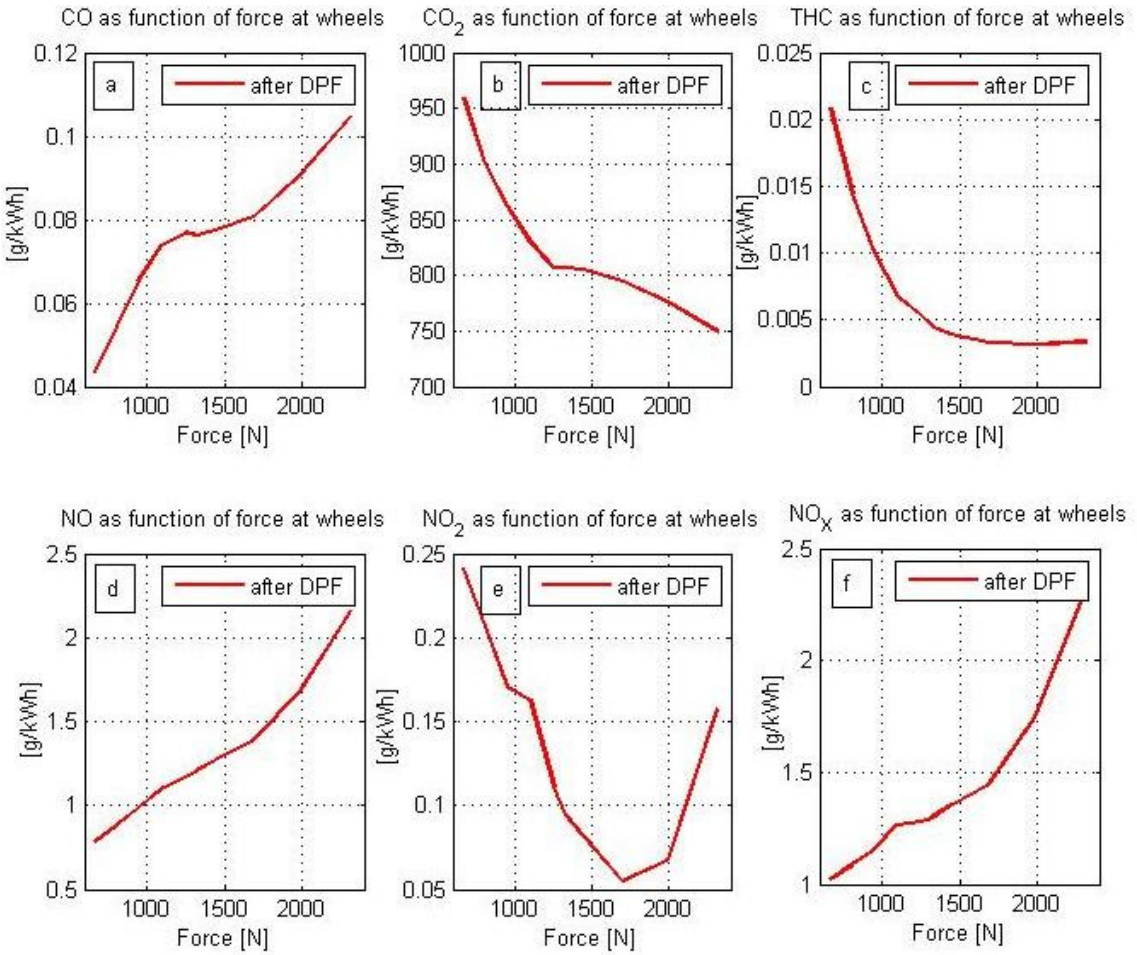

Fig. 4: CO, CO_2, THC, NO, NO_2 and NO_X specific mass emissions after DPF

The specific mass emitted after DPF of CO, NO and NO_2 are strong influenced by the passive regeneration, with an increasing of CO and NO emission due to the soot oxidation and a reduction of NO_2, which is involved in the soot oxidation reactions.

The PM number filtration efficiency defined as the ratio of the filtered to the inlet PM number and has values between 99.8 and 99.99%. The soot mass filtration efficiency is defined as the ratio of the filtered soot mass to the inlet and has values between 99.998 and 99.999%. Therefore quasi all the produced soot from the engine is mechanically filtered by the DPF. The PM number drops at around 3% to 4% and the soot mass remains unchanged along the DOC.

Active regeneration. The active regeneration of the DPF is induced from the ECU once the parameters which characterize the particle filters stored soot loading overcome the admitted limits; and for this experiment is the measured backpressure of the entire after treatment system (DOC and DPF). The aim of the ECU is to provoke very high exhaust gas temperature before the DPF which consents the oxidation of the stored soot by the oxygen presents in the exhaust gas, this maximizing the engine efficiency and reducing the noise and the feel of an active regeneration. The active regeneration was induced by driving with constant speed of 70km/h and a force at the wheels of 650±10N, for more than 27h with a new DPF; therefore loading the soot in the new DPF with low exhaust gas temperatures.

The active regeneration is trigged by the ECU with a higher fuel injection (trough a post injection, the ratio of THC in the exhaust gas flow increase) and a reduced air mass flow (the intake air throttle must reduce the increased air mass flow caused from the hotter exhaust gas coming into the turbo charger, consenting rich mixtures combustion and lower fuel oxidation during the expansion stroke). During active regeneration the exhaust gas composes then with a larger part of THC and CO which will be oxidized in the DOC, the consequent high heat released from the exothermic reactions increase the exhaust gas temperature which will then cause the active regeneration start.

The drawback of the active regeneration is lower power measured at the wheels and higher specific fuel consumption.

The higher concentration of THC and CO into the exhaust gases coming from the engine are not completely oxidized into the DOC. Therefore the THC and CO emissions after DPF during an active regeneration are higher. Fig. 5 reports the specific mass emitted during normal engine conditions, active regeneration and the mean of both.

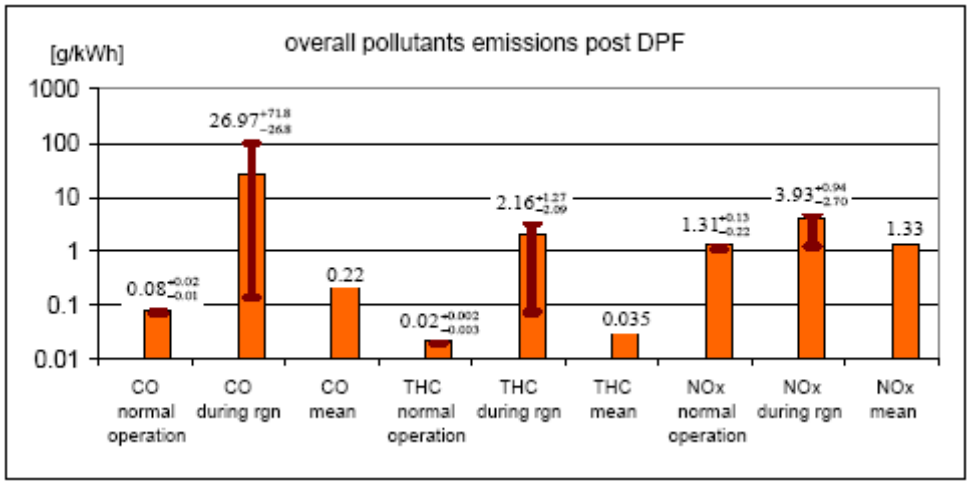

Fig. 5: Overall pollutant emission value after the DPF

Particularly the CO emissions after DPF are strong affected from the soot oxidation, which then increases the CO emitted. Fig. 5 shows that the mean emission of CO, THC and NO_x are higher taking into account the major emission due to the active regeneration: 175% more CO emissions (0.22g/kWh instead of 0.08g/kWh), 75% more THC emissions (0.035g/kWh instead of 0.02g/kWh) and 1.5% more NO_x emissions (1.33g/kWh instead of 1.31g/kWh).

The filtration efficiency is very high also during the active regeneration, starting with values of 99.9 % then decreasing up to 86.9 % and after the regeneration back to values around 98 % and successively 99.9 %. The filtration efficiency after an active regeneration could be lower respect the value before the regeneration; this is because the filter is emptier than before. During the active regeneration there is soot emission after the DPF of 49mg; this related to the total energy spent for the soot loading and the regeneration phase; the result is a mean soot emission of 0.137±0.001mg/kWh.

The mean emission results of CO, THC, NO_X (Fig. 5) and soot mass (0.137±0.001mg/kWh) calculated taking into account the emissions and transient conditions are lower than the Euro 3, Euro 4 or Euro 5 emission limits of the European emission regulations for heavy-duty diesel truck under steady state conditions (Tab. 1).

Conclusions

The investigations proposed in this work show that the investigated after treatment system is a robust and efficient system. The DOC shows high pollutant conversion efficiency for the entire exhaust gas temperature range and the DPF high PM number and soot filtration efficiency.

DPF passive regeneration characteristics were investigated under steady state conditions by driving at constant speed (70km/h), varying the engine load and therefore the delivered force at the wheels from 650 to 2317N. The emissions after the DPF, increasing the delivered force at the wheels, are for: THC between 0.021 and 0.003g/kWh for the fifth gear, CO between 0.104 and 0.043g/kWh and NO_X between 1.02 and 2.32g/kWh. The DOC conversion efficiency is between 93.9 and 98.8% for CO, between 92 and 95.7% for THC and lowers than 35% for NO. The soot mass doesn't vary along the DOC but the PM number reduce of 3 to 4%. The DPF filtrates more than 99.998% of soot and between 99.98 and 99.99% of the PM number for both gears.

DPF active regeneration is induced by passing the after treatment's backpressure limit and has duration of 520s, with higher mean specific fuel consumption and lower mean power delivered at the wheels. The active regeneration is trigged by a post injection and a reduced air mass flow. These engine parameters have the consequence of higher THC and CO engine emissions. Therefore the exothermic oxidation reactions occurring in the DOC increase the exhaust gas temperature more than during normal engine conditions. During the active regeneration the DPF heats up and empties out the stored soot. The thermal expansion of the silicon carbide filter and the high exhaust gas volume flow reduces the DPF PM number filtration efficiency from 99.9 to 86.9% during the last phase of the active regeneration. Nevertheless after few minutes the PM number filtration efficiency is back to 99.9%. The DPF under normal engine conditions shows very high soot filtration efficiency, but during the active regeneration 49mg of soot were emitted, corresponding to a mean soot emission of 0.137mg/kWh. After DPF the mean emitted amount increases of 175% for CO, 75% for THC and 1.5% for NO_X, due to the higher CO, THC and NO_X emissions during the active regeneration.

For both regeneration modes, the emission restriction Euro 5 of the European emission regulations for heavy-duty diesel truck under steady state conditions is satisfied.

Acknowledgements

I would like to thank the entire department of Internal Combustion Engines Laboratory (Abt137) and particularly Daniel Schreiber for the essential technical support during this work, Jacqueline Tschudin for the filter assemblage and Anthi Liati for the soot characterization.

I owe the greatest thanks to Panayotis Dimopoulos, first for his undisputed theoretical background on diesel engines and after treatment systems, second for his constant and helpful availability during my whole master thesis and third for his pleasant company.

References

Després, J., M. Elsener, M. Koebel, O. Kröcher, B. Schneider, and A. Wokaun, "Catalytic oxidation of nitrogen monoxide over Pt/SiO_2," *Applied Catalysis B-Environmental* **50**, 73-82 (2004).

Dieselnet (2010) http://www.dieselnet.com Accessed February 2010.

Jacqot, F., Logie, V., Brilhac, J.F. and Gilot, P., "Kinetics of the oxidation of carbon black by NO_2 - Influence of the presence of water and oxygen," *Carbon* **40**, **335-343** (2002).

Setiabudi, A., M. Makkee and J.A. Moulijn, "An optimal NO_x assisted abatment of diesel soot in an advanced catalytic filter design," *Applied Catalysis B-Environmental* **42**, 35-45 (2003).

Online characterization of gas and solid unregulated emission from 2-Stroke mopeds

*M. Clairotte[*1], T. Adam[1], U. Manfredi[1], R. Chirico[2-3], P.F. DeCarlo[2], M.F. Heringa[2], R. Zimmermann[4-5], A.S.H. Prevot[2], G. Martini[1], C. Astorga[1]*

[1] EC Joint Research Centre Ispra, Institute for Environment and Sustainability, Transport and Air Quality Unit, 21027 Ispra (VA), Italy
[2] Paul Scherrer Institut, Laboratory of Atmospheric Chemistry, CH-5232 Villigen, Switzerland
[3] Italian National Agency for New Technologies, Energy and Sustainable Economic Development (ENEA), FIS-LAS, Via E. Fermi 45, 00044 Frascati, Italy
[4] Analytical Chemistry, Institute of Chemistry, University of Rostock, 18051 Rostock, Germany
[5] Institute of Ecological Chemistry, Helmholtz Zentrum München, 85764 Neuherberg, Germany
*Corresponding author: michael.clairotte@jrc.ec.europa.eu

Introduction

Emissions from transport is one of the main contributors to atmospheric pollution and regarding greenhouse gases, road transport remains the first source of long term pollution (more than 20 years time horizon). The contribution of vehicles to urban transport pollution is far to be equal, and it is largely admitted that 2-stroke, 50cc mopeds can be high emitters, becoming a problem mainly in southern Europe and East and South of Asian countries. Indeed, Powered Two Wheels (PTW) is very popular to resolve traffic problem in congested cities. Whereas European legislation became more stringent for passenger car and heavy duty vehicle (EURO 6 / EURO VI respectively), new steps of regulation for PTW will still take some time to come into force (Euro 3 expected in 2013). This delay has been build on by the scientific community to understand in detail the emission characteristics from PTW. Although many studies give valuable data to adjust the future emission standards, most of them are obtained from offline measurement system after a collection step (i.e. Bags, cartridges…). Despite of the poor time resolution available along considered cycle, a cold start effect has emerged (Adam et al. 2009). The aim of this study is to go further in the characterization of emission yields from mopeds by taking advantage of real time measurement of gas and solid phases. To achieve our goal, an original set of measurements have been carried out to monitor online gas and particle emitted during different cycles. The large real-time dataset created during this campaign has been processed by multivariate statistical method in the way to extract a correlation between solid and gas emissions.

Material and Methods

In term of emission regulation, the principal contribution from the European Directive 97/24/EC EURO2 was the substantial reduction of the carbon monoxide (CO) standard, and in less extend the sum of hydrocarbons (HC) with mono-nitrogen oxides (NO_x). To comply with the new directive, solutions available to manufacturers were to adapt converter catalyst at the 2 wheeler tailpipe, associated with different technology like a Secondary Air Injection or Direct Injection engine system. Indeed, reduction of CO and HC can be promoted by leaner condition of engine combustion stoichiometry. In return, this Fuel/Air ratio enhances NO_x emission but concerning European standards, the contribution of nitrogen oxides in the sum ($HC+NO_x$) remains poor. Two particular mopeds have been selected for this study in order to register a very different behavior along test cycles. Hence 2 mopeds complying with EURO 1 and EURO 2 emissions standard have been used. The first EURO 1 moped was motorized with a 50 cc carburetor engine (Cb), without catalyst (Euro1-Cb). The EURO 2 was a 50cc with Direct Injection engine (DI) followed by an oxidant catalyst and a Secondary Air Injection system (Euro2-DI). Mineral oil was used for the Cb Euro 1 and semi-synthetic for DI Euro 2. The whole study has been conducted in the Vehicle Emission Laboratory (VELA - JRC Ispra), on a chassis dynamometer (Roller bench 48"; AVL Zoellner GmbH, Germany) using a Constant Volume Sampling (CVS, flow 4.4 m3/min) dilution tunnel system. The analytical instruments have been either connected to the tailpipe or to the dilution tunnel. A cyclone (cutoff size > 20 µm) has been added between the tailpipe and the dilution tunnel in order to protect from droplet analytical instrument connected directly to the CVS. A full description of the experimental system is illustrated in figure 1. Vehicles have been tested along different cycles: ECE47, WMTC and Steady States (0/35/50 km) but the results presented in this study will focus on the statutory ECE47 cycle.

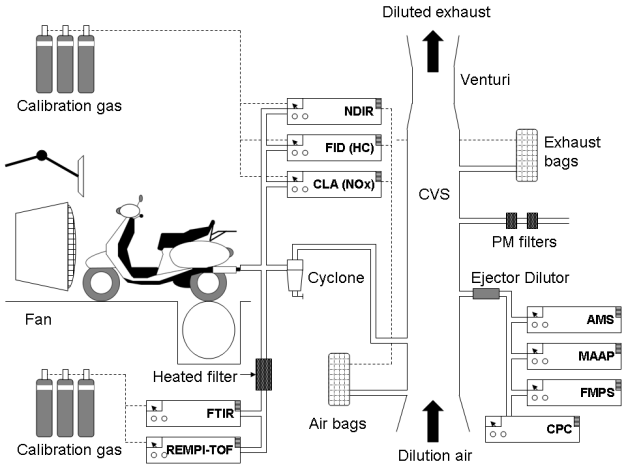

Figure 1: Schematic diagram of the experimental setup

Analytical instrumentation:

The gas sampling point was placed directly at the tailpipe, in order to avoid any losses all along the surface of the sampling equipment or the dilution tunnel. Indeed, some compounds like ammonia or nitrogen dioxide are well known for their capacity to remain adsorbed on the sampling system surface, mostly in the presence of condensed water (Hoard et al. 2007). Firstly, small chain HC (saturated and unsaturated with less than 4 carbons), nitrogen species (NO, NO_2, N_2O, NH_3 and HCN) and other oxygenated small compounds (Formaldehyde, Acetaldehyde, Methanol) have been monitored by a High Resolution Fourier Transform Infrared spectrometer (HR-FTIR - MKS Multigas analyzer 2030, Wilmington, MA). This system is a semi-quantitative technique based on a PLS model which allows predicting the concentration of 20 exhaust compounds from gasoline engine. A minor amount of exhaust flow is constantly aspirated into the FTIR multipath optical cell (5.11m) at 4.5-5 L/min and atmospheric pressure, through a PTFE heated line (191°C). Then, gas sample absorbs a part of an IR beam, generated by a Michelson interferometer. Then, transmitted signal is registered by a MCT detector with a frequency of 1Hz. The absorbance spectrum is obtained after a mathematical Fourier Transformation of the beam detected. A real time prediction is run based on spectrum detected; the predictive model is supported by a Labview developed software MG2000 (MKS).

Heavier Polycyclic Aromatic Hydrocarbons (PAH) were measured by REMPI (Resonance Enhanced Multi-Photon Ionisation) technique coupled with a TOF (Time-Of-Flight) mass spectrometer (prototype). This technique is known to be a soft and sensitive on-line method for the detection of gaseous aromatic compounds. The REMPI-TOFMS was also directly connected to the tailpipe of the vehicle by a heated transfer line consisting of a deactivated silica capillary (length 1.5 m; i.d. 0.32 mm; T = 220°C). A constant volume of exhaust was continuously drawn into the instrument (flow 8 mL/min; residence time < 1 s) in order to analyze undiluted, unfiltered and non-aged exhaust. The principle of REMPI-TOFMS is described in detail in the literature (Muhlberger et al. 2001), therefore, only a brief description is given here. Fundamental Nd:YAG laser pulses (1064 nm) are used for non-linear generation of UV light (266 nm). The UV pulses are directed into the ionization chamber straight underneath the inlet needle of the transfer line. Soft photoionization of the aromatics in the exhaust is induced by a sequential two-photon absorption process via an electronic transition state. The generated molecular ions are extracted into the flight tube of the reflectron TOFMS (Kaesdorf Instruments, Germany). Mass spectra are recorded via a transient recorder PC card whereby data processing is done by a LabView (National Instruments, USA) based custom-made software. Calibration is carried out by applying external gas standards. In principle, 20 complete mass spectra per second can be recorded since a 20 Hz laser was used. To complete gas measurement system, regulated emission were recorded according to legislative methods like Non-Dispersive Infra Red spectrometer (NDIR), chemiluminsecence detector (CLD) and heated flame ionisation detector in order to monitor CO/CO_2, NO_x, and non-methane hydrocarbon respectively. These data issued from the Steady States cycles were used as quality control to validate some of the HR-FTIR results. Differences between both measurements for common

compound available were confirmed to be below 3 % in volumetric concentration (data not shown).

Finally, aerosol emitted was sampled from diluted exhaust at the CVS, after an additional dilutor injector (Dekati) to avoid saturation of the dedicated analytical systems. The particle concentration was measured by a TSI 3022A Condensation Particle Counter (CPC). In order to measure particle size distribution along the cycles, a TSI 3091 Fast Mobility Particle Sizer (FMPS) have been chosen. This system allows the detection of particle within a range of 5.6 to 560 nm size diameter, with 32 channels resolution. Despite of less accurate results in comparison to a SMPS and possible artifact in the low diameter detection (<10nm)(Jeong and Evans 2009), the high acquisition frequency of 1Hz made it more appropriate for the fast changing of size distribution along speed profile. Anyway, these disadvantages cannot change the conclusion of this study. In order to monitor aerosol Black Carbon, a Thermo 5012 Multi-Angle Absorption Photometer (MAAP) was used. This analytical technique consists in collecting aerosol on a glass fiber filter tape and measure light absorption through the filter. Light scattered is measured simultaneously with different detection angles to reduce cross–sensitivity and improve black carbon detection (Petzold and Schönlinner 2004). Concerning the chemical composition of particles, a High-Resolution Time-of-Flight Aerosol Mass Spectrometer (HR-ToF-AMS) was set to monitor the organic fraction as well as nitrate and chloride species. This technique presents two main advantages for our application which are i/ a high time resolution and ii/ a low detection limit. A full description is available in the literature (DeCarlo et al. 2006) hence a short description is given here. Diluted emission is sampled from the CVS through an aerodynamic lens. Particles within the range from 30 nm to around 1 µm vacuum aerodynamic diameter are measured. After a first step through a mechanical rotating chopper (time 0 of the flight), particles reach a 600C heated plate where a thermal vaporization occurs followed by electron ionization at 70ev. During this process, only non-refractory species, like organic species, are vaporized. Then, ions are extracted into a time-of-flight spectrometer and mass spectrum is detected by a Multichannel Plate Detector (MCP). In order to reach the higher time resolution, the instrument was used in V-mode (flight distance around 1.9m), with a frequency of 0.2Hz. In the end, to complete physical particle characterization, total mass was determined by a weighted method, according to legislated method in force for the light duty vehicles (ECE/TRANS/WP29/2009/57).

Data pre-processing

Since our instruments set presents a heterogeneous acquisition frequency, a common time table of 1 Hz as been fixed in order to apply a Principal Component Analysis (PCA) in the database. The REMPI-TOF real-time data were converted to fit 1 Hz frequency by an average of 4 Hz measurement. In the case of solid phase measurement, the lowest data frequency fixed by the CPC, the AMS and the MAAP instruments (0.2Hz) were linearly interpolated to fit in our common database. Brief losses of record due to instrument malfunction were also filled by linear interpolation. This interpolation was only applied when time gaps were shorter than 5s and 10s, for gas and solid measurement respectively. All concentration measurements were transformed in mass emission by using exhaust and CVS flow rate from the VELA laboratory sensor. Finally, signal from each system were precisely synchronized with the VELA data. Instruments connected directly at the tailpipe (FTIR, REMPI-TOFMS) were adjusted thanks to the common NO measurement between FTIR and CMD detector. However, an additional CO_2 gas analyzer (LI-7000, LI-COR Biosciences) has been connected to the CVS in a way to correct from time shift CVS sampling instrument (CPC, FMPS, HR-ToF-AMS and MAAP).

Results and Discussion

Regulated and a selection of unregulated emission for the 2 mopeds along the official ECE47 cycle are presented in the table 1. According to the European legislative 97/24/EC, only the hot phase is taken in account, hence the second half of the ECE47 cycle. Considering emission from Euro1-Cb and Euro2-DI, efforts to reduce emission are evident; probably largely attributed to the engine technology (DI) and the supplementary post-treatment technology (catalyst + SAI). Considering unregulated emission, despite of a noticeable decrease of CH_4, the Euro2-DI moped presents non negligible production of nitrous oxide, another strong greenhouse gas. However, even if the global warming potential are taken into account (310 and 21 eq.g CO_2 for N_2O and CH_4 respectively in 20 years time horizon), nitrous oxide plays a minor role in the total

balance. This difference integrated in the whole cycle is not compensated in term of CO_2 equivalent and the Euro2-DI moped remains "greener" compare to the Euro1-Cb. On the other hand, ammonia appears in the Euro1 exhaust which could be explained by the reaction between largely emitted CO and NO_x (Livingston et al. 2009). Anyway, calculation of the lambda factor thanks to modal emission confirms that Euro2-DI moped was running in leaner condition which greatly limit ammonia apparition.

Table 1: Regulated and Unregulated emission factor from the 2 mopeds during the official ECE47 cycle (mean of 2 tests, standard deviation in parenthesis) - SAI: Secondary Air Injection, nd: non detectable (methods: * according to 94/24/EC, $^{\Delta}$ HR-FTIR, $^{\bullet}$ NDIR, $^{\circ}$ according to 98/69/EEC)

Emission in g/km		**Euro 1 - Carburetor without catalyst**		**Euro 2 - Direct Injection with oxidant catalyst and SAI**	
		Cold Phase	Hot Phase	Cold Phase	Hot Phase
Regulated	CO *	6.0 (0.4)	8.7 (0.2)	2.3 (0.3)	0.60 (0.06)
	CO Standards		**6**		**1**
	HC *	5.037 (0.004)	2.134 (0.003)	1.87 (0.03)	1.2 (0.2)
	NO_x *	0.037 (0.005)	0.019 (0.003)	0.352 (0.005)	0.391 (0.008)
	HC+NO_x Standards		**3**		**1.2**
Unregulated	CO_2 $^{\bullet}$	47 (2)	40 (1)	47.8 (0.8)	42.20 (0.03)
	CH_4 $^{\Delta}$	0.054 (0.005)	0.09 (0.02)	0.014 (0.002)	0.0079 (0.0002)
	N_2O $^{\Delta}$	nd	nd	0.0026 (0.0002)	0.0021 (0.0002)
	NH_3 $^{\Delta}$	0.0020 (0.0006)	0.006 (0.001)	nd	nd
	PM $^{\circ}$	0.090 (0.002)	0.014 (0.002)	0.053 (0.005)	0.117 (0.008)

The Direct Injection moped emits more particle matter (PM) during the hot phase. This tendency was already reported in different studies (Spezzano et al. 2008; Adam et al. 2009). Comparison of PM values with the sum of organic aerosol and black carbon estimated by HR-ToF-AMS and MAAP respectively, show a systematic lower estimation with the legislative method (data not shown). According to the directive, a period of 2 hours must be respected between the collection and the weighing step (at 22ºC and 50% of humidity), which allows the loss of the most volatile organic compounds from particles collected on the filter surface. This result confirms that methodology followed for the light duty vehicle cannot be transposed directly for mopeds PM mass determination. Size distribution evolution is presented in figure 2 for the two mopeds along the ECE47 cycle. The mopeds emit equivalent particle number in the beginning of the cycle; this number decreases largely along the followed acceleration in the case of the Euro1-Cb. Whereas Euro2-DI scooter yields continuously the same number of particle during subsequent acceleration. Moreover, the median diameter of the Euro1-Cb presents a substantial decreasing and the Euro2-DI median diameter increase slightly. It is assumed that particles from 2-stroke mopeds are mainly unburned fuel and oil droplet. Exhaust temperature registered at the tailpipe of each moped shows a divergent trend starting at the third acceleration (around 300s) and the Euro1-Cb moped exhaust was reached higher temperature (up to 300C) compare to the Euro2-DI moped (less than 200C). Hence, exhaust temperature can explain partially the decreasing of the particle median diameter for the Euro1-Cb moped. In addition, data from AMS present in figure 3 show the aerosol organic mass variation along the cycle for each moped. This graphic highlights the common trend of organic aerosol and median diameter of particle for both mopeds. Therefore, the evaporation or condensation of organic matter on the particle surface can be an explanation of such particle diameter variation.

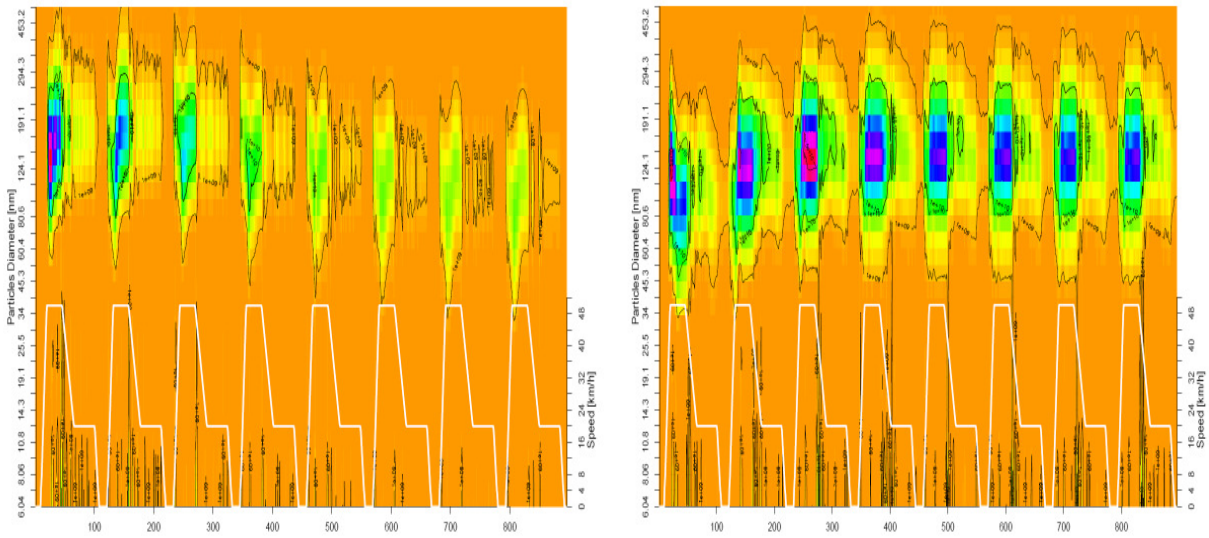

Figure 2: Particle size distribution along ECE47 cycle - Euro1-Cb on the left and Euro2-DI on the right (FMPS data - mean of 2 tests)

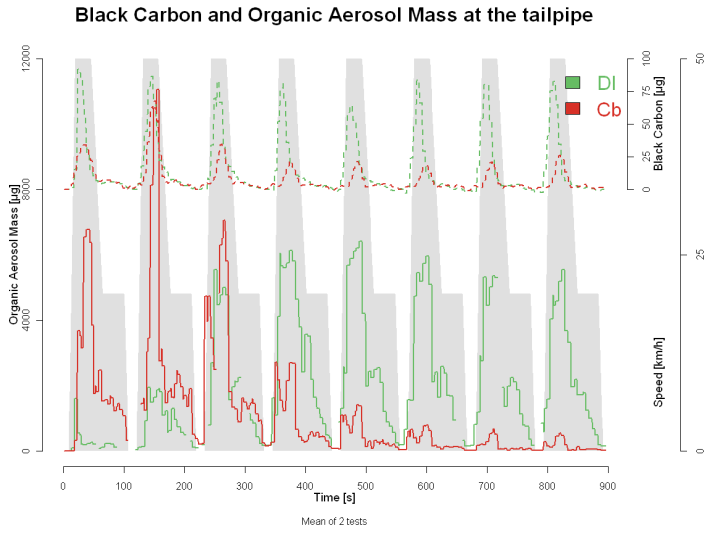

Figure 3: Organic Aerosol (bottom) and Black Carbon (top) mass at the tailpipe from the 2 mopeds during ECE47 cycle (HR-Tof-AMS data - mean of 2 tests)

To take advantage of the detailed online database collected during this campaign, PCA model has been applied. In addition with modal data from the different instruments, 3 explanatory variables have been included in the dataset: Speed, Exhaust Temperature and Vehicle Specific Power. Within this abstract, only results from the Euro1-Cb moped during ECE47 cycle are presented. The PCA model explains 80% of the total variance with 2 components (67% and 13% for PC1 and PC2 respectively). Figure 4 presents the loadings for a selection of variables. From this graph, 4 groups can be distinguished: **Group A** in the top left including Aerosol-Organic, Aerosol-Nitrate, and particle volume (calculated from the FMPS data considering particle shape as spherical), that confirm the correlation between particle volume and organic aerosol emitted. Not so far on the right of this group, the median diameter is present which confirm the same tendency. NO_2 and O_2 are also correlated with this group which verify that higher particle diameter is promoted during the leaner condition, or during the first part of the cycle when engine temperature is not hot enough. Indeed, exhaust temperature is present in the opposite part of the graph with ammonia (**Group B**) which means that these 2 groups present an opposite correlation. Another interesting **Group C** appears on the left, with particle number, black carbon, benzene and naphthalene. Finally, a last **Group D** can be extracted and

is shown at the bottom of the graphic with CO_2 and Speed. The position of this group demonstrates the independence of the other solid and gas emission with the consumption (except obviously CO_2, HC, and HCN to a lesser extent). Finally, to illustrate the “Cold Start” effect during the ECE47 cycle, total variance has been discriminated in 8 sub-classes (as many as acceleration repetition during the official cycle). This approach has plenty of advantages compared to the real time data, considering ECE47 as 8 phases cycle. This representation shows an equivalent variance distribution for the 2 first accelerations close to the **Group A**, followed by an intermediate third acceleration and a cluster including accelerations 4 to 8, closer to **Group B**.

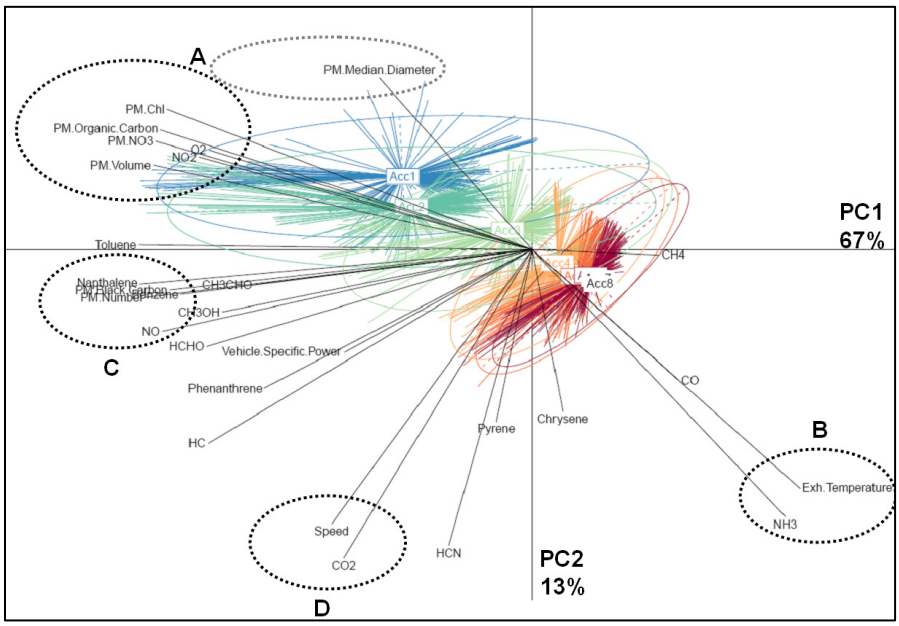

Figure 4: PCA score for the Cb-Euro1 moped during ECE47 cycle (2 tests dataset)

ReferencesEN.REFLIST

The Influence of Traffic Conditions on Primary NO_2 Tailpipe Emissions and Road-Side Pollutant Concentrations

P. K. Hardy[1], G. Harrison[1], H. C. James[1], H. Li[2], T. O. Lynch[1], S. C. Pickard[1], J. Tate[3], A. S. Tomlin[2], S. M. Weekes[1].*

[1]Doctoral Training Centre in Low Carbon Technologies, SPEME, University of Leeds, Leeds, LS2 9JT, UK

[2]Energy and Resources Research Institute, SPEME, University of Leeds, Leeds, LS2 9JT, UK

[3]Institute for Transport Studies, University of Leeds, Leeds, LS2 9JT, UK, j.e.tate@its.ac.uk

Introduction

Although European directives to reduce the total NOx emissions from vehicles have been in operation for over a decade, a lack of regulation on the NOx composition has caused vehicle manufacturers to focus primarily on total NOx, disregarding any increase in the fraction of NOx that is NO_2. Many fleets across Europe have seen an increased uptake in diesel vehicles and tailpipe modifications aimed at reducing CO_2 and particulate emissions. This has resulted in an increase in 'primary' NO_2 emitted directly from vehicles and hence overall ambient NO_2 concentrations (Grice et al., 2009). However, the EU First Daughter Directive recently came into force, stipulating that by 1st January 2010, ambient NO_2 concentrations must not exceed an annual mean of 40 μgm^{-3} and an hourly mean may not exceed 200 μgm^{-3} more than 18 times per year. Despite the potentially damaging effects of NO_2 exposure, the UK and many other European countries are not on course to meet their obligations under this Directive and have filed for an extension to avoid fines for non-compliance (DEFRA, 2009).

Ambient NO_2 concentrations are extensively monitored in the UK and vehicle manufacturers routinely conduct engine dynamometer tests to establish the exhaust composition from their engines, yet these studies often remain disconnected. A range of factors may influence roadside concentrations of traffic related pollutants. It is well established that urban geometries can influence pollutant dispersion due to local meteorological effects (Tomlin et al, 2009), while traffic characteristics as well as levels of congestion can all act to increase local pollutant concentrations relative to a background level. In this study we present measurements of real-world driving emissions from a diesel vehicle within an urban area along with in-street and background NO_2 measurements in an attempt to create a more holistic picture, linking vehicle emissions to ambient pollutant concentrations.

Methodology

The Leeds Instrumented Junction was established in 2007 as a cooperative effort between the University of Leeds and Leeds City Council (LCC) and is situated in the often heavily-congested Headingley district, 3km North-West of the city centre (illustrated in Figure 1). Local pollutant concentrations were measured at Environmental monitoring station 1 (ENV1 in Figure 1) including NOx, NO_2 (chemiluminescent analysers, APIM200E) and O_3 (UV analysers, APIM400E), along with local wind speed and direction (sonic anemometers-Gill WindMaster measuring at a frequency of 10Hz). Vehicles entering and exiting the site are counted and their vehicle class identified using a pair of inductive loop detectors (GoldenRiver M661, two per lane). Traffic monitoring data from the unit to the South of the experimental area (TMU South in Figure 1) was used in this study. The prevailing wind speed and direction were measured from a 12m high mast operated by LCC, located approximately 4 km to the south of the measuring site. The road section being studied has been characterised as a non-uniform street canyon with an unbroken office/shopping complex of height ≈ 20m demarcating the Eastern side and irregularly spaced set-back buildings lining the Western side (Tate et al., 2009). The background pollutant measurement is taken in a residential area away from the roadside (ENV4 in Figure 1). Pollutant and traffic measurements are synchronised to an atomic clock while in-street meteorology measurements are GPS time-stamped. Measurements are averaged over 15 minute intervals and collated to a central synchronised database. Traffic data represents the six month period from January to June 2009 while all other monitoring data is drawn from the 18-month period January 2008 to June 2009.

Vehicle tailpipe emissions measurements were carried out using a 1.8 litre, Euro 3 Ford Connect TDCi, diesel van, defined as a Class 1-iii Light Commercial Vehicle. The vehicle was fitted with a two-way oxidation catalyst for the control of CO and THC (Total Hydrocarbon) emissions. Measurements were made directly from the exhaust system using a portable Fourier Transform Infrared spectrometer (FTIR) system (Temet Gasmet CR 2000) that was able to measure regulated CO, CO_2, NOx (NO_2 and NO), 27 individual hydrocarbons and other non-regulated species at 0.5 Hz, with a sensitivity of 0.5-3 ppm and an accuracy of 3% within calibrated measurement ranges (see Li, 2009 for further details). The FTIR system was used in conjunction with a Horiba On-Board measurement System (OBS-1300), which was used for measuring tailpipe exhaust flow rate, air fuel ratio, CO, CO_2, and determination of the road speed and location of the vehicle using an incorporated GPS unit. The CO and CO_2 measured by both the FTIR and OBS systems were used for time alignment between the two systems. An offset of 2 seconds was given to FTIR emissions data for time alignment with air fuel ratio, exhaust flow and GPS measurements as the response time of the FTIR was estimated to introduce a 2 second lag time. The on-board emission measurement systems were powered by two on-board 12V batteries to avoid drawing power from the vehicle's electrical system which would otherwise add an additional load on the engine. In addition, a sample handling unit was used to hot filter the exhaust gases to remove particulates and maintain the wet gases at a temperature of 180^0.

Emission measurements were made during three replications of a journey on a typical commuter route which passes through the instrumented traffic junction in Headingley Leeds. This allowed an integrated approach for measuring roadside pollutant concentrations and traffic emissions on the same section of road. The road is subject to a speed limit of 48km/h (30mph), is often heavily congested, and passes through a number of junctions and traffic signals. The return journey is a repeat of the outward journey but travelling in the opposite direction. The total distance of the route is 8.9 km. The drives were carried out on three separate consecutive days around midday. The test vehicle had been driven in urban conditions for approximately 20 minutes before the test drive negating any cold-start effects.

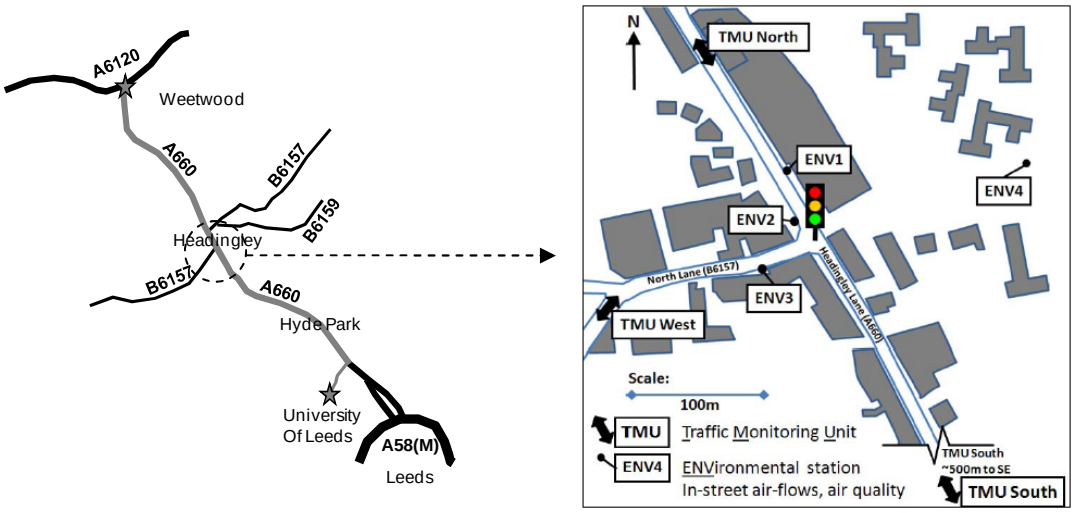

Figure 1: (left) The drive cycle route including the instrumented junction site in Headingley. The grey line represents the outward and return route; the stars mark the start and end points of the route. (right) Schematic diagram of the instrumented junction site, ENV1 (roadside), ENV4 (background) and TMU South (classified traffic flow) were used in this study.

Results and Discussion

Primary NO_2 fraction of total NOx (f-NO_2)

NO_2 concentrations measured in polluted areas are due to primary NO_2 emitted directly from vehicle exhausts and secondary NO_2 formed by reactions in the troposphere. Clapp and Jenkin, (2001) showed that the total oxidant (OX = NO_2 + O_3) measured at the roadside varies linearly with NOx. OX is made up of NOx-independent and NOx-dependent fractions, with the former identified from the intercept of the OX vs NOx curve and the latter from the gradient. The NOx-

independent fraction is related to regional concentrations of O_3, while the NOx-dependent fraction is related to the ambient level of primary NO_2. In the present study we use the extended method proposed by Carslaw and Beevers, (2004) to estimate the direct contribution to primary NO_2 from the road by subtracting the measured local background concentrations (from ENV4 in Figure 1). Using this method we calculated the average primary NO_2 fraction of total NOx (f-NO_2) as 14.1% with an interquartile range of 11-22% as shown in Figure 2.

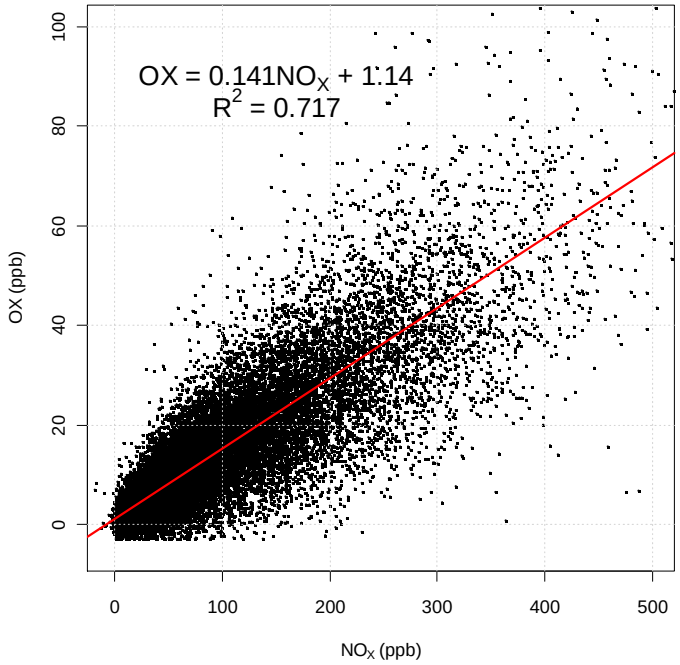

Figure 2: OX and NOx concentrations for the 18 month period after subtracting the ENV4 local background pollutant concentrations. The gradient indicates an average f-NO_2 value of 14.1%.

Comparison with previous work

It is useful to compare the results here with a similar highly polluted urban site at Marylebone Road, London. Carslaw and Beevers, (2004) used the total oxidant approach to estimate roadside f-NO_2 on Marylebone Road between 1998 and 2002. Weekday f-NO_2 values of 8.7-9.7% were calculated. These values are of a similar order of magnitude to those calculated at the Headingley site with the difference consistent with observations that f-NO_2 is generally increasing in urban areas (Grice et al., 2009). A more recent study of the Marylebone site by El Rashidy, (2009) concluded that the weekday p-NO_2 in 2008 had risen to almost 23% at the Marylebone road site. The large increase between 2002 and 2008 has been attributed in part to the introduction of catalytic regenerative particle traps on London buses.

Primary NO_2 and traffic characteristics

The calculated f-NO_2 (14.1%) was used to determine the average diurnal concentration of primary NO_2 (p-NO_2) from the measured roadside NOx concentrations. In order to account for different meteorological conditions throughout the data set, the p-NO_2 concentration was multiplied by the background wind speed resulting in a p-NO_2 parameter. The diurnal variation of the p-NO_2 parameter alongside average traffic flow and vehicle speed is presented in Figure 3. It was found that at low traffic flow and high speed (free-flow conditions), the p-NO_2 parameter was lower; conversely at high traffic flow and low speed (congested flow) the p-NO_2 parameter was higher (see Figure 3).

The exception to this finding was that the p-NO_2 parameter decreased at an earlier time than the total traffic flow. As the p-NO_2 contribution from commercial vans, heavy-duty vehicles and buses/coaches is known to be high (Carslaw and Beevers, 2004), their average diurnal flow profiles were examined. It is evident (Figure 3) that the p-NO_2 parameter correlates more closely with the flow of vans and buses than with the total traffic flow. The peak flow of vans and buses is between 08:00-16:00 hrs, which approximately correlates with the observed peak

(07:00-15:00 hrs) and reduction (from 15:00 hrs) in the p-NO_2 parameter. Between 20:00-24:00 hrs the oscillations in the flow of buses and vans appears to be reflected in the p-NO_2 parameter, despite the low traffic numbers.

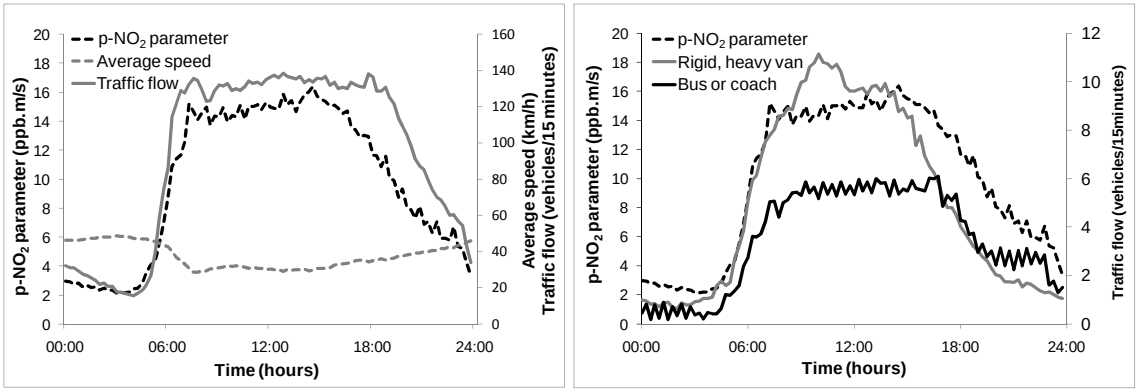

Figure 3: (left) Average speed and total traffic flow compared to p-NO2 parameter. Total traffic flow and total speed accounts for cars, motorcycles, buses/coaches, heavy vans, lorries and cars with trailers. (right) Average traffic flow of buses, coaches and heavy vans compared to p-NO2 parameter.

Primary NO_2 as a fraction of total NO_2

While concentrations of p-NO_2 may be mitigated by reducing the emissions contribution locally, the secondary NO_2 contribution may require action to reduce precursors on a regional or national scale. Thus it is important to understand the fraction of total NO_2 that is p-NO_2. The average p-NO_2 fraction of total NO_2 concentrations was calculated as 33% at the roadside and is shown to vary diurnally (Figure 4). The diurnal profile is similar to that of the traffic flow. These results imply that in Headingley one third of NO_2 at the roadside is directly emitted from transport, with the maximum fraction of NO_2 from vehicles occurring at 08:00hours at over 40%. The relatively high contribution of p-NO_2 to overall NO_2 concentrations indicates that significant air quality improvements could be made by reducing primary emissions at the Headingley site.

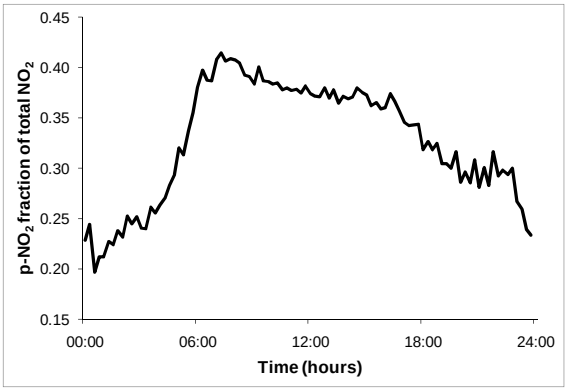

Figure 4: Average diurnal p-NO_2 as a fraction of total NO_2 at the roadside.

Tailpipe NO_2 emissions

To supplement the results from air quality monitoring the tailpipe emissions data for free-flow and congested conditions were analysed. A clear definition of what constitutes congestion is not simple to formulate and often open to debate. In the context of this study, a convenient definition is when, "*a vehicle is forced to wait through more than one signal cycle*" (Roess et al. 2004). From this definition a coarse measure of congestion can be formulated as a journey time

of twice the free-flow journey time. Or equivalently, an average speed of half the legal limit for the road, making the assumption that the free-flow speed is equal to the legal speed limit.

Using this approach, a 60 second running average velocity was calculated for each of the test journeys so that brief periods of stoppage at junctions and traffic lights would not be classified as congestion. The sectors of the drive cycle were classified as congested when the 60-second moving average speed measure was less than 24 km/h, while all other sectors where considered to be free-flow. While this approach does have its limitations, it allows some distinction to be made between emissions made in free-flow and congested conditions. An example of this analysis is shown for a single journey in Figure 5 along with the averaged emissions data for the three replications of the test journey.

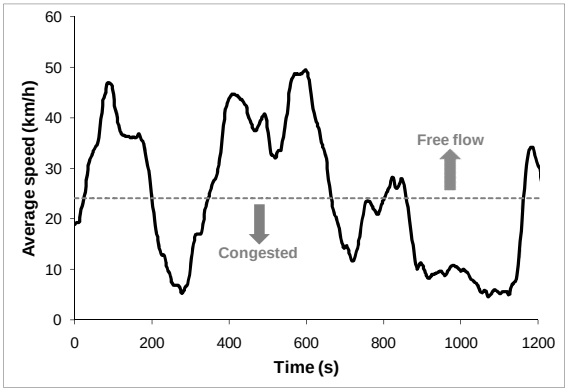

	Congested	Free-flow	Average
NOx (g/km)	0.43 (0.08)	0.34 (0.03)	0.36
NO (g/km)	0.34 (0.06)	0.28 (0.02)	0.30
NO_2 (g/km)	0.09 (0.03)	0.06 (0.01)	0.06
f-NO_2 (%)	20 (3)	17 (1)	18
Average speed (km/h)	15	36	26

Figure 5: (left) Representative velocity profile for a single journey. (right) Average emissions and speed for congested and free-flow traffic conditions. Values in parentheses represent the standard deviation across the three journeys.

The average emissions over the three journeys show an increase in NO_2 as a percentage of NOx (f-NO_2) from 17% to 20% in congested conditions as well as an overall increase in NOx emissions. Given the variability between journeys of real-world emissions measurements, statistical tests were used to investigate the significance of these differences between congested and free-flow conditions. Independent samples t-tests were carried out using SPSS 17.0 for Windows for each of the three journeys. For the first and third replications of the journey, the difference in f-NO_2 between congested and free flowing traffic conditions was significant at the $p<0.001$ level. For the second replication, the difference was not statistically significant ($p = 0.752$). The failure of the second replication of the journey to show a statistically significant difference between congested and free-flow conditions may have been due to an increase in the average speed during the sectors classified as congested during this journey.

While three journeys provides only a small data set on which to base conclusions, the results do indicate that for the vehicle studied both the total NOx and the f-NO_2 increases in congested conditions. Hence measures which relieve congestion and aid free-flow conditions, even with no reduction in total traffic volume, could have an impact on local p-NO_2. Since p-NO_2 accounts for a significant percentage of the total roadside NO_2 concentration, any measures to reduce p-NO_2 emissions would have beneficial impact on meeting air quality targets.

Comparison with previous work

In a recent study by Grice et al., (2009) trends in the measured roadside f-NO_2 across Europe were investigated with reference to a number of case studies. Their work showed an average f-NO_2 value of 12.4% measured across monitoring sites in 2004 with a general trend of increasing f-NO_2. Measurements in Headingley seem consistent with a small increase compared to this value due to a general upward trend, whereas recent values at Marylebone Road seem higher due to additional pollution control measures for particulates. With regard to tailpipe emissions, Grice et al., (2009) also reported average f-NO_2 values of 30% for Euro 3 diesel vans, which is greater than the values presented here.

Conclusions

In-street pollutant concentrations were monitored over an 18 month period at a busy urban junction in Leeds. Using a total oxidant approach, the average f-NO_2 was calculated as 14% at the Leeds roadside. On average, p-NO_2 as a fraction of the total in-street NO_2 concentration was calculated to be 33% with a diurnal trend which corresponds with the observed traffic flows. This indicates that significant improvements in total NO_2 concentrations could be achieved by implementing measures to reduce primary NO_2 emissions. In addition, the in-street p-NO_2 parameter exhibited a strong relationship to traffic flows with congested conditions leading to the highest values. The parameter was particularly strongly related to flows of commercial vans, heavy-duty vehicles and buses/coaches highlighting the disproportionate effect of diesel vehicles on NO_2 concentrations. Comparisons with recent f-NO_2 calculated at Marylebone Road in London suggest that where additional particulate controls are used they need to be coupled with primary NO_2 controls in order to avoid increasing primary NO_2 concentrations at the roadside.

Air quality data was supplemented with direct emission measurements from a Euro III diesel light goods vehicle monitored over three replications of a test journey which included the Instrumented Junction air quality test site. While only limited emissions measurements were undertaken, these indicated a correlation between driving conditions and p-NO_2 emissions. Congested conditions resulted in an average f-NO_2 of 20% while free-flow conditions resulted in average f-NO_2 of 17%. The grams per km increase in NOx and primary NO_2 emissions indicate that mitigating congestion would most likely result in lower in-street NO_2 concentrations even if traffic volumes remain unchanged.

It is expected that more detailed emissions measurements under real-world driving conditions for a range of vehicle classes and fuel types would be beneficial in understanding more fully the impact of congestion on in-street pollutant concentrations.

References

Carslaw, D.C. and S.D. Beevers (2004), Investigating the potential importance of primary NO_2 emissions in a street canyon, *Atmospheric Environment*, 38(22), 3585-3594.

Clapp, L.J. and M.E. Jenkin (2001), Analysis of the relationship between ambient levels of O_3, NO_2 and NO as a function of NOx in the UK, *Atmospheric Environment*, 35(36), 6391-6405.

Department for Environment, Food and Rural Affairs, (DEFRA), (2009), UK approach to its application for time extension notification to nitrogen dioxide limit value deadline, version 1.0, R. Vaughan, *Air quality and industrial pollution programme.* Available at: www.defra.gov

El Rashidy, R. (2009), The Influence of traffic and urban air flows on roadside concentrations of traffic related pollutants at a busy junction in Leeds (Headingley), Unpublished Master's thesis, SPEME, University of Leeds, Leeds, UK.

Grice, S., J. Stedman, A. Kent, M. Hobson, J. Norris, J. Abbott and S. Cooke (2009), Recent trends and projections of primary NO_2 emissions in Europe. *Atmospheric Environment*, 43(13), 2154-2167.

Li H., G.E. Andrews, D. Savvidis, B. Daham, K. Ropkins, M. Bell and J. Tate (2009), Impact of driving cycles on greenhouse gas (GHG) emissions, global warming potential (GWP) and fuel economy for SI car real world urban driving. *SAE Int. Journal of Fuels and Lubricants,* 1(1), 1320-1333.

Roess R.P. E.S. Prassas and W.R. McShane (2004), *Traffic Engineering*, Third Edition, Published by Prentice Hall, ISBN 0-13-142471-8.

Tate, J., K. Ropkins, P. Goodman, C. Oates, H. Chen, M. Bell, A.S. Tomlin, A. Balogun and R. Smalley (2009), The influence of traffic congestion, synoptic and in-street winds on nitrogen dioxide concentrations around a congested intersection: a measurement study. Air Quality Conference 2009, Istanbul, March 2009.

Tomlin, A.S., R.J. Smalley, J.E. Tate, J.F. Barlow, S.E. Belcher, S.J. Arnold, A. Dobre and A. Robins (2009), A field study of factors influencing the concentrations of a traffic-related pollutant in the vicinity of a complex urban junction, *Atmospheric Environment*, 43(32), 5027-5037.

PORTABLE EMISSION MEASUREMENT SYSTEMS (PEMS) FOR PM MEASUREMENTS: COMPARISON OF DIFFERENT TECNIQUES

Lauretta Rubino

Sensors Europe GmbH, Feldheider Str. 60, 40699 Erkrath, Germany

Abstract

The use of PEMS represents a robust and accurate solution to study gaseous and particulate emissions from combustion engines. Increasing health concerns in urban areas associated to particulate emissions, and more stringent regulations both in Europe and the US, are pushing towards real world measurements of PM emissions.
This work focuses on the latest portable PM measurements systems from Sensors such as the SEMTECH Laser Aerosol Monitor (LAM) and the Portable Particulate Measuring Device (PPMD); the former is based on Laser Light Scatter Photometry (LLSP) for real time PM measurements, with an accuracy of 0.01 mg/m^3 in the particle size range 100-10,000 nm, the latter is based on the Quartz Crystal Microbalance (QCM) technique for continuous PM measurements on-road. Their performance is compared to standard laboratory instrumentation.
The LAM and the PPMD are used in combination with the exhaust flow meter (EFM), for exhaust mass measurements and may be also operated with standard gravimetric filter-based instrumentation for PM collection.
In this context, testing has been carried out in the laboratory, on standard cycles, such as the World Harmonized Transient Cycle (WHTC), using Euro III engines with partial filter, running on low sulfur fuel to check the performance and sensitivity of the devices at different PM levels. Data are compared with standard gravimetric mass measurements, using a CVS full flow dilution tunnel and partial flow dilution systems, such as the AVL Smart Sampler SPC472. For the standard gravimetric method, PM was collected on a Teflon-coated glass fibre filter (PallflexEMFABTX40HI20) and weighted on a microbalance according to procedures currently in use in the Particulate Measurement Program (PMP) for filter weighting, conditioning and handling. A comparison with PM measurements techniques, other than gravimetric, such as the photo-acoustic principle of operation for soot measurements (AVL Micro Soot Sensor (MSS)) is also presented. Good agreement was found between the standard laboratory instrumentation and the PM PEMS. Preliminary results are reported and discussed.

Introduction

Portable Emission Measurement Systems (PEMS) have become an important tool to monitor the in-service conformity of large on-road and off-road engines from heavy-duty vehicles, construction and agricultural equipment. PEMS are envisaged as a tool to check the emissions from heavy-duty engines during their real operation and, more recently, programs have also been launched to evaluate the feasibility of PEMS also for non-road equipment and light-duty vehicles [1,2].
To measure PM emissions on-board several technologies and instruments are currently available and more effort is ongoing to make these technologies more compact and suitable for on vehicle testing. A wide variety of instruments and measurement techniques have historically been used to characterized compressed ignition combustion generated PM. These techniques range from the simple filter sampling to highly sophisticated instrumentation. In this context, only a brief overview is provided more can be found in [3].
Optical methods, including light extinction (opacity) and laser scattering can be used to measure the carbonaceous mass of PM (i.e. soot). Until now, opacity was widely used as the indirect mass measurements and opacity meters were the only on-line instruments; nowadays, with the introduction of after-treatment systems, they are facing problems with the detection limit in presence of low mass concentration and NO_2 [3,4]. Absorption measurements can be used to determine the carbon mass. A number of techniques have been developed for absorption measurements. However, besides difficulties with data interpretation, the method is not sensitive enough to measure low concentration, typical of modern and trap equipped engines. Hence, optical techniques are very suitable when soot concentrations are prominent but can be insensitive when PM is dominated by volatile species, such as downstream of Diesel Particulate Filters (DPFs) [3,4,5].

Photo-acoustic spectroscopy is a technique where particles are heated by absorption of light from a chopped light beam. The resulting acoustic wave is then measured by a microphone. This principle has been largely used to measure diesel particles in the past for laboratory applications [6] and more recently, thanks to technical progress in high power laser diodes and sensitive miniature electret microphones, a commercial device, the Micro Soot Sensor (MSS), has been introduced on the market [7].
Laser-induced Incandescence (LII) and Photoelectric Aerosol Sensor (PAS) [8, 9] could also be considered but data interpretation is complex, limited to a certain particle size and shape and with a response that may vary in presence of high Soluble Organic Fraction (SOF).
Techniques for particulate mass determination in real time are the Tapered Element Oscillating Microscope (TEOM) [10] and the Quartz Cristal Microbalance (QCM), both based on a change in resonance frequency of a collecting device due to acquired mass. They both offer a good resolution and sufficient sensitivity. The main drawbacks of the TEOM are uptake of water and other volatile material, which may lead to artifacts and, for on-vehicle application, interferences caused by vibrations and vehicle movements; its sensitivity to fluctuations in pressure and temperature causes problems with diesel particle measurements application.
The Electrical Tailpipe PM Sensor (ETAPS), based on electrostatic principles for particle detection in real time has been introduced by Dekati [11]; Other recent instruments include the Horiba OBS TRPM, which combines the gravimetric principle of depositing and measuring PM on filter with real time measurements of particle length through a diffusion charge sensor (DCS) that is used as PM detector, with the assumption that the mass accumulated on the filter is proportional to the PM length parameter [12].The recent introduction of the SEMTECH Portable Particulate Mass Device (SEMTECH-PPMD), which includes a micro-proportional sampling system (MPS), an Exhaust Flow Meter (EFM) and a QCM by Sensors Inc. seems very promising for exhaust PM measurements above all at low emission levels [3]. In addition to mass, particle number and size measurements are of increasing importance because of adverse health effects associated with ultrafine particle emissions [13,14**]** and a variety of aerosol instrumentation is available for particle number and size measurements. However, so far, all the official PM emission limits are still defined in terms of total mass, as determined by gravimetric analysis, specific to either distance for light-duty vehicles or work for heavy-duty vehicles.
To judge whether the improvements are sufficient to foresee a short term introduction in the European legislation, The European Commission has launched a Call for expression of interest to participate in the EU-PEMS PM evaluation program where several commercially available PM PEMS, were submitted by instrument manufacturers. These are: Control Sistem m-PSS, AVL Micro Soot Sensors (MSS), DEKATI DMM, DEKATI ETaPS, Horiba OBS TRPM and Sensors SEMTECH-PPMD as reported in [3].
This paper focuses on the SEMTECH LAM and SEMTECH PPMD, based on LLSP and QCM respectively and their comparison to both gravimetric (CVS) and non-gravimetric techniques such as the photo-acoustic principle of operation for soot measurements (AVL Micro Soot Sensor (MSS)). A brief description of the two systems is provided below.

SEMTECH-PPMD

The portable particulate mass measuring device (PPMD) by Sensors is based on the QCM technique for PM mass measurements. It is composed of two micro-proportional sampling systems (MPS) for exhaust dilution and a carousel quartz crystal microbalance (CQCM) consisting of eight quartz crystals [15, 16]. Figure 1 illustrates the MPS design. It is adapted from Brockmann [16] and it is based on laminar flow capillary. The second MPS is to allow for additional dilution. The initial dilution is at the downstream end of the sample inlet capillary (for capillary flow control). The second is at the upstream end of a venturi throat (downstream of the transport capillary containing the sample and primary dilution). This secondary dilution creates a pull or suction on the end of the second or transport capillary. The constraints for this diluter are the total flow through the sampler, i.e., sample flow plus primary dilution flow plus secondary dilution flow, is held constant and the sample flow is controlled to always be proportional to the exhaust flow. The equations for the flow through the sampler can be determined by applying Bernoulli's equation along with the requirements of constant total flow and that the sample flow must be proportional to the exhaust flow [15, 16]. A schematic of the PPMD is shown in figure 2. The SEMTECH-PPMD consists of 2 MPS and a carousel QCM including 8 crystals to measure mass continuously by switching to the next available crystal. It is attached to the SEMTECH

EFM for exhaust mass measurements based on the “averaging pitot” technique [3]. The QCM technique employs a piezoelectric crystal as a sensitive microbalance. Electrostatic precipitation collects aerosol particles on the surface of the piezoelectric crystal; the crystal is excited in its natural frequency, which decreases with increasing mass load on its surface. Thus, the particulate mass collected on the crystal can be determined by measuring the change in the crystal natural frequency. The frequency to mass relationship is defined according to the Sauerbrey fundamental equation as [17]:

$$(\Delta f)/(\Delta m) = -C_f / A_d \qquad \text{(i)}$$

$$\text{For } A_d \geq A_a \quad C_f = f^2/Nq \qquad \text{(ii)}$$

Where f = crystal resonant frequency; Δf = change in frequency due to a change in mass per unit area on the crystal; q = density of the quartz; N =frequency constant for AT-cut quartz; C_f = sensitivity; A_a= active (or vibrating portion) of the crystal surface, A_d = area covered by deposit Δm [17].The SEMTECH-PPMD system determines mass over NTE events or any other user-defined sample intervals by measuring the mass before and after the sample interval. This method most closely simulates the standard gravimetric sampling method, where filters are allowed to equilibrate with a standard condition. The SEMTECH-PPMD has been submitted for evaluation within the EU PM PEMS program as well as the US Measurement Allowance Program.

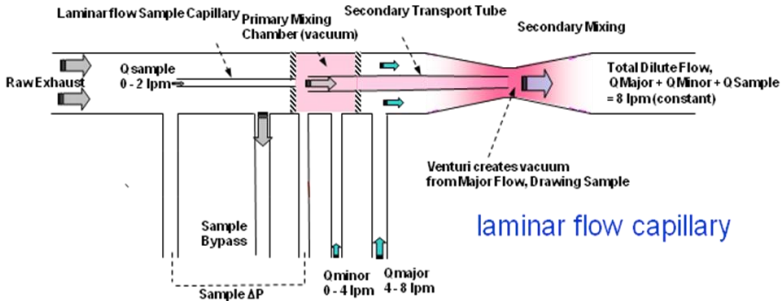

Figure 1: Schematic of the Micro-proportional Dilution system (MPS) based on laminar flow capillary. It illustrates the sample and transport capillaries, the primary and secondary dilution, and the venturi [17].

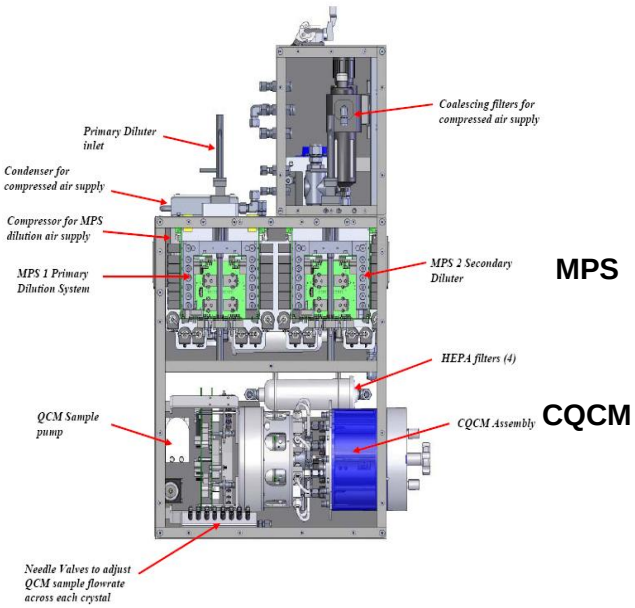

Figure 2: SEMTECH-PPMD schematic including MPS and Carousel QCM (CQCM) [3, 15].

SEMTECH-LAM

The LAM operating principle is laser scattering photometry where a laser beam is aimed into a controlled sample of the particle stream. The particles reflect and refract the laser light, a portion of which is collected through a lens and focused on a very sensitive photo-detector. The electrical signal generated by the photo-detector is amplified and analysed in a high-speed microprocessor to calculate the particle concentration in mg/m^3 as reported in the schematic below (Figure 1). It measures particle size in the range 100-10,000 nm, with an accuracy of 0.01 mg/m^3; its Technical specifications are reported below in Table 1. The SEMTECH LAM may be used as stand-alone or in combination with other instrumentation of the SEMTECH family such as the SEMTECH-FS based on the gravimetric method and /or the PPMD as in this case.

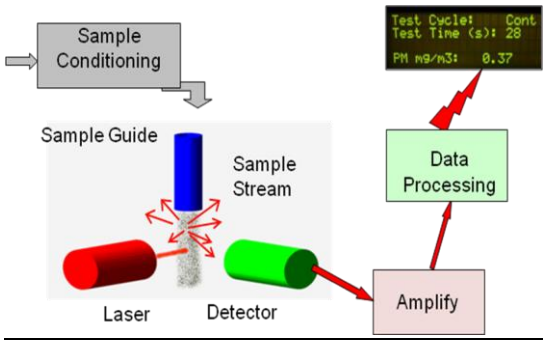

Figure 3: Schematic of the laser light scattering photometry principle of operation.

Table 1: SEMTECH-LAM Specifications.

- Range: 0-40 mg/m^3 / 0-700 mg/m^3- auto ranging
- Dilution: selective ratio
- Aerosol size: 100 to 10,000 nm
- Resolution: 0,01mg/m^3
- Drift: <0,25 mg/m^3 per 6 hours
- Sample rate: 5 Hz
- Sample Flow: 1.5 l/min
- Output: Analogue: 0 to 5 VDC / RS 232
- Power Supply: 12-24 VDC or 110-240 VAC
- Operating T: 0-40°C operating temperature
- Weight: 6 kg /10 lb
- Size: 44cm x 18cm x 55cm

Experimental

Testing was carried out with a EU V engine (MAN, 10 litre 6 cylinder, no DPF) with SCR and a EU III engine (IVECO Cursor 8 litre, 6 cylinder) provided with partial filter running on low sulphur fuel (S < 10 ppm); the EU III engine is the “golden” engine used for the PMP program. This preliminary testing with the LAM was carried out during the EU PM-PEMS program at the JRC vehicle emission laboratory (VELA5) in Ispra. Tests were carried out on both the WHTC and ETC cycles. For the standard gravimetric method (PTS) PM was collected on a Teflon coated glass fiber filter (PallflexEMFABTX40HI20 and weighted on a microbalance according to procedures currently in use in the Particulate Measurement Program (PMP) for filter weighting, conditioning and handling. The standard gravimetric method using the conventional Constant Volume Sampling (CVS) for dilution was compared to portable instruments such as the AVL Smart Sampler (SPC) using the partial flow sampling (PFS) principle. The AVL Smart Sampler (SPC 472) was used as reference instrument for the PFS principle; it is a partial-flow tunnel for gravimetric measurement of diluted particulates. Figure 4 shows a schematic of the experimental arrangement at VELA 5 (JRC); the CVS flow was set to 80 m^3/min.

,

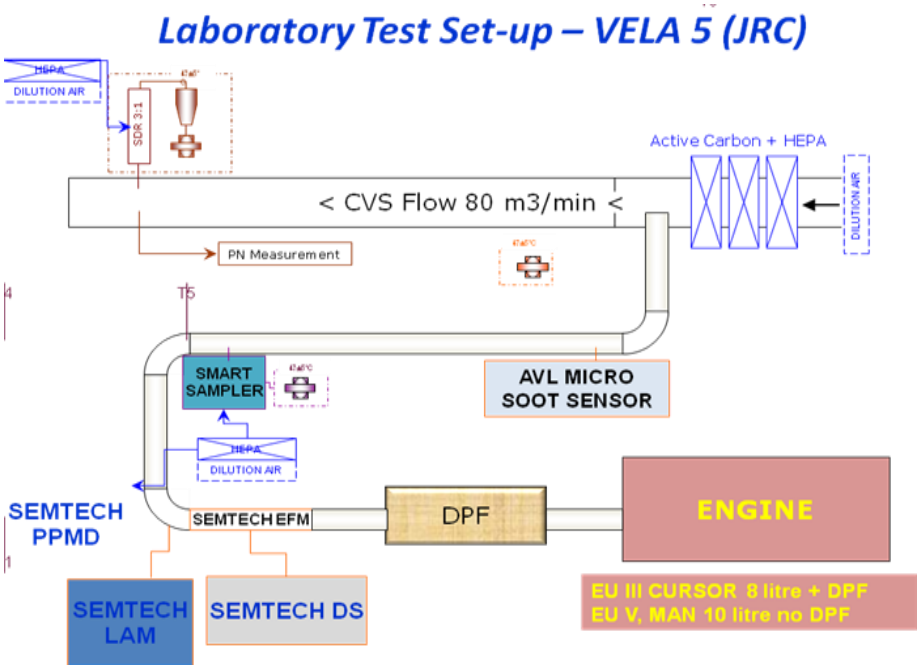

Figure 4: Laboratory experimental set-up.

Preliminary Results

Preliminary results are shown for the EU V engine and the EU III engine with partial filter. Figure 5 shows a comparison between LAM and the MSS in concentration (mg/m^3) over the WHTC cycle. The engine speed (rpm) is reported on the right-hand axis. The two profiles are very similar and zooming in the first 600 sec (Figure 6) of the cycle there is a good agreement between the two concentration values. A comparison of the integrated values (g/test) over the WHTC cycle is reported in Figure 7 where comparison is made among LAM, MSS and the gravimetric filter method (CVS and SPC). It seems that the LAM is able to distinguish between cold and hot WHTC cycles compared to the MSS. Data are reported for direct sampling (test 1-4) and for sampling with a heated extension line (5 m).
Good agreement between LAM (grey line) and MSS (black line) was also found during EU III engine testing. Similarly to the EU V engine testing, the LAM was able to distinguish between cold and hot WHTC cycle as shown in Figure 7. Comparison between LAM over a cold and a hot cycle (Figure 8) and between LAM and MSS over a cold WHTC cycle is shown in Figure 9; comparison over a hot WHTC cycle is presented in Figure 10. Good agreement was found also over the ETC cycle as shown in Figure 11.
A comparison of the integrated values over the WHTC cycle is shown in Figure 12. A comparison is provided not only with the gravimetric filter method but also with the QCM technique that is the working principle of the SEMTECH PPMD distinguishing between cold and hot WHTC cycle and ETC. The PPMD well follow CVS and SPC, and the LAM is very similar to the MSS over hot cycle and around 15% higher concentration values were found over cold WHTC cycles.
An example of LAM combined to PPMD data is shown in Figure 13; instantaneous (g/s) LAM values are compared to PM mass measured on a 2-min based by the PPMD; PM mass values over the WHTC cycle are provided over 2 min to allow for crystal stabilization. Accumulated values are shown as well. Good agreement was found between LAM and MSS as well as between PPMD and CVS and SPC values. Further engine testing and analysis is on-going. Further results will be published in a later stage.

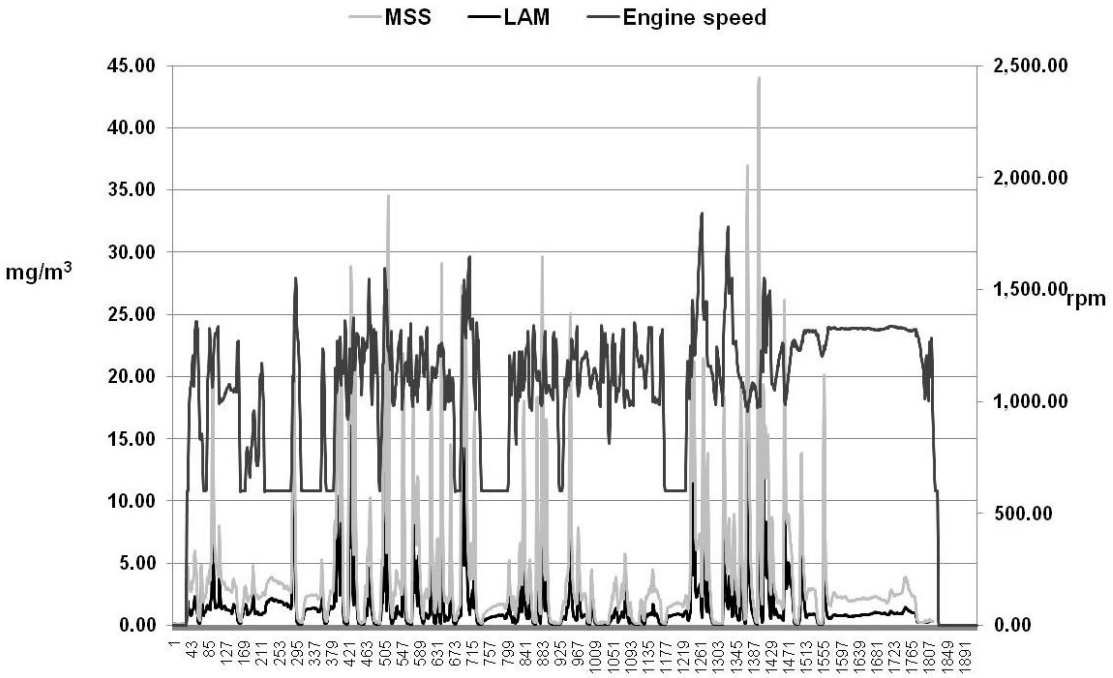

Figure 5: Comparison between LAM and MSS over the WHTC cycle – EU V engine.

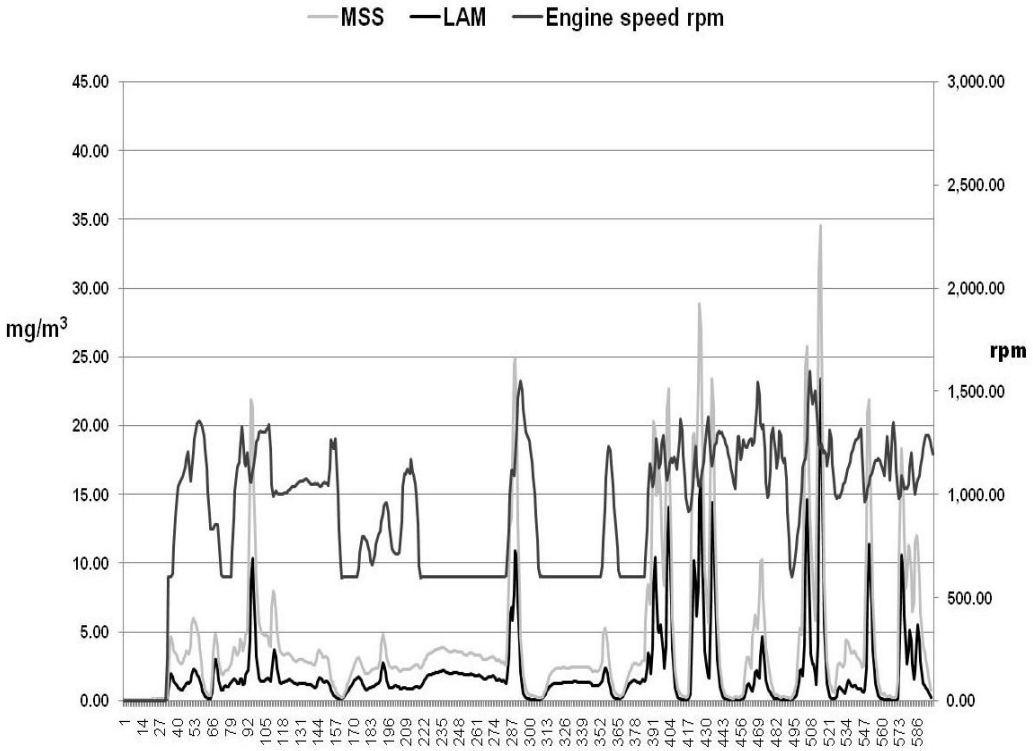

Figure 6: Zoom in the first 600 seconds of the WHTC cycle- EU V engine.

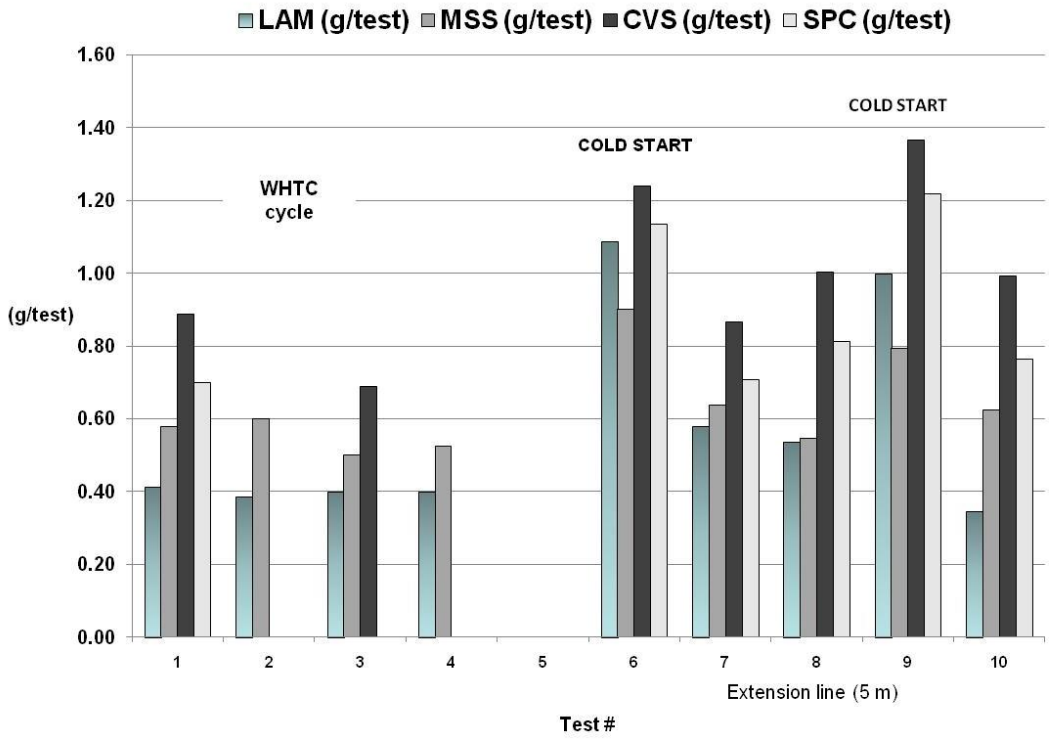

Figure 7: Comparison of the integrated PM values (g/test) among LAM, MSS; and gravimetric filter methods (CVS and SPC).

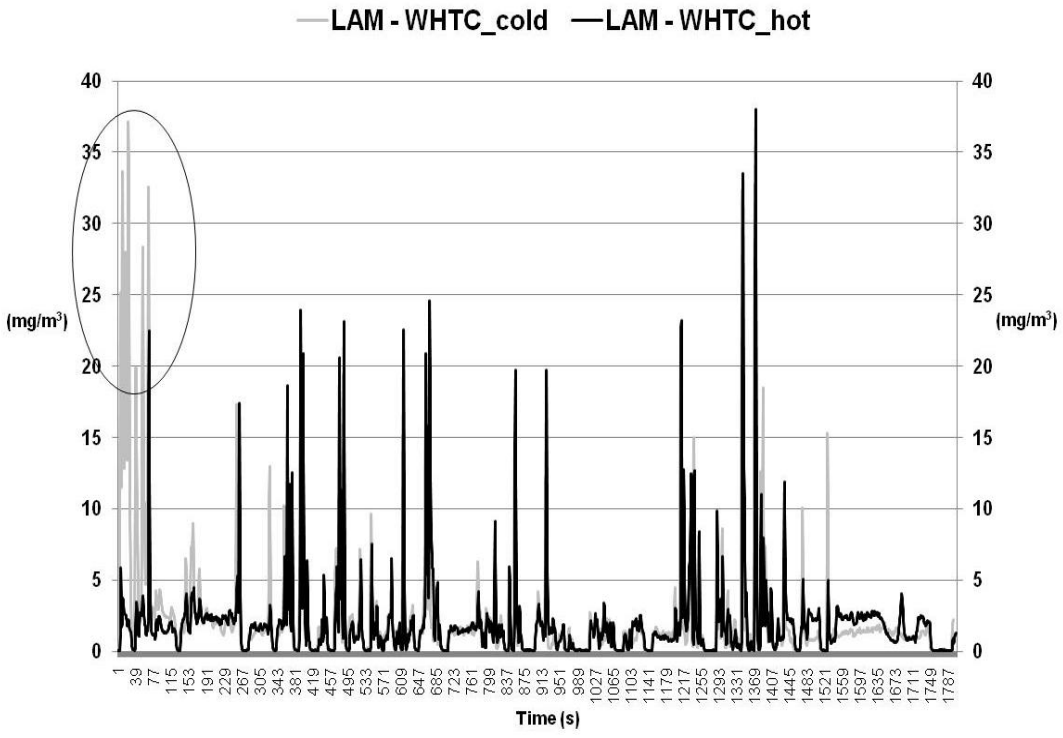

Figure 8: Comparison between LAM over the WHTC cycle – EU III engine with partial filter.

.

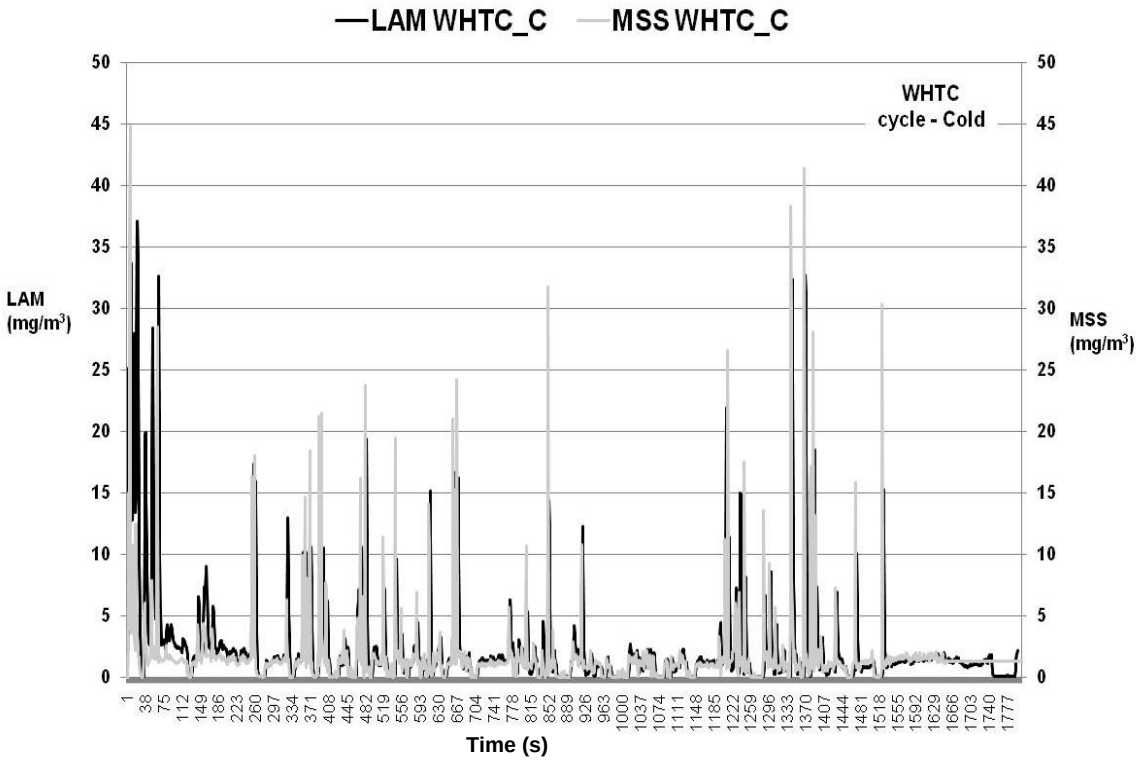

Figure 9: Comparison between LAM and MSS over the WHTC cycle, cold start – EU III engine with partial filter.

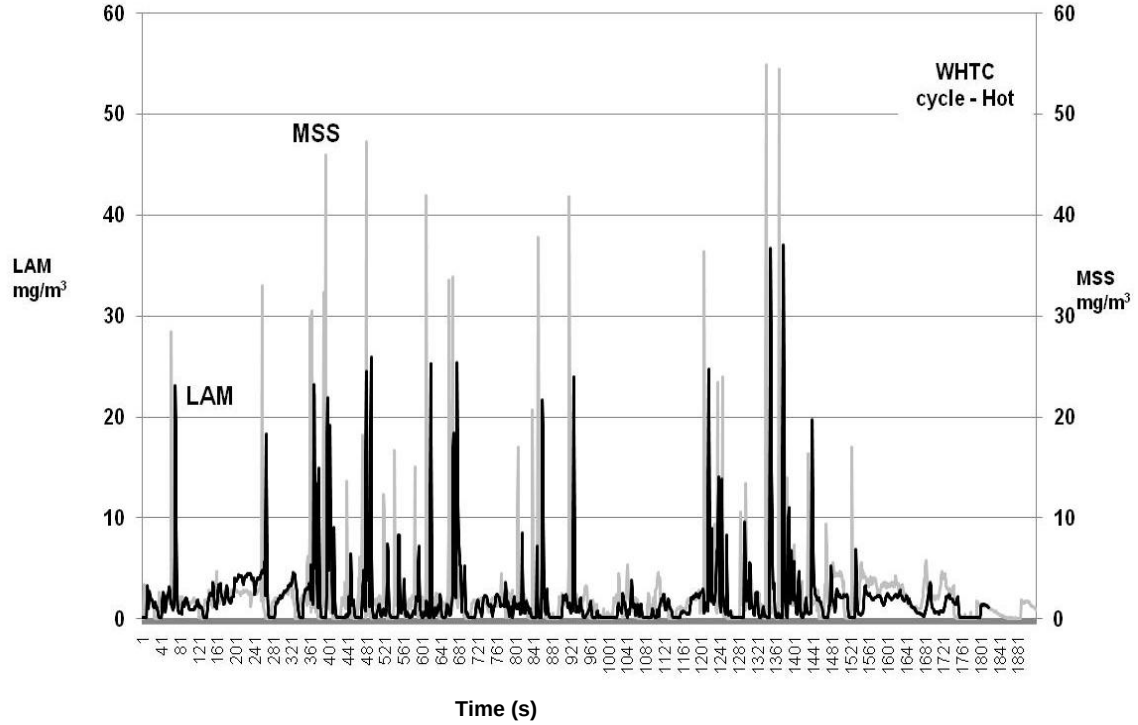

Figure 10: Comparison between LAM and MSS over the WHTC cycle, cold start – EU III engine with partial filter.

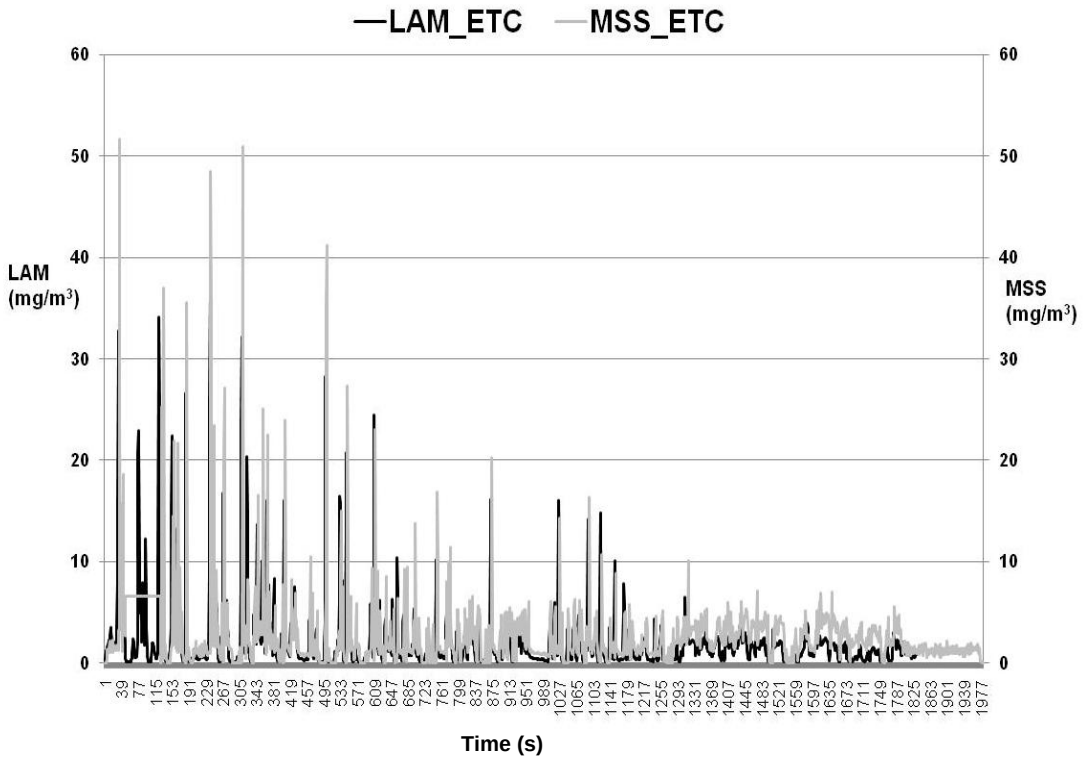

Figure 11: Comparison between LAM and MSS over the WHTC cycle, cold start – EU III engine with partial filter.

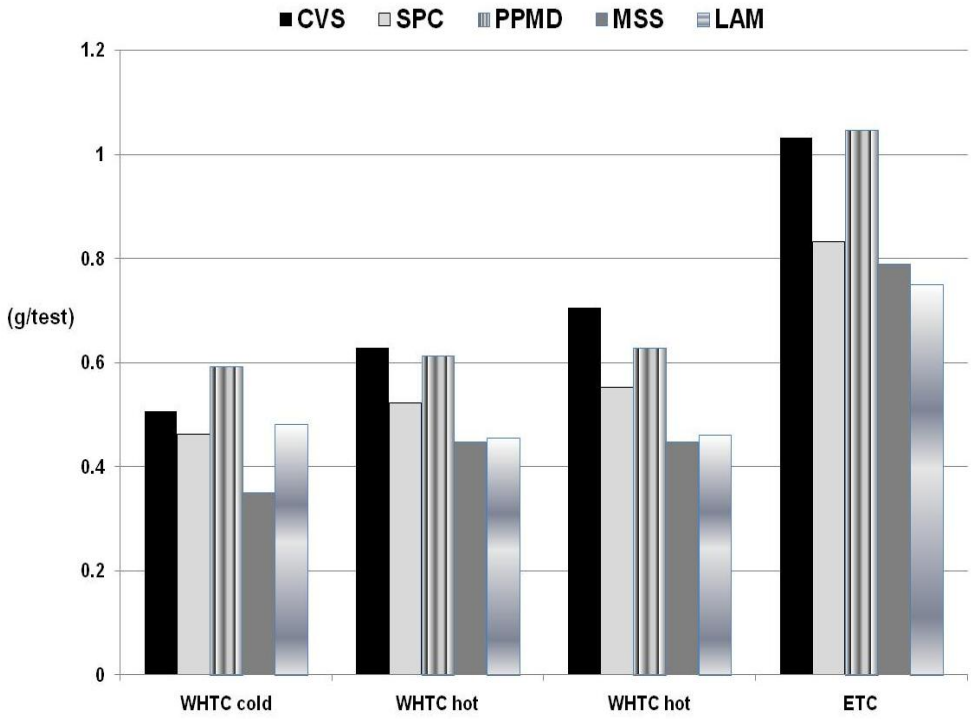

Figure 12: Comparison of the integrated PM values (g/test) among LAM, MSS, PPMD and gravimetric filter methods (CVS and SPC) over WHTC and ETC cycle.

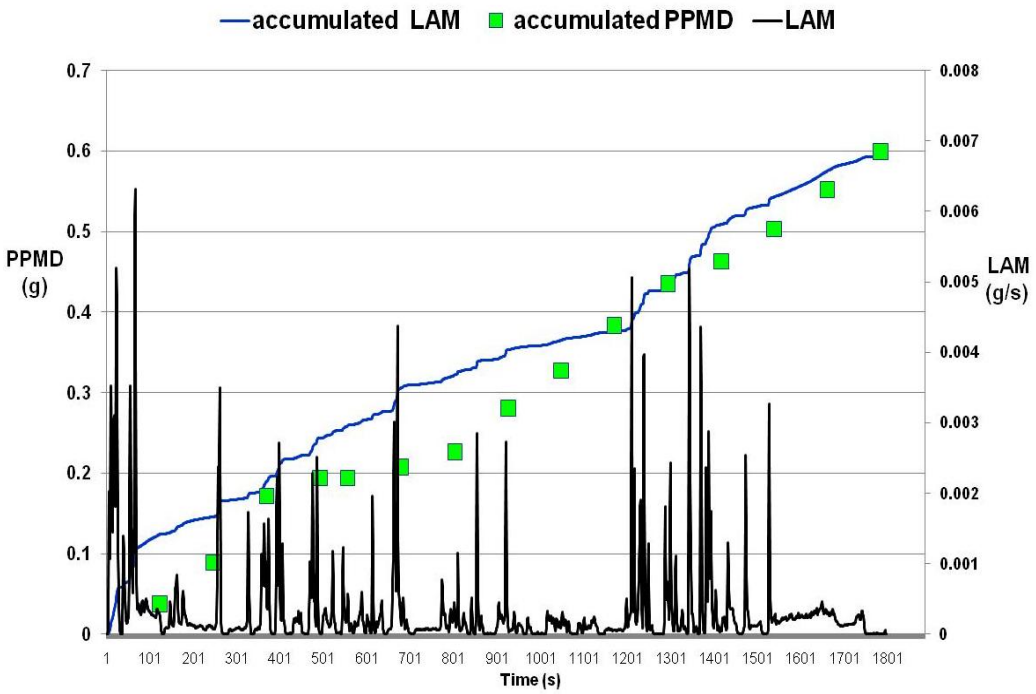

Figure 13: An example of LAM and PPMD data over the WHTC cycle; The LAM is providing instantaneous concentration (g/s) while the PPMD provides PM mass measurements (g) every 2 min (sampling time for quartz crystal stabilization). Accumulated values are shown as well.

Conclusions

Preliminary laboratory testing using the SEMTECH LAM with a EU V engine with no DPF and a EU III engine with partial filter showed good agreement of the device with the MSS over both WHTC and ETC cycle. The LAM was able to distinguish between cold and hot start and better follow the gravimetric filter method over cold start. Good agreement was found also between the SEMTECH PPMD based on the QCM technique and the gravimetric filter methods (both CVS and SPC) with the EU III engine with partial filter. Further data analysis is ongoing and further testing both in the laboratory and on road is planned for the near future.

Acknowledgements

Special thanks to the European Commission DG Joint Research Centre Vehicle Emission Laboratory (VELA) and in particular to Mr. Pierre Bonnel, Massimo Carriero and Alois Krasenbrink. The support of the EU PM-PEMS program is highly acknowledged.

References

1. L. Rubino, P. Bonnel, A. Krasenbrink, M. Carriero, J. Kubelt, I. Fumagalli, F. Montigny, G. De Santi. “Development of an official test method for on-board PM measurements from Heavy-Duty diesel engines in the European Union”, SAE paper No. 2007-01-1946 Kyoto, July, 2007.
2. L. Rubino, P. Bonnel, R. Hummel, A. Krasenbrink, U. Manfredi, G. De Santi. “On-Road Emissions and Fuel Economy of Light Duty Vehicles using PEMS: Chase-Testing Experiment”, SAE paper No. 2008-01-1824, SAE International Powertrains, Fuels and Lubricants Congress Shangai 23-25 June 2008.
3. L. Rubino, P. Bonnel, M. Carriero, A. Krasenbrink “Portable Emission Measurement System (PEMS) for Heavy Duty Diesel Vehicle PM Measurement: The European PM PEMS Program” SAE paper No. 2009-24-0149.
4. Mohr M., and Lehmann U. (2003). Comparison study of particle measurements systems for future type approval application. Research report no. 202770, EMPA.

5. Chase, R.E., Duszkiewicz, G.J., Richert, J.F.O., Lewis, D., Maricq, M.M., Xu, N. (2004). PM measurement artifact: organic vapor deposition on different filter media. SAE paper No. 2004-01-0967.
6. Kramer, L., Bozoki, Z., Niessner, R.(2000). Set-up, calibration and characterization of a mobile photoacoustic soot sensor. *Journal of Aerosol Science*, 31S1, 72-73.
7. Schindler W., Haisch C., Beck H.A., Niessner R., Jacob E. and Rothe D. A 'Photoacustic Sensor System for Time Resolved Quantification of Diesel Soot Emissions' SAE paper No. 2004-01-0968.
8. Moosmuller, H., Arnott W.P., and Rogers C.F. (1997). Methods for real time, in situ measurement of light absorption. *Journal of the Air and Waste Management Association*, 47, 157-166).
9. Crua C., Kennaird, D.A., and Heikal, M.R. (2003). Laser-induced incandescence study of diesel soot formation in a rapid compression machine at elevated pressures. Combustion and Flame, 135, 475-488.
10. Witze, P.O., Chase, R.E., Maricq, M.M., Podsiadlik, D.H., Xu, N. (2004). Time resolved measurements of exhaust PM for FTP-75: comparison of LII, ELPI, and TEOM techniques. SAE Paper No. 2004-01-0964.
11. Niemela V. (2006). Electrical tailpipe PM sensor for diesel engine emissions measurements; 10th ETH Conference on Combustion-generated Nanoparticles, Zurich 21-23, 2006.
12. Qiang Wei, M. Akard , S. Porter, H. Nakamura "The Development of an On-Board Instrument for On-Road Diesel Particulate Measurement" SAE paper No. 2008-36-0273E, Sao Paulo, Brasil, 2008.
13. Rubino, L., Phillips P.R., Twigg, M.V. (2005). Measurements of ultrafine particle number emissions from light-duty diesel engines using SMPS, DMS, ELPI and EEPS. ICE2005, SAE/NA Paper No. 2005-24-015.
14. Burtscher H. (2005). Physical characterization of particulate emissions from diesel engines: a review. Aerosol Science, 36, 896-932.
15. D. Booker, R.A. Giannelli, and J.Hu, "Road Test of an On-board Particulate Matter Mass Measurement System", SAE 2007-01-1116.
16. J.E.Brockmann, B.Y.H.Liu, P.H.McMurray, "A Sample Extraction Diluter for Ultrafine Aerosol Sampling", Aerosol Science and Technology, vol 3-4, pp441-451 (1984).
17. Sauerbrey, G.Z.: Measurements of the amplitude distribution of vibrating AT-cut crystals by means of optical observations Proc. Of the 17th annual frequency control symposium (1963)

Contact

Lauretta Rubino, Sensors Europe GmbH, Erkrath, Germany – email: lauretta.rubino@sensors-europe.eu.

Netherlands In-Service Testing Programme for Emissions of Heavy-Duty Engines and Vehicles; developments from on-cycle to real world emissions

R.Vermeulen[1], H.L. Baarbé[2], R. Verbeek[3], H.J. Dekker[4] and N.E. Ligterink[5]

[1, 3, 4, 5] TNO, Netherlands Organisation for Applied Scientific Research, Environmentally and Sustainable Transport, P.O. Box 155, 2600AD Delft, Netherlands, Robin.Vermeulen@tno.nl.
[2] VROM, P.O. Box 20951, 2500 EZ Den Haag, The Dutch Ministry of Spatial Planning and the Environment, Henk.Baarbe@minvrom.nl

Abstract

From 1993 to 2009 a large number of heavy-duty engines (Pre-Euro I to Euro V certified) has been tested over the steady state legislative emission test cycle in an In-Service Emission Test Programme. The tests were carried out on a chassis dynamometer. In addition in 2009, a number of Euro V certified vehicles has been tested in the real world, using a Portable Emission Measurement System.

In contrast to the emission tests as performed over the legislative test cycle, the real world tests revealed an in-effective NO_x control system mainly at low and medium vehicle speeds for most of the tested Euro V engines equipped with an SCR system. At low speeds, typical for urban operation, NO_x emission levels were up to three times higher than the emission limit for the legislative test cycle. The real world results were calculated using the on-road data and a new calculation method based on averaging the emission data in speed bins. This method made it possible to reveal the typical emission behaviour of the vehicles over the speed range.

Emission behaviour like a high NO_x emission at low vehicle speeds is commonly unwanted; in the Netherlands Environmental zones have been established in city centres, especially to reduce pollutant emissions in areas with a dense population. Therefore, the results highlight the need for including real world emissions in legislation beyond Euro V, not only controlling averaged emissions over accurately defined driving cycles, but also separately controlling for instance real world urban emissions.

Introduction

In 1993 the Dutch heavy-duty In Service testing programme was started on behalf of the Dutch Ministry of the Environment to investigate the emissions of heavy-duty vehicles of the Dutch vehicle fleet and at that time in particular those vehicles stimulated by the Dutch national subsidy scheme for clean and low-noise trucks. Gradually, the programme started to focus on durability and maintenance effects on emissions of vehicles in the Dutch fleet, also delivering data for the development of emission factors serving national and international emission models. With the introduction of electronic engine control, it was observed that some manufacturers optimized their engines only on the test cycle points and so starting as of Euro II off cycle emissions became an important part of the test programme.
Until now, within the ongoing programme of the Dutch government, over 250 trucks and almost 100 engine types have been tested in the ESC (European Steady State Test Cycle) test on the chassis dynamometer. Over the years, real world emissions of trucks gained more and more attention. Besides investigating the compliance of truck engines in service on the ESC test according to the TNO Diesel Control Method (Verbeek, 1993), new measurements and measurement methods were added to the programme to improve insight in real world emissions. In the recent years, with the introduction of Euro-IV and, in particular, Euro-V trucks on the road, efficiency of SCR and slip of ammonia, N_2O and NO_2 have become part of the test programme.
Due to the introduction of advanced aftertreatment systems and engine control systems to meet the current and future EU emission regulations, the test method with steady state test points (ESC) is deemed no longer suitable as a basis to predict real world emissions of heavy-duty vehicles. Testing an engine on a test bed or in a vehicle over steady state test points makes it harder to transform results to real world emission performance. Especially the emission

behaviour of modern engines and their aftertreatment systems under dynamic conditions have become far more complex and their performance is influenced by real world conditions like the vehicles driving pattern and payload. Hence, modern engines need to be investigated in a more sophisticated way, preferably in their vehicles under real world conditions.
With the development and introduction of measurement systems like the Portable Emission Measurement System (PEMS), remote emission sensing systems and the full climate power train transient test bed a new, more advanced approach of the current in service testing programme is possible and necessary to fulfil one of the most important requirements: gain insight in real world emissions of heavy-duty and making sure that in the future steps of emission legislation result in a decrease of emissions in the real world and not only on well defined test cycles.

This paper highlights the trends from the emission test programme that has been running in the laboratory for many years, testing engines in their trucks on a steady state test cycle. The paper also shows the results of real world emission tests as recently performed with 10 heavy-duty vehicles on the road. Using a new calculation method, also briefly discussed in this paper, the recent emission tests revealed real world emission behaviour of heavy-duty vehicles equipped with SCR systems to reduce NO_x over their operating speed range.

In-Service Testing on the chassis dynamometer

With the Netherlands In-Service Emission Testing Programme for heavy-duty vehicles running over more than a decade, trends can be shown of the emission performance over the steps in emission legislation. Figure 1 below shows the evolution of the EU emission limits as applicable for the engines as tested over the steady state test cycles.

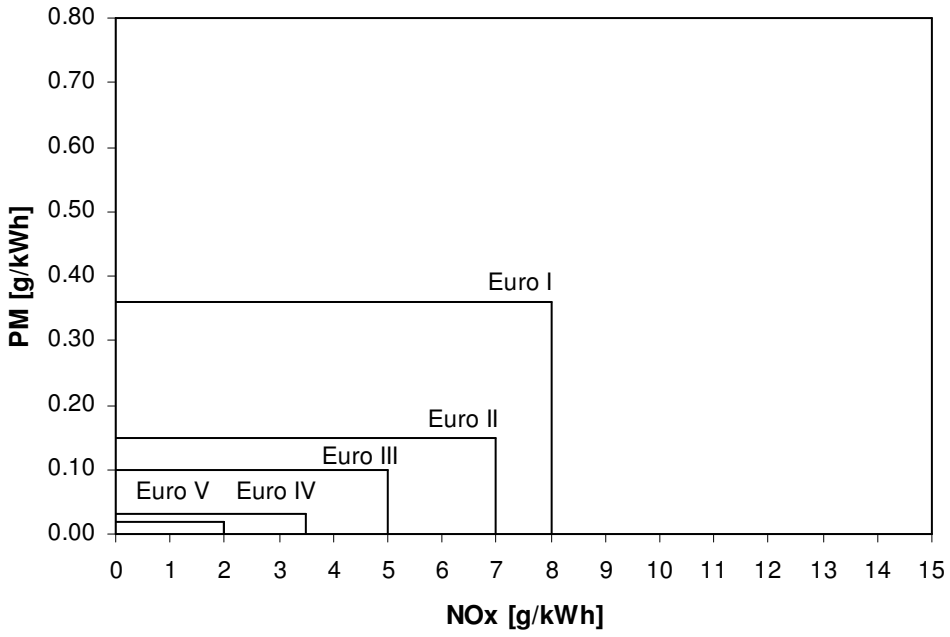

Figure 1: Evolution of the EU emission limits for NO_x and PM as applicable for the steady state test cycles (13-mode up to Euro II and ESC up to Euro V).

Going from pre-Euro I engines to Euro V engines Figure 2 clearly shows a trend towards lower PM and NO_x emissions and, with the exception of a few outliers, the scatter of each category becomes smaller as well. For the Euro V certified engines tested in-use over the ESC the average NO_x emission lies just above the applicable limit.

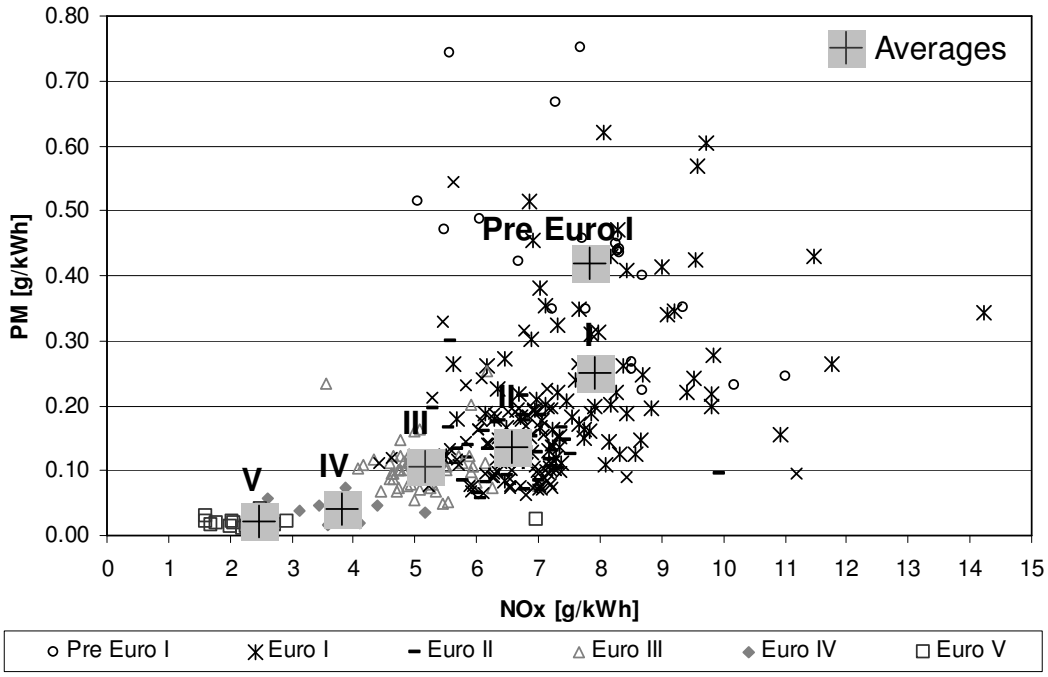

Figure 2: A clear downward trend can be observed from the NO_x and the PM emissions over the steady state test cycle, going from pre-Euro I (1990-1993) to Euro V (2009) certified engines. The results are from the trucks as they are taken from the road (in-use) and tested, without any corrective measures (adjustments, repair, and maintenance).

Until Euro II heavy-duty engines were rather conventional with mechanically controlled fuel injection. With Euro II electronic control was introduced on many engines and at that legislative step, it was for the first time observed that some manufacturers optimized their engines only in the area of the prescribed test points of the steady state driving cycle, resulting in elevated emissions outside the test cycle points (Riemersma et al., 2000), (Riemersma and Staats, 2006).

With the introduction of Euro IV and Euro V more advanced emission control systems were fitted. It was suspected that their control, operation and overall efficiency could be largely sensitive to the operating conditions, like driving patterns and payload. Therefore it was decided to test emissions under real world driving conditions and not only under accurately defined conditions within the laboratory.

Real world emission testing

In the EU within the PEMS Pilot Programme a procedure has been developed for testing the In-Service Conformity of engines installed in vehicles on the road using a Portable Emission Measurement System (PEMS). For the Dutch Programme it was decided at the end of 2008 to abandon the method simulating the legislative test cycle (ESC) on a chassis dynamometer and to start using PEMS as developed for checking EU In-Service Conformity, so as to gain experience with the tool. The PEMS method has evolved in a technical procedure able to test and accurately assess the gaseous emissions of heavy-duty engines and vehicles in a vehicle in the field. But the pass-fail procedure developed for Euro V In Service Conformity is aimed at averaged driving conditions and cuts out events with a low average power, hereby leaving out possibly important emission events, like for instance at low engine load and at cold start. For the

measurement of particulate matter no choice regarding the required system set up has been made yet. But the coming Euro VI standards, which are expected to require wall flow type particulate traps, may reduce the need to measure the emission of particulates under real world driving conditions, because the efficiency of this after treatment technology is largely insensitive to the duty cycle.

The PEMS method is rather different from laboratory testing. Differences can be noted for reproducibility, repeatability, robustness, workability and more. Especially repeatability and reproducibility are lacking compared to lab testing due to effects of ambient conditions, weather, traffic, the driver etc. But there are some clear advantages too. PEMS delivers real world data, under real world circumstances. When trips are selected with care, most traffic situations can be covered to find out all about emission behaviour under a wide range of conditions. When a representative trip is driven, emission data can become representative for a certain application or usage (e.g. bus line 77). And, as will be shown in the next paragraphs, if a new method is used to analyze the data of the real world testing, vehicles and driving circumstances can be discriminated with ease. The PEMS testing performed during this programme was mainly to gain experience with the tool. But next to 'experience' it already delivered great insight in emission behaviour of HD vehicles under real world driving conditions and it contributed to discussions at EU level as well.

On road trips

With most vehicles a reference trip as well as a representative trip was driven.

The reference trip is every time the same trip, hence the name reference, and includes almost all traffic conditions as well as special conditions like idling, a coast down etc.

For the representative trip the vehicle is operated in the real world as well, following distribution routes, bus lines or whatever trip is typical for the vehicle. This is prescribed in the EU PEMS technical procedure. For this procedure the required pay load is 50% of the maximum pay load and in a few cases, more or less payload was applied to experience possible differences in emission behaviour caused by this payload.

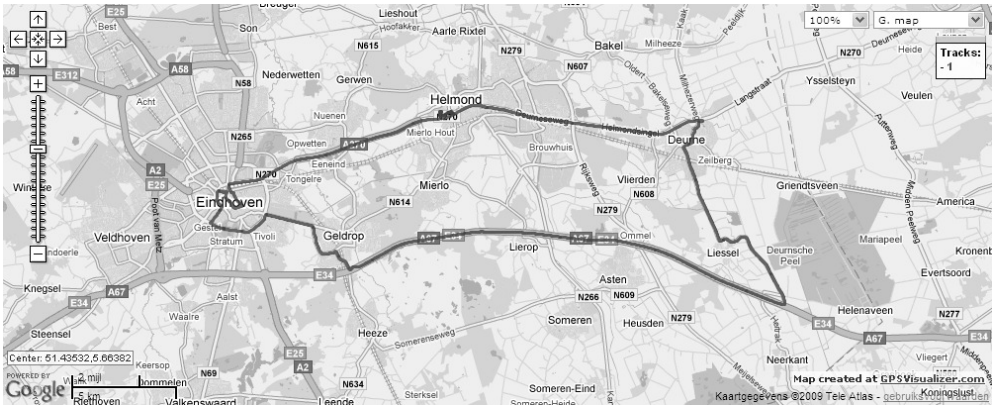

Figure 3: The reference trip starting at the TNO location in Helmond, driving the trip clockwise.

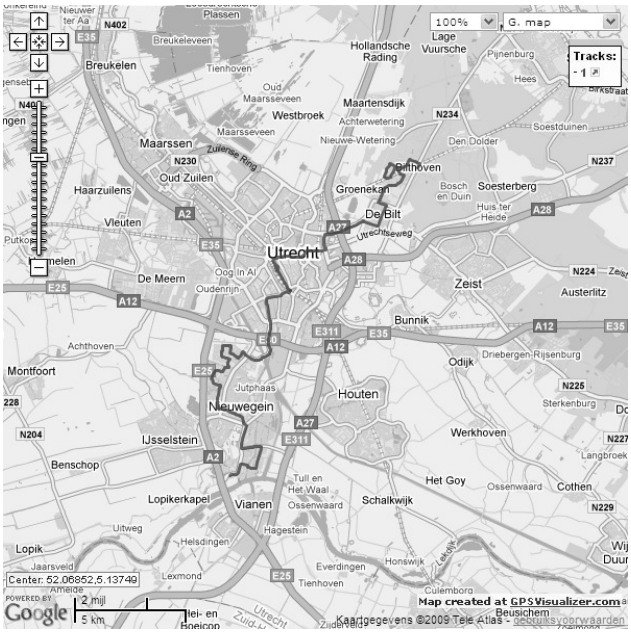

Figure 4: An example of a representative trip; bus line 77.

Vehicles

All of the selected vehicles have engines satisfying the latest heavy-duty emission standard: Euro-V. One small distribution truck and the city bus are labelled Environmentally Enhanced Vehicle or EEV, which implies however the same NO_x limit. From the 10 vehicles all but one were equipped with an SCR (Selective Catalytic Reduction) system to reduce the NO_x emissions. The one exception was equipped with an EGR (Exhaust Gas Recirculation) system serving the same purpose as the SCR system. This vehicle selection is considered to represent the Dutch fleet composition reasonably well. At the side of small distribution trucks only one vehicle was measured. A future programme should aim at testing more vehicles from this category, typically operating in urban environment. The kerb weight of the rigid trucks and truck-trailers ranged between 5.8 ton and 17.8 ton and the rated engine power ranged from 118 to 324 kW.

Table 1: Tested heavy-duty engines and vehicles over legislative categories for the on road tests.

Emission class	Number of Vehicles	
EURO V (B2 D, E and G)	8	2 rigid trucks, 6 tractor trailer combinations
EURO V EEV (B2 I)	2	1 bus and 1 distribution truck
Total	10	

A method to analyse real world emission data; CO_2 specific NO_x emissions

On road emission measurements as performed with PEMS deliver a huge and valuable amount of data. Not only second by second emission data is sampled but also many engine and vehicle parameters. The huge amount of data makes it a challenge to derive meaningful results. For the purpose of the pass-fail evaluation for In-Service Conformity according to the procedure developed within the EU the EMROAD tool is available. This tool is flexible and calculates

emissions online and integrated over user selectable trips and over especially for the EU ISC procedure defined averaging windows. However, the tool relies on engine work derived from the vehicles ECU to calculate brake specific emissions. The work is not very well defined; it is derived from engine load as broadcasted by the ECM according SAE J1939 and is rather unreliable due to lacking requirements regarding accuracy of the signals.

The emission values of trucks vary greatly with velocity, work (kWh) and vehicle mass (pay load). To be able to compare the emissions of different trucks, and judge their performance against emission limits, a uniform analysis method is required. To compare the respective NO_x emissions of different trucks, the ratio of the masses of NO_x and CO_2 emissions is suitable, as this ratio is relatively invariant over a wide range of trucks and varies only slowly with ambient test conditions and driving circumstances. In this analysis, the total NO_x and total CO_2 emissions for particular velocity bins are summed, and the fraction NO_x/CO_2 is determined per bin. These bins have a 5 km/h spacing, in which both the average emission and the corresponding average velocity are determined.

Formula;

$$gNOx\ per\ kgCO2 = \frac{\sum_{v=vi}^{v=vi+5} NOx[g/s]}{\sum_{v=vi}^{v=vi+5} CO2[kg/s]}$$

The current emission standard is based on the determination of brake specific emissions (g/kWh). In order to relate the emission results to an equivalent of the Euro V emission limit, the emission limit must then also be expressed in terms of the NO_x/CO_2 fraction. For this, the efficiency of the engine (i.e. the amount of CO_2 emitted per kWh) must be estimated and used as a default for determination of an equivalent limit value. Under an assumption of a brake specific fuel consumption for a diesel engine of 210 g/kWh during the ETC (or ESC), the specific CO_2 is about 666 grams per kWh. This value can be used to convert the emission limits to emission per kg CO_2. The relation between NO_x per CO_2 and NO_x per kWh of engine work is as follows;

$$\frac{NOx[g]}{Work[kWh]} = \frac{NOx[g]}{CO_2[kg]} \cdot \frac{CO_2[kg]}{Work[kWh]}$$

The Euro-V limit of 2.0 g/kWh, to which these trucks have to comply, then corresponds to a level of 3.0 g NO_x per kg CO_2. An In-Service limit applying a compliance factor of 1.5, as currently proposed for EU legislation, would yield a level of 4.5 g NO_x per kg CO_2. In practice engine efficiency can be lower and hence, the equivalent of the emission limit would become lower.

Real world emission measurements; results

The data gathered during the real world trips was analysed using the special method as described above. To exclude effects from a cold start all data where the engine coolant temperature was below 70 °C was excluded from the analyses. Figure 5 shows the average NO_x emission per kg CO_2 emission for different velocities (bins) and different vehicles:

- At lower velocities emissions are very high compared to the emission standard and still much higher than the currently proposed limit for vehicles In-Service Conformity, which lies 1.5 times higher than the applicable emission limit for Euro V engines.
- Only on the motorway, at 80 km/h or higher, the emissions on average near the equivalent of the emission limit.
- The results show a clear spread between the NO_x performances of vehicles. The single truck with the EGR system (Tractor trailer 2 in the picture below) seems to function better, however, trucks with this technology are less common in The Netherlands and on the basis of the results of one vehicle conclusions for that specific technology cannot be drawn. The small distribution truck (Small rigid 3 in the picture below) seems to be in-effective over almost the complete speed range.
- The Euro V EEV city bus managed to stay at an agreeable level below the equivalent of the emission standard.

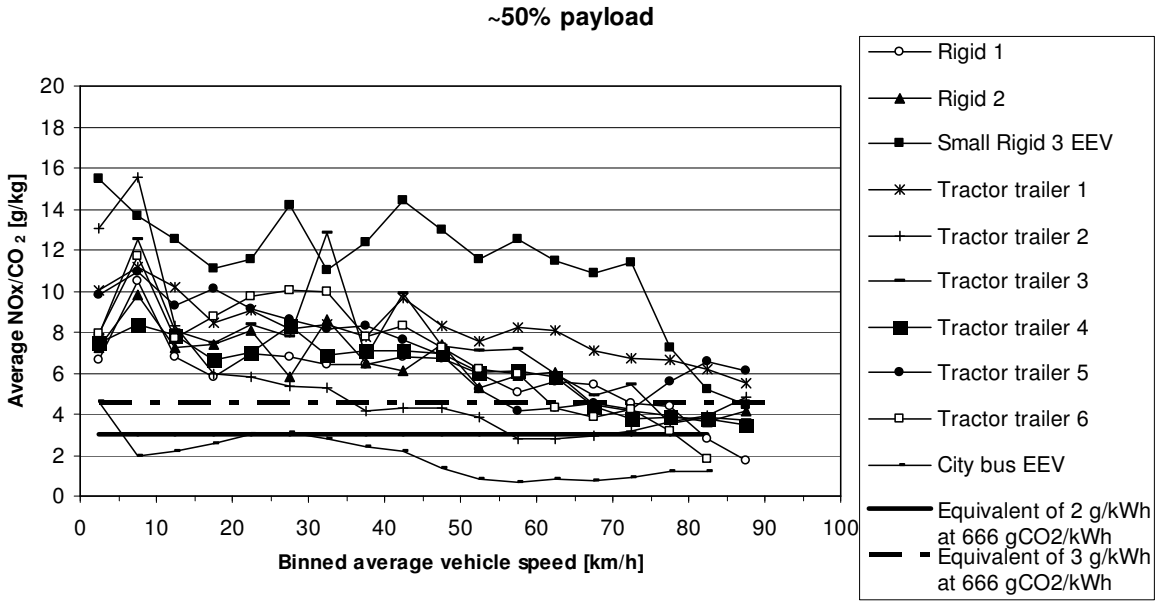

Figure 5: Binned average NO_x as a function of vehicle speed for Euro V and EEV vehicles. All trips are with 50% payload (coolant temperature > 70 °C).

Although the number of trucks is limited, straightforward statistical analysis showed a common trend of NO_x emissions appearing around two times higher than anticipated at speeds around 60 km/h and around three times higher at speeds below 30 km/h as they occur mostly in the urban environment. The different traffic circumstances are roughly distinguished by their speeds.

Apart from the trucks, also an EEV city bus has been measured with PEMS. The NO_x emissions of this bus was below the value corresponding with the emission limit across almost the entire speed range, demonstrating that it is possible to have good real-world NO_x emissions. The bus was not tested on the same reference trip, but on an urban bus route. It is not expected that this is a reason for the difference in NO_x emission performance though.

Further analyses revealed the influence of payload, as is shown in Figure 6. For one vehicle the reference trips were driven with 0, 50 and 100% payload (the last corresponds to a Gross Vehicle Weight of 50 tonne). At a higher payload the emission of NO_x per CO_2 decreases but still does not come close to 3 g/kg CO_2 at lower speeds. The higher the payload, the higher the average engine load, the higher the exhaust temperature is and hence the higher the working temperature of the SCR catalysts is.

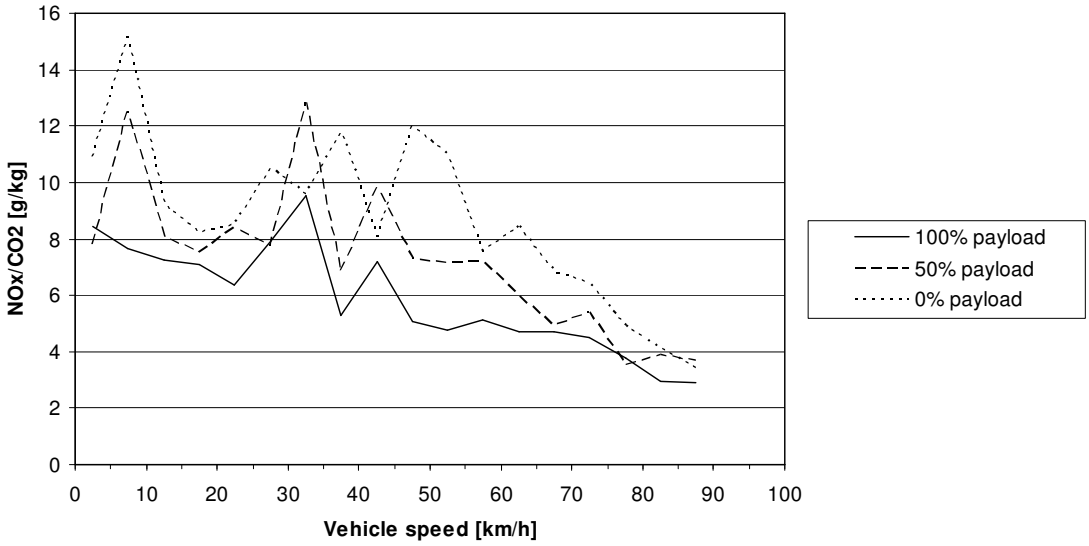

Figure 6: Example of binned average NO_x emission as a function of vehicle speed, for a Euro V vehicle with different payloads.

Discussion

The Dutch In-Service Testing programme for heavy-duty emissions from 1994 to 2009, included testing of engines mounted in complete vehicles on a chassis dynamometer, and recently testing of Euro V vehicles on the road. This has yielded clear insights in emission behaviour of conventional up to modern heavy-duty vehicles.

In the past, simple test cycles, using steady state test points, could easily check the emission performance of conventional diesel engines. Today, NO_x emissions of modern engines with advanced aftertreatment systems appear sensitive to operating conditions like vehicle speed and payload. Obviously, an important part of the explanation for this sensitivity can be found in the way the SCR system works (Helden, 2004). If the temperature of the SCR catalyst is too low to convert NO_x with ammonia, dosage of reagent should be stopped to avoid either slip of ammonia or the formation of deposits on the catalyst, the last leading to an even worse efficiency. Higher payloads and high vehicle speeds lead on average to a higher engine load and higher exhaust gas temperatures and hence, under these conditions reagent can be dosed and the SCR catalyst is able to reduce NO_x efficiently.

Current emission test cycles (ESC and ETC) generally contain engine load collections that lead to sufficiently high exhaust gas temperatures so that over a complete test cycle NO_x can easily be reduced with a high efficiency. With that in mind the new test cycle for Euro VI, the WHTC, was developed and already contains more low load operation and even includes a cold start to provide more demanding operating conditions with respect to NO_x control.

But, as shown in this paper, real world NO_x emissions can at low speeds be up to three times higher then anticipated for Euro V engines equipped with an SCR system. From the point of view of air quality this is commonly unwanted; For NO_2, the noxious component of NO_x, limits have been defined and those limits are still exceeded along busy roads in many cities in the Netherlands. The recent results from the on-road emission test therefore highlight the need for

including real-world emission evaluation in emission legislation beyond Euro V and the real world emissions should not be averaged over large time windows or driving cycles so that important emission events, like those occurring under urban driving conditions, are compensated. Instead, urban driving conditions should be analyzed separately or at least given enough weight in the procedure so that urban emissions are controlled to an agreeable extend.

Further possible causes for the elevated NO_x emissions are still under examination and special attention is given to the potential of the existing systems to be further optimized for proper operation under most driving conditions.

Changing emission control technology applied to heavy-duty engines has led to the need to test engines not only over a well defined test cycle, but also as mounted in their vehicles under transient conditions and in the real world on the road. The PEMS measurement technique has made this possible. Other test methods such as remote emissions sensing and a climate test cell can further complete assessment of real world emissions. Remote sensing might reveal trends with respect to the real effectiveness of emission control strategies of the overall vehicle fleet and identify problem areas. The in-depth investigation of these problem areas is possible within the climate test cell under varying and extreme environmental conditions and with laboratory level reproducibility and accuracy.

Other test methods could add further crucial insights for the In-Service Testing Programme in emission behaviour of heavy-duty vehicles in the real world; on the one hand a fully equipped heavy-duty power train emission test cell, able to simulate extreme environmental conditions, will enable in-depth investigation in vehicles emission control strategies and on the other hand remote sensing might reveal trends with respect to the real effectiveness of emission control strategies of the Dutch fleet.

The method relating emissions to CO_2 yields good estimates of the emission performance over the velocity range of modern heavy-duty vehicles and even is able to distinguish between payloads. The method is therefore very suitable to assess and to model heavy-duty emissions for air quality evaluations. As of the end of 2009 the basics of this method were introduced in the Netherlands emission model for road transport Versit+.

Conclusions

An in-use compliance test program with several hundreds of heavy-duty vehicles (pre-Euro I to Euro V) carried out in the Netherlands between 1993 and 2009, demonstrated that the on-cycle emissions have been reduced considerably over time. The average NO_x emission of Euro V engines in their legislative cycles lies only just higher than the applicable emission limit and is at a level of 30% of pre-Euro I engines. For the mass emission of particles the latest heavy-duty engines are at 5% of the pre-Euro I engines.

Measurements with 10 Euro-V heavy-duty vehicles on the road with a Portable Emission Measuring System (PEMS), however, showed that real world NO_x emissions are up to a factor 3 higher than expected on the basis of the limit values at low and medium vehicle speeds, which are typical for urban operation.

In order to secure agreeable real-world emissions, especially for urban driving conditions, it is recommended for future emissions legislation to separately judge emission performance for different driving conditions (e.g. urban, rural and motorway) under real-world operating conditions.

A new calculation method which bins emission data in speed intervals and relates NO_x to the CO_2 emission is able to reveal emission behavior over the speed range of a heavy-duty vehicle.

References

Helden, R. van, (2004), Optimization of Urea SCR deNO_x Systems for HD Diesel Engines, SAE 2004-01-0154.

Ligterink N.E., R. de Lange, R. Vermeulen, and H.J. Dekker (2009), On-road NO_x emissions of Euro-V trucks, TNO report MON-RPT-033-DTS-2009-03840, 2 December 2009

Riemersma I.J., R.C. Rijkeboer and K.H. Jordaan (2000), Final Report In-Use Compliance Programme, 00.OR.VM.077.1/IJR, November 2000

Riemersma I.J., F. Staats (2006), In Use Compliance programme for trucks, 2001-2004, TNO report 06.OR.VM.019.1/IJR, April 18, 2006.

Verbeek R. (1993), Eindrapport Diesel-controle methode; Procedure en nauwkeurigheid van testen, volgens Richtlijnen 88/77/EEG en 72/306/EEG, uitgevoerd op een rollenbank (Final report DCM; Procedure and accuracy of testing, according to 88/77/EEC and 72/306/EEC, carried out at a chassis dynamometer), TNO-report 93.OR.VM.023.1/PvG/RV, 1993.

Influence of Driving Style on Fuel Consumption and Emissions in Diesel-Powered Passenger Car

N. Fonseca[1], J. Casanova[1] and F. Espinosa[2]*

[1] Department of Energy and Fluid Mechanics Engineering. Universidad Politécnica de Madrid. C/José Gutiérrez Abascal, 2. 28006 Madrid. Tel: 34913363155. Email: jesus.casanova@upm.es

[2] Department of Electronics. Universidad de Alcalá. Campus Universitario. Ctra. Madrid-Barcelona, km. 33,600 | Alcalá de Henares (Madrid) Tel: 34918856545. Email: felipe.espinosa@uah.es

Abstract

This paper presents the main results of a study on the influence of driving style on fuel consumption and pollutant emissions of diesel passenger car in urban traffic. Driving styles (eco, normal or aggressive) patterns were based on the "eco-driving" criteria. The methodology is based on on-board emission measurements in real urban traffic in the city of Madrid. Five diesel passenger cars, have been tested. Through a statistical analysis, a Dynamic Performance Index was defined for diesel passenger cars. Likewise, the CO, NO_X and HC emissions were compared for each driving style for the tested vehicles.

Eco-driving reduces by 14% fuel consumption and CO_2 emissions, but aggressive driving increase consumption by 40%. Aggressive driving increases NO_X emission by more than 40%. CO and HC, show different trends, but being increased in eco-driving style.

Introduction

The Driving style of the driver refers to aspects of the actual driving action, where the driver can exercise their free will, although he is conditioned by external agents such as the configuration of the streets and roads (slope, crossroads per kilometre, etc.) and traffic congestion. Thus, the dynamic behaviour of the driver is reflected in how he acts on the vehicle controls such as: throttle, clutch, brake, gear shift and steering wheel. In order to asses the benefits of one driving style versus another, some real data were needed. Nevertheless, this study is not based on actual measurements of driver direct actuation on the vehicle controls, but on dynamic variables, recorded in real time, that are directly affected by the way the vehicle engine is operated, such as vehicle acceleration, engine speed and current gear shift.

Three different driving styles have been studied: eco-driving –in which shifting is made as soon as possible at a maximum of 2000 rpm for diesel engine to as high a gear as possible as defined by TNO (Vermeulen, 2006; Van Mierlo et al., 2004), normal driving and aggressive driving. Aggressive driving is defined as the driving style contrary to eco-driving, characterized by hard accelerations, increased use of first and second gear and driving at high engine speed (Casanova et al., 2005).

In order to have real figures of some relationships between real driving style and fuel consumption and emissions, data collected in real traffic conditions and using different diesel powered vehicles of different technology level were needed. Then, five different diesel passenger cars have been tested in real traffic use along two circuits in the city of Madrid. The testing methodology and the main results are presented.

Methodology

This study is based on about 1000 km driven in real traffic, equivalent to approximately 100 hours of emission measures, consumption and dynamic variables with five light duty diesel vehicles whose characteristics are presented in the table 1. Also, five different drivers have driven the cars, to somehow reduce the bias that could cause their own way of driving. Three different circuits have been used in the city of Madrid, the Madrid-UPM circuit (Casanova et al., 2009), Tetuan circuit and extraurban circuit, whose characterizations are shown in Figure 1 and Table 2 and 3. These circuits were chosen because they include the different types of streets normally found in a city like Madrid (local streets, secondary, main, arterial and highway),

allowing to analyse the influence of road infrastructure. All trials were made with the engine at normal operating temperature to avoid the inherent variability of the cold start.

Table 1: Overview of the tested passenger cars

Make and model	Year of manufacture	Engine: make / model	Engine displacement (cm^3)	Max. power (kW)	Weight (kg)	Emission legislation EURO
PEUGEOT 406 BK STDT 2,1	1998	PEUGEOT / D-P8C	2088	80	1485	Euro 2
RENAULT LAGUNA	2005	RENAULT / D/F 9Q D6	1870	88	1350	Euro 3
CITROEN C4 HDI92 LX	2007	CITROEN / D-9HX	1560	66,2	1332	Euro 4
RENAULT LAGUNA	2008	RENAULT / D/K 9K 37	1461	81	1386	Euro 5
SEAT LEON	2008	VOLKSWAGEN /(D) BKD	1968	103	1315	Euro 4

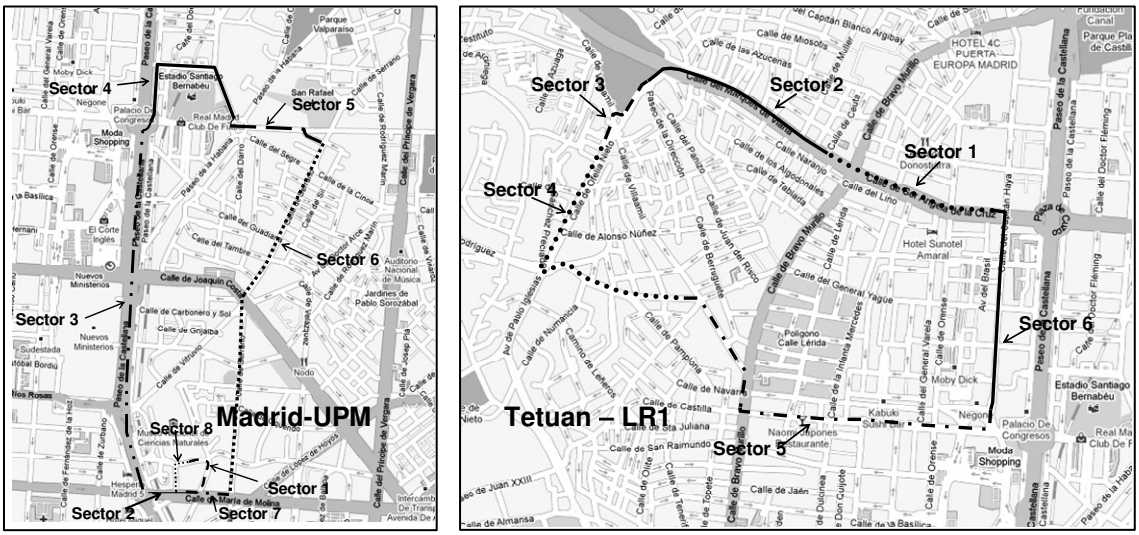

Figure 1: Madrid-UPM and "Tetuán" LR1 circuits.

Table 2. "Tetuan" – LR1 circuit. Table of characteristics per sector.

Sector	Distance (m)	Crossroads per km	Average Slope (%)	Average speed without traffic km/hr)	Lanes
1	610	8.2	0.86	31.6	3
2	680	7.6	-2.84	35.5	2
3	340	2.9	-0.63	42.5	2
4	1080	8.3	2.33	30.9	1
5	1400	6.4	-1.69	17.2	4
6	890	4.5	1.76	28.0	4
TOTAL	5000	6.6	0.02	25.6	---

Table 3. Madrid-UPM circuit. Table of characteristics per sector.

Sector	Distance (m)	Crossroads per km	Average Slope (%)	Average speed without traffic km/hr)	Lanes
1	517	5.80	-1.58	35.36	1
2	271	7.38	-2.81	30.63	3
3	1881	5.32	2.40	34.57	8
4	230	4.35	1.75	38.66	2
5	303	13.20	-2.78	18.06	3
6	385	10.39	2.53	22.95	3
7	796	12.56	-2.53	23.24	3
8	761	6.57	-2.06	41.10	4
9	289	3.46	-3.05	44.28	3
10	257	3.89	1.02	25.14	1
TOTAL	5690	7.21	0.00	32.31	----

The five cars tested, were instrumented with a self-developed non-intrusive universal on-board emission measurement system (MIVECO-PEMS) and a portable global activity measurement system (PGAMS), described by Casanova et al. (2009). So, The most important variables that ware recorded in real time at 10 Hz have been: exhaust gas flow, exhaust gas temperature, and exhaust gas pressure; concentration of CO (ppm), CO_2 (%), HC (ppm), NO_X (ppm) and air/fuel ratio (lambda); engine speed (rev/min), vehicle speed (km/h), oil and cooling water temperatures and weather conditions such as atmospheric pressure, humidity, temperature and headwind speed. As part of signal post-processing work (synchronization of real time recorded signal and thermodynamic and fluid mechanics calculations), the instantaneous mass emissions, total emissions and emission factors were calculated, both for each trial and for each of the sectors studied into each circuit.

Results and discussion

In a preliminary study presented in ETTAP09 (Casanova et al, 2009) a dynamic performance index "DPI" for a light duty gasoline vehicle was experimentally determined to evaluate the specific driving style used in a specific trial. In this work, a new dynamic performance index has been defined for light duty diesel vehicles. It is based on emission and dynamic measurements done in real traffic conditions for 5 light duty diesel vehicles (see Table 1). Various dynamic variables have been analysed over each entire circuit and over each sector in which it was divided. These are: average speed, positive average acceleration, percentage of time above a certain engine speed, percentage of time in each gears (first, second, third, etc.) and power demand (speed x acceleration) as defined by Ericsson (2001). The percentage of time does not include the time when car is stopped. So the Dynamic Performance Diesel index "*DPDi*" can be expressed as:

$$\textbf{\textit{DPDi}} = 1.58e\text{-}3 * \textbf{\textit{\%\_time\_1gear}} + 2.05e\text{-}3 * \textbf{\textit{\%\_time\_2gear}} + 1.48e\text{-}3 * \textbf{\textit{\%\_time\_>1850rpm}} + 5.82e\text{-}2 * \textbf{\textit{Average\_acceleration}}$$

Where it appears that the most influential parameters to quantify the driving style are the percentage of time that the driver runs in the first gear *(%_time_1gear*), in second gear *(%_time_2gear*), the percentage of time that leads to more than 1850 rpm *(%_time_>1850rpm*) and the positive mean acceleration (*Average_acceleration*) - that does not include periods of deceleration. The DPDi thus defined let to distinguish typical ranges of average accelerations that can occur in the three driving styles for the range of average speeds that can be had downtown in a city like Madrid, as shown in Figure 2.

The DPDi takes values in a range between 0 and 1.2 approximately, as shown in Figure 3, where in addition, the probability distribution of the DPDi according to the intention of the driver for eco and aggressive driving is shown.

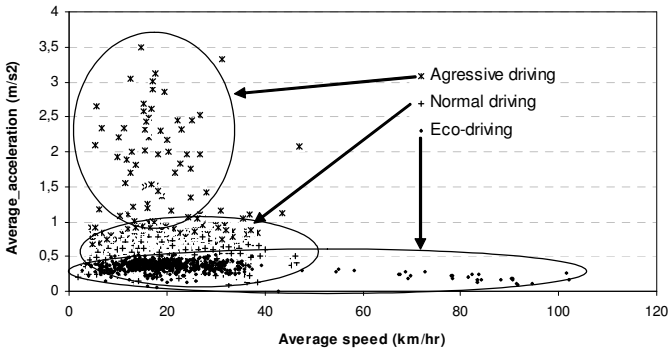

Figure 2: Average acceleration in real urban traffic for different driving styles.

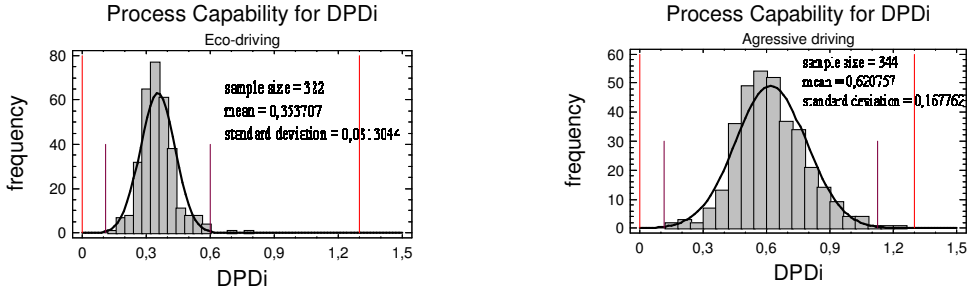

Figure 3: Probability distribution of the DPDi according to the intention of the driver for eco and aggressive driving.

The driver cannot always drive with his desired style due to the randomness characteristic of real traffic, as can be shown in figue 3. Thus the DPDi allows to reclassify each driving pattern according to driving style as follow: eco-driving DPDi ≤ 0.4, normal driving 0.4 < DPDi <0.6 and aggressive driving DPDi ≥ 0.6. As an example, figure 4 shows the effect of the driving style on fuel consumption for one of the tested cars.

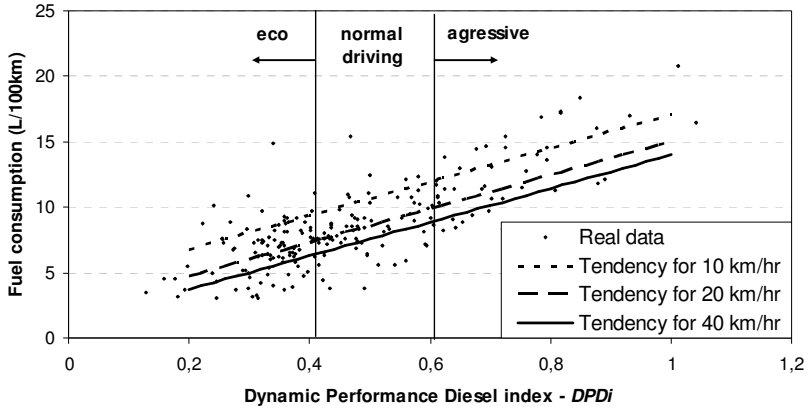

Figure 4: Influence of the dynamic behavior of the driver on fuel consumption in real traffic. Measurements made on Renault Laguna 2005 in Madrid City, 30 trials and 200 km of travel. Trends calculated for 0% slope.

One of the features of the DPDi is that it let us to compare the different vehicles in real traffic, because guarantees the equality of the driving style used in each route. Moreover, as discussed in the previous paper (Casanova et al., 2009), driving in real traffic is determined by three factors: driving style, road and traffic congestion. The congestion is reflected in the relationship between real traffic average speed and average speed without traffic, where real traffic average speed is independent of the driving style and average speed without traffic depends on the type of street. Based on these ideas, there was made a statistical study for each of the cars, of which the follow empirical equation was obtained:

Consumption (L/100 km) = k0 + k1 * (1/average_speed) + k2 * %slope + k3 * DPDi

Where k0, k1, k2 and k3 are the constants calculated by multiple regression analysis. The constants for each of the vehicles tested are shown in Table 4.

Table 4. Fuel consumption of cars tested. Coefficients of empirical equation of multiple regression.

Test vehicle	k0	k1	k2	k3	Model P-Value	R-squared (%)	Confidence level
Peugeot 406	-0.3474	48.2355	0.5899	12.8849	0.0000	90.1	99%
R_Laguna 2005	0.1196	41.1305	0.6620	12.8349	0.0000	84.6	99%
Citröen C4	0.4077	39.0072	0.6390	8.8021	0.0000	87.1	99%
R_Laguna 2008	-0.9273	41.9819	0.7481	14.9574	0.0000	87.3	99%
Seat León	-1.6971	34.6786	0.8766	17.6009	0.0000	90.8	99%

The figure 5 shows graphically the previous fuel consumption tendencies, for streets with slope of 0% and for the three driving styles: eco-driving (DPDi = 0.33), normal driving (DPDi = 0.49) and aggressive driving (DCI = 0.74).

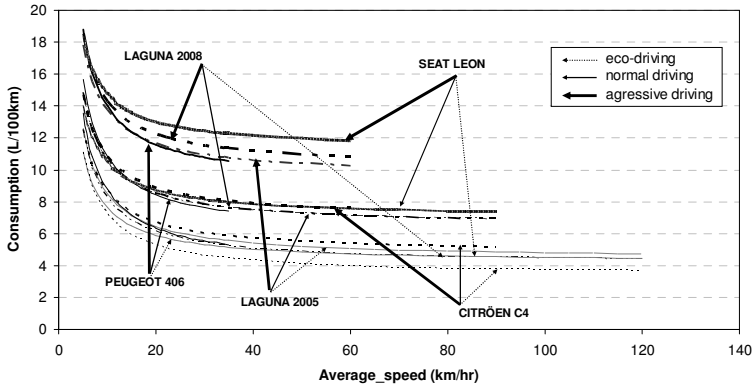

Figure 5: Fuel consumption tendencies for tested vehicles, based on urban and extra-urban routes in Madrid City.

It confirms that the driving style has a very high influence on fuel consumption and hence over carbon dioxide emissions. This graph shows that in normal driving conditions, fuel consumption are very similar for all tested vehicles, except for the Citroën C4 that is a car with energy classification A (lowest consumption in its range).

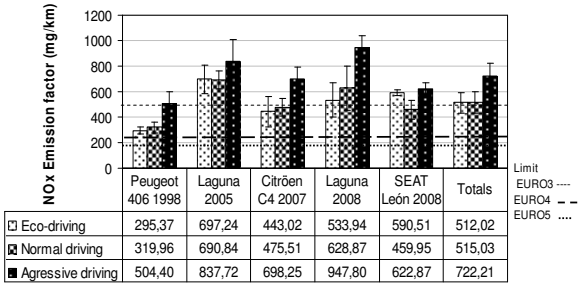

	Peugeot 406 1998	Laguna 2005	Citröen C4 2007	Laguna 2008	SEAT León 2008	Totals
Eco-driving	295,37	697,24	443,02	533,94	590,51	512,02
Normal driving	319,96	690,84	475,51	628,87	459,95	515,03
Agressive driving	504,40	837,72	698,25	947,80	622,87	722,21

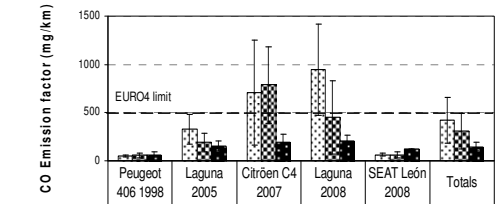

	Peugeot 406 1998	Laguna 2005	Citröen C4 2007	Laguna 2008	SEAT León 2008	Totals
Eco-driving	49,13	329,49	711,86	948,07	66,55	421,02
Normal driving	56,82	191,27	787,22	453,32	60,19	309,77
Agressive driving	66,12	151,50	196,32	202,10	122,30	147,67

Figure 6: Influence of driving style on NO_X and CO emission factors for urban traffic.

Additionally, based on the total results of each of the circuits, comparative studies were made between vehicles tested, as seen in Figure 6, for CO and NO_X emissions, with average speed of 19.3 km/h. The effect of driving style is not the same in all cars for those emissions, which

agrees with the TNO results (Vermeulen, 2006). The reason could be the different calibration of each engine electronic control. In eco-driving pattern when low engine speed and medium to high gas pedal positions are used, CO and NO_X emissions can increase, probably because of mixture enrichment, due to low oxidation catalyst efficiency at high combustion temperature at high fuel/air equivalence ratio.

Conclusion

Figure 7 shows a summary of the influence of driving style on emissions, which shows that for all the cars tested, the advantage of eco-driving is clear in terms of reducing consumption and CO_2 emissions by 14%, and the disadvantage of aggressive driving that increases consumption and CO_2 by about 40% (Figure 7), which agrees with De Vlieger (2000) and Van Mierlo et al. (2004). But CO, HC and NO_X emissions depend on the engine design and calibration. Anyway, on average for NO_X emissions, eco-driving do not have advantages, but aggressive driving increases this emission by more than 40%. Another important aspect observed is that NO_X emissions in real traffic generally exceed the statutory emission limits.

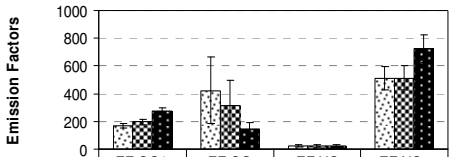

	EF CO2 (g/km)	EF CO (mg/km)	EF HC (mg/km)	EF NOx (mg/km)
Eco-driving	166,22	421,02	22,86	512,02
Normal driving	194,93	309,77	22,24	515,03
Agressive driving	274,90	147,67	20,01	722,21

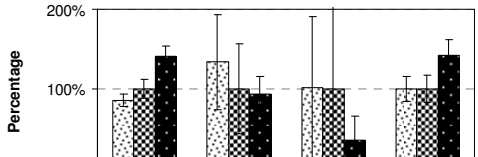

	EF CO2	EF CO	EF HC	EF NOx
Eco-driving	85,7%	133,8%	100,9%	99,9%
Normal driving	100,0%	100,0%	100,0%	100,0%
Agressive driving	141,1%	93,7%	36,2%	142,4%

Figure 7: Summary of influence of driving style on emission factors for urban traffic.

Dynamic Performance Diesel index "*DPDi*" determined experimentally, is a tool that could be used to develop an eco-driving assist system, similar to that developed by Mukai et al. (2009).

Acknowledgments

This project was supported by the Spanish Ministry of Environment. The authors wish to acknowledge the contributions of Victor Pozo, Victor Criado, Emilio Cano, Pedro Rodrigo and Cesar Chacón for carrying out of tests and driving the cars.

References

Casanova J., N. Fonseca and F. Espinosa (2009), Proposal of a dynamic performance index to analyze driving pattern effect on car emissions, *Proceedings 17th Transport and air pollution symposium and 3rd Environment and Transport Symposium*, Actes INRETS n°122.

Casanova J., S. Margenat and J. Ariztegui (2005), Impact of driving style on Pollutant Emissions and Fuel Consumption for Urban Cars. *Proceedings of the 1st International Congress of Energy and Enviroment Engineering and Management*. Portalegre, Portugal. 2005. p175

De Vlieger I., D. De Keukeleere & J. G. Kretzschmar (2000), Environmental effects of driving behaviour and congestion related to passenger cars. *Atmospheric Environment*. Volume 34, Issue 27, 2000.

Ericsson E. (2001), Independent driving pattern factors and their influence on fuel-use exhaust emission factors. *Transportation Research Part D: Transport and Environment*. Volume 6, Issue 5, September 2001.

M. Mukai, J. Murata and T. Kawabe (2009), Driving Assist System for Ecological Driving Using Model Predictive Control. *Proceedings of SICE 9th Annual Conference on Control System*.

Van Mierlo J., G. Maggetto, E. van de Burgwal and R Gense (2004), Driving style and traffic measures—influence on vehicle emissions and fuel consumption, *Proceedings of the Institution of Mechanical Engineers, Part D: Journal of Automobile Engineering*, Volume 218, Number 1.

Vermeulen R.J. (2006), The effects of a range of measures to reduce the tail pipe emissions and/or the fuel consumption of modern passenger cars on petrol and diesel. *TNO report*, IS-RPT-033-DTS-2006-01695.

Improvements in Hydrocarbon measurement in exhaust tailpipe emissions

Blanc J.L., M. Benoît, V. Bossoutrot, S. Lombard, J.M. Rabillier

Air Liquide – Research Centre Claude Delorme – Chemin des loges – 78354 JOUY-EN-JOSAS- FRANCE.
Jean-luc.blanc@airliquide.com

Introduction

International regulations focus on air pollution with more and more drastic requirements. In March 2001 Clean Air For Europe (CAFE) programme was launched and four years later a thematic strategy on air pollution was adopted in 2005, September 25th.

Since 2005, International regulations have restricted the fuel engine emission tolerance. European Regulation no 715/2007 of the European Parliament and of the Council of 20 June 2007 on type approval of motor vehicles with respect to emissions from light passenger and commercial vehicles (Euro 5 and Euro 6) defines a maximum concentration of hydrocarbons (THC), carbon dioxide (CO_2) and nitrogen oxides (NOx). And the objective of the commissions is clearly announced as a continuing effort to reduce vehicle emissions.

Table 1: Evolution of the engine emissions limits value (category N2, reference mass inferior to 1305 kg, positive ignition)

Pollutants ($mg.km^{-1}$)[1]	Symbol	Euro 3	Euro4	Euro 5	Euro 6
Carbon dioxide	CO_2	2300	1000	1000	1000
Total Hydrocarbons	THC	200	100	100	100
Nitrogenous oxides	NO_x	150	80	60	60
Particule matter				5	5

In this context of more restrictive vehicles emissions, the lower levels of analysis required have a direct impact on the expected sensitivity of analysis. The usual detection of hydrocarbons is the Flame Ionization Detection. The required levels of hydrocarbon measurements are closed to the quantification limits of such analytical method.

The analysis of hydrocarbons and volatile organic carbons (VOCs) is widespread for regulation compliance and air quality monitoring. These compounds are measured using Flame Ionisation Detection (FID) that requires feed gases to ignite the flame. The fuel is typically a mixture of hydrogen and helium.

As emission limits continuously decrease, the sensitivity of the analysers must be adjusted to comply with these requirements. The analytical technique used to measure hydrocarbons based on a Flame Ionisation Detector (FID) requires a mixture, which is called fuel gas, composed of 40% H2 and 60% He. The US Code of Federal Regulations Title 40 Part 1065 dedicated to Engine Testing Procedures specifies the uncertainty of H2 content at 1% (in absolute value) and the total hydrocarbon content (THC) to be less than 50 ppb equivalent C1 in this H2 / He mixture. This regulation becomes effective in 2010.

Results

1) Hydrogen concentration in fuel gas

Flame Ionization Detection (FID) is sensitive to the hydrogen concentration in fuel gases. Experiments show that the variation of hydrogen concentration in the gas mixture has a consequence on FID response.

[1]http://europa.eu/legislation_summaries/internal_market/single_market_for_goods/motor_vehicles/interactions_industry_policies/l28186_fr.htm

In the experiment, the proportion of hydrogen in helium is increased by increments of 0.5% absolute from 38% to 42%. The total FID response is registered and compared with the response of a reference of 40% hydrogen concentration in fuel gas. Figure 1 shows the variation of the response in function of the concentration of hydrogen. A variation of 1% absolute Hydrogen concentration has a corresponding variation of 10% relative signal.

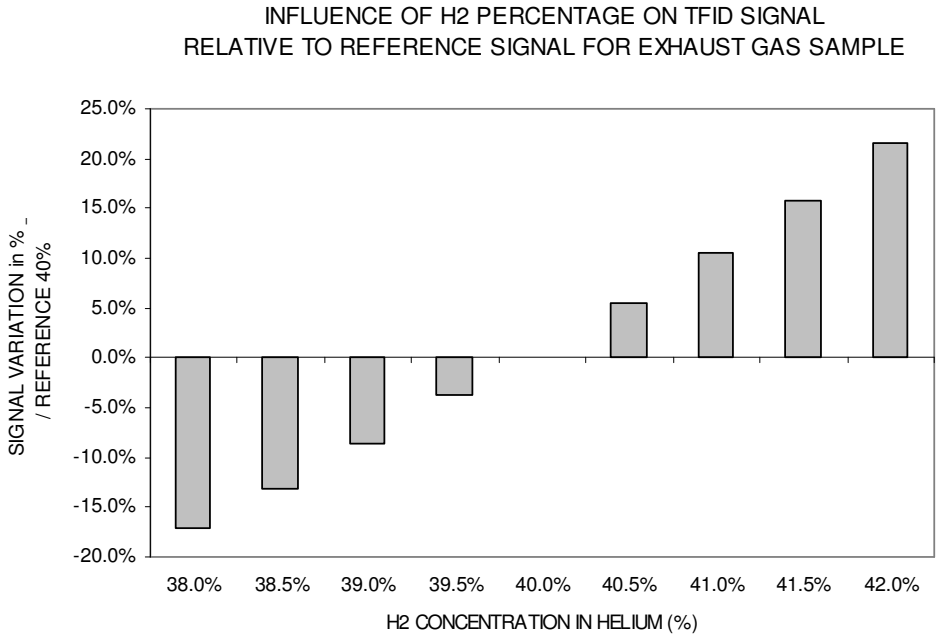

Figure 1: Variation of FID response with increasing percentage of hydrogen in helium – the referenced concentration of hydrogen is 40%.

This result highlights the importance of the accuracy of the composition of the fuel gas mixture (hydrogen and helium) in FID measurements, which is in agreement with the request US code of Federal Regulations on H2 content of 40% +/- 1%(absolute). For this reason, Air Liquide has designed a solution to accurately mix the hydrogen and helium.

The equipment is supplied with pure gases hydrogen and helium. The fluids are continuously mixed, into a buffer tank which stabilizes the flow in case of outlet flow variation. The analysis of gas mixture is driven with Flame Ionization Detector (FID) coupled with a Varian 3800 GC. The analyzer is equipped with a Molsieve 5A column (Chrompack/Varian).

Various experiments (measurements on 8 days, different flow rates of fuel gas) have validated the accuracy of the gas mixture.

The analysis of the gas mixture shows a variation independent of the flow rate of the gas mixture. The calculated uncertainty following ISO 13005 recommendations is less than 0.4% (absolute) during the period of analysis. The uncertainty is compliant with (US) CFR 1065 part 40 (1% absolute). The results are illustrated in Figure 3.

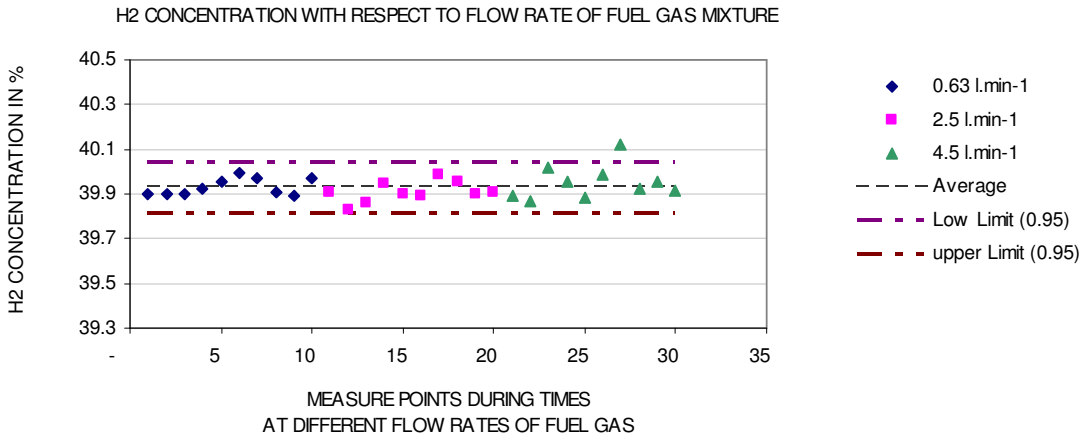

Figure 2: Variation of real time hydrogen concentration at various gas mixture flow rates.

The hydrogen concentration of the fuel gas mixture is within the limits of variation defined for a confidence of 0.95. The concentration of mixture is not influenced by the variation of the flow rate of the mixture following the analysis of variance.

2) Impact of hydrocarbons in fuel gas on TFID response

TFID response is influenced by additive concentration of hydrocarbons as impurities carried by fuel gas. The concentration in hydrocarbons has a significant influence on TFID signal without any sample and with a representative mixture of engine exhaust gases, as shown in figure 3.

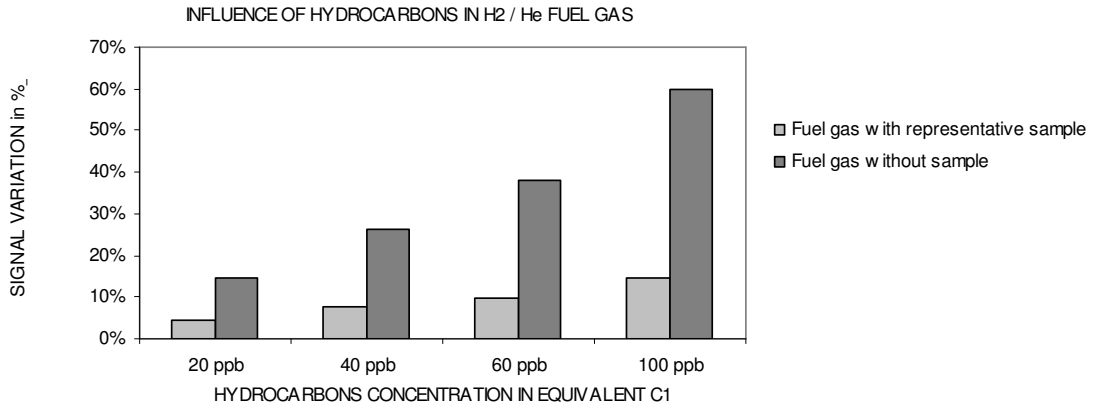

Figure 3: Influence of hydrocarbons (< C4) in H2/He fuel gas on the TFID signal

20 ppb of hydrocarbons concentration (equivalent C1) increases TFID signal of 14% without any sample and 6% with a representative mixture of engine exhaust gas. For 100 ppb, these values increase of 14% and 60% respectively. This situation justifies using purified gases for a better performance of TFID analysis.

To reach the purity of a maximum concentration of 50 ppb of total hydrocarbons, the gas is purified just after mixing hydrogen and helium flows. In this way, the distance to point of use is reduced, decreasing the probability to introduce impurities in purified fuel gas.

Different level of hydrocarbons impurities have been tested with the dynamic purifying system. Hydrocarbons concentration after purification stays under the upper limit of 50 ppb THC equivalent C1, as shown in figure 4.

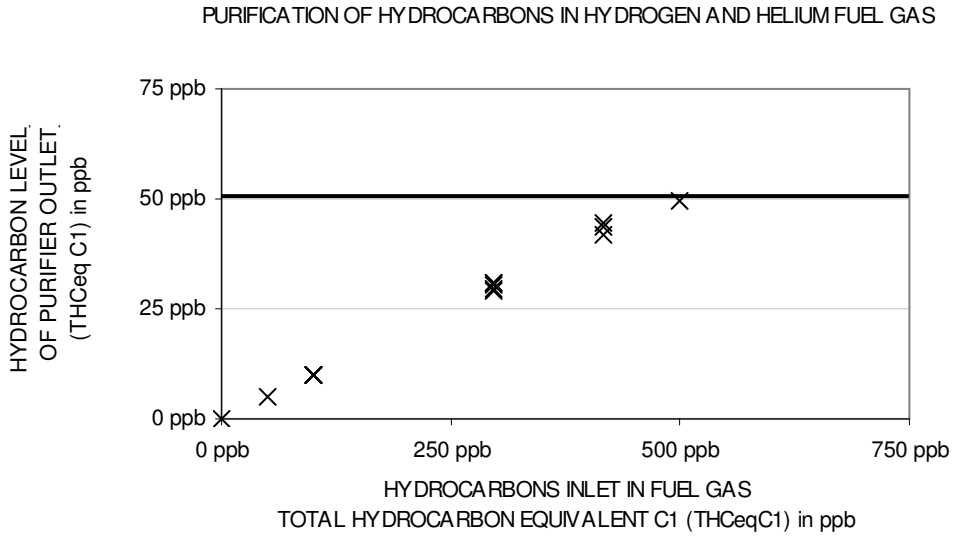

Supplied with Air Liquide standard quality in Specialty Gases, the fuel gas mixture is inferior to 50 ppb of total hydrocarbons equivalent C1 after purification.

Conclusion

To obtain more sensitivity in analysis requires optimizing fuel gas and purity of air and carrier gas. Experiments on hydrogen concentration in fuel gas demonstrate that the TFID response is influenced by gas mixture concentration. A 1% variation of hydrogen concentration generates a TFID signal variation of 10% with respect to reference. Air Liquide has designed a solution which mixes hydrogen fuel gas with helium and purifies the mixture at the limit value required by (US) CFR 1065 part 40. The solution consists in equipment which mixes fuel gas at the targeted concentration of 40% of hydrogen in helium with an uncertainty of 0.4% in absolute value. The system supplied with standard quality Specialty Gases furnishes a gas mixture of less 50 ppb of total hydrocarbons equivalent C1. The solution is compact (19" rack) and easy to handle. The solution is adapted to automotive engine emission testing supplying fuel gas to various bench tests. The solution is compliant with international regulations applied in Northern countries and Asia, including Australia.

Reference

Bossoutrot V., M. Carré and S. Lombard (2008), Influence of fuel gas specifications on Flame Ionization Detectors, *Pittcon*, New Orleans.

Bossoutrot V., A. Grimberg and S. Cochet (2007), Influence of feed gas mixture blending tolerance on Flame Ionisation Detector Signal, *Gas Analysis Symposium*, Rotterdam.

The on-road emission characteristics of UK passenger cars: The application of a remote sensing vehicle emission measurement system.

J. Tate.

Institute for Transport Studies, University of Leeds, Leeds, LS2 9JT, UK, j.e.tate@its.leeds.ac.uk

Introduction

It has long been established that exposure to air pollutants can have a detrimental impact upon health (UK NAO, 2009). The UK and European Union aims to achieve levels of air quality that do not result in unacceptable impacts on, and risks to, human health and the environment. European policies aim to improve air quality by setting various legally binding limit values and target reductions for different air pollutants. The UK is not meeting EU limit values or UK objectives for particulate matter (PM_{10}), nor on track to meet EU limit values or UK objectives for nitrogen dioxide (NO_2) by the 2010 deadline (UK NAO, 2009). Despite the implementation of measures to reduce total PM and NO_X emissions from the transport sector, recent evidence suggests an unwanted side-effect of new diesel pollution abatement technologies, as well as the greater uptake of diesel vehicles observed both in the UK and throughout Europe, has given rise to the increased emission of Nitrogen Dioxide (NO_2) directly from vehicles (Grice et al, 2009). There is clearly a need to better understand the emissions from vehicles on the road. Vehicle emission Remote Sensing Device instruments that measure the tailpipe emissions of vehicles as they drive-through a monitoring site are now available in the EU. The technology works by scanning the exhaust plume trailing the vehicle. This approach is commonly used in the U.S. and Canada in large-scale pre-screening testing for vehicle inspection and maintenance emission programs. Manufactured by http://www.esp-global.com/ the RSD-4600 instrument used in this study is able to characterise emissions from 1000's of vehicles per day. The measurements, when combined with detailed Vehicle Registration Information allow the on-road vehicle fleet emissions to be characterised, broken down by vehicle type (Car, Van, light and heavy commercial vehicle, Bus), age, fuel type and emission standard (e.g. Euro 0 - 5). This combination of RSD emission measurements and detailed vehicle registration information provides a rare opportunity to:

- Study the composition of the vehicle fleet being driven on the road in detail. This is important as for example, modern diesel passenger cars are known to typically complete more miles per year than comparable petrol cars, or indeed older diesel cars. As it is newer passenger diesel cars that are now understood to be one of the main contributors towards the increase in primary NO_2 emissions, and hence worsening of roadside NO_2 concentrations, it is important to develop an accurate and up-to-date knowledge of their proportions on the road;
- Study the emission characteristics of each vehicle fuel type and Euro standard on the road. Whilst the RSD is not able to measure NO_2 directly, with knowledge of a vehicles' fuel type, Euro standard, nitrogen oxide (NO) emissions and recommended primary NO_2 fraction (Grice et al, 2009), it is possible to predict the NO_2 contribution.

With an improved evidence base and understanding of the proportion of vehicle miles driven by different vehicle type sub-categories (fuel type and Euro standard) and characterization of on-road vehicle emissions in Air Quality Management Areas, Authorities will be able to design targeted and more effective management strategies.

Methodology

Materials - ESP Remote Sensing Detector

The vehicle-emission Remote Sensing Device (RSD) used in this study is able to measure ratios of Carbon Monoxide (CO), Hydrocarbons (HC), Nitric Oxide (NO) to Carbon Dioxide (CO_2) in motor vehicle exhaust. The measurement ratios therefore reflect the pollutant emissions per unit of fuel used. The system is also able to study coarse particle emissions (smoke). The RSD-4600 instrument used in this study is a dedicated across road vehicle emissions monitoring system. It comprises: A Source/ Detector Module incorporating infrared and ultraviolet source/ detector arrays; A Mirror Box of 'corner cube' configuration; A Across

road Vehicle Detector speed/acceleration bar; and a Camera system. The basic deployment configuration is similar to the Source/Detector and Mirror Box arrangement shown in Figure 1. A record is defined as a beam block (by a vehicle) followed by a half second of data collection. If the data collection is interrupted by another beam block, i.e. a following vehicle with a headway less than 0.5 seconds, the measurement attempt is aborted. A measurement is declared 'valid' when: the size of the observed emission plume (CO_2) is sufficient to allow emission ratios to be calculated (i.e. the maximum CO_2 concentration in the measurement open-path is > 10% and the mean of 5 consecutive 50Hz CO_2 measurements is > 5%); a speed/ acceleration measure is present with the speed is in the range 5 to 60kmh^{-1} and the vehicle is accelerating; and a clear 'static' digital image of the number plate is captured. The collection of a high proportion of 'valid' measurements requires:

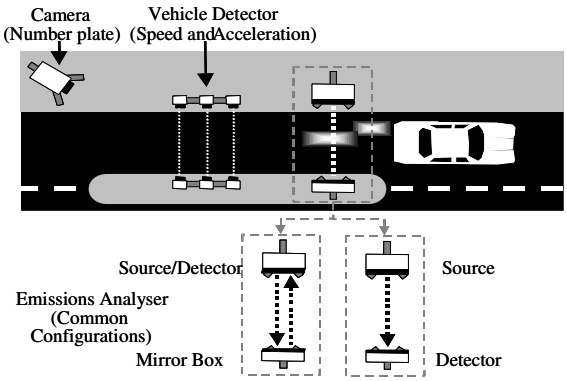

Figure 1: RSD instrument schematic

- The remote sensing beam to be located in a position where it will intersect a significant proportion of exhaust gas. It is typically aligned less than 300mm from the road surface. Emissions from vehicles with elevated tail-pipes, cannot be studied in this configuration;
- Study sites are restricted to "single-file" (single lane) operation;
- The optical beam path distance is limited to less than 10 metres;
- The majority of vehicle engine's being under load as they drive through the measurement site. Sites should therefore have an uphill grade;
- Weather and environmental conditions to be favourable. High wind speeds rapidly disperse exhaust plumes and the equipment is not weather-proof.

At the start of each RSD 4600 sampling session, ambient conditions were logged. The Source/Detector arrays were calibrated hourly using the instruments internal reference cell. The 'static' digital image of each 'drive-through' measured was viewed off-line and the number plate alphanumeric character string added to the measurement dataset. The Society of Motor Manufacturers and Traders (http://www.smmt.co.uk/) matched the number plate registration record (Vehicle Registration Mark) with the UK Motor Vehicle Registration Information database. The database is the result of co-operation between the SMMT, vehicle manufacturers/ importers and the DVLA (http://wwwdvla.gov.uk). The information fields made available include: vehicle details (manufacturer/ model, date of 1st registration, size, weight), engine specification (fuel type, capacity, No. cylinders, Euro status), performance/ transmission (manual/ automatic/ semi-automatic) and environmental details (e.g. fuel consumption for the New European Drive Cycle).

Study Site and Data Collection

The study site is in the Salterhebble district of Halifax (UK), located on the North-bound carriageway of Huddersfield Rd (A629) at coordinates 53°42'07.31"N – 1°51'13.60"W. The urban arterial road is an important link between the M62 motorway to the South and the town centre. The site has an up-hill gradient of +1.8degrees. A central traffic island separates the North and South-bound traffic lanes at this location, which provides a refuge for the "mirror box" and "speed – acceleration reflector bar" components. The surveys took place on Thursday the 1st and Thursday the 8th of October 2009 between 0800 and 1800 hrs. The passenger car database of 'valid' RSD measurements successfully matched with SMMT Vehicle Registration information was 4819 records.

Results

Fleet characteristics

The detailed Vehicle Registration Information (VRI) allows the on-road vehicle fleet proportions to be studied in detail, including: vehicle type, age, Euro emission standard and fuel type. Vehicle emission standards are defined in a series of European Union Directives (e.g. 98/69/EC and 1999/96/EC) staging the progressive introduction of increasingly stringent standards. Currently, emissions of NO_X, HC, CO and PM are regulated for most vehicle types. For each vehicle type different standards apply. In this conference paper only the passenger car fleet is

considered. The sample size of other vehicle type (Light Commercial Vehicle, Heavy Commercial Vehicle) sub-categories was in-sufficient for any meaningful analysis.

Figure 2 illustrates the observed passenger car fleet proportions, broken down by Euro standard and fuel type. The 'on-road' passenger car fleet is dominated by Euro3 classification or better vehicles. These cars registered in 2000 onwards comprise 90.6% of the 'on-road' passenger car fleet. The detailed Vehicle Registration information (VRI) includes the reported vehicle specific fuel consumption for the New European Drive Cycle (NEDC) including the combined (urban ECE and EUDC), extra-urban and urban (cold) drive cycles. The VRI fuel consumption figures (units - litres per 100km) have been converted into carbon dioxide (CO_2) emissions per unit distance (grams per km). The distribution of carbon dioxide emission per unit distance for each fuel type and Euro standard combination, for the NEDC combined drive cycle is presented in the Figure 3 (a) boxplots. The bold horizontal line shows the median value. The bottom and top of the box show the 25th and 75th percentiles respectively. The vertical dashed lines, termed 'whiskers', present the 1.5 times the interquartile range of the data. Outliers are not plotted to truncate the y-axis scale. Both the petrol and diesel passenger cars are progressively becoming more fuel efficient with each successive Euro standard. It is surprising that there's little difference between the median CO_2 per km for the observed petrol and diesel cars, however the diesel cars are typically larger, with a higher kerb weight and engine capacity, as illustrated in Figures 3(b) and (c). There's little trend over time in the median engine capacity of either petrol or diesel engines, approximately 1.6litres and 2.0litres respectively. The vehicle mass of both the observed petrol and diesel engine passenger cars is however steadily increasing with each successive Euro standard.

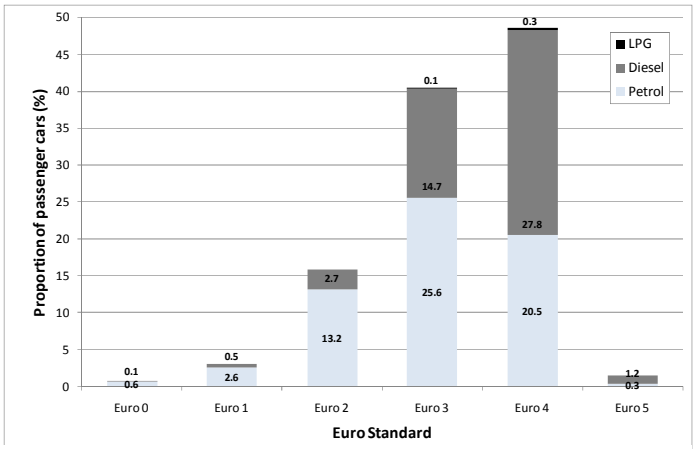

Figure 2: Passenger car fleet proportions

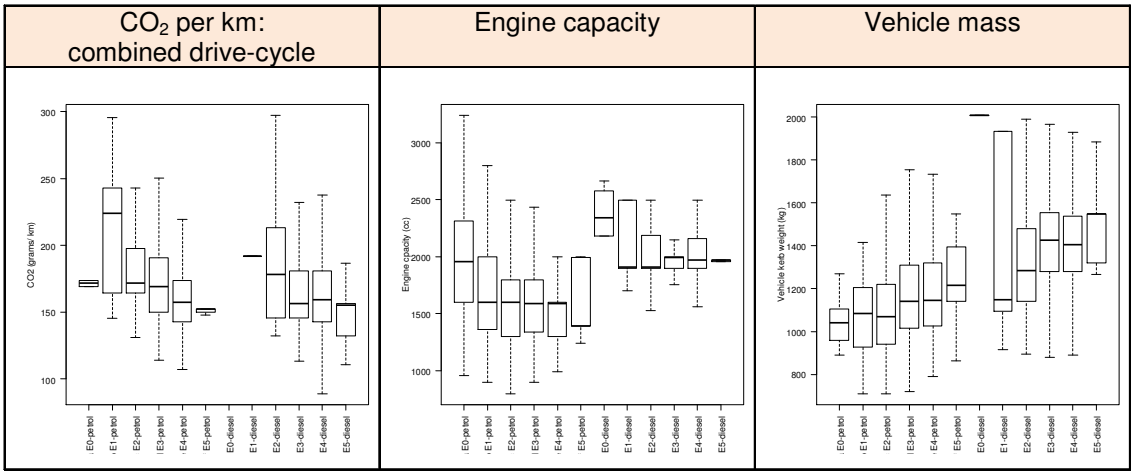

Figure 3: The distribution of (a) reported CO_2 per km (b) engine capacity (c) vehicle mass, for the observed passenger car fleet categorized by fuel type and Euro standard

Emission Measurements

The distribution of emission measurements, categorised by fuel type and Euro standard, are illustrated in Figure 4. The notches drawn as a 'waist' on either side of the median give a rough indication of the 95% confidence interval of the median. Emission ratios for passenger cars are falling broadly in-line with Euro classifications and Emission standards. Improving car engine and emission abatement technology is clearly significantly reducing the on-road emission ratios of Hydrocarbons (HC), Carbon Monoxide (CO) and coarse PM (visible smoke) from both petrol and diesel cars. Nitric Oxide (NO) emissions from petrol cars are also reducing in-line with

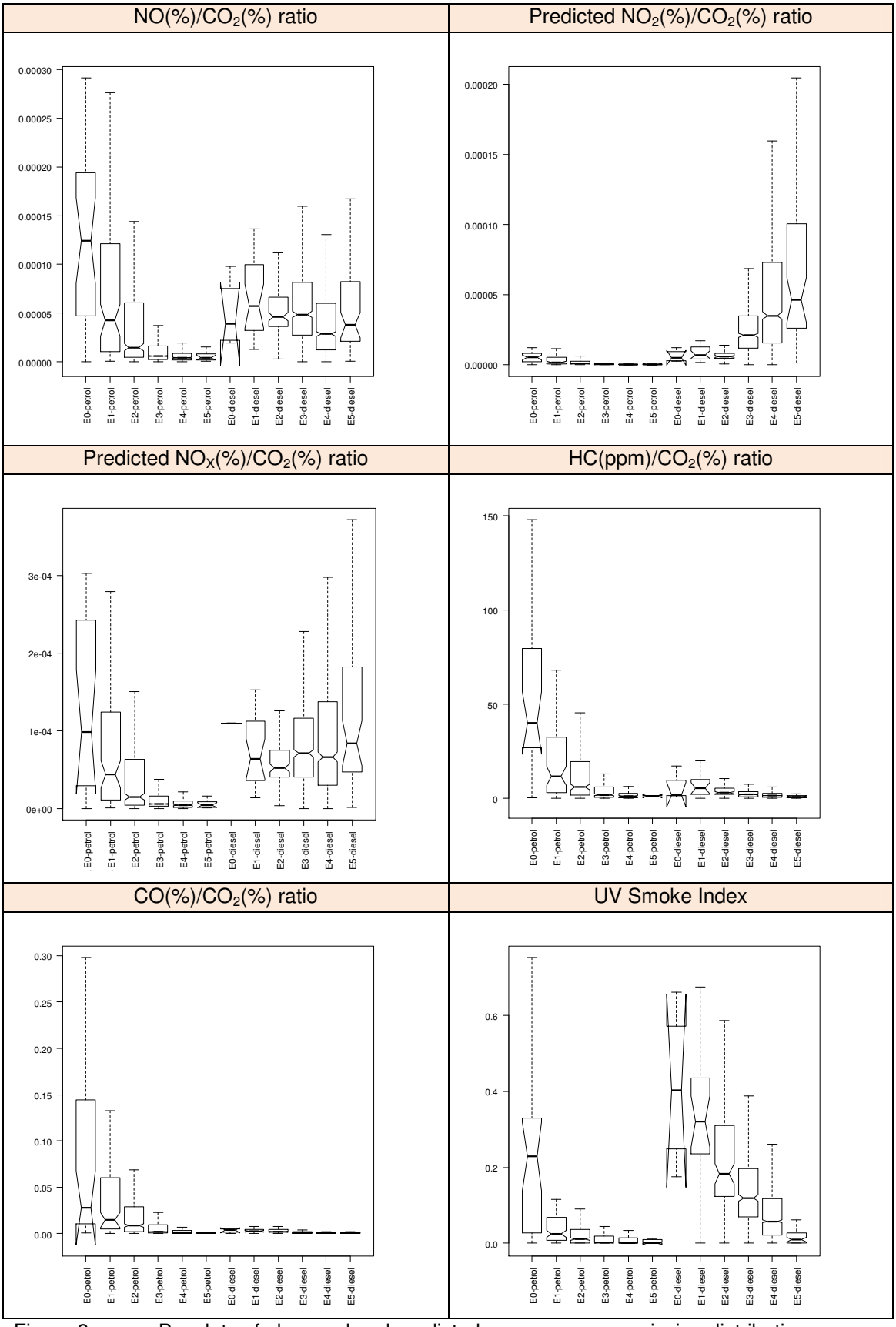

Figure 3: Boxplots of observed and predicted passenger car emission distributions, categoried by Euro standard and Fuel type.

emission standards. There is weaker evidence of a reduction in the NO/CO_2 ratio from newer diesel Cars. It should be noted that the Euro 5 Emission standards only came into force in September 2009, therefore the measurement sample size for this sub-category is limited (sample 15 petrol, 55 diesel). The confidence range for the median values for Euro5 Cars is consequently greater (as illustrated by the 'notches'). Whilst the RSD is not able to measure NO_2 directly, with knowledge of a vehicles' fuel type, Euro standard, nitrogen oxide (NO) emissions and recommended primary NO_2 fractions f-NO_2(%) (Grice et al, 2009 e.g. Euro 4 petrol = 3%, diesel 55%), it is possible to predict the NO_2 and NO_X contribution. The predicted NO_2/CO_2 and NO_X/CO_2 ratio distributions are also presented in Figure 4.

Whilst the engine and exhaust after-treatment systems of petrol passenger cars have reduced the fuel based NO, NO_2 and NO_X ratios in-line with each successive and more stringent Emission standard, the downward trend in the observed NO and predicted NO_X emission charactistics of diesel passenger cars is significantly weaker. Diesel NO_X reduction technologies are shown to be less effective in limiting on-road NO_X emissions, which are not falling in-line with the standards. The surge in vehicle miles driven by modern diesel vehicles, are predicted to contribute worryingly increasing amounts of nitrogen dioxide directly from the tail-pipe (termed primary NO_2). There's little forecast improvement in the primary NO_2 emission characteristics of diesel cars yet to be introduced (Euro 6 standards come into effect from September 2014).

Summary and Conclusions

Improving car engine and exhaust after-treatment technologies have been shown to significant reduce the on-road emission ratios of Hydrocarbons (HC), Carbon Monoxide (CO) and coarse PM (visible smoke) from both petrol and diesel cars. Nitric Oxide (NO) emissions from petrol cars are also reducing in-line with emission standards. There is weaker evidence of a reduction in the NO/CO_2 ratio from newer diesel Cars. The UK is not on track to meet EU limit values or UK objectives for NO_2 by the 2010 deadline (National Audit Office, 2009). It is well known that NO_2 levels in urban streets are dependent on: vehicle emissions of Nitric Oxide (NO) which quickly reacts with available Ozone (O_3) to form secondary NO_2 (sNO_2), and primary NO_2 (pNO_2) emitted directly by vehicles. Whilst NO_X emissions from passenger cars with petrol engines have been shown to fall in line with Euro standards, this work has shown there's little change in the on-road NO_X emission characteristics of passenger cars with diesel engines.

The detailed Vehicle Registration information has demonstrated the surge in the proportion of vehicle miles driven by modern diesel vehicles at this urban arterial study site. The analysis has demonstrated that whilst a diesel passenger car is more fuel efficient than a comparable (vehicle mass and engine size) petrol vehicle, they contribute worryingly high amounts of nitrogen dioxide directly from the tail-pipe. Diesel passenger cars are also typically larger (vehicle mass and engine size) than petrol cars. This leads to the median fuel consumption and CO_2 per km figures for diesel and petrol passenger cars being comparable for each successive Euro standard. These findings are in-line with other work that indicates that an unwanted side-effect of new diesel engine emission abatement technologies is an increase in primary NO_2 emissions, for example the increase in the NO_2/NO_X ratio at UK roadside sites (Carslaw, 2005). There's little forecast improvement in the primary NO_2 emission characteristics of diesel cars yet to be introduced e.g. Euro 6 standards come into effect from September 2014. With a growing share of vehicle miles being completed in modern diesel vehicles, with high primary NO_2 emissions, it is considered there'll be little improvement/ a worsening of roadside NO_2 concentrations at heavily trafficked UK and EU locations over the period 2010 – 2105 and beyond. Without a radical shift in direction, EU and UK NO_2 limit values are likely to be exceeded at the most polluted sites over the next 10 years.

Low Emission Zone policies that restrict or deter older vehicles (e.g. Euro 2 and older) that are considered to be more polluting from accessing environmentally sensitive areas may actually exacerbate the NO_2 problem. The resulting number and fleet share of modern diesel engine vehicles for example, that emit significantly more NO_2 directly will increase.

This is believed to be the first study that has combined on-road (RSD) vehicle emission measurements with detailed Vehicle Registration data. With for example, the primary NO_2 emission characteristics of vehicles changing rapidly, it is increasingly important to have up-to-date information and knowledge. This new approach offers an opportunity to extend the

evidence base and contribute towards the development of more targeted and effective management strategies.

Recommendations for Future Work

- Amass a larger dataset so the difference in Emission ratios between vehicle types and Emission standard sub-categories can be studied with greater certainty. A 10day measurement campaign has been carried out in March 2010;
- Integrate ANPR (Automatic Number Plate Recognition) with the RSD instrument and logging system, to cut-down the data entry task and reduce the measurement/ identification of high-emitters/ analysis turn-round period;
- Making good use of DVLA vehicle specific information (e.g. vehicle weight, fuel type and engine size), explore whether a Vehicle Specific Power (VSP) metric considering speed, acceleration, estimate of gearing and vehicle weight could be used to better explain and understand the variations in vehicle emissions; and
- Emerging research instruments (Burgard et al, 2006) in the US have recently extended the RSD capability to sense the interesting species nitrogen dioxide (NO_2) and ammonia (NH_3). The application of this enhanced RSD technology, coupled with DVLA vehicle specific information would be a significant step towards better understanding vehicle emissions in real-world operation (on-road).

Acknowledgements

The author gratefully acknowledges Calderdale Council for funding the on-road vehicle emission measurement and analysis project (ITS research contract RG.TRAN. 478550). Dr David Carslaw (Kings King's College London, Environmental Research Group) and the Society of Motor Manufacturers and Traders are thanked for sourcing the detailed Motor Vehicle Registration Information. The author would also like to thank the ITS research technicians Colin Oates and Paul Cockerill for the survey work.

References

Burgard, D.A.; Dalton, T.R.; Bishop, G.A.; Starkey, J.R.; Stedman, D.H. (2006), A NO_2, SO_2 and NH_3 Detector for Remote Sensing of Vehicle Emissions. Rev. Sci. Instrum., 2006, 77, 014101/1-014101/5.

Carslaw, D. 2005. Evidence of an increasing NO_2/NO_X emissions ratio from road traffic emissions. Atmospheric Env. 39, pp. 4793 – 4802.

Carslaw, D. and Beevers, S. 2005. Estimations of road vehicle primary NO_2 exhaust emission fractions using monitoring data in London. Atmospheric Env. 39, pp 167-177

Grice, S., Stedman, J., Kent, A., Hobson, M., Norris, J., Abbott, J., Cooke, S. 2009. Recent trends and projections of primary NO_2 emissions in Europe. Atmospheric Env. 43, pp. 2154 – 2167.

UK National Audit Office. 2009. Briefing for the House of Commons Environmental Audit Committee. December 2009. http://www.nao.org.uk/publications/0910/eac_briefing_-_air_quality.aspx

Electric Vehicles Environmental and Energy Assessment: Methodological focusing and application

M.L Picherit[1,3], D. Le Boulch[1], T. Brincourt[1], M. André[2], J. Bourgois[3]*

[1] EDF R&D - Ecoefficiency and Industrial Processes Department, Moret sur Loing, France, E-mail contact: marie-lou-externe.picherit@edf.fr
[2] INRETS Laboratory Transport and Environnement, Bron, France
[3] Ecole des Mines de Saint-Etienne, centre SITE, Saint Etienne, France

1. Background, aim, and scope

The Internal Combustion Engine Vehicles (ICEV) are responsible for 12% of the total emissions of greenhouse gases, and their local emissions have important sanitary impacts in urban areas (respiratory problems, lung irritations…)

Electrical vehicles (EV) and plug-in electric hybrid vehicles (PHEV) appear to be a possible answer for this environmental challenge: they thus deserve a detailed evaluation.

Among the various conceivable methodological approaches (direct emissions, « well to wheel », Life Cycle Assessment etc.), the LCA is the most exhaustive one. It considers the whole vehicle and takes into account the impacts of batteries.

Nevertheless the EV LCA presents various methodological difficulties: in this paper, we intend to highlight the different issues related to LCA for EV by proposing a suitable methodology which has been applied, as an example, on a small urban electric vehicle with a lithium-ion battery (lithium iron phosphate or LFP) manufactured by MICROCAR (France)

2. Methodological framework

2.1 Issue

The analysis of the LCA application for an EV reveals that the prospective character of the studied system engenders multiple difficulties. Indeed, EV studied in this paper are still prototypes, and are not based on mature or well-established technologies.

We identified the following difficulties:

- **Few EV are used by private people today and we have to consider EV performances with insufficient feedback of experience**. For example, the vehicle lifetime has yet to be estimated. Furthermore, EV uses are not well known yet: they must be determined from sociological and sector-based studies. To conclude, it's difficult to fix EV consumptions and therefore representative data must be obtained per experimental means.

- **Some elements of the traction chain are still under development.** It's not easy to obtain data about their composition.

- **The EV development depends on socioeconomic conditions in the near future.** For example, evolution of the CO2 content of the medium term kWh must be considered.

In this paper, two essential items are presented:

- For a more in-depth assessment of the use phase, experimental test bench trials were carried out.

- Key parameters for the use of the LCA method have been identified in order to manage all the difficulties of the study.

2.2. Experimental tests

EV consumption varies with the use and the efficiency of the elements of the traction chain (batteries, charger, motor…) and also with the battery weight.

For a more in-depth assessment of the use phase, roll-bench tests were carried out in INRETS laboratories on the chosen urban EV and its internal combustion engine equivalent (figure 1). Consumption, autonomy, braking recovery and the influence of the vehicle auxiliaries were measured with the ARTEMIS (urban and road) driving cycle (André, 2004) and the ECE cycles. The ARTEMIS cycles are representative of real driving conditions in Europe. They are used to assess consumption and pollutant emissions of touring vehicles. For the ICEV, exhaust emissions were measured. The performances of the two vehicles were compared

Figure 1: Roll-bench tests at INRETS laboratory with the MICROCAR vehicles

Figure 2 presents the measured EV consumption in kWh per kilometre covered and takes into account the energy efficiency of the whole traction chain. The ARTEMIS road cycle was adapted because the performances of the EV were not sufficient enough to follow the compulsory speed profile. It was limited to 60 km/h which was the maximum speed of the tested vehicle. As a consequence, this modification impacted the duration of the cycle: the driving cycle was set so that the same distance than the original cycle was travelled, but with a longer duration. In summary, the same trip was made but with different vehicle performances.

To validate the choice of the ARTEMIS urban cycle, a cycle (which we called "experimental cycle") was made from real-world data recorded on-board the EV in the streets of Lyon and its suburbs via a simple GPS logger. We tried to represent all the kinematics of driving of the urban Artemis cycle. The results confirm the representativeness of the ARTEMIS urban cycle:

- The drivers of the tested vehicle confirm that it fits well into the urban traffic without slowing it down
- The results obtained with the “experimental cycle” show that the characteristics duration-speed averages, as well as the specific consumption were similar to those of the ARTEMIS’ urban cycle (table 1).

Table 1: Main characteristics of the experimental and the urban Artemis cycles

	Experimental cycle	Urban Artemis Cycle
Average speed	19,1	17,6
Maximal speed	52,4	57,7
Stop duration %	26	28,4
kilometre covered	5,3	4,9

The various tested cycles give different specific consumptions (figure 1), which shows that expressing vehicle consumption without specifying its uses, makes little sense. Besides, the results obtained with the experimental cycle show that the ARTEMIS cycles are the most adapted to estimate urban use in Europe, and that the cycle ECE underestimates the real specific consumption.

These experiments also allowed us to demonstrate the influence of various parameters, which have more energy consumption impact on EV than on ICEV:

- The user driving behaviour, because the specific consumption is not only connected to the acceleration of the driver, but also to the way he uses the regenerative braking capability of the EV.
- The use of the auxiliaries, such as the air conditioning, which will more or less rapidly decrease the autonomy of the vehicle. The use of air-conditioning will considerably limit this one.
- Gradient, never considered for vehicles tested on bench also have influence

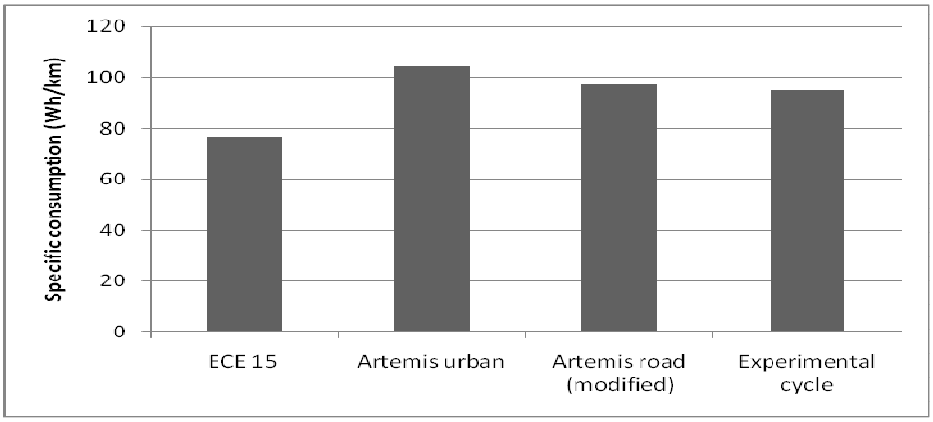

Figure 2: Measured vehicle specific consumption (Wh/km)

Roll-bench emission tests were also performed with the ICE equivalent version of the EV. The exhaust gases were collected and analysed in order to characterise the nature and the quantity of pollutants avoided by the EV in urban areas. Finally, all these results were integrated in our LCA model.

2. 3 Identification of key parameters and how the LCA method manages to take them into account

Figure 3 identifies the key parameters for the Life Cycle Inventory (LCI) of the EV use phase.

EV specific consumptions were already identified and treated with the trials, but three other parameters are essential to consider:

- **The influence of electricity production means**. Current mix or prospective ones should be assessed
- **The EV vehicle lifetime**
- **The number of batteries used during the EV life.**

The environmental assessment of EV is complex, but the LCA method allows us to handle those difficulties (Frischknecht and al., 2009):

- Via **sensitivity studies** for items on which we do not have enough certainty such as battery life, energy mix, EV lifetime and the number of batteries will be considered with this approach.
- Via **establishment of scenarios** to assess EV potential uses and the improvement of the technology in the near future (vehicle use and consumptions) (figure 3).

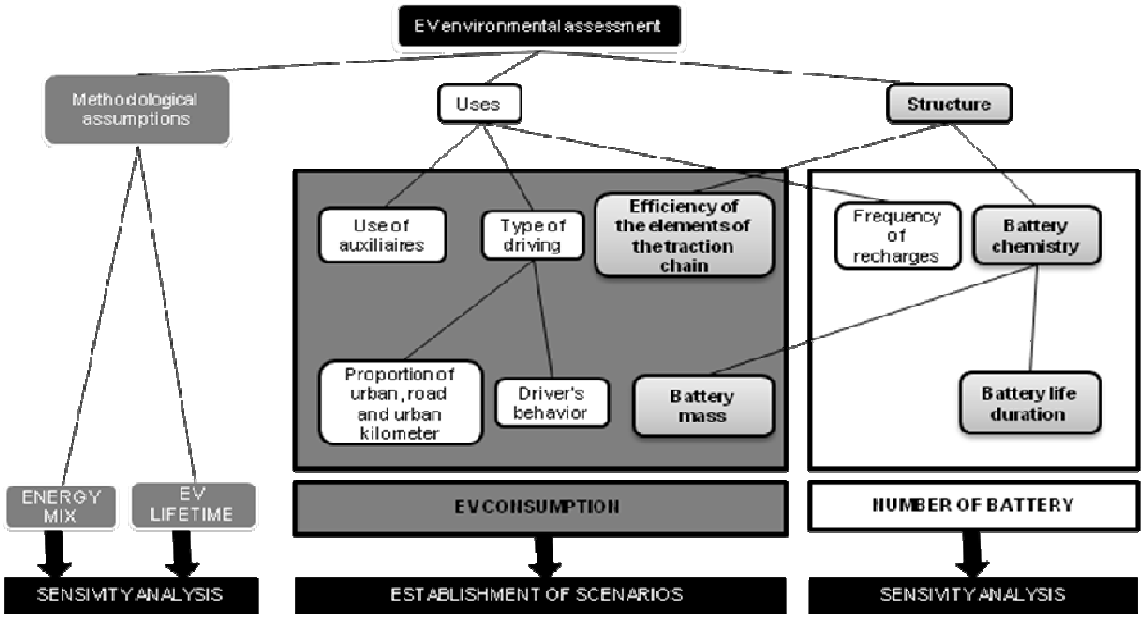

Figure 3: Identification of key parameters

3. An example: Influence of the battery chemistry – Parameters and results

We present some results to highlight the importance takeoff the taking into account of the identified key parameters. The results were obtained with the urban small EV (8 kWh of lithium-iron phosphate (LFP) battery) and its internal combustion engine equivalent.

When analysing an EV, the battery is often considered as the main environmental concern (Van den Bossche, 2005). Thus, we have to present the environmental burden expressed in CO2 content of different traction batteries to show that multiple parameters have to be considered.

3.1 Identification of the main parameters

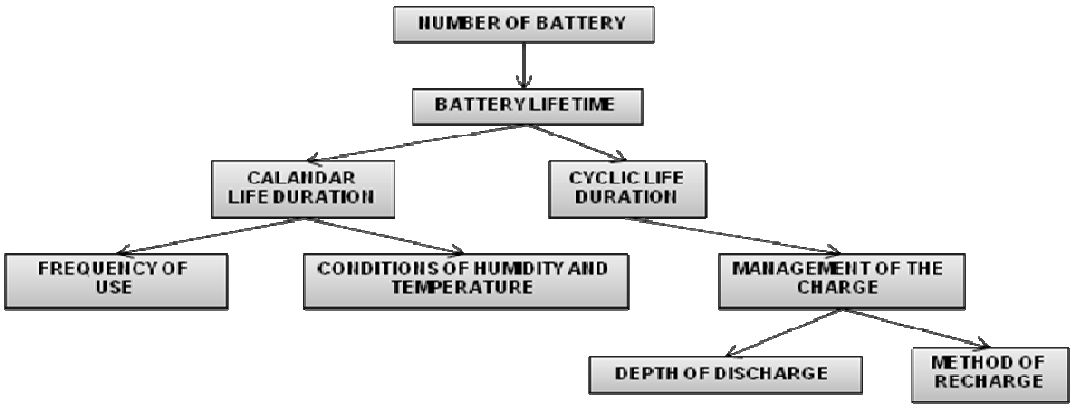

Figure 4: Multiple influential parameters on the batteries life duration

The number of batteries needed during the whole EV life only depends on the battery lifespan. This is an essential figure, because it defines the number of batteries to produce and recycle during the EV life. With time and use, battery performances (power, energy and safety) will decrease. In any case, it is a difficult parameter to fix because it is dependent on multiple elements (Rantik, 1999) (figure 4).

Two types of lifetime related information have to be considered: the calendar life duration (in years) and the cycle life duration (Number of cycles). For example, we can assume that for a normal EV use (< 200 full cycles per year), a recent lithium-ion battery which can achieved more

than 2000 full charge/discharge cycles will be more limited by its calendar cycle rather than its cycle life. On the opposite, valve-regulated lead-acid batteries (often used for this type of small EV) are more sensitive to the number of charge/discharge cycles (Rantik, 1999).

3.2 First results and discussions

In our model, we consider a maximal depth of discharge (DOD) of the battery of 80%. Self-discharge, is not taken into account. We chose to assess the vehicle for a half road (ARTEMIS road) and half urban (ARTEMIS urban) use. The EV lifetime is fixed at 10 years, and 100 000 km (10 000 km per year). The additional energy consumption due to the battery mass is also taken into account with our consumption model. Regarding electricity consumption, the European electricity producing mix has been chosen.

The main technical characteristics for different battery chemistries are listed in table 2.

Table 2: Main characteristics of the considered batteries

	Lead-acid (VLRA)	Ni-MH	Lithium-ion (LFP)
Energy density (Wh/kg) **Battery efficiency (%)** **Battery energy (kWh)** **Battery weight (kg)**	40 75 8 200	75 75 8 107	118 95 8 68
Determined minimum and maximum battery lifetime (years)	3-5	7-8	5-10
Determined number of batteries	2-4	1-2	1-2

Data availability is a major problem for establishing a high quality inventory and it's difficult to find reliable and verifiable data on lithium-ion traction battery production process because the technology is still under development. Careful analysis was conducted to determine the minimum and maximum lifetimes of batteries. These are based calendar life duration, cycle life duration, depth of discharge applied to the battery, number of kilometre travelled per year.

Sensibility analysis showed that energy consumption in lithium-ion traction battery production process is a very important issue in our study, and we conclude that more reliable inventory data on battery is required. In the meantime, we use figures found in the literature (Hischier and al., 2009 and Ishihara and al.) and propose the results obtained with each of them. It must be noted that ECOINVENT data is applicable to batteries phone and laptop. It may not be extrapolated to traction batteries, but we will consider it to test the sensitivity of our results to this parameter. Lithium-ion battery recycling is not considered because little information is available.

Figure 5 shows the whole life cycle results of our EV, expressed per kilometre, with different battery technologies. The values are normalised (lead-acid battery EV=100 and battery lifetime= 3 years). It is noticeable that the battery lifetime parameter does not have the same impact for the different traction batteries. Ni-MH and lead-acid battery impacts are less dependent on the number of batteries than the lithium technology ones.

The figure highlights the impact of the battery weight on the vehicle consumption. The lead-acid battery has the largest energetic density, and therefore the vehicle consumption is higher than those obtained with the other vehicles.

These results also confirm the importance of energy consumption in the process of lithium-ion traction batteries: this is the only data which differs between the life cycle inventories of the lithium vehicles (ECOINVENT or Japanese data) ant the obtained results are really different.

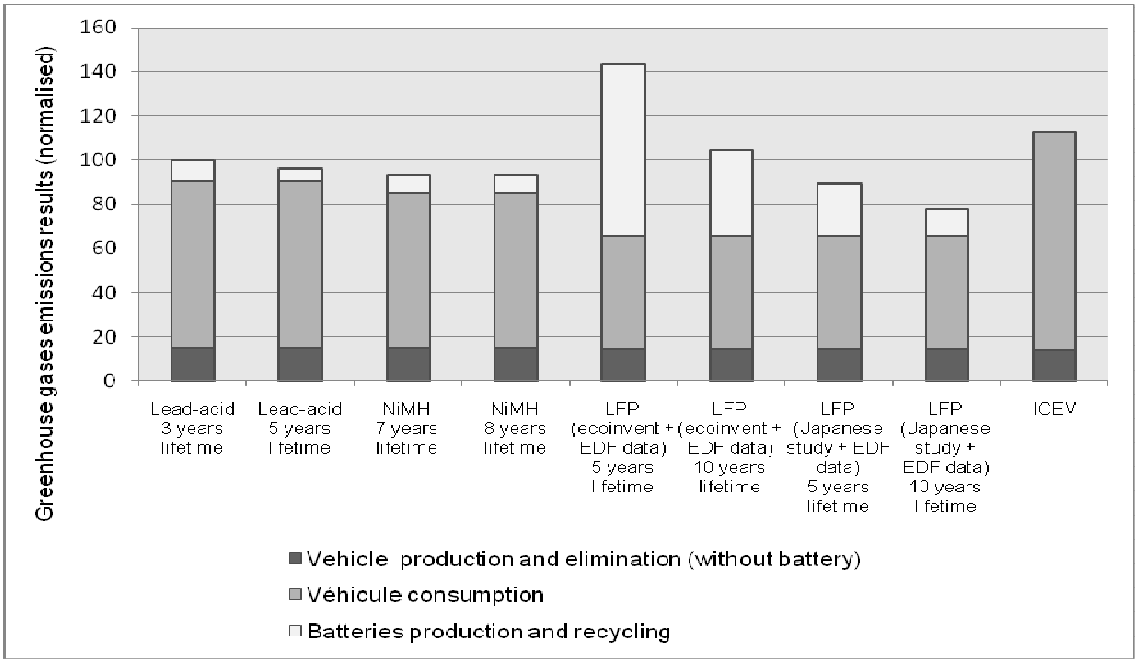

Figure 5: Results from applying the LCA method for the whole life cycle vehicle and for different battery technologies (amount of greenhouse gases emissions produced per kilometre)

Finally, these initial results show the importance of the battery for the EV assessment. Indeed, life duration, capacities, production energy, and number of batteries used during the EV life vary according to the type of battery considered and can also depend on the type of vehicle uses.

4. Conclusions and future prospects

By identifying the environmental advantages / benefits but also weaknesses of various electric solutions in regard to their equivalent combustion engine vehicles, this research attempts to contribute to an exhaustive and objective assessment of EV and other alternative technologies, depending not only on their technological characteristics, but also on the uses envisaged for such vehicles.

The results presented in this paper only assess the impact of greenhouse effect, but our study also includes atmospheric acidification, energy, and local impact (particles, SOx, NOx, and noise).

Finally, we hope to publish all our results, on experiments as well on our LCA and their sensibility analysis (kilometre covered per year, vehicle life duration, uses, energy mix...).

5. Reference

M. André, 2004, The ARTEMIS European driving cycles for measuring car pollutant emissions. In : *Science of the Total Environment*

R. Frischknecht, S.Büsser, W.Krewitt, 2009, Environmental assessment of the future technologies: how to trim to fit this goal ? In: *International Journal of LCA*

R. Hischier, M. Classen, M. lehmann, W. Scharnhorst, 2007, ECOINVENT Report n°18: Electronics Modules, part 2

K. Ishihara, N. Kihira, N. Terada, T. Iwahori, Environmental burdens of large Lithium-Ion Batteries Developed in a Japanese National Project

M. Rantik, 1999, Life Cycle Assessment of Five Batteries for Electric Vehicles under different charging regimes, *KFB*

P. Van den Bossche, F. Vergels, J. Van Mierlo, J. Matheys, W. Van Autenboer, 2005, SUBAT: An assessment of sustainable battery technology In: *Journal of power source*

Influence of the Aging of Tractor Engines on Performance, Fuel Consumption and Exhaust Emissions

M. Landis, I. Schiess and M. Hatt*

Agroscope Reckenholz-Tänikon Research Station ART, CH-8356 Ettenhausen, Switzerland,
marco.landis@art.admin.ch

Introduction

The combustion process in combustion engines can be adversely affected by wear phenomena in injection nozzles, by changes to the injection pump or by alterations to valve clearance. The current understanding of performance, consumption and emission characteristics during running time is based mainly on endurance runs on engine test benches. We have only a rudimentary knowledge of the practical effect of operation and maintenance on engines. There has in particular been little research into the influence of the periodic exhaust-emission servicing compulsory in Switzerland (Swiss Confederation 2009). In order to assess these influences under working conditions the Federal Office for the Environment (BAFU) sponsored a project in which twenty tractors with tractor test results available for 1994-2002 were traced to their present owners and re-tested on the same test bench using an identical measuring technique.

Methodology

Vehicles selected

20 vehicles were selected at random from a data base of 130 tractors tested in the period between 1994 and 2002 (Fig. 1). The tractors had performance ratings ranging between 37 and 118 kW and came from various manufactures like Deutz, Sisu, Iveco and John Deere. The tractors incorporated both air-cooled (n= 4) and water-cooled (n= 16) engines with capacities of between 3000 cm^3 and 7500 cm^3. 16 engines had an exhaust gas turbocharger and three of these had an intercooler as well.

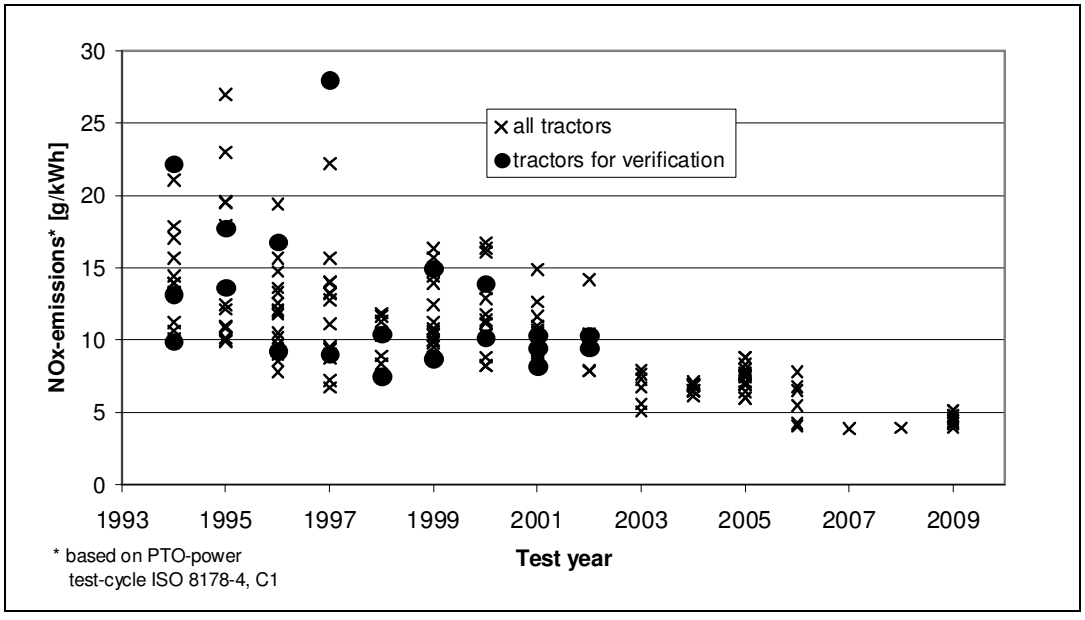

Figure 1: Vehicles selected from the extensive data base, as exemplified by NOx emissions.

Parameters surveyed and measurement methodology

Measurements were taken on the tractor test bench at Agroscope ART Research Station in Tänikon. For measurements taken on tractors between 6 and 14 years of age the identical measurement technology was used as in the original as-new test. The variables measured and the methodology used are shown in Figure 2 and Table 1.

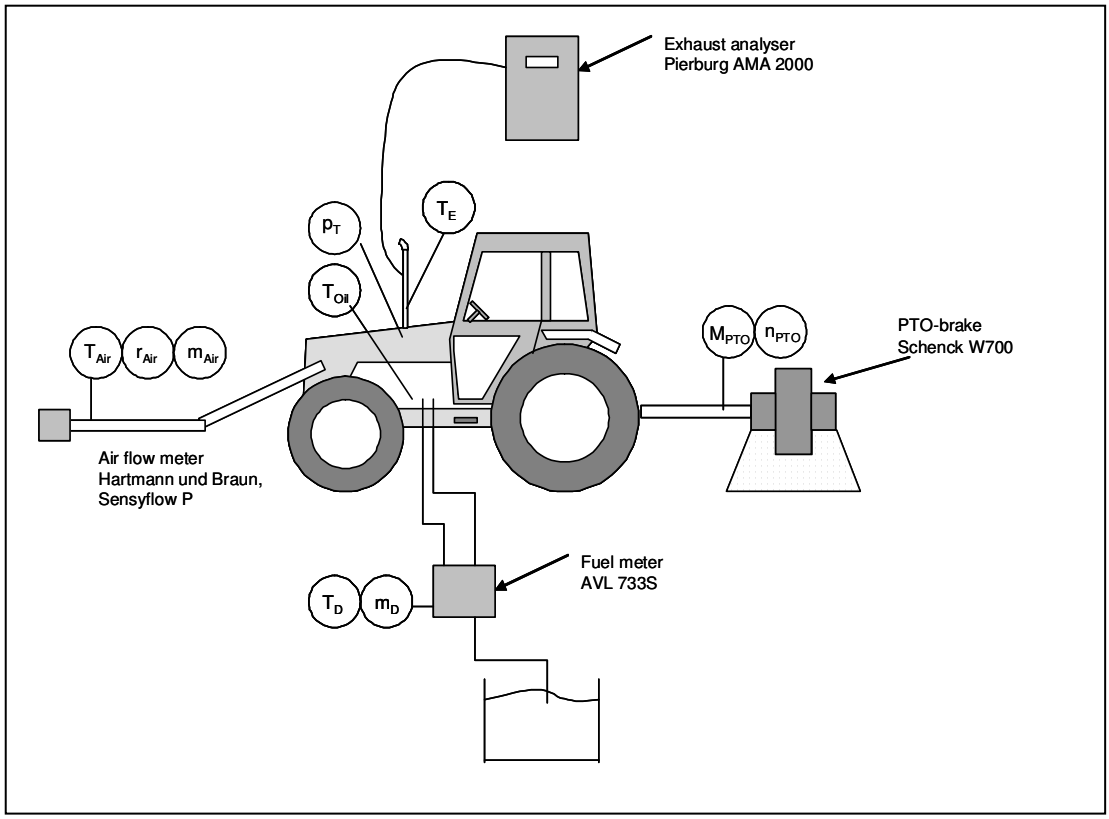

Figure 2: Measurements taken on the test bench (See Tab. 1 for explanations)

Table 1: Measured variables and methodology used

Measured variables		**Abbrev.**	**Sensor**
PTO power		n_{ZW} M_{ZW}	Schenck W700 eddy current dynamometer
Fuel consumption		m_D	AVL 733S fuel mass flow meter
Intake air volume		m_{Air}	Hartmann & Braun Sensyflow P, nominal diameter 100 mm
HC, NOx, CO exhaust gas emissions			Pierburg AMA 2000 exhaust measurement system comprising: FID analyser for THC NDIR analyser for CO CLD analyser for NOx
Smoke measurement			Bosch filter pump V = 330 cm^3
Temperatures	Ambient	T_U	Thermocouples, Type K
	Intake air	T_{Air}	
	Fuel	T_D	
	Exhaust gas	T_A	
	Engine oil	T_{Oil}	
Ambient air pressure		p_U	Mercury barometer, R. Fuess Type 11a-9 VTK
Boost pressure		p_T	Analog manometer 0 – 1.6 bar
Intake air humidity		r_{LF}	Rotronic hygroscope, Type DAG-020A

Measuring performance and consumption
Tractor performance and consumption were measured as specified in OECD Code 2 (OECD 2008)

Exhaust gas measurement (HC, NOx, CO)
Exhaust gas measurement was based on Directive 97/68/EC (European Parliament and Council 1997), with the power being measured at the tractor PTO shaft instead of the engine flywheel. The measuring cycle used was the stationary 8-stage test conforming to ISO 8178-4, C1 (ISO 2007). In each case the measuring points were recalculated on the basis of the full load characteristic curve. The measurement points of the first and second measurement differed according to the power developed by the engine.

Smoke measurement
Smoke measurement was carried out with filter paper on the full load curve at an engine speed of 70 % of the rated rpm. Filter paper blackening was converted into exhaust gas carbon black concentration by means of AVL correlation (Technische Universität Graz 2007). Conversion is only possible to carbon black, as this causes the blackening. Conversion to particulate volume is almost impossible, since exhaust gas constituents which do not cause blackening (volatile constituents) are not taken into account. The measurement was taken at only one measuring point and is not comparable with a cyclic value.

Effect of power loss at the PTO shaft
The power loss measured was at the PTO shaft. Power at the PTO shaft is less than engine power, as the power flow goes via the gearbox where losses are incurred as soon as auxiliaries such as hydraulic pumps and fans are running at the same time. At rated power the readings taken at the PTO shaft in accordance with OECD Code 2 came to between 77 and 83 % of the engine power measured in accordance with Directive 97/68/EC (Lampel 2006; Lossie 2006). The influence of the lower power measured at the PTO shaft also has an impact on the specific emissions. As division is by a lower rating, specific emissions increase. Since fan power loss has a disproportionate effect at partial load points of the measuring cycle, the losses in the 8-stage measuring cycle would probably turn out higher. The exact conversion of emissions to engine power is not possible, so all the specific emission values measured relate to power at the PTO shaft.

Fuel
Commercial diesel fuel was used for the measurements. During initial measurements in 1994 the sulphur content of the fuel fluctuated at a level above 1000 ppm. In the later measurements it was around 300 to 400 ppm. In the second measurement in 2008 and 2009 the sulphur content amounted to less than 10 ppm. As the effects of sulphur content are mainly restricted to particulate emissions (Tan et al. 2009), the influence of fuel on the results is estimated to be very low.

Results

Tractor operating hours

In the first measurement the engines had a running time of between five and 330 operating hours (Fig. 3). In the second measurement engine running time was between 1600 and 14,000 hours. This gave an annual operating hour count of between 130 and 1000 hours.

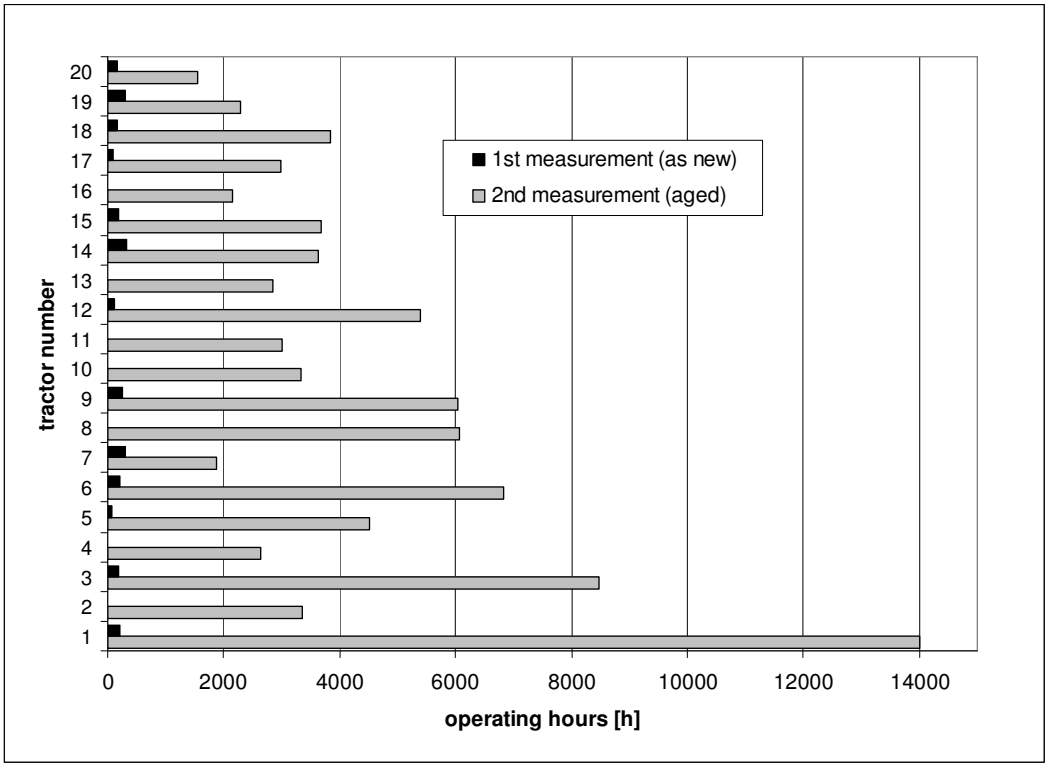

Figure 3: Tractor operating hours on first measurement between 1994 and 2002 and on second measurement between 2008 and 2009.

PTO power and specific consumption

On second measurement the performance of most tractors fluctuated within the range of the first, with tendencies to a slight increase in power (Fig. 4). Improved performance was recorded in two tractors due to a deliberate increase in the quantity of fuel injected. In one case improved performance was attributable to the governor, which had adjusted itself. A reduction in power of up to 15 % was measurable in three vehicles. In two tractors the owners said that the power had deliberately been throttled, as the engines tended to overheat during heavy work. This was why cylinder liners and pistons already had to be replaced in one instance, the cylinder head in another.

The partial slight increase in measurable performance can stem from the gearbox and auxiliaries, which run in during operation and thus cause less frictional loss.

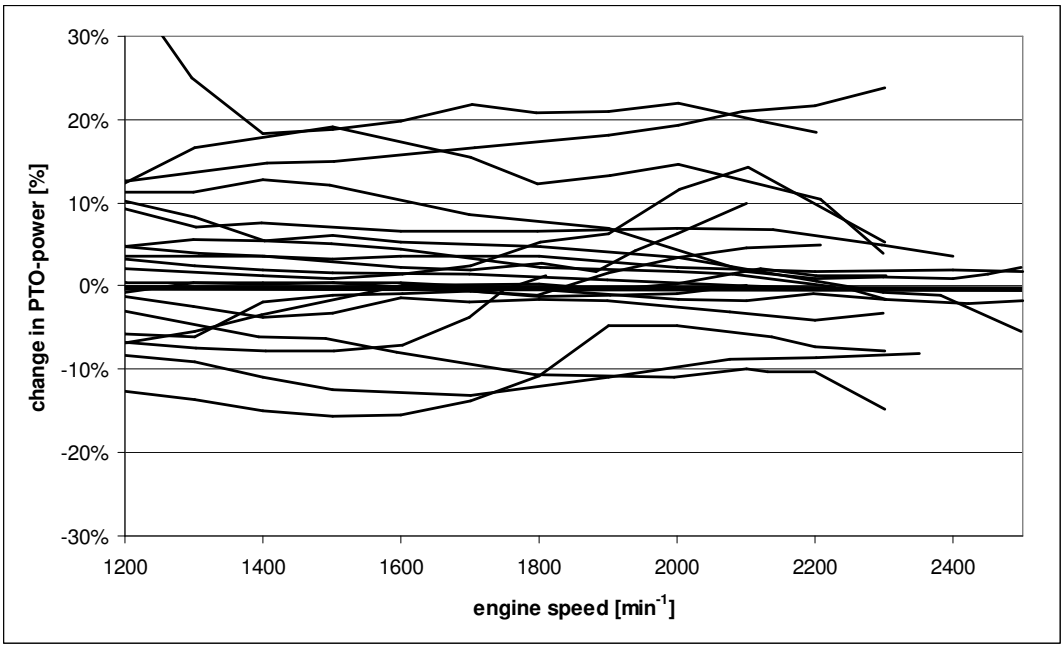

Figure 4: Change in PTO power between first and second measurement. The values of the first measurement (as-new condition) are given as 0 %.

In most of the tractors specific consumption compared with the first measurement varied in the range of ± 5 %, with no definite trends being identifiable. (Fig. 5). It is assumed that the lower specific consumption values of up to 12 % in one tractor are attributable to the new injectors. No adjustment of injection timing was discernable, either at the injection pump or during exhaust gas measurement (the NOx values were even slightly lower).

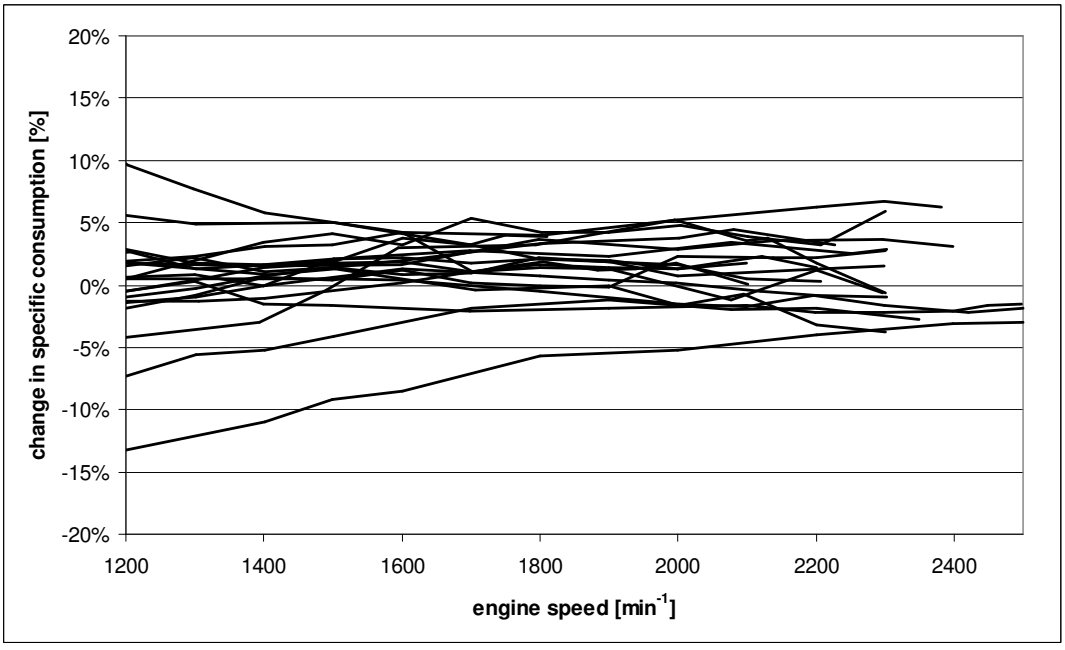

Figure 5: Change in the specific consumption of the 20 tractors tested compared with the as-new condition.

Gaseous emissions

Hydrocarbons HCs

The change in HC emissions between the first (as-new) and second measurement (with aged engines) varied between -50 % and +240 %, the median being -14 %. Apart from three greatly inflated values, no major variations were found in the others. The variations should be

relativised with reference to the absolute values as they were consistently below 0.8 g/kWh, which represents no great change.

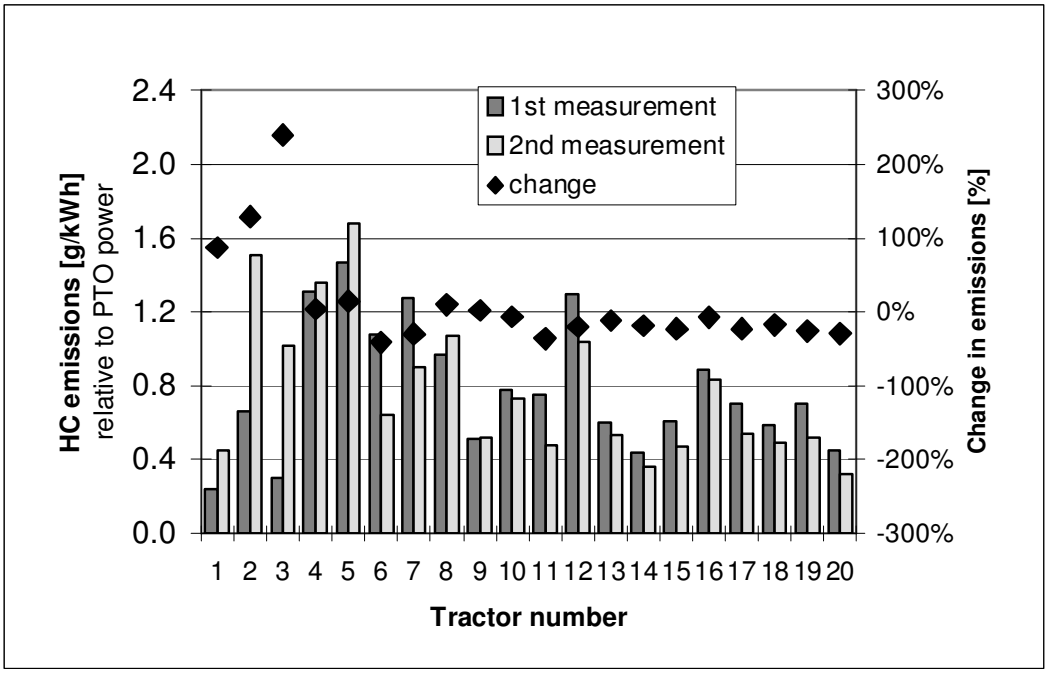

Figure 6: Weighted HC emissions in the test cycle conforming to ISO 8178-4,C1 on first and second measurement together with percentage change.

Nitrogen oxides NOx

NOx emissions fluctuated largely within the range of the first measurement. The percentage changes fluctuated within the range of ± 20 %, with a median of -6 %. No significant outliers were noticeable in any of the tractors. This indicates that the injection timings were not altered, as otherwise the NOx values would have changed.

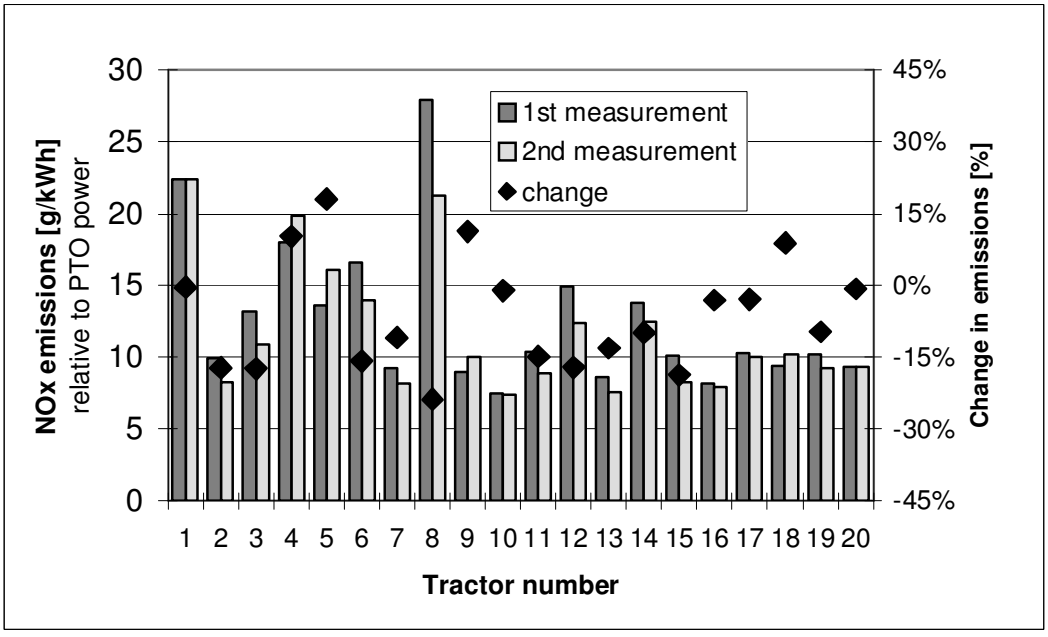

Figure 7: Weighted NOx emissions in the test cycle conforming to ISO 8178-4,C1 on first and second measurement together with percentage change

Carbon monoxide CO
The changes in carbon monoxide emissions were in the range between -40 % and +200 % with a median of +38 %. The increase in CO emissions was particularly marked at measurement points five and six of the 8 stage test. The deteriorations were due to increased injection amounts (performance increase).

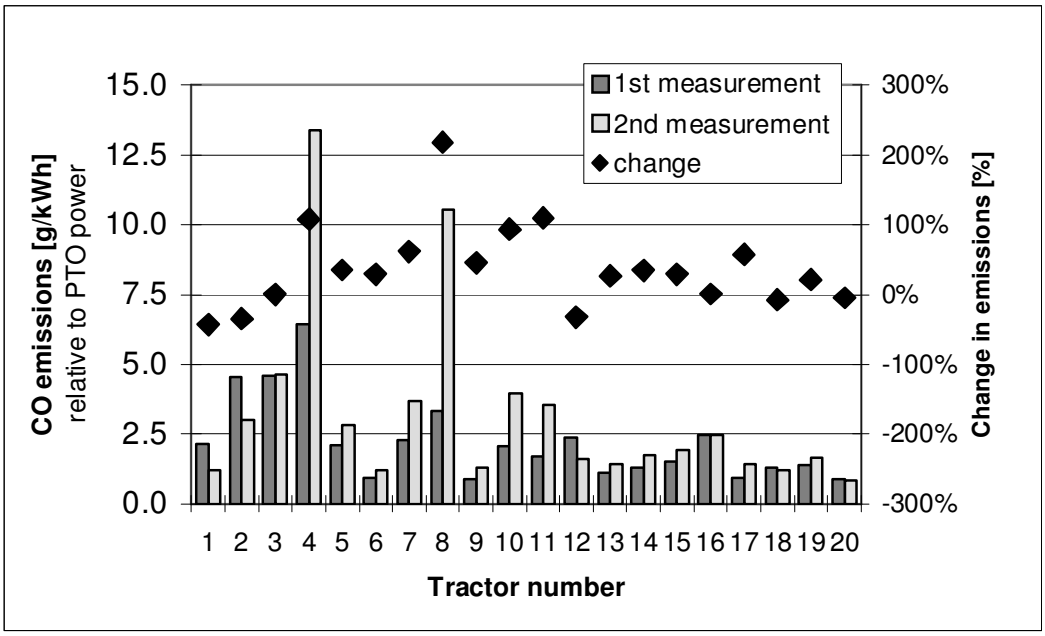

Figure 8: Weighted CO emissions in the test cycle conforming to ISO 8178-4,C1 on first and second measurement together with percentage change.

Full load carbon black
In some cases there were considerable changes to carbon black emissions at full load and an engine speed of 70 % of the rated rpm. Due to the inaccuracy of the measurement method slight changes have a very strong impact, particularly when carbon black emissions are low.

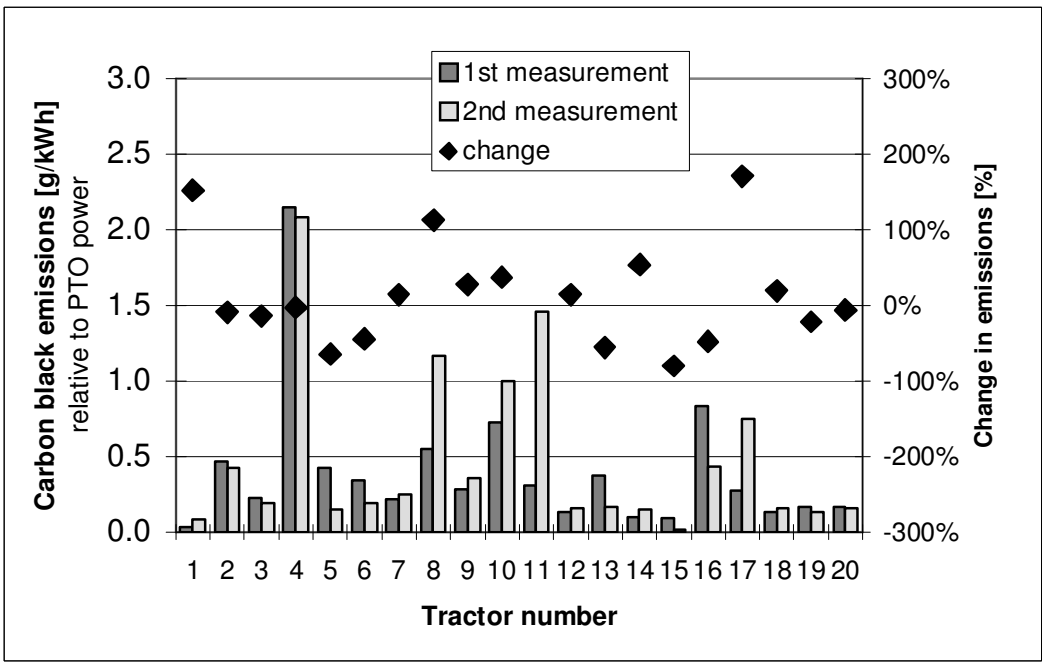

Figure 9: Carbon black emissions at full load and 70 % of rated rpm on first and second measurement together with percentage change.

Discussion

In general no major differences were found between the measurement in the as-new condition of the tractors compared with their used condition. The exception was two tractors in which a deliberate boost in performance was found as the result of an increase in the amount of fuel injected. The small increase measured in the performance of individual tractors can be due to the development of play in the injection pump control rod or to a reduction of spring tension in the injector, which causes a fractionally longer injection period. Two engines tended to overheat during practical operation. The amount of fuel injected was subsequently reduced in order to decrease the thermal load. When measurements are taken at the PTO shaft a slight positive influence on performance caused by the running-in of gearbox and auxiliaries cannot be ruled out. As the greatest losses are caused by the fan, radiator and auxiliaries such as hydraulic pumps, however, the influence of any possible self-adjusting minor transmission loss is probably very low. When power is measured at the PTO shaft according to OECD Code 2, the influence of intake air temperature and air pressure on performance is not offset. Since similar ambient conditions prevail for all the measurements, the effect is minimal at most.
An adjustment to start of delivery was not found in any of the tractors. An earlier start of delivery would have caused lower specific consumption with a simultaneous increase in NOx emissions. No doubt an important role here is played by the exhaust-emission servicing compulsory in Switzerland at regular intervals (every four years for tractors with a maximum speed of 30 km/h and every two years for tractors with a maximum speed of 40 km/h). Injection timing must be checked during exhaust-emission servicing.

Higher hydrocarbon emissions could be due to dripping injection nozzles.
Carbon monoxide emissions rose, particularly at measurement point five of the 8-stage test. In most of the tractors this was attributable to slightly better performance and the higher amount of injected fuel needed to achieve it. The air/fuel ratio then deteriorates, which can lead to local air deficiency in the combustion chamber. This behaviour is very marked, particularly in the range of maximum torque. The steep rise in emissions at measurement point five also impacts cycle emissions. This meant that in the cycle individual tractors showed a noticeable deterioration compared with the first measurement. Since measurement point five is of hardly any significance in agricultural practice, as the gear has already been changed or the rpm of powered implements cannot drop so low, the deterioration at this measurement point should not be overemphasised.
The carbon black emissions calculated from the blackening figures rose significantly in individual tractors. In a test encompassing several measurement points this cannot be used to reach any conclusion on cycle emissions. Soluble exhaust gas constituents are not taken into consideration when determining the blackening figure, so it is not possible to say anything about particulate emissions. The reasons for the partial rise in carbon black emissions will be found in a less efficient combustion process. This is caused, for example, by local air deficiency in the combustion chamber or poor fuel atomisation due to worn injection nozzles.

The changes measured in emission behaviour are very consistent with existing data (U.S. Environmental Protection Agency 2004) and (Schäffeler and Keller 2008). These studies show predominantly neutral behaviour in the nitrogen oxides and a slight increase in hydrocarbons, carbon monoxide and particulates. The importance of engine maintenance and any necessary repairs is shown by the fact that the injection nozzles already had to be replaced in several tractors. On the basis of this study no universal statement can be made on the right time to change the injection nozzles. Nozzle service life was between 2000 h and 6000 h. The unloaded engine opacity test carried out during compulsory exhaust-emission servicing plays a key role in the prompt identification and replacement of worn engine and injection components.

Summary

In order to investigate the influence of aging on tractors, 6 to 14 year-old used tractors tested in the as-new condition were re-measured on the test bench at Agroscope Reckenholz-Tänikon ART Research Station, and these values were compared with those of the as-new condition.
The performance of most of the tractors changed within the range +/-10 %. Higher performance was attributable to increased amounts of fuel injected and, to a minor extent, to reduced frictional losses (run-in gearboxes). Specific consumption and NOx emissions stayed approximately the same in all the tractors. Considerably higher hydrocarbon HC and carbon monoxide CO values were recorded in individual tractors than from measurements over ten

years previously. This was caused by wear phenomena in the injection nozzles, resulting in poorer fuel atomisation and increased injection amounts, which had a particularly negative influence on CO and carbon black figures.

References

European Parliament and Council (1997), Directive 97/68/EC of the European Parliament and of the Council of 16 December 1997 on the approximation of the laws of the Member States relating to measures against the emission of gaseous and particulate pollutants from internal combustion engines to be installed in non-road mobile machinery. Brussels, 84 pp.

ISO (2007), ISO 8178-4 C1: Reciprocating internal combustion engines-Exhaust emission measurement-Part 4: Steady-state test cycles for different engine applications. Test cycle C1. 25 pp.

Lampel H. (2006), Was sagen die Leistungsdaten eines Traktormotors aus? Wieselburgtagung 27.2.2006, Power Point Presentation, Wieselburg.

Lossie U. (2006), Durchblick im PS-Dschungel. *top agrar*, 1/2006, p. 108-109.

OECD (2008), CODE 2, OECD Standard code for the official testing of agricultural and forestry tractor performance. Paris, 87 pp.

Schäffeler U. and M. Keller (2008), Treibstoffverbrauch und Schadstoffemissionen des Offroad-Sektors, Studie für die Jahre 1980–2020. Bundesamt für Umwelt, *Umwelt-Wissen* Nr. 0828., Bern, 172 pp.

Schweizerische Eidgenossenschaft (2009), Verkehrsregelnverordnung (VRV). Bern, 64 pp.

Tan P.-Q., Hu Z.-Y. and D.-M. Lou (2009), Regulated and unregulated emissions from a light-duty diesel engine with different sulfur content fuels. *Fuel, 88*, 6, p. 1086-1091.

Technische Universität Graz (2007), Vorlesungsunterlagen Abgastechnik, Chapter 12.3. Graz.

U.S. Environmental Protection Agency (2004), Exhaust and Crankcase Emission Factors for Nonroad Engine Modeling-Compression-Ignition. NR-009c, *EPA420-P-04-009*, 135 pp.

Lidar Observations of Ship Plumes in the English Channel

M. Bennett and S. Christie*

Centre for Air Transport and the Environment, Manchester Metropolitan University, John Dalton Building, Chester Street, Manchester M1 5GD, UK, m.bennett@mmu.ac.uk

Introduction

Emissions of nitrogen oxides (NO_x) and sulphur dioxide (SO_2) from shipping in the European Union are expected soon to exceed those from all land based combustion sources (Agren, 2000). And indeed, these expectations might have been serious *under*-estimates (Corbett and Köhler, 2003). Ships are also a major source of particulate matter (PM), which may be a globally significant source of mortality (Corbett et al., 2007). They represent a major gap in the otherwise successful efforts to reduce emissions of photochemical precursors, acidifying species, and aerosol loads in Europe. The chemistry and dispersion of ship plumes is, however, poorly understood and largely unquantified. There are critical gaps in our understanding of the processes involved: mixing and entrainment within the plume, for instance, greatly influence the chemistry within the plume and ultimately its effect on the atmosphere over the spatial and temporal scales pertinent to most current atmospheric models - current models are largely unable to reproduce such small-scale processes. On more local scales, the fumigation and hence health impacts (e.g. from NO_2 and respirable particulate), of ship plumes will depend critically on plume buoyancy, dispersion, and chemical gradients within the plumes.

The key to modelling these chemical observations lies in being able to construct a realistic model of the plume dispersion, internal mixing, and entrainment of air from outside the plume. A typical scheme within existing models might use Briggs-type Gaussian parameters for the cross-sectional area of the dispersing plume (e.g. Franke et al., 2008) and then assume that the primary emissions are well mixed with ambient air within this volume. A difficulty with such schemes, however, is that the Gaussian plume strictly only arises as a result of time-averaging over an ensemble of random dispersion events. Plume spread parameters are thus strictly only relevant to time-averaged behaviour, typically over 30 min. Much (if not most) of the plume spread over such a period arises from looping or meandering of the short term plume, which is clearly irrelevant to the intimate mixing required for in-plume chemistry to take place. There is thus a clear need to make some high resolution measurements of the dispersion of marine plumes at some point relatively close to the point of emission, and to observe how they evolve.

Dispersion of the emissions from a large commercial vessel travelling at full power is subject to several factors. Initially, it will be dominated by competition between the thermal buoyancy of the emission and entrainment into the turbulent wake of the ship. Further downwind, the near-field plume will gradually be broken up and dispersed by ambient turbulence in the marine boundary layer: it is some trial observations of this process which we shall be reporting in this paper. For light to moderate winds, such dispersion will be dominated by the relative temperatures of sea and air. Where ships are near the coast, however, the overall flow may also be affected by subsidence and divergence in the sea breeze circulation (Simpson, 1994). In strong winds, of course, diabatic effects become irrelevant, the sea surface roughens, and the plume disperses neutrally.

We have therefore initiated a programme of backscatter Lidar measurements of the dispersion of smoke from ocean-going vessels in the English Channel.

Methodology

The Dover Strait is the busiest international shipping lane in the world, being the principal route to most of the major container ports in Northern Europe and the UK: about 295 vessels transit each day (Squire, 2003). For this reason traffic is segregated, with westbound shipping restricted to a lane on the English side. Dungeness, on the Kent coast, is only 7.5 km from the landward side of this shipping lane and 33 km across the bay from the busy ferry port of Dover (Figure 1).

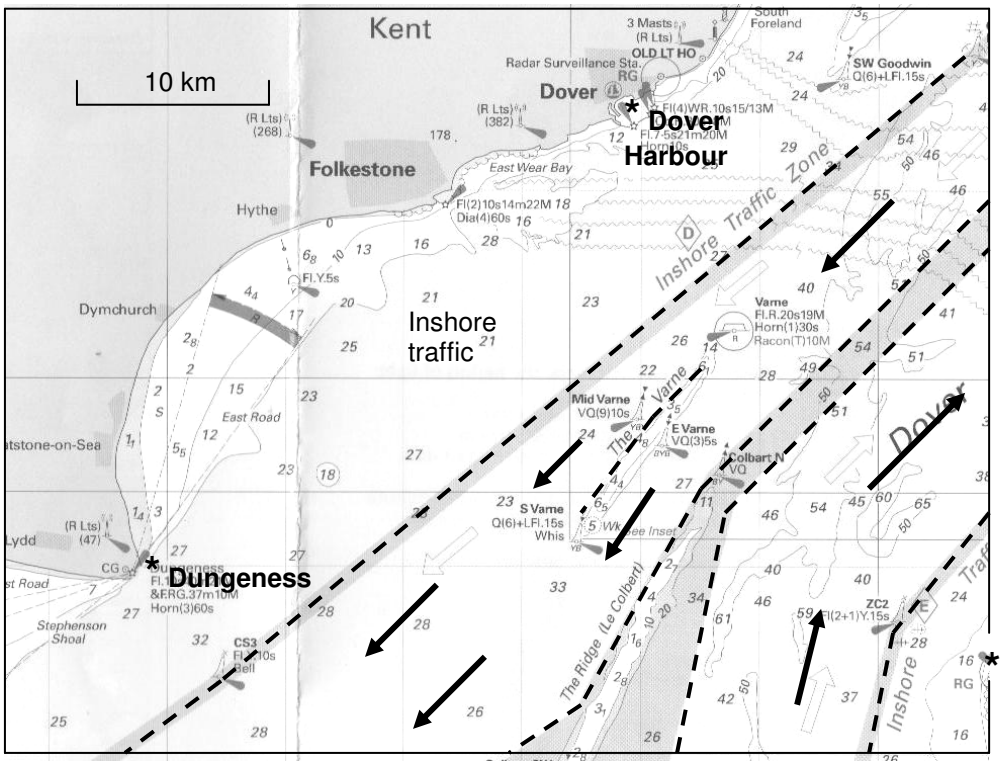

Figure 1: Shipping lanes in the eastern English Channel.

Our field site is on the foreshore at Dungeness Point, where the outbound shipping lane reaches its closest approach to the coast (Figure 2). There is an open aspect to the sea from the SW through to the NE.

Figure 2: Shipping viewed from Dungeness Point, September 2009.

For the measurement of dispersion in the marine boundary layer, we need a long upwind fetch over the sea. Our site can offer this, since the fetch varies from a minimum of 43 km in E winds, to 105 km in S winds, 225 km in SW winds and the full width of the Atlantic at WSW. SW winds

would also have the virtue of being relatively clean. From SSW and eastwards, we may suffer increasing background interference from the emissions of NE-bound shipping and from continental sources: the refineries near Le Havre lie at a distance of 170 km SSW.

The nearby synoptic station at Herstmonceux records a 38% occurrence of winds between S and WSW. Ship plumes will therefore be encountered frequently at this site. With an onshore breeze of (say) 5 m s^{-1}, ship plumes would be advected to within range of the Lidar after a travel time of order 20-30 min.

MMU's Rapid-scanning Lidar is vehicle-mounted, with an on-board electrical generator, and is thus easily deployable at remote sites (Figure 3). The Lidar is eye-safe, being built around a frequency-tripled YAG laser (λ = 355 nm), with a laser pulse power of 33 mJ. The system also has an on-board weather station with a 10 m mast (not fully extended in Figure 3).

Figure 3: Lidar in operation at Dungeness, 19 June 2008.

In this application, the Lidar was set to detect the return signal using two photomultiplier tubes with a range resolution of 5 m. Each tube could then return signals over a range span of 1250 m, with the minimum possible range being ~175 m. Three scanning modes were employed:-

- Near-horizontal scans across the sea surface to provide a plan view of offshore plumes. Both detectors were then set to the same range span, typically 750-2000 m, and with similar sensitivities.

- Vertical scans from the sea surface up to an elevation of 10-15^{o} at an azimuth approximately normal to the wind direction. This should provide vertical cross-sections of any offshore plumes and also some indication of the structure of the marine boundary layer.

- Vertical scans through the horizon at azimuths close to that of the nearest approach of the shipping. The two detectors would then be set with offset range spans (e.g. 7000-8250 m and 7750-9000 m) in order to maximize the chance of catching a ship. By scanning alternately at two azimuths, typically separated by 10^{o}, the range, speed and heading of a vessel can in principle be estimated.

An extensive suite of numerical analysis tools has been developed for the Lidar. On a scan-by-scan basis, we can readily identify individual plumes and parameterize them in terms of height, spread, plume area, intermittency etc. (Bennett et al., 1992; Bennett, 2004).

Besides meteorological measurements, the Lidar scans were supplemented with onshore measurements of SO_2 (API model M100E, UV fluorescence) and fine particulate (Osiris). The latter is a particle counter/sizer and reported concentrations of PM_{10}, $PM_{2.5}$ and PM_1. Both instruments were logged at 1 min intervals. In addition, we deployed two ultra-fast UVIC point samplers (Griffiths et al., 1998). These detect all species with a first ionization potential of less than 10.2 eV (typically unsaturated hydrocarbons). It was hoped that these would provide information on the small-scale structure of any plumes as they came ashore.

Observations

After a pilot study on the afternoon of 19 June 2008, a series of measurements was made in the week 14-18 September 2009. A further week is planned for 20-24 April 2010.

With some practice, it was found that clear signals could be obtained from shipping, as hard targets, at ~7.5 km range. Their stack emissions, however, could not be detected with the Lidar at that range (although they were often visible through binoculars).

Unfortunately, the winds over the September survey period were uniformly unfavourable for detecting shipping plumes: they were mostly offshore, between N and NE. On the final day of the trial, however, the wind veered to between NE and ENE. Typical results are shown in Figures 4 and 5. The EEE and NNN axes in these Figures correspond to eastings and westings relative to the measurement site. We may note that the reported signal here has been corrected for atmospheric extinction and for the $1/r^2$ geometric decay of the signal with range – such corrections lead to the noise being amplified at greater ranges. At all ranges, the corrected signal has been normalized by the ambient backscatter from clear air: a value of 0.06 thus corresponds to a plume backscatter of 6% that from clear air.

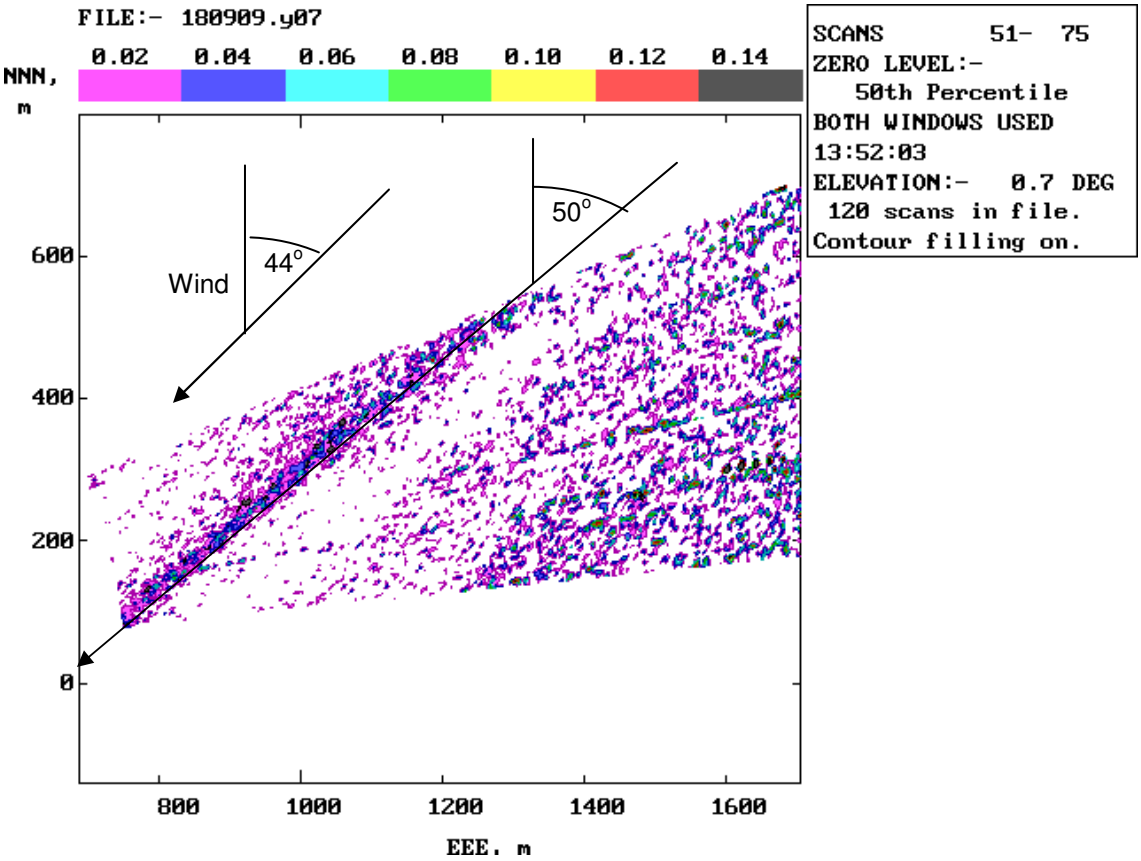

Figure 4: Near-horizontal Lidar cross-section of a marine plume from near Dover. Average of 25 scans over 130 s centred on 13:51:00 (BST): the plume would have lain 600 m S of the Lidar by this time. Wind speed 8.3 m s^{-1} @ 10 m; wind direction 44° (true); air temperature 15.1°C; sea surface temperature 17°C. The SO_2 concentration, measured at the Lidar, peaked at 2.8 ppb at 1349 with a duration (FWHM) of 12 min. Dover Harbour lies on a bearing of 51° from the Lidar at a distance of 33 km.

When optimized for recent studies at airports (Graham et al., 2006), we found that the limiting sensitivity for an individual scan was about 3% of the clear air background at a range of 200 m. In the present application, we are attempting to detect plumes at a substantially greater distance (> 1 km) against a bright sky (cf. Figure 2). It is thus necessary to average over a significant number of scans before plumes may be seen consistently.

Figure 4 shows a plume apparently arising from the Dover area – it is not clear whether this is from ships in harbour or from some nearby land-based source. Note that over the rather long averaging time, any plume element may have been advected by ~1100 m. This corresponds to at least the length of the plume seen in the Figure. Inspection of individual scans, however, does not reveal a single compact puff of smoke advecting with the wind. Plume elements seem to have been reasonably well dispersed along the wind direction. What is striking is the modest width (~30 m) of the plume, even after a probable advection distance of >30 km. We may note that this was despite a choppy sea surface and some slight instability in the marine boundary layer.

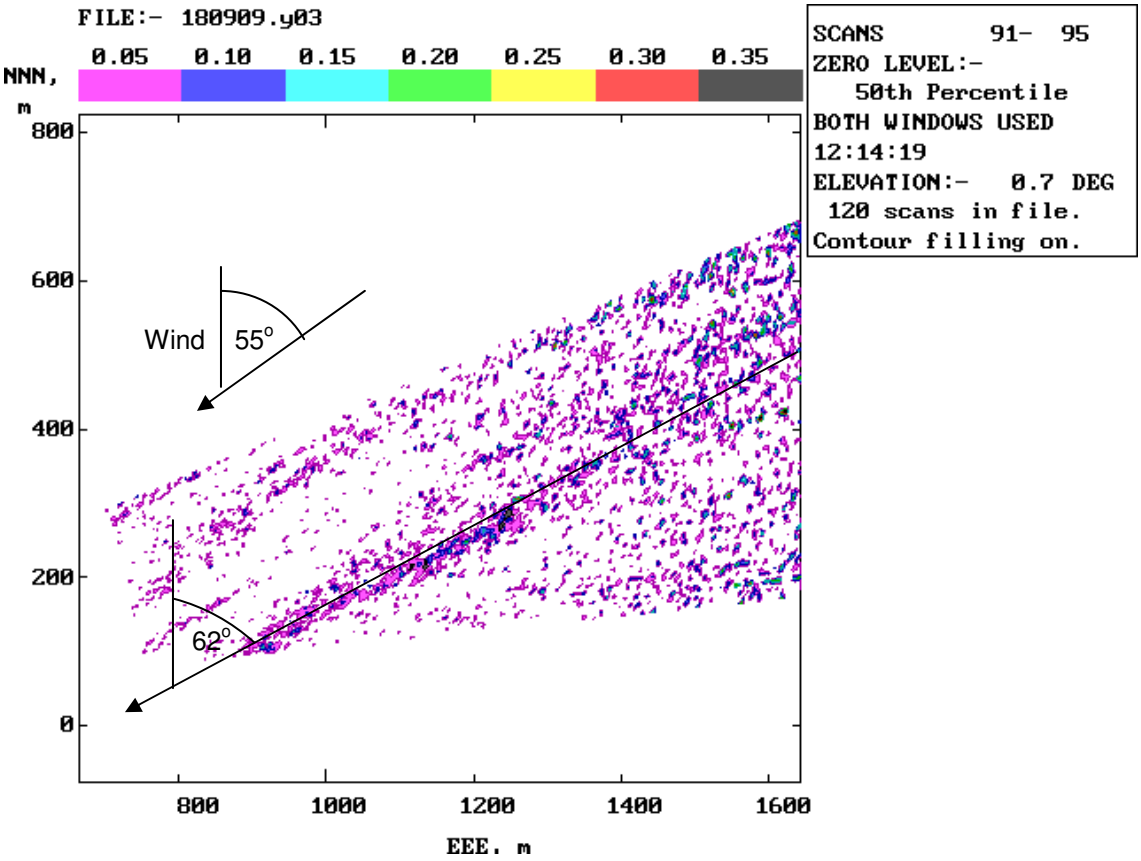

Figure 5: Near-horizontal Lidar cross-section of plumes from shipping off Dover. Average of 5 scans over 25 s. Wind speed 9.8 m s^{-1} @ 10 m; wind direction 55° (true); air temperature 14.6°C (all met. variables averaged over 3 min); sea surface temperature 17°C. Peaks in SO_2 concentration were typically ~1.5 ppb above a baseline of ~0.5 ppb.

Around midday on 18 September, the wind veered to ENE and the Lidar could survey a longer offshore fetch. This may be seen in Figure 5. The plumes now shown have ostensibly come from several km offshore from Dover and must thus originate from shipping. Again the time-averaged plumes shown have a length comparable to the advection length over the averaging time. We seem here to be looking at plume elements looping into the scanning plane. Again, their width is only ~1% of their advection distance.

It is worth noting that the observed direction of a plume need not necessarily match that of the wind: from a moving source, the plume direction should be the vector sum of the source and wind velocities. In the case of Figure 5, this implies that the source cannot have had a substantial cross-wind component. This is consistent with its being an outbound ship, mid-channel off Dover (cf. Figure 1).

Discussion

It was obviously disappointing that adverse winds did not permit us to monitor shipping plumes over the short fetch from the shipping lane to the shore at Dungeness. Nevertheless, it is clear that, given favourable winds, the system has sufficient sensitivity to be able to do so. Ship plumes which have travelled over more than 30 km of marine fetch show peak backscatter in excess of 10% of the ambient scattering; this is detectable by the Lidar at a range of >1 km.

The observed plumes were surprisingly compact, their short term width being typically only ~30 m, even over a rough surface in slightly unstable conditions. Associated peak concentrations of SO_2 were typically less than 2 ppb from ships offshore but possibly ~3 ppb from Dover Harbour.

The Lidar was capable of obtaining hard returns off ships in the main shipping lane at a range of 7.5 km; their aerosol emissions, however, could not be detected at this range. With a suitable scanning procedure, the range, speed and bearing of ships could be estimated.

Further field trials are planned.

Acknowledgements

We are grateful to the Romney Marsh Countryside Project for permission to make measurements from the foreshore and to the Environment Agency for provision of secure parking for the Lidar system.

References

Agren C. (2000), The harm of emissions, *Swedish NGO Secretariat on Acid Rain,* www.seaat.org.

Bennett M. (2004), Lidar cross-sections of a marine boundary-layer, *Weather,* 59, 42.

Bennett M. and S. Christie (2006), Optical measurements of pollution dispersion at commercial airports, *Photon06,* Manchester, 4-7 September 2006.

Bennett M., S. Sutton and D.R.C.Gardiner (1992), An analysis of Lidar measurements of buoyant plume rise and dispersion at five power stations, *Atmos. Environ.,* 26A, 3249-3263.

Corbett J.J. and H.W. Köhler (2003), Updated emissions from ocean shipping, *J. Geophys. Res.,* 108, D20 4650.

Corbett J.J., J.J. Winebrake, E.H.Green, P. Kasibhatla, E. Eyring and A.Lauer (2007), Mortality from ship emissions: a global assessment, *Environ. Sci. Technol.* 41, 8512-8518.

Franke K., V. Eyring, R. Sander, J. Hendricks, A. Lauer and R. Sausen (2008), Toward effective emissions of ships in global models,, *Meteor. Zeits.,* 17, 117-129.

Graham A., D.W. Raper, S. Christie and M. Bennett (2006), Lidar Study Report, 'Air quality at Heathrow Airport: impact of emissions from aircraft in ground run and flight', Annex 7 of *Project for the Sustainable Development of Heathrow: Air Quality Technical Report.* UK Department for Transport.

Griffiths R.F., I. Mavroides and C.D. Jones (1998), The development of a fast-response portable photo-ionization detector: a model of the instrument's response and validation tests in air, *Meas. Sci. & Technol.,* 9, 1369-1379.

Simpson J.E. (1994), Sea breeze and local winds. *Cambridge University Press.*

Squire D. (2003), The hazards of navigating the Dover Strait (Pas-de-Calais) traffic separation scheme, *J. Navigation.* **56,** 195-210.

Air pollution by fine particles (PM-10, PM-2,5 and PM-1), size distribution and associated trace metals evaluation in the great area of Algiers.

Rabah Kerbachi, Ali Bitouche, Dalila Belhout, Nassima Oucher, , Nassim Berkouki, Ménouer Boughedaoui
Laboratory LSTE, Ecole Nationale Polytechnique, El-Harrach, Alger, Algérie Fax +213 21 522973
email : r_kerbachi@yahoo.fr

Abstract :

The study presents the levels of air pollution by fine particulates matters PM-10, PM-2.5 and PM-1 at six different sites in the great Algiers. The results reveal that pollution by PM-10 and PM-2.5 is very high and exceeds the European and WHO guidelines. At urban site, the average content of PM-10 rises up to 65 µg/m^3 but values higher than 100 µg/m^3 were often reached. The (PM-2.5) average content is 35 µg/m^3 which constitute more than 50 % in mass of the PM-10. The ratio PM-2.5/PM-10 is a characteristic of an urban area influenced by the road traffic. Moreover, it is noted that approximately one third of the PM-10 is composed of very fine fraction of PM-1. It is shown that PM-10 are distributed according to a bimodal distribution with a good correlation between the very fine (PM-1) and the respirable particles (PM-2.5).

The size range analysis of trace metals (Fe, Mn, Pb, Cu, Co and Cd) associated to these particles shows high pollution by lead which is due to the very low use of unleaded fuel in Algeria. It is noticed that major part of toxic metals (Pb and Cd) are distributed on the very fine particles. The heavy metals of soil dust of earth's crust Fe and Mn are enriched in the coarse particles (range 3 - 10 µm). Data of the mass median diameter and the size distribution of trace metals are also discussed.

Key–words: Air pollution, fine particles, PM-i, trace metals, size distribution, Algiers

1- Introduction :

Fine particles of different size fractions PM-10, PM-2.5 and PM-1 are an important factor in air pollution, particularly in urban areas with high road traffic density. In health, they represent a major indicator of the quality of the air (Schroeder et al. 1987; Jansen et al. 1997; Chiron et al., 1997). Numerous and consistent studies attribute their greater responsibility in the occurrence of a wide range of biological and health effects (Dockery et al. 1993; Pope et al., 1995). Due to their physico-chemical properties, they exert on the respiratory and cardiovascular system high potential for harm. The European Commissioner for Environment, estimated in 2007 that each year 370,000 people in Europe die prematurely from diseases linked to air pollution, including 350,000 of them because of respirable particles PM-2.5. Also, after the USA and WHO, the European Union is studying the feasibility of more rigorous standards in effect since 2000.
In Algeria, where urbanization and motorization is expanding rapidly, the degradation of air quality and pollution are already perceived. Studies have shown that the Greater Algiers (3.5 million inhabitants, 1000,000 vehicles), like any large city, facing a severe air pollution (Boughedaoui et al. 2004; Kerbachi et al. 2006a and 2006b). The main emission source is road traffic. The fine particle pollution has not been the subject of special attention.
And also to have accurate data on levels and types of pollution and to achieve a strategy of prevention, we have from 2002 to 2007 conducted a large study on contamination of the atmosphere with PM10, PM-2, 5 and PM-1 in different types of sites in the Greater Algiers. Heavy metals associated with these particles and their contributions to global pollution were also studied.

2. Methodology:

The study was conducted at six sites: three urban sites U1, U2 and U3 for assessing the exposure rate of urban population to pollution, one site close to road traffic S (site under the direct influence of cars emissions) and two peri-urban sites PU1 and PU2 located at the limit of the urban city (Fig1)

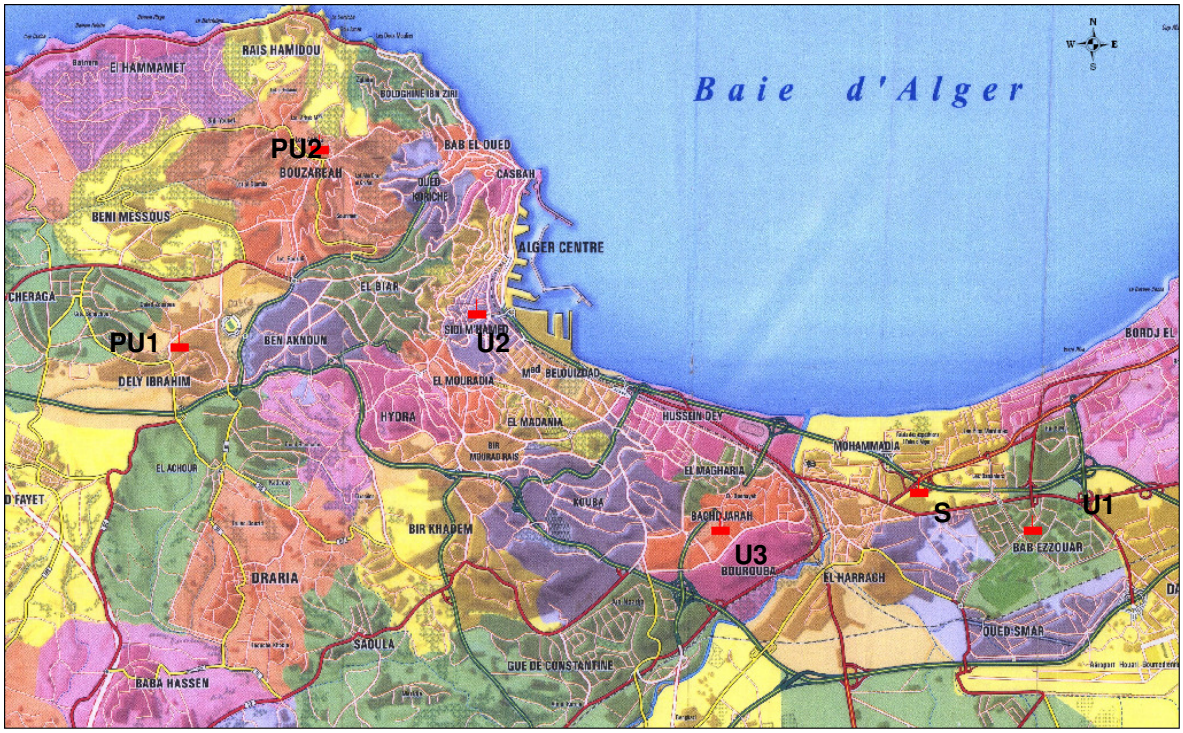

Figure 1 : Localisation of measurement sites in Great-Algiers (sampling site)

S: The sampling station is located at the campus of Ecole Nationale Polytechnique (ENP) south-east at about 10 km from central Algiers and directly (8 m) along the main road RN5. This important road is frequented by more than 25,000 vehicles per day with approximately 15% of buses and heavy vehicles diesel. This site is also exposed to natural ventilation.
U1: The station is located at the university campus of Bab-Ezzouar about 15 km southeast of Algiers. It is an urban site with high resident population density (45,000 inhabitants per Km2).
U2 : The sampling site is located within the hospital Mustapha Bacha in central Algiers. This position overlooking the bay of Algiers is undergo to a very good natural ventilation
U3 : this site is like U1, an urban site with high resident population density in the district Badjarah.
PU1 :The peri-urban site is located in the district of Dely Brahim (south-Algiers) at the Institute ISMAL.
PU2 : This site is located at the end of the district Bouzaréah at the research centre CDER. This well ventilated site, which is the highest point of Algiers, is not under the influence of direct emissions of particles.

In all these sites, sampling is performed at a height of 4 to 12 m from the ground. Samples are taken using a high volume sampler HVS-PM-10 equipped with a Sierra-Andersen cascade impactor with four stage (< 1um, 1-1.5 um, 1.5 - 3 µm, 3 -7.2 µm et 7.2 - 10 µm). The sampling time is 24 hours and the flow 1 m3/mn. Measurements are carried out for a period of one year at each site (with a sampling average frequency of six daily samples a month). After acid digestion of the collected particulate filters, heavy metals Fe, Pb, Mn, Cu and Cd, are analyzed by atomic absorption spectrophotometry

3 - Results and discussion

Levels of air pollution by fine particles

The results show that in all sites concentrations vary daily in a wide range. The diurnal variation is due, firstly, changes in the intensity of emission sources (road traffic), and other meteorological influences (wind, rain,...). For all sites studied, the mean levels of the three size fractions PM-10 PM-3 and PM-1 are summarized in table 1.

Table 1: Atmospherics mean levels of PM-i in µg/m^3 measured in ambient air in Algiers

Sites	PM-1	PM-3	PM-10	PM-1/PM-10	PM-3/PM-10
S	27.1	43.3	80.4	0.34	0.54
U1	22.2	35.6	69.3	0.32	0.51
U2	18	28.1	48	0.37	0.58
U3	22	38	73	O,30	0,52
PU1	13.1	18.3	27	0.48	0.67
PU2	1O.4	20	30	0.35	0.66

It follows that the atmospheric concentrations of PM-i in road traffic site S (site under direct influence of vehicle emissions) are the highest. The lowest levels are measured in peri-urban sites. They are on average two times lower than in urban areas.
The ratios PM-1/PM-10 and PM-3/PM-10 giving the mass of fine particles contribute to PM-10 are similar for all sites and show that in the PM-10, the very fine particles are predominant. The very harmful PM-1 are about a third of PM-10 and PM-3 more than half. Figure 2 shows the average mass contributions to PM-10 of different size fractions measured in urban areas.

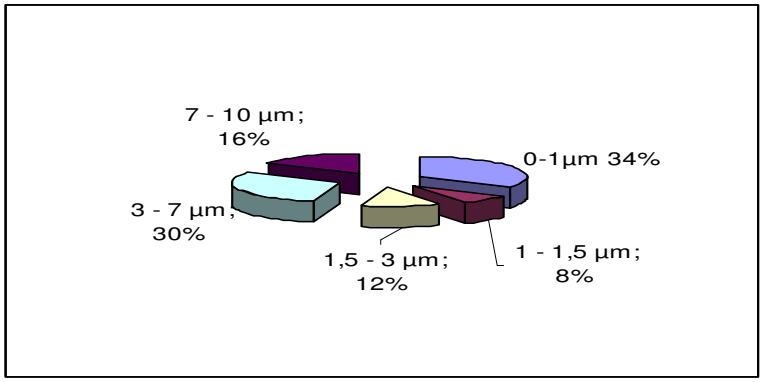

Figure 2 : Mass distribution of the PM-10 per size range in urban site

The respirable fraction PM-2.5 that standards take into consideration is not accessible experimentally by our sampler. It is determined graphically from plotting data for the five size classes on a log-probability diagram the di diameter of particles based on the percentage of the cumulative mass of particles with a diameter ≤ di (Butler, 1979). The results obtained show that the PM-2, 5 are, according to the type of site, approximately 92 to 94% of PM-3. Thus, by equating the PM-3 to PM-2.5, the error is acceptable.
The comparisons of measured atmospheric concentrations with the PM-10 and PM-2.5 standards of Algeria (JO-RADP, 2006), U.S. (U.S. EPA, 1997), European (CE JO-1999) and WHO standards (WHO, 2005) show that compared with the strong guide values of health protecting by of WHO, the average annual levels of PM-10 and PM-2.5 are substantially exceeded in all types of sites. The European and U.S. standards are met in peri-urban sites. The very little binding Algerian standard (80 µg/m3 for PM-10) is respected at all sites. Overall, we find that the fine particle pollution is excessive in both types of site, traffic station as well as urban sites.
This pollution is alarming in its scale, but also because of the strong presence of very fine particles which increase the potential harm of airborne particles.
A comparison with other cities also shows that Algiers accuses a high rate of pollution. The PM-10 levels measured in Algiers are indeed much higher than those observed in European cities like Paris, Lyon and Marseille (22 to 40 ug/m3) (MEEDA, 2006), but lower than in some cities emerging countries known for their high pollution as Beijing (135.9 g/m3) and Cairo (130 to 250 g/m3) (Gertler and al, 2006).

Correlations between different size classes
The daily evolution of particulate levels in PM-1, PM-3 and PM-10 shows a similarity in their evolution, particularly between the PM-1 and PM-3. Figure 3 presents some correlations calculate at road traffic site. We notice that for both types of sites, we get very good linear correlations between PM 1 and PM-3 and on other hand between PM-(3-10) and PM-10. The correlation

between PM-1 and PM-10 is not satisfactory. This result suggests that very fine particles PM-1 and PM-3 were probably the same origin, road traffic and the secondary particles. The fractions PM-10 and PM-(3-10) which are less fine particles are highly enriched in particles of terrestrial origin and resuspension.

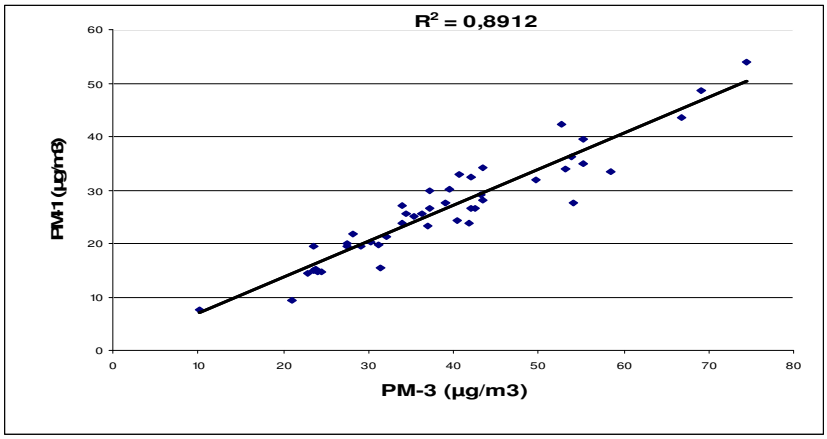

a)

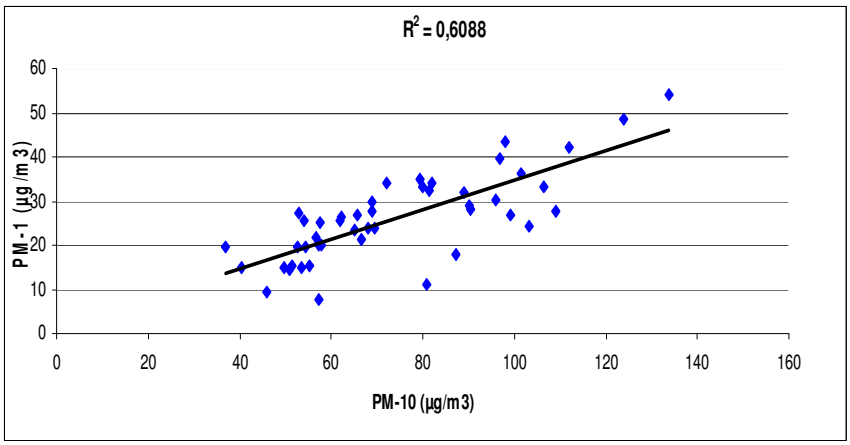

b)

Figure 3 : PM-i correlations at traffic station: a) PM-1 / PM-3 b) PM-1 / PM-10

Particle size distribution

The study of the frequency distribution of levels of different size classes can access the modality of the size distribution of particles measured in Algiers (Zhuyun Xu et al. 2002). The statistical analysis of data shows that the particles studied follow a bimodal distribution curve centred on 0.6 and 6µm modes (Figure 4) for urban sites and modes centred on 0.8 and 6 µm on the road traffic site.
The literature reports similar bimodal distributions. In some cases, it leads to a trimodal curve when considering also the ultrafine particles.

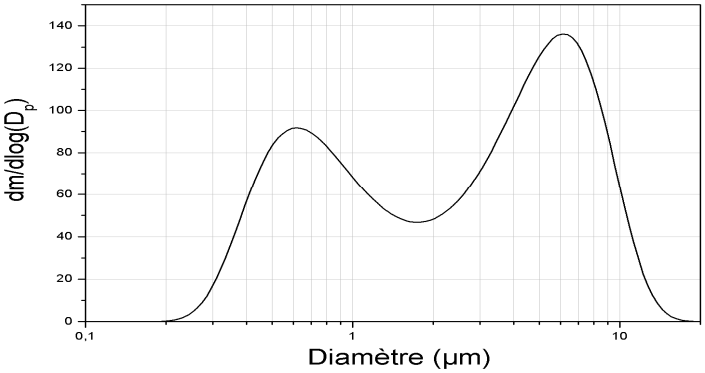

Figure 4: bimodal size distribution of PM-10 in Algiers

Heavy metals associated with PM-i

The study of heavy metals by particle size (table 2) shows that in almost all fractions and at all sites, the iron is, among the elements studied, the most abundant metal. In urban areas, with an average content of 470 ng/m3, it is rising 0.64% of PM-10. Lead, in abundance, following the iron. From 300 ng/m3 content at road traffic site, it has now dropped to about 6 ng/m3 in peri-urban site. In urban area, lead levels measured are relatively high and exceed the new European standard of 0.2 µg/m3.

Table 2: Atmospherics levels of heavy metals associated to the PM-i size fractions

		Average concentrations (ng/m^3)				
		Fe	Pb	Mn	Cu	Cd
PM-1	Traffic station	148.9	150.8	16.8	32.7	7.4
	urban	106.7	117.4	11.3	20.1	0.6
	Peri-urban	146.6	Nd	15.3	7.9	nd
PM-3	Traffic station	282.9	208.9	31.2	63.2	12.8
	urban	193	147.6	27.3	41.3	1.1
	Peri-urban	251.4	4.2	28.7	12.8	nd
PM-10	Traffic station	639.8	299.3	57.3	98.9	21.2
	urban	467.1	231.2	41.3	60.8	1.4
	Peri-urban	440.3	6.1	61.4	22.6	0.3

Analysis of these data shows that heavy metals are distributed differently on the size classes. So in urban areas, the ratio $Pb_{PM\text{-}3}/Pb_{PM\text{-}10} = 0.66$ means that 66% of global atmospheric lead has a particle size less than 3µm. In the case of iron, 60% fall on the coarser fraction PM-(3-10). Manganese behaves like iron. This difference in the size of heavy metals is related to their emission source. The metals of the earth's crust (Fe, Mn, Cu) are associated with coarse particles (3-10µm) while lead enriches especially fine particles from road traffic (Figure 5).

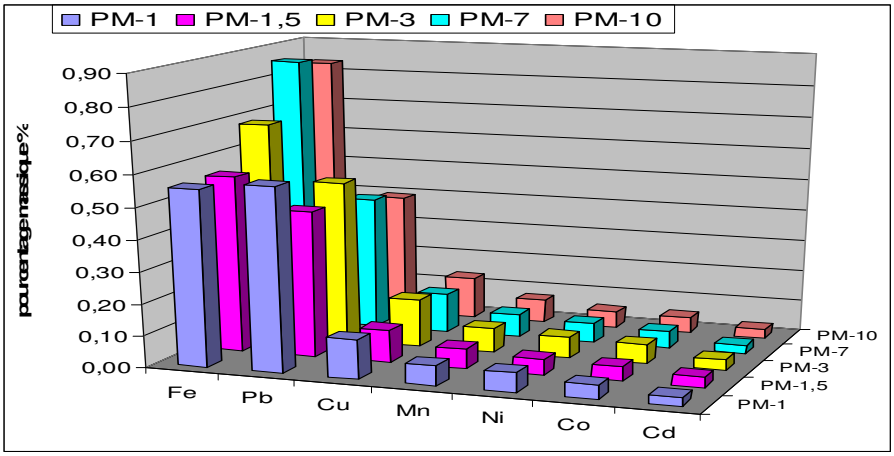

Figure 5 : Mass fractions of heavy metals in the PM-i at traffic station

Conclusion

The study conducted over several years has allowed access to levels of air pollution by particulate matter (PM-10, PM-2.5 and PM-1) met in Algiers in different types of sites. In urban and at station traffic site, levels of PM-10 and PM-2.5 are excessive and exceed largely international and WHO standards. This pollution is particularly worrying that over 60% of PM-10 particles are respirable. In peri-urban sites, the pollution levels are indeed reduced by half, but reached the levels measured

in magnitude in urban sites in major European cities. It also shows that PM-10 following a bimodal distribution centred on 0.6 and 6µm. There are probably three major sources of pollution: road traffic and the secondary particles to PM-3 and terrigenous sources for PM-(3-10). The study of heavy metals showed the presence of high levels of lead associated with very fine particles and Fe-Mn crust in the coarse particles. In Algeria, the vehicle fleet is rather old with a low level of maintenance and the use of leaded fuel are the main reasons of high pollutant emissions of fine particles associated to high levels content of lead particles. In addition, arid climate is a source of a large part of air pollution by coarse particles.

Références

Boughedaoui M., R. Kerbachi.et R. Joumard (2004) : Mesure de la pollution plombifère dans l'air ambiant d'Alger, *Poll. Atm.,* N°121,105-111

Butler J.D. (1979): Air pollution chemistry, *Academic Press ,* London, 345-352

Chiron M., P. Quenel et D. Zmirou (1997) : La pollution atmosphérique d'origine automobile et la santé publique. *Poll. Atm.,* Janvier-mars, 41-52.

Dockery D.W., C.A. Pope, X. Xu, J.D. Spengler, M.E. Ware, B.G. Fay, Jr. Ferris and F.E. Speizer (1993) : An association between air pollution and mortality in six US cities. *N. Eng. J. Med.,* 329, 1753 –1759.

Gertler A.W., M. Abu-Allaban and D.H. Lowenthal (2006), The mobile source contribution to observed PM-10, PM-2,5 and VOCs in The greater Cairo area, 15e Colloque international *" Transport et pollution de l'air", proceedings N°107*, Vol. 1, Inrets Ed., Arcueil, France, 2006, 263-269

Janssen N. A. H., D. F.M. Van Mansom, K. Van Der Jagd, H. Harsema and G. Hoek (1997): Mass concentration and elemental composition of airborne particulate matter at street and background locations. *Atm. Env.,* vol. 31, N°8, 1185-1193.

Journal officiel des Communautés européennes (1999): L 163/41, directive 1999/30/CE du 27 avril 1999, Bruxelles.

Journal officiel de la République algérienne démocratique et populaire (2006), Décret N° 06-02 du 7 janvier 2006 définissant les valeurs limites, les seuils d'alerte et les objectifs de qualité de l'air en cas de pollution atmosphérique

Kerbachi R., M. Boughedaoui, L. Bounouna, M. keddam (2006a), Ambiant air pollution by aromatic hydrocarbons in Algiers, *Atm. Env.,* 40, 2006 , 3995-4003

Kerbachi R., M. Boughedaoui, A. Bitouche et R. Joumard (2006b) : Etude de la pollution de l'air par les particules fines PM-10, PM-2,5 et PM-1 et évaluation des métaux lourds qu'elles véhiculent en milieu urbain, 15e Colloque international "*Transport et pollution de l'air", proceedings N°107*, Vol. 2, Inrets Ed., Arcueil, France, 2006, 213-218

Ministère de l'Ecologie, de l'Energie, du Développement durable et de l'Aménagement du territoire, France (2007), Bilan de la qualité de l'air 2006, rapport du 7 mars 2007

Pope C.A., M.J. Thun, M. Namboodira, D.W. Dockery, J.S. Evans, F.W. Speizer and Jr. C. W. Heath (1995) : Particulate air pollution as a predictor of mortality in a prospective study of U.S. adults. *Am. J. Respir. Crit. Care Med., vol. 151, N°3*, 669-674.

Schroeder W.H. et al. (1987): Toxic trace elements associated with airborne particulate matter, A review. *JAPCA*, 37, 11, 1267 – 1285.

U.S.- Environmental Protection Agency (1997): National ambient air quality standards (NAAQS) for particulate matter, *Federal Register,* vol.62, N° 138.

WHO, Air quality guide line, *Global update 2005*, particulate matter, ozone, nitrogen dioxide and sulphur dioxide, Genova 2005.

Zhuyun Xu, M. Gautam and S. Mehta (2002), Cumulative frequency fit for particle size distribution, *Appl. Occup. Env. Hyg.,* volume 17(8), 538-542

Emission Factors Derived from Measurements in the Gubrist Road Tunnel

Markus Meier[1], Roy Eugster[1], Urs Schaufelberger[1], Peter Maly[1], Urs Steinemann[2], Franz Zumsteg[2]
[1] OSTLUFT, Switzerland, [2] US+FZ Consultants, Switzerland

The Campaign

Since 1990 the office of waste, water, energy and air of the Canton Zurich has conducted measuring campaigns in the Gubrist tunnel near the city of Zurich. The measurements of the year 2008 were undertaken in cooperation with OSTLUFT. With the gathered data the emission factors of motor vehicles under real conditions were calculated. The campaigns focus on the driving situation 'highway, 100 km/h, uphill slope of 1.3 %' relating to the 3.2 km long, unidirectional two lane tube.

The most recent campaign was led from April 19th to June 30th, 2008. The emitted pollutants resulted from the difference between the concentrations at the exit portal and the entrance portal. As the vehicle passage time is approximately 2 minutes, an averaging sequence of 5 minutes was chosen. Thus around 10,000 data points could be validated for the directly measurable substances NO, NO_2, NO_x, CO and TVOC. Additionally PM10 and the opacity of the tunnel air were recorded. The fractions of elementary carbon EC and organic carbon OC resulted from the analyses according to TOT (EUSAAR2) of the PM10. The emission factors resulted from these data together with detailed traffic counts according to Swiss10 and the air flow through the tunnel. The chosen method allows to determine emission factors for vehicles shorter than 7 m, mainly personal cars and light duty vehicles, as well as for heavy duty vehicles longer than 7 m.

The Results

1 - Emission reduction of gaseous substances

The results show a tremendous reduction of the total NO_x-, CO- and TVOC-emission factors since 1990.

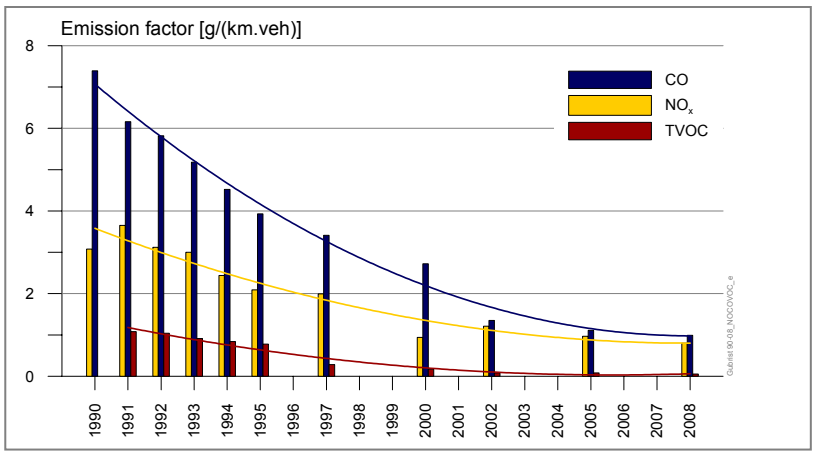

Development of the average emission factors of NO_x, CO and TVOC since 1990 in the uphill tube of the Gubrist tunnel

2 - Emission increase of small particles

Based on the Swiss motor vehicle statistics of September 2007 the Diesel-fraction of personal cars was 13 % and of light duty vehicles 61 %. The tendency to more Diesel driven engines is still strong. The results of the EC-analyses performed since the year 2002 reflect this development clearly.

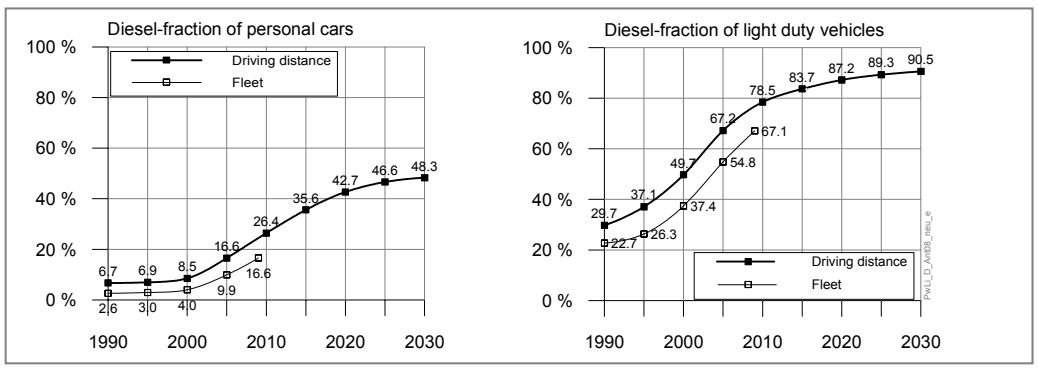

Rise of the Diesel-fraction of personal cars and light duty vehicles in Switzerland. The driving distance of Diesel driven vehicles is remarkably higher than their fraction in the car fleet.

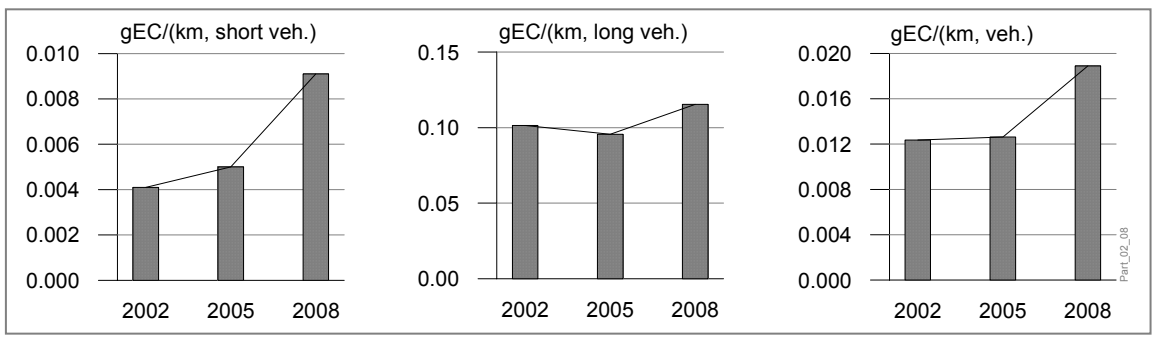

Development of EC-emissions since 2002 in the Gubrist tunnel

Between 2002 and 2008 the values for short vehicles were doubled.

3 - Comparison with Data from the Handbook Emission Factors 3.1

The measurement report update of April 2010 (www.ostluft.ch) includes the comparison of the evaluated emission factors with the indications in the recently published Handbook Emission Factors (HBEFA) Version 3.1. The values for NO_x, CO and TVOC relate exclusively to the situation with free flowing traffic with 100 km/h on a highway with a slope of +1.3 % as in the Gubrist north-bound tube.

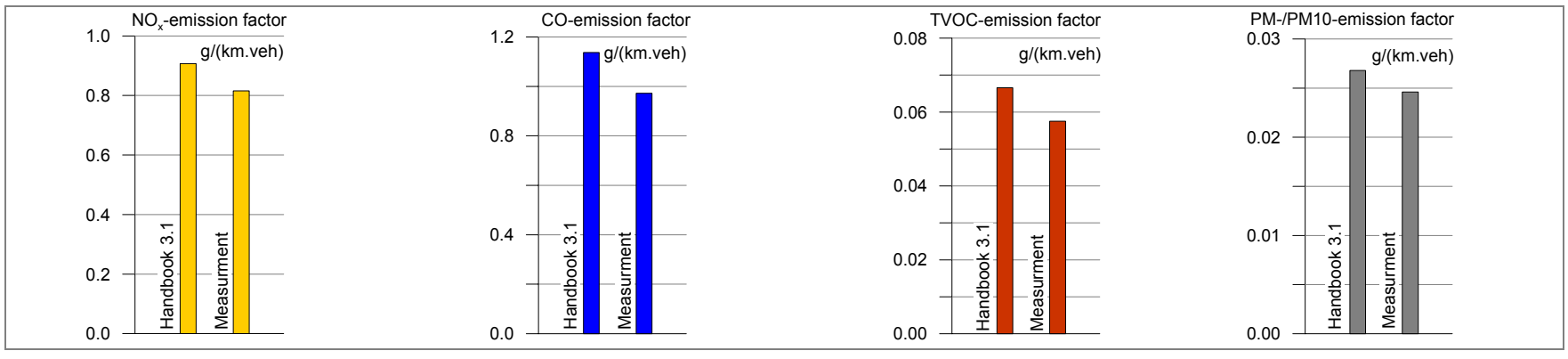

NO_x: 10 % lower | *CO: 15 % lower* | *TVOC: 14 % lower* | *PM10: 8 % lower than PM in HBEFA*

Emission factors: For the traffic with 6 % of long vehicles through the Gubrist tunnel the measurements indicate slightly lower values than the Handbook calculated at (Land/AB/100/flüssig; „BAU" (CH); 1.292 %; Klimaanlage Frühling). PM does include neither friction nor resuspension contributions.

Long-term Trends in Nitrogen Oxides, total-NMVOCs and Ozone in the Swiss Planetary Boundary Layer deduced from the NABEL-Network

J. Staehelin [1], B. Struchen [1] and C. Hueglin [2]

[1] Institute for Atmospheric and Climate Science, Swiss Federal Institute of Technology Zuerich (ETHZ), 8092 Zuerich, Switzerland, Johannes Staehelin@env.ethz.ch
[2] Empa, Swiss Federal Laboratories for Materials Testing and Research, CH-8600 Duebendorf, Switzerland

Introduction

Ozone is the most important air pollutant of photochemical smog. High ozone concentration in ambient air can affect human health and significantly reduces agricultural crop yields (e.g. Roy. Soc, 2008). Ozone and other photooxidants are formed in the troposphere from its precursors (nitrogen oxides (NO_x: $NO+NO_2$), volatile organic compounds (VOCs) and carbon monoxide (CO)) under the influence of solar ultraviolet radiation.

Between the late 1950s and the early 1990s surface ozone concentrations more than doubled in the Swiss resort village Arosa and similar changes were documented at other rural, remote and alpine sites in Europe (Staehelin et al., 1994). This large ozone increase is commonly attributed to the large increase in anthropogenic ozone precursor emissions which took place in all industrialized countries in the period of the extraordinary economic growth following World War II. Measures to reduce anthropogenic emissions of ozone precursors were introduced in Europe in the late 1980s and they were particularly successful in the early 1990s in Germany, Switzerland and England and some other European countries (EEA, 2009), e.g. as consequence of the successful introduction of catalytic converters in gasoline driven road traffic vehicles (e.g. Colberg et al., 2005). A decrease in NO emissions leads to increasing ozone concentrations in urban areas (due to less effect of the fast reaction of NO with O_3, called titration), whereas at rural sites decreasing ozone concentration are expected downwind of decreasing large emission sources of VOC and NO_x if photochemical ozone production becomes more effective than the effect of titration. Ox ($O_3 + NO_2$) can be used instead of ozone in order to compensate the effect of titration of ozone caused by close NO emission sources.

Decreasing ozone concentrations as expected from the decrease in ozone precursor emission were reported from monitoring sites in England (e.g. Derwent et al., 2003). Ordóñez et al. (2005) analyzed long-term daily ozone summer maxima from 12 Swiss ozone (and Ox) monitoring sites located in Switzerland north of the Alps (covering the period 1990 to 2003) using ANCOVA for meteorological adjustment. They found only small decreases at suburban and rural sites when restricting the measurements to the 90th percentile of daily ozone maxima. In this study we use generalized additive models (GAM) instead of ANCOVA for adjustment of the effect of meteorology on ozone summer maxima. This study covers an extended time period from 1990 to 2007, and we include two additional monitoring sites located in the Southern part of Switzerland. Our findings for meteorologically adjusted ozone maxima are compared with recent numerical simulations (EEA, 2009). Finally, the trend of ozone precursors (NO_x and t-NMVOC) is also investigated.

Measurements and Methods

The Swiss national air pollution monitoring network (NABEL) operated by Empa and the Swiss Federal Office for the Environment (FOEN) provides continuous high quality ambient air pollutant measurements. The sites are selected to provide an overview in ambient air pollutant concentrations at different representative conditions in Switzerland and their long-term changes. The sites (see Fig. 1) are classified into *Urban traffic related*: Bern (BER): Lausanne (LAU); *Urban background*: Zuerich (ZUE) Lugano (LUG); *Suburban*: Basel (BAS), Duebendorf (DUE), *Forest site:* Laegern (LAE): Rural *traffic related*: Haerkingen (HAE), Sion (SIO); *Rural*: Taenikon

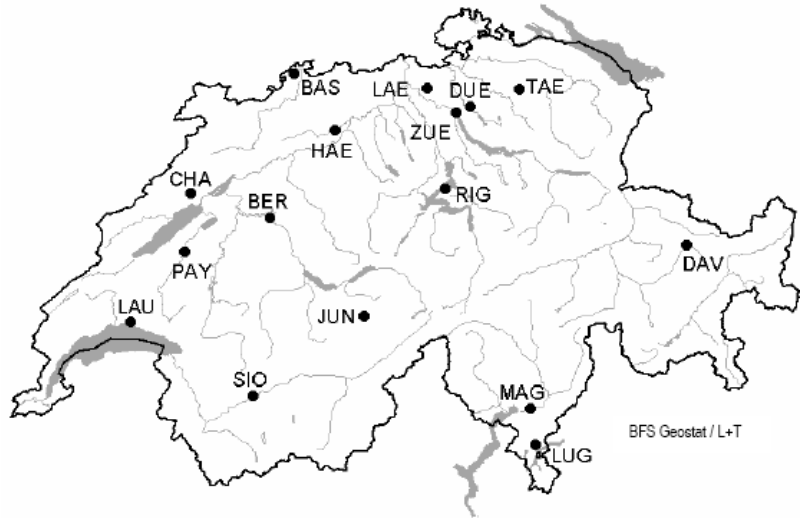

Figure 1: Sites of the Swiss ambient air pollutant monitoring network NABEL (see text).

(TAE), Payerne (PAY), Magadino (MAG); *Rural above 1000m a.s.l.:* Chaumont (CHA), Rigi (RIG); *Alpine*: Davos (DAV); *High alpine*: Jungfraujoch (JUN). The compounds analyzed in this study include O_3, NO_x, total non methane volatile organic compounds (t-NMVOC) and Ox. Conventional type of measurement methods are applied (see Empa, 2009).

Ambient air concentrations strongly depend on prevailing meteorological conditions. For meteorological adjustment GAM models (Wood, 2006, p.121) were used. We analyzed summer measurements and applied GAM models to every station and species separately. The target values of the study were: daily means for NO_x and t-NMVOC, and the mean and 90^{th} percentile of the daily maximum hourly average of O_3 and Ox. The meteorological covariates for the individual sites and species were determined by forward selection testing approximately 60 meteorological quantities using the same meteorological variables as described by Ordóñez et al. (2005). For summer daily ozone maxima the most often selected meteorological covariates were: afternoon temperature, global radiation, water mixing ratio or relative humidity, wind direction and/or wind speed, day of the week, and days after frontal passage. In the final models only 4-5 meteorological predictors were used which explained the largest part of meteorological variability. For trend determination several approaches were tested, it turned out that trend results were robust and did not depend much on the chosen method; for more details see Struchen (2009).

Results

Fig. 2 shows that a substantial part of interannual variability in ambient air concentration of t-NMVOC (available only for Dübendorf, Zürich and Locarno) can be explained by applying the GAM model; note that the downward trends were large (relative decrease for the period 1990 to 2007 around 50% in Zürich and 60% for Duebendorf). For NO_x the reductions were determined to be 32-55%. The large reductions are consistent with the information of the anthropogenic emission inventory of FOEN documenting the successful reduction of ozone precursors in Switzerland.

Total NMVOC measurements for Lugano are only available since 2000 showing a very fast decrease (around 60%); note, that Lugano is located in the Ticino area which is South of the Alps. Ambient air concentrations in the Ticino area can be influenced by the emissions of the close Milan capital area which is strongly industrialized. It was documented earlier, that polluted air masses from the Milan area can be transported to the Southern part of Switzerland (Prevot et al., 1997). The decrease in t-NMVOC in Lugano might be partially attributable to primary

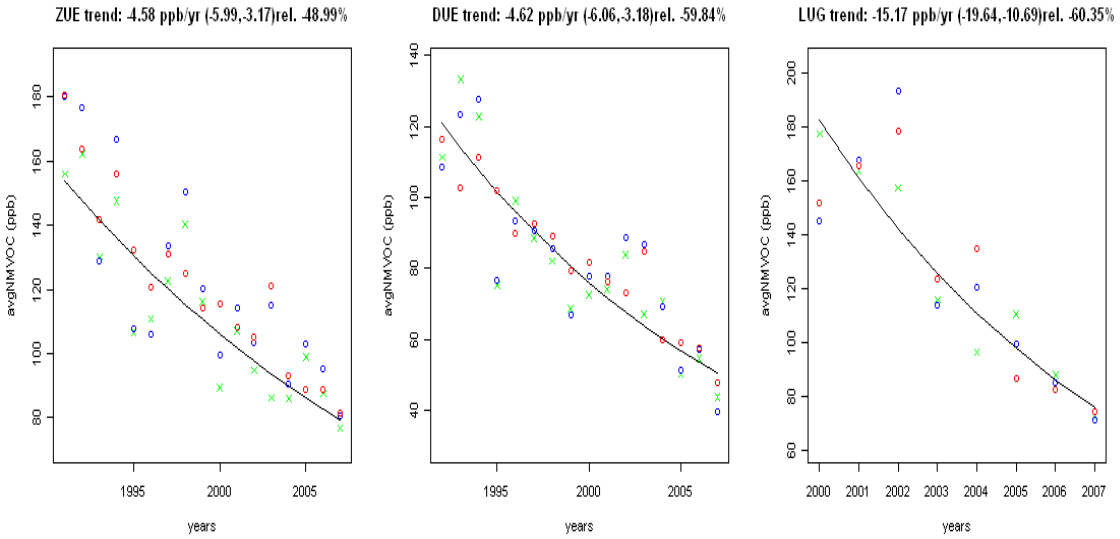

Figure 2: Long-term trends for summer t-NMVOC measurements of the NABEL sites Zürich (left side), Duebendorf (middle) and Lugano (right side). The circles denote the measured seasonal averages and the fitted values, the crosses denote the meteorologically adjusted seasonal t-NMVOC values. The lines represent a fit to the meteorologically adjusted data.

emission decrease in Northern Italy if it is assumed that a reduction in primary emission occurred later in Northern Italy than in Switzerland

The results of the GAM model when applied to the seasonal mean of the daily O_3 maxima (see Fig. 3) show increases at urban sites which are expected because of the decrease in NO emissions leading to less titration. For O_x no significant increases in daily maxima were found at polluted sites confirming that decreasing NO emissions are mainly responsible for O_3 increases at urban areas. However, despite the large decreases in ozone precursor concentrations no significant decrease at rural monitoring ozone time series was found. Only when using the 10% of highest daily maxima of O_3 (90 percentiles) the meteorologically adjusted ozone measurements are in (qualitative) agreement with the expectation from ozone precursor decreases: they show decreasing ozone concentrations at suburban, rural and prealpine series, from which, however, only three are statistically significant. These results are similar to earlier findings reported by Ordóñez et al. (2005).

Discussion and Conclusion

Ozone decreases of the summer daily ozone maxima deduced from the Swiss monitoring network are only significant at a few rural sites if the GAM model is applied to 90th percentile values. The magnitude of the decrease at suburban and rural sites is in the order of 10% (90th percentiles) which is rather small compared to the decrease in t-NMVOC (50-60%) and NO_x (32-55%) (period: 1990-2007). The European Environmental Agency recently published a report on ground level ozone in the EEA member countries (EEA, 2009). They modeled ground level ozone concentrations from 1995-2005 on a 50*50km grid using the regional EMEP Unified Chemical Transport Model. In the numerical simulations meteorology as well as the decrease in emissions of ozone precursors was described. They compared the modeling results with measurements of 40 rural background stations with at least 10 years of data in 8 countries. Besides modeling the long term trends of surface ozone, also statistical trend estimation by linear regression of monitoring measurements was done. The comparison of modeled trends and statistically estimated trends showed reasonable agreement for several countries, however, large inconsistencies were found for Switzerland and Austria. Different ozone quantities were modeled, including the mean of the ten highest daily maximum ozone concentrations (MTDM) (based on one hourly mean data) for April – September. This measure is comparable to the 0.9 percentile of daily maximum ozone concentrations during summer used in this study. In

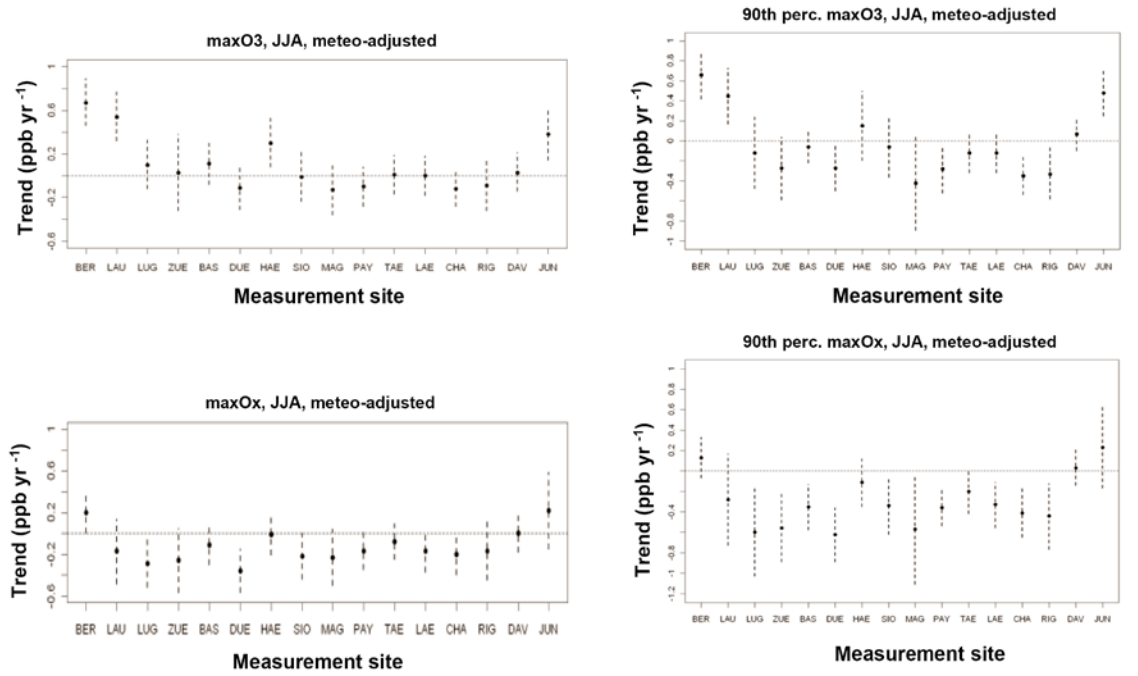

Figure 3: Trends of the mean of daily maxima (left side) and 90 percentile of daily maxima (right side) of O_3 (top panel) and Ox (bottom panel) for summer values (JJA - June, July and August) determined by meteorological adjustment using the GAM model for individual NABEL sites (period 1990-2007) (see text). The individual NABEL sites are grouped according to NO_x concentrations decreasing from the left to the right (NO_x concentrations are largest at BER (Bern) and lowest at JUN (Jungfraujoch)).

particular for Switzerland a trend of about -1.25 pbb/yr was predicted whereas the trends derived from the measurements were almost zero and statistically insignificant.Downward surface ozone trends from our study based on the meteorologically adjusted 90th percentiles are around a factor three smaller than the predictions of the numerical simulations. During the 1990s ozone concentrations at the high alpine site Jungfraujoch increased as first noted by Brönnimann et al. (2002). Ozone measured at Jungfraujoch represent to a large extent free tropospheric air. Upward mixing of air from the polluted boundary layer (PBL) of the Swiss plateau into the free troposphere was studied in detail (so called mountain venting, e.g. Henne et al.). If mixing of polluted PBL air into the free troposphere is enhanced by mountains (such as the Alps) it is reasonable to assume that high mountains are also leading to enhanced downward mixing of free tropospheric air into the PBL of the Swiss plateau. Such a downward mixing of increasing ozone might have partially compensated the expected effect of ozone precursor reduction in the Swiss planetary boundary layer air. A similar hypothesis was presented by comparison of numerical simulations with ozone measurements (Andreani-Aksoyoglu, 2008). (Note that the Emep model (EEA, 2009) did not account for the increase in ozone concentrations in free tropospheric air.)

Another question concerns the scientific causes that have been responsible for increasing ozone in free tropospheric air advected from the Atlantic. Ordóñez et al. (2007) provided evidence from empirical analysis that ozone changes in the lower stratosphere could have caused the ozone increase found during the 1990s at high Alpine sites such as Jungfraujoch, Zugspitze (Germany) and Sonnblick (Austria).

References

Andreani-Aksoyoglu, S., J. Keller, C. Ordóñez, M. Tinguely, M. Schultz, and A.S.H. Prévôt (2008), Influence of various emission scenarios on ozone in Europe, Ecol. Model., doi:10.1016

Brönnimann, S., B. Buchmann, and H. Wanner (2002), Trends in near surface ozone concentrations in Switzerland: the 1990s, *Atmos. Env*., 36, 2841-2852.

Colberg, C.A., B. Tona, W.A. Stahel, M. Meier, J. Staehelin (2005), Comparison of a road traffic emission model (HBEFA) with emissions derived from measurements in the Gubrist road tunnel (Switzerland), *Atmos. Environm*., 39, 4703-4714.

Derwent, R.G., M.E. Jenkin, S.M. Saunders, M.J. Pilling, P.G. Simmonds, N.R. Passant, G.J. Dollard, P. Dumitrean, A. Kent (2003), Photochemical ozone formation in north west Europe and its control, *Atmos. Environ*., 37, 1983-1991.

Empa (2009), Technischer Bericht zum Nationalen Beobachtungsnetz für Luftfremdstoffe (NABEL), Empa, Dübendorf.

European Environmental Agency (EEA 2009), Assessment of ground-level ozone in EEA member countries, with a focus on long-term trend technical report series: ISSN 1725-2237.

Henne, S., J. Dommen, B. Neininger, S. Reimann, J. Staehelin and A. S.H. Prévôt (2005), Influence of mountain venting in the Alps on the ozone chemistry of the lower free troposphere and the European pollution export, *J. Geophys. Res*., 110, D22307, doi:10.1029/2005JD005936.

Ordóñez, C., H. Mathis, M. Furger, S. Henne, C. Hüglin, J. Staehelin and A. S.H. Prévôt (2005), Changes of daily surface ozone maxima in Switzerland in all seasons from 1992 to 2002 and discussion of summer 2003. *Atmos. Chem. Phys.*, 5, 1187-1203.

Ordóñez, C., D. Brunner, J. Staehelin, P. Hadjinicolaou, J.A. Pyle, M. Jonas, H. Wernli, A. S.H. Prévôt (2007), Strong influence of lowermost stratospheric ozone on lower free tropospheric ozone changes over Europe, *Geophys. Res. Lett*., 34, L07805, doi:10.1029/2006GL029113.

Prévôt, A.S.H., J. Staehelin, G.L. Kok, R.D. Schillawski, B. Neininger, T. Staffelbach, A. Neftel (1997), The Milan phootoxidant plume, *J. Geophys. Res.,* 102, 23,375-23,388.

Royal Society, Ground-level ozone in the 21st century: future trends, impacts and policy implications, 2008.

Staehelin J., J. Thudium, R. Bühler, A. Volz-Thomas, and W. Graber (1994), Trends in surface ozone concentrations at Arosa (Switzerland), *Atmos. Environ*., 28, 75-87.

Struchen, B. (2009), Long-term surface trends of ozone and its precursors species in Switzerland, A GAM model approach, Master thesis, Institute for Atmospheric Science, ETHZ.

Wood, S.N. (2006), Generalized Additive Models – An Introduction with R. Chapman & Hall/CRC. ISBN: 1-58488-474-6.

Meteorological influences upon airport air quality in Zurich, Paris CDG, Athens and Mexico City

Klaus Schäfer[*1], Carsten Jahn[1], Maria Hoffmann[1], Edgar Flores-Jardines[1], Stefan Emeis[1], Michel Grutter[2], Ralf Kurtenbach[3], Peter Wiesen[3]; Costas Helmis[4], Maria Tombrou[4], Dimosthenis Asimakopoulos[4], Evi Anamaterou[5], Michael O'Connor[5], Richard Ramaroson[6], Emanuel Fleuti[7], Christoph Münkel[8]*

[1] Karlsruhe Institute of Technology, Institute for Meteorology and Climate Research, Atmospheric Environmental Research (KIT/IMK-IFU), 82467 Garmisch-Partenkirchen, Germany

e-mail: klaus.schaefer@kit.edu

[2] Centro de Ciencias de la Atmósfera (CCA), Universidad Nacional Autónoma de México (UNAM), México D.F. 04510, México

[3] Bergische Universität Wuppertal (BUW), Faculty of Natural Sciences and Mathematics, Department of Chemistry, Laboratory for Physical Chemistry, 42097 Wuppertal, Germany

[4] National and Kapodistrian University of Athens (NKUA), Department of Environmental Physics and Meteorology, Faculty of Physics, 15784 Athens, Greece

[5] Athens International Airport S.A. (AIA), Environmental Services Department, 19019 Spata, Greece

[6] Harvard University, SEAS, Cambridge, MA 02138, USA

[7] Unique (Flughafen Zürich AG), CH-8058 Zurich, Switzerland

[8] Vaisala GmbH, 22525 Hamburg, Germany

Abstract

The meteorological influences upon airport air quality were studied in several regions characterised by different weather situations. The particulate and trace gas load was measured together with the mixing layer height as well as the emissions at Zurich airport in 2004, at CDG airports near Paris in 2005, at the Mexico City International Airport in 2006 and at the Athens International Airport in 2007. The continuous determination of the mixing layer height was performed by a ceilometer on the basis of a software for routine retrieval of measured data. Further, mixing layer height was determined by remote sensing with a Doppler-sodar (sound detection and ranging). Vertical wind profiles and turbulence parameters up to 1300 m maximum were measured by this method too.

The continuous MLH data were correlated with simultaneous measured air pollutants.

The influences of mixing layer height upon air quality are relevant. The detailed results of these influences in relation to the airport and aircraft emissions are shown and discussed. It is concluded that at an airport with widespread emission sources the air quality is influenced by the meteorological conditions as at urban background regions which were studied also.

1. Introduction

To study meteorological influences upon airport air quality measurement campaigns were performed in several regions characterised by different weather situations. The main idea is to investigate the local air quality, the emission sources and the transport of the air pollutants. On the basis of this information the environmental impact should be studied and the future development predicted.

The objectives of the study presented in this paper are:

- Measurements and determination of mixing layer height (MLH), and
- Correlation of air pollutants with MLH.

An air quality monitoring campaign was performed at Zurich airport from 30 June until 15 July 2004 (see also Schürmann et al. (2007)). The particulate (PM_{10}) and trace gas load (NO_x, CO,

O_3, HC) was measured by in situ instrumentation and the MLH by the Vaisala ceilometer LD40. The measurement site was nearby a terminal building which was not in normal operation during that time.

From 15 June until 12 July 2005 a field campaign was organized at CDG airports near Paris (see also Ramaroson et al. (2009)). Air quality and ground air traffic emissions were measured continuously at terminals, taxiways and runways by DOAS (NO, NO_2) and FTIR (CO, CO_2) along with meteorological parameters and MLH by a Doppler-sodar. The following locations were used for the open-path concentration measurements by DOAS and FTIR: Test pen measurements from 15 until 17 June 2005, across a taxiway from 20 until 24 June 2005, near a gate from 27 June until 04 July 2005 and across another taxiway from 04 until 11 July 2005.

A one-week-campaign at the Mexico City International Airport (MCIA) was performed from 12 until 16 April 2006 (see also Schäfer et al. (2009a)). Air pollutants like NO, NO_x, CO and O_3 as well as meteorological parameters like wind, temperature and irradiance were measured at the airport by in situ instrumentation in addition to the air quality monitoring network RAMA in Mexico City. The MLH was measured by the ceilometer LD40.

To detect air quality (NO, NO_x, CO, O_3 and PM_{10} measured by in situ instruments at three sites at the airport area) and meteorological data a measurement campaign was carried out at the Athens International Airport (AIA) from 13 until 25 September 2007 (see also Schäfer et al. (2009b)). The campaign was realised with the aid of existing monitoring equipment at the AIA as well as at the participant partners that was transferred to the AIA and operated at two sites.

The assessment of urban air quality requires not only the knowledge of the temporal and spatial structure of meteorological parameters like wind direction and wind speed but also of the MLH, because this variable controls the vertical space for rapid mixing of near-surface pollutants. It was demonstrated that the lowest stable layer or inversion limits the vertical exchange of primary pollutants emitted at or near the surface (Schäfer et al., 2006) and thus controls the near-surface pollutant concentrations. Because MLH is a consequence of vertical temperature and moisture profiles in the lower atmosphere, remote sensing is a suitable tool to monitor MLH (Emeis et al., 2004; Emeis et al., 2006). Monitoring of mixing layer height was performed as during other measurement campaigns in urban and sub-urban areas (Hannover, Munich, Budapest, Augsburg; see Schäfer et al. (2006)) by the Vaisala ceilometer LD40. It is an eye-safe commercial mini-lidar and designed originally to detect cloud base heights and vertical visibility for aviation safety purposes. These measurements of the vertical aerosol distribution are routinely retrieved for MLH by a software which was improved continuously and compared with radiosonde data. Further, MLH was determined by remote sensing with the Doppler-sodar (sound detection and ranging) DSD3x7 from Metek (see also Schäfer et al. (2006)). Vertical wind profiles and turbulence parameters up to 1300 m maximum were measured by this method too.

2. Measurement campaign and methodology

The Vaisala Ceilometer LD40 applied here is described in more detail in Münkel (2007). It is a compact mini-lidar with a diode laser of 855 nm wavelength capable to cover an altitude range higher than 4000 m. The lowest detectable layers are around 150 m. The minimum range resolution is 7.5 m. The eye-safety class is 1M. The ceilometer backscatter profiles of the fully automated instrument are usually used to detect vertical visibility and cloud characteristics. To detect the heights of the near surface aerosol layers and the MLH the gradient method is used. The minima of the vertical gradient (the term ‘gradient minimum’ is used here to denote the most negative value of the gradient) is given as an indication of MLH or upper edge of up to 5 lifted layers (Emeis et al., 2007). An averaging over time and height enables the suppression of noise generated artefacts. A sliding averaging is done and minimum accepted attenuated backscatter intensities are set. The MLH retrieval algorithm works appropriate during nearly cloudless conditions.

MLH was determined solely from sodar data as the minimum of the height of the ground-based echo layer and the height of an elevated echo maximum (if present). The top of the lowest stable layer, the lifted inversion and the top of the turbulent layer are given. If the MLH was higher than the instrument’s range it could not be determined from sodar data and the MLH was set at this range. These problems caused an ambiguity of MLH parameters if the MLH is large.

Details on the determination and statistical evaluations of the resulting MLH are reported in Emeis and Türk (2004).

Multiple layer detection is important if residual layers are available during the late night. These conditions enable the contribution of air pollutants emitted during the day before during mixing around noon to the current air quality. One- or half-hourly-mean values are determined from these data as well as from the concentration data and applied for the correlation analyses of data.

An estimation of the total error of the correlation values is necessary to demonstrate the reliability of the determined correlation coefficients. The concentrations of NO_x, CO and PM_{10} are measured with a standard error in the order of 5 % (S_1 = 0.05). The determination of MLH from SODAR and ceilometers data has an error of about 10 % (S_2 = 0.10) if MLH is within the detection range. Thus, the overall error of correlation between the concentrations and MLH can be estimated from the following equation

Overall Standard Error = $1 - \{(1 - S_1) \cdot (1 - S_2)\}$

which is giving a value of 14.5 % for NO_x, CO and PM_{10}. Only such correlation coefficients between concentrations and MLH which are higher than this value are significant i.e. showing dependence between these data.

3. Results

3.1 Mixing layer heights

Figure 1 shows a typical evolution of a daytime convective boundary layer at AIA with increasing MLH up to 14:00. The afternoon was characterized by convective conditions. The MLH during the morning was between 600 and 900 m but during the afternoon up to about 1800 m. During the night the MLH went down to 300 m.

It can be summarized at MCIA (see Schäfer et al. (2009a) for more details) that the height of the near-surface layer during the night and the morning was between 300 m and 600 m. From the morning until about 14:00 the MLH is increasing. During the afternoon convective conditions existed and the MLH was around 2000 m or higher.

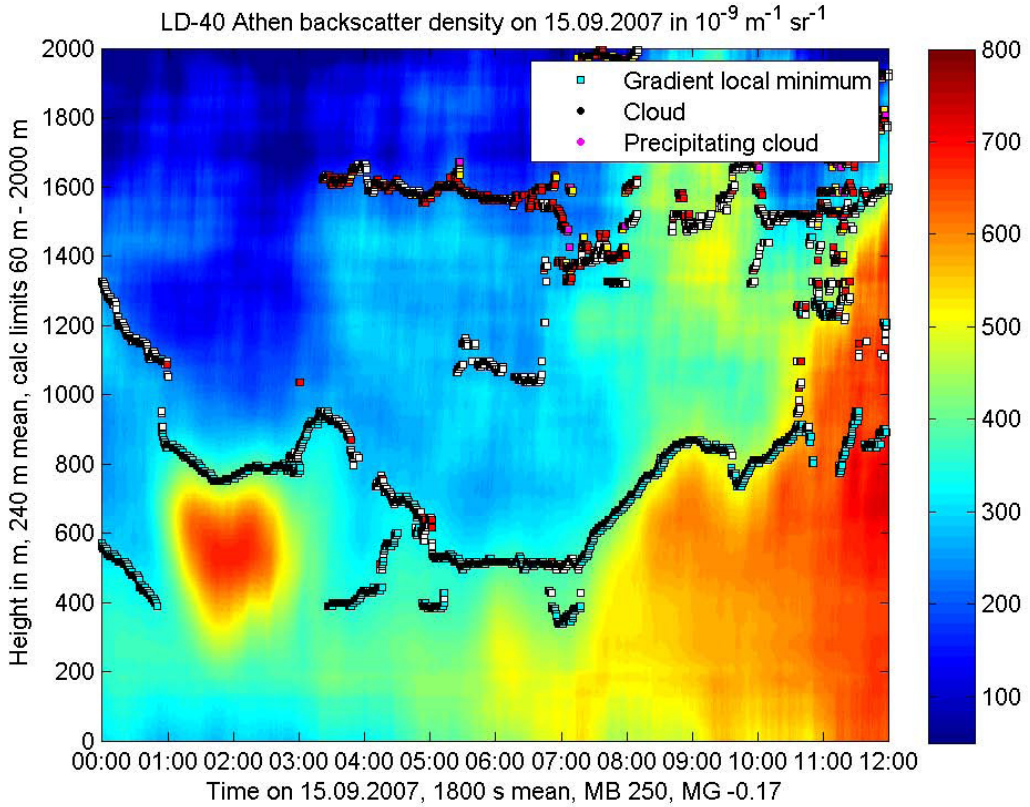

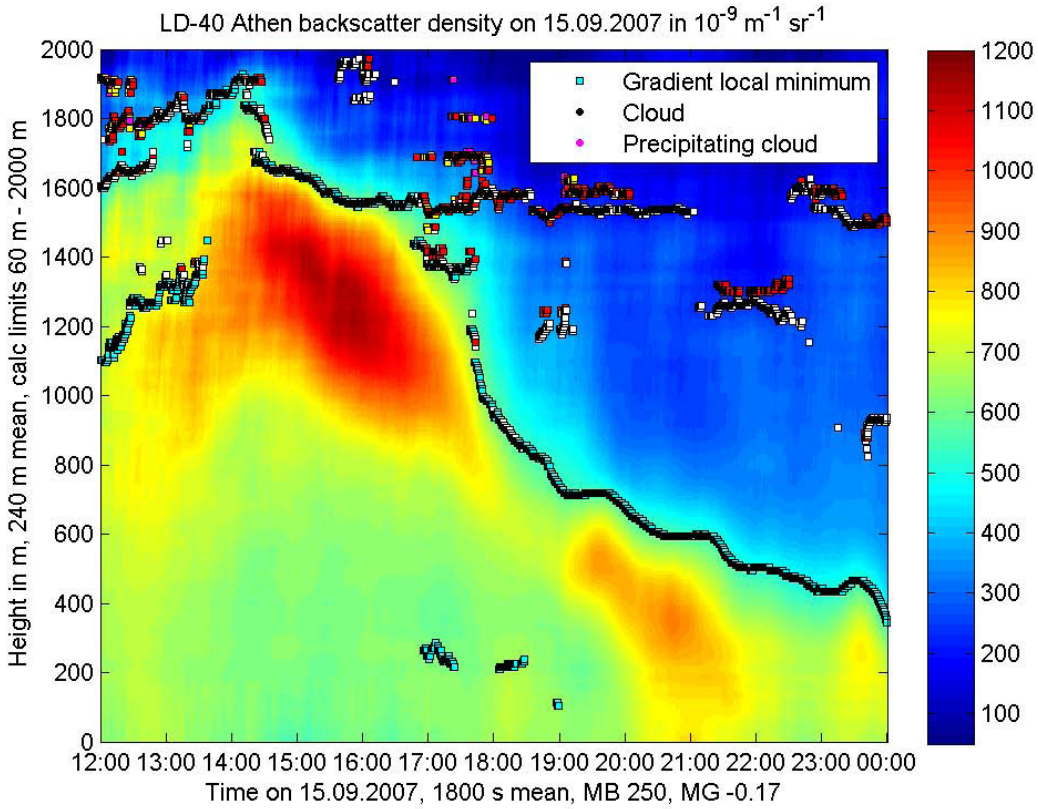

Fig. 1. Measurement results of ceilometer Vaisala LD40 at Athens International Airport to observe the vertical aerosol distribution on 15 September 2010 (00:00 - 12:00 above, 12:00 – 24:00 below). The mixing layer height is given from the local minimum of the gradient of the backscatter data of the ceilometer. The time scale is in local time.

3.2 Mixing layer height influences upon airport air quality

The correlations of one- or half-hourly-mean values of concentrations (y, in µg/m^3) and MLH (x, in m) at MCIA are the following:

CO: y=-0.51·x+3100, R^2=0.23;

NO: y=-0.01·x+21, R^2=0.08; NO_x: y=-0.04·x+87, R^2=0.16; NO_2: y=-0.02·x+54, R^2=0.19.

Consequently, the influence of the MLH upon the CO, NO_x and NO_2 concentrations is relevant (see Schäfer et al. (2009) for more details).

At AIA the CO concentrations and MLH are presented in Figure 2. The data analyses show the following results (see Figure 3 for NO_2 as an example) with y in µg/m^3 and x in m:

CO: y=-0.12·x+260, R^2=0.14;

NO: y=-0.01·x+9, R^2=0.04; NO_x: y=-0.03·x+47, R^2=0.11; NO_2: y=-0.03·x+47, R^2=0.20;

PM_{10}: y=-0.02·x+46, R^2=0.14.

The influences of the MLH upon pollutant concentrations are relevant for CO, NO_2 and PM_{10} only. In all cases an exponential dependence of the concentrations on MLH does not show a better correlation.

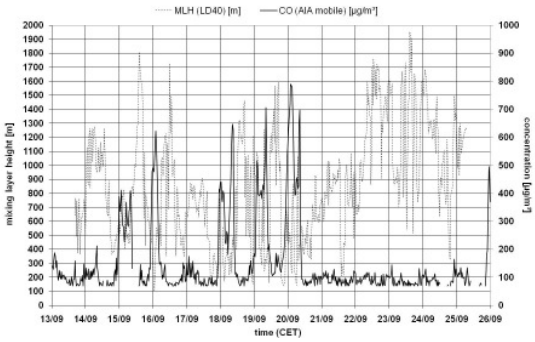

Figure 2: Concentrations of CO and mixing layer heights at Athens International Airport during the measurement campaign.

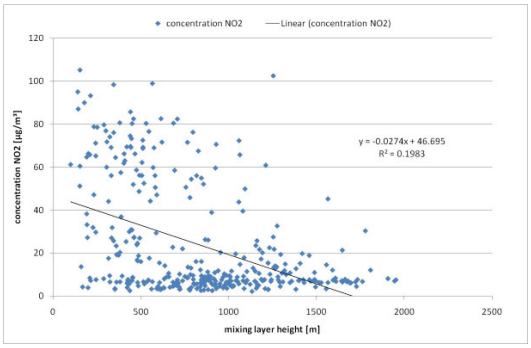

Figure 3. Correlation of NO_2 concentration and mixing layer height at Athens International Airport. The parameters of a linear regression function and the square of the correlation coefficient are given.

At Zurich airport the comparisons of half-hourly-mean values of concentrations and MLH show no significant correlation. This is not surprising because during summer time the correlations were found as the lowest ones (see Schäfer et al., 2006). The influence of MLH upon pollutant concentrations is relevant for NO_x daily-mean values only (with y in µg/m^3 and x in m):

NO_x: $y=-0.01 \cdot x+41$, $R^2=0.29$.

At Paris CDG airports the vertical range of the sodar soundings limited the availability of MLH data to night time hours only. Further, the atmosphere was well mixed during this summer time and low level jets were formed very often so that strong turbulences were available (see also Reitebuch and Emeis (1998)). Consequently, no significant correlations of concentrations with MLH were found.

4. Conclusions

The airport air quality is not only determined by the emissions and chemical transformations mainly within the frame of the ozone chemistry but also by the meteorological conditions. The influences of wind speed and MLH are significant for CO, NO_2 and PM_{10} load at MCIA, AIA and Zurich airport also. The influences of MLH upon one- or half-hourly-mean CO, NO_2 and PM_{10} concentrations at MCIA and AIA are in the order of 20 % and upon daily-mean NO_x concentrations at Zurich airport significant also.

A continuous measurement of MLH is possible by ceilometers - such instruments are available at each airport.

The significant influences of MLH upon air pollutant concentrations are in good agreement with the results described in Schäfer et al. (2006) for urban and rural background stations in the region of Munich and Hannover. It was found there that mainly during winter the MLH determines the concentration of air pollutants near the surface by about 50 % in areas which are not influenced by strong emissions and during time periods without strong vertical mixing and advection.

But the findings described here at airports that an exponential dependence of the concentrations on MLH does not show a better correlation is in contradiction to the findings in Schäfer et al. (2006). It was a hint there for a non-perfect mixing of a pollutant in the boundary layer caused by continuous emissions near the ground. It seems that the emissions of air pollutants at the airports are not so relevant in comparison to the emissions in the surroundings.

References

Emeis, S., Münkel, C., Vogt, S., Müller, W., Schäfer, K. (2004), Determination of mixing-layer height, *Atmospheric Environment*, 38, 273-286.

Emeis, S. and Türk, M. (2004): Frequency distributions of the mixing height over an urban area from sodar data. *Meteorol. Z.*, 13, 361-367.

Emeis, S. and Schäfer, K. (2006), Remote sensing methods to investigate boundary-layer structures relevant to air pollution in cities, *Bound-Lay. Meteorol.*, 121, 377-385.

Emeis, S., Jahn, C., Münkel, C., Münsterer, C., Schäfer, K. (2007), Multiple atmospheric layering and mixing-layer height in the Inn valley observed by remote sensing, *Meteorol. Z.*, 16, 415-424.

Emeis, S., Schäfer, K., Münkel, C. (2008), Surface-based remote sending of the mixing-layer height, *Meteorol. Z.*, 17, 621-630.

Münkel, C. (2007), Mixing height determination with lidar ceilometers - results from Helsinki Testbed, *Meteorol. Z.*, 16, 451-459.

Ramaroson, R., Gouriou, F., Talbaut, M., Puente Lelievre, C., Magnani, G., Fréjafon, E., Schäfer, K., Jahn, C., Schürmann, G., Hoffmann, M., Copalle, A., Vannier, F., Paux, E., Perros, P. (2009), Field experiments at Roissy CDG airports: Commercial engine emissions and Air quality, in: Proceedings of the 19th International Symposium on Air Breathing Engines (ISABE) "Technology & Skills Challenge: Powering out of turbulence", American Institute of Aeronautics and Astronautics (USA), ISABE-2009-1117; Proceedings CD.

Reitebuch, O., Emeis, S. (1998), SODAR-measurements for atmospheric research and environmental monitoring. *Meteorol. Z.*, NF, 7, 11–14.

Schäfer, K, Emeis, S., Hoffmann, H., Jahn, C. (2006), Influence of mixing layer height upon air pollution in urban and sub-urban areas, *Meteorol. Z.*, 15, 647-658.

Schäfer, K., Flores-Jardines, E., Emeis, S., Grutter, M., Kurtenbach, R., Wiesen, P., Münkel, C. (2009a), Determination of mixing layer heights by ceilometer and influences upon air quality at Mexico City airport, in: R.H. Picard, K. Schäfer, A.T. Comeron, E. Kassianov, C.J. Mertens (eds.), Remote Sensing of Clouds and the Atmosphere XIV, *Proc. SPIE* Vol. 7475 (SPIE, Bellingham, WA, USA) 74750M-1 – 74750M-11.

Schäfer, K., Emeis, S., Jahn, C., Hoffmann, M., Heyder, C., Haas, F., Helmis, C., Scouros, G., Kurtenbach, R., Niedojadlo, A., Wiesen, P., Bennett, M., Christie, S., Graham, A., Anamaterou, E., O'Connor, M. (2009b). Airport air quality data bank for modelling studies, in: *Proceedings of the 3rd conference Environment and Transport and of the 17th conference Transport and Air Pollution (ETTAP2009)*, Aurielle Charron (ed.), Actes INRETS, Institut National de Recherche Sur les Transports et leur Securite, Bron cedex, France, Vol. 122, paper-28; Proceedings CD.

Schürmann, G., Schäfer, K., Jahn, C., Hoffmann, H., Bauerfeind, M., Fleuti, E., Rappenglück, B. (2007) The impact of NO_x, CO and VOC emissions on the air quality of the airport Zurich, *Atmospheric Environment* 41, 103-118.

Meteorological influences and role of emissions within the context of air quality in Beijing

K. Schäfer[*1], Y. Wang[2], S. Norra[3], R. Shen[1], J. Xin[2], H. Ling[2], G. Tang[2], C. Münkel[4], N. Schleicher[5], Y. Yu[5], S. Emeis[1], P. Suppan[1]*

[1] Karlsruhe Institute of Technology, Institute for Meteorology and Climate Research, Atmospheric Environmental Research (KIT/IMK-IFU), 82467 Garmisch-Partenkirchen, Germany

e-mail: klaus.schaefer@kit.edu

[2] Chinese Academy of Sciences (CAS), Institute of Atmospheric Physics, LAPC, 100029 Beijing, P. R. China

[3] Karlsruhe Institute of Technology, Institute of Geography and Geoecology (KIT/IGG), 76128 Karlsruhe, Germany

[4] Vaisala GmbH, 22525 Hamburg, Germany

[5] Karlsruhe Institute of Technology, Institute of Mineralogy and Geochemistry (KIT/IMG), 76128 Karlsruhe, Germany

Abstract

Two campaigns were performed in 2009 to analyse the vertical distribution of atmospheric particles by various methods. Particles were sampled by passive sampling methods on adhesive acceptor plates in various heights. The filters were weighed before and after sampling to determine the mass concentration of sampled particulates. $PM_{2.5}$ was sampled by active samplers and by TEOM instruments during the same time.

Furthermore, a ceilometer was used to analyse the actual development of the mixing layer height and boundary layers as well as the vertical distribution of aerosols and particles.

To study the gaseous pollutants and those compounds important for secondary aerosol formation like SO_2, NO, and NO_2 or O_3, benzene, toluene, xylene, and formaldehyde a DOAS is operated since beginning of April 2009. Three open paths of the DOAS are installed to get information from air pollutants at a busy road of Beijing (connecting northern third ring road and northern forth ring road) and the living area nearby. This is supported by in situ monitoring of air pollutants at a station nearby the DOAS site.

These data are used to show the meteorological influences and the role of emissions within the context of the air quality in Beijing relevant for measures to reduce the air pollution.

1. Introduction

Beijing air quality suffers from frequently occurring air pollution events. Local and regional wind systems are able to bring fresh air masses or at least to limit air pollution over Beijing. Presumably, one main local wind system occurs in Beijing, which is a sort of mountain-valley wind system. This wind system is induced by the more than 2000 m high mountain ridge of the north-western Yundu and Xishan Mountains. On the other hand, this mountain ridge acts as a barrier for air masses coming from south-eastern directions with low velocities. During those meteorological conditions, air pollution can accumulate in the region of Beijing. Several field visits were carried out to investigate the air quality during different meteorological situations and to assess their potential impacts on Beijing's atmosphere and air pollution.

One of the important scientific questions for high air pollution in Beijing is: Which regional meteorological situations (transport and exchange conditions) and which emission processes cause high particulate matter (PM) exposures? Although it was shown for a short period in winter 2005 that intensive $PM_{2.5}$ mass concentrations are associated to southern wind directions and low $PM_{2.5}$ mass concentrations to north-western wind directions (Norra et al., 2007), many questions on the impact of meteorological conditions on the aerosol pollution in Beijing are still

not sufficiently answered. This means in detail: How much do the local wind systems influence the PM load? How much does the mixing layer height (MLH) influence the PM exposure?

To find answers for these questions two campaigns were performed in 2009 to analyse the vertical distribution of atmospheric particles by various methods. Coarse geogenic, biogenic and anthropogenic particles were sampled by passive sampling methods on adhesive acceptor plates in various heights at 8 (roof of the LAPC building) and 80 m height (at the 325 m meteorological tower) from February until April. $PM_{2.5}$ was sampled by active samplers and by TEOM instruments during the same time. Furthermore, a ceilometer was installed at the roof of the LAPC building nearby the 325-m-tower to analyse the actual development of the MLH and boundary layers as well as the distribution of aerosols and particles. Also radiosonde data from a meteorological observatory in the southern suburb of Beijing were used. To study the gaseous pollutants and those compounds important for secondary aerosol formation like SO_2, NO, and NO_2 or O_3, benzene, toluene, xylene, and formaldehyde a DOAS is operated at the roof of the LAPC building since beginning of April 2009. The DOAS measurements are performed along three different open paths across and away from the third ring road of Beijing so that horizontal spatial variations of air pollutants and the contribution of traffic emissions to air quality can be estimated. This is supported by in situ monitoring of air pollutants at a station nearby the DOAS site.

Some results of these studies of air pollution by particulate matter in various heights, composition of particles during different meteorological situations as well as of gaseous air pollution nearby a major traffic emission source will be presented to show the meteorological influences and the role of emissions within the context of the air quality in Beijing relevant for measures to reduce the air pollution, such as:

- High particulate load, when MLH is much lower than 1000 m and winds reach Beijing from the North-East;
- Low particulate load and winds from the West / North-West, transporting dry air masses;
- Higher particulate loads during winds from the South-West, transporting particulate loaded air masses;
- “Dust clouds” transported by winds from the West / North-West;
- Multiple layering of the lower atmosphere.

First results of these investigations were presented already (Schäfer et al., 2009).

2. Methodology

Air pollution episodes in urban areas often occur during low wind speeds and low MLH and can not only be ascribed to increased local anthropogenic emissions. An important factor, which influences exchange processes of ground level emissions, is the MLH whose quantitative knowledge is important for the understanding and analysis of air pollution episodes (Schäfer et al., 2006). Air pollutants emitted from the ground can accumulate up to the MLH and if the MLH is located near to the ground air pollution can be high due to a strongly limited air mass dilution. To study these processes in more detail, the correlations of particulate concentrations with MLH are investigated.

One-hourly-mean and daily-mean-values are determined from these data as well as from the concentration data and applied for the correlation analyses.

An estimation of the total error of the correlation values is necessary to demonstrate the reliability of the determined correlation coefficients. The concentrations of $PM_{2.5}$ and trace gases are measured with a standard error in the order of 5 % ($S_1 = 0.05$). The determination of MLH from ceilometer data has an error of about 10 % ($S_2 = 0.10$) if MLH is within the detection range. Thus, the overall error of correlation between the concentrations and MLH can be estimated from the following equation

$$\text{Overall Standard Error} = 1 - \{(1 - S_1) \cdot (1 - S_2)\}$$

which is giving a value of 14.5 % for all compounds. Only such correlation coefficients between concentrations and MLH which are higher than this value are significant i.e. showing dependence between these data.

2.1 Mixing layer height

Remote sensing capabilities were used here to monitor MLH (Emeis et al., 2004; Emeis et al., 2006). The ceilometer Vaisala LD40 was operated to observe the vertical aerosol distribution (Emeis et al., 2007). The performance of the compact lidar working with a diode laser at 855 nm wavelength called ceilometer is originally used to investigate cloud layers, vertical visibility, and cloud cover is sufficient to determine convective layer depths exceeding 2000 m. It enables the detection of nocturnal stable layers down to 150 m. The two lens optical design of this ceilometer provides sufficient overlap of the transmitter and the receiver field-of-view over the whole measuring range and allows reliable detection of nocturnal stable layers. The instrument runs in fully automated, hands-off operation mode. Laser power and window contamination are permanently monitored to provide long-term performance stability.

The heights of the near surface aerosol layers and the MLH can be analyzed from optical vertical backscatter profiles (Emeis et al., 2008). Here the gradient method is used (Münkel, 2007). In this method these heights are characterized by minima of the vertical gradient (the term 'gradient minimum' is used here to denote the most negative value of the gradient) of the optical attenuated backscatter intensity. This approach has been refined and extended to enable the calculation of up to five lifted inversions (Emeis et al., 2007).

For a better understanding of the results presented here, the applied method is shortly summarized in the following. Prior to the determination of gradient minima the overlap and range corrected attenuated backscatter profiles are averaged over time and height to suppress noise generated artefacts. Therefore the height values of the aerosol layers are determined in a two-step procedure. Between ground and 900 m height sliding averaging is calculated over 20 min for a variable height interval Δh. Up to 200 m height Δh is 80 m; every 100 m it is increased by 20 m. Above 900 m, Δh is 240 m. Two additional parameters have been introduced to further reduce the number of false hits. The minimum accepted attenuated backscatter intensity right below a lifted inversion is set to $300 \cdot 10^{-9}$ $m^{-1}sr^{-1}$. Additionally, the threshold determining whether a vertical gradient minimum of the backscatter intensity is reported as a lifted inversion is set to $-MB \cdot 0.625 \cdot 10^{-4}$ m^{-1}, where MB is the mean backscatter intensity up to a height of 1000 m.

2.3 Particulate concentrations

At LAPC $PM_{2.5}$ was collected on quartz fibre filters (Whatman) by means of a Mini-Volume Sampler (Leckel GmbH, Berlin). The pump rate was 200 l/h. According to the duration of the sampling interval filters of 25 mm or 50 mm in diameter were used. The necessary weighing procedures were carried out at the IMG. $PM_{2.5}$ was sampled on the roof-top of the LAPC building in 8 m height and on the LAPC meteorological tower at 80 m height in parallel to in situ measurements of $PM_{2.5}$ concentrations by TEOM instruments. Both methods to determine concentrations (weighing of filters and in situ measurements) were compared and showed a mean deviation of 0.83 and 0.82 in 8 m and 80 m height correspondingly.

2.4 Particle composition

The quartz fibre filters were analysed by ICP-MS for trace elements and main elements (Norra et al., 2007).

2.5 Gaseous concentrations

To study different emission sources by one instrument an open-path DOAS (providing a path-integrated air pollution information in different directions) was used for measurements of NO, NO_2, SO_2, O_3, Benzene, Toluene, Xylene and HCHO concentrations. The DOAS from OPSIS GmbH contains an analysator (AR 500) and an emitter/receiver unit (ER 130) pointing to three retroreflectors. One retroreflector was installed at a lamp mast on the other side of the motorway (568 m path length, path 3) so that the path was about 10 m above motorway level and perpendicular across the motorway which is connecting northern third ring road and northern forth ring road. Another retroreflector was set up for a path (126 m path length, path 1) in nearly the same direction across a normal street with shops and restaurants and the third retroreflector was used to operate a path (266 m path length, path 2) perpendicular to and away from the motorway. The emitter/receiver unit was in a distance of about 20 m to an air pollution monitoring station at the roof of that building.

3. Results

The measurement results of the ceilometer Vaisala LD40 at LAPC to observe the vertical aerosol distribution are presented below. These results and their comparisons with radiosonde data (wind vector, relative humidity and potential virtual temperature) from a meteorological observatory in the southern suburb of Beijing are plotted in the same figure and described in detail in Schäfer et al. (2009).

3.1 Particulate load and mixing layer height

3.1.1 High particulate load and low mixing layer height

During winds from the North-East near the surface and from the South-West in higher heights as on 04 March 2009 relatively high backscatter intensities can be found i.e. there is a high particulate load near the surface. The mixing layer heights during these events are up to about 700 m during the early afternoon.

3.1.2 Low particulate load and winds from West / North-West

Winds from the West / North-West in all heights transport continental air masses which are much dryer than from other directions. The backscatter intensities go down dramatically indicating much cleaner air. The MLH was in much higher heights.

3.1.3 Higher particulate loads during winds from South-West

Winds from the South-West transport more particulate loaded air so that the ceilometer backscatter intensity is increased showing relatively high particulate loads and coupled with a MLH between 600 m and 1000 m. Such a situation was on 07 March 2009 which is shown in Figure 1. The particulate load was still growing during the day indicated by the increasing ceilometer backscatter intensity. The MLH increased during the day. The relative humidity, the virtual potential temperature and wind vectors from radiosonde measurements at 08:00 and 20:00 local time are given too. At 20:00 the decreasing relative humidity and increasing potential virtual temperature with height agreed well with the height of the near-surface layer detected from ceilometers data (600 m).

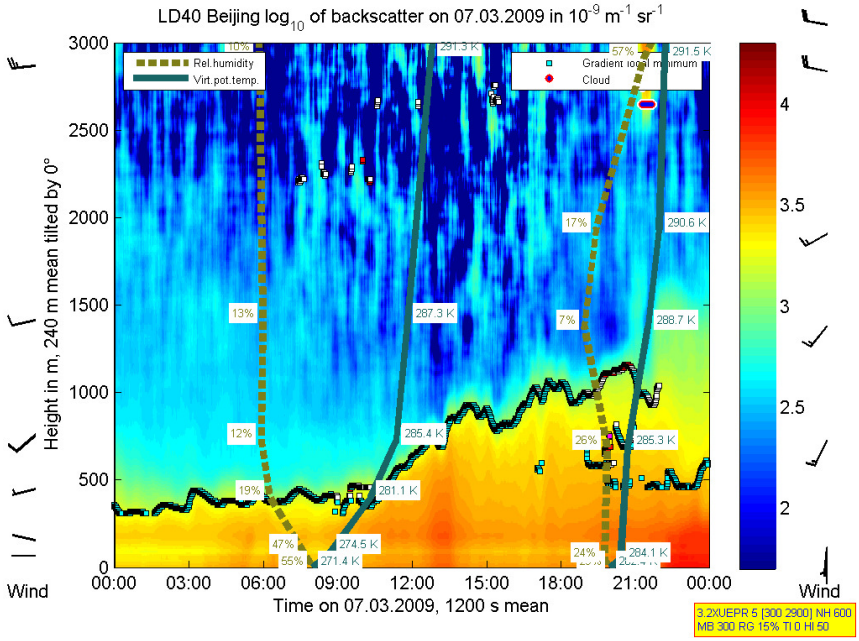

Fig. 1. Measurement results of ceilometer Vaisala LD40 at LAPC to observe the vertical aerosol distribution together with radiosonde data (wind vector, relative humidity and potential virtual temperature) from a meteorological observatory in the southern suburb of Beijing at 07 March 2009. The mixing layer height is given from the local minimum of the gradient of the backscatter data of the ceilometer as well as the relative humidity and the virtual potential temperature. The time is given as local time. The backscatter intensity is presented in different colours (see right part of the figure).

3.1.4 Dust cloud

On 15 March 2009 winds blew from West / North-West bringing dry continental air masses. During the morning hours, the backscatter intensities from the ceilometer measurements in heights above 500 m were higher than those in lower heights. The reason could be a particulate or dust cloud originated from the desert regions in that direction. During the late morning hours the dust cloud was sinking down to the surface. The relative humidity was lowest and the virtual potential temperature was highest within the dust cloud. Above the cloud both values were nearly constant. The signs “cloud” here are not real because the ceilometer signals were detected also in heights much higher than the given “cloud” level (up to 1500 m). During the afternoon hours the near-surface atmosphere became cleaner.

3.2 Multiple layering of the lower atmosphere

Multiple layers within the planetary boundary layer (up to 2000 m) height were observed when winds were from the South / South-West. The relative humidity was decreasing during the day. During the night of that day a near-surface layer was developed. All layers determined from ceilometer backscatter intensities agreed well with increasing virtual potential temperature. Above the MLH the relative humidity and the virtual potential temperature were nearly constant.

3.3 Correlations of particulate concentrations with mixing layer heights

The $PM_{2.5}$ concentrations determined by weighing were corrected by humidity and temperature. The temporal periods of the $PM_{2.5}$ samplings were the following: 26-27/02, 27-28/02, 28/02-02/03, 02-09/03, 09-16/03, 16-23/03, 23-30/03, 30/03-02/04, 02-03/04, 03-07/04, and 07-08/04. The concentrations of $PM_{2.5}$ at 8 and 80 m height and the MLH were averaged during the same measurement time periods. During high MLH (1000 – 1200 m) the concentrations were relatively low (20 – 40 µg/cm^3) and during low MLH (600 – 1000 m) the concentrations were relatively high (40 – 140 µg/m^3). The correlations between $PM_{2.5}$ concentrations from TEOM and MLH were calculated by using a linear regression. The correlations of $PM_{2.5}$ concentrations (y, in µg/m^3) with MLH (x, in m) are described by the equation
$y=-0.14\cdot x+186$ with a square of the correlation coefficient $R^2=0.41$ in 8 m height and
$y=-0.14\cdot x+182$ with a square of the correlation coefficient $R^2=0.45$ in 80 m height
i.e. the correlations in both heights are significant (see also Schäfer et al. (2009)).

Using daily mean data it was found from the TEOM $PM_{2.5}$ concentration data that there is also a significant correlation in both heights (see Figure 2). The correlation coefficients are a little bit smaller than those for averages over some days as described before. The parameters are different also. An exponential regression does not provide better correlations.

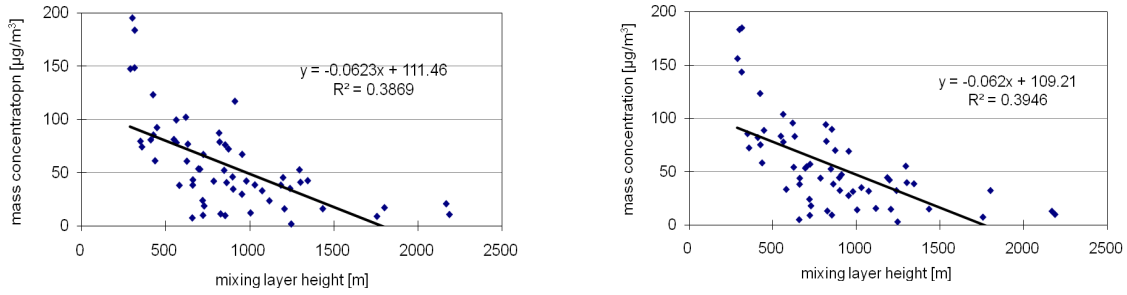

Figure 2: Correlation of daily averaged $PM_{2.5}$ mass concentrations measured by TEOM with mixing layer heights measured by ceilometers at 8 m height (left) and 80 m height (right).

To investigate the influence of temporal averaging periods the correlations of hourly mean values (y, in µg/m^3) with MLH (x, in m) were investigated with the following result:
in 8 m height $y=-0.03\cdot x+94$, $R^2=0.21$;
in 80 m height $y=-0.03\cdot x+92$, $R^2=0.23$.

3.4 Correlations of element concentrations with mixing layer height

Further, the correlations of element concentrations analysed from these $PM_{2.5}$ samples MLH were studied. There were similar linear regressions as mentioned before for the mass concentration of the ^{65}Cu and ^{66}Zn mass concentrations in both altitudes, of the ^{34}S, ^{47}Ti, ^{55}Mn, ^{56}Fe, ^{75}As, ^{111}Cd and ^{207}Pb mass concentrations in 8 m altitude only but no regressions for ^{27}Al,

^{39}K and ^{42}Ca. The main reason for these differences is the source of the elements: if it is the soil the source dominates (no MLH influence), if it is the traffic and the industry the transport dominates (no MLH influence in higher altitudes) and if it are widespread area sources the MLH dominates.

3.5 Correlation of gas concentrations from DOAS with mixing layer height

The correlations of hourly mean concentrations (y, in µg/m^3) with MLH (x, in m) within the time period 07 – 30 April 2009 for the different paths are the following:
NO_2, 1: y=-0.03·x+178, R^2=0.30; 2: y=-0.03·x+116, R^2=0.26; 3: y=-0.04·x+145, R^2=0.20;
SO_2, 1: y=-0.01·x+38, R^2=0.03; 2: y=-0.01·x+36, R^2=0.17; 3: y=-0.01·x+37, R^2=0.16.
Consequently, the influence of the MLH upon the concentrations of these gases is relevant (with the exception of path 1 for SO_2). The correlations of NO with MLH are not significant. The concentrations of benzene, toluene, xylene, and formaldehyde are near the detection limit.

4. Conclusions

High particulate ($PM_{2.5}$) load near the surface is coupled with MLH if it is much lower than 1000 m. During conditions characterised by MLH higher than 1000 m a multiple layering of the planetary boundary layer was observed. It can be concluded that an important part of the variance of the observed $PM_{2.5}$, SO_2 and NO_2 concentrations is caused by the MLH i.e. that the influence of MLH upon $PM_{2.5}$, SO_2 and NO_2 concentrations is significant. The dependence of element concentrations from MLH is different and significant only for those compounds which are not emitted from sources nearby the measurement site as ^{65}Cu and ^{66}Zn. The most appropriate temporal averaging period for the correlation of concentrations with MLH are daily mean values. This is caused by missing data during certain weather situations like well-mixed conditions and some very rapid temporal variations of MLH.

In addition to the MLH also the wind direction had a considerable influence on the particle concentrations. During winds from westerly directions the air was relative dry and clean. Sometimes particulate clouds from desert regions were transported to Beijing so that the backscatter intensity increased rapidly. During winds from other directions, especially from the ocean, the relative humidity was high. Higher particulate loads were observed during winds from south-westerly directions which transported particulate loaded air masses.

References

Emeis, S., Münkel, C., Vogt, S., Müller, W., Schäfer, K. (2004), Determination of mixing-layer height, *Atmospheric Environment*, 38, 273-286.

Emeis, S. and Schäfer, K. (2006), Remote sensing methods to investigate boundary-layer structures relevant to air pollution in cities, *Bound-Lay. Meteorol.*, 121, 377-385.

Emeis, S., Jahn, C., Münkel, C., Münsterer, C. and Schäfer, K. (2007), Multiple atmospheric layering and mixing-layer height in the Inn valley observed by remote sensing, *Meteorol. Z.*, 16, 415-424.

Emeis, S., Schäfer, K., Münkel, C. (2008), Surface-based remote sending of the mixing-layer height, *Meteorol. Z.*, 17, 621-630.

Münkel, C. (2007), Mixing height determination with lidar ceilometers - results from Helsinki Testbed, *Meteorol. Z.*, 16, 451-459.

Norra, S., Hundt, B., Stüben, D., Cen, K., Liu, C., Dietze, V., Schultz, E. (2007), Size, morphological and chemical characterization of aerosols polluting the Beijing atmosphere in January/February 2005, in: G.M. Morrison, S. Rauch (eds.), *Highway and Urban Environment*, Springer, Berlin.

Schäfer, K, Emeis, S., Hoffmann, H., Jahn, C. (2006), Influence of mixing layer height upon air pollution in urban and sub-urban areas, *Meteorol. Z.*, 15, 647-658.

Schäfer, K., Wang, Y., Münkel, C., Emeis, S., Xin, J., Tang, G., Norra, S., Schleicher, N., Vogt, J., Suppan, P. (2009), Evaluation of continuous ceilometer-based mixing layer heights and correlations with $PM_{2.5}$ concentrations in Beijing, in: R.H. Picard, K. Schäfer, A.T. Comeron, E. Kassianov, C.J. Mertens (eds.), Remote Sensing of Clouds and the Atmosphere XIV, *Proc. SPIE* Vol. 7475 (SPIE, Bellingham, WA, USA) 74750N-1 – 74750N-12.

Modeling Air Pollutants and Greenhouse Gas Concentration Fields using Non-linear Prediction Chaos Theory Methods

A. Glushkov[1], O. Khetselius[1,2], V. Khokhlov[2] , N. Loboda[2] and Yu. Bunyakova[2]*

[1] OSEU, Odessa, Institute of Applied Mathematics, P.O.Box 24a, 65009, Odessa, Ukraine
dirac13@mail.ru
[2] OSEU Odessa, Institute of Hydrometeorology, P.O.Box 24a, 65009, Odessa, Ukraine
*nuclei08@mail.ru

1. Introduction

Example In order to facilitate important decision-making platforms for scenarios for the reduction of emissions, corresponding technical solutions and political decisions related to the environment there is required an extending analysis and consideration to different aspects of sustainability and the preservation of resources, global systems. An accurate identification of problematic sources affecting outdoor air should be studied and based on a high level of competence in analyses and modeling, naturally combined with process measurement techniques and corresponding interpretation (c.g. Ajavon et al, 2008; Balzani Lööv et al, 2008 ; Glushkov et al, 2004; Loboda et al, 2006 ; Khokhlov et al, 2008). New perspectives in analysis and modeling atmospheric pollutants are opened by using modern non-linear analysis methods, including a chaos theory ones. We use these methods to investigate air pollutants, greenhouse gas (CO2, CO; NO2, SO2 , ozone O3 etc) concentrations fields and chaotic behaviour in concentration time series Glushkov et al, 2004; Loboda et al, 2006 ; Khokhlov et al, 2008). As an example below we present some results regarding cited effects in the NO nitrogen dioxide and sulphurous anhydride concentration time series at two sites in Gdansk region. To reconstruct an attractor, the time delay and embedding dimension are needed. The former is determined by the methods of autocorrelation function and average mutual information, and the latter is calculated by means of correlation dimension method and algorithm of false nearest neighbours. It is shown that the low-dimensional chaos exists in the time series under investigation. The spectrum of Lyapunov exponents is reconstructed as well as both Kaplan-Yorke dimension and Kolmogorov entropy that inversely proportional to the predictability limit are calculated. Non-linear prediction method is used for the time series. It is shown that even though the simple procedure is used to construct the non-linear model, the results are quite satisfactory.

2. Data

The nitrogen dioxide (NO_2) and sulphurous anhydride (SO_2) concentration data observed at the sites of Gdansk region (Poland) during 2003 year are used. There are ten sites in the region, but the time series are continuous at two ones only, Sopot (site 6) and Gdynia (site 9). We use one year hourly concentrations, consisting of a total of 8760 data points. Table 1 presents some of the important statistics of the series.

Table 1 : Some statistics of air pollutant concentrations at the sites of Gdansk region (Poland) during January-December 2003

Statistics	Site 6 (Sopot)		Site 9 (Gdynia)	
	NO_2	SO_2	NO_2	SO_2
Number of data	8760	8760	8760	8760
Mean ($\mu g/m^3$)	15.46	9.13	17.04	11.84
Maximum value ($\mu g/m^3$)	107.53	111.99	101.13	95.47
Minimum value ($\mu g/m^3$)	2.29	3.99	3.92	5.59
Standard deviation ($\mu g/m^3$)	11.99	6.94	11.22	7.19
Skewness	2.26	4.79	1.81	3.89
Kurtosis	7.61	38.15	4.43	22.78

Indeed the concentrations exhibit significant variations without any apparent cyclicity, i.e. a visual inspection of the (irregular) concentration time series does not provide any clues regarding its dynamical behaviour, whether chaotic or stochastic. In the figure, horizontal dashed lines indicate the lower limits (96 μg/m^3 for NO_2 and 89 μg/m^3 for SO_2 and) for the index 2 of air pollution as provided by the EU Directives on Air Quality. A few events with values exceeding these limits have occurred during the year, and all the events were registered in winter or early spring, whereas in summer and autumn the concentrations of the pollutants were on the average lower especially for the sulphurous anhydride. Although the distance between the sites 6 and 9 is only about 7 km and they are located on the beach of Gdansk Bay (the coordinates of sites 6 and 9 are 54°24'54"N, 18°34'47"E and 54°29'40"N, 18°33'15"E, respectively), there is indeed some significant differences. For example, the absolute maxima (minima) at the site 6 are slightly higher (lower) that those at the site 9 (see Table 1). Also, the early December considerable increase of SO_2 concentration was only registered at the site 6, whereas the middle November peak have only occurred at the site 9. The overall variations of the pollutants at the two sites are nearly coherent with the exception of the above-mentioned cases and the lack of SO_2 concentration increase at the site 6 at the end of March. It is noteworthy that the time series of the concentrations not obey the Gaussian distribution (see Table 1).

3. Testing for chaos in time series

Let us consider scalar measurements $s(n) = s(t_0 + n\Delta t) = s(n)$, where t_0 is the start time, Δt is the time step, and n is the number of the measurements. In a general case, $s(n)$ is any time series, particularly the concentrations of atmospheric pollutants. Since processes resulting in the chaotic behaviour are fundamentally multivariate, it is necessary to reconstruct phase space using as well as possible information contained in the $s(n)$. Such a reconstruction results in a certain set of d-dimensional vectors $\mathbf{y}(n)$ replacing the scalar measurements. In 1980 it was (Packard et al, 1980) introduced the method of using time-delay coordinates to reconstruct the phase space of an observed dynamical system. The main idea is that the direct use of the lagged variables $s(n + \tau)$, where τ is some integer to be determined, results in a coordinate system in which the structure of orbits in phase space can be captured. Then using a collection of time lags to create a vector in d dimensions,

$$\mathbf{y}(n) = [s(n), s(n + \tau), s(n + 2\tau), \ldots, s(n + (d-1)\tau)],$$

the required coordinates are provided. In a nonlinear system, the $s(n + j\tau)$ are some unknown nonlinear combination of the actual physical variables that comprise the source of the measurements. The dimension d is also called the embedding dimension, d_E. The example of the Lorenz attractor given by Abarbanel et al. (1993) is a good choice to illustrate the efficiency of the method.

3.1. Time lag

The choice of proper time lag is very important for the subsequent reconstruction of phase space. If τ is chosen too small, then the coordinates $s(n + j\tau)$ and $s(n + (j + 1)\tau)$ are so close to each other in numerical value that they cannot be distinguished from each other. Similarly, if τ is too large, then $s(n + j\tau)$ and $s(n + (j + 1)\tau)$ are completely independent of each other in a statistical sense. Also, if τ is too small or too large, then the correlation dimension of attractor can be under- or overestimated respectively. It is therefore necessary to choose some intermediate (and more appropriate) position between above cases.

First approach is to compute the linear autocorrelation function

$$C_L(\delta) = \frac{\frac{1}{N}\sum_{m=1}^{N}[s(m+\delta) - \bar{s}][s(m) - \bar{s}]}{\frac{1}{N}\sum_{m=1}^{N}[s(m) - \bar{s}]^2}, \qquad (1)$$

where $\bar{s} = \frac{1}{N}\sum_{m=1}^{N} s(m)$, and to look for that time lag where $C_L(\delta)$ first passes through zero. This gives a good hint of choice for τ at that $s(n + j\tau)$ and $s(n + (j + 1)\tau)$ are linearly independent. However, a linear independence of two variables does not mean that these variables are nonlinearly independent since a nonlinear relationship can differs from linear one. It is therefore preferably to utilize approach with a nonlinear concept of independence, e.g. the average

mutual information.

Briefly, the concept of mutual information can be described as follows. Let there are two systems, A and B, with measurements a_i and b_k. The amount one learns in bits about a measurement of a_i from a measurement of b_k is given by the arguments of information theory as

$$I_{AB}(a_i, b_k) = \log_2\left(\frac{P_{AB}(a_i, b_k)}{P_A(a_i)P_B(b_k)}\right),$$

where the probability of observing a out of the set of all A is $P_A(a_i)$, and the probability of finding b in a measurement B is $P_B(b_i)$, and the joint probability of the measurement of a and b is $P_{AB}(a_i, b_k)$. The mutual information I of two measurements a_i and b_k is symmetric and non-negative, and equals to zero if only the systems are independent. The average mutual information between any value a_i from system A and b_k from B is the average over all possible measurements of $I_{AB}(a_i, b_k)$.

To place this definition into the context of observations from a certain physical system, let us think of the sets of measurements $s(n)$ as the A and of the measurements a time lag τ later, $s(n + \tau)$, as the B set. The average mutual information between observations at n and $n + \tau$ is then

$$I_{AB}(\tau) = \sum_{a_i, b_k} P_{AB}(a_i, b_k) I_{AB}(a_i, b_k). \quad (2)$$

Now we have to decide what property of $I(\tau)$ we should select, in order to establish which among the various values of τ we should use in making the data vectors $\mathbf{y}(n)$. The known Fraser's and Swinney's suggestion is to choose that τ where the first minimum of $I(\tau)$ occurs.

3.2. Embedding dimension

The goal of the embedding dimension determination is to reconstruct a Euclidean space R^d large enough so that the set of points d_A can be unfolded without ambiguity. In accordance with the embedding theorem, the embedding dimension, d_E, must be greater, or at least equal, than a dimension of attractor, d_A, i.e. $d_E > d_A$. In other words, we can choose a fortiori large dimension d_E, e.g. 10 or 15, since the previous analysis provides us prospects that the dynamics of our system is probably chaotic. However, two problems arise with working in dimensions larger than really required by the data and time-delay embedding (Abarbanel et al., 1993). First, many of computations for extracting interesting properties from the data require searches and other operations in R^d whose computational cost rises exponentially with d. Second, but more significant from the physical point of view, in the presence of noise or other high dimensional contamination of the observations, the extra dimensions are not populated by dynamics, already captured by a smaller dimension, but entirely by the contaminating signal. In too large an embedding space one is unnecessarily spending time working around aspects of a bad representation of the observations which are solely filled with noise. It is therefore necessary to determine the dimension d_A. There are several standard approaches to reconstruct the attractor dimension.

The correlation integral analysis is one of the widely used techniques to investigate the signatures of chaos in a time series. The analysis uses the correlation integral, $C(r)$, to distinguish between chaotic and stochastic systems. To compute the correlation integral, the algorithm of Grassberger and Procaccia (Grassberger et al, 1983) is the most commonly used approach. According to this algorithm, the correlation integral is computed as

$$C(r) = \lim_{N\to\infty} \frac{2}{N(n-1)} \sum_{\substack{i,j \\ (1\le i<j\le N)}} H\left(r - \| \mathbf{y}_i - \mathbf{y}_j \|\right), \quad (3)$$

where H is the Heaviside step function with $H(u) = 1$ for $u > 0$ and $H(u) = 0$ for $u \le 0$, r is the radius of sphere centered on $\mathbf{y}_i$ or $\mathbf{y}_j$, and N is the number of data measurements. If the time series is characterized by an attractor, then the correlation integral $C(r)$ is related to the radius r given by

$$d = \lim_{\substack{r\to 0 \\ N\to\infty}} \frac{\log C(r)}{\log r}, \quad (4)$$

where d is correlation exponent that can be determined as the slop of line in the coordinates $\log C(r)$ versus $\log r$ by a least-squares fit of a straight line over a certain range of r, called the scaling region. If the correlation exponent attains saturation with an increase in the embedding

dimension, then the system is generally considered to exhibit chaotic dynamics. The saturation value of the correlation exponent is defined as the correlation dimension (d_2) of the attractor. The nearest integer above the saturation value provides the minimum or optimum embedding dimension for reconstructing the phase-space or the number of variables necessary to model the dynamics of the system. On the other hand, if the correlation exponent increases without bound with increase in the embedding dimension, the system under investigation is generally considered stochastic.

Another method for determining d_E comes from asking the basic question addressed in the embedding theorem: when has one eliminated false crossing of the orbit with itself which arose by virtue of having projected the attractor into a too low dimensional space? In other words, when points in dimension d are neighbours of one other? By examining this question in dimension one, then dimension two, etc. until there are no incorrect or false neighbours remaining, one should be able to establish, from geometrical consideration alone, a value for the necessary embedding dimension. Such an approach was described by Kennel et al. (1992).

In dimension d each vector $\mathbf{y}(k)$ has a nearest neighbour $\mathbf{y}^{NN}(k)$ with nearness in the sense of some distance function. The Euclidean distance in dimension d between $\mathbf{y}(k)$ and $\mathbf{y}^{NN}(k)$ we call $R_d(k)$:

$$R_d^2(k) = [s(k) - s^{NN}(k)]^2 + [s(k+\tau) - s^{NN}(k+\tau)]^2 + \\ ... + [s(k+\tau(d-1)) - s^{NN}(k+\tau(d-1))]^2. \tag{5}$$

$R_d(k)$ is presumably small when one has a lot a data, and for a dataset with N measurements, this distance is of order $1/N^{1/d}$. In dimension $d+1$ this nearest-neighbour distance is changed due to the $(d+1)$st coordinates $s(k+d\tau)$ and $s^{NN}(k+d\tau)$ to

$$R_{d+1}^2(k) = R_d^2(k) + [s(k+d\tau) - s^{NN}(k+d\tau)]^2. \tag{6}$$

We can define some threshold size R_T to decide when neighbours are false. Then if

$$\frac{|\, s(k+d\tau) - s^{NN}(k+d\tau)\,|}{R_d(k)} > R_T, \tag{7}$$

the nearest neighbours at time point k are declared false. In practice, the percentage of false nearest neighbours is determined for each dimension d. A value at which the percentage is almost equal to zero can be considered as the embedding dimension.

3.3. Results for atmospheric pollutant time series

Table 2 summarizes the results for the time lag calculated for the first thousand values of the time series. It is noteworthy that the autocorrelation function crosses the zero only for the NO_2 time series at the site 9, whereas this statistic for other time series remains positive. Of course, the values, where the autocorrelation function first crosses 0.1, can be chosen as τ, but Islam and Sivakumar (2002) showed that an attractor cannot be adequately reconstructed for very large values of τ. Before making up final decision we therefore calculate the dimension of attractor for all values in Table 2 using methods described in Sec. 3.2.

Table 2: Time lags (hours) subject to different values of autocorrelation function, C_L, and first minima of average mutual information, I_{min1}, for the time series of NO_2 and SO_2 at the sites of Gdansk region (Poland) during January-December 2003

	Site 6 (Sopot)		Site 9 (Gdynia)	
	NO_2	SO_2	NO_2	SO_2
$C_L = 0$	—	—	102	—
$C_L = 0.1$	136	232	53	147
$C_L = 0.5$	6	12	4	26
I_{min1}	9	19	8	17

The large values of τ result in impossibility to determine both the correlation exponents and the attractor dimensions (see Table 3) using the method of Grassberger and Procaccia (1983). Such an outcome can be explained not only inappropriate values of τ but also shortcomings of correlation dimension method (see e.g. Sivakumar, 2000; Khokhlov et al., 2008).

Table 3: Correlation exponents (d_2) and embedding dimensions determined by false nearest neighbours method (d_N) with percentage of false neighbours (in parentheses) calculated for various time lags (τ) for the time series of NO_2 and SO_2 at the sites of Gdansk region (Poland) during January-December 2003 (Note: * The saturation is not registered).

Site 6 (Sopot)						Site 9 (Gdynia)					
NO_2			SO_2			NO_2			SO_2		
τ	d_2	d_N	τ	d_2	d_N	τ	d_2	d_N	τ	d_2	d_N
136	n/s*	11(6.2)	232	n/s*	10 (8.8)	53	7.62	9 (9.2)	147	n/s*	10 (9.8)
6	5.42	6 (1.3)	12	1.64	6 (1.2)	4	5.29	6 (1.1)	26	3.95	6 (1.1)
9	5.31	6 (1.2)	19	1.58	6 (1.2)	8	5.31	6 (1.1)	17	3.40	6 (1.2)

Moreover, if the algorithm of Kennel et al. (1992) is used, then the percentages of false nearest neighbours are comparatively large in the case of large τ. On the other hand, if the time lags determined by the average mutual information are used, then the algorithm of false nearest neighbours provides the embedding dimension $d_E = 6$ for all air pollutants. Since we assume that the dynamics of system is preferably non-linear, the latter value will be used.

4. Model of non-linear prediction

Before building a model of non-linear prediction, it is important to define how predictable is a chaotic system? The predictability can be estimated by the Kolmogorov entropy, which is proportional to the sum of positive Lyapunov exponents. The spectrum of Lyapunov exponents is one of dynamical invariants for non-linear system with chaotic behaviour. The chaotic motion of physical system is not unpredictable even all the instabilities one encounters in phase space. The limited predictability of the chaos is quantified by the local and global Lyapunov exponents, which can be determined from the measurements.

4.1. Lyapunov exponents

The Lyapunov exponents measure the average local rates of expansion and contraction of chaotic syste. The Lyapunov exponents are related to the eigenvalues of the linearized dynamics across the attractor. Negative values show stable behaviour while positive values show local unstable behaviour. For chaotic systems, being both stable and unstable, the Lyapunov exponents indicate the complexity of the dynamics. The largest positive value determines some "average" prediction limit. High dimensional chaotic systems tend to have very large positive exponents and predictions may be of little use. Since the advent of chaos, the spectrum of Lyapunov exponents can be considered a measure of the effect of perturbing the initial conditions of a dynamical system. Positive and negative Lyapunov exponents can coexist in a dissipative system, which is then chaotic. Since the Lyapunov exponents are defined as asymptotic average rates, they are independent of the initial conditions, and hence the choice of trajectory, and therefore they do comprise an invariant measure of the attractor. In fact, if one manages to derive the whole spectrum of Lyapunov exponents, other invariants of the system, i.e. the Kolmogorov entropy and the attractor's dimension can be found. The Kolmogorov entropy measures the average rate at which information about the state is lost with time. An estimate of this measure is the sum of the positive Lyapunov exponents. The estimate of the dimension of the attractor is provided by the Kaplan and Yorke (1979) conjecture

$$d_L = j + \frac{\sum_{\alpha=1}^{j} \lambda_\alpha}{|\lambda_{j+1}|}, \tag{8}$$

where j is such that $\sum_{\alpha=1}^{j} \lambda_\alpha > 0$ and $\sum_{\alpha=1}^{j+1} \lambda_\alpha < 0$, and the Lyapunov exponents are taken in descending order. The dimension d_L gives values close to the dimension estimates discussed earlier and is preferable when estimating high dimensions.

There are a few approaches to computing the Lyapunov exponents. One of them computes the whole spectrum and is based on the Jacobi matrix of system. In the case where

only observations are given and the system function is unknown, the matrix has to be estimated from the data. In this case, all the suggested methods approximate the matrix by fitting a local map to a sufficient number of nearby points. In this study, we use the method with the linear fitted map proposed by Sano and Sawada (1985).

4.2. Non-linear modelling

Non-linear modelling of chaotic processes is based on the concept of compact geometric attractor on which observations evolve. Since the orbit is continually folded back on itself by the dissipative forces and the non-linear part of the dynamics, some orbit points $\mathbf{y}^r(k)$, $r = 1, 2, \ldots, N_B$ can be found in the neighbourhood of any orbit point $\mathbf{y}(k)$, at that the points $\mathbf{y}^r(k)$ arrive in the neighbourhood of $\mathbf{y}(k)$ at quite different times than k. One can then choose some interpolation functions, which account for whole neighbourhoods of phase space and how they evolve from near $\mathbf{y}(k)$ to whole set of points near $\mathbf{y}(k+1)$ (Abarbanel et al., 1993).

The implementation of this concept is to build parametrized non-linear functions $\mathbf{F}(\mathbf{x}, \mathbf{a})$ which take $\mathbf{y}(k)$ into $\mathbf{y}(k+1) = \mathbf{F}(\mathbf{y}(k), \mathbf{a})$ and then use various criteria to determine parameters $\mathbf{a}$. Further, since one has the notion of local neighbourhoods, one can build up one's model of the process neighbourhood by neighbourhood and, by piecing together these local models, produce a global non-linear model that capture much of the structure in the attractor itself. It is noteworthy that no clue is given by the data as to the kind of model that would be appropriate for the source of chaotic data. The most widespread form of local model is quite simple:

$$s(k+\Delta k) = a_0^{(k)} + \sum_{j=1}^{d_A} a_j^{(k)} s(k-(j-1)\tau), \tag{9}$$

where Δk is the time over which predictions are being made. The coefficients $a_j^{(k)}$, may be determined by a least-squares procedure, involving only points $s(k)$ within a small neighbourhood around the reference point. Thus, the coefficients will vary throughout phase space. The fit procedure amounts to solving $(d_A + 1)$ linear equations for the $(d_A + 1)$ unknowns.

When fitting the parameters a, several problems are encountered that seem purely technical in the first place but are related to the nonlinear properties of the system. If the system is low-dimensional, the data that can be used for fitting will locally not span all the available dimensions but only a subspace, typically. Therefore, the linear system of equations to be solved for the fit will be ill conditioned. However, in the presence of noise the equations are not formally ill-conditioned but still the part of the solution that relates the noise directions to the future point is meaningless.

4.3. Short-range forecast of atmospheric pollutant time series

Table 4 shows the global Lyapunov exponents. It can note that the Kaplan-Yorke dimensions, which are also the attractor dimensions, are smaller than the dimensions obtained by the algorithm of false nearest neighbours. Also, there are the two positive λ_i for the each time series under consideration. Since the Lyapunov exponents determine conversion rate from a sphere into an ellipsoid, then the smaller sum of positive exponents results in the more stable dynamical system and, correspondingly, the higher predictability. The presence of the two (from six) positive λ_i suggests the system broadens in the line of two axes and converges along four axes that in the six-dimensional space. The time series of SO_2 at the site 9 have the highest predictability (slightly more than two days), and other time series have the predictabilities slightly less than two days. Such the predictability is quite sufficient.

Table 4: First two Lyapunov exponents (λ_1 and λ_2), Kaplan-Yorke dimension (d_L), and average limit of predictability (Pr_{max}, hours) for the time series of NO_2 and SO_2 at the sites of Gdansk region (Poland) during January-December 2003

	Site 6 (Sopot)		Site 9 (Gdynia)	
	NO_2	SO_2	NO_2	SO_2
λ_1	0.0184	0.0164	0.0189	0.0150
λ_2	0.0061	0.0066	0.0052	0.0052
d_L	4.11	5.01	3.85	4.60
Pr_{max}	40	43	41	49

To use the non-linear prediction method, it is necessary to solve another one problem which can be defined as how much exactly nearest neighbours, *NN*, must be considered to obtain satisfactory results of the forecasts? The solution can be arrived at if a few forecasts are

accomplished with various number of *NN*, and their results are compared with original data. As a rule, the coefficient of correlation rises to a maximum (Islam and Sivakumar, 2002). In the current study, we use this approach the last one hundred points of the time series; the 24-hour forecasts are accomplished on the basis of previous 8660 data points. Table 5 summarizes the results of our experiments. As it was expected, the coefficients of correlation rise to the maxima at some number of *NN*. It is noteworthy that these coefficients are both large and significant. Thus, we further use $NN = 180$ for NO_2 and $NN = 260$ for SO_2 at the site 6, as well as $NN = 2100$ for NO_2 and $NN = 250$ for SO_2 at the site 9.

Table 5: Coefficient correlation (*r*) between actual data and 24-hour forecast subject to number of neighbours (*NN*) for last one hundred points of the time series of NO_2 and SO_2 at the sites of Gdansk region (Poland) during January-December 2003

	Site 6 (Sopot)						Site 9 (Gdynia)					
	NO_2			SO_2			NO_2			SO_2		
NN	80	180	200	80	260	280	80	210	230	80	250	270
r	0.95	0.96	0.96	0.91	0.94	0.94	0.96	0.97	0.97	0.93	0.94	0.94

Figure 1 shows, as an example, the original data and 24-hour forecasts of pollutants sat the site 6. As can see, almost all the maxima in the original data have the counterparts in the forecast, but the differences between them can be sufficiently great. Nevertheless, the root-mean-square errors are 6.025 and 5.636 for NO_2 and SO_2 respectively. The results of the short-range forecasts can be thus considered as quite acceptable.

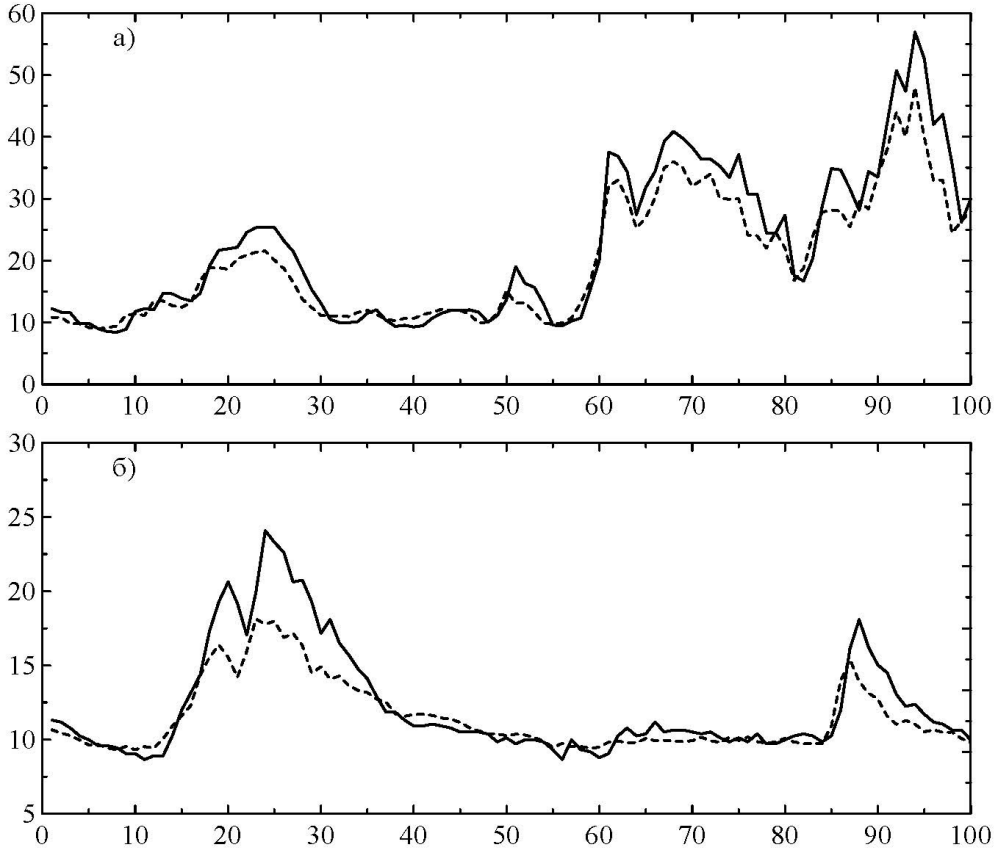

Figure 1: Original data (solid lines) and 24-hour forecasts (dashed lines) for last one hundred data points of (a) NO_2 and (b) SO_2 from 2003 at site 6 of Gdansk region, Poland.

5. Conclusions

In our study we use the modern non-linear analysis methods, including a chaos theory ones, to investigate air pollutants, greenhouse gas (CO2, CO; NO2, SO2 , ozone O3 etc) concentrations

fields and chaotic behaviour in concentration time series. As example above, we have presented an analysis of the time series of pollutants in the atmosphere using methodology from chaos theory. Our results show that these time series are resulted from the low-dimensional chaos. In spite of the fact that the embedding dimensions for each time series are identical ($d_N = 6$), this outcome is not regularity. Also, the correlation dimensions were calculated using the algorithm of Grassberger and Procaccia (1983). It is noteworthy that the nearest integer above the saturation value provides the minimum or optimum embedding dimension for reconstructing the phase-space or the number of variables necessary to model the dynamics of the system. This concept can be applied to the dynamics of NO_2 time series, since the embedding dimension determined by both the correlation dimension method and the algorithm of false nearest neighbours are identical. In this case, the number of variables necessary to model the dynamics of the system equals six. From the other hand, the analysis of correlation dimension provides only the number of variables, but not their physical meaning.

Also, our results can be considered as the example of quite successful short-range forecast for the concentrations of atmospheric pollutants. It is noteworthy that the non-linear prediction method provides the satisfactory results in the case, when the concentrations are sharply rising; at least, all the tendencies to the rising were revealed by the method

References

Ajavon,A.N.; Jucks,K.W.; Kurylo,M.J.; Lambert,J.C.; Newman,P.A.; Piekutowski,T.; Peter,T.; Pyle,J.;Ravishankara,A.R.; Reimann,S.; Shanklin,J.; van der Leun,J.C; Veefkind,P.; Velders,G.J.M., Report of the seventh meeting of the ozone research managers of the parties to the vienna convention for the protection of the ozone layer, 2008, *Report number* 51, WMO/TD-No. 1437, 367pp.

Abarbanel, H.D.I., Brown, R., Sidorowich, J.J., Tsimring, L.Sh., 1993. The analysis of observed chaotic data in physical systems. *Rev. Mod. Phys.*, 65(4), 1331-1392.

Balzani Lööv,J.M.; Henne,S.; Legreid,G.; Staehelin,J.; Reimann,S.; Prevot,A.S.H.; Steinbacher,M.; Vollmer,M.K. 2008, Estimation of background concentrations of trace gases at the Swiss Alpine site Jungfraujoch (3580 m asl), *Journal of Geophysical Research* D, Vol, 113, P. D22305.

Glushkov A.V. , Loboda N.S., Statistical Modelling and Estimating the Irrigation Effects on Annual Runoff and Water Resources, 2004 *Water resources in Asia Pasific Region* (Kyoto, Japan) 1359-1362.

Glushkov A.V, Khokhlov V.N., Prepelitsa G.P., Tsenenko I.A., 2004, Temporal variability of the atmospheric methane content, *Optics of atmosphere and ocean* 14, 219-223.

Grassberger P., Procaccia I., 1983. Measuring strangeness of strange attractors. *Physica* D 9, 189-208.

Islam M.N., Sivakumar B., 2002. Characterization and prediction of runoff dynamics: a nonlinear dynamical view. *Advances in Water Resources* 25, 179-190.

Kaplan J.L., Yorke J.A., 1979. Chaotic behavior of multidimensional difference equations, in: Peitgen H.-O., Walter H.-O. (Eds.), Functional Differential Equations and Approximations of Fixed Points. *Lecture Notes in Mathematics* No. 730. Springer, Berlin, pp. 204-227.

Kennel M.B., Brown R., Abarbanel H.D.I., 1992. Determining embedding dimension for phase-space reconstruction using a geometrical construction. *Physical Review* A 45, 3403-3411.

Khokhlov V.N., Glushkov A.V., Loboda N.S., Bunyakova Yu.Ya., 2008, Short-range forecast of atmospheric pollutants using non-linear prediction method. *Atm. Environment (Elsevier)*, 42, 7284–7292.

Loboda N.S., Glushkov A.V., Khokhlov V.N., Lovett L. 2006, Using non-decimated wavelet decomposition to analyse time variations of North Atlantic Oscillation, eddy kinetic energy, and Ukrainian precipitation, *Journal of Hydrology (Elsevier)*, 322, 14-24.

Paluš, M., Pelikán, E., Eben, K., Krejcír, P., Juruš, P., 2001. Nonlinearity and prediction of air pollution. In V. Kurkova, N.C. Steele, R. Neruda, M. Karny (editors), *Artificial neural nets and genetic algorithms.* Springer, Wien, pp. 473-476.

Packard N.H., Crutchfield J.P., Farmer J.D., Shaw R.S., 1980. Geometry from a time series. *Physical Review Letters* 45, 712-716.

Sano M., Sawada Y., 1985. Measurement of the Lyapunov spectrum from chaotic time series. *Physical Review Letters* 55, 1082-1085.

Effects of Temperature and of Different Pollution Sources on Particle Size Distributions in Grisons (Switzerland)

J. Thudium [1], C. Chelala [1], H. Lötscher [2]*

[1] Oekoscience, Werkstrasse 2, CH-7001 Chur, Switzerland, Thudium@oekoscience.ch

[2] Amt für Natur und Umwelt, Gürtelstrasse 89, CH-7001 Chur, Switzerland

Introduction

Many Europeans Cities are equipped with measurements of PM10 and PM2.5. Yet, these particles matter are not representative of the presence of ultrafine particles that are more and more emitted in the atmosphere due to the growth of the number of diesel vehicles. Until now, in Europe, there is no legislation that limits the air pollution of fine particles but several objectives at long term (with EU Directive going till 2020) including emissions reduction of diesel vehicles (norms Euros 5 for particles filters). However, the study of this pollution is very important knowing that it can lead to lung cancer, heart diseases and asthma attacks (Pope et al., 2002).

Objectives and Methodology

The present study is made in the canton of Grisons in Switzerland (Fig. 1) where most of the particles are emitted, not only by road traffic, but also by heating especially by wood. This is a seasonal pollution that affects the resident population and the winter tourists.

The main objectives of the present study are to discern the relation between particle size distribution and meteorological parameters (such as temperature, wind speed and rain), nitrogen pollution level and accumulation mode, all in dependency to the week-day (workings days or Sundays/holidays) and to the measurements site classification (traffic, interurban, rural).

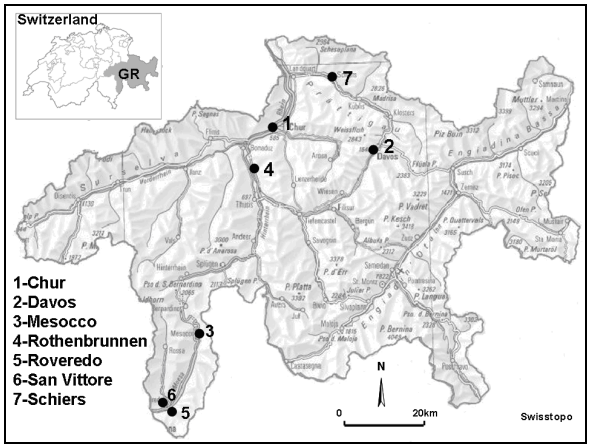

Figure 1: Localization of the measurements stations of ultrafine particles in the Grisons canton (Switzerland).

The measurements were made by the Department of Nature and Environment of Canton Grisons (Amt für Natur und Umwelt Graubünden) using the technique of Scanning Mobility Particle Sizers (SMPS) with a mobile Condensation Particle Counter (CPC) (for further information: Grimm Aerosol Technik, 2006). Measurements campaigns for seven stations of several days have been made from 2005 till 2010. There are three types of stations: traffic (station No. 1-3-4), interurban (station No. 2) and rural with essential wood heating (station No. 5-6-7) (Fig.1). The measurement interval is for seven minutes resumed to hourly values. Their size range is 11-1110 nm in a resolution of 44 channels. Furthermore, at each measurement site, a continuous monitoring of many pollutants and metrological components is available. The NOx, the temperature, the wind speed and the precipitation (in duration/h) will be taken into consideration in this study.

Main Results

Figure 2 represents an example of the size distribution for the three stations types. In fact, the traffic nearby station (4: Rothenbrunnen) shows that the peak of particles concentration is between 10-20 nm and the interurban station (2: Davos) shows a peak at about 20 nm. The station at Davos had a distance of about 40 m to the nearest street, whereas the station at Rothenbrunnen is at about 5 m from the highway. This may explain the shift in the peak between these two stations: at Davos, the coagulation has more progressed. But the rural station (6: San Vittore) with dominant wood heating shows a very different response as the peak is at 60-100 nm.

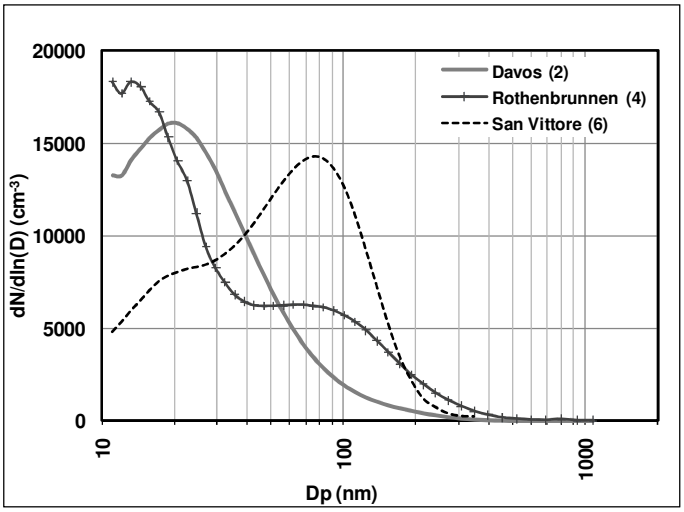

Figure 2: Particle size distribution for workdays at three types of station: Davos (11.-22.12.2009), Rothenbrunnen (15.11.2005 - 20.12.2005), San Vittore (22.12.2006-12.01.2007).

(a)

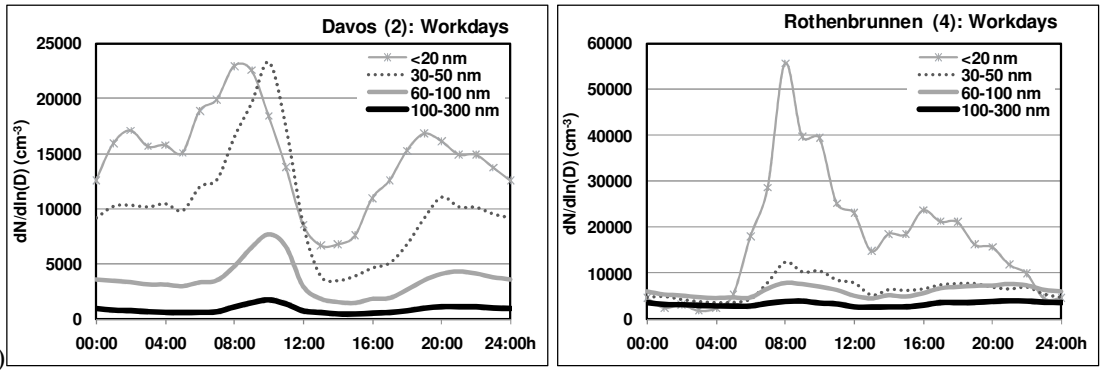

(b)

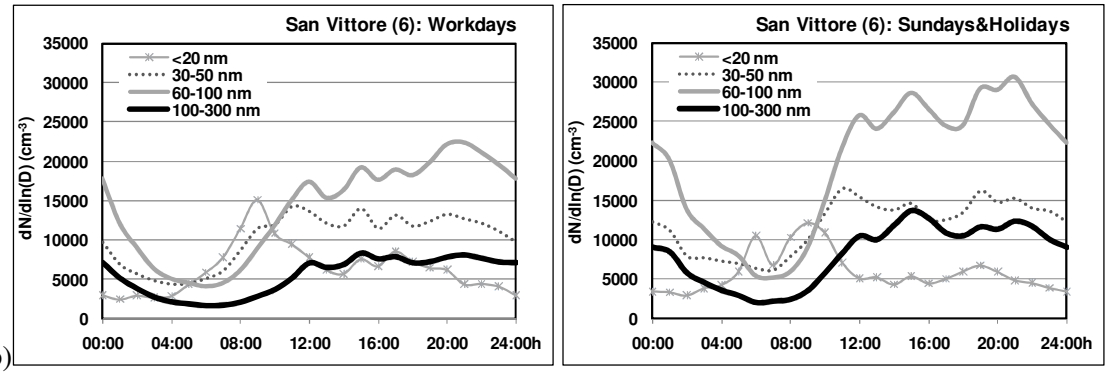

Figure 3: Daily variation of 4 classes of particle size distribution for (a) workdays at Davos (11.-22.12.2009) and Rothenbrunnen (15.11.2005 - 20.12.2005), and (b) for workdays (left-hand) and Sundays/holidays (right-hand) at San Vittore (22.12.2006-12.01.2007).

Daily variation of particles concentration in four size classes shows the integrated effect of variation of emissions and of meteorological conditions. Figure 3 shows that both the traffic exposed and the interurban station confirm the traffic induced daily variation at the two finest size classes (<20 nm) and (30-50 nm). The morning and afternoon rush hours are evident for the interurban and traffic stations (Fig. 3 (a)). In the very cold winter nights of Davos, apparently strong nucleation processes take place, leading to the formation of ultrafine particles, together with the continuous heating (often oil); this behavior have been reproduced in four different winter measurement campaigns at this station. At San Vittore (rural with wood heating dominant) (Fig. 3 (b)), particles in the size range of 60-100 nm are most numerous especially in Sundays and holidays where people tend to more heating. Their presence lasts all the afternoon till late evening. This is also typical for the two other stations with essential wood heating, Roveredo and Schiers.

Effect of studied parameters on particles size distribution

For each parameter, a sorting has been made for the lowest and highest 30% of existing data. So, three classes are obtained showing the less, medium and higher values of the studied parameter. Also, due to the lack of data and to the sorting, some hours are not well representative for all classes. Therefore, only a section of day hours has been taken into consideration. In addition, correlation between parameters and particles concentrations (see e.g. Fig 4(c)) has been done to illustrate the response of each parameter in terms of class-average values. The figures included in this study are few sampling showing the general case of study for all the station types.

The relation with NOx concentration: The level of nitrogen oxides affects the particles size distribution for all the studied stations and all the measurements phases. This analyse has been also made to NO_2, the results are very similar to NOx response. There is no relationship between NOx and particles number concentration common to all stations, but at a certain station, particles concentration increase clearly with increasing NOx, above all in the small size ranges in the case of the traffic exposed and interurban stations (Fig. 4 (a) and (b)).

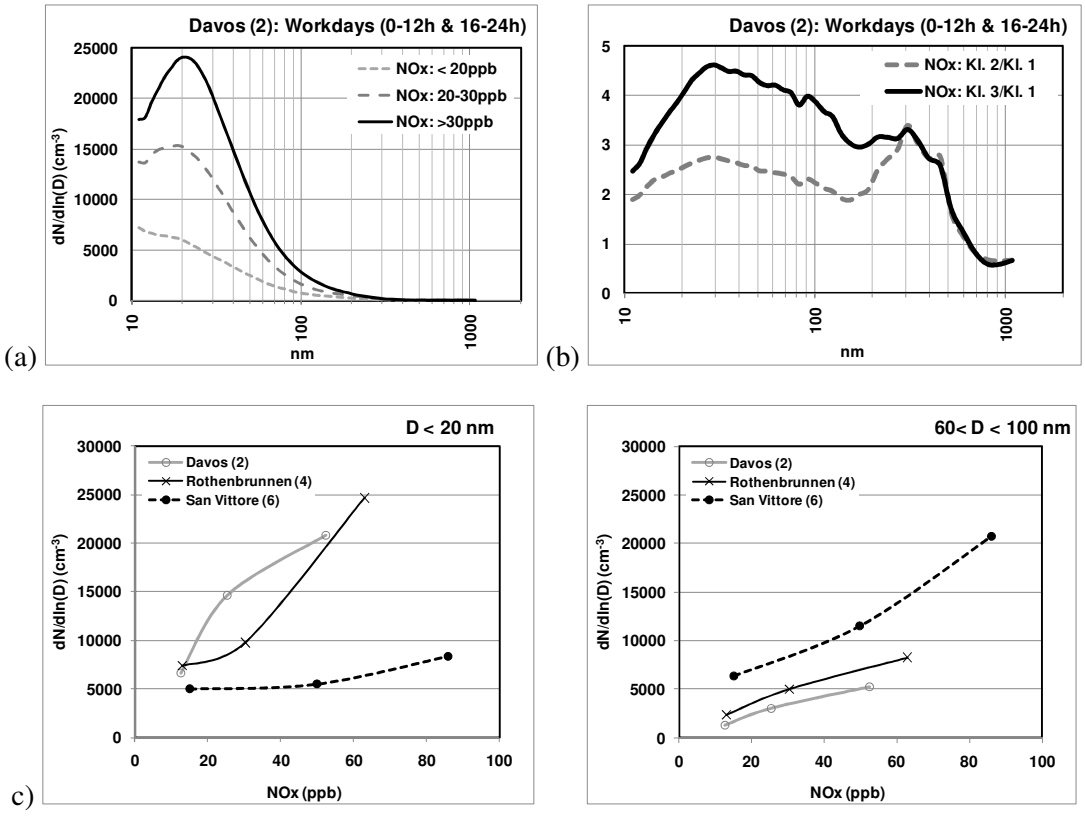

Figure 4: (a) Particle size distribution for workdays (0-12h & 16-24h) in relation with NOx classes and (b) relationship between the NOx classes, at Davos (11.-22.12.2009) and (c)

correlation between NOx concentration and particle size classes (D < 20 nm: left-hand and D: 60-100 nm: right-hand) for the three stations (see Fig. 2).

Fig 4 (c) shows a high correlation between particles concentrations (for diameters D less than 20 nm and diameters D between 60 and 10 nm) and NOx level. At the stations with wood heating dominant, it is more the particles in the accumulation mode which are increasing with NOx (San Vittore, Fig. 4 (c), right-hand). This can be explained by the emission of NOx by wood heating too and the stronger coagulation that can happen in the inversion layers. In fact, the temperature inversions are frequent in wintertime in alpine valleys.

The relation with temperature: The temperature showed a strong relationship with the wind speed, especially during daytime (between 10-20h) where the wind speed is higher. In order to focus only on the temperature effect on particles size distribution, the investigation takes in consideration the intervals from 0-10h and 20-24h. Therefore, all stations with similar wind speeds over all temperature ranges showed a clear increase of the number of particles until 60 nm with decreasing temperature (Fig. 5). For particles higher than 100 nm the behaviour was not uniform. In some cases, colder temperatures may have led to more heating emissions, warmer to more suspension from the soil. In any case the temperature dependency of particles with size ranges less than 100 nm is very strong. Hence, to compare particles number concentrations, temperature information should exist.

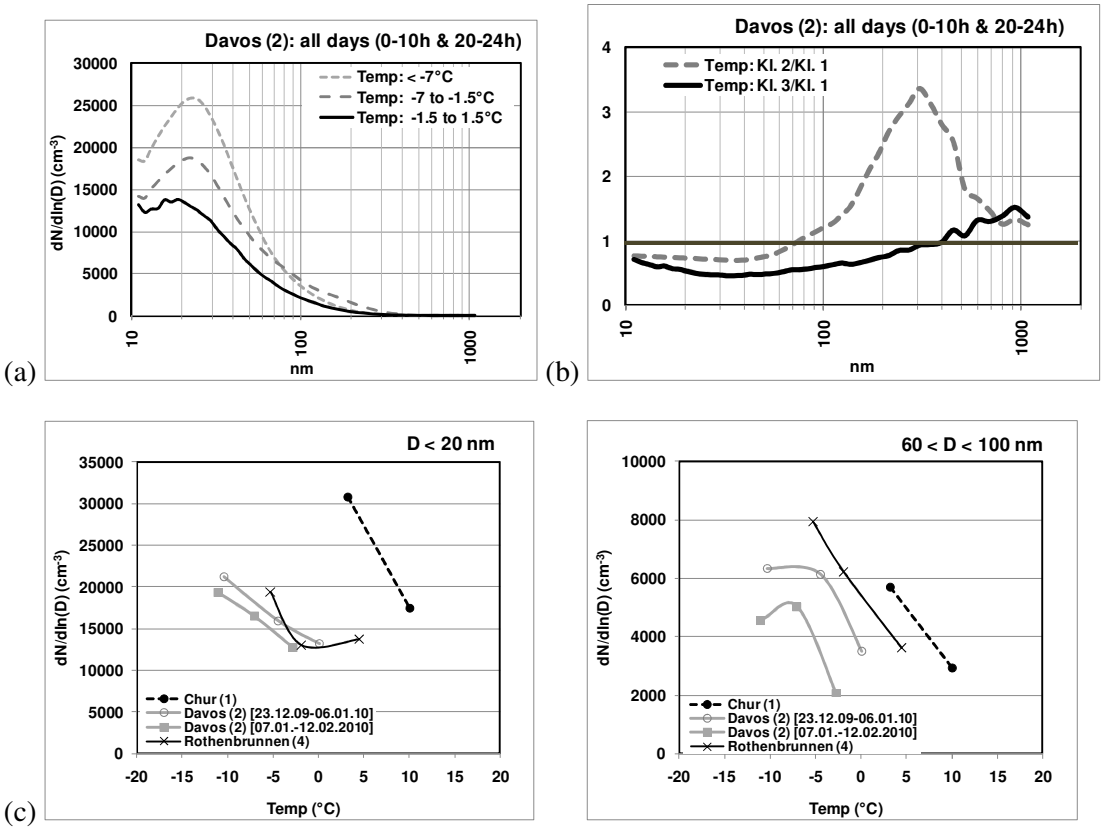

Figure 5: (a) Particle size distribution for all days (0-10h & 20-24h) in relation with temperature classes and (b) relationship between the temperature classes, at Davos (23.12.2009-06.01.2010) and (c) correlation between temperature and particle size classes (D < 20 nm: left-hand and D: 60-100 nm: right-hand) for four measurements campaigns (s. Fig. 2).

Influence of particles in the accumulation mode: The class of 82 nm is selected for it is representative of the accumulation mode. The number concentration of this size was divided in three classes of low, mean and high values for each station. In nearly all cases, increased concentration in the accumulation mode indicates an increased concentration for all particle sizes, whereby the ultrafine particles (less than 30 nm) increase less in concentration compared with the accumulation mode.

The smaller increase of ultrafine particles concentration could occur due to the fact that more particles surface in the air may enhance condensation and reduce nucleation of new particles.

Also, this could come out from additional wood heating sources. But since this behaviour is shown throughout day (Fig. 6 (c)), (because during night time we consider that there are no wood burnings), it is indicated that the first effect also takes place (Charron and Harrison, 2003).

Only at stations with wood heating as really dominant particle source (as San Vittore and partially Roveredo), the concentration of ultrafine particles (< 30 nm) decreases with increasing concentration in the accumulation mode.

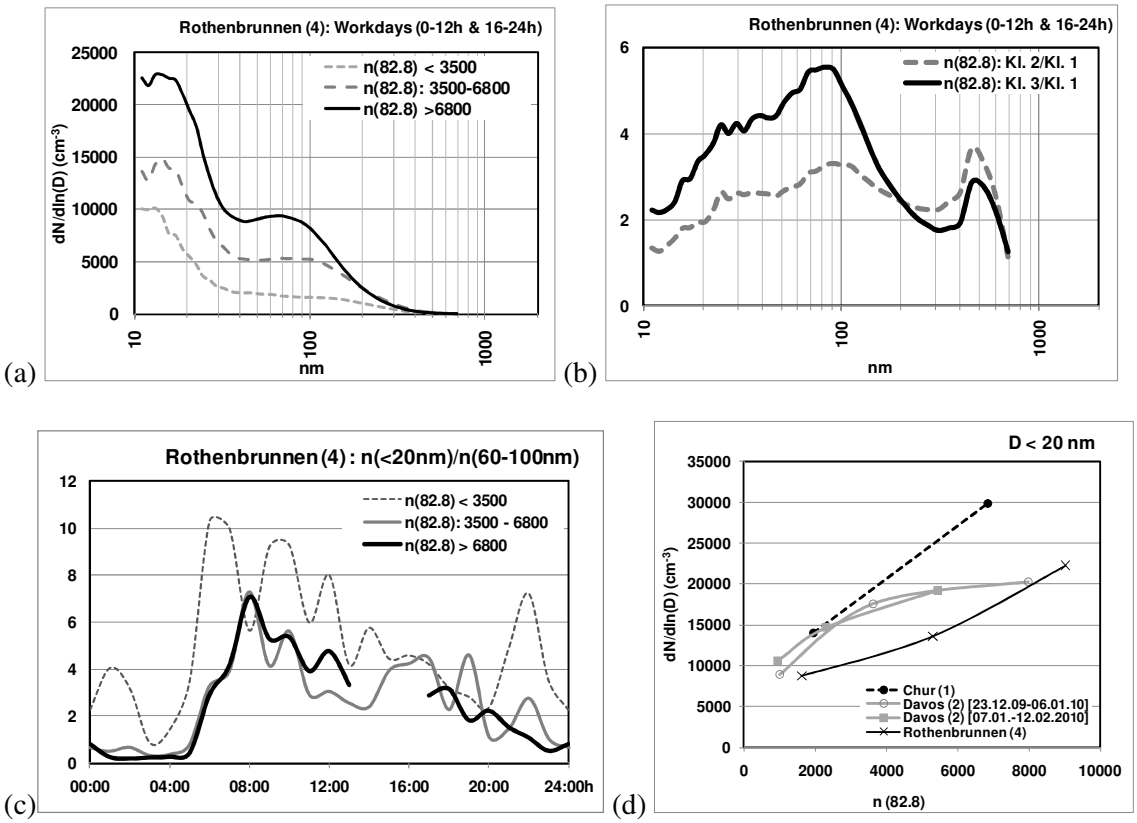

Figure 6: (a) Particle size distribution for workdays (0-12h & 16-24h) in relation with accumulation mode classes and (b) relationship between the accumulation mode classes, at Rothenbrunnen (15.11.2005 - 20.12.2005) and (c) daily variation of relation n(<20nm)/n(60-100nm) for Rothenbrunnen at workdays and (d) correlation between accumulation mode concentration and particle size class (D < 20 nm) for four measurements campaigns (s. Fig. 2).

Also the effect of the wind speed on particle size distribution has been analyzed. The results are homogeneous for all the stations at all phases of time. More wind leads to less particles numbers for all the particle sizes. However it seems that this effect is smaller for the ultrafine particles (< 30 nm). Only large particles (> 700 nm) may increase with the wind, this could be due to resuspension in the air.

Precipitation leads to smaller particle concentrations for all sizes at all stations except at one. Wash out is expected to be responsible for this effect, but it has also to be considered that in winter time in Grisons, it is colder without than with precipitation, so that the temperature effect of particle formation (s. above) overlays the precipitation effect.

Conclusion

The relation between NOx and particles number concentration is not homogenous for all the measurements sites. But at each station, the particle concentrations of all size increase clearly with increasing NOx, in particular in the small size ranges for the traffic and interurban stations. As traffic is the main source for NOx it is also a main source for ultrafine particles.

Concerning temperature effects on particle size distribution, an evidence for an increase of the smallest particles (<60 nm) with decreasing temperature was founded. This is in good

agreement with Charron and Harrison (2003) who found an inverse relationship between particle numbers from 11-30 nm and temperature for measurements at London, as well as with Bukowiecki et al. (2003) who found in the Zurich region that low temperatures led to enhanced numbers of the smallest particles.

There is evidence too that more particles surface may enhance condensation and reduce nucleation of new particles. So the presence of a wood burning aerosol with many larger particles influences the development of a traffic induced particle collective. This is in agreement with Charron and Harrison (2003) who found a favoured formation of ultrafine particles in "cleaner atmospheres".

Acknowledgments

This study has been funded by the “Amt für Natur und Umwelt Graubünden” of the Grisons canton.

References

Bukowiecki, N., J. Dommen, A. Prevot, E. Weingartner and U. Baltensperger (2003), Fine and ultrafine particles in the Zürich (Switzerland) area measured with a mobile laboratory: an assessment of the seasonal and regional variation throughout a year, Paul Scherrer Institut (Villigen), in *Atmospheric Chemistry and Physics,* 3, 1477–1494.

Charron A., R.M. Harrison (2003), Primary particle formation from vehicle emissions during exhaust dilution in the roadside atmosphere, *Atmos. Environ.*, 29, 4109-4119.

Grimm Aerosol Technik (2006), Scanning Mobility Particle Sizer (SMPS+C), Size distributions of airborne nano- to micrometer particles with high sensitivity and resolution from Grimm-aerosol, *software manual*, 4.

Pope C.A., R.T. Burnett, M.J. Thun, E.E. Calle, D. Krewski, K. Ito and G.D. Thurston (2002), Lung cancer, cardiopulmonary mortality, and long-term exposure to fine particulate air pollution, *JAMA*, 297(9), 1132-1141.

Thudium J. (2009), Zusammenfassung zu Untersuchungen atmosphärischer Partikel im Gebiet von OSTLUFT, 75.

Thudium J. and C. Chelala (2009), Partikel in der Bündner Luft, Eine Zusammenfassung bisheriger Untersuchungen, 42.

Concentrations of Platinum Group Metals from Transport in the Environment

V. Adamec[1], R. Licbinsky[1], L. Sikorova[1,2], J. Huzlik[1], I. Dostal[1]*

[1] Transport Research Centre, Lisenska 33a, 636 00 Brno, Czech Republic, roman.licbinsky@cdv.cz
[2] Laboratory of Risk Research and Management, Faculty of Safety Engineering, VSB-Technical University of Ostrava, Lumirova 13, 700 30 Ostrava, Czech Republic

Introduction

Catalytic converters are used in effort to decrease gaseous pollutants emissions such as carbon monoxide, nitrogen oxides and hydrocarbons originating during the fuel combustion. Converters are formed by steel carrier with honeycomb structure with highly porous layer (so-called washcoat) of aluminium oxide resistant to both high temperatures (highly above 800°C) and frequent temperatures changes. Catalytic layer formed by very fine scattered platinum group metals (PGE) especially platinum (Pt), palladium (Pd) and rhodium (Rh) is deposited on this porous part. Converter is during the vehicle operation chemically and mechanically stressed by quick changing of oxidative and reduction conditions, high temperature and mechanical abrasion. These processes are the reason of PGE emission primarily to the atmosphere with consequent contamination of other environmental matrices especially road neighbourhood and city agglomerations with high traffic intensity (Ravindra 2004). PGE are emitted from converters in the amount of $ng.km^{-1}$ in the form of fine dispersed metal nanoparticles adsorbed on aluminium oxide particles from washcoat (Artelt 1999; Moldovan 2002; Palacios 2000). Wide range of studies indicates accumulation of PGE in separate environmental matrices such as particulate matter (PM) in the atmosphere (e.g. Rauch 2006; Gómez 2002), road dust (e.g. Leśniewska 2004; Djingova 2003), soil (e.g. Wichmann 2007) or sediments (e.g. Prichard 2009). PGE were found out also in plants (e.g. Leśniewska 2004; Djingova 2003) and in organism bodies (e.g. Ek 2004). Higher PGE concentrations are not restricted to emission sources surroundings but these were determined also in distant localities in central Greenland (Barbante 2001). Pt in metal form is considered to be biologically inert (Ravindra 2004) but contact with soluble compounds induce irritation and origin of hypersensitivity mostly in the form of rashes and due to longer exposition also breathing complications such as rhinoparynx and lower air passages inflammation (Nordberg 2007). Share of PGE soluble fraction in overall emissions varied from 1 % (Artelt et al., 1999) to 10 % (Moldovan 2002). Catalytic converters in vehicles so transport is considered the main source of environment pollution by PGE and this is supported by the fact that the Pt/Rh rate determined in separate environmental matrices was till 1999 the same as the rate of these elements in catalytic converters (Ravindra 2004). Results of studies focused on PGE contents in selected environmental matrices on localities burden by traffic in the Czech Republic in years 2002 – 2009 are presented in this paper.

Methods

Samples of separate environmental matrices were taken on selected sites in the Czech Republic and consequent analyses have proceeded with the aim of determination of environmental burden by PGE. Potential health risks related to this anthropogenic burden in connection with transport were taken into account during the localities selection hence the most of the sampling points were situated in the city of Brno and its surroundings. Soil was sampled also next to main highway connecting the capital city (Prague) and the second largest city of the Czech Republic (Brno) to determine the accumulation of PGE during the period of using the catalytic converters in vehicles.

Particulate matter (PM)

Middle volume samplers Leckel MVS6 were used for PM sampling in 24 hours intervals. Devices were placed just next to roads with different traffic intensities and PM were captured on nitrocellulose filters. Exposed filters were transported to the laboratory in ice box and placed here in constant temperature and humidity. PM concentrations were determined after 48 hours under these conditions using gravimetric method (Mettler-Toledo MX5/A balances). Weighted filters were digested using ultrapure water, hydrofluoric and nitric acid under higher pressure and temperature in ultraClaveIII® device. PGE concentrations were consequently measured using ICP – MS Agilent 7500 device.

Soil

Soil sampling was conducted under stabile grass stand on localities with different burden by traffic in the urban area. Samples were taken from three depths of 0 – 2 cm, 0 – 5 cm a 0 – 20 cm using boring bar Eijkelkamp. Samples on all localities were collected from approximately 10m2 area and quartering was done to obtain suitable amount of the sample right on the locality. Samples were dried up under room temperature, homogenized and lay down through 2 mm screen to separate off coarse particles and organic matter. Prepared samples were melted to nickel sulphide (docimastic method) that allows efficient extraction and concentration of PGE. PGE concentrations were consequently measured using ICP – MS method VG Elemental plasma Quand 3 device. Soil was also sampled in exits from D1 highway connecting Prague and Brno, two largest cities in the Czech Republic. Samples were collected as 10 separate samples taken 0,5 m from each other in the line of 4,5 metres parallel to road in two distances from road – 5 and 10 m and from two depths 0-2 cm a 2-5 cm using boring bar Eijkelkamp. Samples were dried up under room temperature, homogenized and lay down through 2 mm and 1 mm screens to separate off coarse particles and organic matter. Quartering was done to obtain suitable amount of the sample for analyses by ICP – MS method.

Tunnel dust

Samples were swept down on the roads surface (raod dust) and also were taken from air conditioning system (fine dust). After drying were samples laid down through 5,6 mm screens to separate off coarse particles and organic matter. Prepared samples were as well as soils melted to nickel sulphide and PGE concentrations were determined by ICP-MS method on VG Elemental plasma Quand 3 device.

Runoff waters

Runoff waters were sampled both from drainage systems in tunnels and from storm water setting tanks along the highways to polyethylene bottles. Superpure nitric acid was used for sample stabilization. PGE concentrations were determined by ICP-MS method on Elan 6000 device.

Data statistical evaluation

Statistical evaluation of obtained data sets was conducted using QC Expert 3.0 software. To gain the proper information about PGE concentrations in separate environmental matrices, the different statistical approaches were used to determine the most accurate mean value. Geometrical mean was calculated when the set contained more than 20 data or less than 2 data. Horn procedure for mean value calculation of small sampling was used when the set contained from 4 to 20 data and median was calculated when there were only 3 results.

Results and Discussion

PGE in the air are mostly adsorbed on particulate matter in all fractions and their concentrations range for Pt <0.093 – 32.4 $pg.m^{-3}$, Rh <0.18 – 13.2 $pg.m^{-3}$ and Pd 0.2 – 166.1 $pg.m^{-3}$. PGE concentrations in waters were for Pt <0.01 – 0.208 $\mu g.l^{-1}$, Pd <0.02 – 0.80 $\mu g.l^{-1}$ and Rh <0.005 – 0.01 $\mu g.l^{-1}$. PGE are not naturally contained in these matrices so measured concentrations represent environmental burden by anthropogenic processes and in these cases by transport. PGE concentrations in dust sampled in road tunnels range in interval of 67.79 – 637 $ng.g^{-1}$ for Pt, 19.93 - 705.2 $ng.g^{-1}$ for Pd and 15 – 564.6 $ng.g^{-1}$ for Rh. PGE concentrations in soil sampled in urban area were determined for Pt in interval between 0.4 – 39.6 $\mu g.kg^{-1}$, for Pd in interval between 0,5 – 12,2 $\mu g.kg^{-1}$ and for Rh in interval between 0.06 – 4.89 $\mu g.kg^{-1}$. These element mean concentrations in Earth crust, just for comparison, are averaged at about 0.01 ppm of Pt, 0.015 ppm of Pd and 0.0001 ppm of Rh. Concentration data in separate environmental matrices were analysed of dispersion (ANOVA) to find out factors affecting PGE concentrations. Due to considerable asymmetry of statistical distribution Napierian logarithms of concentrations that have normal distribution necessary for usage of ANOVA process were analysed.

Multifactor ANOVA for PGE concentrations data in the air indicate that their concentrations in separate PM fractions are statistically significantly different with 95% probability. As it is showed in fig. 1 the most of PGE is adsorbed to coarse PM fraction PM2.5-10. Time progress is inconclusive although time factor is statistically significant and for its more accurate determination would be

necessary longer sampling periods in separate years. Results also indicate significantly higher concentrations of Pd adsorbed to PM than other PGE elements. Transport intensity influence is also significant described by the positive prediction factor 0.043 that indicates higher PGE concentrations on localities with higher traffic intensity.

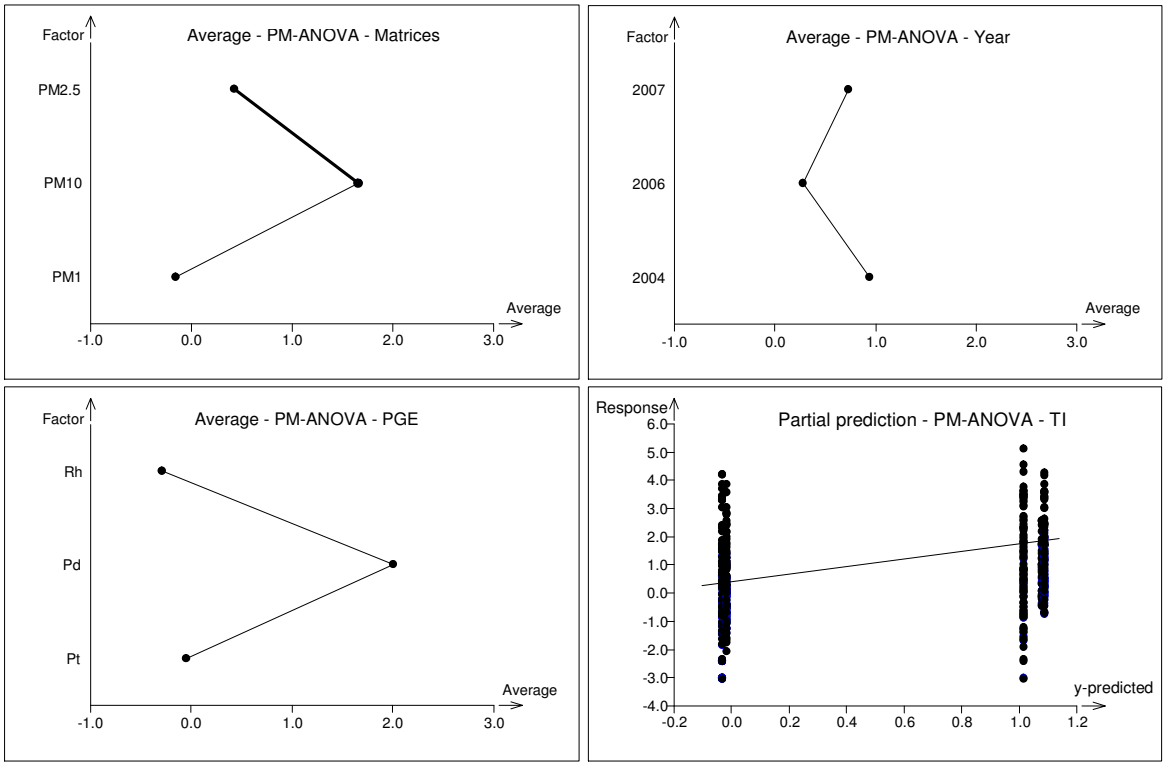

Fig. 1: Multifactor ANOVA analysis for PGA concentrations adsorbed on PM.

Multifactor ANOVA for PGE concentrations in tunnel dust indicate no statistically significant differences among road dust (from road surface in tunnels), fine dust (air conditioning system in tunnels), year of sampling and locality. Two factor ANOVA analyses (fig. 2) shows statistically significant higher concentrations of Pt than Pd in contrast to their concentrations in the air (Factor 1). Rh concentrations in tunnel dust are the lowest as well as for air concentrations. Concentrations were 1,5 times higher than in 2003 and this difference is statistically significant (Factor 2).

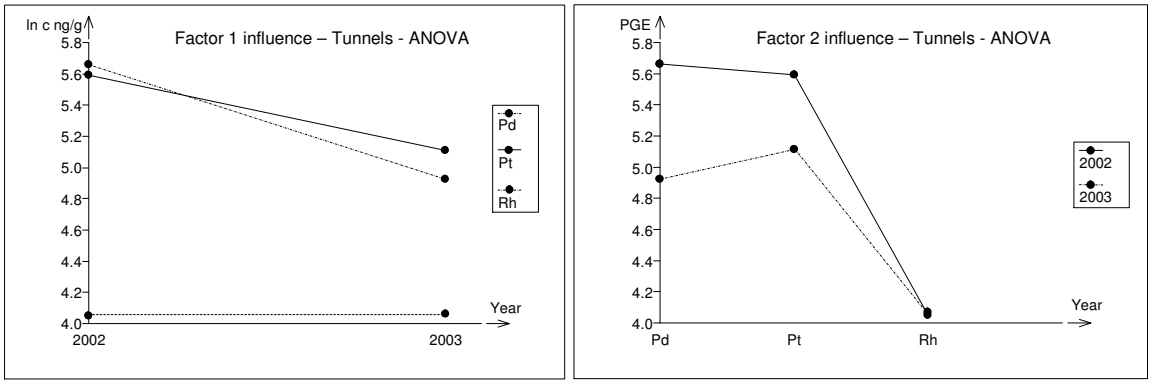

Fig. 2: Two factor ANOVA analysis for PGE concentration in tunnel dust.

Evaluation of PGE concentrations in soils data indicates that depth of sampling was not statistically significant. Statistically significant factors were sampling locality, PGE concentrations and transport intensity. Variation of PGE concentrations Napierian logarithms mean values according to localities is shown in fig. 3. Localities with high traffic intensities especially crossroads are the most contaminated sampling sites. Pt concentrations in soils were the highest, Pd concentrations were

lower and Rh concentrations were the lowest. Transport intensity influence is statistically significant described by the positive prediction factor 0.019 that indicates higher PGE concentrations on localities with higher traffic intensity.

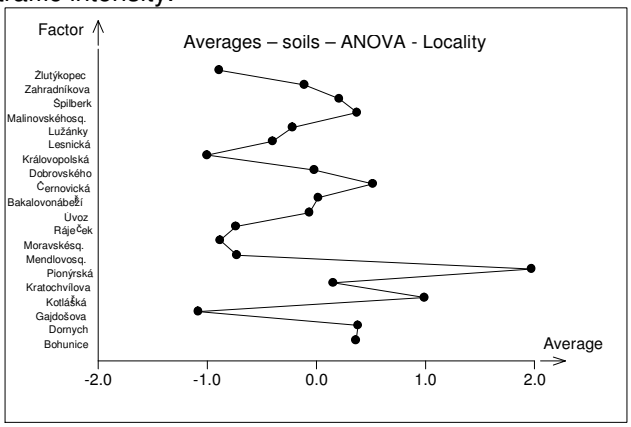

Fig. 3: Multifactor ANOVA analysis for PGE concentrations in soils – localities variability.

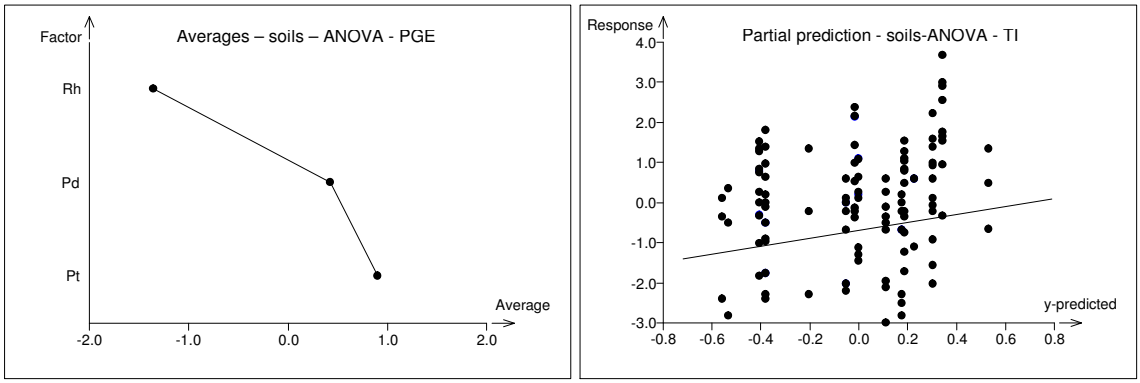

Fig. 4: Multifactor ANOVA analysis for PGE concentrations in soils – PGE concentrations variability and transport intensity.

PGE concentrations in runoff waters and porous waters were mostly under the detection limits for analytical method except Pd concentrations.

Measured concentrations of PGE adsorbed to PM in the air are in a good accordance with concentrations data published in literature (see table 1). Especially Pt concentrations in PM10 in Brno are nearly similar with concentration measured in Wien and significantly lower than concentrations measured in Madrid probably due to much higher transport intensities. Pt concentrations in tunnel dust mean values measured in Brno are the highest comparing with data from other European countries whereas the highest Pd concentrations were determined in Munich where the highest transport intensity among compared sites was. PGE concentrations in soils in urban area in Brno belong to the lowest in compared set of data, lower concentrations were determined only in the United Kingdom. The highest PGE concentrations were measured next highways in Germany and Athens in Greece. Large fluctuation of PGE concentrations in separate environmental matrices can be found in results in table 1. Some of the data show significant increase in different years especially in Germany. However this fact was not documented in samples taken in the Brno and its surroundings.

Table 1: PGE concentrations in separate environmental matrices in different European cities (Ravindra et al., 2004; Lesniewska et al., 2004; Riga-Karandinos et al., 2006; Wichmann et al., 2007; Gómez et al., 2002)

Environmental matrices	Locality	Year	TI	Pt			Pd			Rh			Unit
				mean value	lower limit	upper limit	mean value	lower limit	upper limit	mean value	lower limit	upper limit	
PM10	Wien, Austria		high	4.30			2.60			0.40			pg.m^{-3}
	Madrid, Spain	1998-1999	75 - 100	12.80	<0.1	57.1				3.30	<0.2	12.20	
	Brno, Czech Republic	2004-2007	8 - 34	3.3	0,047	32,4	23.7	0,195	166	1.9	00,9	13,2	
Tunnel dust – road dust	Steiermark, Austria, Tanzenberg tunnel	1997	high	55.00	47.00	63.00	4.00	2.70	5.30	10.30	8.90	11.70	µg.kg^{-1}
		1998	high	81.3	78.9	83.7	6.00	4.20	7.80	12.80	11.60	14.00	
	Germany, Frankfurt am Main, Harbor tunnel	1994	high	165	137	193	113.7	78.30	149.1	24.00	20.00	28.00	
	Bialystok, Po land	2000	28	23.30	19.50	27.10	23.90	22.70	25.10	6.76	5.48	8.04	
	Brno tunnels, Czech Republic	2002-2003	26.5	205.0	67,8	638	124.8	19,9	705	70.7	15	565	
Soil	Braunschweig, Germany	2005	16	50.30			43.30			10.70			µg.kg^{-1}
	Frankfurt am Main, Germany	1991	15	6.00	3.00	13.00		2.00	4.00				
		1994	15	46.00	12.00	82.00	4.00	2.00	8.00	9.00	3.00	19.00	
	Richmond, United Kingdom	1995	high	1.51	0.30	8.00		2.10	28.7				
	Athens, Greece	2003	48.6	141.1	73.3	254	125.9	25.40	239				
	Brno, Czech Republic	2006	11 - 46.5	2.46	0,4	39,6	1.53	0,5	8,2	0.26	0,05	4,89	

TI.....transport intensity [thousands of vehicles.day^{-1}]

Conclusion

Pt concentrations are higher than Pd concentrations in soils and in tunnel dust (road dust) whereas in waters and PM in air are concentrations of these metals reverse. So Pd is probably occurred in the environment in mobile forms and it can spread to longer distances from the source than Pt. Rh concentrations are nearly order of magnitude lower. Transport intensity is the important factor that influences PGE concentrations in the environment and it was confirmed also by the measurements conducted in Czech Republic in Brno. PGE concentration values determined in Brno and its surroundings are nearly similar to data from other European cities published in literature. Some studies also indicate increase of PGE concentrations in the environment but this fact was not explicitly documented by measures conducted during the period of 2002 – 2007 in Brno area. Longer measurements of PGE concentrations in separate environmental matrices seem to be necessary to find out time dependency progress.

References

Artelt, S.; Kock, H., König, H. P., Levsen, K., Rosner, G. (1999), Engine dynamometer experiments: platinum emissions from differently aged three-way catalytic converters. *Atmospheric Environment*, 33, 3559-3567.

Barbante, C., Veysseyre, A., Ferrari, C., van de Velde, K., Morel, C., Capodaglio, G., Cescon, P., Scarponi, G., Boutron, C. (2001), Greenland Snow Evidence of Large Scale Atmospheric Contamination for Platinum, Palladium and Rhodium.*Environmental Science & Technology*, 35, 835-839.

Djingova, R., Kovacheva, P., Wagner, G., Markert, B. (2003), Distribution of platinum group elements and other traffic related elements among different plants along some highways in Germany. *Science of the Total Environment*, 308, 235-246.

Ek, K. H., Rauch, S., Morrison, G. M., Lindberg, P. (2004), Platinum group elements in raptor eggs, faeces, blood, liver and kidney. *Science of the Total Environment*, 334-335, 149-159.

Gómez, B., Palacios, M.A., Gómez, M., Sanchez, J.L., Morrison, G., Rauch, S., Mcleod, C., Ma, R., Caroli, S., Alimonti, A., Petrucci, F., Bocca, B., Schramel, P., Zischka, M., Petterson, C., Wass, U. (2002), Levels and risk assessment for humans and ecosystems of platinum-group elements in the airborne particles and road dust of some European cities.*Science of the Total Environment*, 299, 1-19.

Leśniewska, B. A., Godlewska-Żyłkiewicz, B., Bocca, B., Caimi, S., Caroli, S., Hulanicki, A. (2004), Platinum, palladium and rhodium content in road dust, tunnel dust and common grass in Białistok area (Poland): a pilot study. *Science of the Total Environment*, 321, 93-104.

Moldovan, M., Palacios, M. A., Gómez, M. M., Morisson, G., Rauch, S., Mcleod, C., Ma, R.; Caroli, S., Alimonti A., Petrucci F., Bocca B., Schramel P., Zischka M., Pettersson C., Wass U., Luna M., Saenz J. C., Santamaría J. (2002), Environmental risk of particulate and soluble platinum group elements released from gasoline and diesel engine catalytic converters. *Science of the Total Environment*, 296, 199-208.

Nordberg, G. F., Fowler, B. A., Nordberg, M., Friberg, L. T. (2007) Handbook on the Toxicology of Metals. Elsevier.

Palacios, M., Gómez, M., Moldovan, M., Morrison, G., Rauch, S., McLeod, C., Ma R., Laserna J., Lucena P., Caroli S., Alimonti A., Petrucci F., Bocca B., Schramel P., Lustig S., Zischka M., Wass U., Stenbom B., Luna M., Saenz J. C., Santamaría J., Torrens J. M. (2000), Platinum group elements: quantification in collected exhaust fumes and studies of catalyst surfaces. *Science of the Total Environment*, 257, 1-15.

Prichard, H. M., Sampson, J., Jackson, M. A (2009), further discussion of the factors controlling the distribution of Pt, Pd, Rh and Au in road dust, gullies, road sweeper and gully flusher sediment in the city of Sheffield, UK. *Science of the Total Environment*, 407, 1715-1725.

Rauch, S., Peucker-Ehrenbrink, B., Molina, L. T., Molina, M. J., Ramos, R., Hemond, H. (2006), Platinum group elements in airborne particles in Mexico City. *Environmental Science & Technology*, 40, 7554-60.

Ravindra, K., Bencs, L., van Grieken, R. (2004), Platinum group elements in the environment and their health risk. *Science of the Total Environment*, 318, 1-43.

Riga-Karandinos, A. N., Saitanis, C. J.; Arapis, G. (2006), First study of anthropogenic platinum group elements in roadside top-soils in Athens, Greece. *Water, Air and Soil Pollution*, 172, 3-20.

Wichmann, H., Anquandah, G. A. K., Schmidt, C., Zachmann, D., Bahadir, M. A. (2007), Increase of platinum group element concentrations in soils and airborne dust in an urban area in Germany. *Science of the Total Environment*, 388, 121-127.

Impact of Land Use on Urban Mobility and Air Quality in a Portuguese Medium-sized City

C. Borrego[1], E. Sá[1], R. Tavares[1], J. Bandeira[2] and M. C. Coelho[3]*

[1] CESAM & Department of Environment and Planning, University of Aveiro, Campus Universitário de Santiago, 3810-193 Aveiro, Portugal

[2] Centre for Mechanical Technology and Automation, University of Aveiro - Campus Universitário de Santiago, 3810-193 Aveiro, Portugal, JorgeBandeira@ua.pt

[3] Centre for Mechanical Technology and Automation & Department of Mechanical Engineering, University of Aveiro - Campus Universitário de Santiago, 3810-193 Aveiro, Portugal

Abstract

The main purpose of this research was to evaluate the impact of current and future mobility pattern scenarios on air quality in Aveiro, a medium-sized Portuguese city. A sequential modelling process, comprising: i) land use and transportation – TRANUS model, ii) road traffic air pollutants emissions – TREM model and iii) air quality – TAPM model, was applied to assess the baseline situation and two future scenarios. The traffic modelling results of the baseline situation was based on traffic monitoring data gathered during October and November of 2008. The future scenarios consisted on different mobility patterns and vehicle technology characteristics, according to developing trends: (1) the "car polling" scenario", which imposes a mean occupancy rate of 3 passengers by vehicle and (2) the "Euro 6 scenario", which establish that all the vehicles accomplish at least Euro 6 standard technology. Present and future mobility patterns during a morning peak hour were evaluated according to the development trends. Fuel consumption and road traffic emissions were also estimated. A preliminary study of the base scenario modelled data showed a reasonably consistency which allowed the use of the system for the future scenarios. Regarding modelled CO concentrations an underestimation was observed. Nevertheless, the modelled PM10 levels were coherent with the monitored data. Reductions of 54% and 83% for CO, 44% and 95% for PM10, 44% and 87% for VOC and 44% and 79% for NO_x emissions were observed in the car pooling and Euro 6 scenarios, respectively. Changes of traffic volume, by increasing the vehicles occupation rates (car pooling scenario) resulted in a higher decrease of fuel consumption, when compared with a vehicle technology renewal (Euro 6 scenario). Concerning air quality, CO and PM10 annual average concentrations were estimated and compared with the baseline scenario. A reduction of 100 $\mu g.m^{-3}$ of CO annual average concentration was observed in both scenarios. The results of PM10 annual concentrations showed a reduction of 1.35 $\mu g.m^{-3}$ and 2.7 $\mu g.m^{-3}$ for car pooling and Euro 6 scenarios, respectively. This research allowed to conclude that, even new European standards emissions fulfilment will be a basic step in order to reduce local air pollution, the modification of urban mobility patterns is a key factor for this contribution.

Introduction and research objectives

Medium-sized cities (defined as having population of up to 250,000 in Europe) are facing increasingly traffic congestion and mobility problems. Besides the struggle related with land use, urban sprawl or low density areas, this type of cities face problems of financial support and road-space re-allocation for new Transit systems (Vougioukas et al, 2008). In Portugal half of the urban population lives in cities with 20,000-110,000 inhabitants (INE, 2001), where usually the main patterns of residential urbanization are diffuse settlements disconnected from concentrated urban centers. The city of Aveiro, located in the central coast of Portugal is a Portuguese medium-sized city (55,000 inhabitants) facing this type of urban development.

Over the last years several empirical and modeling studies have been performed, integrating land use, mobility, emissions and its relationship with urban structures (Johnston and de la Barra, 2000, Lam and Niemeier, 2005, Morton et al, 2007). However, available literature

focusing land use and transport planning impacts on environmental sustainability an air quality and population exposure to atmospheric pollutants (Marquez and Smith, 1999, Marshal et al. 2005, Borrego et al. 2006, EC, 2007, De Ridder et al. 2008a) are still scarce. Furthermore, most the work was performed for imaginary cities (Borrego et al. 2006; Martins et al., 2007), existing highly urbanized metropolitan regions (Civerolo et al. 2007, De Ridder et al. 2008a, 2008b) or at a local scale (Borrego et al 2003), but none for medium-sized cities.

Taking into account the problems that medium-sized cities face and the lack of research focused on this type of urban systems, the main purpose of this research was to evaluate the impact of current and future mobility pattern scenarios on air quality in Aveiro, a medium-sized Portuguese city.

Methodology

To evaluate the potential impacts of land use on urban mobility and air quality in a medium-sized city, a sequential modeling process was used, comprising: i) the land use and transportation – TRANUS model, ii) the road traffic air pollutants emissions – TREM model, and iii) the air quality –TAPM model, was applied to a baseline scenario (present situation) and two future scenarios ('car pooling' and 'EURO 6'), as shown in Figure 1.

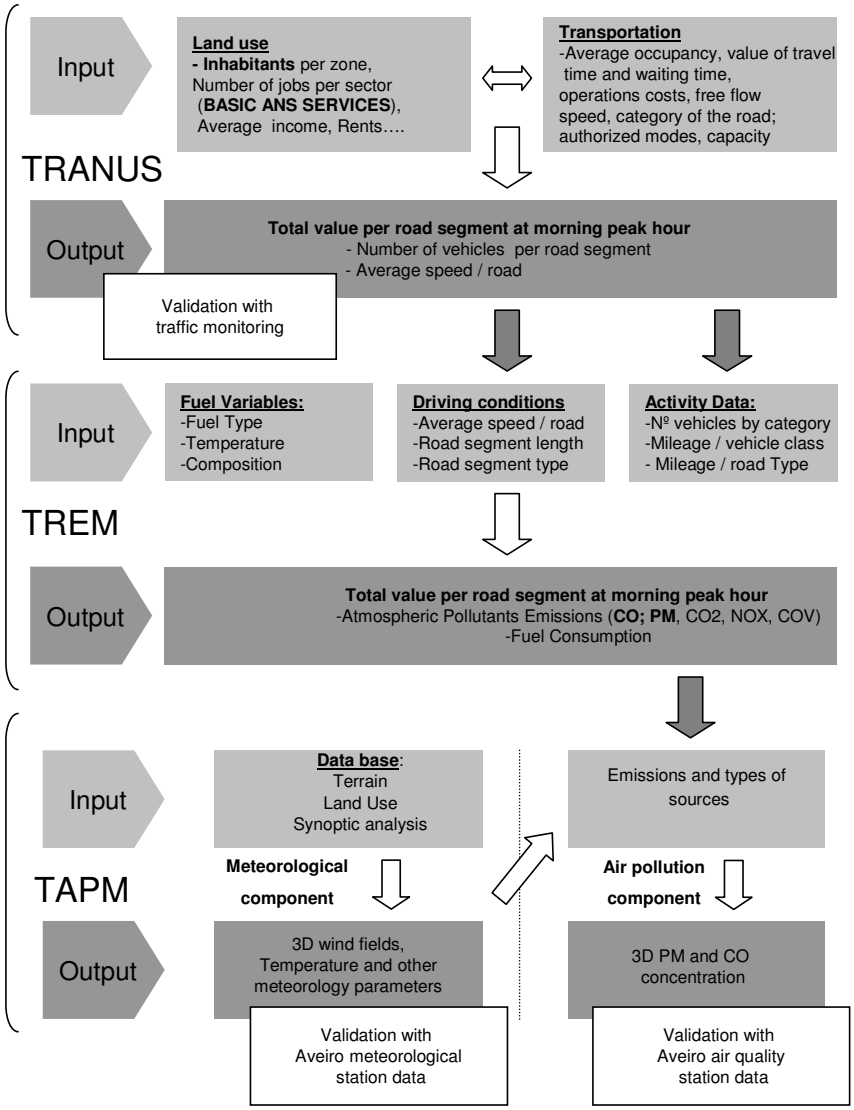

Figure 1: Structure of the methodology, with indication of the used modelling platforms and correspondent main inputs and outputs.

The **TRANUS model** was developed by Modelistica, to simulate land-use and transport (Modelistica, 2007). Mobility patterns are estimated based on the spatial distribution of activities, the real estate market and transportation system. People displacements are explained according to the economic and spatial interactions between activities and the transport system. Due to the lack of data for the urban neighborhoods, empirical factors and a simple structure constituted by four sectors: Population (number of inhabitants), Basic employment (jobs in the primary and secondary sectors), Service employment and Land (available construction area) were used. In order to evaluate TRANUS outputs, modelled traffic fluxes were compared with traffic monitoring performed on the six main intersection of the urban core (DE counts) and on the 5 main arterials that converge into the city center (VR counts) (see Figure 2).

The **Transport Emission Model for Line Sources (TREM)** was developed at the University of Aveiro, to support the quantification of emissions induced by road traffic with high temporal and spatial resolution to be used in air quality modelling (Borrego et al. 2003). The emission rates for several atmospheric pollutants and fuel consumption are estimated as a function of average speed. Average speed and traffic flow per road segment were introduced using TRANUS outputs. To characterize fleet composition, statistical data from insurance companies and the Portuguese automobile commercial association (ACAP, 2008) were applied using the same proportional sharing for vehicle technologies in the road network. Such approach is based on the preliminary analysis of the monitored data, which presented slight oscillations in both spatial and temporal dimensions regarding the fleet composition.

The **Air Pollution Model (TAPM)** is a 3-D Eulerian model which predicts meteorology and air pollution concentrations, based on the fundamental fluid dynamics and scalar transport equations (Hurley, 2005). The model integrates two modules: the meteorological and the air pollution component. The first predicts the meteorology input data for the second plus the emissions files, which estimates concentration and deposition of air pollutants. Atmospheric concentrations of carbon monoxide (CO) and particulate matter (PM10) were modelled. These were the selected pollutants due to their relevance within the scope of road traffic emissions but also for the availability of monitored data at the Air Quality Monitoring Station located within the study domain. To study the influence of the PM10 and CO traffic emissions in the road network, TAPM was applied over the region of Aveiro for the winter period (November and December). The application considers four domains with different sizes and resolution, (from 750×750 km^2 of area and 30×30 km^2 of resolution for Domain 1 until 25×25 km^2 and 1×1 km^2 for the domain 4). For the domain 4, area-sources annual emission data are obtained from the updated Portuguese national inventory, spatially downscaled to the sub-municipality level for pollutant and each activity sector. The disaggregation was made until 1×1 km^2, needed for the chemistry mode with sulphur and fine particle chemistry and for the tracer mode simulations. Although the simulation was performed for all the four domains only the domain 4 will be analysed in detailed, to validate both components of TAPM.

Regarding the future scenarios, two situations were defined. The ‘car pooling’ scenario aims to evaluate the effects resulting from the increase of vehicle occupancy rate (car pooling). An increase of 1.5 to 3 was considered for the mean vehicle occupancy rate. The ‘EURO 6’ intended to evaluate the pollutants emissions and its effect on air quality if all vehicles met the most recent European emissions standard. Therefore, the fleet composition was changed so that all passenger cars belong to the class EURO 6 and vehicles would meet the most stringent criteria according to the available information.

Results

TRANUS generated two origin destination matrices, i) home based work (HBW) and ii) home based services (HBS), which were created based on the relationships between the defined sectors and a trip generation function. TRANUS assigned 80% for HBW trips and 20% for HBS. Regarding the comparing between monitoring and assigned traffic in TRANUS, the overall Percent Root Mean Square of Error (%RMSE) value was 31.9% using both the DE and VR counts (sample of 21121 vehicles). Considering just VR counts a %RMSE of 25.9% was obtained (sample of 11951 vehicles). The internal cordon line allowed evaluating the model behaviour considering the total amount of traffic fluxes entering and leaving the urban core at

the morning peak hour (Figure 2). For this assumption, deviations were rather low (1% and 12% for inputs and the outputs, respectively).

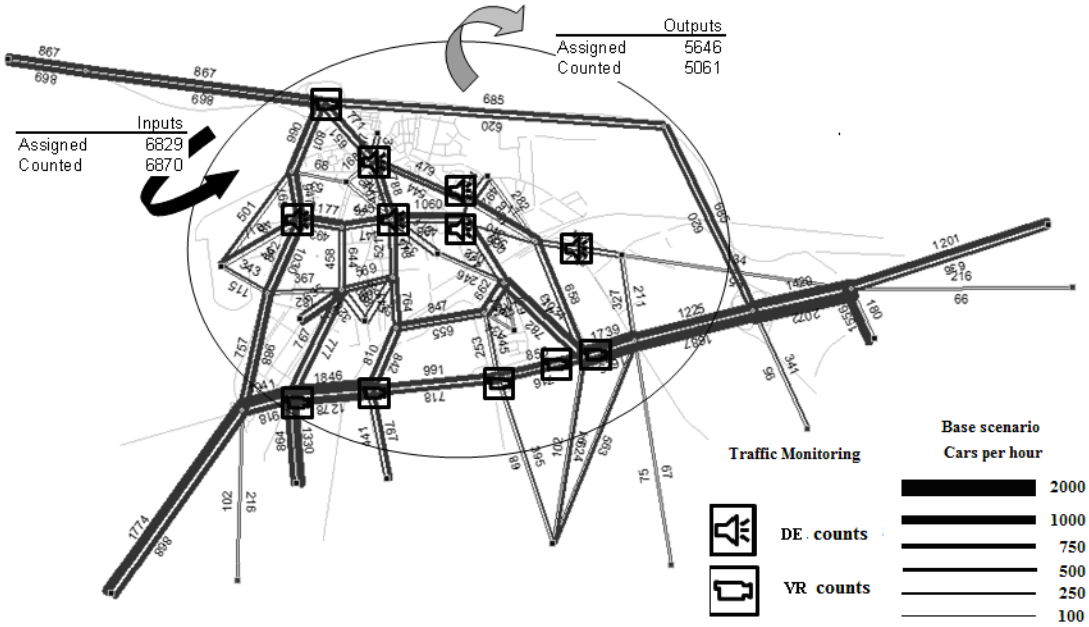

Figure 2: Assigned traffic at the morning peak hour for the baseline scenario.

Regarding the car pooling scenario, the most striking feature is that there is an average reduction by 45% in the total number of vehicles circulating in the city during the morning rush hour.

A total of 12 tons for CO_2 emissions, corresponding to around 7.8 tons of fuel consumption was estimated by TREM for the road network at the morning peak hour. In the same period, were also estimated: 99 $kg.h^{-1}$, 2.7 $kg.h^{-1}$, 49.2 $kg.h^{-1}$ and 1.51 $kg.h^{-1}$, for CO, PM10, NOx and VOC, respectively. Reductions of 54% and 83% for CO, 44% and 95% for PM10, 44% and 87% for VOC and 44% and 79% for NO_x emissions were observed in the car pooling scenario and Euro 6 scenarios, respectively. Fuel consumption and CO_2 emissions do not suffer significant reductions in EURO 6 scenario.

Air pollution module validation was performed by a comparison between the monitoring data in the air quality station of Aveiro and the model results for two months, considering the pollutants CO and PM10 (see Figure 3).

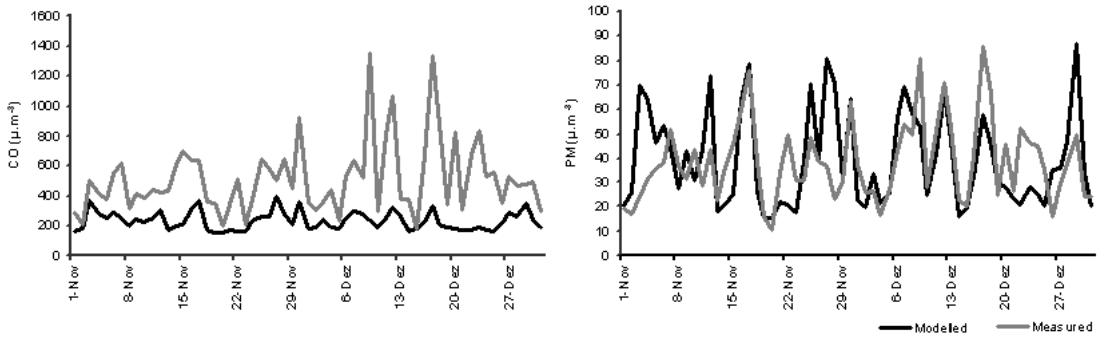

Figure 3 Comparison between the model results and the measured values on the air quality station of Aveiro for CO and PM10.

Regarding a qualitative analysis of CO, TAPM always underestimate the concentrations values. A first explanation to some of the observed divergences is connected to the model characteristics, in particular, its low resolution cell (1 km x 1 km). This characteristic does not

allow simulating the local environment of the air quality station with enough accuracy. It is known that the speed variations, namely accelerations, influence CO emissions (Coelho et al, 2005). The air quality station is located near a traffic light intersection, typically a stop-and-go "hotspot", which increases CO emissions. Another possible explanation for these deviations is the lack of a strong based knowledge on the source of exceptional emissions and the background pollutant concentrations, particularly concerning CO. The results also suggest that TAPM has better performance when use the chemistry mode instead of the tracer mode. The PM10 concentration model results were consistent with the reality. The two curves show an equivalent behaviour, indicating a higher correlation between the modelling results and the measured values. Figure 4 shows annual average concentrations for CO and PM10. For CO the maximum concentration is predicted for the city center (235µg.m^{-3}). The highest annual average concentration for PM10 is observed southeast from the city center (44 µg.m^{-3}).

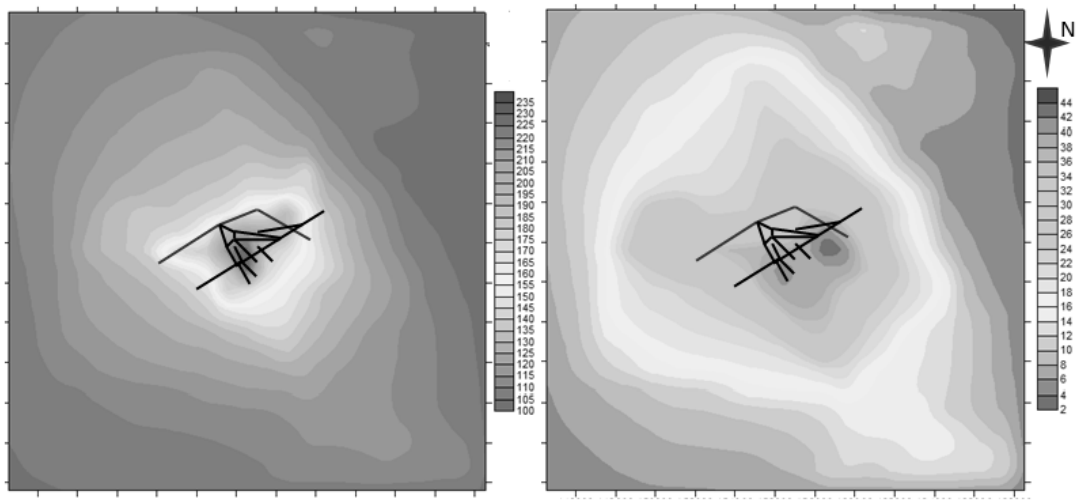

FIGURE 4 CO (left) and PM10 (right) annual concentrations (µg.m^{-3}) for: baseline scenario

Taking into account the outputs of TREM for the simulated scenarios a reduction of 100 µg.m^{-3} of CO annual average concentration was observed in both cases. Regarding PM10 annual concentrations, maximum reductions of 1,35 µg.m^{-3} and 2,7 µg.m^{-3} for car pooling and Euro 6 scenarios, respectively, are observed.

Conclusions

From the preliminary analysis of the baseline scenario outputs, it was possible to conclude that the developed methodology provided reasonably consistent results when compared with the measured data. It was proved that it can be possible to develop a methodology able to simulate the mobility patterns and air quality in a medium-sized city. Concerning the land use and transportation modelling, although the socioeconomic component was based on empirical approaches, it was achieved very acceptable results. Regarding air quality results, the simulation of CO concentrations showed an underestimation when compared with the experimental values. However, the modeled PM10 concentrations were consistent with the reality.

This research also allowed to conclude that, even new European standards emissions fulfilment will be a basic step in order to reduce local air pollution, the modification of urban mobility patterns is a key factor for this contribution. In both simulated scenarios the annual average concentration of PM10 remains high, showing that probably will be relevant to implement other measures outside the scope of transportation aiming the reduction of PM concentration.

References

ACAP: Portuguese Association of Car Manufacturers [Internet]. Statistics on Fuel Economy [cited 2008 Nov 20]. Available from: http://www.acap.pt

Borrego C., Tchepel O., Costa A., Amorim J. and A. Miranda (2003), Emission and dispersion modeling of Lisbon air quality at local scale. *Atmospheric Environment* , 37, 5197-5205.

Borrego C., H. Martins, O. Tchepel, L. Salmim, A. Monteiro, A, and A. Miranda (2006), How urban structure can affect city sustainability from an air quality perspective. *Journal of Environmental Modeling and Software* 2006, 21: 461-467.

Civerolo K., C. Hogrefe, B. Lynn, J. Rosenthale, J-Y Ku, W. Solecki, J. Cox, C. Small, C Rosenzweig, R. Goldberg, K. Knowlton, and P. Kinney. (2007), Estimating the effects of increased urbanization on surface meteorology and ozone concentrations in the New York City metropolitan region. Atmospheric Environment,; 41 1803-1818.

Coelho M., T. Farias, and N. Rouphail (2005), Impact of Speed Control Traffic Signals on Pollutant Emissions. *Transportation Research Part D*, 4, 323-340.

De Ridder K., F. Lefebre, S. Adriaensen, U. Arnold, W. Beckroege, C. Bronner et al (2008a), Simulating the impact of urban sprawl on air quality and population exposure in the German Ruhr area. Part I: Reproducing the base state. *Atmospheric Environment* , 42 (30), 7059-7069.

De Ridder K., F. Lefebre, S. Adriaensen, U. Arnold, W. Beckroege, C. Bronner et al (2008b), Simulating the impact of urban sprawl on air quality and population exposure in the German Ruhr area. Part II: Development and evaluation of an urban growth scenario. *Atmospheric Environment*,; 42: (30), 7070-7077

EC – Commission for the European Communities, Green Paper – Towards a new culture for urban mobility [internet]. Brussels 2007 [cited 2008 Sep 22]. Available from: http://ec.europa.eu/transport/clean/green_paper_urban_transport/

Hurley P. (2005a) The Air Pollution Model (TAPM) Version 3. Part 1: Technical Description, CSIRO *Atmospheric Research,* Technical Paper, 71, 54

Hurley P. (2005 b), The Air Pollution Model (TAPM) Version 3. User Manual, CSIRO *Atmospheric Research*, Technical Paper 31: 37

Hurley P., W. Physick and K. Luhar (2005c), TAPM: a practical approach to prognostic meteorological and air pollution modelling. *Environmental Modelling & Software*, 20, 737-752.

Hurley P., W. Physick, A. Luhar and M. Edwards (2005d), The Air Pollution Model (TAPM) Version 3. Part 2: Summary of Some Verification Studies, CSIRO *Atmospheric Research*, Technical Paper, 72: 54.

Johnston A. and T. de la Barra (2000), Comprehensive regional modeling for long-range planning: linking integrated urban models and geographic information systems. *Transportation Research Part A*, 34 (2): 125-136.

INE – Portuguese Statics – [cited 2008 Oct 09], Available from: http://www.ine.pt

Lam T. and D. Niemeier (2005), An exploratory study of the impact of common land-use policies on air quality. Transportation Research Part D 2005, 10 (55), 365-383.

Marquez L. and N. Smith (1999), A framework for linking urban form and air quality. Environmental Modeling and Software, 14 (6), 541-548.

Martins H., A. Miranda and C. Borrego (2007), Linking urban structure and air quality. Transport/Land Use Planning and Air Quality 2007. 9-11 July, Orlando, USA

Modelistica TRANUS: Integrated Land Use and Transport model – General description [internet] Caracas 2007, [cited 2008 Oct 09]. Available from: http://www.modelistica.com/tranus_english.htm.

Morton B., D. Rodriguez, Y. Song, and E. Cho (2007), Using TRANUS to Construct a Land Use-Transportation-Emissions Model of Charlotte, North Carolina. Proceedings of the Transportation Land Use, Planning, and Air Quality Conference 2007, Orlando, FL.

Reid E, Bartholomew K, Winkelman S, Walters J, and d. Chen (2008) The evidence on urban development and climate change. Washington, DC Urban Land Institute, Smart Growth America, Center for Clean Air Policy and National Center for Smart Growth Education and Research.

Vougioukas M., G. Sammer, A. Monzon, E. Evans and G. Ambrosino (2008), Quality public transport systems in medium size cities: socio–economic development and urban regeneration impacts, funding and implementation advances, Proceedings of European Transport Conference 2008, Leiden, Netherlands.

Influence of Street Canyon Geometries on the Dispersion of Nanoparticles

Ali Abdulsaheb and Prashant Kumar

Division of Civil, Chemical and Environmental Engineering, Civil Engineering (C5), University of Surrey, Guildford, UK, GU2 7XH

Emails:aa00101@surrey.ac.uk (Ali Abdulsaheb); p.kumar@surrey.ac.uk (Prashant Kumar)

Introduction

The adverse impacts of atmospheric nanoparticles on public health, climate change and urban visibility have attracted substantial attention of the air quality management and regulation authorities. Health issues become even more critical when people living or travelling nearby its sources (mainly vehicles) are exposed to high concentrations. One such place is urban street canyons where dispersion is limited by surrounding built–up environment. Hence, it is important to control their emissions in the urban environment. Several street canyon studies have looked into factors affecting the flow and dispersion conditions of gaseous pollutants, but very few have considered the influence of street canyon geometries on the dispersion of nanoparticles. Such information is critical for nanoparticle dispersion models that are required for designing mitigating policies in future.

The objective of this study is to apply a computational fluid dynamics (CFD) code FLUENT (using k-ε model) in a two–dimensional (2D) domain to study the flow and dispersion characteristics of nanoparticles in urban street canyon having four different shapes of upwind and downwind roofs. Different roof shapes have been selected to analyse the changes in distribution of nanoparticle concentrations in an idealised and more complex geometry. The other aim of this study is to analyse the effect of various sizes of emission sources on dispersion of nanoparticles, because there is no standard practise to select the source sizes while performing CFD simulations.

Methodology

Site description and measurements

Figure 1 shows the simple schematic diagram of a street canyon (Pembroke Street, Cambridge) that is used for CFD simulations. Both the height (H) and width (W) of the canyon is 11.6 m. The length of the canyon is about 167 m. The street canyon is orientated southwest (SW) – northeast (NE) and one–way traffic is running from SW to NE.

Particle number and size distributions were measured using a fast response differential mobility spectrometer (DMS500) in the 5-2738 nm size range. Measurements of meteorological parameters (wind speed, wind direction, temperature and pressure) have been taken at a height of 16.6 m above the road level. Detailed description of the canyon and measurements can be seen in Kumar et al. (2008b; 2009).

CFD simulations

A CFD code FLUENT is used to predict the dispersion of particle number concentrations (PNCs) in the selected street canyon with a combination of four types of roof tops. The flow field was calculated using steady Reynolds Averaged Navier Stokes (RANS) with the standard k-ε turbulence model. The dispersion of the particles was simulated with the 'user defined scalar (UDS)' option in FLUENT. An advection-turbulent diffusion equation was solved using the mean velocity field from the k-ε model and with a turbulent Schmidt number set to unity (i.e., the turbulent diffusivity was set equal the effective kinematic viscosity, also calculated by the k-ε model).

Computational domain and boundary conditions

Figure 1 shows the computational domain that represents four different roof top configurations for the same street canyon. The canyon is considered as an infinitely long canyon to model the distribution of nanoparticles in cross-wind conditions. This allows us to use a 2D domain. Table

1 explains the four different geometrical forms of the street canyon. A uniform velocity profile was set as a boundary condition at the inlet; a symmetry condition is assumed at the top of the flow domain. No slip conditions are considered at the side walls, street floor and roof in the upstream and downstream region of the domain. A background concentration (1.88×10^9 # m^{-3}) was set at all points in the grid at the inlet.

Emission sources

There is no standard practice to assign the size of an emission source in CFD simulations. In this study, we use four different sizes of finite cross–section line emission sources with constant discharge on the centre-line of the canyon, as were used in our earlier study (Kumar et al. 2009). All sources are located 0.20 m above the road level to simulate the height of the exhaust pipe. A description of four different sizes of emission sources is presented in Table 1. The strength of the sources CFD_Sa, CFD_Sb, CFD_Sc and CFD_Sd were taken as 3.086×10^{11}, 1.79×10^9, 2.4×10^{10} and 5.99×10^9 # $m^{-1}s^{-1}$, respectively (Kumar et al. 2009).

It should be noted that the intermediate and largest sizes of sources (i.e. CFD_Sb, CFD_Sc and CFD_Sd) intend to mimic the rapid dilution (in the region of the source) just after the rear end of the vehicle, but not the effect of traffic-produced turbulence in the rest of the vehicle wake. For simplicity, no extra source of turbulence is used in CFD simulations.

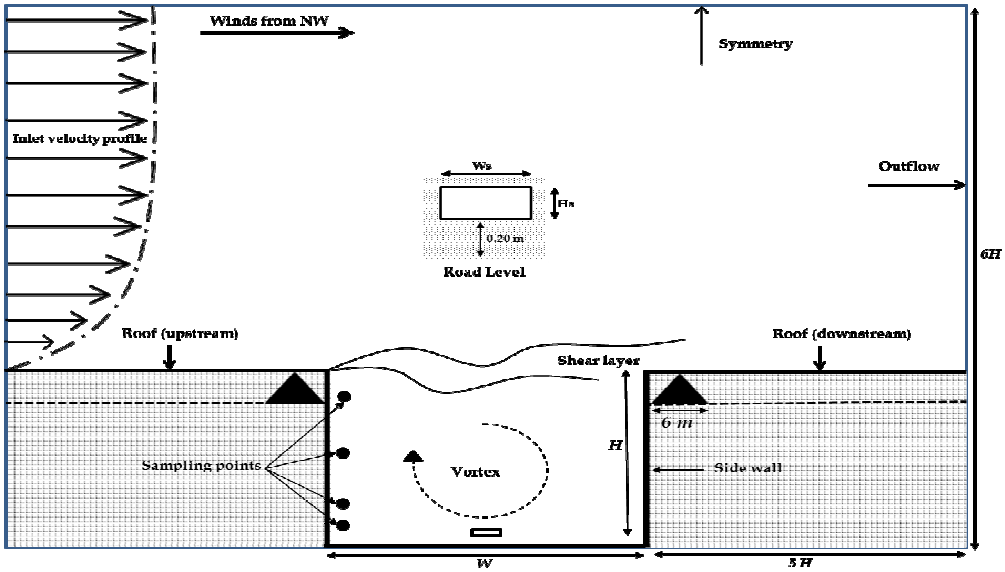

Figure 1: Schematic diagram of computational domain representing the dimensions of Pembroke Street. The black triangles show the modifications to the roof tops for defining four different canyon geometries; the height of the triangle is 1.7m, details can be seen in Table 1. H_s and W_s are the height and width of the source, respectively. Note that the figure is not to scale.

Table 1: Description of different canyon geometries used along with their associated emission sources.

Canyon	Roof Geometrical Form	Emission Source	Source Size			Emission Sources Installed
			Height (m)	Width (m)	Comments	
Canyon_1	Both sides flat	CFD_Sa	0.11	0.53	Smallest	CFD_(Sa,Sb, Sc & Sd)
Canyon_2	Upwind tapered and downwind flat	CFD_Sb	1.98	5.08	Largest	CFD_(Sa,Sb, Sc & Sd)
Canyon_3	Both sides tapered	CFD_Sc	0.75	1	Intermediate	CFD_(Sa,Sb, Sc & Sd)
Canyon_4	Upwind flat and downwind tapered	CFD_Sd	1.5	2	Intermediate	CFD_(Sa,Sb, Sc & Sd)

Results and Discussions

Flow characteristics

Figure 2 shows the distribution of mean velocity vectors in the selected street canyon geometries. One common observations from all four cases is that the mean velocity vectors shows an expected primary clockwise canyon vortex, with its centre being about the mid–building height, and small recirculation zones at the bottom corners of each canyon. These observations are in accordance to numerous field (De Paul and Sheih 1986; Kumar et al. 2008a) and computational studies (Huang et al. 2009; Kastner-Klein et al. 2004) that were carried out for a regular street canyons having an aspect ratio of about unity. The wind velocity is relatively slower at the centre of the vortex in each canyon compared to windward or leeward side walls. Interestingly, changes in the shape of roof tops do not seem to affect the presence of the primary canyon vortex but do appear to affect the magnitude of wind velocity flow field closer to pitched portion of the roofs and inside the canyon. Canyon_3 is having tapered roofs on both sides; the nature of canyon vortex is similar to those in other cases except the distortion along the sloping roofs of the building. Similar vortex characteristics were observed by Xie et al (2005) and Huang et al (2009) in their work for such geometries. For all cases studied with pitched roofs, a recirculation zone can be seen in upwind and downwind edges of the pitched roofs. This also influenced the wind velocity and turbulence levels (Fig. 3) at different parts in the canyon (Xie et al. 2005). For example, the wind velocity dramatically increases from the initial inlet velocity (3.8 m s^{-1}) to the maximum of 4.3, 4.4 and 4.1 m s^{-1} over the pitched roofs in Canyon_2, Canyon_3 and Canyon_4, respectively.

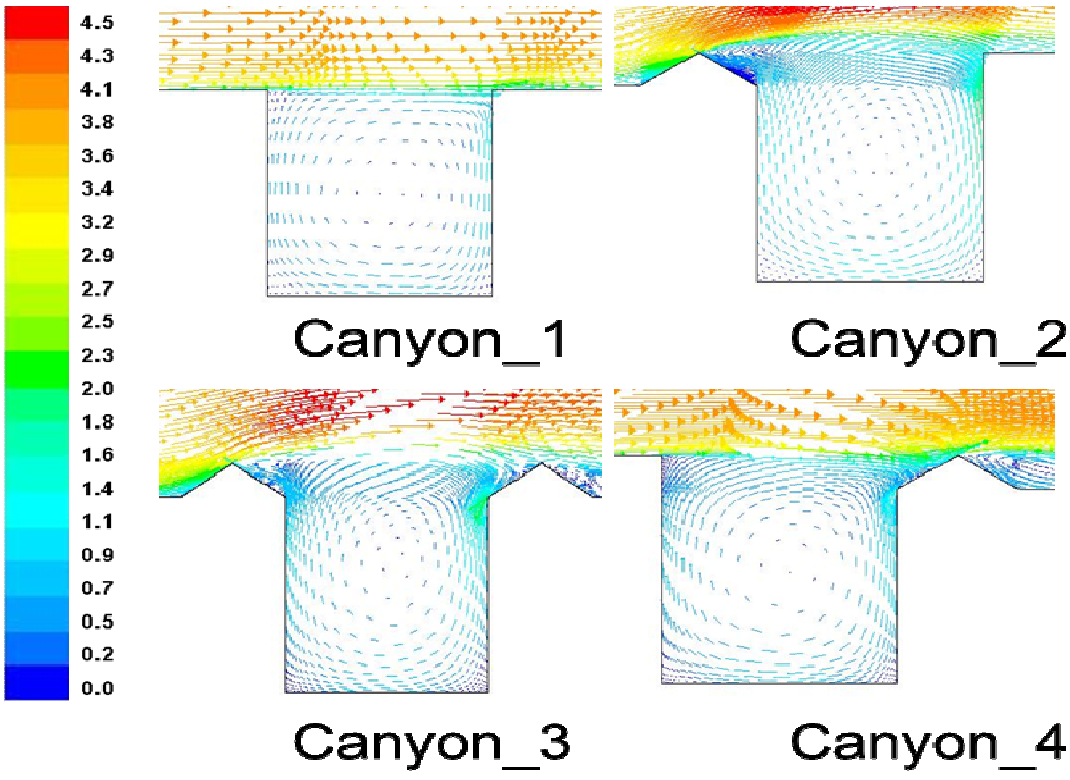

Figure 2: Flow distribution showing mean velocity vectors (m s^{-1}). This figure is for a constant inlet velocity 3.8 m s^{-1}. Note that high density of vectors means the grid spacing is close.

Turbulent kinetic energy (TKE)

The distribution of TKE is shown in Figure 3. A shear layer can be seen at the top of each canyon. However, the thickness of the shear layer changes with the change in canyon geometry. The TKE produced in this shear layer is dissipated when swept by the canyon vortex along the downwind side of the canyon. The dissipation rate of TKE is different for each canyon depending on the shape of the roof top. Canyon_1 and canyon_4 show nearly identical

dissipation pattern except the increased TKE along the windward tapered side where it increases to about 0.7 m^2 s^{-2} from 0.1 m^2 s^{-2} at the corner of the downwind side wall. The other two canyons show a different behaviour. For example, these got relatively high turbulence on the windward side of the canyon whereas it is nearly negligible on the leeward side. For example, the TKE at the top left corner of the tapered roof in Canyon_3 is about 0.5 m^2 s^{-2} which increased to about 0.7 m^2 s^{-2} at the top of right hand tapered roof due to increased velocity and then decreasing to about 0.01 m^2 s^{-2} at the bottom corner of windward wall. The above observations clearly indicate that change in rooftop geometries affect the TKE distributions within the canyon; this effect is largest in Canyon_3 and smallest in Canyon_1.

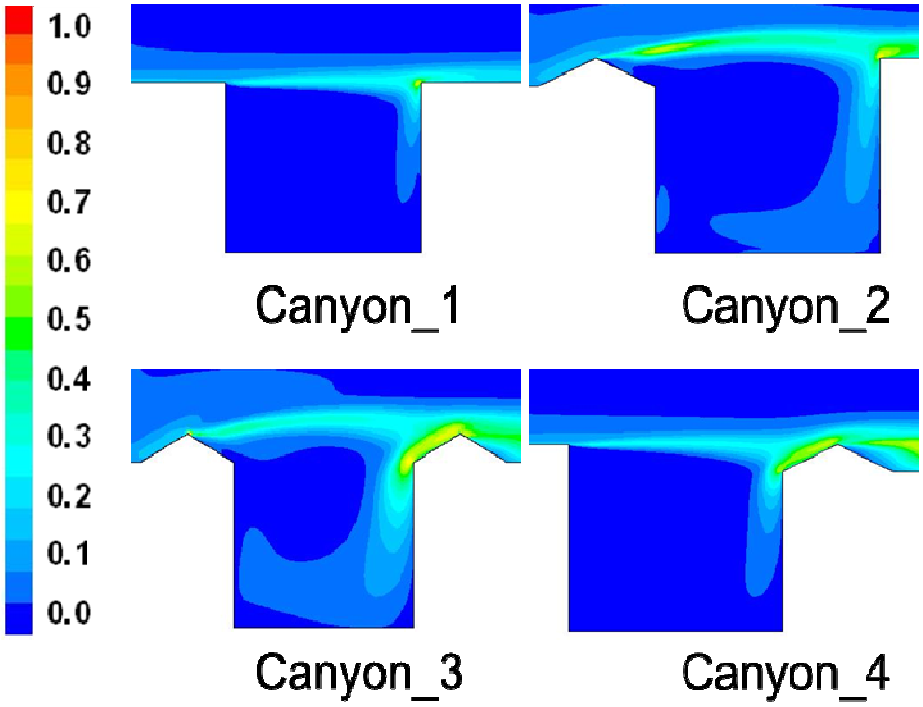

Figure 3: Distribution of turbulent kinetic energy (m^2 s^{-2}) in different canyon geometries.

Concentration distributions of nanoparticles

Figure 3 shows the concentration distributions of nanoparticles in all 16 cases, including a combination of four different shapes of roof tops and four different sources. Concentration distributions are expected to be dependent on intensity of turbulence (i.e. larger the TKE, larger will be the mixing and smaller the concentrations of nanoparticles) and the strength of the canyon vortex. Concentration distributions follow the above described relationship with the TKE distributions (Figure 3) and the strength of the vortex (Fig. 1). For example, greater turbulence occurred on the windward wall in canyon_1 causing a rapid dilution of the nanoparticles in that region and resulting in smallest concentrations compared to other canyons. On the other hand, concentrations are relatively larger at the leeward side of the walls in this canyon due to reduced TKE as compared with windward walls.

Average levels of turbulence were larger along the entire windward side of Canyon_2 as compared to its leeward side (Figure 3), resulting in much lesser concentrations at windward side. Similar patterns can be observed in Canyon_3 and Canyon_4. However, the change in the magnitude of concentrations is different in each canyon. For example, average concentrations on the leeward side of Canyon_1 at 1 m away from the wall are about 30, 60 and 40% larger than the average concentrations in Canyon_2, Canyon_3 and Canyon_4, respectively.

Influence of source size on the dispersion of nanoparticles

Figure 4 demonstrates the effect of different sizes of emission sources on the dispersion of nanoparticles. All the figures, irrespective of their source sizes, show the advection of

nanoparticles number concentrations from the sources to the leeward wall. However, the distribution of concentrations varied with the change in height and width of the sources. The smallest source (CFD_Sa), lead to largest concentrations in the bottom left hand corner of the canyon, irrespective of any roof top shape. This is because the smallest source is close to the ground and hence the particles are emitted into the edge of the vortex sweeping around the canyon and leading to high concentrations there. In cases with larger source areas, the particles first accumulate one the upper leeward side corner of the source where the concentrations are the largest, and then advected upwards on the leeward side by the canyon vortex (Figure 4). Moreover, the larger sources are centred further away from the ground and emit the particles nearer to the centre of the vortex, leading to higher concentrations further away from the leeward wall. However, the effects of source sizes are relatively smaller on windward side compared to leeward side because of the clockwise advection of particles by the canyon vortex.

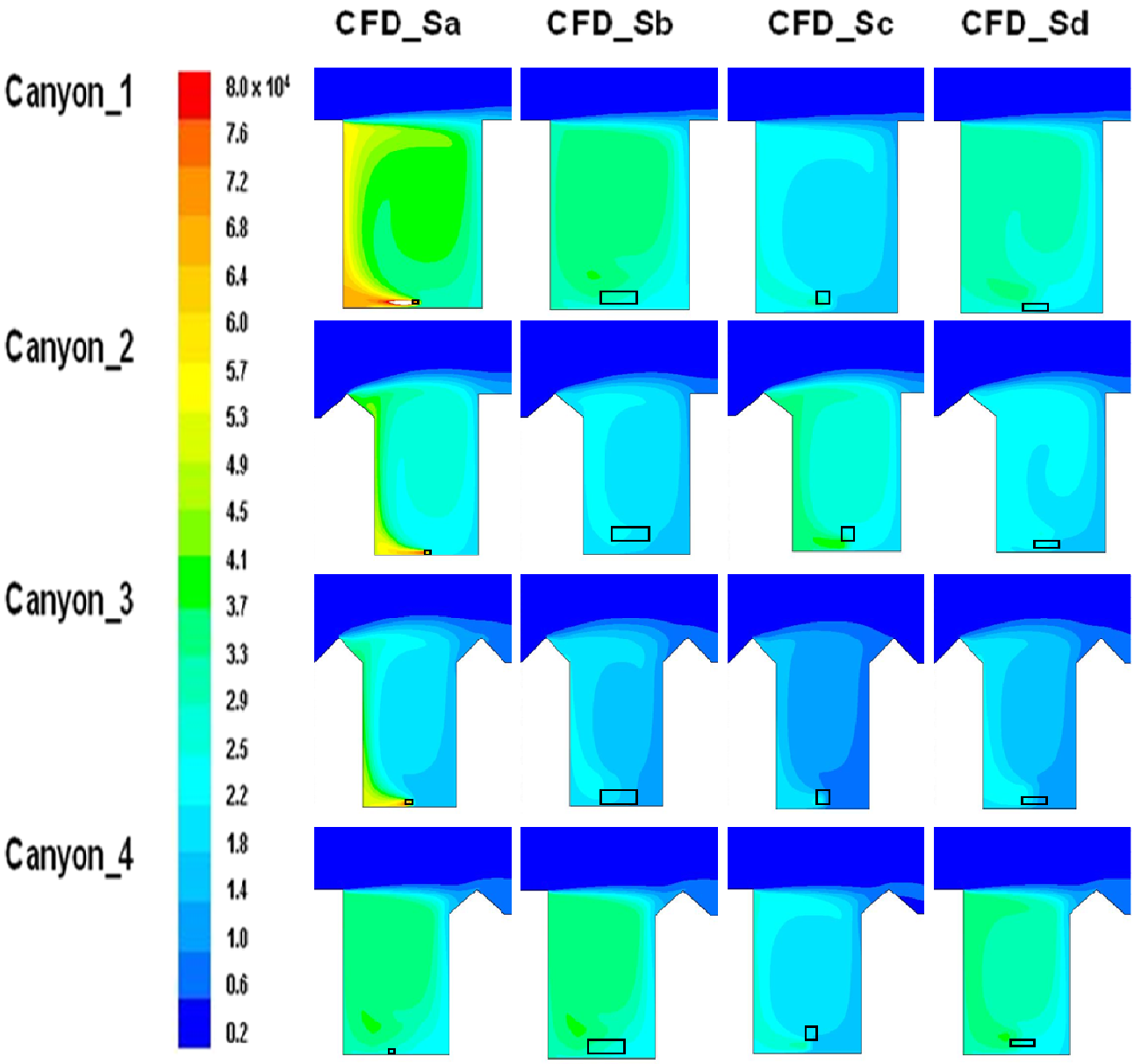

Figure 4: Typical distribution of mean PNC (# cm^{-3}) contours for 16 cases. Rectangular boxes represent the area of the sources. (Figure not to scale).

Summary and Conclusions

This study investigated the effect of the street canyon roof shapes (e.g. flat and pitched) on wind flow and dispersion of nanoparticles using a CFD code FLUENT. Four different sizes of emission sources were used in CFD simulations to assess their influence on distributions of mean nanoparticle number concentrations in selected street canyon geometries. As expected, a primary canyon vortex was observed in all types of canyons. However, the pitched roofs distorted the canyon vortex close to the roof top and influenced the magnitude of wind velocity in the canyon. Changes in the shape of rooftops (i.e. from flat to pitch) also altered the thickness of shear layer and distribution of turbulent kinetic energy that in turn affected the dispersion of nanoparticle concentrations. It is generally expected that larger turbulence levels lead to increased mixing of pollutants and results in smaller concentrations. In case of a flat roof canyon, advection of the nanoparticles from the source towards the leeward side of the canyon was higher and turbulent levels were the smallest that corresponded to the largest concentrations close to the leeward wall as opposed to other cases with pitched roofs. Pitched roofs positively influenced the strength of the canyon vortex and the advection of nanoparticles from the source towards the leeward wall; this is clearly evident from the colour contours in Fig. 4 as these are lighter in Canyon_2, Canyon_3 and Canyon_4 than those in Canyon_1. The canyon geometry having pitched roof on either side (i.e. Canyon_3) showed maximum turbulent kinetic energy (see Fig. 3) and corresponded to smallest concentrations. It can be concluded that changing the shapes of the rooftop, rather than assuming an ideal flat canyon, can affect the distribution of turbulent kinetic energy and concentrations. A detailed analysis of its quantitative impact on concentration distribution is under analysis. For all the studied cases, the changes in source size alter the distributions of concentrations substantially, indicating that selection of an appropriate source size is important in CFD simulations. The influences of source size on concentrations are much greater close to leeward side of the canyon compared to modest effect close to the windward side. These results support our previous findings (Kumar et al. 2009) that a source size scaling the dimension of the vehicle, not the size of the exhaust pipe, appears to be better representing the measured nanoparticle concentrations since this accounts for the effect of traffic–produced turbulence through rapid mixing in the source region.

References

De Paul F. T., C.M. Sheih (1986), A tracer study of dispersion in an urban street canyon, *Atmospheric Environment,* 20, 455-459.

Huang, Y., X. Hu and N.. Zeng (2009), Impact of wedge-shaped roofs on airflow and pollutant dispersion inside urban street canyons, *Building and Environment*, 44, 2335-2347.

Kastner-Klein, P., R. Berkowicz and R. Britter (2004), The influence of street architecture on flow and dispersion in street canyons, *Meteorology and Atmospheric Physics*, 87, 121-131.

Kumar, P., P. Fennell and R. Britter (2008a), Effect of wind direction and speed on the dispersion of nucleation and accumulation mode particles in an urban street canyon, Science of the Total Environment, 402, 82-94.

Kumar, P., P. Fennell, D. Langley and R. Britter (2008b), Pseudo-simultaneous measurements for the vertical variation of coarse, fine and ultra fine particles in an urban street canyon, *Atmospheric Environment*, 42, 4304-4319.

Kumar, P., A. Garmory, M. Ketzel, R. Berkowicz and R. Britter (2009), Comparative study of measured and modelled number concentrations of nanoparticles in an urban street canyon, *Atmospheric Environment*, 43, 949-958.

Xie, X., Z. Huang, J. Wang and Z. Xie (2005), Thermal effects on vehicle emission dispersion in an urban street canyon, *Transportation Research Part D: Transport and Environment*, 10, 197-212.

Continuous measurement of coarse, fine, and ultrafine particulate matter, gaseous pollutants and meteorological conditions at multiple locations in Antwerp, Belgium

Vinit K.Mishra[a,b], Luc Int Panis[a] , Martine Van Poppel[a], Evelien Frijns[a], Roland O'Donoghue[a] , Patrick Berghmans[a], Jan Theunis[a] , Nico Bleux[a], Roeland Samson[b]*

[a]VITO, Flemish Institute for Technological Research Boeretang 200, B-2400 Mol, Belgium
(*Corresponding authors: Ph:+32-14-33-5357, e-mail: vinitmishra@gmail.com)
[b]Department of Bioscience Engineering, University of Antwerp, Antwerp, Belgium

Introduction

The spatio-temporal variability of various pollutants were measured during a measurement campaign in Antwerp. The main objective was to determine spatial variation of various pollutants within one square kilometre urban grid. The measurement campaigns were carried out in order to evaluate error (co-)variances, including those related to the spatial representativity error associated with point measurements as compared to the volume averages found in air quality model grids. To do so, a measurement campaign was set up around a monitoring stations (VMM stations) of the Flemish Environment Agency, at an urban location, (Borgerhout, Antwerp). PM2.5, NO_2 and O_3 concentrations were monitored at four locations and UFP levels at three locations out of the four, in a buffer of 1 km (model fine grid size) around VMM measurement site, over a period of 3 weeks during Summer.

Methodology

Borgerhout is a district of the municipality and city of Antwerp in the Flemish Region of Belgium. The district houses 41,614 inhabitants (as of 31 May 2006). Borgerhout is a typical busy urban commercial/residential area with heavy traffic activity, it is located at 51°13"N and 4°26"E. The measurement campaign for PM2.5 and gaseous pollutants at Borgerhout was started on 24th June and completed on 12th July 2009. In total measurement was performed at four locations around VMM measurement station at Borgerhout.

Fig. 1: Map of the measurement grid around VMM in Borgerhout.

The four locations and their characteristics are described below:

1.Turnhoutsebaan-heavy traffic with separate tram lane in the middle, two lanes for other traffic, one in each direction.
2.Provinciestraat-street canyon with heavy traffic and tram, road with two lanes on in each direction
3.Platin &Moretuslei- very busy traffic intersection with train lines close to it, four lanes, two in each direction.
4.Kleine Beerstraat-street with moderate traffic with tram, with two lanes one in each direction.

Table 1: The list of instruments installed at four sampling sites in Antwerp.

S.No.	Location	Instruments	Parameter
1	Kleine Beerstraat- OCMW	Partisol	PM2.5 gravimetric
		Air pointer	Meteo, NO,NO_2, O_3
		GRIMM	PM1,2.5,10, TSP-real time
		CPC-Butenol	UFP number concentration
2	Provinciestraat Kleuterschool	Partisol	PM2.5 gravimetric
		GRIMM	PM1,2.5,10, TSP-optical
		Air pointer	Meteo, NO,NO_2, O_3
		UFP monitor	Size resolved UFP concentration
3	Turnhoutsebaan-The court	Partisol	PM2.5 gravimetric
		Air pointer	NO,NO_2, O_3
		GRIMM	PM1,2.5,10, TSP-real time
		CPC-Water based	Number concentration
4	Plantin n Moretuslei Zwembad	Partisol	PM2.5 gravimetric
		Air pointer	NO,NO_2, O_3
		TEOM-FDMS	PM 2.5 real-time
		GRIMM	PM1,2.5,10, TSP-optical
5	VMM	Partisol	PM2.5 gravimetric

The meteorological parameters were measured by meteo instruments mounted on Air Pointers, at two sites (Provinciestraat & Kliene beerstraat) out of the four. During the measurement period, the mean temperature was about 21˚C and relative humidity 64%. The wind rose diagram shows that the predominant wind direction was from North and South East at Provinciestraat and West North West at Kliene Beerstraat (fig. 2.10). The wind directions were different at the two locations as the wind directions were influenced by the specific local orientation of buildings around the measurement sites.

Result and Discussion

Particulate concentrations (PM2.5) at different sites in Borgerhout

The continuous measurement (gravimetric) for PM2.5 was performed at all the five sampling location, including one at VMM, with partisol. The temporal pattern of PM2.5 at all the five sites are given in the fig. 2 below.

The PM 2.5 concentration derived from partisol shows that although PM 2.5 levels were almost uniform within the grid of 1 Km around VMM station, but there were slight variation in the concentration levels according to the levels of traffic in the area. All the four locations showed strong correlations with the PM2.5 levels at VMM.

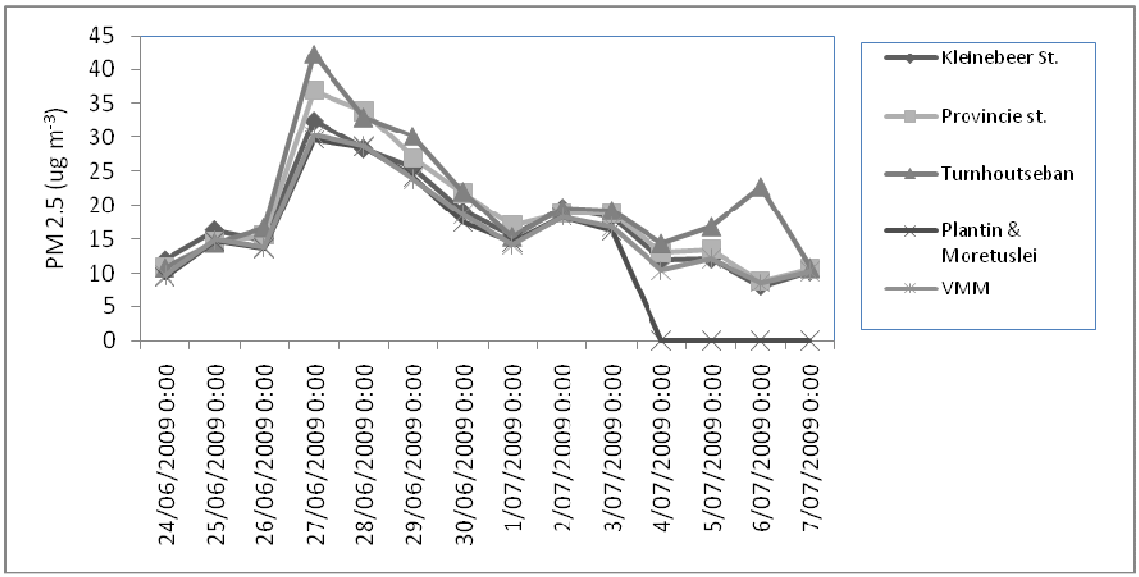

Fig. 2: Temporal variation in PM2.5 levels (partisol) at the five sites including VMM.

The temporal trend of real time PM2.5 levels measured with TEOM at three sites VMM, Provincistraat and Zwembad were slightly higher in comparison to the one measured with partisols. But TEOM derived PM 2.5 levels also showed similar temporal trend during entire campaign.

Gaseous Pollutants

The gaseous pollutans were measured at the three sites out of the four and were compared against the VMM data. The gaseous pollutants followed the similar diurnal trend at the five sites (including VMM), although their levels were slightly different from each other and also the wind directions associates with the highest concentration were found to be different from each other, which was expected at high traffic urban location.

The Correlation Aanalysis was performed on the gaseous pollutant data of all the four sites (including VMM). The correlations between NO and NO_2 between Provinciestraat and Kliene beerstraat were higer(>80%) than Provinciestraat and Turnhoutsebaan (57%). Correlation between NO_2 at Turnhoutsebaan and Kliene beerstraat were also lower (60%). The correlation between Turnhoutsebaan and VMM were low (57%) but the correlation between Kliene beerstraat and VMM were not significant. Probable reason for good correlation between VMM and Turnhoutsebaan can be the similar high levels of traffic crossing these sites. The traffic density was lowest at Kliene beerstraat.

The O_3 levels at the four sites showed good correlation with each other. Probably because O_3 levels follow the diurnal temperature pattern (sunlight).

Measurement of UFP

The fine-scale spatial and temporal variability of the number of ultra-fine particles (UFP) were measured during campaigns in Antwerp. The focus was on traffic-related particles and typical urban locations, like a busy crossing, a street canyon, and background streets. It was examined how the variability of number concentrations within the urban environment is affected by location within the same microenvironment in the city. In order to determine regional vs. local contributions to particle number levels, highly time-resolved data for particle number together with size distribution was analyzed using several measuring and statistical techniques.

The same locations where instruments for PM2.5 and gaseous pollutants were installed, were also used for simultaneous measurement of UFP levels, in order to find out possible correlations between different pollutants and UFP and also to examine short term variation in UFP concentrations. Traffic counts were also performed at these locations to correlate the observed variation in pollutant level with the variation in traffic. Out of the four measurement locations three were used to measure UFP concentration which were Turnhoutseban (Water

based CPC), Klienebeer straat (OCMW) (Butenol CPC), and Provinciestraat (UFP monitor). Typical diurnal variation of UFP levels at the three location has been given in the figure 3 below.

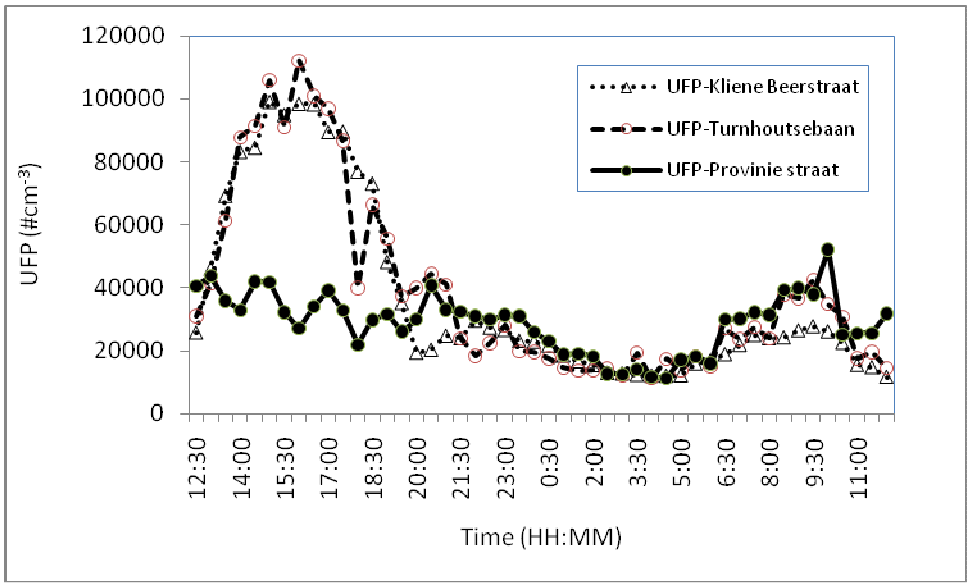

Fig. 3: Typical diurnal pattern of UFP levels (30 min Average) on 29th & 30th June 2009 at three locations in Borgerhout.

As expected the correlation between UFP levels at Provinciestraat (measured with UFP monitor) were not significant. On the other hand the two CPCs located at Turnhoutsebaan (WCPC) and OCMW (Butenol-CPC) showed good correlation with each other. The reason for the low correlation between Proviciestraat and other two sites was the fact the UFP monitor which was used to measure UFP levels at this site, had a lowest cut-off size of 30nm, on the other hand the two CPCs have lowest cut off of 2.5nm. The traffic locations usually have a large number of particles below 30nm and that was the reason why the levels of UFP were much higher at the other two sites in comparison to Provinciestraat and they also showed higher correlation with each other.

In order to understand UFP dynamics correlations between different gaseous pollutants (NO, NO_2, NO_x, and O_3) and UFP, were examined. There were significant correlations between different gases and UFP levels, for example NO and NO_2 showed strong correlation with UFP at different sites, at Klienebeerstraat, O_3 showed substantial correlation with UFP. While correlation between UFP and different NO species show common source of their origin(vehicular traffic), the higher correlation between UFP and O_3 indicate towards major role of photochemical processes behind the formation of UFP in the area. The correlation between different gases and UFP helps us to understand the formation and transformation mechanism behind UFP dynamics in an urban microenvironment. It was also observed that UFP poorly correlates with fine and coarse PM fractions at all the three sites. This further proves the transient and very local nature of UFP in comparison to fine and coarse fraction of particles which generally tend to have a uniform regional nature.

Conclusions

It can be concluded from the correlation analysis and also by observing the temporal trend in PM 2.5 concentration at the five sites that the PM2.5 concentration were rather constant within the Grid of 1 km around VMM measurement station. The temporal variation in PM2.5 concentration levels within the grid follow the same trend at all the sites even if the measurement was performed with three different types of instruments. The similarity in the temporal trend of real time (TEOM) data further established the fact that PM 2.5 concentration were less impacted by very short term local changes in the traffic conditions. Therefore the PM 2.5 levels were observed as more or less a constant over a small region and less impacted by very local sources, both building up and dispersion of PM 2.5 was found to be slower in contrast to gaseous and ultrafine concentration levels, which are highly impacted by very local sources.

Regarding within grid variation in UFP levels, it was established that the UFP do have a very strong and clear diurnal pattern which follows the traffic variation more closely than fine and coarse fractions of particles. The strong correlation between two sites measuring with CPC indicates the fact that the two locations although having different levels of traffic and hence different UFP levels, follow exactly the same diurnal pattern. The correlation between two sites with completely different levels of anthropogenic activities also indicates that UFP also have a regional characteristics in addition to very strong local nature. The high correlation with O_3 levels at one of the site (Kliene Beerstraat) indicates significant role of photochemical processes in UFP formation at this site.

References

Charron, A., Harrison, R.M., Moorcroft, S., Booker, J., 2004. Quantitative interpretation of divergence between PM10 and PM2.5 mass measurement by TEOM and gravimetric (Partisol) instruments. Atmospheric Environment 38 (3), 415–423.

Price, M., Bulpitt, S., Meyer, M.B., 2003. A comparison of PM10 monitors at a kerbside site in the northeast of England. Atmospheric Environment 37, 4425–4434.

Pinto JP, Lefohn AS, Shadwick DS. Spatial variability of PM25 in urban areas in the United States. 2004. J Air Waste Manage (54): 440–9.

Direct implementation of non-linear chemical reaction terms for ozone chemistry in CFD-based Air Quality modelling

B. De Maerschalck[1], S. Jannssen[1], M. Clemens[1]*

[1] VITO, Dep. Of Atmospheric Modelling , Boeretang 200, 2400 Mol, Belgium, bart.demaerschalck@vito.be

Introduction

The last decade Computational Fluid Dynamics (CFD) has gained interest as a practical tool for local air quality modelling in complex environment like street canyons, urbanized areas industrial plants. CFD-based air quality models are capable of solving complex three-dimensional flows around obstacles like buildings, trees and vehicles. After solving the wind and turbulence field, the dispersion of pollutants in the atmosphere can be simulated either in a Lagrangian approach, tracking individual particles after release, or an Eulerian approach, that is solving a 3D scalar advection equation. Until now, most CFD-based air quality models solve for an inert gas, similar to wind tunnel modelling. However, it is well understood that nitrogen oxides are reacting fast with ozone while a European air quality directive is specific for NO_2. Regarding to traffic emissions about 80% of NO_x emission is NO, but depending on the ozone background concentrations and meteorological conditions this will react and for secondary NO_2 which can have a significant effect on the local air quality.

In this paper we present a model that transforms the NO_x composition dynamically during transportation. For that, the scalar advection equations for NO, NO_2 and O_3 are coupled by non-linear reaction terms and solved simultaneously. The model is implemented and tested in the Envi-met local air quality and micro climate model (Bruse 2007; De Maerschalck, Janssen et al. 2009).

Ozone chemistry in the troposphere

Nitrogen oxides are ubiquitous urban air pollutant mainly emitted by traffic, power plants and industry. Nitric oxide is on mass basis the most important nitrogen compound emitted into the atmosphere. Nitric oxide is formed from atmospheric nitrogen (N) at high temperatures as in combustion processes. More than 90 percent of the emitted oxide consists of nitrogen oxide (NO), while the remaining party is emitted as nitrogen dioxide (NO_2) (Berkowicz 1998). Once emitted from the tail pipe, nitrogen oxide will react with ozone:

$$\mathrm{NO} + \mathrm{O_3} \quad \longrightarrow \quad \mathrm{NO_2} + \mathrm{O_2}\ . \tag{1}$$

Under typical tropospheric boundary layer conditions, this reaction takes place within a time span of a couple of seconds till minutes, depending on the background concentrations NO, NO_2 and O_3 and meteorological conditions.

NO_2 is the first reaction product of the atmospheric oxidation process of the emitted NO. However, the freshly formed nitrogen oxide will absorb solar ultraviolet radiation ($200nm \leq \lambda \leq 420nm$) and forms again NO and O_3:

$$\mathrm{NO_2} + h\nu \longrightarrow \mathrm{NO} + \mathrm{O}\ . \tag{2}$$
$$\mathrm{O} + \mathrm{O_2} + \mathrm{M} \longrightarrow \mathrm{O_3} + \mathrm{M}\ . \tag{3}$$

Reaction (3) happens quasi immediately. Therefore, in general reactions (2) and (3) are considered as one and O_2 in the atmosphere is accepted as being constant.

The reaction of NO with O_3 and the photolysis of NO_2 form a cycle which occurs rapidly over the timescales of seconds till minutes. Under most tropospheric conditions, NO and NO_2 will coexist as a mixture, called NO_x. If a steady state is reached, the following equilibrium holds:

$$\frac{[\mathrm{NO}][\mathrm{O_3}]}{[\mathrm{NO_2}]} = \frac{j_{NO_2}}{k_{NO}}\ . \tag{4}$$

where the parentheses indicate the number concentration of the compound in molecules/cm³. k_{NO} is the second order or bimolecular reaction rate coefficient in (1) and is dependent on the ambient temperature (Seinfeld and Pandis 2006):

$$k_{NO} = A_0 \exp\left(-\frac{E}{R}\frac{1}{T}\right) . \tag{5}$$

with

$$\begin{aligned} A_0 &= 2.2 \times 10^{-12} \frac{cm^3}{molecule\ s} . \\ \frac{E}{R} &= 1430\ K \end{aligned} \tag{6}$$

Figure 1 plots the reaction rate as a function of the temperature.

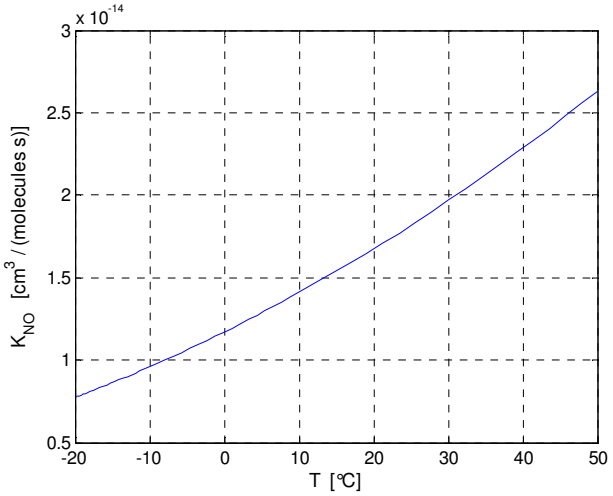

Figure 1 : Bimolecular reaction rate coefficient as function of the temperature

j_{NO_2} is the photolysis coefficient of equation (2) and is dependent on the solar ultraviolet radiation. The computation is rather complicated. Theoretically one should integrate over the product of the NO_2 specific absorption cross section with the quantum yield for photolysis and the spectral actinic flux within the limits of the ultraviolet spectrum (Seinfeld and Pandis 2006).

However, for a fast estimate different parameterisations are available based on solar angel, solar radiation and cloud coverage (Berkowicz and Hertel 1989; de Leeuw 1995; van Ham and Pulles 1998)

For the implementation in the Envi-met model, the following empirical formulation based on the solar radiation is used:

$$j_{NO_2} = 0.8 \times 10^{-3} \exp(-10/R_s) + 7.1 \times 10^{-6} R_s . \tag{7}$$

with R_s the solar radiation measured in $[W/m^2]$. In ENVI-met in every cell the solar radiation is calculated based on the positions of the sun, cloud cover, local shadows and reflections. Figure 2 shows the estimated values during two different days at a location in the Netherlands based on different parameterization schemes. The red line is the one according to (7) where R_s is dynamically computed by the Envi-met model.

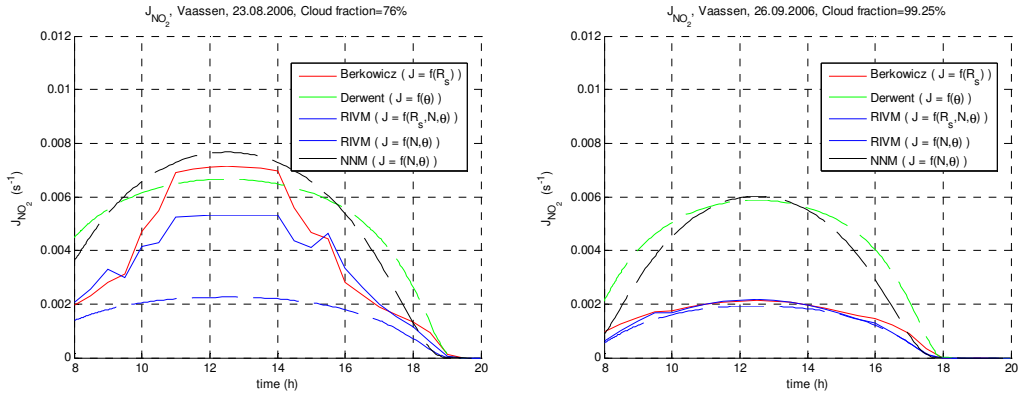

Figure 2: Computed photolysis coefficient during the day for Vaassen, The Netherlands (Left: 23/08/2006, mean cloud coverage 76%; Right: 26/09/2006, 99%)

Chemical equilibrium

Assume that $[NO]_0$, $[NO_2]_0$ and $[O_3]_0$ are the initial number concentrations put in a reactor of constant volume at constant temperature and radiation. After a short time a steady state will be reached for which the photostationary state relation (4) holds. From the conservation of nitrogen and the stoichiometric reaction of O_3 with NO follows (Seinfeld and Pandis 2006):

$$\begin{aligned} [NO] + [NO_2] &= [NO]_0 + [NO_2]_0 \,. \\ [O_3]_0 - [O_3] &= [NO]_0 - [NO] \,. \end{aligned} \tag{8}$$

One can solve now the chemical equilibrium in the reactor and gets:

$$\begin{aligned} [NO_2] &= [NO_2]_0 + \frac{1}{2}\left([O_3]_0 + [NO]_0 + \frac{j_{NO_2}}{k_{NO}}\right) - \frac{1}{2}\sqrt{D} \,. \\ [NO] &= -\frac{1}{2}\left([O_3]_0 - [NO]_0 + \frac{j_{NO_2}}{k_{NO}}\right) + \frac{1}{2}\sqrt{D} \,. \\ [O_3] &= -\frac{1}{2}\left([NO]_0 - [O_3]_0 + \frac{j_{NO_2}}{k_{NO}}\right) + \frac{1}{2}\sqrt{D} \,. \end{aligned} \tag{9}$$

with

$$D = \left([NO]_0 - [O_3]_0 + \frac{j_{NO_2}}{k_{NO}}\right)^2 + 4\frac{j_{NO_2}}{k_{NO}}\left([NO_2]_0 + [O_3]_0\right) \tag{10}$$

One can assume that for a rural background concentration, NO, NO_2 and O_3 are in equilibrium. We now can verify that the parameterisation in (7) together with the modelled solar radiation holds by using the computed photolysis coefficients to estimate the equilibrium state according to (9) and (10). The initial numbers are taken from nearby rural measurement stations. Theoretically, if the measured background concentration is in equilibrium and the photolysis coefficient is estimated well, the computed equilibrium should not differ from the local measurements.

The measured background concentrations are compared to the modelled equilibrium state for two days at the location of Vaassen, the Netherlands (Janssen, De Maerschalck et al. 2008). The measured background concentration is the mean from three Dutch rural background concentrations. Again the red line is based on the parameterisation in (7). The red line with the bullets is the measured mean background concentration.

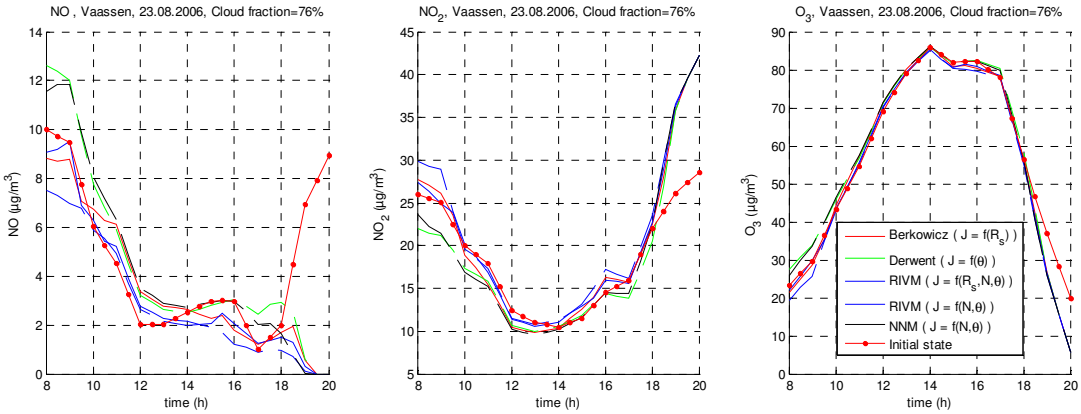

Figure 3: Measured rural background concentrations and computed equilibrium for NO (left), NO2 (middle), and O3 (right). (Vaassen, The Netherlands, 23/08/2006, 76% cloudiness)

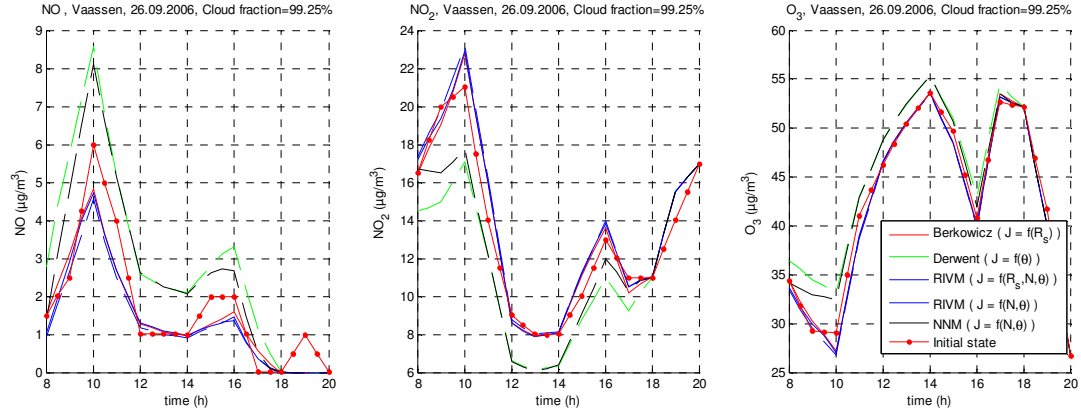

Figure 4: Measured rural background concentrations and computed equilibrium for NO (left), NO2 (middle), and O3 (right). (Vaassen, The Netherlands, 26/09/2006, 99% cloudiness)

Dynamic chemical transformation processes in CFD based air quality models

The dispersion of a certain gas i can be described by a scalar dispersion equation for the concentration $C_i(x, y, z)$:

$$\frac{\partial C_i}{\partial t} + \boldsymbol{u} \cdot \nabla C_i + \nabla \cdot (\boldsymbol{K_i} \cdot \nabla C_i) - E_i - S_i + R_i \ . \tag{11}$$

with $E_i(x, y, z)$ the local emissions of compound i and $S_i(x, y, z)$ the sum of all sink terms (deposition, interaction with vegetation, sedimentation, ...). R_i is the chemical reaction term and is in general dependent on the concentration of all compounds involved in the reaction. The advection velocity and the turbulent reaction terms are computed by the flow solver of the CFD model.

For the photochemical reactions described above the dispersion equations for NO, NO_2 and O_3 have to be solved simultaneously. The partial differential equations are coupled with the following non-linear reaction terms:

$$R_{NO} = \left(\frac{\mathrm{d}\,[\mathrm{NO}]}{\mathrm{d}t}\right)_R = -k_{NO}\,[\mathrm{NO}][\mathrm{O_3}] + j_{NO_2}[\mathrm{NO_2}] \ . \tag{12}$$

$$R_{NO_2} = \left(\frac{\mathrm{d}\,[\mathrm{NO_2}]}{\mathrm{d}t}\right)_R = k_{NO}\,[\mathrm{NO}][\mathrm{O_3}] - j_{NO_2}[\mathrm{NO_2}] \ . \tag{13}$$

$$R_{O_3} = \left(\frac{\mathrm{d}\,[\mathrm{O_3}]}{\mathrm{d}t}\right)_R = -k_{NO}\,[\mathrm{NO}][\mathrm{O_3}] + j_{NO_2}[\mathrm{NO_2}] \ . \tag{14}$$

Notice that these reaction terms are given in number concentration while equation (11) is typically describing conservation of mass. In Envi-met all concentrations are mixing ratios measured in $\mu g/kg_{air}$, Therefore, equations (12) to (14) have to be converted to mass concentrations first.

Figure 5 (Janssen, De Maerschalck et al. 2008) illustrates the local effect of oxidation of traffic emitted NO on the local air quality. The continuous lines show the modelled NO and NO_2 concentrations downwind of a motor way. The green lines are for a motorway with a vegetation barrier, the red lines without a vegetation barrier. The position of the driving lanes and vegetation barrier are indicated by the red and green blocks. The green and red dots with error bars are the measured concentrations.

One can see that NO is decreasing faster than the NO_2 concentrations, both with and without a vegetation barrier. This is due to the fact the NO is reacting with ozone and forms secondary NO_2. One can also notice that due to the vegetation the effect is even stronger. The vegetation slows down the local wind speed, so there is more time for the chemistry. At the same time, due to increased turbulence, more fresh ozone is mixed in which enhances the oxidation process as well.

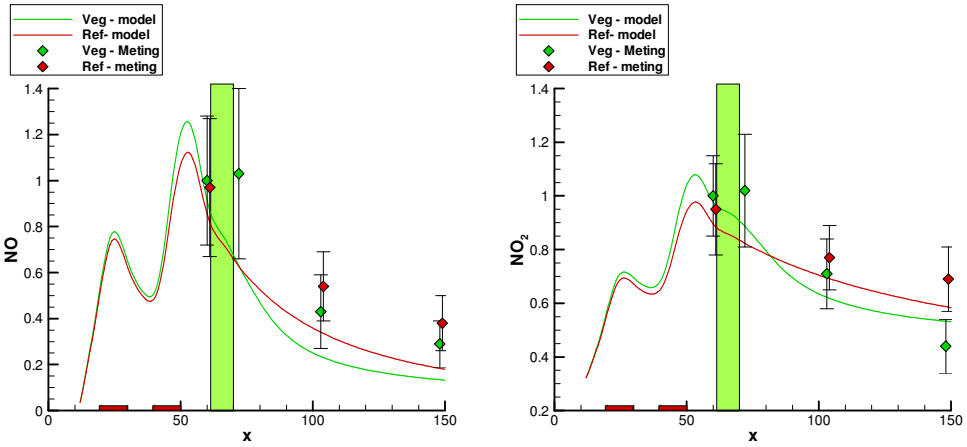

Figure 5: NO and NO_2 concentrations downwind of a highway with an without a vegetation barrier.

References

Berkowicz, R. (1998), Street Scale Models in *Urban Air Pollution - European Aspects*, J. Fenger, O. Hertel and F. Palmgren, Kluwer Academic Publishers, 223-251.

Berkowicz, R. and O. Hertel (1989), *Technical Report DMU LUFT – A131*, National Environmental Research Institute, Roskilde, Denmark,

Bruse, M. (2007), Particle filtering capacity of urban vegetation: A microscale numerical approach. *Berliner Geographische Arbeiten* 109, 61-70.

de Leeuw, F. A. A. M. (1995), *Parametrization of NO2 photodissociation rate*, Technical Report, 722501004, Dutch National Institute for Public Health and Environment (RIVM), Bilthoven, The Netherlands

De Maerschalck, B., S. Janssen, et al. (2009), *CFD Simulations Of The Impact of a Vegetation Barrier Along a Motor Way on Local Air Quallity*. Air Quality, Science and Application, Istanbul, Turkey, University of Hertfordshire.

Janssen, S., B. De Maerschalck, et al. (2008), *Modelanalyse van de IPL meetcampagne langs de A50 te Vaassen ter bepaling van het effect van vegetatie op luchtkwaliteit langs snelwegen*, DVS-2008-044, VITO rapport : 2008/IMS/R/241, VITO, Mol, Belgium

Seinfeld, J. H. and S. N. Pandis (2006), *Atmospheric chemistry and physics*, New Jersey, John Wiley.

van Ham, J. and M. P. J. Pulles (1998), *Nieuw nationaal model*, Technical Report, TNO R 98/306, TNO, KEMA, KNMI, VNONCW, RIVM, Apeldoorn, The Netherlands

Concentrations of traffic-related air pollution along motorways and motorway viaducts : a comparative study

M. Van Poppel[*1], *L. Int Panis*[1,2], *P. Berghmans*[1]

[1]VITO – Flemish Institute for Technological Research, 2400 Mol, Belgium, martine.vanpoppel@vito.be
[2]IMOB – Transportation Research Institute, University of Hasselt, Hasselt, Belgium

Introduction

Epidemiological studies have suggested associations between living near busy roads and respiratory health. Studies have shown that air pollution concentrations are significantly associated with distance to a motorway. (Janssen et al., 2001; Hagler et al., 2009) However, not much is known about the difference in concentrations between normal motorways and motorway viaducts with the same amount of traffic. Hence, the question is whether motorway viaducts have a positive impact on people's exposure to air pollution as compared to normal motorways.
In this study, we examined the effect of the position of a motorway, i.e. ground level versus viaduct, on $PM_{2.5}$ and NOx ground level concentration within about 100 m from the road.

Methodology

Measurements were performed in February – April 2009. During the measurement period, two cases were studied consecutively: one motorway at ground level and one motorway viaduct (see Figure 1). In each case study, $PM_{2.5}$ and nitric oxides (NO, NO_2 and NO_X) were measured at both sides of the motorway. $PM_{2.5}$ was measured using a TEOM-FDMS, nitric oxides were measured using a mobile platform Airpointer, both using an averaging time of 30 minutes. The measurement locations at each side of the road were located at 29 m and 102 m from the motorway at ground level and at 60 m and 120 m from the motorway viaduct. Data on wind direction and wind speed was available from a nearby monitoring site.

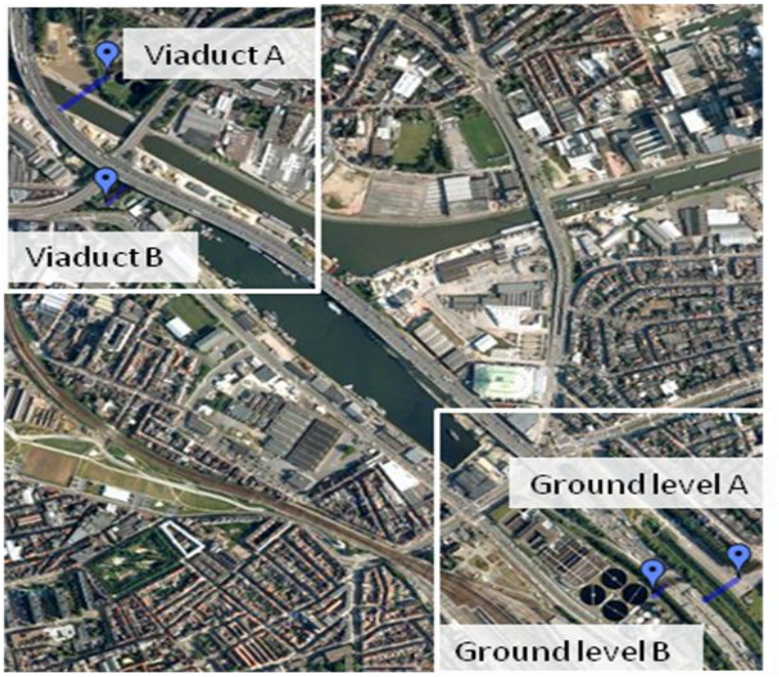

Figure 1: Sampling locations near the motorway for the two cases on the same motorway stretch: (1) motorway viaduct (top left) and (2) motorway at ground level (bottom right)

In a first step, the average of the 30-minute data per 15° wind sector were plotted in a pollution rose to check if pollutant concentrations had increased in the direction of the road.

Next, the the difference in concentration between both sides of the road (ΔC) for $PM_{2.5}$, NO, NO_2 and NO_x was studied using multivariate linear regression. ΔC, which can be seen as the contribution of road traffic to the pollutant concentration, was calculated as $C_{downwind} - C_{upwind}$. C_{upwind} and $C_{downwind}$ are the concentrations measured at the site respectively upwind and downwind of the road taking into account prevailing wind directions. Only data for which wind was within 60° from perpendicular to the road was taken into account for statistical analysis. Due to a bend in the road, for some of the receptor points a wind sector of only 55° or 50° from perpendicular to the road was taken into account.

The multivariate linear regression takes into account influencing parameters such as time of day, day of the week, distance to the road and wind speed, to correct for non-identical conditions in the consecutive measurement campaigns. Time of day is included using two dummy variables to distinguish between peak hours (7.00 – 9.00 and 16.00 – 18.30), night time (22.00 – 6.00) and non-peak hours. The day of the week variable makes a distinction between weekdays and weekend days or holidays. Distance to the road is integrated as a continuous linear variable, with only two distances for each case study.

Results and discussion

Pollution roses showed increased average concentrations in the direction of the road for nitric oxides and $PM_{2.5}$ (see Figure 2). The impact of road traffic seems higher at the measurement location closest to the road. The increased pollutant concentration from traffic appeared to be higher in the case at ground level compared to the viaduct.

The results of the linear regression analysis indicated that taking into account the influencing parameters listed above, the contribution of the motorway to pollutants is significantly higher when the motorway is at ground level. Furthermore, time of day and day of the week also showed to have a significant effect on ΔC.

Figure 3 shows an example of the estimated impact of road traffic to the pollutant concentration (ΔC) for $PM_{2.5}$, NO and NO_2, as estimated by the linear regression model. As can be seen in Figure 3, ΔC is higher for the motorway at ground level for all pollutants.

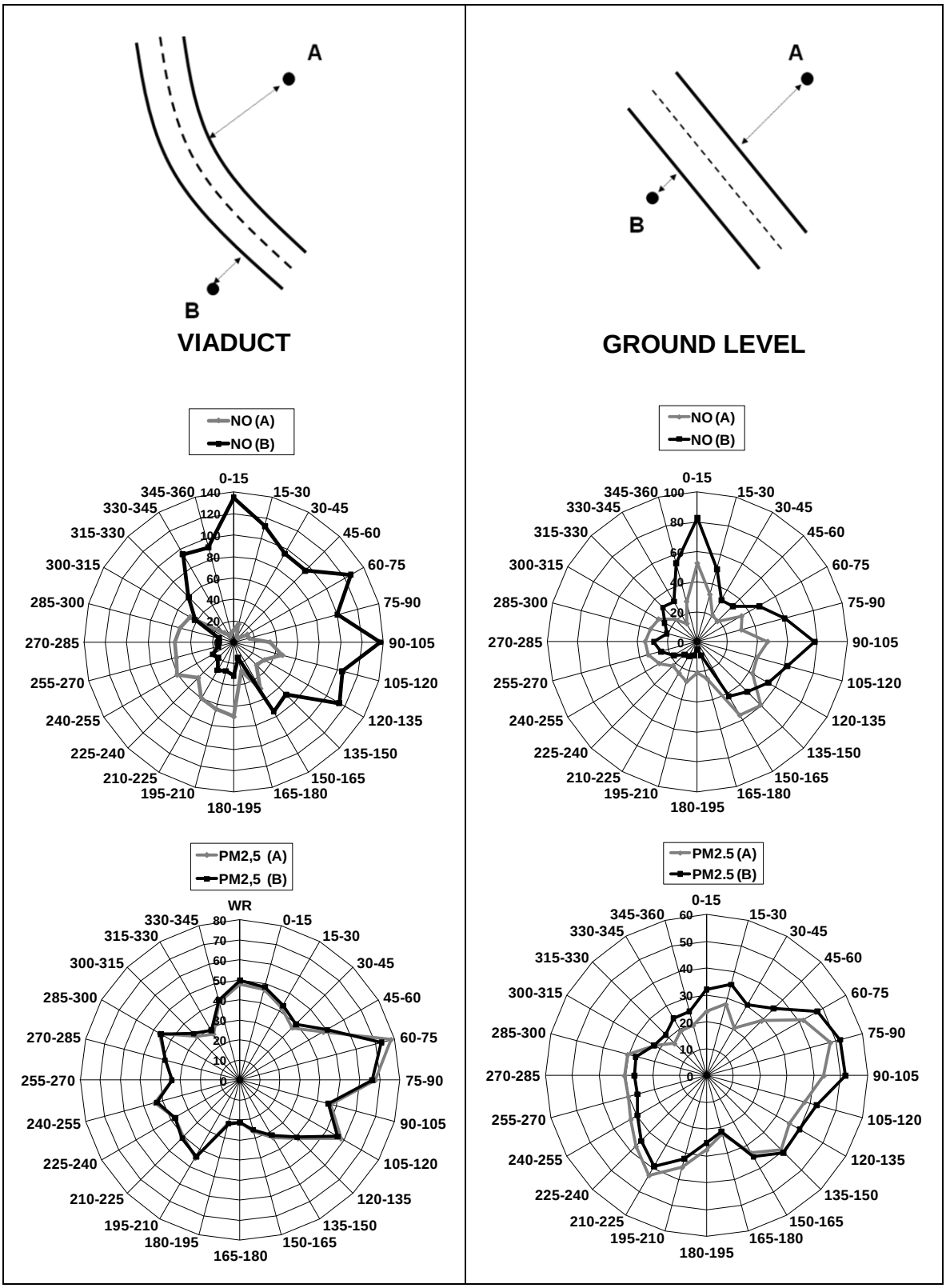

Figure 2: Pollution roses for $PM_{2.5}$ ($\mu g/m^3$) and NO (ppb) near a highway at ground level (right) and highway viaduct (left)

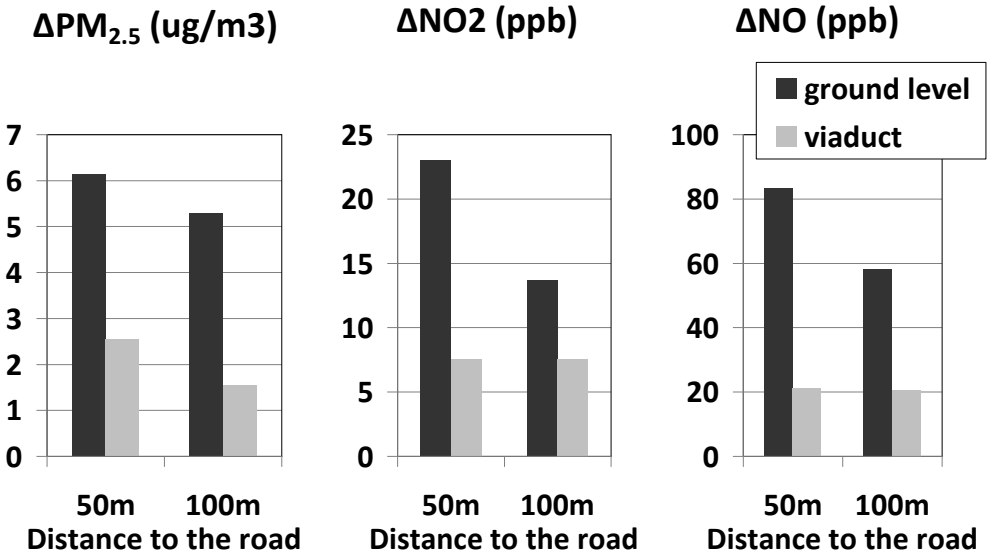

Figure 3 : Contribution of road traffic to concentrations of $PM_{2.5}$ and nitric oxides at a distance of 50 m and 100 m from a motorway at ground level and a motorway viaduct as estimated by the multiple regression model for a weekday, during peak hours and at a wind speed of 3 m/s

The results of this study seem to indicate that a viaduct has a positive impact on people's exposure to traffic related air pollution compared to a highway at ground level.

Acknowledgments

This work was funded by BAM (Management Company Mobility Antwerp).

References

N. A. H. Janssen, P. H. N. van Vliet, F. Aarts, H. Harssema, B. Brunekreef, 2001. *Atmos. Environ.,* 35, 3875-3884

Hagler G. S. W., Baldauf R. W., Thoma E. D., Long T. R., Snow R. F., Kinsey R. F., Kinsey J. S., Oudejans L., Gullet B. K. (2009), *Atmos. Environ*., 43, 1229 – 1234.

Modeling Pollutant Dispersion from Roadway Traffic using a Line Source Gaussian Formula

*R. Briant[1] *, I. Korsakissok[1] and C. Seigneur[1]*

[1] CEREA, Centre d'Enseignement et de Recherche en Environement Atmosphérique, Joint Laboratory École des Ponts ParisTech / EDF R&D, Université Paris-Est, 6-8 avenue Blaise Pascal, Cité Descartes Champs-sur-Marne 77455 Marne la Vallée Cedex 2 FRANCE

** briantr@cerea.enpc.fr*

Introduction

Roadway traffic may adversely impact air quality and it is essential to be able to predict with reasonable accuracy the pollutant concentrations associated with vehicle emissions.

Gaussian plume models are widely used to model atmospheric dispersion. They are based on an analytical formula to model dispersion from pollution sources represented by points. To model a line emission such as a road, the use of point sources implies to discretize it and to use a large number of points. The precision of the results is related to the discretization step which means that the more point sources per road section we use, the more precise the concentration will be. Because the computational time required for a simulation increases linearly with the number of sources, such an approach may become cumbersome for a large road network.

Using a line source Gaussian formula would then be an efficient alternative because we would have only one source per road section. However, the analytical solution for a line source is only exact when the wind direction is perpendicular to the road (Yamartino, 2008). Indeed, the approximation required to be able to compute an analytical formula for a line source, induces some error when the wind direction is not perpendicular to the road and it also makes the solution diverge when the wind direction is parallel to the road.

We present here a novel approach to reduce the error in the line source formula when the wind direction is not perpendicular to the road. We estimated this error on a case study, it was then parameterized and generalized so that it can be applied to every wind direction.

Gaussian plume model using line sources

Gaussian models in general require some hypotheses in order to lead to an analytical formula. We first assume that the emission rate and meteorological parameters are constant so that the plume is at steady state and doesn't change with time. Then we assume that the wind is strong enough so that the turbulent diffusion in the wind direction is not significant compared with the advection (slender plume approximation) (Arya, 1999; Seinfeld et Pandis 1998).

The Gaussian analytical formula used to compute concentrations (C in $g.m^{-3}$) at a receptor point due to a line source is obtained by solving equation 1. It represent the integral along the line source of a continuous point source.

$$C(x,y,z) = \frac{Q}{2\pi u \sigma_y \sigma_z} \exp\left(\frac{-z^2}{2\sigma_z^2}\right) \int_{y_1}^{y_2} \exp\left(\frac{-(y_{wind}-s)^2}{2\sigma_y(s)^2}\right) ds \quad \text{(Eq: 1)}$$

- x, y, z : coordinate of the receptor point in the reference system of coordinates (m).
- Q : emission rate ($g.s^{-1}$).
- u : wind speed ($m.s^{-1}$).
- y_1 and y_2 : ordinates of source extremities (m).
- σ_y and σ_z : the dispersion coefficients along y and z axes (m).
- y_{wind} : coordinate y in the wind system of coordinates (m).
- s : variable of integration representing all points of the line source.

To solve this equation for cases when the wind is not perpendicular to the road, another approximation is required. Here we selected the HV approximation (Venkatram and Horst, 2005). It consists in using the effective distance between the receptor and the source in the wind direction, to compute dispersion coefficients. This simplifies equation 1 and makes it possible to solve it by the use of a variable change (equation 2).

$$C(x,y,z) = \frac{Q}{2\sqrt{2\pi}u\cos\theta\sigma_z} \exp\left(\frac{-z^2}{2\sigma_z^2}\right) \left[erf\left(\frac{(y-y_1)\cos\theta - x\sin\theta}{\sqrt{2}\sigma_{y_1}}\right) - erf\left(\frac{(y-y_2)\cos\theta - x\sin\theta}{\sqrt{2}\sigma_{y_2}}\right)\right] \quad \text{(Eq: 2)}$$

- θ : the angle between the normal to the source and the wind direction (rad).

We notice that when the wind direction is parallel to the road, the computed concentration is infinite ($\cos\theta = 0$). Therefore, we assume that the solution can then be approximated by that for $\theta = 89°$. When the wind direction is perpendicular to the road, Equation 2 become identical to the basic analytical solution.

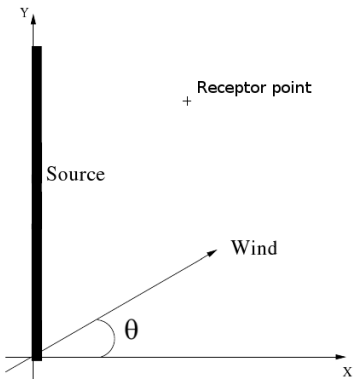

Figure 1: θ is the angle angle between the wind direction and the direction perpendicular to the road.

We wish to estimate the error by comparing the solution of Equation 2 to an "exact" solution. This reference solution was obtained by representing the line source by a very large number of point sources until convergence was obtained (i.e., when doubling the number of point sources did not lead to a significant change on the solution). To estimate the error, we assume heteroscedasticity and the error between the line source analytical formula and the reference solution is computed as in equation 3. Equation 3 computes a relative error so that it does not depend on the multiplicative factor in front of the equation (e.g., emission rate, wind speed and σ_z).

$$Error(x,y,z) = \frac{C_{line}(x,y,z) - C_{reference}(x,y,z)}{C_{reference}(x,y,z)} \quad \text{(Eq: 3)}$$

- C_{line} : Concentration computed with a line source.
- $C_{reference}$: Concentration computed with a discretized source (see text).

This error was computed at several distances from the source (along the wind direction) and it was parameterized with analytical functions. Figure 2 shows two examples of parameterized error curves.

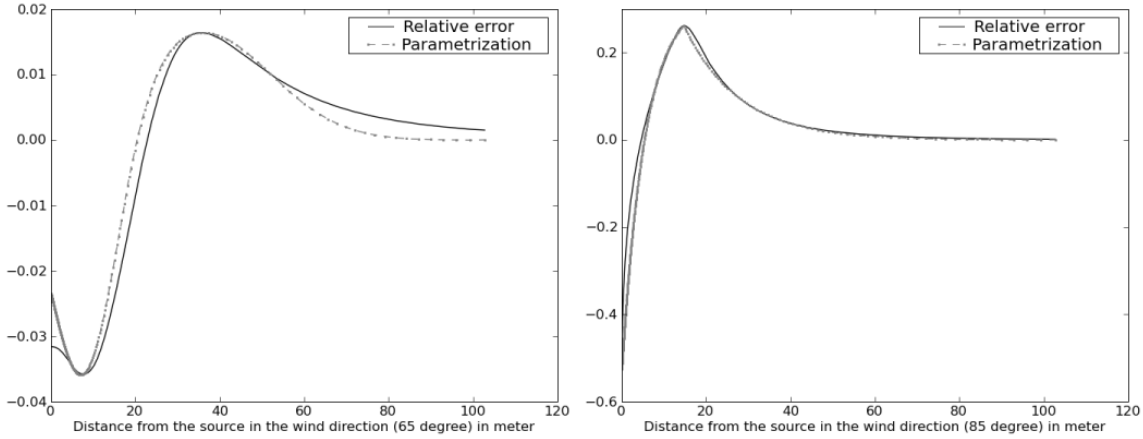

Figure 2: Curve of relative error as function of the distance from the source along the wind direction with a wind angle equal to 65 degrees (left) and 85 degrees (right).

These parametrizations were developed with wind angles in the first quadrant and, by symmetry, were used for the others quadrants. For small wind angles (i.e.,wind direction nearly perpendicular to the road) the error value is small (less than 0,01%) so no correction is needed. We chose to apply the correction for wind angles greater than 40°. Different parametrizations were used for wind angles in a range of 40° to 74° (Figure 2, left) and for angles in a range of 74° to 90° (Figure 1, right).

These parametrizations (refered to as "corrective term"), were then applied to the computed concentrations as in Equation 4.

$$Ccorrected(x,y,z) = \frac{C_{line}(x,y,z)}{1 + Corrective\ term(x,y,z)} \quad \text{(Eq: 4)}$$

- Corrective term(x,y,z) : correction computed from the parametrization.

Results

To evaluate this new model, it was implemented into the Gaussian plume model (Korsakissok and Mallet, 2009) of the modeling platform Polyphemus (Mallet and al., 2007). Concentrations are computed at several distances to the middle of the line source along the wind direction and we compared the results obtained with the new model (Equation 4) with the reference :

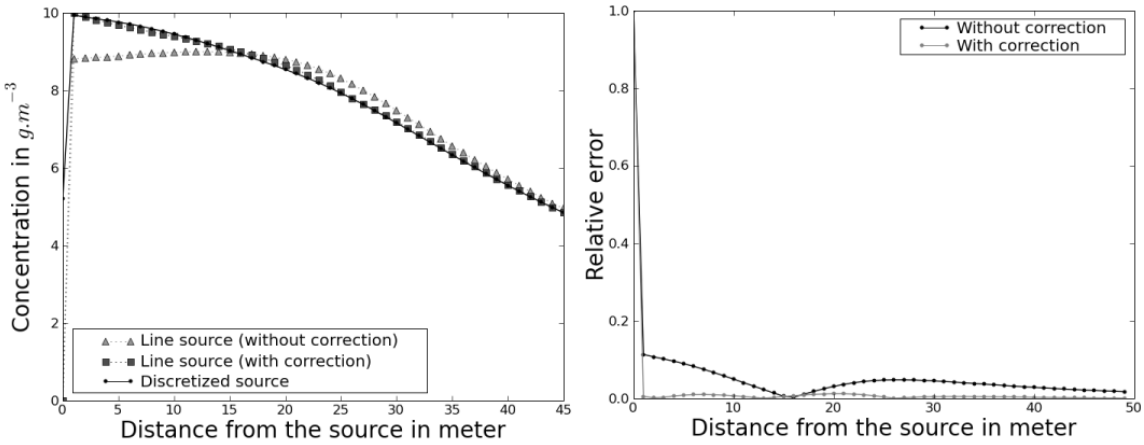

Figure 3: Concentration (left) and relative error (right) as a function of the distance of the receptor from the center of the source (θ = 75°).

Figure 3 shows that, the corrected concentration profile is very close to the reference and the relative error is significantly reduced.

We can see in figure 4 that the error is also reduced when applying the correction on the whole simulation domain.

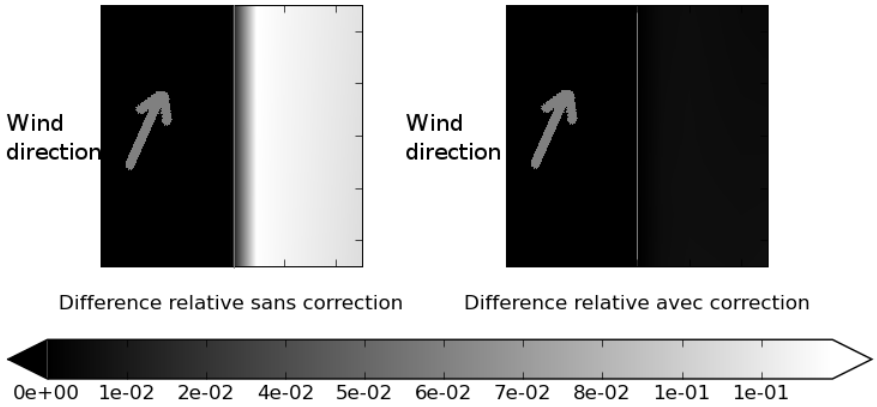

Figure 4: Relative error of line source formula with (right) and without (left) correction. (the line source is shown in gray in the figure). Here θ = 75°.

Figure 4 shows the results for θ = 75° in the middle of a road section. The correction term does not completely attenuate the error near the ends of the road section and an additional correction is then needed. Ongoing work addresses the extension of this model to other atmospheric stability conditions.

Conclusion

The results presented here are very promising because the error associated with an analytical solution is negligible and it is valid for the entire range of angles. In terms of computational time, the computation of the correction to the HV analytical formulation is negligible compared with the computational time required to perform a simulation with a high number of point sources. The new analytical formulation corresponds to the computational time for 3 point sources.

References

Arya S., (1999), Air pollution meteorology and dispersion, *Oxford University press*.

Korsakissok I. and V. Mallet, (2009), Comparative study of Gaussian dispersion formulas within the Polyphemus platform: evaluation with Prairie Grass and Kincaid experiments, *jam.*, 48, 2459-2473.

Mallet V., D. Quélo, B. Sportisse, M. Ahmed De Biasi, É. Debry, I, Korsakissok, L. Wu, Y. Roustan K. Sartelet, M. Tombette and H. Foudhil (2007), Technical note : The air quality modeling system Polyphemus, *Atmos. Chem. Phys.*, 7(20), 5479-5487.

Seinfeld J.H., S.N. Pandis (1998), Atmospheric chemistry and physics : from air pollution to climate change, Willey-Interscience.

Venkatram A., T.W. Horst (2005), Approximating dispersion from a finite line source, *Atmos. Environ.*, 40, 2401-2408.

Yamartino R., (2008), Air Quality Modeling – Theories, Methodologies, Computational Techniques, and Available Databases and Software, *vol III.*, Published by *The EnviroComp Institute and the Air & Waste Management Association*.

Can particulate matter be used to evaluate traffic related abatement measures? Conclusions of three recent case studies in the "hot spot" Flanders, Belgium.

Stijn Janssen[1], Wouter Lefebvre[1], Frans Fierens[2], Bart De Maerschalck[1]*

[1] VITO, Boertang 200, 2400 Mol, Belgium – stijn.janssen@vito.be
[2] Belgian Interregional Environment Agency (IRCEL), Kunstlaan 10-11, B-1210 Brussels, Belgium

Introduction

Member States are obliged to look for all possible measures that can be implemented to improve the ambient air quality and to meet the EU air quality limit values. In many cases, abatement measures have a focus on traffic related pollution. Since particulate matter is one of the most important air pollutants in Flanders (Northern part of Belgium), mitigation strategies are evaluated on the basis of PM concentration reductions.

Very recently, three case studies were set up in Flanders. In each case, a traffic related abatement measure was evaluated. More specifically the cases consists of a low emission zone in the city centre of Antwerp, the closure of the Ring road of the city of Antwerp and a speed limit reduction from 120 to 90 km/h on several major highways during particulate matter smog episodes.

Methodology

The impact of each of those traffic related measures was evaluated by means of an air quality modelling system. The emission model MIMOSA, based on the COPERT 4 methodology, is used to model the traffic emissions (both exhaust and non-exhaust) in the different scenarios. The MIMOSA model calculates geographically and temporally (hourly) distributed emissions for Flanders. It employs detailed mobility data (traffic volumes per road segment, fleet composition, traffic speed on road segments, …) and emission factors following the COPERT methodology. MIMOSA can hence generate hourly emissions for different traffic scenario's.

The regional air quality models AURORA or BelEUROS were used to simulate the regional background concentrations. The regional air quality models are prognostic 3-dimensional Eulerian chemistry-transport models, designed to simulate urban- to regional-scale concentration fields both for gaseous pollutants and particulate matter. They take into account emissions of all air pollutants and hence can assess the change in concentration levels due to changing emission patterns.

Coupled to these regional models, the bi-Gaussian plume model IFDM was used to simulate the air quality patterns at high resolution along the highways on an hourly basis. Using this procedure, concentration maps for the Flemish region with a resolution up to 30 m for the hot spots were obtained.

Case studies

Recently, three different scenario studies were implemented in the Flanders region to assess the impact of traffic related mitigation measures.

A first case study was related to the closure of the northwestern part of the Ring road of Antwerp. The closure of the Ring road of Antwerp via the so called "Oosterweelverbinding" is one of the main projects in the Master plan of Antwerp. This master plan is initiated to solve the serious traffic congestion problems which are faced today in and around the city of Antwerp. In this study, the impact assessment of the Oosterweelverbinding is tested with respect to these evolutions for $PM_{2.5}$. Model calculations are preformed for two different situations: the "Oosterweel" scenario for 2015 in which the Ring is closed and an "Autonomous" scenario for 2015 in which the Ring is not closed. The model calculations pointed out (Figure 1) that the impact of traffic related measures on the local PM concentrations (PM_{10} and $PM_{2.5}$) are rather limited and of the order of a few percent level.

In a second case, the implementation of a low emission zone (LEZ) for the city centre of Antwerp is examined. The LEZ is defined as a restriction for heavy duty vehicles and busses with a Euro label lower than EURO IV. The measure is intended to be in force in the year 2015. EURO IV vehicles will be older than 10 year at that time. In combination with the LEZ, a reorganisation of the local traffic flows in the city centre is implemented as well. Local traffic circulation plans are developed by the city authorities and are designed to discourage people entering the city centre by cars.

A third case study is related to a short term emission reduction strategy taken by the Flemish government which decided to introduce speed reducing measures (maximum 90 km/h instead of 120 km/h on certain sections of motorways) during PM_{10} smog episodes. Since May 2006, the measure has been into force a couple of times during predicted smog episodes.

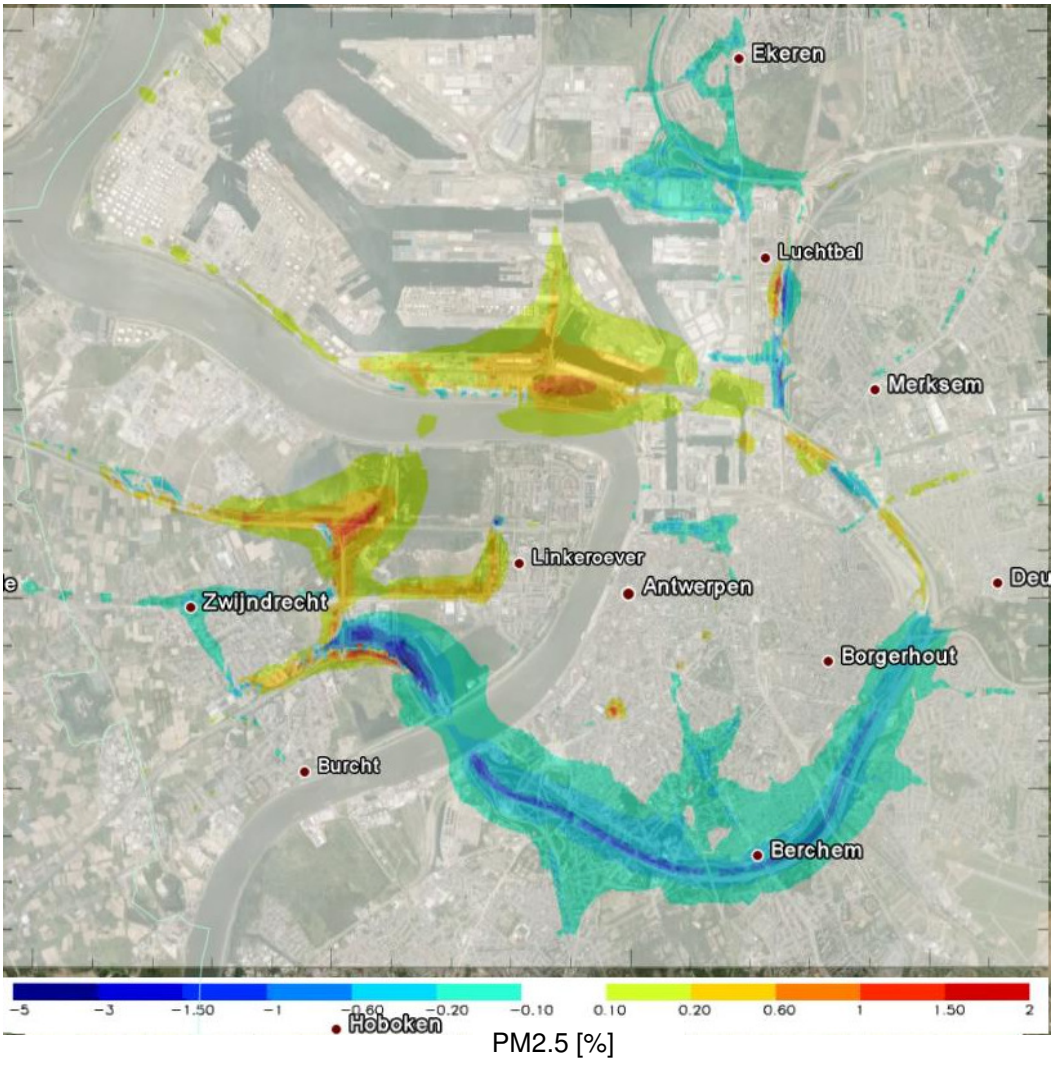

Figure 1: Relative differences (in %) in PM2.5 concentrations after closure of the north-western part of the ring way of Antwerp, Belgium.

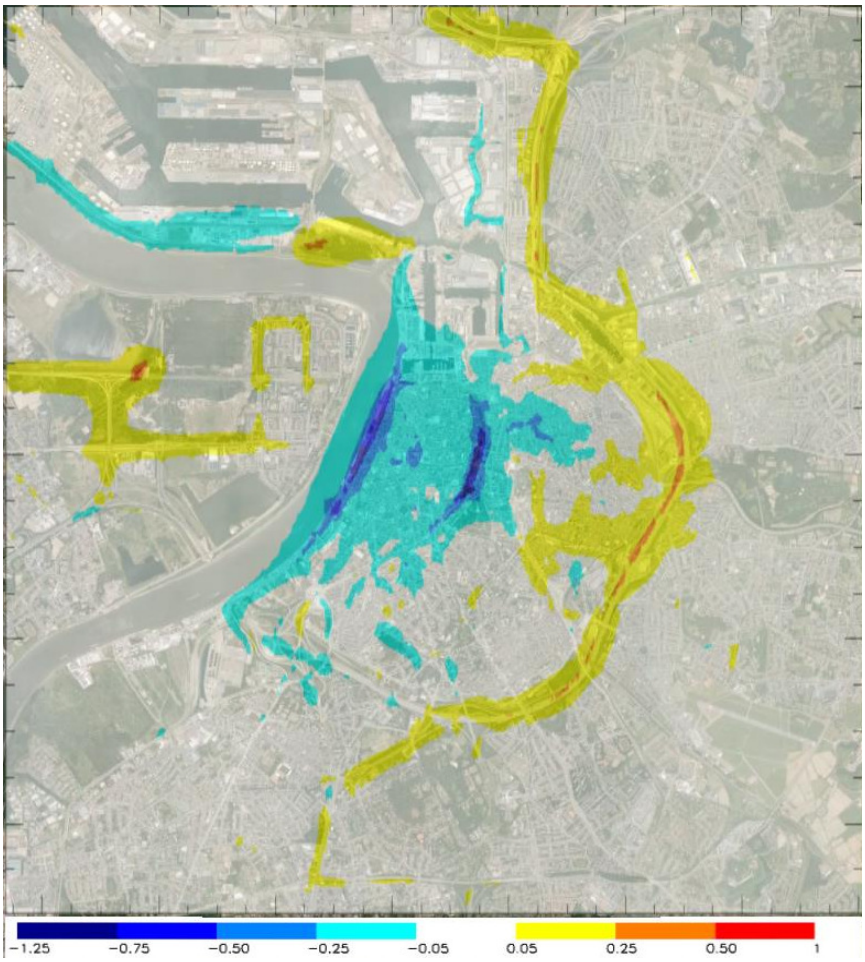

Figure 2: Relative differences (in %) in PM10 concentrations after implementation of a low emission zone in the city centre of Antwerp, Belgium.

Results and discussion

For each of the three case studies, the relative impact of the mitigation measure on PM_{10} or $PM_{2.5}$ concentrations is simulated. In all cases a base case and a scenario analysis including the specific measure is modelled. A relative comparison of those results is presented in Figure 1 - Figure 3.

The model predicts a limited impact of the Oosterweelverbinding on $PM_{2.5}$ (Figure 1): increased concentrations of a few percent along the new northern segment of the Ring and decreased concentrations along the southern part of the Ring due to the reduction of traffic (in particular heavy duty vehicles) on this part.

For the implementation of the LEZ and the implementation of local traffic plans, model simulations estimate a reduction of about 1% of PM_{10} concentrations in the city centre (Figure 2). Maximum reductions are obtained on the most busy traffic lanes which are used most frequently by trucks and busses to cross the city centre. It is interesting to note that the implementation of the LEZ combined with the local traffic plans also causes an increase in PM_{10} concentrations in the outside regions of the city and on the Ring road.

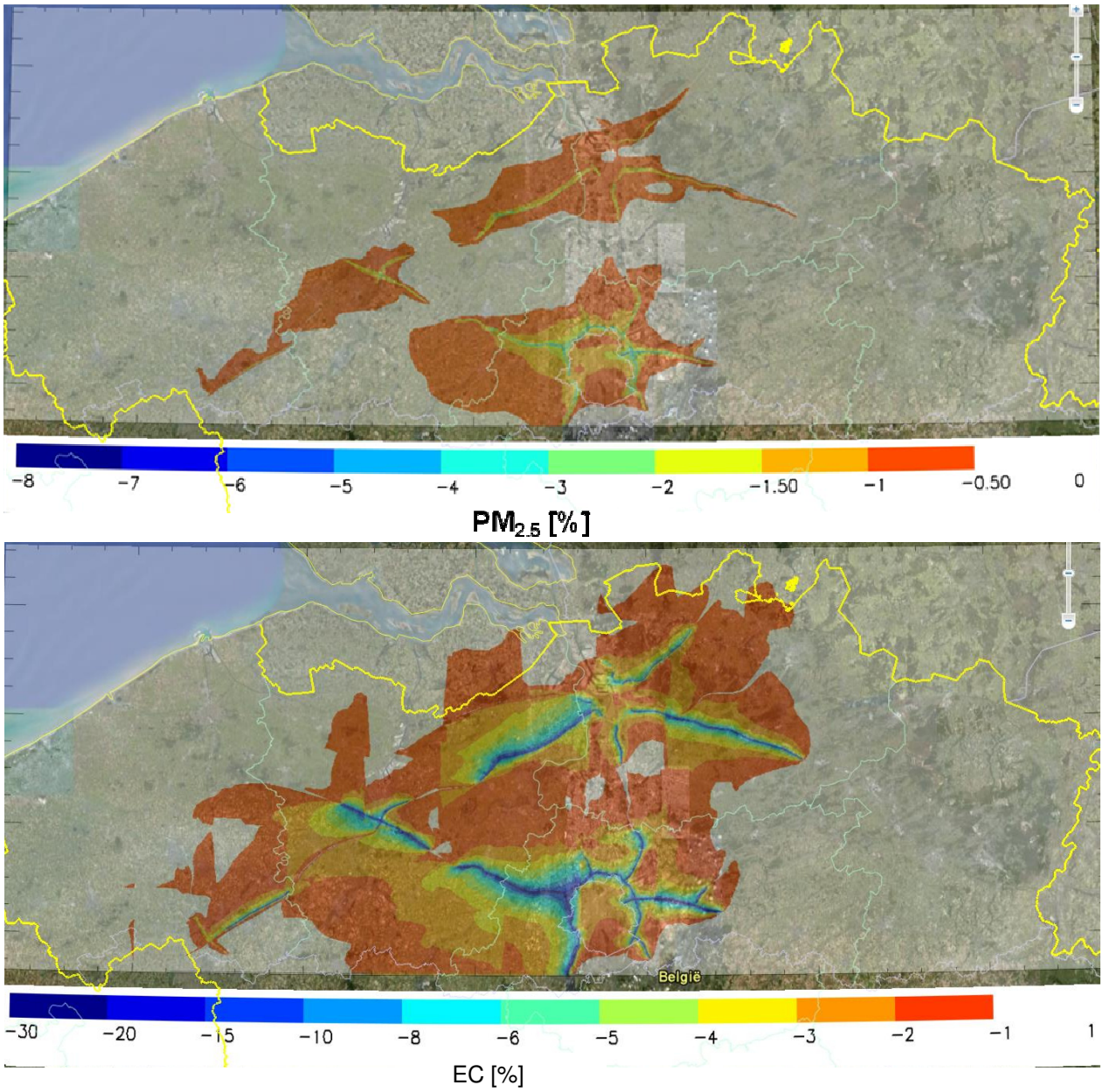

Figure 3: Relative differences (in %) in PM2.5 (upper panel) and Elemental Carbon (EC, lower panel) concentrations after imposing a speed limit reduction from 120km/h to 90km/h.

For the speed limit reduction case, model simulations are not performed for a whole year as in the first two cases but for two smog episodes in 2007 and 2008 only. Model calculations point out that a decrease in the traffic emissions is up to about 30% (somewhat higher for $PM_{2.5}$) on the highways where the speed limit enters into force. However, the decrease in PM_{10} concentrations is only visible close to the highways where the speed reductions have been applied. In the direct vicinity of most of these highways, the changes are not higher than 1.5% with a maximum close to 5%. The difference is larger for $PM_{2.5}$, although the effects remain also limited (Figure 3). Maximum changes for $PM_{2.5}$ increase up to 8%.

As an overall conclusion of those three case studies, it can be stated that the impact of traffic related mitigation strategies on PM_{10} and $PM_{2.5}$ levels is limited. In the three examples for which an impact assessment was calculated, the maximum reduction is only a few percent. As such, it is questionable if these particulate matter parameters are most suited to evaluate such kind of measures.

To further pin down this assumption, the third case study (speed limits on highways), is used to model the impact on the elemental carbon (EC) component of PM. After all, it is assumed that

this EC content directly emitted by traffic, is one of the most harmful for the exposed population. Model simulations point out that in this case the measure can have a significant impact on the EC concentrations. EC concentration decreases up to 30% were modelled in a wider vicinity of the highway. This is in sharp contrast with the reduction levels that are seen for the more classical PM pollutants such as PM_{10} and $PM_{2.5}$. The reason for this can be attributed to the high secondary particulate matter fraction and the large background contribution which are observed for both PM_{10} and $PM_{2.5}$. For EC, a primary pollutant, the overall background is estimated to be very low and local contribution of traffic emissions have a clear signal on the concentrations in ambient atmosphere.

Conclusions

In this paper, three different case studies are examined implementing traffic related mitigation measures for air pollution. The mitigation measures cover the redistribution of traffic on the Ring road of Antwerp due to the closing of the Antwerp ring road, the implementation of a low emission zone in the city centre of Antwerp and the the enforcement of a speed limit reduction of 90 km/h on a number of highway segments in Flanders.

For all cases, a relatively low impact (percent level) of the measures is observed for the classical total mass PM_{10} and $PM_{2.5}$ pollutants. However, a much higher impact (up to ~30%) is observed on the elemental carbon (EC) fraction of particulate matter, which is assumed to be more harmful for population exposure. It turns out that EC is a better traffic related air quality indicator which contains a much more pronounced signal of traffic emissions. Therefore it is questionable if the classical pollutants such as total mass PM_{10} and $PM_{2.5}$ are well suited to evaluate traffic related measures for air pollution reductions. As a result of the current legislation, policy makers are facing the situation that mitigation strategies do not help very much in meeting the EU air quality limit values but might be relevant in reducing the health impact of the exposed population.

Simulation of commute patterns and commute exposure to air pollution

M. S. Ragettli[1,2], M. Ritter[1,3], C. Braun-Fahrländer[1,2], L. Grize[1,2], N. Künzli[1,2], L.-J. S. Liu[1,2]*

[1] Swiss Tropical and Public Health Institute, Department of Epidemiology and Public Health, Environmental Exposure Sciences, CH-4002 Basel, Switzerland, Martina.Ragettli@unibas.ch
[2] University of Basel
[3] Institute for Meteorology, Climatology, and Remote Sensing, University of Basel, Klingelbergstrasse 27, 4056 Basel, Switzerland

Abstract

Background: Air pollution exposure during commuting may be associated with adverse health effects. So far, only little attempt has been made to model commute exposure to air pollution for a large population and its sub-groups.
Aim: Our objective is to simulate personal exposure to air pollution based on commute patterns of the Swiss population. In particular, we aim to a) build a commute model to simulate commute route and mode of transportation from one location to another, and b) to simulate the air pollution exposure during commute based on simulated routes, modes and predictions of traffic air pollutants.
Methods: Commute patterns will be simulated by means of a Geographic Information System (GIS) model using extensive information from the Swiss 2005 Microcensus on travel behavior. Exposure to traffic-related air pollution will be estimated based on pertinent literature and by using a fine-scale air pollution dispersion model. Simulated estimates will be validated with personal measurements. The models will be built for the cantons of Basel-Stadt and Basel-Land including about 700 subjects. Simulating variations of commute routes from one location to another will allow us to test scenarios of change in commute patterns on exposure distribution.
Conclusion: This study will contribute to a better understanding of population exposure to harmful pollutants during daily commuting which is crucial for health risk assessments as well as for the elaboration of policy recommendations.

Introduction

Urban transport microenvironments likely contain high concentrations of harmful air pollutants, and are therefore considered as one of the most important microenvironments for air pollution exposure (WHO, 2006). Even though people usually spend only a small amount of their time commuting, the relatively short traffic participation contributes considerably to their 24-hour average personal exposure to traffic-related air pollution (Gulliver and Briggs, 2005; van Roosbroeck et al., 2008). There is growing evidence from epidemiological studies that not only long-term exposure to traffic-related air pollutants but also short-term increases of exposures during traffic participation have a potential for cardiovascular (Peters et al., 2004; Riediker et al., 2004) and respiratory health impacts (McCreanor et al., 2007; Strak et al., 2010). In recent years, a growing number of personal monitoring studies exploring levels and determinants of air pollution exposure during commute have been published. However, these investigations provide only limited information on the commute exposure levels of an entire urban population (Kaur et al., 2007). On one hand, exposure estimates are related to a small number of individuals. On the other hand, measurements were carried out mostly along predefined routes rather than representing real population-based activity patterns. There is clearly a need for improved journey-time exposure estimates and information on time-activity patterns for both epidemiological and health risk assessments (Gulliver and Briggs, 2005; Jerrett et al., 2005; Zou et al., 2009).

The aim of our project is to develop a multi-modal commute model which is able to simulate both travel patterns and commute exposure. The focus of the analysis will be on trips undertaken for working purposes and leisure time activities because these travel purposes account for most of the trips and cover the longest distances travelled in Switzerland (FSO, 2007). An assessment of the energy expenditure during active and passive modes of commuting is also planned.

Methods

Study area. The model will be built for the region of Basel, Switzerland including the Cantons of Basel-Stadt and Basel-Land. The area covers about 550 km2 and has approximately 470'000 inhabitants. While the Canton Basel-Stadt is predominantly an urban area and a major centre for pharmaceutical and chemical industries, Basel-Land is largely rural in character. The region is located at the border triangle with Switzerland, Germany and France. In recent years, the expansion of the public transportation network as well as the bicycle use promotion is a major theme of traffic policy in the city of Basel. For Basel-Stadt it has been estimated that the residents mainly use public transport to go to work and that 40% of the households have no private car. In the Canton Basel-Land, individual motor vehicles are used more often. According to cantonal statistics, about 50% of the population uses the car to go to work. Despite efforts made to improve the urban air quality, air pollution and especially NO_2 levels still exceed Swiss federal standards.

Simulation of commute routes. A commute model will be built in order to simulate commute routes and mode of transportation from one location to another by means of a Geographic Information System (GIS) model. Tele Atlas Mulinet road network data (Tele Atlas Inc., Lebanon, NH, USA) as well as VECTOR25 data from Swisstopo (Swiss Federal Office of Topography, Wabern, Switzerland) will be used to develop a multi-modal network dataset. It will include various street types as well as public transport such as train, bus and tram lines. Commute patterns will be simulated using extensive information on the Swiss travel behavior from the Microcensus on Travel Behavior 2005. It is a statistical survey carried out by the Swiss Federal Statistical Office (FSO) every five years since 1974. The Microcensus data provide temporally and spatially resolved data on the travel behavior of a representative number of individuals in the Swiss population. In 2005, about 33'390 persons in 31'950 households were interviewed about their travel behavior by telephone. The interviews were performed throughout the year, including Sundays and holidays. Detailed information (among others) is available on daily travel patterns (number of trips, duration of trips, distance travelled) the purpose of the trips, and the modes of transport used. For the majority of the study population residence and work places, destinations of leisure time activities as well as places where the study participants changed modes of transport have been geo-coded in 2005. Additionally, the interviewers collected the coordinates of all start and target locations of trips and legs undertaken during the day before the interview. Trips are defined by the purpose of commuting and consist of one or more legs. Legs are pieces of the trip travelled using the same mode of transport (FSO, 2007). For the Cantons of Basel-Stadt and Basel-Land, data on trips and legs are available from 691 persons aged 6 to 65+. An overview of the number of trips and legs to be simulated is provided in Table 1.

Table 1: Number of subjects, trips and legs by purpose of trip

	All purposes	Working	Leisure time	Working and leisure time
Subjects (n)	787			
Subjects with geocoded trips (n)	691	202	473	567
Trips (n)	2'524	528	1'102	1'630
Trips within study area* (n)	2'209	467	934	1'401
Legs (n)	4'251	948	1'850	2'798
Legs within study area* (n)	3'606	856	1'577	2'433

*with start and target location within Basel-Stadt or Basel-Land

Trips of the study population will be determined based on the information on mode of transport and geo-coded start and target locations of trips and legs using the GIS based route finder "ArcGIS

Network Analyst" by ESRI (Redland, CA, USA). An example of a simulated trip and corresponding legs are displayed in Figure 1.

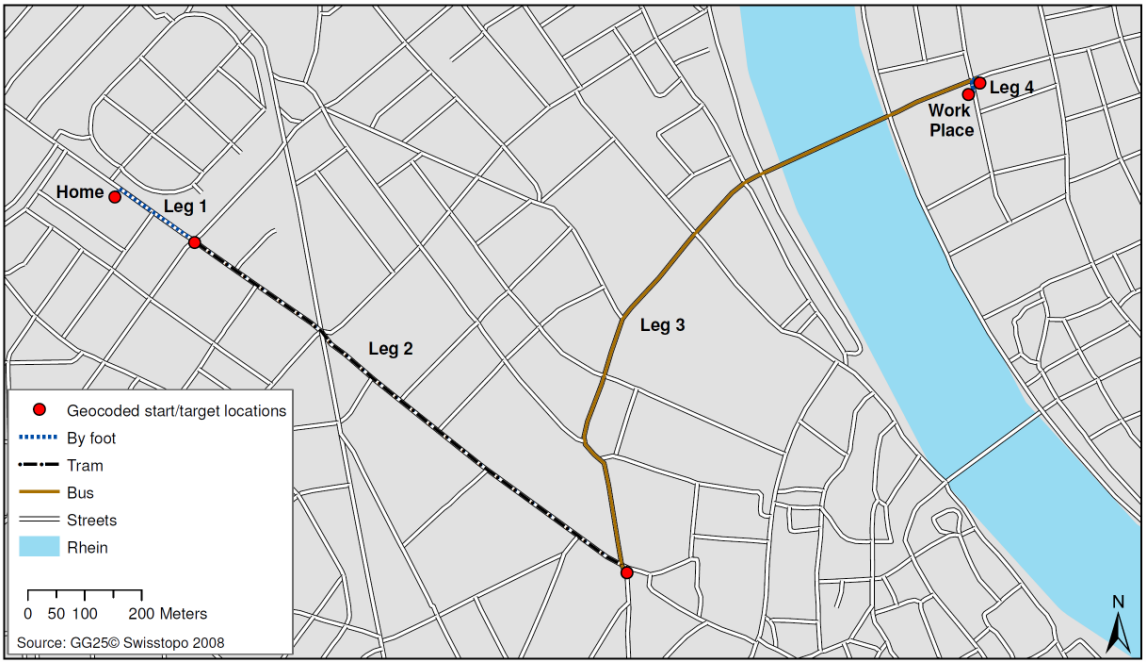

Figure 1: Example of simulated trip in the city of Basel. The trips with associated legs are displayed on the basis of the Swiss map VECTOR25 (Swiss Federal Office of Topography, Wabern, Switzerland, 2008).

Simulation of commute exposure to traffic related air pollution. The exposure to traffic-related air pollution during commute will be modeled on the simulated commute routes and modes of transport. Two different approaches for the simulation of exposure will be adopted. First, the exposure to traffic-related air pollution will be estimated based on pertinent literature. This includes an extensive literature review and evaluation of factors determining and modifying personal exposure during traffic participation. Since a geographic information system is used for the analysis, special focus will be attached to spatial determinants of traffic-related air pollution such as land use or street density. Attention will be paid to factors that have been documented to modify the spatial extend of the health impact from pollutants. Exposure modification on different modes of transportation (bus, tram, train, car, bike, foot) will be also accounted for. The second approach is to model the commute exposure to air pollutants using ambient air data from various monitoring campaigns carried out at the Swiss Tropical and Public Health Institute and city of Basel. Measurements include particulate matter (PM), nitrogen dioxide (NO_2), nitrogen oxides (NO_x) as well as various PM source components. In addition, personal measurements will be carried out in order to validate the commute exposure estimates.

An assessment of alternative commute patterns regarding effects on population exposure distribution and energy expenditure is also part of the study. Evaluating different scenarios of population exposure with respect to traffic routes should enable the identification of key determinants of personal exposure that might be the subject of policy interventions.

Conclusion

The study will contribute to an enhancement of the quality of exposure and corresponding health risk assessments. Moreover, an understanding of how activity patterns affect population exposure in space and time is very valuable for the evaluation and elaboration of urban policies that address public health, environmental quality and quality of urban living.

Collaboration

This study is part of the international project “Transportation, Air Pollution, and Physical Activities; an integrated health risk assessment programme of climate change and urban policies (TAPAS)”. It is led by the by the Centre for Research in Environmental Epidemiology (CREAL) in Barcelona.

References

Swiss Federal Statistical Office (FSO) (2007), Mobilität in der Schweiz. Ergebnisse des Mikrozensus 2005 zum Verkehrsverhalten, *Statistik der Schweiz*, Neuchâtel, Bern, 1-98.

Gulliver J. and D. J. Briggs (2005), Time-space modeling of journey-time exposure to traffic-related air pollution using GIS*, Environmental Research*, 97, 10-25.

Jerrett M., A. Arain, P. Kanaroglou, B. Beckerman, D. Potoglou, T. Sahsuvaroglu, J. Morrison and C. Giovis (2005), A review and evaluation of intraurban air pollution exposure models, *Journal of Exposure Analysis and Environmental Epidemiology*, 15, 185-204.

Kaur S., M. J. Nieuwenhuijsen and R. N. Colvile (2007), Fine particulate matter and carbon monoxide exposure concentrations in urban street transport microenvironments, *Atmospheric Environment*, 41, 4781-4810.

McCreanor J., P. Cullinan, M. J. Nieuwenhuijsen, J. Stewart-Evans, E. Malliarou, L. Jarup, R. Harrington, M. Svartengren, I. Han, P. Ohman-Strickland, K. F. Chung and J. F. Zhang (2007), Respiratory effects of exposure to diesel traffic in persons with asthma, *New England Journal of Medicine*, 357, 2348-2358.

Peters A., S. von Klot, M. Heier, I. Trentinaglia, A. Hormann, H. E. Wichmann and H. Lowel (2004), Exposure to traffic and the onset of myocardial infarction, *New England Journal of Medicine*, 351, 1721-1730.

Riediker M., W. E. Cascio, T. R. Griggs, M. C. Herbst, P. A. Bromberg, L. Neas, R. W. Williams and R. B. Devlin (2004), Particulate matter exposure in cars is associated with cardiovascular effects in healthy young men, *American Journal of Respiratory and Critical Care Medicine*, 169, 934-940.

Strak M., H. Boogaard, K. Meliefste, M. Oldenwening, M. Zuurbier, B. Brunekreef and G. Hoek (2010), Respiratory health effects of ultrafine and fine particle exposure in cyclists, *Occupational and Environmental Medicine*, 67, 118-124

van Roosbroeck S., G. Hoek, K. Meliefste, N. A. H. Janssen and B. Brunekreef (2008), Validity of residential traffic intensity as an estimate of long-term personal exposure to traffic-related air pollution among adults, *Environmental Science & Technology*, 42, 1337-1344.

Zou B., J. G. Wilson, F. B. Zhan and Y. N. Zeng (2009), Air pollution exposure assessment methods utilized in epidemiological studies, *Journal of Environmental Monitoring*, 11, 475-490.

Propene Adsorption On Different Zeolites And Silicoaluminophosphates Under Cold Start Conditions

J.M. López[1], M.V. Navarro[1], T. García[1], R. Murillo[1], A.M. Mastral[1], F.J. Varela-Gandía[2],D. Lozano-Castelló[2], A. Bueno-López[2], D. Cazorla-Amorós[2]*

[1] Instituto de Carboquímica, CSIC, M Luesma Castan 4, 50015-Zaragoza, Spain
[2] Departamento de Química Inorgánica, Universidad de Alicante, Apartado 99, E-03080, Alicante, Spain, d.lozano@ua.es

Introduction

Three-Way Catalysts (TWC) for gasoline vehicle emission control usually start working at around 200 ºC. The catalyst requires a period of 1 to 2 minutes to reach this temperature; during that time, up to 80% of hydrocarbons (HCs), mainly toluene and propene, in a drive cycle are emitted (Park et al., 2007). The emissions control during this "cold start" period is essential to reduce the environmental impact of gasoline engines.

The use of ''hydrocarbon traps", before the TWC seems to be the most relevant solution from a scientific-technological point of view. The critical factors for any emission trap are: (i) high adsorption capacity of HCs at low temperatures, (ii) desorption starting at temperatures higher than 200 ºC, (iii) a reversible adsorption process and (iv) solid material resistant at temperatures higher than 750 ºC. Zeolites have been found to be the preferred adsorbents for these applications, mainly due to their stability under severe process conditions. The general finding in different hydrocarbon traps is that while the heavier exhaust HCs (e.g. toluene) are adequately trapped by the zeolites, the light HC components (i.e. propene) often desorb from the HC trap before the catalyst has reached its light-off temperature (Baek et al., 2004; Burke et al., 2003; Iliyas et al., 2007).

Then, to increase the temperature of propene release, it is important to optimize the propene adsorption equilibrium and kinetics, which depend, among other properties, on specific surface area and pore volume (Baek et al., 2004), Si/Al (Burke et al., 2003) and pore network connectivity (Iliyas et al., 2007). Thus, the objective of the present work is to analyze how each of these properties affects the equilibrium adsorption capacity, molecular diffusion and desorption temperature of propene.

Experimental

Four zeolites (Na-Mordenite, high alumina Na-ZSM-5, Silicalite-1 and Na-Beta) and two silicoaluminophosphate (SAPO) molecular sieves (SAPO-5 and SAPO-41) have been synthesised according to the methods described elsewhere (López et al. 2010).

The crystal structure of zeolites and SAPO molecular sieves were characterised by X-ray powder diffraction (XRD), using a 2002 Seifert powder diffractometer. Morphology and crystal sizes were examined by scanning electron microscope (SEM) in a HITACHI microscope (model S-3000N). The micro-chemical characterization was made by energy-dispersive X-ray analysis (EDX) for Si/Al atomic ratio determination. The EDX analysis was performed in an analyzer associated with the SEM. The textural characterization of the zeolites and SAPO molecular sieves was carried out by means of the adsorption of N_2 (-196 ºC) and CO_2 (0 ºC). Surface area was calculated from N_2 adsorption isotherms using the BET equation (S_{BET}). Total micropore volume (V_{DR} (N_2)) and narrow micropore volume (V_{DR} (CO_2)) were calculated applying the Dubinin–Radushkevich (DR) equation to the N_2 adsorption (-196 ºC) and the CO_2 adsorption (0 ºC), respectively.

A fixed bed reactor was used to obtain propene adsorption and desorption data over the materials using a Flame Ionization Detector (FID). Propene adsorption was carried out at atmospheric pressure with different concentrations of propene (50 ppmv to 500 ppmv, in He). Adsorption experiments were conducted at 30 ºC ± 1 ºC with a constant gas flow of 30 ml/min, by passing propene through an adsorbent bed of 0.20 g of zeolite placed in a reactor (0.457 cm inner diameter, Di). Propene TPD processes were performed in He atmosphere (gas flow

30ml/min) after the adsorption step increasing the reactor temperature from 30 ºC to 350 ºC at 50 ºC/min and this temperature was hold during 60 min.

Similar conditions were used to perform the cold start tests (CST). However, 500 ppmv of propene in He atmosphere (gas flow 30 ml/min, 0.20 g of sample and 0.457 cm of Di) was employed in this case so that propene was applied together with a heating ramp. It is worth commenting that a CST procedure allows investigation of competitive adsorption and desorption from an initially empty zeolite, which is closer to the conditions that would be experienced by an in-line hydrocarbon trap in an automobile (Park et al., 2007). In order to simulate this ‘‘cold start” conditions, four cycles of adsorption/desorption were run with a constant inlet of 500 ppmv of propene using He as carrier gas. Previous to start each experiment, gas stream was passed through an inert bed reactor during 1.6 min in order to stabilize the propene concentration. First cycle (named cycle 0) was done to get a real used solid and after that three more cycles were done to test the ageing process of the materials. CST cycles were analysed to determine the amount of remaining adsorbed propene at two different temperatures (250 ºC and 300 ºC).

Results and discussion

The phase purity and crystallinity of the samples prepared in this study have been confirmed by XRD (López et al. 2010). The morphology and crystal size obtained by SEM is according to these materials (López et al, 2010). Table 1 summarises the BET surface areas (S_{BET}), the total micropore (V_{DR} (N_2)) and narrow micropore volume (V_{DR} (CO_2)). The data corresponding to N_2 adsorption on Mordenite crystals synthesized has not been included because diffusional problems were found during the measurements done for that sample. Table 1 also contains the Si/Al atomic ratio estimated by EDX. BETA is the zeolite with the highest surface area and pore volume of the present study. Silicalite-1 and ZSM-5 present similar surface area. Furthermore, Silicalite-1 is also a zeotype of the MFI zeolite structure with no aluminum content, so the pore size distribution is the same as in the ZSM-5.

Among the two different silicoaluminophosphate molecular sieves prepared (SAPO-5 and SAPO-41), SAPO-5 has much higher porosity than SAPO41. The surface area for the sample SAPO-5 is similar to that for Silicalite-1 and ZSM-5, although in the case of SAPO-5 it has much higher narrow micropore volume (V_{DR} (CO_2), which is higher than (V_{DR} (N_2). The pore size of SAPO-5 and its pore volume, together with the one-dimensional nature of this type of molecular sieves make very interesting to analyze the performance of this material as hydrocarbon trap.

Table 1: Porous texture characterization results, Si/Al atomic ratios and NH_3 desorbed during TPD.

Sample	S_{BET} (m^2/g)	V_{DR} (N_2) (ml/g)	V_{DR} (CO_2) (ml/g)	Si/Al	Total NH_3 desorbed (mmol/g)
Silicalite-1	323	0.14	0.17	-	-
ZSM-5	319	0.15	0.11	16.7	0.25
Mordenite	-	-	0.15	7.7	0.45
SAPO-5	352	0.17	0.23	0.2	0.24
SAPO-41	55	0.03	0.05	0.1	0.12
BETA	564	0.28	0.25	12.6	0.29

TPD of ammonia was used for the characterization of samples in terms of the nature and number of surface acid sites (Thompson and Mathews, 1989). As shown in Table 1, the amount of ammonia desorbed from the prepared solids ranges from 0.12 (SAPO-41) to 0.45 (Mordenite) mmol NH_3/g. Mordenite zeolite appears to have the highest concentration of acid sites, which is consistent with the high Al content of this zeolite. For the rest of zeolite samples, the amount of acid sites estimated by ammonia TPD decreases with the increase of Si/Al ratio (see Table 1). In the case of SAPO materials, it has been seen in the literature that a progressive substitution of silicon in a neutral aluminophosphate provides acidity ranging from weak to strong acid sites (Elangovan et el., 1995). The area of the NH_3-desorption peaks indicates that the number of acid sites increases in the order of SAPO-41 < SAPO-5, which agrees with the results published by other researchers (Yunfeng et al., 2005).

Figure 1 shows the experimental propene adsorption isotherms on the six inorganic adsorbents (symbols) obtained at 30 ºC. All the isotherms are of type I and characteristic of microporous adsorbents. Propene was more adsorbed by BETA zeolite in all the partial pressure range investigated. Adsorption capacity decreased dramatically for the rest of adsorbents following the trend ZSM-5 > Mordenite > SAPO-5 > SAPO-41 > Silicalite-1. The amount adsorbed of propene reached the plateau at higher pressure following the trend ZSM-5 > Mordenite > SAPO-5 > SAPO-41 > Silicalite-1. Moreover, saturation plateau was not reached for BETA material in the partial pressure range investigated.

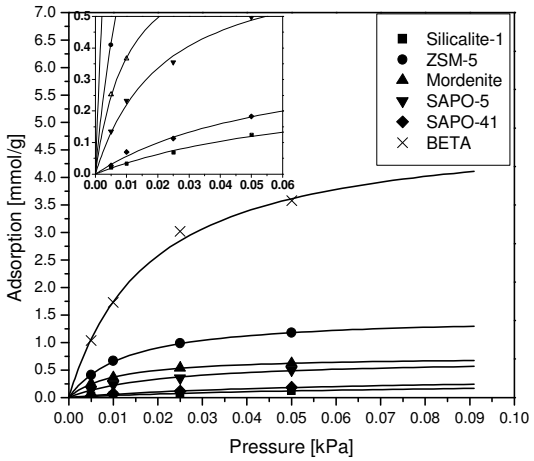

Figure 1: Propene adsorption isotherms for different zeolite materials. Symbol: experimental data; line: Langmuir fitted.

The experimental isotherms (Figure 1) can be fitted to a Langmuir equation and then, the adsorption capacity of the theoretical monolayer (W_0) can be obtained. The BETA zeolite presented a W_0 value (4.94 mmol/g) around three times higher than the next one, ZSM-5 (1.48 mmol/g). This high value can be explained taking into consideration the porosity, structure and aluminium content of this zeolite. ZSM-5 has lower content of acid sites than BETA and also much lower surface area and pore volume (see Table 1). These characteristics could explain the much lower propene adsorption capacity. Furthermore, the effect of Si/ Al ratio is clearly observed in the case of Silicalite-1, which has the same framework and pore size distribution than ZSM-5 but with no aluminium content. This material showed the lowest W_0 (0.30 mmol/g). Thus, not only the porosity but also the strength of the adsorption, explains the results for these materials. Mordenite zeolite presents a low W_0 value (0.40 mmol/g) due to the blockage of a large part of the micropore volume has occurred during the synthesis.

SAPO-5 and SAPO-41 (0.75 mmol/g and 0.40 mmol/g, respectively) points out the important effect of the pore size (pore size, 7.3 Å and 4.3 x 7.0 Å, respectively). However, other important differences between both molecular sieves are: (i) the specific surface area and micropore volume: SAPO-5 has much higher porosity than SAPO-41 (see Table 1); and (ii) the content of acid sites: area of the NH_3-desorption peak for SAPO-5 is double than for SAPO-41 (see Table 1). Then, these three factors (pore size, micropore volume and acid sites) can explain the almost double propene adsorption capacity of SAPO-5 compared to SAPO-41.

Experimental breakthrough curves were obtained for the six materials at different concentrations of propene, ranging from 50 ppmv to 500 ppmv. The results are shown in Table 2 expressed as $g_{propene}/g_{adsorbent}$. BETA zeolite presented the highest adsorption capacity (0.151 g/g), being three times higher than the next one, ZSM-5 (0.050 g/g). SAPO-41 and Silicalite-1 zeolites showed the lowest adsorption capacities with only 0.008 and 0.005 g of propene adsorbed per gram of adsorbent, respectively. Propene breakthrough curves can be used to determine the role of the diffusion on the performance of hydrocarbon traps. It is well-known that there is a direct relationship between the length of the mass transfer zone (MTZ) and the diffusion of the molecules into the pores. So, narrow MTZ lengths are convenient for an effective use of the adsorbent. Table 2 includes the MTZ length and the ratio to the total bed length for all the zeolite materials used. SAPO-5, Mordenite and SAPO-41 zeolites present the most severe diffusion problems with less than 25% of the bed length being used for the

adsorption process. These three materials have one-dimensional channel networks and therefore a more acute molecular sieving behaviour. Diffusion of propene molecules in these adsorbents is more restricted. On the other hand, ZSM-5, BETA and Silicalite-1 zeolites have three-dimensional channel networks and present less diffusion problems, especially ZSM-5 with more than 80% of the bed length being used.

Table 2: Adsorption capacity (W) at P = 0.05 kPa, MTZ length (L_T) and bed length (L).

Trap	*W (g/g) x 10^3*	*L_T (cm)*	*L (cm)*	*L_T/L*
Silicalite-1	5	1.35	2.63	0.51
ZSM-5	50	0.46	2.63	0.17
Mordenite	26	1.60	2.01	0.80
SAPO-5	25	1.40	1.86	0.79
SAPO-41	8	1.46	1.91	0.76
BETA	151	0.66	1.26	0.52

The desorption profiles have been obtained for the six zeolite materials and Table 3 summarizes the temperatures at which the different peaks appear, propene desorbed and propene recovering efficiency determined form the TPD experiments.

Table 3: Desorption temperature maxima, propene desorbed and propene recovering efficiency determined from the TPD experiments.

Trap	*Desorption T (ºC)*	*Total amount of propene desorbed* (g_{des}/g)x10^3*	*Propene recovering efficiency (g_{des}/g_{ads})*
Silicalite-1	135	4	0.77
ZSM-5	201, 350	7	0.13
Mordenite	213	25	0.96
SAPO-5	319	18	0.72
SAPO-41	142, 229, 273	8	0.95
BETA	218, 245, 318	14	0.09

* assuming that only propene is released.

Additional CST experiments have been carried out using conditions that more closely mimic the automotive ‘‘cold start”, i.e. increasing the temperature under 500 ppmv propene/He gas flow. Figure 2 shows the CST profiles for the different materials. All the adsorbents, except Silicalite-1, showed more than one desorption peak. Table 4 summarizes the different temperatures at which those peaks appeared. According to Tables 3 and 4, these peaks could be associated to the presence of different active sites in the adsorbents, where propene molecules can be chemisorbed. Table 4 also includes the amount of propene adsorbed and desorbed in the CST. It is important to remark that these amounts are much lower than those obtained from the breakthrough curves (Table 2) and the TPD (Table 3).

Several cycles have been performed and Table 5 includes the remaining adsorbed propene (%), assuming that only propene is desorbed, at two selected temperatures (250 and 300 ºC). These values were calculated from the amount of propene released and the amount that is fed into the adsorption reactor until the system has reached the selected temperatures. These temperatures were selected in order to check if the adsorbents still trap the propene at those temperatures when an aged TWC starts to operate. Note that the first cycle named cycle 0 was done to get a real used solid and after that three more cycles were done to test the ageing process of the materials. Table 5 includes the results corresponding to the next three cycles. It can be said that the six zeolite materials keep a constant adsorption capacity with a very low ageing effect after the four cycles but with different results at both selected temperatures. Then, we can distinguish two groups of samples, those which trap more than 60% of propene up to 300ºC (SAPO-5, ZSM-5 and BETA) and those with a much lower retention capacity that, up to 300 ºC is around 30% (Silicalite-1, Mordenite and SAPO-41).

Table 4: Real test desorption temperature (ºC), cold start releasing rate (μmol_{C3H8}/min) and total amount of propene adsorbed and desorbed during a CST.

Trap	T_0-T_f	T_{max}	r_{C3H8}[a]	*Propene ads*[b] (g_{ads}/g) x 10^3	*Propene des*[c] (g_{ads}/g) x 10^3
Silicalite-1	183-277	206	6.22	0.6	0.4
ZSM-5	272-350	297, 344	2.73	1.1	1.0
Mordenite	179-350	222, 300	0.97	0.7	0.8
SAPO-5	188-350	343	0.26	0.9	1.0
SAPO-41	184-350	215, 240, 286	1.85	0.5	0.2
BETA	247-350	311, 350	0.68	1.0	0.8

(a) Calculated from the slope of the first releasing peak during the cold start test ; (b) Total amount of propene adsorbed; (c) Total amount of propene desorbed, assuming that only propene is released.

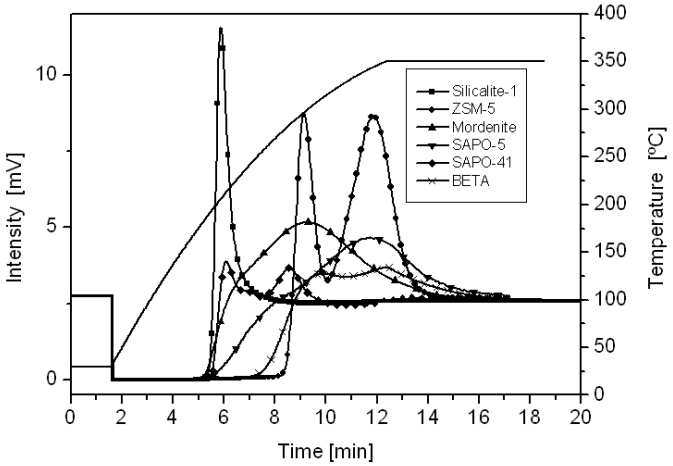

Figure 2: Cold start cycle for different zeolite materials.

In Table 5 it can be observed that SAPO-5, a solid material with high diffusion problems, shows a very good performance during a CST. It is worth to point out that although propene is starting to be released at quite low temperature compared to other traps, such as ZSM-5 and BETA (see Table 4), the releasing rate is very low, only reaching ca. 15% of the total propene emitted at 250ºC and ca. 40% at 300ºC. A similar behaviour can be observed in the case of Mordenite and SAPO-41 materials. Then, it is apparent that those materials with higher kinetic restrictions have a slower propene releasing rate, calculated as the slope of the first peak released in a CST (see Table 4). Therefore, kinetic restrictions also seem to be a key parameter since they determine the propene releasing rate once the propene molecules start to leave the hydrocarbon trap.

Table 5: Remaining adsorbed propene* (%) at selected temperatures (ºC) and different cycles calculated from the CST.

Trap	*Cycle 1*		*Cycle 2*		*Cycle 3*	
	250	*300*	*250*	*300*	*250*	*300*
Silicalite-1	32	24	32	24	33	25
ZSM-5	99	80	99	76	99	77
Mordenite	62	29	61	28	64	27
SAPO-5	90	69	87	62	86	61
SAPO-41	67	42	64	38	62	37
BETA	100	87	100	86	99	83

*assuming that only propene is released

Comparing TPD and CST results (see Tables 2–4), it can be observed that the relationship between TPD and CST is not straightforward. In the standard TPD measurement, the sample is first equilibrated with constant concentrations of propene species, which provide adsorbed propene molecules on different sites of the materials (most and less favourable sites). On the other hand, during a CST experiment, propene diffuses into an empty sample at low temperatures and it is first preferentially adsorbed in the most favourable sites. Then, as the temperature of the adsorbent increases, the equilibrium adsorbed loading decreases and the less favourable sites are not significantly used. The fact that disagreements between the offset temperatures in both types of experiments are associated to the presence in the TPD profiles of low temperature peaks can be easily confirmed in the case of ZSM-5, SAPO-41 and BETA materials, where the contribution of physical adsorption to the TPD profiles can be identified. Accordingly, offset temperatures in the second peak of the TPD profiles and offset temperature in the CST are in good agreement for these materials, i.e. 285 ºC vs. 272 ºC in the case of ZSM-5; 180 ºC vs. 184 ºC in the case of SAPO-41; and 236 ºC vs. 247 ºC in the case of BETA. Therefore, it can be concluded that only the most stable sites where chemisorption takes place, seem to be used for the retention of propene during a CST, where the amount adsorbed is, at least, one order of magnitude lower than the total coverage of propene at equilibrium conditions.

Conclusions

In this work propene adsorption isotherms and desorption profiles for six materials have been obtained and the relationship between these experimental data and the performance of these materials during a CST has been studied. The results point out that CST should be recommended for the evaluation of porous materials as cold start traps. From the analysis of the results it can be said that the requirements for a propene trap under cold start conditions are: (i) high equilibrium propene adsorption capacity, where propene should be mainly chemisorbed and; (ii) kinetics restrictions. Therefore, the results obtained for BETA and ZSM-5 zeolites and SAPO-5 are promising since they accomplish some of these requirements.

Acknowledgements

The authors would like to thank Spanish Ministerio de Medio Ambiente y Medio Rural y Marino (Project 331/PC08/3-13.1), Generalitat Valenciana (PROMETEO/2009/047) for financial support and F.J. Varela-Gandía thanks U.A. for the thesis grant.

References

Baek S.W., Kim J.R., Ihm S.K. (2004), Design of dual functional adsorbent/catalyst system for the control of VOC's by using metal-loaded hydrophobic Y-zeolites, *Catal. Today*, 93–95, 575–581.

Burke N.R., Trimm D.L., Howe R.F. (2003), The effect of silica:alumina ratio and hydrothermal ageing on the adsorption characteristics of BEA zeolites for cold start emission control, *Appl. Catal., B*, 46, 97–104.

Elangovan S.P., Krishnasamy V., Murugesan V. (1995), SAPO-5 and SAPO-11: Synthesis, characterization and camphene isomerization activity, *React. Kinet. Catal. Lett.*, 55, 153–159.

Iliyas A., Zahedi-Niaki M.H., Eic M., Kaliaguine S. (2007), Control of hydrocarbon cold-start emissions: A search for potential adsorbents, *Micropor. Mesopor. Mater.*, 102, 171–177.

López J.M., Navarro M.V., García T., Murillo R., Mastral A.M., Varela-Gandía F.J., Lozano-Castelló D., Bueno-López A., Cazorla-Amorós D. (2010), Screening of different zeolites and silicoaluminophosphates for the retention of propene under cold start conditions, *Micropor. Mesopor. Mater.*, 130, 239-247.

Park J.H., Park S.J., Nam I.S., Yeo G.K., Kil J.K, Youn Y.K. (2007), A fast and quantitative assay for developing zeolite-type hydrocarbon trap catalyst, *Micropor. Mesopor. Mater.,* 101, 264-270.

Thompson S.C., Mathews J.F. (1989), Characterization of hydro-cracking catalysts by acidity measurement, *Appl. Catal.,* 47, 45–57.

Wesson P.J., Snurr R.Q. (2009), Modified temperature programmed desorption evaluation of hydrocarbon trapping by CsMOR zeolite under cold start conditions, *Micropor. Mesopor. Mater.*, 125, 35–38.

Yunfeng H., Xiangsheng W., Xinwen G., Silue L., Sheng H., Haibo S., Liang B. (2005), Effects of channel structure and acidity of molecular sieves in hydroisomerization of n-octane over bi-functional catalysts, *Catal. Lett.*, 100, 59–65

Influence of the Three Way Catalyst Design Parameters on the Conversions During Cold Start and Hot Engine Operations

*H. Santos[1], M. Costa[2]**

[1] Mechanical Engineering Department, School of Technology and Management, Polytechnic Institute of Leiria, Morro do Lena – Alto Vieiro Apt. 4163, 2411-901 Leiria, Portugal
[2] Mechanical Engineering Department, Instituto Superior Técnico, Technical University of Lisbon, Avenida Rovisco Pais, 1049-001 Lisbon, Portugal, mcosta@ist.utl.pt

Abstract

Exhaust after-treatment systems will have to become increasingly efficient during both cold start and hot engine operation in order to comply with the strict emission limits that will apply in the Europe and worldwide in future. The main objective of this article is to study the influence of the three way catalyst (TWC) precious metal loading (PML), on the TWC conversions during both cold start and hot engine operating conditions. To this end, this article reports transient and steady-state experimental data for two TWC with different PML. The experimental data revealed that the PML influences both the ignition location and propagation during cold start. It was observed that: (i) for low PML the ignition starts at the TWC back-end and for high PML the ignition starts at the TWC front-end; (ii) for high PML the ignition occurs at lower inlet gas temperatures and propagates faster which reduces both the heat-up time and the ignition propagation time. Under hot engine operating conditions, it was observed that the influence of the PML on the TWC conversions is marginal, which can be attributed to the insignificant reaction resistance as compared to the transport phenomena resistances.

Introduction

As world-wide automobile emissions legislation becomes stepwise tightening, the need to achieve higher catalytic efficiencies of the exhaust gas after-treatment systems becomes more critical, both during cold start and under normal operating temperatures (i.e., after light-off, when the catalyst temperature allows for conversions above 50%). The conversion of the exhaust gas pollutants in a three way catalyst (TWC) channel is controlled by three sequential processes, namely: external mass transfer (between the bulk gas and the washcoat surface), internal mass transfer (pore diffusion) and chemical reactions (Hayes and Kolaczkowski, 1994).

The TWC light-off occurs typically at temperatures between 200 and 300 ºC (Shelef and McCabe, 2000; Kašpar et al., 2003). A decrease in the light-off temperature with an increase in the PML has been already established based on temperature and chemical species composition measurements upstream and downstream of the TWC (Kašpar et al., 2003). However, the study of ignition characteristics based in such measurements does not provide information about the ignition location and propagation. In the present work, in addition to measurements upstream and downstream of the TWC, solid wall temperature measurements within the TWC substrate have been also performed in order to enhance the understanding of the TWC ignition characteristics.

The TWC light-off is mainly controlled by chemical kinetics. As the operating temperature increases, the operation of the TWC moves from the kinetic to the mass transfer controlled regime (West et al., 2003). As a result, above light-off temperature the TWC conversions are mainly limited by transport phenomena (e.g., Umehara et al., 2000; Brück et al., 2001 and Ramanathan et al., 2003). Recently, Santos and Costa (2008) have studied two TWC with identical characteristics (*e.g.*, dimensions, PML, etc.), with the exception of the substrate type. The authors have concluded that at high space velocities, the metallic substrate presents better conversions as compared to the ceramic substrate, mainly because of its larger geometric surface area. In addition, a number of literature studies have concentrated on the influence of the TWC design parameters on the conversions during hot engine operations. However, these studies do not disclose the influence of the PML on TWC conversions for different hot engine operating conditions that correspond to real engine operating conditions (engine speed and load). This work studies the influence of the PML on the TWC conversions during hot engine operation through the experimental characterization of two TWC with different PML.

Experimental

In this work, we have studied two commercial TWC and Table 1 lists their main characteristics. The two TWC have identical characteristics (e.g., dimensions, substrate type, etc.), with the exception of the PML. One of them has a PML of 50 g/ft^3 (referred to here as TWC-L – low PML) and the other 100 g/ft^3 (referred to here as TWC-H – high PML).

Table 1: Main technical characteristics of the TWC studied.

Substrate Type	Square Cell Ceramic
Cell density (cells/cm^2)	62 (400 cpsi)
Substrate dimensions (mm)	Diameter = 10.5 Lenght = 11.5
Catalyst volume (dm^3)	1.0
Uncoated geometric surface area (m^2/m^3)	2740
Uncoated wall thickness (mm)	0.1651 (6.5 mil)
Mean washcoat thickness (mm)	0.0228
Open frontal area uncoated (%)	75.7
Cell hydraulic diameter uncoated (mm)	1.105
Washcoat material	CeO_2-Al_2O_3
Precious metal loading	5 Pd/1 Rh TWC-L: 50 g/ft^3 TWC-H: 100 g/ft^3

The measurements were carried out on a vehicle equipped with a 2.8 liter DOHC V6 spark ignition engine that has multipoint fuel injection. Figure 1 shows a schematic of the vehicle and TWC experimental setup. In order to perform the experiments, each TWC was in turn placed in the so called under-floor position replacing the original TWC installed on the vehicle. The vehicle was tested on a chassis dynamometer. The transient operating conditions were imposed by a servo that actuates the engine throttle. A dedicated software was used to control the servo and also for data acquisition. The data obtained include inlet mass flow rates, manifold absolute pressures, engine operating temperatures, engine speeds, signals from the lambda sensors, exhaust gas species concentrations and temperatures taken both upstream and downstream of the TWC, as well as temperatures in various locations within the substrate of the TWC.

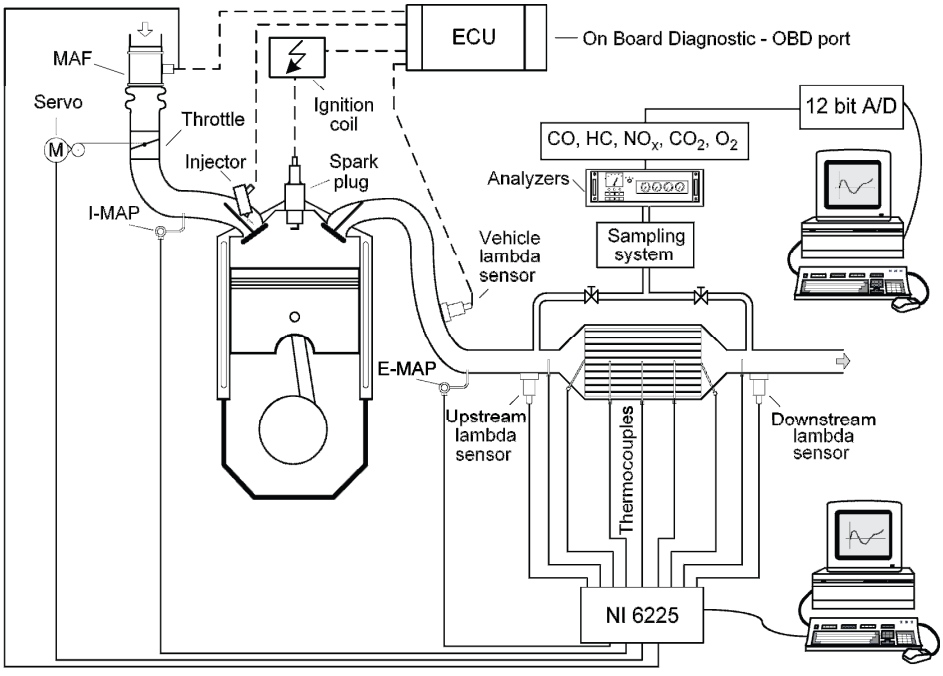

Figure 1: Schematic of the vehicle and TWC experimental setup.

Cold Start Engine Operation

The cold start measurements were carried out during extended engine idle periods. These modes provided exhaust conditions of temperature and flow that proved very valuable in evaluating the TWC low temperature activity and deducing the sensitivity of TWC to ignition with respect to PML, exhaust temperatures and other implied factors.

Figures 2 and 3 show the time variation of the gas and solid temperatures for the TWC-L and TWC-H at idle, respectively. Note that these figures include a schematic of locations of the thermocouples used to measure the exhaust gas and the solid wall temperatures in the vehicle exhaust after-treatment system. As can be seen in Figures 2 and 3, thermocouples Tgi and Tgo allowed for the measurement of the inlet and outlet gas temperatures, and thermocouples Twi and Two allowed for the measurement of the solid wall temperatures along the centreline at the TWC inlet and outlet, respectively.

During the trials it was observed that the time required to reach steady-state operating temperatures and downstream emissions at idle was 2800 s so that measurements were taken during this period of time.

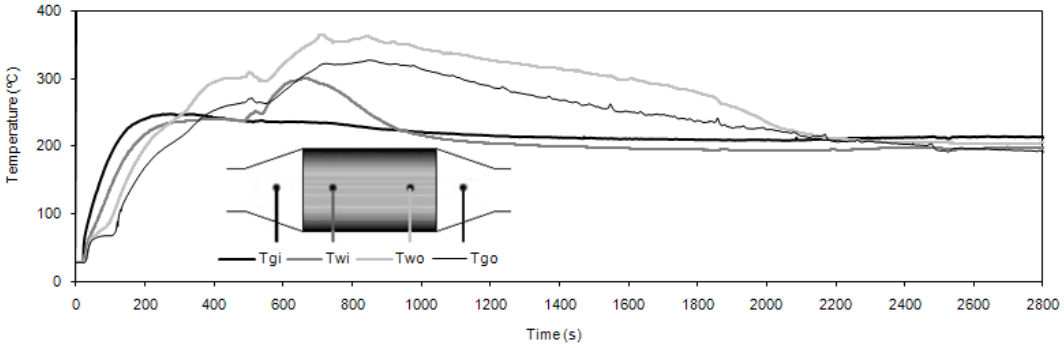

Figure 2: Time variation of the gas and solid temperatures for the TWC-L at idle.

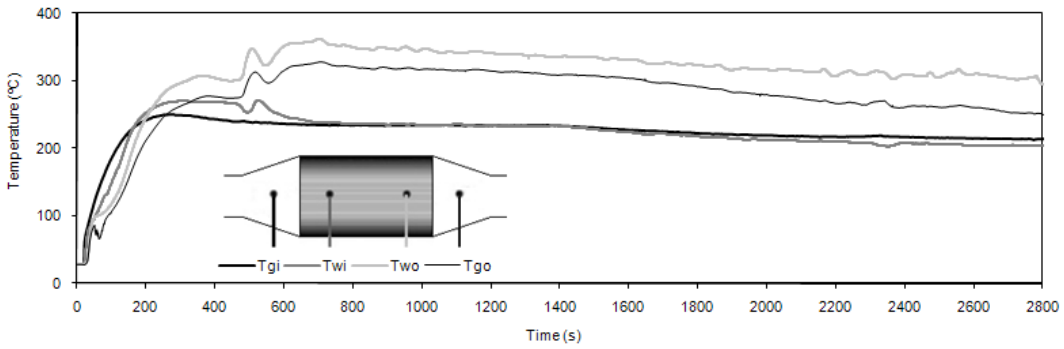

Figure 3: Time variation of the gas and solid temperatures for the TWC-H at idle.

Figures 2 and 3 show that after engine being switched on (t = 20 s), the inlet gas temperature (Tgi) starts to increase as a consequence of the hot exhaust gas flow. The start of the ignition can be identified from the measured gas and solid temperature profiles. When ignition occurs, the heat generated by the gas pollutants conversion within the porous washcoat leads to a rapid solid wall temperature increase. The instant and location where the solid wall temperature rises above the inlet gas temperature indicates that the heat transfer occurs from the solid wall to the fluid and the occurrence of the TWC ignition.

The solid wall temperature profiles reveal distinct ignition characteristics for the TWC-L and TWC-H. Indeed, the temperature profiles displayed in Figure 2 for the TWC-L reveal that the ignition takes place first at the substrate outlet, the so-called back-end ignition, while for the TWC-H, Figure 3 indicates that ignition starts at the substrate inlet, the so-called front-end ignition.

The temperature profiles in Figures 2 and 3 also indicate that the TWC-H ignites at lower inlet gas temperatures, as compared to the TWC-L. This observation indicates that the use of a

higher PML contributes to reduce the heat-up time required for ignition. In fact, a comparison between Figures 2 and 3 shows that the start of the ignition in the TWC-H occurs several seconds before it starts in the TWC-L. It is important to point out that the reduction of the heat-up time required to achieve TWC ignition is crucial to diminish vehicle emissions during cold start periods.

Figure 2 shows that when the ignition starts at the TWC-L outlet, the inlet gas temperature is already decreasing after reaching the maximum. This indicates that the low PML of the TWC-L does not favor ignition near the substrate inlet for temperatures below 250 ºC. As for the TWC-H, Figure 3 shows that the ignition starts (at inlet gas temperatures of about 230 ºC) before the inlet gas temperature reaching the maximum. In this case, the inlet gas temperature remains increasing after the start of the ignition. This means that the high PML of the TWC-H presents two important advantages: it decreases the inlet gas temperature required for the start of the ignition and favors the front-end ignition.

In addition to the influence of the PML on the ignition location it is also important to know the influence of the PML on the ignition propagation. The temperature profiles displayed in Figures 2 and 3 reveal that the temperature front propagates faster for the case of the front-end ignition (see Figure 3), as compared to the TWC back-end ignition case (see Figure 2). Please not that for the case of back-end ignition, the heat produced by the pollutants conversion at the reactor outlet is convected downstream of the TWC. Therefore, when the ignition starts at substrate outlet the only driving force for the temperature front moving from the outlet towards the inlet is the conduction through the solid.

Hot Engine Operation

The vehicle was tested under several steady-state hot engine operation conditions. Table 2 summarizes the test conditions. For each engine speed (2000, 3000 and 4000 rpm), tests were made for six different break mean effective pressures (BMEP), corresponding altogether to eighteen test conditions. Note that the Re and SV are the same for both TWC-L and the TWC-H because these two TWC have the same substrate and washcoat characteristics and only differ on the PML.

Table 2: Test conditions.

Vehicle		TWC-L and TWC-H			
Engine Speed (rpm)	BMEP (bar)	Re	SV (s^{-1})	TWC-L Solid Wall Temperature (K)	TWC-H Solid Wall Temperature (K)
2000	0.0	56.7	30.8	758	769
	0.9	78.9	47.4	809	809
	1.8	97.6	63.3	844	855
	2.3	104.6	70.2	865	865
	2.9	114.0	19.3	882	883
	3.2	120.2	86.7	888	899
3000	0.0	83.0	50.9	805	820
	1.0	110.9	81.0	910	913
	1.9	135.0	105.2	939	947
	2.9	159.2	132.0	975	977
	3.6	180.9	155.3	999	1012
	4.4	115.4	178.3	1021	1031
4000	0.0	115.0	78.5	864	873
	1.0	155.4	130.5	981	989
	2.0	178.0	160.0	1022	1024
	3.0	206.0	191.6	1041	1048
	4.1	233.3	229.6	1072	1077
	5.3	261.0	263.6	1095	1100

For all test conditions listed in Table 2, the Reynolds number within the TWC channels is < 261 (laminar flow). The space velocities are in the range of 30.8 to 263.6 s^{-1}. The solid wall temperatures included in Table 2 were taken as the mean value of the various solid wall

temperatures measured within the TWC. Table 2 reveals that the measured values for the solid wall temperature for both TWC (TWC-L and TWC-H) are rather similar. The solid wall temperatures are in the range of 758 to 1095 K and 769 to 1100 K for TWC-L and TWC-H, respectively.

Figures 4 and 5 show the measured CO and NO_x conversions as a function of the space velocity in the TWC-L and TWC-H, respectively. It is seen that for both TWC the conversions are higher for NO_x than for CO. In addition, Figures 4 and 5 reveal that for both TWC the conversions tend to decrease for higher space velocities, regardless of the chemical species. Furthermore, the NO_x conversions present a more monotonous dependence of space velocity.

The substrate volume of the TWC studied in this work is just 36% of the engine displacement volume. Marsh *et al*. (2001) also measured the TWC conversions in warmed-up conditions using a TWC with a low substrate volume. In good agreement with the present findings these authors verified that even under high load conditions, like driving on the highway, small substrates with volumes of 50-60% of the engine displacement yield conversions over 96% for HC and CO and close to 100% for NO_x.

A comparison between Figures 4 and 5 indicates that the decreasing of the NO_x conversion for higher space velocities is slightly less marked for the TWC-H than for the TWC-L. On the other hand, these figures indicate that the CO conversions are rather similar for both TWCs. This indicates that the TWC-L (with 50 g/ft^3, PML) and TWC-H (with 100 g/ft^3, PML) performs similarly during hot engine operation. This result reveals that for the two TWC studied the reaction resistance can be considered negligible as compared to the transport phenomena resistances (external and internal mass transfer).

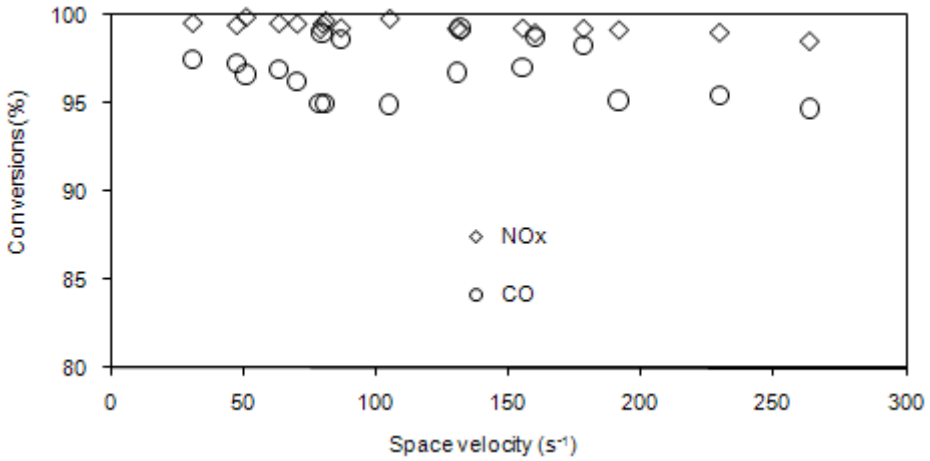

Figure 4: Conversions of CO and NO_x for the TWC-L as a function of space velocity.

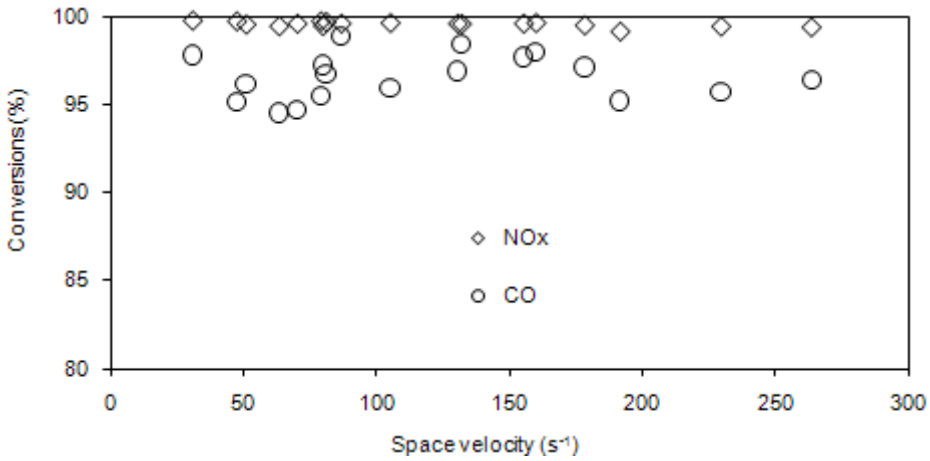

Figure 5: Conversions of CO and NO_x for the TWC-H as a function of space velocity.

Conclusions

During the cold start operation it was found that: (i) the PML influences both the ignition location and propagation; (ii) for low PML the ignition starts at the TWC back-end and for high PML the ignition starts at the TWC front-end; (iii) for high PML the ignition occurs at lower inlet gas temperatures and propagates faster which reduces both the heat-up time and the ignition propagation time. Under hot engine operating conditions, it was observed that the influence of the PML on the TWC conversions is marginal, which can be attributed to the insignificant reaction resistance as compared to the transport phenomena resistances (external and internal mass transfer).

Acknowledgments

The first author (H. Santos) is pleased to acknowledge the Fundação para a Ciência e a Tecnologia (FCT) for the provision of a scholarship (SFRH/BD/32851/2006).

References

Brück R., F. Kaiser, R. Konieczny, C. Webb and A. Anderson (2001), Study of modern application strategies for catalytic aftertreatment demonstrated on a production V6 engine, SAE Paper 2001-01-0925.

Hayes R.E., S. T. Kolaczkowski (1994), Mass and heat transfer effects in catalytic monolith reactors, *Chemical Engineering Science*, 49, 3587-3599.

Kašpar J., P. Fornasiero and N. Hickey (2003), Automotive catalytic converters: current status and some perspectives, *Catalysis Today*, 77, 419-449.

Marsh P., F. Acke, R. Konieczny, R. Brück and P. Hirth (2001), Application guideline to define a catalyst layout for maximum catalytic efficiency", SAE Paper 2001-01-0929.

Ramanathan K., V. Balakotaiah and D. H. West (2003), Light-off criterion and transient analysis of catalytic monoliths", *Chemical Engineering Science*, 58, 1381-1405.

Santos H., M. Costa (2008), Evaluation of the conversion efficiency of ceramic and metallic three way catalytic converters, Energy Conversion and Management, 49, 291-300.

Shelef M., and R.W. McCabe (2000), Twenty-five years after introduction of automotive catalysts: what next?, *Catalysis Today*, 62, 35-50.

Umehara K., M. Makino, M. Brayer, E. R. Becker and R. Watson (2000), Prediction of catalytic performance for ultra thin wall and high cell density substrates, SAE Paper 2000-01-0494.

West D.H., V. Balakotaiah and Z. Jovanovic (2003), Experimental and theoretical investigation of the mass transfer controlled regime in catalytic monoliths, *Catalysis Today*, 88, 3-16.

Reduction of Air Pollution Inside a Vehicle by Using Nano-Particle Filter

L. Tartakovsky[1], V. Baybikov[1], J. Czerwinski[2], M. Gutman[1], M. Kasper[3], M. Veinblat[1] & Y. Zvirin[1]*

[1] Technion – Israel Institute of Technology, Technion City, 32000 Haifa, Israel, tartak@technion.ac.il

[2] Laboratory for IC-Engines and Exhaust Emission Control (AFHB), University of Applied Sciences, Biel-Bienne, Gwerdtstrasse 5, CH-2560 Nidau, Switzerland

[3] Matter Engineering AG - Nanoparticle Management, Bremgarterstrasse 62, CH-5610 Wohlen, Switzerland

Introduction

It is quite well established now that road users, such as cyclists and especially professional drivers, are exposed to higher levels of air pollution than background or curbside data might suggest, Chan et al (1991), Colwill and Hickman (1980), Kingham et al (1998), Rudolf (1994),Van Wijnen et al. (1995), Taylor and Fergusson (1998). According to the latter source, road users in the center of the roadway are likely to be travelling through a tunnel of the most polluted air and this is the principal reason for their raised relative exposure to pollutants – see Fig. 1.

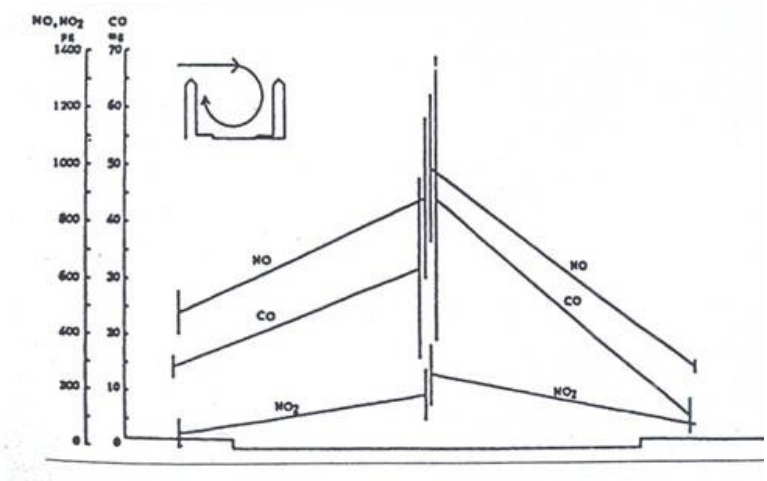

Figure 1: Comparison of differences in CO, NO and NO2 concentrations on the sidewalk and inside a car (Taylor and Fergusson, 1998).

In countries with hot climate conditions, almost the entire vehicle fleet is equipped with air conditioning (AC) systems, and the driver usually makes a decision about the desired method of car ventilation: without AC and opened window, with AC and internal recirculation of air, or with AC and introduction of outdoor air into the car. Recent research works studied the effects of the car ventilation method on air pollution inside a car (Tartakovsky et al., 2006). Significant influence of car ventilation method on the inside air quality was found with relatively high levels of particle concentrations inside a vehicle.

Objectives

The main goal of this study was to assess the possibilities to reduce air pollution by nano-particles inside a vehicle with aid of a special particles filter. The data collected in this research can be used to evaluate exposure levels of professional drivers to air pollution inside a vehicle during driving in urban areas and city centers.

Methodology

The experiments have been performed with 4 vehicles of different makes and types: 3 passenger cars (PC) and one van serving as a shuttle taxi. Main data of these vehicles are summarized in Table 1.

Table 1: Vehicles that have been used in experiments

Vehicle model	Type	Engine type	Engine volume	Production year	Traveled distance, km
Renault Megane	PC	SI	1.6	2005	130000
Citroen C4	PC	SI	1.6	2009	10000
Peugeot 206	PC	SI	1.4	2002	150000
Volkswagen Transporter	Van	CI	2.5	2008	130000

The experiments have been carried out in two Israeli cities: Haifa and Tel-Aviv; both characterized by heavy traffic conditions in city centers and differ in topography: very hilly in the former and flat in the latter. Driving routes in both cities have been selected in collaboration with local transport planning authorities and based on previous road gradient measurements (Tartakovsky et al., 2000) and traffic counts. Average road gradient of two driving routes in Haifa used for experiments with PC and shuttle taxi was found to be about 6% compared with 0.5% at driving route in Tel-Aviv. Experiments with a shuttle taxi have been performed on a real taxi route and in a real-world driving regime with frequent doors opening at taxi stops.

Concentrations of CO, NO, NO_2, and nano-particles PN (particles number) were measured in this study. Average size of nano-particles was assessed as well. Interscan gas analyzers of models 4140, 4540 and 4150 with electrochemical cells served for measurements of CO, NO and NO_2 concentrations, respectively. Nano-particles concentrations and their average size were measured by the Matter Engineering diffusion size classifier (DISC).

All readings of the gas analyzers, and DISC, as well as stop events, were logged at 1 Hz frequency by a Squirrel 1023 and DISC built-in data loggers, and subsequently analyzed after downloading to a computer. Sampling collection was performed in the driver's breathing zone. Experiments were carried out during all working days of the week, from 7 AM till 7 PM.

In part of experiments a novel nano-particle filter system (Nanocleaner) developed by the Matter Engineering AG was used, in order to reduce air pollution by particulates inside the vehicle. The Nanocleaner system contains input backpressure monitor, in order to prevent filter clogging. In all experiments with the Nanocleaner, the vehicle's air conditioning (AC) system operated in internal air recirculation mode and a fresh air was supplied inside a vehicle by the Nanocleaner. The filter system installation in the tested vehicle is shown on Fig.2. Filters supplied by the Matter Engineering AG for experiments were designed for use in the PC's, therefore in experiments with the shuttle taxi van two filter systems were used and operated simultaneously.

Comparative noise measurements inside the vehicle were performed with the nano-particle filter system switched on and off. The measurements have been done in proximity of the driver head by sound level meter IEC 651 type d ,Luton SL 4022.

The testing program included measurements outside the vehicle and inside a vehicle at different ventilation modes with the Nanocleaner switched on and off. The following ventilation modes were studied: AC switched on and introduction of outdoor air into the car; AC switched on, internal air recirculation; AC switched off, vent off, window of the driver fully open.

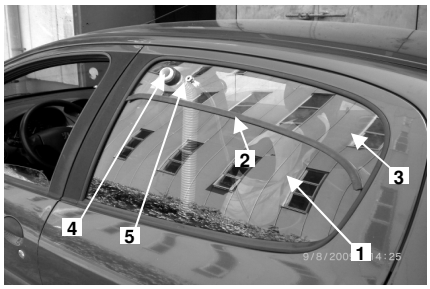

1 – vehicle original window; 2 – seal;
3 – insertion window; 4 – air inlet to nanocleaner;
5 – air inlet to diffusion size classifier

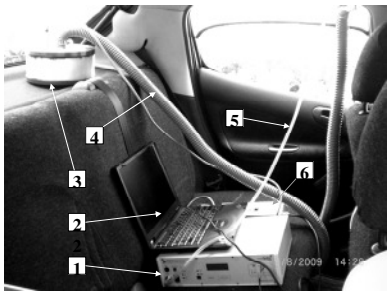

1 – diffusion size classifier; 2 – laptop with DiSC software;
3 – Nanocleaner; 4 – Nanocleaner inlet line;
5 – DiSC sample line; 6 – Nanocleaner control unit.

Figure 2: Nanocleaner installation in tested vehicle.

Results and discussion

Results of nano-particles concentration and size measurements that have been performed with PC in Haifa and Tel-Aviv are presented in Fig. 3. The Figure shows PN concentrations and size, as were observed outside and inside the vehicle, with the Nanocleaner switched on.

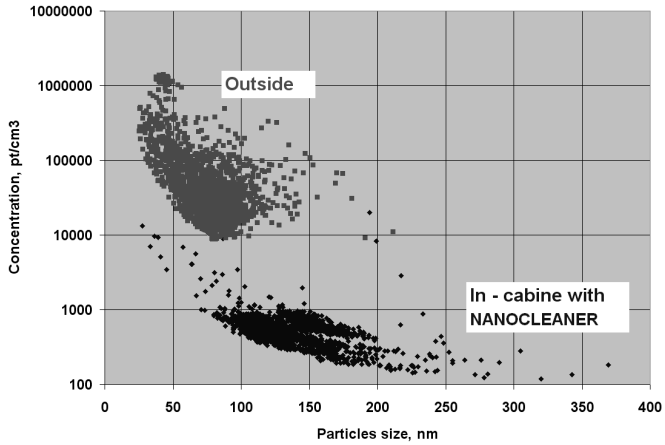

Figure 3: Results of nano-particle measurements outside and inside passenger car.

The experiments results show clearly that the use of the nano-particle filter system allowed significant reduction of up to 95-99% of PN concentrations inside the car, compared with outside readings. The achieved levels of PN concentrations inside the car that were reduced by using the Nanocleaner to values below 250 cm^{-3} are typical for a clean office. Along with this, some minimal time is required, in order to achieve maximal cleaning effect. The experiments on the long Tel-Aviv driving route (route length 15 km) have shown that minimal PN concentrations inside the car (about 230 cm^{-3}) were achieved after about 25 min of filter operation – see Fig. 4.

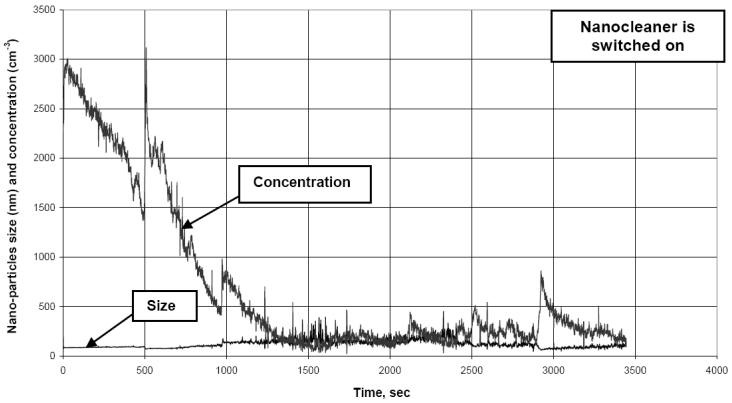

Figure 4: Results of nano-particle measurements inside the car – Tel-Aviv driving route.

Thus, in shorter urban driving trips it will be impossible to achieve a maximal cleaning effect. This was confirmed by the results of experiments on the short Haifa driving route (length of 4.1 km), where time of one driving run usually did not exceed 12-13 min. As a result, minimal PN concentrations that were achieved inside the car in these trips did not fall below 3000 cm^{-3}.

The data in Fig. 3 clearly show that use of nano-particle filter leads to some increase in size of particles measured inside the vehicle, compared with ambient air data. Average nano-particles size outside the vehicle was measured to be 70-80 nm compared with 120-130 nm inside the vehicle after Nanocleaner operation. This result may be explained by increase of the relative contribution of dust particles settled down on seats and other surfaces inside the vehicle and resuspended due to human activities and air movement, as the filter cleans air entering vehicle cabine. Fig.5 shows distribution of nano-particle sizes as was measured outside and inside the vehicle with the Nanocleaner switched on.

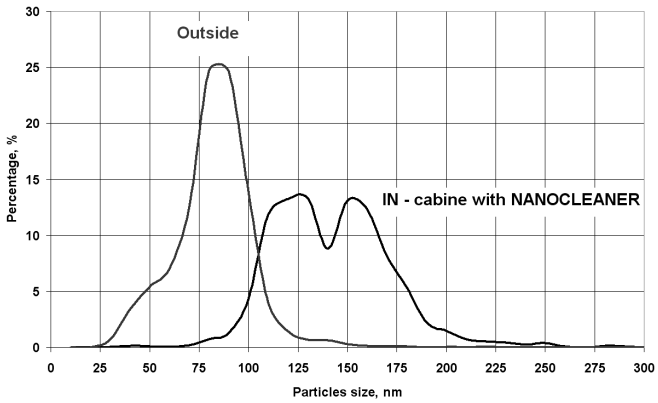

Figure 5: Distribution of nano-particles size inside and outside a vehicle.

Drivers and operators, who took part in the road tests, noted the noise generated by operation of the nano-particles filter. In order to assess this noise level, some preliminary measurements have been performed during experiments with passenger cars. Their results are summarized in Table 2.

Table 2: Noise level inside a car

Operation mode	Noise level, dB
Nanocleaner switched off	66 – 71
Nanocleaner switched on	68 – 73

The measured noise levels with and without nano-particle filter operation indicate some tendency of noise intensification with the Nanocleaner switched on. More detailed study of this issue with frequency analysis of the noise spectrum and development of appropriate noise mitigation measures, if necessary, may be recommended.

As anticipated, no effect of the nano-particle filter system on concentrations of gaseous pollutants was observed.

Results of experiments with the Nanocleaner in the shuttle taxi are shown in Fig. 6. As mentioned above, in these tests two Nanocleaner units were used and operated simultaneously, due to the big volume of the passenger space in this shuttle taxi van. The measured results show a significant influence of the frequent door openings on the cleaning effect. During the major part of the test, PN concentrations did not fall down below 8000 cm^{-3} with a rise back to the almost ambient levels with door opening. It can be assumed that average levels of PN concentrations inside a shuttle taxi may be reduced by appropriate adoption of the filter productivity (filtered air flow rate) to air exchange volume during a shuttle taxi operation.

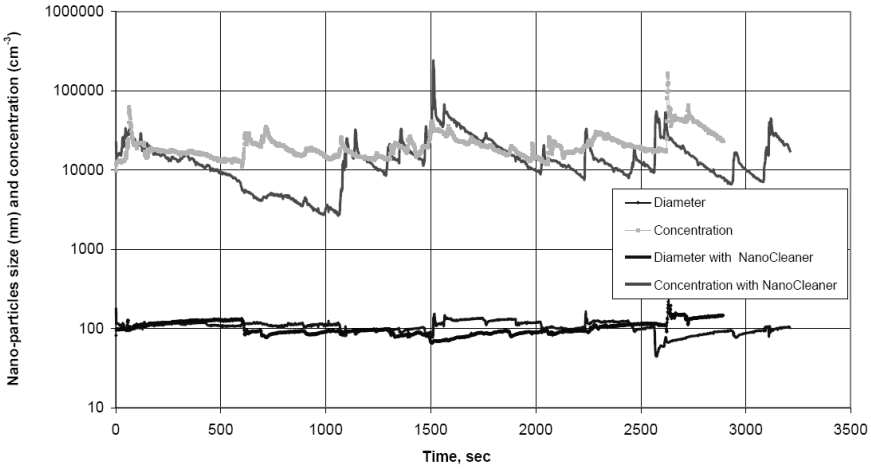

Figure 6: Measurements of nano-particles size and concentrations inside a shuttle taxi.

Conclusions

Results of experiments demonstrated that dedicated nano-particle filter system allows significant reduction up to 99% of particle number concentrations inside a vehicle. Some minimal time is required, in order to achieve maximal cleaning effect. The results of experiments show that minimal PN concentrations inside a car (about 230 cm^{-3}) were achieved after about 25 min of filter operation. Use of nano-particle filter leads to some increase in size of particles measured inside a vehicle compared with ambient air data.

The measured noise levels with and without nano-particle filter operation indicate some tendency of noise intensification with Nanocleaner switched on. A more detailed study with frequency analysis of the noise spectrum and development of appropriate noise mitigation measures, if necessary, may be recommended.

Acknowledgements

The financial support of the Israeli Ministry of Environment Protection is highly appreciated. The authors wish to thank the Matter Engineering AG and Israeli Taxi Drivers Association for their technical support.

References

Chan C., H. Ozkaynak, J. Spengler and L. Sheldon (1991), Driver exposure to volatile organic compounds, CO, Ozone, and NO2 under different driving conditions, *Environmental Science and Technology*, vol. 25, n° 5, p 964-972.

Colwill D., J. Hickman (1980), Exposure of drivers to Carbon Monoxide, *Journal of the Air Pollution Control Association*, vol. 30, n° 12, p 1316-1319.

Kingham S., J. Meaton, A. Sheard and O. Lawrenson (1998), Assessment of exposure to traffic-related fumes during the journey to work, *Transportation Research*, part D, vol. 3, n° 4, p 271-274.

Rudolf W. (1994), Concentrations of air pollutants inside cars driving on highways and in downtown areas, *Science of the Total Environment*, vol. 146/147, p 433-444.

Tartakovsky L., M. Gutman, Y. Aleinikov, M. Veinblat, Y. Zvirin, B. Flicstein and B. Ben David (2000), The Effect of Road Profile on Passenger Car Emissions, *Transport and Air Pollution, 9th International Scientific Sumposium*, Avignon, France, 445 – 449.

Tartakovsky L., Y. Aleinikov, V. Baybikov, E. Berlin, B. Flicstein, Z. Fuhrer, M. Gutman, M. Veinblat and Y. Zvirin (2006), Driver exposure to air pollution inside a car – effects of ventilation method, *Proceedings ACTES – INRETS No. 107 of the 2nd Conf. Environment & Transport*, Vol. 2 Arcucil, France.

Taylor D., M. Fergusson (1998), The comparative pollution exposure of road users – a summary, *World Transport Policy and Practice*, 4/2.

Van Wijnen J., A. Verhoeff, H. Jans and M. Van Bruggen (1995), The exposure of cyclists, car drivers and pedestrians to traffic-related pollutants, *International Archives of Environmental Health*, vol. 67, p 187-193.

Uncatalysed and Catalysed Soot Combustion under $NOx+O_2$: Real Diesel versus Model Soots.

I. Atribak, A. Bueno-López and A. García-García.*

MCMA Group, Department of Inorganic Chemistry, Faculty of Sciences, University of Alicante, Ap.99-E-03080, Alicante, Spain, a.garcia@ua.es

Introduction

Soot abatement in diesel exhaust conditions commonly consists of the separation of carbonaceous particles by mechanical filtration using a diesel particulate filter (DPF) and subsequent burning of the soot particles in order to avoid pressure drops by filter plugging. Since this material burns at roughly 550-600ºC with oxygen, while diesel exhaust gases temperature most of the time lie between 200-400ºC, a suitable catalyst is needed to promote soot combustion (Atribak et al., 2008).

In this context, the NOx present in the exhaust gases (typically, 100-600 ppm, mainly as NO) are of interest. If NO is catalytically oxidised to NO_2, the combustion of soot proceeds efficiently, even in the loose-contact mode between soot and catalyst, as NO_2 is very oxidant at low temperatures (Krishna et al., 2007; Atribak et al., 2008).

The catalytic combustion of soot in NOx/O_2 gas streams has been extensively studied employing catalysts of different chemical nature, most of them able to oxidise NO to NO_2 (Krishna et al. 2007; Atribak et al. 2009). The majority of these studies were conducted on readily available model soot samples. The use of model soot, such as a carbon black, as a surrogate of real soot can be considered suitable for catalysts screening, since real diesel soot features are heterogeneous. However, available model soot samples can present great discrepancies with real soot, from a microstructure and reactivity viewpoint. The physico-chemical properties of a real soot depend on several aspects such as the quality of the fuel and lubricating oil used, which contribute to the soluble organic fraction (SOF) content, the type and age of the engine or the engine operating conditions (Collura et al., 2005).

In general, model and real soots differ in several aspects. One of them is the amount and type of ashes, since real soot incorporates into the structure the metals that diesel fuels and lubricating oils contain. On the other hand, real soot contains a variable amount of adsorbed hydrocarbons, which are denoted by SOF (soluble organic fraction), and this amount varies from only 5%, for a loaded engine, to 60%, for an idle engine, of the total mass (Stanmore et al., 2001).

In our previous works, different ceria and ceria-zirconia catalysts were prepared and tested for a model soot (Printex-U by Degussa) catalytic combustion [Atribak et al. 2008 and 2009), with promising results in terms of high catalytic activity and high thermal stability. One of our previous conclusions was that the soot reactivity imposes a minimum combustion temperature that cannot be additionally lowered by using a catalyst. This limit temperature depends on the soot features, and therefore, it is expected to be different for each soot sample. In order to deepen into this aspect, and also to test our most promising catalysts with both real and model soot samples, the present study is devoted to analyse the uncatalysed and catalysed combustion of three different diesel soot samples and two commercial soot samples, whose physico-chemical properties have been characterised by different techniques.

Experimental

Five soot samples were selected for this study. Two of them are commercial carbon blacks from *Degussa* (Printex-U) and *Cabot* (Vulcan XC-72R). The rest of carbon materials studied, denoted by MCMA-soot, A-soot, and B-soot, are real diesel soot samples. MCMA-soot was collected at the exhaust pipe of a test bench equipped with a turbo-diesel Nissan 2.0 engine running under idle conditions (steady state 880 rpm) at our laboratory. A-soot and B-soot were supplied by Renault S.A., and were collected at the exhaust pipe of a test bench equipped with a F9Q diesel engine of 1900 cm^3 running at 2000 rpm. The samples were trapped on a SiC filter placed before (B-soot) or after (A-soot) a $Pt/CeO_2/Al_2O_3$ cordierite oxidation catalyst.

Two home-made $Ce_{0.76}Zr_{0.24}O_2$ catalysts and a commercial sample of composition $Ce_{0.80}Zr_{0.20}O_2$, supplied by Rhodia, were used in this work. The home-made samples were prepared from $Ce(NO_3)_3{\cdot}6H_2O$ and $ZrO(NO_3)_2{\cdot}xH_2O$ as precursors, following two different preparations procedures: i) co-precipitation route and ii) reversed micro-emulsion route. The nomenclature of the catalysts is COP (prepared by co-precipitation; 67 m^2/g), RH (commercial sample; 113 m^2/g) and RME (prepared by reversed micro-emulsion; 128 m^2/g). The characterization of these catalysts and the details related to the preparation procedures were reported elsewhere (Atribak et al., 2009).
The C, H, N, S elemental compositions of the soot samples were determined by elemental analysis (Carlo Erba Instruments equipment -model EA 1108-).
Proximate analysis of the soot samples were performed in a Thermogravimetry-Differential Thermal Analysis equipment from METTLER TOLEDO (model TGA/SDTA851e/SF/1100).
BET surface areas were measured by multi-point N_2 adsorption at -196ºC using an automatic Autosorb-6B (Quantachrome equipment). The samples (both soot samples and catalysts) were previously degassed for 4 hours at 250ºC under vacuum.
TEM analyses of the soot samples were performed with a JOEL (JEM-2010) microscope, which works under an acceleration voltage of 200 kV. The maximum resolution obtained between lines is of 0.14 nm and between points of 0.25 nm.
Raman spectra of the soot samples were recorded in a Bruker RFS 100/S Fourier Transform Raman Spectrometer with a variable power Nd:YAG laser source (1064 nm). 64 scans at 85 mW laser power (70 mW on the sample). No heating of the sample was observed under these conditions.
The soot combustion tests were performed in a tubular quartz reactor (inner diameter = 10 mm) coupled to specific NDIR-UV gas analysers for CO, CO_2, NO, NO_2 and O_2 monitoring. For the uncatalysed reactions, 20 mg of soot were diluted with SiC to avoid pressure drop and favour heat transfer. For the catalysed reactions, 20 mg of soot were mixed with 80 mg of the selected catalyst in the so-called *loose contact* conditions (Atribak et al., 2008) and the soot-catalyst mixture is diluted afterwards with SiC. The gas mixture used contained 500 ppm NOx, 5% O_2 and balance N_2, and the gas flow was fixed at 500 ml/min (Gas Hourly Space Velocity –GHSV- of 30000 h^{-1}). The experiments consisted of Temperature Programmed Reactions, where the gas mixture was fed to the reactor at room temperature and then the temperature was increased until 750ºC at 10ºC/min.

Results and discussion

3.1. Characterisation of soot samples.

TEM micrographs (not shown for the sake of brevity) were taken in order to deduce the microstructure of the different soot samples. It can be commented that the primary soot particles are spherules and that these primary particles have about the same size for all soot samples. A deeper analysis of all the pictures taken allows concluding that the size of the primary particles is between 10-50 nm, and among the five soot samples, significant differences on particles size are not inferred. The primary particles present a core-shell structure, where long-range layers are concentrically arranged along the outermost periphery, and short layers are amorphously arranged inside the core, in agreement with the description reported by some other authors (Song et al., 2006). The spherules form chain-like aggregates (secondary particles) composed of several tens or hundreds of primary spherical particles. The TEM images suggest that the degree of agglomeration is highest for MCMA-soot, and its primary particles seem to present the most irregular surface. However, clear differences among the remaining soot particles can be hardly deduced from the TEM images.
Raman spectroscopy was also used as a tool for the structural characterisation of the soot samples. This technique is sensitive not only to crystal structures but also to molecular structures (short-range order). The Raman signals of graphite crystals result from lattice vibrations and are very sensitive to the degree of structural disorder (Sadezky et al., 2005).
The spectrum of a highly ordered graphite would present a unique strong band at around 1580 cm^{-1} (G-mode), corresponding to the “in-plane” displacement of the carbon atoms strongly coupled in the hexagonal “short” sheets, that is, ideal graphitic lattice vibration mode with E_{2g}-symmetry. This kind of Raman profile is observed in the spectrum of the pure commercial graphite sample included in Figure 1 for comparison purpose.
Figure 1 shows the Raman spectra of the five soot samples, where two main broad bands are identified. Besides the so-called G-band, an additional first order-band (D or “Defect” band) appears, which is characteristic of disordered graphite and corresponds to a graphitic lattice vibration mode with A_{1g} symmetry.

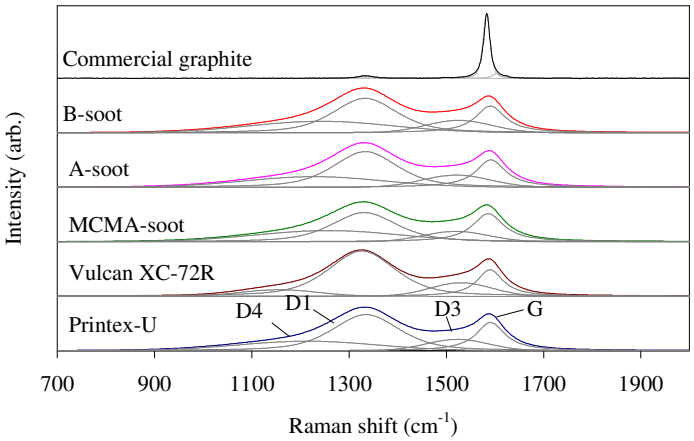

Figure 1: Raman spectroscopy characterization of the soot samples (a commercial graphite sample (by Alfa Aesar) is included for comparison).

In Figure 1 the Raman spectra are drawn along with the corresponding curve fitting results. For the soot samples, four different bands were deconvoluted in the spectral region between 700 and 1900 cm^{-1} (G, D1, D3 and D4 bands). Among the four deconvoluted bands, the most intense one is the D1 band, which appears at around 1320 cm^{-1}. The broad band at 1500-1520 cm^{-1} is associated with amorphous sp^2-bonded forms of carbon and will be referred to as the D3-mode in this paper. Finally, a band near 1200 cm^{-1} can be discerned, attributed to disordered graphitic lattice (with A_{1g} symmetry), polyenes or ionic impurities (D4).

Table 1 compiles several Raman parameters obtained after curve fitting. First of all, it is known that an increase of disorder in carbonaceous materials is reflected by an increase in the frequency of the G mode, being 1582 cm^{-1} for single hexagonal crystal graphite. The peak position of the soot samples (1585.9-1590.5 cm^{-1}) suggests a relative disorder compared to ordered-graphite, and all the soot samples present similar values. However, differences in the G-band width are observed among our five soot samples. For Vulcan, the FWHM measured is of 62.9 cm^{-1}, somewhat lower than those of the rest of samples analysed (72.2-78.9 cm^{-1}) suggesting that Vulcan XC-72R presents the most ordered structure. In line with these results, Sadezky et al. (Sadezky et al., 2005) also reported values of the G band FWHM for different types of soot from 46 to 101 cm^{-1}. Meanwhile, significant lower values were measured for a graphite bar (20-22 cm^{-1}) and for a highly-ordered graphite (15-16 cm^{-1}) than for the remaining carbon materials studied. From our results, the lowest value of G-band width for Vulcan XC-72R could be ascribed to a slightly higher graphitic order.

Table 1: Parameters obtained from Raman spectroscopy after deconvolution of the spectra

Sample	**G (ν cm^{-1})**	**FWHM G (cm^{-1})**	**D1 (ν cm^{-1})**	**FWHM D1 (cm^{-1})**	**I_{D1}/I_G**
Vulcan XC-72R	1590.5	62.9	1327.2	160.8	3.60
Printex-U	1590.5	72.2	1334.2	163.1	2.35
MCMA-soot	1585.8	78.9	1331.9	157.4	1.77
B-soot	1590.5	72.2	1334.2	155.0	2.30
A-soot	1590.5	74.6	1331.9	156.1	2.30

An attempt was made to obtain a correlation among the L_a parameter (the average in-plane microcrystallite dimension) values and the soot properties. According to Ferrari et al. (Ferrari et al. 2000), when defects are progressively introduced in the graphite layer and reducing L_a below 2 nm, the number of ordered rings now decreases and the net result is the decreasing of I_{D1}/I_G with increasing amorphisation. The Tuinstra Koening equation is no longer valid. A new relationship is accepted, since the samples are in the regime where I_{D1}/I_G values are proportional to L_a^2 [Ferrari et al., 2000). According to this approximation and taking into account the I_{D1}/I_G values compiled in Table 1, the order of L_a values for the soots studied is as follows:

Vulcan XC-72R > Printex-U > Soot-A = Soot-B > MCMA-soot

This trend is in agreement with the idea that Vulcan XC-72R presents the most graphitic structure while the real diesel soots are more disordered materials.

Table 2 shows the elemental analysis of the five carbon materials used. The results evidence differences among the commercial carbon blacks and the diesel soot samples. As expected, commercial samples present a higher percentage of carbon and less hydrogen and nitrogen. Conversely, the real soot samples present a higher proportion of oxygen (estimated by difference). Among real soot samples, the slightly lower oxygen content of A-soot should be related to the influence of the oxidation catalyst. Several effects might be invoked, including the oxidative cracking, dehydrogenation, alkylation and oxidation of some compounds constituting the soluble organic fraction, and a partial oxidation of soot to CO and CO_2 by the NO_2 formed by catalytic oxidation of NO by O_2 over platinum (Collura et al., 2005).

Table 2: Elemental analysis of the different soot samples

Sample	C (%)	H (%)	N (%)	S (%)	O* (%)
B-soot	85.0	1.2	0.9	<0.2	12.7
A-soot	87.9	0.9	0.4	0.2	10.6
MCMA-soot	84.7	1.1	0.5	0.8	12.9
Vulcan XC-72R	98.0	0.1	0.1	0.5	1.3
Printex-U	92.2	0.6	0.2	0.4	6.6

* estimated by difference

More accentuated differences regarding composition can be noted when the proximate analyses are compared (listed in Table 3). A negligible amount of ashes was estimated for commercial carbon blacks. On the contrary, ash percentages between 1.2 and 2.2 % were determined for the diesel soot samples. These ashes come from the diesel fuel and from the lubricating oil used, as widely reported (Collura et al., 2005). Commercial carbon blacks present a higher amount of fixed carbon (96.5% for Vulcan XC-72R against 67.3% for MCMA-soot) and a lower amount of volatile matter (3.5% against 30.8% for Vulcan XC-72R and MCMA-soot, respectively). As the volatile matter could influence the kinetics of the uncatalysed and catalysed soot combustion and some authors point out that the mass lost by soot during solvent extraction, (for SOF determination), was almost the same than the mass lost by thermal treatment under inert gas at 600°C (Stanmore et al., 2001), these data were estimated and included in Table 3.

Table 3: BET surface areas, proximate analysis and SOF contents of the soot samples

Sample	BET (m^2/g)	Fixed carbon (%*)	Ash (%*)	Volatile matter (%*)	Wetness (%)	SOF (%)
B-soot	161	74.2	2.2	23.6	2.5	13.0
A-Soot	160	80.3	1.2	18.5	1.3	8.9
MCMA-soot	86	67.3	1.9	30.8	1.4	26.9
Vulcan XC-72R	234	96.5	0.0	3.5	0.5	0.4
Printex-U	100	91.8	0.1	8.1	0.9	3.2

* dry basis.

The MCMA-soot presents the highest mass loss, from which a SOF amount of 26.9% is estimated. This is consistent with the fact that the engine operating mode was idle, which can lead to an extra consumption of fuel due to inadequate diesel combustion. The B-soot presents a lower amount of SOF (13.0%) according to the load operating mode of the engine generating the soot. The contact of B-soot with the oxidation catalyst has led to a significant decrease of its SOF amount (13.0 % versus 8.9% for B-soot and A-soot, respectively), as expected.

The textural characterisation was accomplished by determining the BET surface area of the five materials under study. Otto et al. (Otto et al., 1982) found BET surface areas for different soots in the range 20-230 m^2/g. Ahlström et al. (Ahlström et al., 1989) reported that the BET surface area of a diesel soot increased from about 35 to 270 m^2/g by heating soot to 600°C under nitrogen, that is, after SOF release. This implies that the SOF present is plugging some already-existing micropores and could explain the very low BET value of MCMA-soot (86 m^2/g against 161 m^2/g for B-soot). This would also explain the highest BET surface area of Vulcan XC-72R (234 m^2/g).

3.2. Uncatalysed/catalysed soot combustion.

Figure 2a presents the uncatalysed soot conversion profiles. As a general trend, model soot samples are less reactive than real soot samples. This can be attributed to the lower content in heteroatoms (O, H and N) of the former samples and, in the case of Vulcan XC-72R, to a more ordered structure, according to Raman spectroscopic analysis, as well. According to the combustion profiles the trend in reactivity is as follows: A-soot > B-soot > MCMA-soot > Printex-U > Vulcan XC-72R. Regarding the selectivity towards CO_2 formation as reaction product, real soot samples are more selective than model soot samples.

The least reactive carbon material is Vulcan XC-72R, achieving a 50% of burn-off at a temperature (T50%) as high as 683ºC. This data is consistent with its low oxygen and other heteroatoms content, as well as with the negligible ash content and very high fixed carbon content (96.5%). Printex-U is quite more reactive than Vulcan XC-72R (T50% of 606ºC), and this is the reason why this carbon material is often used as model soot in studies devoted to catalysts for diesel removal. The trend obtained in L_a values was also in agreement with the reactivity trend in catalysed reactions. Vulcan XC-72R and Printex-U present the highest L_a values and the real soots the lowest ones.

Considering the real soot samples, the reactivity order follows the sequence: A-soot > B-soot > MCMA-soot. In order to interpret correctly the reactivity order for real soot samples, it must be paid attention to the temperatures and profiles of volatile compounds emission. The onset combustion temperature (300-350ºC) is similar to that of the volatile matter emission. Up to 400ºC, B-soot and MCMA-soot release volatile matter percentages of 6% and 22%, respectively. However the uncatalysed combustion profiles of both soot samples are identical, evidencing that nearly all these volatile compounds are released during the combustion tests below their light-off temperature. At 450ºC A-soot, which is the real soot presenting the lowest SOF content (8.9%), exhibits the highest slope in its soot combustion curve, and their T50% and T100% values are the lowest ones (511 and 559ºC, respectively). The reason why A-soot is the most reactive material is tentatively explained here. The contact of the virgin soot with the Pt/alumina/ceria catalyst originated not only different kinds of reactions involving SOF, as the oxidative cracking, dehydrogenation, alkylation and oxidation of some compounds constituting the soluble organic fraction, but also the oxidation of soot to CO_2/CO by the NO_2 formed by the catalytic conversion of NO+O_2 over platinum. The latter is supported by a lower O content estimated from Elemental Analysis, as experimental evidence, for A-soot versus B-soot. Therefore, the already-attacked A-soot's surface is more reactive both in uncatalysed and catalysed reactions than B-soot is.

As an example, Figure 2b illustrates the catalysed soot combustion profiles obtained under NOx/O_2 with the most active ceria-zirconia catalysts: RME. As expected, these combustion profiles are shifted towards lower temperatures with regard to the non-catalysed profiles (Figure 2a). This is attributable to the NO oxidation capacity of the catalysts, NO_2 being more oxidant at low temperatures than NO and O_2. The catalytic activity follows the sequence: COP<RH≈RME.

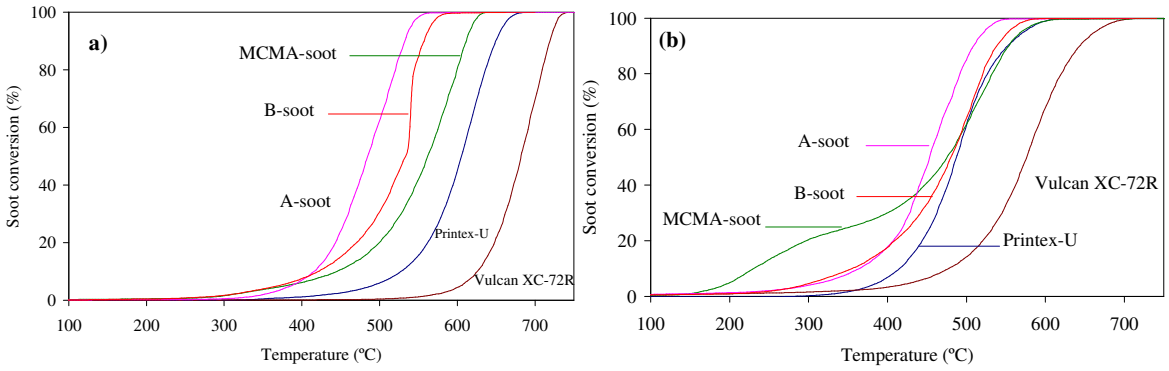

Figure 2: Soot conversion profiles obtained in: a) uncatalysed experiments; b) catalytic experiments (RME catalyst).

By analysing the catalytic profiles in Figure 2, the same trend than that noted in the uncatalysed reactions can be inferred for the different soot samples, with the exception of MCMA-soot. For

this diesel soot, a shoulder in the curve appears in the range 200-400ºC, due to the catalysed combustion of SOF. In fact, as the catalyst used presents a higher surface area (COP < RH < RME), the amount of CO_2 emitted at low temperatures becomes more important (shoulder in the curve) and a decrease in T50% was noted (493ºC > 485ºC > 476ºC). For the uncatalysed reactions, the volatile matter was released before combustion.

By comparing the soot conversion profiles of the catalysed reactions, it is observed that the curves are closer to each other as the catalyst used is more active. They are even overlapped at high temperatures for the most active catalyst (RME). Therefore, the effect of the catalyst is more important as the soot is less reactive. As representative examples, the T50% temperature of Vulcan XC-72R decreases from 683ºC for the uncatalysed reaction to 557ºC for the RME-catalysed reaction (124ºC decrease) while for the B-soot this decrease is of 35ºC, from 485 for the uncatalysed reaction to 450ºC for the RME-catalysed reaction. These experimental data support the hypothesis concerning that soot's inherent reactivity imposes a lower limit of temperature that cannot be additionally lowered by using any catalyst.

As a summary, the reactivity of different soot samples under $NOx+O_2$ follows the same trends both for uncatalysed and catalysed reactions. Whatever the ceria-zirconia catalyst tested, the combustion profiles are always shifted towards lower temperatures, the differences between the different soot samples becoming less important in the presence of catalyst. On the other hand, as the catalyst is more active, the contribution of the volatile matter oxidation to the combustion profile becomes more important, providing evidences of the effectiveness of these catalysts to combust SOF components adsorbed on the soot samples. This is very interesting because when diesel engine operates under idle conditions, the proportion of SOF on particulate matter generated can be as high as 60%.

References

Ahlström A.F., C.U.I. Odenbrand (1989), Combustion characteristics of soot deposits from diesel engines, *Carbon,* 27, 475-483.

Atribak I., A. Bueno-López, A. García-García (2008), Combined removal of diesel soot particulates and NOx over CeO_2-ZrO_2 mixed oxides, *J. Catal.* 259, 123–132.

Atribak I., A. Bueno-López, A. García-García (2009), Further insights into the key features of Ceria-Zirconia mixed oxides governing the catalysed soot combustion under NOx/O_2, Top. Catal. 52, 2088-2091.

Collura S., N. Chaoui, B. Azambre, G. Finqueneisel, O. Heintz, A. Krzton, A. Koch, J.V. Weber (2005), Influence of the soluble organic fraction of the thermal behaviour, texture and surface chemistry of diesel exhaust soot, *Carbon,* 43, 605–613.

Ferrari A.C., J. Robertson (2000), Interpretation of Raman spectra of disordered and amorphous carbon, *Phys. Rev. B: Condens. Matter* 61, 14095-14107.

Krishna K., A. Bueno-López, M. Makkee, J.A. Moulijn (2007), *Appl. Catal. B,* 75, 210-220.

Otto K.,, M.H. Sieg, M. Zinbo, L. Bartosiewicz (1981), The oxidation of soot deposits from diesel engines, SAE Paper 800336.

Sadezky A., H. Muckenhuber, H. Grothe, R. Niessner, U. Pöschl (2005), Raman microspectroscopy o soot and related carbonaceous materials: spectral analysis and structural information, *Carbon,* 43, 1731-1742.

Song J., A. Alam, A.L. Boehman, U. Kim (2006), Examination of the oxidation behaviour of biodiesel soot, *Combust. Flame,* 146, 589-604.

Stanmore B.R., J.F. Brilhac, P. Gilot (2001), The oxidation of soot:a review of experiments, mechanisms and models, *Carbon,* 39, 2247-2268.

Acknowledgements

The authors thank the Ministry of Science and Innovation for financial support (CIT-420000-2009-48 project, partially funded with FEDER resources) and Generalitat Valenciana for Prometeo Programme (Prometeo/2009/047 project).

Preparation and characterization of monolithic catalyst for CNG applications.

M. Adamowska[*1], *L. Gagnepain*[2] *and P. da Costa*[1]

[1] Université Pierre et Marie Curie - Paris 6, Laboratoire de Réactivité de Surface, UMR 7197, 4 Place Jussieu, 75252 Paris cedex 05, France, malgorzata.adamowska@wp.pl, patrick.da_costa@upmc.fr
[2] ADEME – Département Transports et Mobilité, 500 route des Lucioles, 06560 Valbonne, France

1. Introduction

European emission standards like Euro 5 (September 2009) and Euro 6 (September 2014) define the acceptable limits for exhaust emissions of new vehicles sold in EU member states. Natural gas (NG) is a favorable alternative automotive fuel due to its availability, low price, high hydrogen to carbon ratio and lower CO_2 emission than in conventional fuelled vehicles [Winkler et al., 2008]. However, a major disadvantage of using natural gas is the unburned CH_4 emission (effective greenhouse gas). Therefore, to comply with future legislation (EURO 6), highly efficient catalysts for the complete abatement of the unburned methane are needed [Venezia et al., 2009].

The typical three way catalysts (TWC) contain noble metals (Pt, Pd, Rh) deposited together with a washcoat (alumina modified with low loadings of lanthanum or barium and with ca. 10–20% ceria and zirconia) on a ceramic or metallic monolith [Kašpar et al., 2003].

The washcoat is usually applied by impregnation of the honeycomb in slurry of the powder, and subsequent drying and calcination. The last step is very important since the calcination binds the washcoat to the monolith walls, and is usually done at temperatures of 550°C or higher [Pedro et al., 2005]. The quality of the deposited washcoat depends on the slurry properties such as: properties of the solid particles (nature and particle size) [Agrafiotis and Tsetsekou, 2000[a]], properties of the solvent (nature and concentration) [Agrafiotis and Tsetsekou, 2000[b]] and the amount of solids in the slurry [Jiang et al., 2005].

An active element can be incorporated into the layer either during the washcoating step or after the washcoat step, using well-known techniques (wet impregnation, ion exchange or deposition- precipitation) [Nijhuis et al., 2001, Campanati et al., 2003].

In the present work, first of all we tried to develop a simple procedure leading to a reproducible alumina washcoat prepared from the boehmite slurry in the laboratory scale. In this case, we optimized the amount of binding agent, the pH value and procedure conditions. Secondly, we initially modified the slurry composition in order to improve washcoat properties. Finally, we elaborated the preparation procedure of Pd/Al_2O_3/cordierite monoliths. The performance of the washcoating procedure was evaluated by comparing the activity of prepared catalyst with that of a model catalyst provided by an industria. The main objective of these studies is to develop a new catalyst for natural gas vehicle (GNV) applications. So this procedure shall permit to design and prepare any catalyst from the laboratory scale to the industrial scale, in the future.

2. Experimental

2.1. Washcoating of monoliths

The commercial monolithic cordierite provided by Corning with cell density 400 cpsi was used as the support. The boehmite γ-AlOOH (SASOL DISPAL 23N4-80) was chosen as starting material for the washcoat preparation. The γ-alumina was obtained by boehmite transformation during calcination step (550°C for 4 hours). The starting material powder was mixed with the necessary amount of binding agent (20 wt.% colloidal alumina) and other additives. The $Ce_{0.62}Zr_{0.38}O_2$ mixed oxides (5 wt%) provided by Rhodia were added as stabilising agents and as oxygen storage promoters, which is important in TWC applications. According to the literature [Nijhuis et al., 2001], acid should be added to obtain a pH of 3-4 to ensure more effective milling and less difficult coating. However our studies showed that coating process is more effective when the pH of the slurry was adjusted to 4.1 - 4.2 with the appropriate amount of nitric acid (68%). This pH value was optimized during several experiments.

The monoliths (37 mm length, 23 mm diameter) were dipped vertically into the slurry for 2 minutes. The excess of slurry was shaken out of the monolith and the blocked channels were cleared using pressurized air. Then the monolith was dried horizontally in air while being continuously rotated around its axis. Finally, the monolith was dried at 110°C for 2 hours and calcined at 550°C for 4 hours. This step permits to bind the washcoat to the monolith walls and ensures the good transformation of the γ-AlOOH into the γ-Al_2O_3. The monolith was coated

again before the calcination step using the same or a different slurry composition. The washcoat loading was determined by weighting.

2.2. Pd impregnation of monoliths

The monolith was dipped into the Pd catalyst slurry always using the same washcoating procedure. Supported Pd catalyst (1 wt% of Pd referred to the boehmite), prepared by incipient wetness impregnation, was employed as starting material for the washcoat preparation. The Pd catalyst precursor was dried at 110°C for 2 hours and calcined at 550°C for 4 hours in air with temperature ramp of 3°C.min^{-1}. An aqueous solution of tetraammina palladium nitrate solution ($Pd(NH_3)_4(NO_3)_2$) was used as palladium precursor.

2.3. Physicochemical characterizations

The powder X-ray diffraction patterns were recorded on a SIEMENS D500 diffractometer using monochromatised CuKα radiation. Measurements were carried out for 2θ ranging from 10° up to 70°.

The specific surface areas were measured by nitrogen adsorption at 77K using the BET method (Micromeritics ASAP 2010). The samples were previously treated at 350°C under vacuum (2x10^{-3} torr) for 5 hours.

The washcoat quality of the coated honeycombs was studied by a Scanning Electron Microscop JEOL JSM-5510 LV (SEM) equipped for EDS (Energy dispersive spectroscopy) analysis. SEM images of the alumina washcoats were obtained on pieces cut from monolith after metallization of theses samples under an Au film.

Resistance to mechanical vibrations was evaluated using ultrasonic vibrations. A piece of the prepared monolith was treated in an ultrasound water bath (power 220W, frequency 35 kHz). Finally the sample was dried and weighted. The adhesion properties between the catalyst and ceramic surface were determined by weight loss of the monolith as a function of time.

Resistance to high temperature (ageing process) was studied using a piece of the loaded monolith. The ageing process was performed in an oven at 950°C for 4h with heating rate 10°C.min^{-1} using 10% of water in air. These conditions correspond to a real mileage of 50, 000 km.

2.4. Catalytic activity tests

The evaluation of catalytic performance was carried out using the temperature programmed surface reaction (TPSR). The TPSR was performed from room temperature (RT) to 570 °C with a heating rate of 10 °C.min^{-1} using the following gas mixture: 2500 ppm NO, 1700 ppm CH_4, 4800 ppm O_2, 4700 ppm CO, 3400 ppm H_2, 9.25% CO_2 and 18% H_2O. This composition corresponds to a richness of 1.0005. The total flow was 23252 ml·min^{-1} which corresponds to an hour space velocity (GHSV) of 40,000 h^{-1}.

To be close to industrial conditions, our apparatus shows a pre-heater in which the gases are heated up to 790°C. These heated gases flowed through the catalytic bed composed by the carrot of the monolith. Three thermocouples are available to follow the reaction temperature. One is place prior the catalyst, the second one close to the catalyst and the third at the exit of the reactor.

The reactor outflow was analyzed using a set of specific detectors. An Eco Physics NO_x L Chemiluminescence's analyzer (for NO and total NO_x) allowed the simultaneous detection of both NO, NO_2 and NO_x (0-2500 ppm). An IR analyser was used to monitor N_2O and CH_4 (0-2500 ppm). The CO was analyzed by two specific IR analyzer dedicated to low (0-2000 ppm) and high CO concentrations (1-5%). The CO_2 was monitored by Rosemount analytical detector (0-20%).

3. Results and discussion

3.1. Characterization of starting material

The specific surface area of the boehmite is 293 m^2.g^{-1}. Recrystallization to γ-alumina leads to sintering and consequently to a severe drop of boehmite specific surface area (228 m^2.g^{-1}). Average pore diameter ranges from 4.6 nm for the boehmite to 6.2 nm for the γ-alumina. Thus, according to the IUPAC classification, the starting materials studied show mesoporosity.

3.2. Coating of monolith

Two kinds of samples were prepared to investigate the influence of the components used. The first one contains two alumina layers while the second one contains additional ceria-zirconia in the coating.

3.2.1. Boehmite slurry

The washcoated monolith contains 23 wt.% of the alumina layer after two impregnations. It corresponds to 134 g.l^{-1}. The SEM images (Fig. 1 a-b) of the washcoated

monolith, obtained by secondary electrons detection (SEM-SEI images), show that the alumina layer is well deposited on the channel walls and the washcoat is observed in all the corners. However we can also observe cracks in the coat layer.

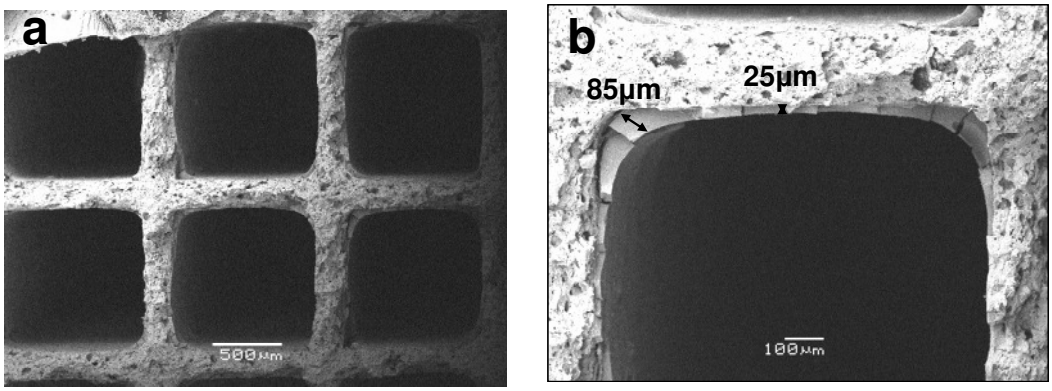

Figure 1: SEM-SEI image: (a) general view of the monolith piece, (b) view of one channel.

The cracks in the corners of the channels can be formed most likely because of a difference in thermal expansion between the cordierite and the alumina, while the cracks in the coat layer can be formed during a too fast drying step. Forzatti et al., 1998, indicate that the drying step requires a careful control of temperature and moisture and the steps must be slow enough to prevent ruptures and cracks.

The thickness of the alumina washcoat varies from 25 µm in the middle of channel up to 85 µm in the corners (Fig. 1b). The distribution of the chemical elements on the sample surface was determined by EDS cartography (Fig. 2).

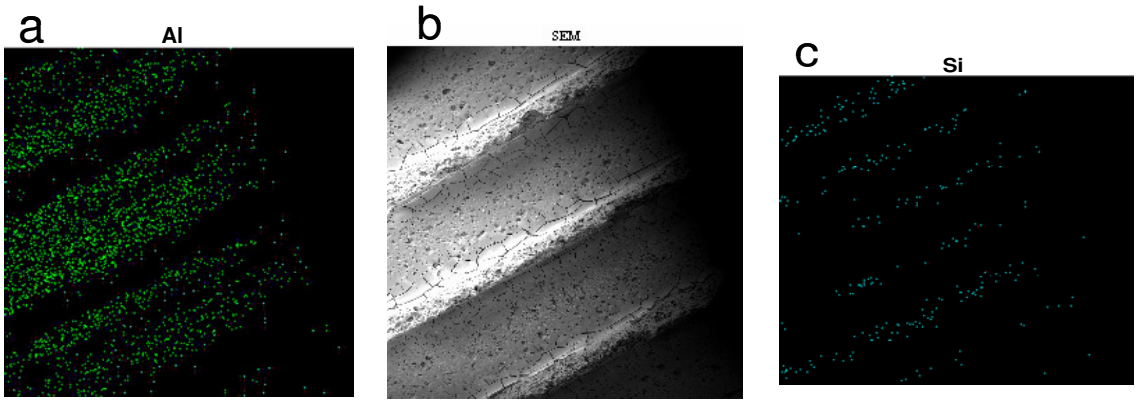

Figure 2: EDS analyse of boehmite coating: (a) EDS Al cartography, (b) general view of bare cordierite, (c) EDS Si cartography.

The results obtained show that the washcoat layer is well deposited over the channel length. However, Fig. 2c shows some areas where the presence of silicon is more significant. So it means that the layer thickness is not homogeneous and this aspect should be studied in future works.

Resistance to mechanical vibrations and resistance to high temperature of the alumina washcoat were determined to simulate, in the laboratory scale, conditions occurring in vehicles. The severe conditions (hot exhaust gases of high velocity and mechanical vibrations) can lead to detachment of the washcoat layer. Therefore, the adhesion of the substrate is a very important requirement. This study was carried out for samples before (fresh catalyst) and after ageing process (ageing catalyst). The weight loss curves of the washcoat are shown in Fig. 3.

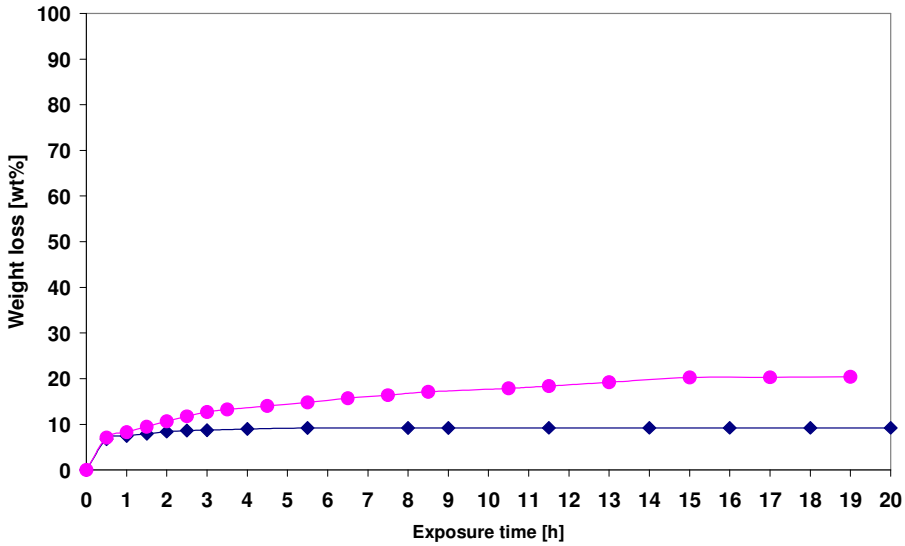

Figure 3: Weight loss of washcoat, as function of time (■- before ageing, •- after ageing).

It can be observed that the washcoat exhibits weight loss in both cases. However, this phenomenon is more significant for the sample exposed to a high temperature treatment. In the case of the fresh catalyst, the washcoat stabilisation is achieved after 2 hours of ultra-sound treatment (the total weight loss around 9 wt %). However, the layer stabilisation of ageing catalyst is observed after 15 hours (the total weight loss around 20 wt %).

3.2.2. Boehmite-ceria zirconia slurry

In order to investigate a possible influence of the $Ce_{0.62}Zr_{0.38}O_2$ on the thermal stability of the coating, we have recorded the XRD pattern of the coating (boehmite/$Ce_{0.62}Zr_{0.38}O_2$) calcined at 1000℃ for 4 hours in air (Fig. 4c). Identification of the diffraction peaks was realized using JCPDS patterns. The comparison of XRD pattern of the coating (Fig.4c) with XRD patterns of the boehmite calcined at 550℃ for 4 hours (Fig.4b), the boehmite calcined at 1000℃ for 4 hours (Fig.4d) and the $Ce_{0.62}Zr_{0.38}O_2$ calcined at 550℃ for 4h (Fig.4a) permits to observe the phase transition. It was shown that pseudoboehmite was transformed into γ-alumina after calcination at 550℃ (Fig.4b).

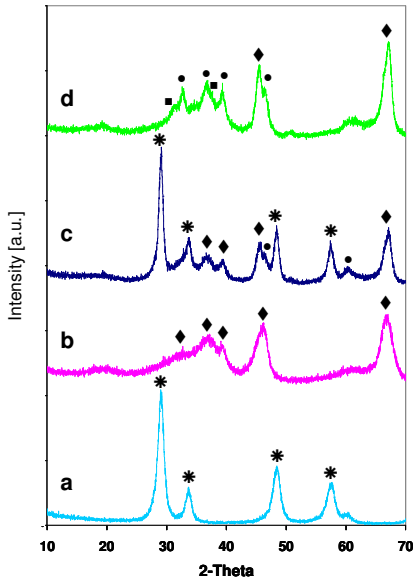

Figure 4: XRD patterns of (a) $Ce_{0.62}Zr_{0.38}O_2$, (b) the boehmite calcined at 550℃/4h, (c) the boehmite -ceria-zirconia calcined at 1000℃/4h (d) the boehmite calcined at 1000℃/4h; (■) θ-Al_2O_3, (•) δ-Al_2O_3, (✱)$Ce_{0.62}Zr_{0.38}O_2$, (♦) γ-Al_2O_3.

However, after calcination at 1000°C (Fig.4d), we can observe the phase transformation of γ-alumina to the δ- Al_2O_3 and θ- Al_2O_3. In this case, Al_2O_3 still exists mainly as the δ- Al_2O_3 phase but with δ and θ- Al_2O_3 phases co-existing (Fig.4d). In the presence of $Ce_{0.62}Zr_{0.38}O_2$ (Fig.4c), we observe mainly the diffraction peaks of γ-Al_2O_3 even after calcination at 1000°C. So we can conclude that the presence of $Ce_{0.62}Zr_{0.38}O_2$ in the washcoat increases the thermal stability of the coating. However, it would be interesting to add another stabilising agent, for example La_2O_3 or BaO, to totally inhibit the phase transformation of γ-Al_2O_3.

3.3. *Catalytic activity tests*

The commercial honeycomb converter is mainly composed by the palladium oxide (2.55 wt.%) and a small amount of rhodium (0.18 wt%) and platinum (0.07 wt%) [Salaün et al., 2009[a]]. Salaün et al., 2009[a], concluded that the palladium is deposited on the alumina whereas rhodium is deposed on the ceria-zirconia.

For CNG applications, methane which is the major component of natural gas is the main pollutant. The palladium in PdO form is presented as the more active phase for methane oxidation [Salaün et al., 2009[a]]. To evaluate the performance of the washcoating procedure, we prepared the catalyst containing 2.5 wt.% of palladium to compare its activity with a model catalyst which contains the same amount of palladium [Salaün et al., 2009[a], Salaün et al., 2009[b]].

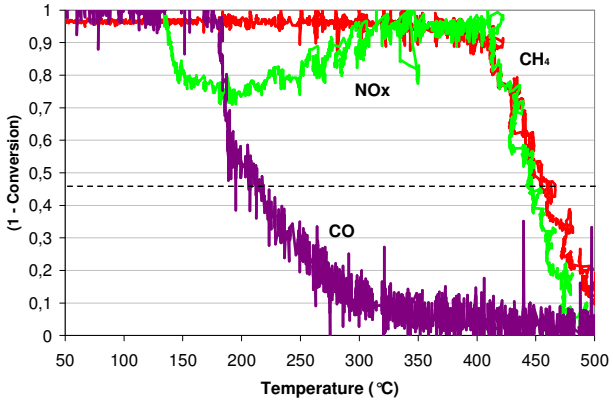

Figure 5: TPSR profile of NO_x,CH_4 and CO. Feed gas: 2500 ppm NO, 1700 ppm CH_4, 4800 ppm O_2, 4700 ppm CO, 3400 ppm H_2, 9.25% CO_2 and 18% H_2O and balance N_2 (GHSV 40,000 h^{-1}).

In Fig. 5, NO_x, CH_4 and CO conversions are reported as a function of the reaction temperature for the Pd-impregnated monolith. At low temperatures, we observe the evolution of the NO_x concentration which is correlated to the N_2O formation. This phenomenon is observed for both catalysts, however the amount of N_2O formed is more important in the case of the model catalyst. According to the literature [Salaün et al., 2009[a], Salaün et al., 2009[b]], at low temperature, the NO can be reduced by hydrogen or carbon monoxide, whereas at high temperature the methane is the reducing agent of NO. Salaün et al., 2009[a], investigated the role of CO and H_2 in NO reduction removing the hydrogen or the oxygen from the feed. In absence of H_2, the NO conversion was decreased significantly and the light off temperature was shifted to higher temperature. In absence of CO, the global trends of the plots of NO reduction and CH_4 oxidation were comparable with those obtained for the total gas mixture. These authors showed that the major reducing agent for NO reduction at low temperature is hydrogen.

At low temperature, we can also observe carbon monoxide conversion which is oxidized by oxygen. Salaün et al., 2009[a], proposed that the CO oxidation and the NO reduction do not take place on the same site (rhodium and palladium sites respectively). Furthermore, these authors supposed that a reaction between CO and N_2O (product of NO decomposition or reduction at low temperature) is possible since less N_2O quantity is detected. However at high temperature, CO could be consumed during the water gas shift reaction. We observed that in the case of the prepared catalyst, the light off temperature is shifted to lower temperature. At high temperature, we can also observe simultaneously NO_x and CH_4 conversion. The methane is completely converted below 550°C. Salaün et al., 2009[a], showed that the main oxidizing agent of methane is NO. However, these authors suggest that at high temperature, the steam effects are not negligible. The evolution of the methane concentration was the same for model and prepared catalysts. So we can conclude that the activity of the catalyst prepared is comparable with the one of the model catalyst.

The prepared catalyst is active in the methane oxidation reaction. However, it is evident that its composition must be optimised to reinforce its catalytic action, to stabilise the alumina transformation and to inhibit the noble metals.

4. Conclusions

On the basis of the results presented in this paper on the preparation and characterisation of monolithic catalyst, it can be concluded that:

1. The washcoat layer is well deposited on the channel walls and in the corners. However the layer thickness is not homogeneous. Additionally, the cracks in the coat layer and in the corners of the channels were observed. So the drying step (temperature and moisture control) has to be optimized.
2. A detachment of the washcoat layer was observed after ultra-sound treatment for fresh and ageing catalysts. However, this phenomenon is more significant for the sample exposed to a high temperature treatment.
3. The XRD results indicate that the presence of ceria-zirconia solid solution can inhibit partially the phase transition of γ-Al_2O_3. However it will be interesting to add another stabilising agent to totally inhibit the phase transformation of γ-Al_2O_3.
4. The prepared catalyst is active in the methane oxidation reaction.

The main goal of our research is to develop a new catalyst for GNV applications. The know-how of the washcoating procedure allows us to optimize the catalyst composition, such as the active phase and the stabilizing agent of alumina. The objective is to improve the catalytic performance and to decrease the price of the catalyst. This monolithic catalyst will be also applied for the methane oxidation and the selective catalytic reduction of NO_x by methane.

References

Agrafiotis C. and A. Tsetsekou (2000)[a], The Effect of Processing Parameters on the Properties of a-alumina Washcoats Deposited on Ceramic Honeycombs, *Journal of Materials Science*, 35, 951-960.

Agrafiotis C. and A.. Tsetsekou (2000)[b], The effect of powder characteristics on washcoat quality. Part I: Alumina washcoats, Journal of the European Ceramic Society, 20, 815-824.

Campanati M., G. Fornasari, A.Vaccari (2003), Fundamentals in the preparation of heterogeneous catalysts, *Catalysis Today*, 77, 299-314.

Forzatti P., D. Ballardini, L. Sighicelli (1998), Preparation and characterization of extruded monolithic ceramic catalysts, *Catalysis Today*, 41, 87-94.

JCPD patterns (00-038-1439,01-074-4629,00-016-0394, 00-011-0517).

Jiang P., G. Lu, Y. Guo, Y. Zhang, X. Wang (2005), Preparation and properties of a γ-Al_2O_3 wascoat deposited on a ceramic honeycomb, *Surface & Coatings Technology*, 190, 314-320.

Kašpar J., P. Fornasiero, N. Hickey (2003), Automotive catalytic converters: current status and some perspectives, *Catalysis Today*, 77, 419–449.

Nijhuis T. A., A.E.W. Beers, T. Vergunst, I. Hoek, F. Kapteijn, J.A. Moulijn (2001), Preparation of monolithic catalysts, Catalysis Reviews, 43 (4), 345-380.

Pedro A., M.Montes and E.E Miró. (2005), Monolithic reactors for environmental applications. A review on preparation technologies, *Chemical Engineering Journal*, 109, 11-36.

Salaün M., A. Kouakou, S. Da Costa, P. Da Costa (2009)[a], Synthetic gas bench study of a natural gas vehicle commercial catalyst in monolithic form: On the effect of gas composition, *Applied Catalysis B: Environmental*, 88, 386-397.

Salaün M., S. Capela, S. Da Costa, L. Gagnepain, P. Da Costa (2009)[b], Enhancement of 3-Way CNG Catalyst Performance at High Temperature Due to the Presence of Water in the Feed: On the Role of Steam Reforming of Methane and on the Influence of Ageing, *Topic in. Catalysis*, 52, 1972-1976.

Venezia A.M., G. Carlo Di, Pantaleo G., Liotta L.F., Melaet G., Kruse N. (2009), *Applied Catalysis B: Environmental*, 88, 430-437.

Winkler A., P. Dimopoulos, R. Hauert, C. Bach, M. Aguirre (2008), Catalytic activity and aging phenomena of three-way catalysts in a compressed natural gas/gasoline powered passenger car, *Applied Catalysis B: Environmental*,84, 162-169.

U.S. EPA's MOVES2010 vehicle emission model: overview and considerations for international application

J. Koupal[1] [*], M. Beardsley[1], D. Brzezinski[1], J. Warila[1], W. Faler[2]

[1] U.S. Environmental Protection Agency, Office of Transportation and Air Quality

2000 Traverwood Drive, Ann Arbor MI, USA 48105

[2] Fluid & Reason LLC, Dearborn MI, USA 48120

Abstract

U.S. EPA recently released its new mobile source emission model, MOVES2010, which reflects several significant updates from its predecessor, MOBILE6. MOVES is a new modelling platform built to support multiple scale analysis, from detailed "project level" assessments to emission inventories at the regional or national level, for greenhouse gases, so-called "criteria" air pollutants, and air toxics. To support multiple scale analysis, MOVES has adopted a "modal" emission approach, which provides more flexibility in predicting emissions for different driving patterns, and allows assessment of emission impacts due to changes in vehicle acceleration as well as vehicle speed. Using a modal approach also enables a much broader assessment of vehicle emissions from multiple data sources, including inspection/maintenance programs, remote sensing data, portable emission measurement systems (PEMS), and traditional laboratory data. The updated emission estimates from MOVES2010 show significant increases in NOx and PM emissions relative to MOBILE6, which have been verified against independent data sources.

MOVES2010 was developed to allow customization to local areas, so that U.S. state and local governmental agencies can satisfy legislative mandates for air quality and transportation planning. These customization features give MOVES broad flexibility for international application as well. This paper discusses different "tiers" for international customization of MOVES. A first level would be to input custom vehicle fleet and activity data such as vehicle age distribution, vehicle distance travelled, and vehicle population; this level of customization could proceed quickly if such local data were already available. A second level of customization would focus on developing vehicle emission rates reflecting the emission standards applicable to the country being modelled. A final level of customization would be to implement more fundamental changes such as adding vehicle types, road types, or driving patterns. This paper will provide details on this tiered approach, with some consideration for the trade-off between increased customization and data collection burden.

Introduction

MOVES (MOtor Vehicle Emissions Simulator) is the U.S. Environmental Protection Agency's (EPA) new model to estimate air pollution emissions from mobile sources. MOVES2010, the first official release of the model, was recently made public and replaces EPA's previous emissions model for on-road mobile sources, MOBILE6.2. A new modelling platform was developed to support multiple scale analysis, from detailed "project level" assessments to emission inventories at the regional or national level, for greenhouse gases, criteria air pollutants, and air toxics. MOVES2010 estimates emissions for all types of on-road vehicles from tailpipe, fuel evaporation, brake wear, and tire wear sources. EPA ultimately plans to expand MOVES to include off-road emissions sources such as construction and agricultural equipment, locomotives and marine vessels.

MOVES development began almost a decade ago, in response to a report from the U.S. National Academy of Science (NAS) that recommended several improvements to EPA's mobile source modelling program. Among the major recommendations were to allow modelling at multiple analysis scales, to address the emerging need to estimate emissions at emission "hotspots" and to assess the local emission impacts of specific transportation projects. Another key recommendation was to develop a system which could be more easily updated with new information. The design of MOVES was greatly influenced by these NAS recommendations.

MOVES employs a completely new software framework that provides more flexibility for model input and output. The model is coded in JAVA, enabling a user-friendly graphical user interface, and stores input and output data in a MySQL relational database structure. This structure means the model is defined by data tables, allowing changes to standard inputs such as vehicle activity and fleet composition, on up to fundamental model elements such as vehicles classes or roadway types. These features will make it easier for users to develop local data for MOVES, and to further customize the model for international application.

The design of MOVES provides international users with a large degree of choice in reflecting their local conditions. Users may wish to rely on U.S. defaults as much as is practical, using local data for only critical inputs such as vehicle distance travelled; or, users may wish to fully customize the model with the driving patterns, emission rates, vehicle classes and road types unique to their area. The degree of customization is of course a function of the time and resources available to the modeler. This paper will lay out a "tiered" approach to customization, consider the types of data needed for each tier, and implications of increased customization.

Overview of MOVES2010

Extensive documentation on MOVES, including a users' guide and design manual, can be found on the MOVES website (http://www.epa.gov/otaq/models/moves). This section gives a brief overview of the model.

For a specified geographic location and time period, MOVES2010 will produce either total inventory (mass emissions), or emission rates (e.g. g/km) for the following pollutants:

- HC (THC, NMHC, NMOG, TOG, VOC)
- CO
- NOx (NO, NO_2)
- NH_3
- SO_2
- PM_{10}, $_{2.5}$ (organic carbon, elemental carbon, sulfate, brake wear, tire wear)
- Greenhouse Gases (CO_2, CH_4, N_2O)
- Toxics: Benzene, Ethanol, MTBE, Naphthalene, 1,3-Butadiene, Formaldehyde, Acetaldehyde, Acrolein

The model estimates energy consumption as well for total, petroleum, or fossil-based energy.

Users can request output in various levels of breakdown, according to the following categories:

- **Vehicle Class** (known in MOVES as "Source Types"), are organized around different patterns of vehicle activity. Source types can be added for further customization. In the default implementation of MOVES these are:
    - Motorcycle, Passenger Car, Passenger Truck, Light Commercial Truck, Bus (Intercity, Transit, School), Heavy Trucks (Single Unit / Combination: Short Haul / Long Haul), Refuse Truck, Motorhome
- **Road Type** is defined by different driving patterns expected to occur on each. These can also be added for further customization. In the default implementation of MOVES these are:
    - Urban Restricted (freeway), Urban unrestricted (non-freeway), Rural Restricted, Rural unrestricted
- **Emission Processes** are defined by unique combinations of how and when emissions are produced. These are:
    - Running, Start, Extended Idle ("hoteling"), Evaporative (Permeation, Vapor Venting, Liquid Leaks), Refueling (Vapor loss, Spillage), Crankcase, Tire Wear, Brake Wear
- **Fuel Types** are defined by unique vehicle technology, and are currently limited to gasoline, diesel, CNG, and electric. Additional fuel technologies, notably FFVs, will be added over time.
- **Model Years** go back 30 years from the calendar year being modeled, and can be output by year.

As noted, one important new feature of MOVES is the option to calculate emissions as emission rates (emissions per unit of distance for running emissions or per vehicle for starts, extended idle and resting evaporative emissions) in a look-up table format.

Analysis Scales

A key feature of MOVES is the ability to assess emissions at different analysis scales. Three analysis scales are supported in MOVES:

- "National" scale is focused on producing national emission inventories for the U.S. down to individual counties, making use of a large database of default information for vehicle fleet, meteorology, fuel and activity data. The defaults are focused specifically on U.S. emission estimation, making this scale less applicable internationally.
- "County" scale is focused on producing regional emission inventories based on pre-defined geographic areas (defined as counties in U.S. implementation), or for "custom domains" defined by the user. The "custom domain" feature is well suited for the development of regional emission inventories outside the U.S. This scale requires local data from the user, such as vehicle distance travelled, fleet age distribution and vehicle speed distributions.
- "Project" scale is focused on smaller-scale environments such as intersections, roadway expansions, or parking lots. Modelling is performed at the individual link level and allows for modelling of custom driving patterns. This scale has the largest demand for user data to define the environment being modelled, making it highly adaptable for international use.

MOVES was developed so that the same calculation procedures are in place for each scale. The different scales are largely defined by the vehicle fleet and activity data required for each, while using a common set of emission rates. Fuel and meteorology data can also be shared between scales.

Figure 1 shows a schematic of the data flow for MOVES at each scale. Increasing levels of data are required from the user as the scale shifts from coarse (national) to fine (project).

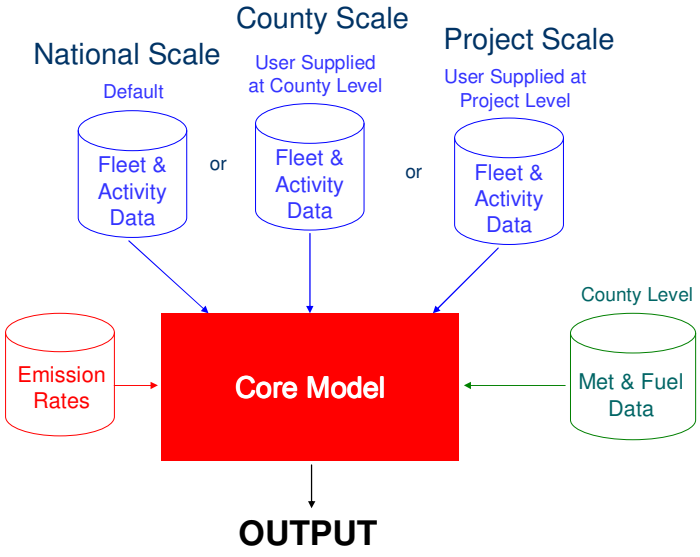

Figure 1: Schematic of MOVES data flow for different analysis scales

Modal Emissions

One of the groundbreaking elements of MOVES is the use of a "modal" emission approach. This allows the fundamental shift from aggregate driving-cycle based emission factors, such as those employed in MOBILE, to a model which can predict emissions over any driving pattern. MOVES uses the metric Vehicle Specific Power (VSP) to do this, enabling emission rates to be developed from a broad range of data, including laboratory, inspection/maintenance, on-board measurement, and remote sensing. For "running" (over the road) emissions, emission rates are characterized by bins of VSP and vehicle speed, as shown in Figure 2.

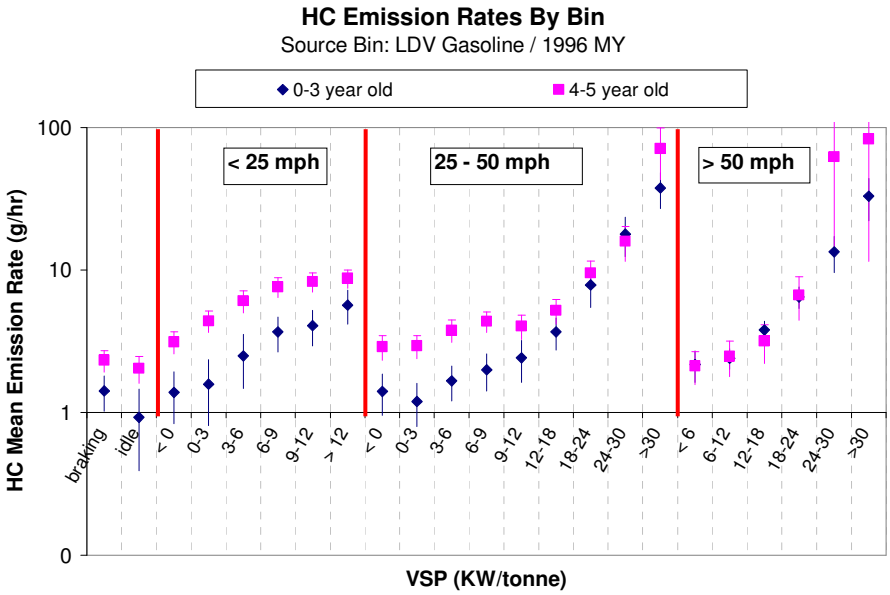

Figure 2: HC emission rates by VSP & Speed bin, shown for two model year groups

Driving activity is then expressed as the distribution of time spent in these bins, as shown in Figure 3. The summed product of emission rate and distribution by bin gives the estimate of average emission rate for a given driving pattern.

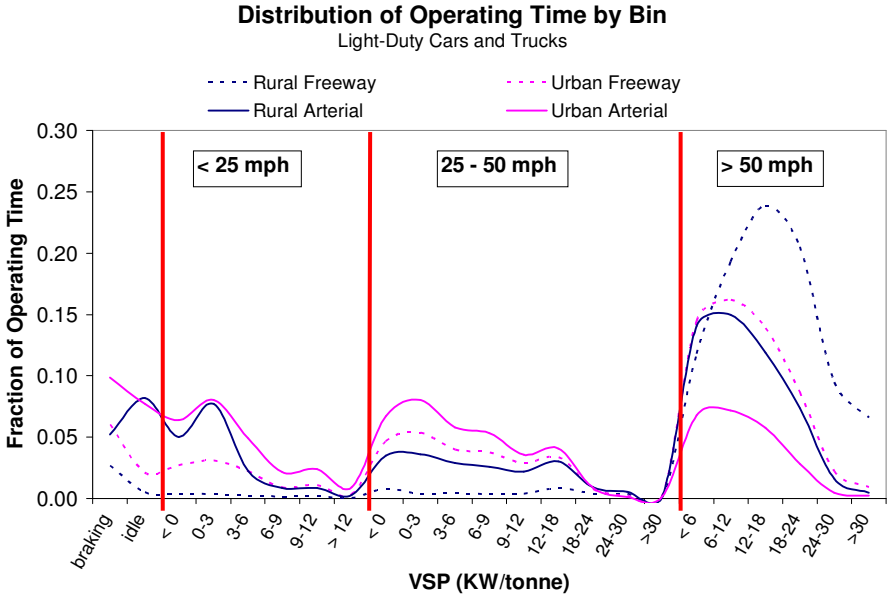

Figure 3: Distribution of time by VSP & Speed bin shown for four road types

This enables a new dimension for vehicle emission modelling – whereas MOBILE could only assess emissions as a function of average speed, MOVES now allows the user to assess emissions by average speed *and* the type of driving that resulted in the average speed – e.g., smooth driving vs. transient driving. This is demonstrated in Figure 4 for CO_2, but applies to nearly all of the pollutants MOVES models.

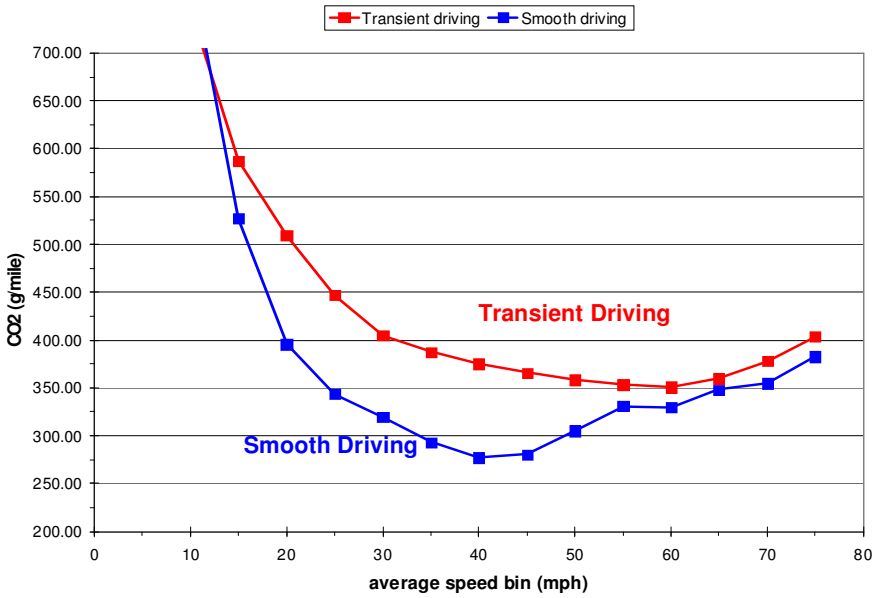

Figure 4: CO2 vs. average speed curve for smooth and transient driving

Customizing MOVES

MOVES was developed to facilitate a large degree of local area customization. The MOVES installation package includes a default database of meteorology, vehicle fleet, vehicle activity, fuel, and emission control program data for the U.S., but localities in the U.S. are encouraged to replace these defaults where better local data is available.

EPA has published technical guidance to assist U.S. areas in developing these improved inputs, centered on a MOVES feature known as the "County Data Manager" (CDM). The CDM is a graphical interface which allows users to import more commonly available data such as vehicle distance travelled, average speed distribution, or vehicle age distributions. The CDM allows easy import of custom data in MS Excel format, and converts to the MySQL data schema used by the model, rather than requiring the user to work directly in MySQL. A screenshot of the CDM is shown below:

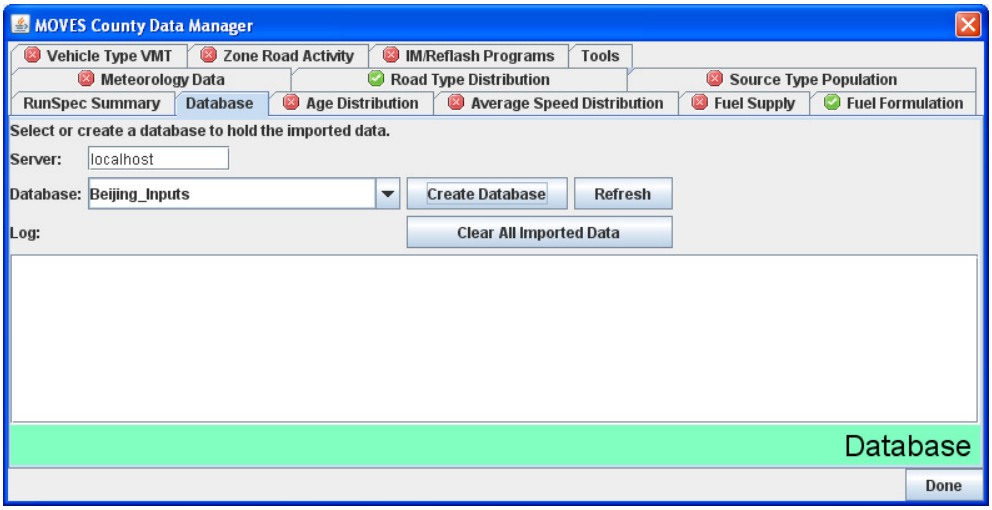

The “Custom Domain” selection under the “Geographic Bounds” panel of the MOVES interface allows the user to define a new geographic area – from a metropolitan area to an entire country - and provide necessary information for the model to produce emissions for that domain. The County Data Manager feature in MOVES is used to enter data for custom domains as well. This feature allows users outside the U.S. to define their own modelling domain, without being constrained by the U.S. - based “county” designations.

Beyond the CDM, further customization of MOVES is possible working directly with the MySQL database. Users can replace all default data if desired, developing an alternate MySQL database to overlay default data in the execution of the model. Alternate databases are specified in the “Manage Input Datasets” panel of the MOVES graphical interface. Potential customization at this level could include new driving patterns, new emission rates, or even fundamental changes such as vehicle classes or road types.

Proposed Approach For International Application

Recognizing that to fully customize MOVES outside of the U.S. would require a substantial data collection effort, a “tiered” approach to customization is recommended, to make use of data that is more likely available in the short term. The focus here is for regional emission inventory development, as project level already requires a great degree of customization. This approach is predicated on the use of the “Custom Domain” option by users to define and customize their region(s) of interest. Once this custom domain is established, the recommended tiers are as follows:

1. **“1st Tier”: Use County Data Manager to input more commonly available local data.** This is the process any U.S. city would use to customize MOVES, as detailed in EPA guidance. Users would supply local activity, fleet distribution, and fuel parameters through the CDM; if these data are available this could be done relatively quickly. However, the resulting model would be based on default U.S. emission rates reflecting U.S. standards, and the driving patterns, vehicles classes and road types already in MOVES2010.

2. **“2nd Tier”: Implement specific emission standards.** Alternate emission rate data tables could be developed to reflect different emission standards (Euro, Asia etc.) and implementation dates. This table could likely be developed from the default U.S. emission rates, by mapping Euro or Asia vehicle technologies or standards to their U.S. counterparts; or, an area that had a body of local emission data could develop all new rates. In combination with the 1st Tier, the resulting model would be highly customized but would still reflect the driving patterns, vehicles classes and road types already in MOVES2010.

3. **“3rd Tier”: Develop alternate MySQL database for more fundamental changes.** For users wishing complete customization, an alternate MySQL database could be developed to add vehicle classes (e.g., taxis, BRTs), road types, or driving patterns. The resulting model could reflect the local situation to a very large degree, but would likely require an extensive research program to generate the data needed for these fundamental changes.

For many international applications, the 2nd tier would likely provide the best trade-off between customization and resource burden. That this would provide good model performance outside the U.S. is based on the hypothesis that individual vehicle emissions differ little between U.S. and other countries, once emission standards are accounted for. Vehicle technologies are similar at comparable standard levels, so differences in deterioration, VSP, temperature, fuel effects would not be expected just because a vehicle is outside U.S. (though this hypothesis could be tested over time by comparing local emission data to MOVES emission rates). Fleet characteristics and activity patterns are a much larger source of difference, and these would be addressed mainly through data entered in the CDM as described in the 1st tier.

Conclusion

The U.S. EPA’s MOVES2010 model reflects many advancements for mobile source modelling, and was developed to allow a large degree of customization, making it highly adaptable outside the U.S. International users will need to consider how much customization is needed, based on an assessment of their local needs, available data and resources. This paper presents a “tiered” approach to aid in this consideration. A first tier would be to input custom vehicle fleet

and activity data such as vehicle age distribution, vehicle distance travelled (e.g., VKT), and vehicle population; this level of customization could proceed quickly if such local data were already available. A second tier would focus on developing vehicle emission rates reflecting the emission standards applicable to the country being modelled. The third tier would address more fundamental changes such as the number and categorization of vehicle classes, road types, and driving patterns. For many international applications, the second tier would likely provide the best trade-off between customization and resource burden. International users are encouraged to develop a plan for customizing MOVES according to these tiers, accounting for the resources and data available to them.

Acknowledgements

The authors gratefully acknowledge the many contributors to the concepts discussed in this paper, including: Gary Dolce, Sean Hillson, Chris Dresser, Gwo-Ching Shyu, Robert Giannelli, Gene Tierney, Harvey Michaels, Mitch Cumberworth, and Chad Bailey, all of EPA; and Chris Frey (North Carolina State University), Matthew Barth (University of California Riverside), and Michael Rodgers (Georgia Technological University).

References

Koupal, et al., "The MOVES Approach to Modal Emission Modelling", presentation at 14th CRC On-Road Vehicle Emission Workshop, March 2004

National Research Council, *Modeling Mobile Source Emissions*, May 2000

U.S. EPA, "Motor Vehicle Emission Simulator (MOVES) 2010 User Guide", EPA-420-B-09-041, December 2009

U.S. EPA, "Technical Guidance on the Use of MOVES2010 for Emission Inventory Preparation in State Implementation Plans and Transportation Conformity", EPA-420-B-10-023, April 2010

Use of Portable Emissions Measurement System (PEMS) for Validation and Development of Passenger Car Emission Factors

M. Kousoulidou[1], L. Ntziachristos[1], S. Gkeivanidis[1], V. Franco[2], Z. Samaras[1], P. Dilara[2],*

[1] Laboratory of Applied Thermodynamics, Dept. of Mechanical Engineering, Aristotle University of Thessaloniki, Greece, email: zisis@auth.gr

[2] Institute for Environment and Sustainability, Transport and Air Quality Unit, EC-Joint Research Centre, Ispra, Italy

Introduction

Traffic emissions are calculated for given vehicle types through the use of emission factors (EFs), which describe the emitted mass of a pollutant per distance driven. EFs can be used to simulate emissions from an entire fleet or vehicles, distinguished according several criteria, such as size, type, cylinder capacity, fuel, type of exhaust technology (e.g. with/without catalytic converter), and driving conditions (acceleration and speed), road gradient and the maintenance condition of the vehicle stock. The diversity of these factors shows that the estimation of air pollutant emissions from traffic is a complex and tedious task.

Emission factors can be derived in a variety of ways. EFs of single vehicles can be measured in dynamometer testing, by either transient chassis or engine emission measurements. The most common approach to obtain emission factors is to sample a range of cars of identical category and emission control technology (e.g. gasoline passenger car 1.4-2.0l, Euro 4), drive them over pre-defined driving patterns (driving cycles) on a chassis dynamometer and record their emissions over such conditions. The total emissions produced divided by the total distance driven leads to an averaged emission factor expressed in g/km which can be considered representative of the particular vehicle technology (provided that the vehicle sample is sufficient large) when driven under conditions similar to the driving cycle selected. The great majority of road transport emission inventories are based on emission factors derived this way.

There are, however, a couple of issues related to the representativity and coverage of these emission factors. The first issue relates to the sample size: Chassis dynamometer measurements are expensive and usually a small number of vehicles are used for the emission factor development in order to reduce the total cost of the study. This may lead to emission factors which are not representative of the particular vehicle class. Another, even more important issue, is whether the driving cycles utilized for testing are representative of real-world driving conditions. It may for example occur that while a driving cycle representing urban conditions is used for the production of an urban emission factor, real-world urban driving conditions are much more transient and therefore the emission factor underestimates the actual emission performance.

A new opportunity develops in the field of emission factor validation, through the use of emission data collected by Portable Emission Measurement Systems (PEMS). PEMS are complete sets of analyzers carried on-board the vehicle which can accurately provide emission rates at a high temporal resolution (i.e. down to 1 Hz). The advantage of this method is that it can provide a long series of emission data of a particular well-known vehicle driven under a multitude of driving conditions. Installation of PEMS setups on several vehicles of various categories can lead to a large database of emission values under different driving and environmental conditions and vehicle technologies. Also, linking this information with Portable Activity Measurement Systems (PAMS) can lead to complete emission-activity information. This means that with a PEMS-PAMS combination, emission rates can be correlated with driving speed, or acceleration/deceleration, or with engine-related parameters.

This paper aims at demonstrating how the instantaneous data from PEMS may be used to develop engine emission maps which are subsequently used as input to a vehicle simulation model (ADVISOR). In addition, the paper compares PEMS derived emission factors with average speed emission factors from an emission model (COPERT 4).

Experimental

A DPF-equipped Euro 5 diesel passenger car (Fiat Bravo 1.6 JTD) was used for testing. The concentration of gaseous exhaust pollutants were measured on-board the vehicle by means of the SEMTECH-DS (Sensors, Inc, Saline, MI) portable emission measurement system. The main unit containing the pumps, the electronic equipment and the analysers were installed in the cabin of the vehicle in order to avoid contamination, excessive vibrations, overheating of the equipment, etc. A GPS and a weather station were installed on the external area of the vehicle.

During the first phase of the program, the vehicle was tested randomly on local routes in the Lombardy region (Italy) designed to include a variety of urban, rural and highway conditions. During the second phase of the program, the following three routes were designed and used as test routes for all vehicles:

- Route 1: Ispra – Milan – Ispra, mix of rural and highway driving conditions;
- Route 2: Ispra – Varese – Ispra, mix of rural and urban driving conditions;
- Route 3: Ispra – Sacro Monte – Ispra, mix of rural driving and uphill-downhill conditions, with an uphill driving section (from 400 to 1200 m).

The vehicle exhaust gas was collected from the tailpipe using a repair-grade probe and sample line. Simultaneously, OBD data such as vehicle speed, engine rpm, intake air mass flow, coolant temperature, and other engine-operating parameters were gathered. Using the intake air mass flowrate, and the measured composition of exhaust gas, a second-by-second exhaust mass flowrate was calculated from the on-board computer. Multiplying the exhaust mass flow by the concentrations of pollutants generates second-by-second emission data in grams (Rakha et al., 2004), which are logged by the instruments.

Method

This paper aims to demonstrate how the instantaneous data values from PEMS equipment may be used to develop engine emission maps which are subsequently used as input to a vehicle simulation model (ADVISOR). In addition the data were also used to test the validity of the corresponding average speed emission factors from an emission model (COPERT). The aforementioned models are briefly introduced in the paragraphs below.

ADVISOR

The Advanced Vehicle Simulator (ADVISOR) is an analysis package for advanced vehicle modelling written in the Matlab/Simulink environment and developed by the National Renewable Energy Laboratory within the US Department of Energy. For the purposes of this research, *engine pollutant maps* were derived from PEMS data using dedicated software specifically developed. This allows for the subsequent simulation and comparison of tailpipe emissions produced under a wide range of conditions (e.g. different regulated test cycles or user-created speed vs. time traces, including road gradient characteristics).

COPERT 4

This is a software program developed and maintained by the Laboratory of Applied Thermodynamics (LAT) at Aristotle University of Thessaloniki which aims at the calculation of air pollutant emissions from road transport. It estimates emissions of all regulated air pollutants (CO, NOx, VOC, PM) produced by different vehicle categories, and CO_2 emissions based on fuel consumption. In this study, only the hot-emission part of COPERT was used in the calculations, thus the cold-start effect of the vehicle at each trip was excluded.

Data analysis (CEMOD and INCERT tools)

Due to the difficulty associated to dealing with the large amount of data gathered during the experimental campaigns, the development of calculation tools to collect, screen and analyze the measured data was required. In line with this, two Matlab-based software applications and their corresponding graphical user interfaces (GUIs) were developed at LAT. The first one, 'CEMOD' (Creation of Engine Maps Using Optimized Data) is intended for the creation of engine pollutant

maps using PEMS measurement data. The created engine pollutant maps are subsequently used as an input to ADVISOR. The second one, 'INCERT' (Interface for the Comparison of Emissions from Road Transport) was created for the comparison between the emission factors (EFs) derived within COPERT and those from real-world operation data (PEMS). Both calculation tools were fed with experimental data collected from the experimental campaign conducted by the EC-Joint Research Centre (JRC), and relevant EFs were produced.

Production of engine pollutant maps

As a case study, the PEMS measurement dataset obtained for the Ispra - Milano route was employed. The engine speed (in rpm), the actual engine torque and the friction torque of the vehicle, as well as the instantaneous pollutant emission, fuel consumption and vehicle speed values were recorded for the entire trip, on a second-by-second basis.

Because the actual emission signal measured by PEMS (or any other similar system) is distorted due to physical limitations of the measurement setup (e.g. the delay of transfer due to the length of the sampling line, mixing phenomena along the flow to the analyzer system, or the response times of the emission analyzers due to both their internal flow characteristics and electronics), the raw measured data were synchronized based on the algorithm previously created and validated by LAT. In particular, the algorithm performs a back correction of the analyzers' signal to correct for time lag and response. This procedure ensures that the instantaneous emission values measured were corrected to their original values and time-aligned to the engine speed, as recorded by the vehicle's on-board diagnostics system (OBD). Further details on the operation of the synchronization model can be found in Geivanidis and Samaras, 2008).

Synchronized data of each pollutant (CO, HC, NO_X and CO_2) were then converted from ppm to g/s in order to be used as input for the creation of the engine maps. A datasheet with the engine speed, the torque and each pollutant expressed in g/km was prepared, in which the highly transient operating modes were filtered out. Several attempts were made before reaching the optimal filtering of the data. These 'optimized' data were then used as input to Matlab, where a mesh was created through extrapolation of the available data points for engine speed, torque and the emission data calculated for each one of the pollutants measured. The pollutant engine map thus extrapolated (plot labelled as 'z_plot') is the first step of the creation of the engine map, which needs to be improved at those (usually several) points were the initial code fails to extrapolate. To solve this, a calculation approach based on a neural network calculation was taken, which extrapolates the proper values (zz_plot) based on the original engine map. Finally, CEMOD calculates the 'zzz_plot' (and its associated data points in tabular form), which is a combination of the 'z plot' and the 'zz_plot'. The user then uses the 'zzz_plot' given by CEMOD as the input for the ADVISOR. Figure 1 shows a screenshot of the CEMOD GUI, which graphically shows the production of a fuel consumption map through the z_plot method.

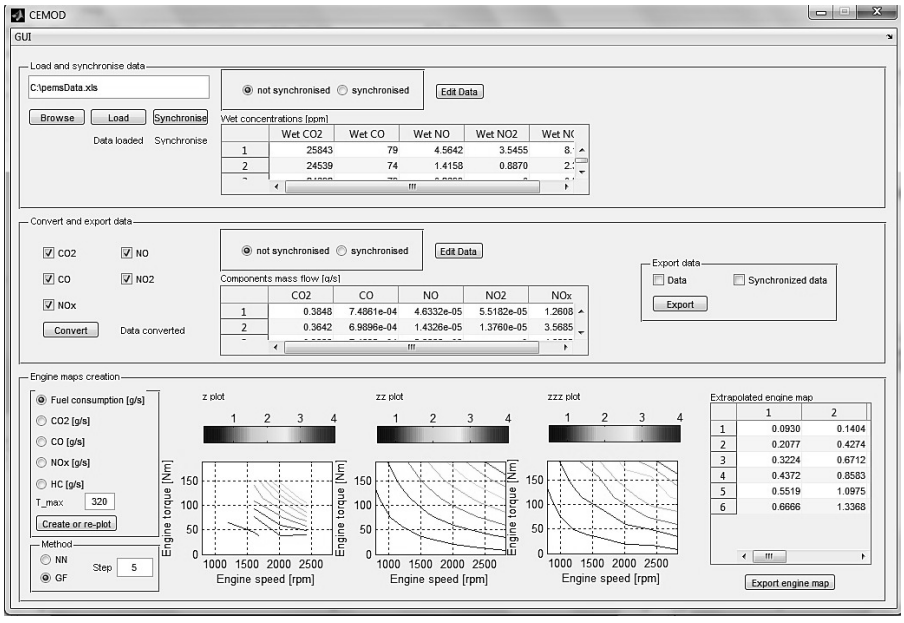

Figure 1: CEMOD tool screenshot

The pollutant engine maps were used as an input in ADVISOR, along with all the relevant vehicle and route data (speed vs. time trace and road gradient as derived from GPS altitude measurements). Finally, the simulation of the trip (Ispra - Milano – Ispra route) was performed in ADVISOR, and the results were compared to the original PEMS data. Moreover, the emission factors calculated for the trip using the INCERT tool (for which three different distance splits of 1, 5 and 10 km were considered) were set side by side with those provided by COPERT for an equivalent trip.

Results and Discussion

PEMS-ADVISOR Comparison

Results indicated a very good correlation between EFs derived directly from PEMS measurements and those provided by ADVISOR, when tested over the same trip (Ispra – Milano). This shows that the method developed is robust by reproducing the data it has been derived from. However, it is more important to validate it over different routes. Results over the Ispra -Varese – Ispra route indicated a very good agreement between PEMS data and ADVISOR, exhibiting very similar deviations to those found for the trip to Milano (in the order of -2%, 21%, 9% and -9% for FC, CO, HC and NOx, respectively).

PEMS-COPERT Comparison

It should be stated upfront that COPERT emission factors represent average values over a vehicle type and are not specific to a particular (single) vehicle. Therefore differences in the levels between the COPERT factors and the particular vehicle should be expected. It is therefore more interesting to compare the shape of the emission factors with average speed between COPERT and PEMS measurements. The following analysis is based on COPERT/PEMS comparison, where PEMS values are expressed as a function of average speed over 1-km trip sections.

With regard to CO (Figure 2.a), both COPERT and PEMS EFs present similar trends, i.e. they consistently decrease as speed increases over a wide speed range. Vehicle emissions measured using PEMS are in this case higher than those predicted by COPERT, but they are both much below the emission standard of 0.5 g/km.

HC emissions measured by PEMS are in practically zero levels (Figure 2.b) with some bursts of emissions occurring erratically during driving. COPERT also predicts very low emissions compared to the emission margin (0.05 g/km calculated as the difference between HC+NOx and NOx emission standards).

The evolution of measured NOx emissions with speed follows a pattern that is similar to COPERT results (Figure 2.c). The emission levels recorded appear to be approximately 60% higher than COPERT values. This increase may be attributed to higher load operation (for example possible uphill driving, which is not included in COPERT simulations). On the other hand, these emission levels are much beyond the emission standard value (0.18 g/km).

Fuel consumption was found to be lower compared to the COPERT values (Figure 2.d). Again, in this case this should be attributed to the fact the vehicle measured was of relatively low engine capacity, size and weight. Such vehicles are poorly represented within the emission factors provided by COPERT, which is based mainly on larger diesel vehicles. Engine downsizing and small capacity diesel engines are new features introduced in the European vehicle market in order to tackle CO_2 emissions. This hints at the need to include new vehicles in COPERT and possibly create an additional category for diesel vehicles of low engine capacity.

On the other hand, the comparison shows that the shape of the COPERT emission factors fairly well represents actual emissions even at short distances (i.e. 1 km trip distance).

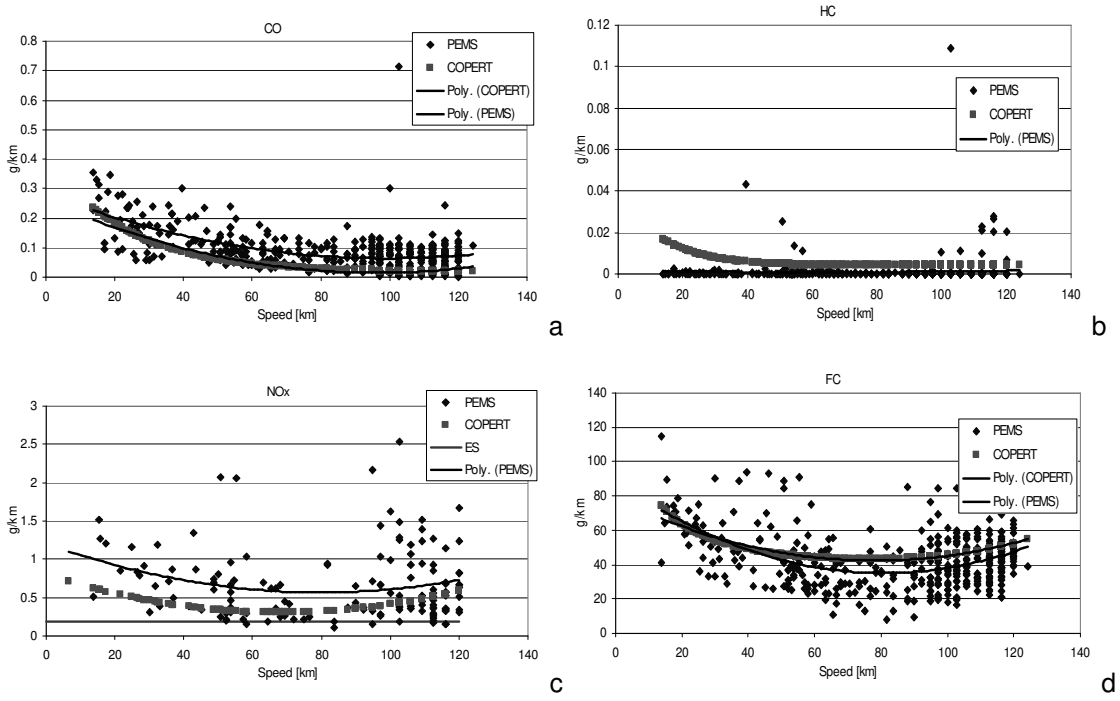

Figure 2: Comparison of a)CO, b)HC, c)NOx and d)FC emission factors between PEMS and COPERT for 1 km distance split.

Conclusions

PEMS measurements are a valuable tool which can help characterize the emissions of regulated pollutants of light-duty vehicles over a wide range of on-road driving conditions. With this type of setup, the emission and fuel consumption characteristics of vehicles can be tested during idling, cruising, accelerating and decelerating modes, on congested versus non-congested roads, and on uphill versus downhill roads. There is, however, some trade-off in that the PEMS measurement methods may not be as accurate or precise as those of the more complex and expensive equipment used in more permanent on-board installations. These shortcomings can be reasonably expected to be overcome as PEMS measurement technology improves with time. Moreover, PEMS measurement campaigns are typically deployed on a small number of vehicles, due to the high cost and complexity of the measurement. This renders them insufficient for the derivation of technology-specific emission factors as those found in COPERT. For this reason, PEMS measurements made during real-world vehicle operation are best used for validating existing emission factors or making relative comparisons of emissions.

In the comparison made in this paper, a good agreement is found between PEMS and COPERT EF values. It is worth noting that, in the case of NO_X, both measured and simulated values are well above the applicable emission limit (0.18 g/km) with 0.69 g/km (i.e. 3.8 times above the limit) for PEMS and 0.43 g/km (i.e. 2.4 above the limit) for COPERT.

References

CATI OEM-2100 Montana System Operation Manual D.V., Clean Air and Technologies International I. 2003, New York.

Geivanidis, S. and Samaras, Z., 2008, Development of a dynamic model for the reconstruction of tailpipe emissions from measurements on a constant volume sampling dilution system, *Meas.Sci.Technol.19* (2008) 015404.

EMEP/EEA (2009), EMEP/EEA. Air pollutant emission inventory guidebook 2009; 1.A.3.b.i, 1.A.3.b.ii, 1.A.3.b.iii, 1.A.3.b.iv Passenger cars, light-duty trucks, heavy-duty vehicles including buses and motor cycles 2009. http://www.eea.europa.eu/publications/emep-eea-emission-inventory-guidebook-2009

Emission Inventory Mobile Sources for Gauteng, South Africa

Tool for Scenario Calculations and Input for Dispersion Modelling

Ralf Kober[1], Yuriy Lozynskyy [2], Josef Brosthaus[3]

[1] TÜV Rheinland Immissionsschutz und Energiesysteme, Carbon Services, D-51105 Cologne, Germany, kober@de.tuv.com

[2] TÜV Rheinland Immissionsschutz und Energiesysteme, Carbon Services, D-51105 Cologne, Germany, yuriy.lozynskyy@de.tuv.com

[3] GECCO, D-51469 Bergisch Gladbach, An der Tent 5a, brosthaus@netcologne.de

1. Introduction

Gauteng is the province in South Africa with the highest population density (StatSA, 2006) and with the largest vehicle fleet among other provinces. This causes high traffic flows on the current road network in the province, and, appropriately, high emission pollution from the transportation sector. As result, this poses a research question on the estimation of emission pollution from road transport in the province, including the analysis of distribution of transport emissions on a microscale level, in order to achieve sustainable transport management in the region.

There is lack of the research on this topic in the recent time. As found the study on the review of South African air quality impact studies relating to vehicle emissions, most of the information available was limited to pre-2006 studies (Stead and Moldan, 2009). Some studies has concentrated on the estimation of the emission factors for different types of vehicles, e.g. Goyns, 2008; Wong,1999; Wong and Dutkiewicz, 2000; Wicking et al., 1997; Stone and Bennett 2002. However, comprehensive and complex research approach on the estimation of the transport emission from road transport on the provincial scale, i.e. for Gauteng province, is still absent by today.

Estimation of transport emissions from transport is a research topic in the framework of the EnerKey project (Energy as a Key Element of an Integrated Climate Protection Concept for the City Region of Gauteng, http://www.enerkey.info) - a German - South African collaboration, which aims to develop and implement innovative pathways and projects in urban energy supply and use in order to improve the sustainability in the province of Gauteng.

Whithin EnerKey Module 4 “Transport and Mobility patterns” the options for the improvements and potentials for air quality and GHG mitigation in the transport and mobility sector are investigated and promoted, considering individual and public transport systems, e.g. the Bus Rapid Transport (BRT). One of the primary goals of the module is the establishment of Emissions Inventory for mobile sources in Gauteng.

On a first step of research, a demo of GIS based tool – Emission Modelling Tool (EMT) 1.0 for Johannesburg was developed in order to estimate emissions from road transport. The reason for the application to the Johannesburg area was that City of Johannesburg, hosting approximately 36,5 % of the population in Gauteng (StatSA, 2006), is the municipality with the largest amount of registered vehicles among other municipalities in Gauteng, making it the most interesting area for the investigations in respect to the emissions from road transport.

2. Methodology

2.1. Input data

For the estimation of the baseline emissions in Johannesburg, three main databases were used as an input data for the modelling:

- HBEFA 2.1: The Handbook Emission Factors for Road Transport for Germany, Switzerland and Austria. This database represents the emission factors, derived from the test results of vehicle emissions on test-beds, for different vehicles classes – passenger cars, light commercial vehicles (LCVs), trucks, buses, minibuses and motorcycles for different traffic situations for different road type classes with different vehicle speed range and traffic type. More detailed information on NATIS can be obtained on the official web-site of HBEFA (e.g. in Keller et al., 2004).

- NATIS - National Traffic Information System of South Africa - database of the registered vehicles in South Africa. It contains information on the type of vehicles, their fuel type (petrol / diesel), engine size and year of vehicle registration. Latest data available for Johannesburg, and which was used in the calculations, is dated by June, 2008.

- EMME 2 data from the application of EMME2 modeling computer program on the travel demand for Johannesburg with the data information on VDF (Volume-Delay Function), vehicle volumes in peak hours and road type. EMME 2 data was created by the application of four basic phases in the traditional travel demand forecasting process on the basis of South African NHTS (National Household Travel Survey) 2003 data with the following updates up to the year 2009.

2.2. Emission modelling

The Emission Modelling Tool (EMT) was created by applying Visual Basic code. Methodology for the modelling is schematically presented on the Figure 1.

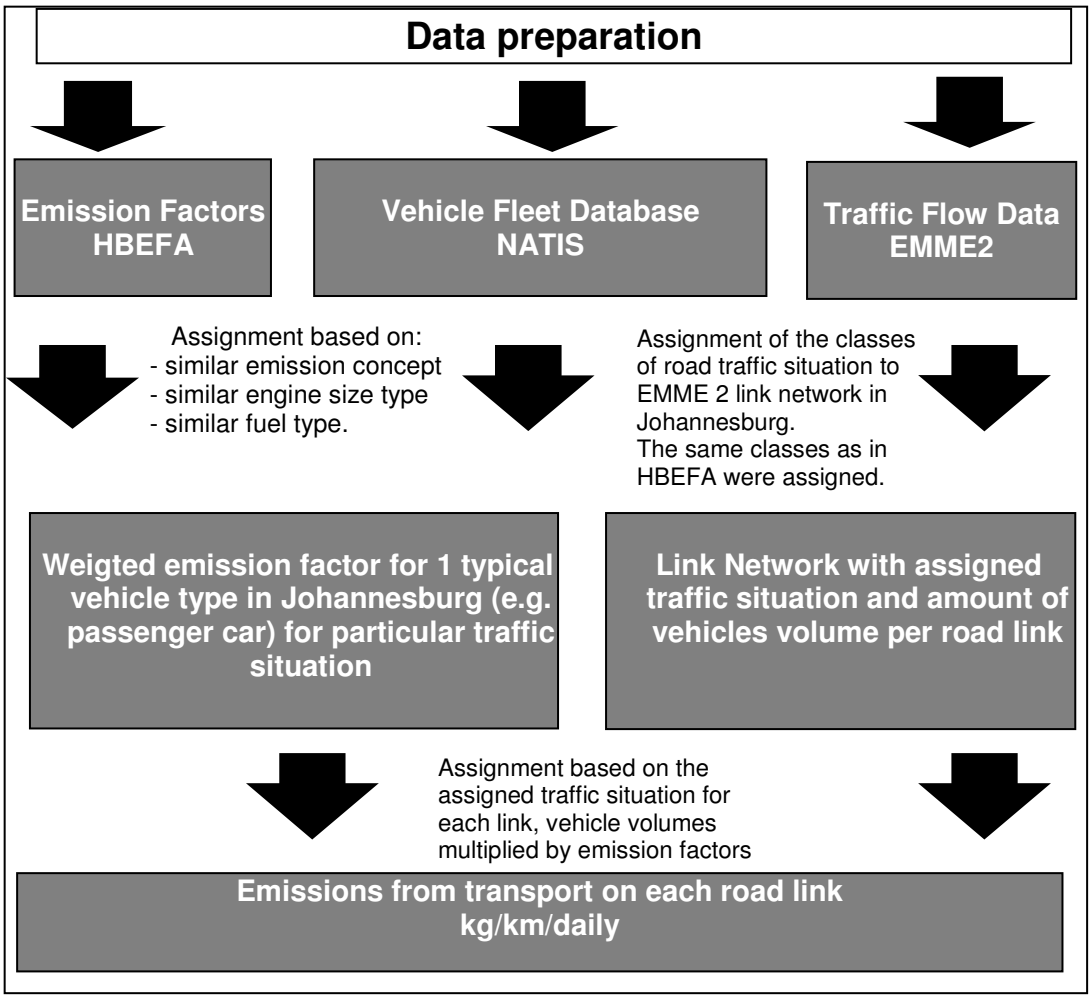

Figure 1:Modelling approach used in EMT 1.0. Demo

The input data for the modelling was prepared in the following steps:

- Transformation of raw EMME 2 data, representing road network in Johannesburg, from tabular format into shapefile format applying Visual Basic Script.

- Extrapolation of EMME 2 data on vehicle volumes in peak hours in Johannesburg to daily values (ADT).

- Vehicle fleet in NATIS database was categorized in the following vehicle classes:

  - Passenger Cars (PCs)
  - Light Duty Vehicles (LDVs)
  - Heavy Duty Vehicles (HDVs) / trucks
  - Heavy Passenger vehicles (HPs) – assumed to be mostly taxies
  - Buses

- Vehicle types in NATIS were appended with engine size categories in liters (L), e.g. for PCs < 1,5 L and vehicle weight categories, as e.g. for trucks 28-32t.

- Vehicle fleet in NATIS was appended with emission concept category for every vehicle (e.g. EURO 1) based on the year of registration. Imported vehicles to South Africa were taken into account (only PCs and LDVs were analyzed as due to the data available), assuming that the percentage of the imported vehicles in South Africa is equal to the percentage of imported vehicles to Gauteng. The absolute figures on the imported vehicles taken from the NAAMSA (National Association of Automobile Manufactures of South Africa) were taken for the years 1995-2007 and the percentage of imported vehicles was derived and applied in the NATIS database in order to identify amount of imported vehicles. The emission concept assignment was done on the basis of assumption that the imported vehicles at the year of their registration would have the emission concept valid in this year in European Union.

- Emission factors from HBEFA database were extracted for every traffic situation (i.e. road type and vehicle speed) for different vehicle types possessing different emission concepts for diesel and petrol vehicles. As result, emission factors for CH_4, CO, CO_2, HC, NO_x, N_2O, NH_3, NMHC, PM, SO_2 pollutants were extracted.

After the preparation of input data, modeling of EMT 1.0. Demo has run through following main steps:

Step 1: Emission factors from HBEFA for different traffic situations after preparation described as above were assigned to each vehicle in the NATIS database. The assignment was made based on the similar emission concept of the vehicles, similar engine size type and similar fuel type. The assumption was made that as due to the current regulation, all new vehicles from 2008 are at least EURO 2 vehicles. It was also assumed, that the inbound and outbound vehicles are of the same type in Johannesburg, as there was no data to assess such differences, if any.

As result of the assignment, there were derived weighted emission factors for different pollutants for one typical vehicle of particular class (e.g. for one typical passenger car) in Johannesburg for a pre-defined traffic situation.

Step 2: For each EMME 2 link there was derived average daily speed through the analysis of VDF. As result, each link got assigned unique average speed category (e.g. 60 km/h). Afterwards, there was made an assignment of classes of road traffic situation to EMME 2 link network in Johannesburg. The classification was made accordingly to the pre-defined classes for traffic situation made for emission factors in HBEFA database.

Step 3: To the categorized by traffic situation EMME 2 links in Step 2 there were assigned weighted emission factors for every vehicle class for appropriate traffic situation on each link. This was followed by the multiplication of the ADT volumes for particular vehicle classes on each road link by the assigned weighted emission factors.
User-friendly interface with ArcGIS 9.2 was created for the EMT 1.0. Demo. It allows the import of the results of the modelling directly to GIS and to vizualize the emissions from road transport

with a predefined legend and classification scheme. The results of the modelling can be seen on the Figures 2a and 2b.

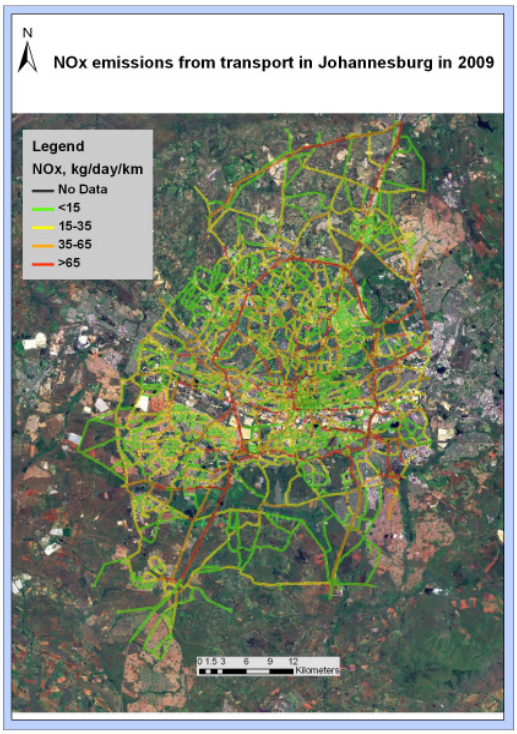

Figure 2a: Example of EMT 1.0 application: NOx emissions from road transport in Johannesburg in 2009

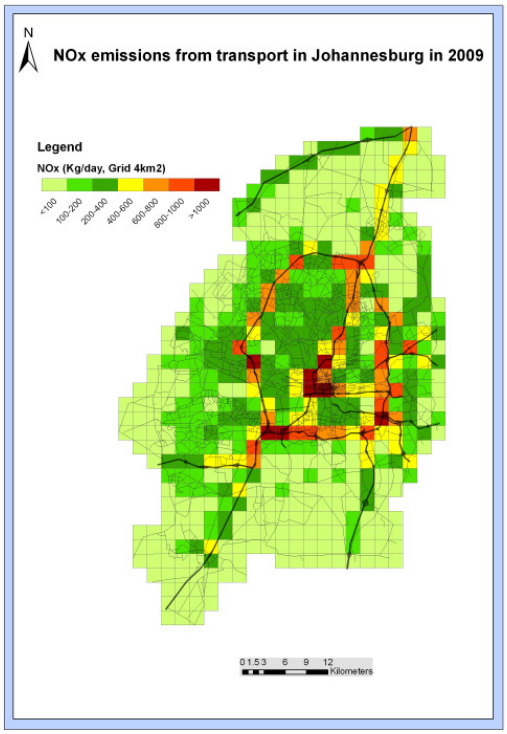

Figure 2b: Example of EMT 1.0 application: NOx emissions from road transport in Johannesburg in 2009, grid size 4 km^2.

Discussion

Presented modelling approach has required a lot of detailed data. Therefore, the results of the analysis were very sensitive to the quality of input data. Most uncertain aspect of modelling remains the assignment to which emission standards the vehicle belongs and whether they are equipped with catalytic converter. No such data was available, and the number of assumption, as described above, was made. In order to fill this data gap, during the EMT modelling the attempt was made to take into account the emission standards of the imported vehicles. This is an important aspect in terms of the assignment of emission concepts to the fleet in Johannesburg – e.g. the amount of imported passenger vehicles to South Africa has risen up to 50 % in the last several years (NAAMSA 2009).

It can be also noted that the results of modelling, i.e. estimation of emissions from road transport, depends largely from the correct estimation of the vehicle volumes. The EMME 2 data is by far the best known and well-documented assignment of the vehicle volumes to the road network in Johannesburg which was made by today.

There were also developed a number of approaches on how to cover the data gaps on volumes not presented by the EMME 2 data. For example, there were no data available on the trucks volumes. Therefore, their proportion was assumed as being a percentage of the total vehicle volumes for rural, urban and highway roads based on traffic counts in Johannesburg taken from the Johannesburg Integrated Transport Plan for the year 2003.

It remains still to investigate the distribution of the emissions from road transport on the streets which are not covered by the existed EMME 2 Link network, being represented by EMME 2 centroids and located mostly in residential areas. It is to expect that the amount of vehicle volumes in those areas will not have a significant impact on the modelling results, since the vehicle volumes are expected to be small.

The EMT tool Demo currently, beside the baseline scenario described as above, incorporates also two scenarios. First scenario allows to construct new fictive vehicle fleet with different amount of vehicles belonging to different emission standards, type of fuel and engine size categories and to calculate and to visualize emissions from transport ones again applying the same modelling approach as presented above. Second scenario allows to analyse the impact of BRT (Bus Rapid Transport) system implementation in Johannesburg (called Rea Vaya) Phase 1a in terms of emission savings from such initiative. The last scenario depends largely on the exact data on the performance level (passenger transported) of BRT.

Conclusions and further work

Applying modelling approach as presented above, there was possible to develop EMT Version 1.0 Demo to categorize the vehicle fleet of Johannesburg into emission concepts and to derive a weighted emission factors for different vehicle classes in the City of Johannesburg for different traffic situations, taking into account the characteristics of the vehicle fleet in the city. Through the analysis of traffic situations in Johannesburg and vehicle volumes, daily emissions from road transport in the city were calculated and visualized on a microscale level. User-friendly interface between EMT 1.0. Demo and ArcGIS 9.2. was established, what allowed to visualize the baseline emissions from road transport in Johannesburg.

It is the intention of Module 4 research team to apply the presented as above modelling approach and to extend and to transform the EMT V.1.0 into a representative Emissions Inventory Mobile Sources Tool. This tool will serve as useful Instrument for traffic regulations in GIS taking into account pollution levels for each road and vice versa. The data on the baseline emission from road transport obtained can be also used for the analysis of impact of pollution on human health on a small-scale level and to model solution for endangered areas. In the future, presented modelling approach will be extended also spatially to the Tshwane and Ekurhuleni municipalities, in that way being applicable, together with Johannesburg, for the most urbanized areas in Gauteng province. The data obtained will serve also as input to air dispersion modelling for the whole Gauteng province on detailed scale.

References

Goyns P. (2008), Modelling real-world driving, fuel consumption and emissions of passenger vehicles: a case study in Johannesburg, PhD Thesis. University of Johannesburg, Unpublished, 223p.

GTS (2006), Executive summary. Summary report. Working Documents, EMME/2 Transportation Model, Gauteng Transportation Study 2000, Unpublished, 96p.

Keller M., de Haan P., Knörr W., Hausberger S., Steven H (2004), Handbuch Emissionsfaktoren des Straßenverkehrs 2.1 Dokumentation, INFRAS, available at http://www.hbefa.net/e/documents/HBEFA21_Dokumentation.pdf

NAAMSA National Association of Automobile Manufacturers of South Africa (2007): NAAMSA Annual Report 2007. Balgair Publications. Available at http://www.naamsa.co.za/papers/, accessed 13th July 2008

Statistics South Africa (2006), Provincial Profile 2004: Gauteng/Statistics South Africa, Pretoria, 99p. Report No. 00-91-07 (2004), available at http://www.statssa.gov.za

Stead M., Moldan A. (2009), Cleaner Fuels for the future – An Oil Industry Perspective. *Proc.of the 28th Southern African Transport Conference (SATC 2009).* Pretoria, South Africa, 117–131.

Stone A., Bennett K. (2002), A bulk model of emissions from South African Diesel Commercial Vehicles, Energy Research Institute (ERI), University of Cape Town, 20p. Available at http://www.erc.uct.ac.za/Research/publications-pre2004/01Stone-Bennett_Diesel_emissions.PDF

Wong C.T. (1999), Vehicle Emissions Project (Phase II), Volume I, Main Report, Engineering Research, Report No. CER 161, February 1999.

Wong C.T., Dutkiewicz R.K (1998), Vehicle Emissions Project (Phase II), Volume I, Main Report, Engineering Research, Report No. CER 161, November 1998.

Vehicle Emission Modelling of Air Toxic and Greenhouse Gases in Porto Metropolitan Area

O.Tchepel[1], D. Dias[1], J. Ferreira[1], R. Tavares[1], A.I. Miranda[1], C. Borrego[1]*

[1] CESAM & Department of Environment and Planning, University of Aveiro, 3810-193 Aveiro, Portugal

* danieladias@ua.pt

Abstract

This work is focused on the development of a modelling approach for traffic-related air toxic pollutants and greenhouse gases with high spatial/temporal resolution including uncertainty quantification, and its application to Porto Metropolitan Area, Portugal, for 2007. The Transport Emission Model for Line Sources (TREM) has been adapted to incorporate air toxics and GHG emissions. Additionally, the model was extended to integrate a probabilistic approach for the uncertainty quantification using the Monte-Carlo technique. The resulting emissions, analysed in terms of cumulative distribution and uncertainty range, pointed out the largest uncertainties for urban roads. Emissions calculated for highways are generally characterised by smaller uncertainty range in comparison with the other types of roads.

Keywords: Road traffic emissions, greenhouse gases (GHG), air toxic pollutants.

Introduction

During the last decades, road traffic has become one of the most important sources of air pollution. Among the extended number of pollutants emitted by vehicles, air toxics and greenhouse gases (GHG) require special attention due to harmful effects on human health and climate change. The most commonly used technique to quantify their emissions is based upon on the principle that the average emission factor for a certain pollutant and a given type of vehicles vary according to the average speed during a trip (Boulter et al., 2007). This approach is usually applied to compile annual national inventories using aggregated information on traffic activity. However, higher temporal and spatial resolution of emission data is necessary for a number of applications, such as population exposure modelling, urban air pollution modelling, definition of sustainable urban development policy, etc.. For these applications, hourly emissions for each road link are usually required. For this purpose, hourly traffic flows attributed to detailed road network should be specified. Uncertainty of these data, as well as uncertainty associated with resulting emissions, is an important issue.

Quantitative methods for dealing with uncertainty in emission estimates involve the characterization of uncertainty in emission factors or activity data and propagation of uncertainty to a total emission inventory. Although numerous probabilistic techniques have been applied, the well-known Monte Carlo approach, which repeatedly takes random samples from the individual distributions and propagates them through the total inventory system, is most often used for this purpose (e.g., Frey and Zheng, 2002a,b; Abdel-Aziz and Frey, 2003).

The IPCC and EPA have developed guidelines recommending the use of Monte Carlo methods as part of a tiered approach to uncertainty estimates for GHGs emissions addressing the quantification of uncertainty in emission and activity factors (IPCC, 2000; EPA, 1997). Monte Carlo simulation methods have been used to estimate uncertainty in inventories, such as for criteria pollutants, hazardous air pollutants (HAPs), and GHGs (e.g., Winiwarter and Rypdal, 2001).

The present work intends to develop a modelling approach for traffic-related air toxic pollutants and GHGs with high spatial/temporal resolution including uncertainty quantification using the Monte Carlo technique. The developed methodology is described and an application to the Porto Metropolitan Area (Portugal), for the year 2007, is presented.

Methodology

TREM Emissions Model

The Transport Emission Model for Line Sources (TREM) was developed at the University of Aveiro based on ARTEMIS methodology. The prime objective of TREM is the estimation of road traffic emissions with high temporal and spatial resolution to be used in air quality modelling. Therefore, roads are considered as line sources and emissions induced by vehicles are estimated individually for each road segment considering detailed information on traffic flow. To develop a consistent model, the methodology was adopted taking into consideration input data availability. Thus, in TREM the average speed approach is used for emission factors estimation, which is considered to be sufficient when the influence of driving dynamics can be neglected (Sturm et al., 1998). In the present work, TREM was updated to include the emissions estimation for air toxics and GHG.

The total emission of the pollutant *p* (E_p) for each road segment is estimated by the model as following:

$$E_p = \sum_i \left(e_{ip}(v) \cdot N_i \right) \cdot L$$

Where $e_{ip}(v)$ is the emission factor for pollutant *p* and vehicle class *i* as a function of average speed *v*; N_i is the number of vehicles of class i and *L* is the road segment length. Besides the average speed, emission rate depends on fuel type, engine capacity and emission reduction technology. Therefore, an adequate aggregation of vehicles by categories and classes is an important task in order to provide an accurate estimation of air pollutant emissions. In TREM, classification of vehicles is performed in order to satisfy two criteria: (i) to maintain the level of detail available from the original methodology for emission factors and (ii) to allow the use of the model when a detailed description of vehicle fleet is not possible (Borrego et al., 2000, 2003, 2004).

Monte Carlo Approach

The Monte Carlo simulation is used to analyse uncertainty propagation, where the goal is to determine how random variations affects the emission estimations. For this purpose, the emissions model has been adapted to use different values randomly for each of the uncertainty input parameters. The values of each of the uncertain input parameters are generated based on their probability distribution. The result is a set of values for each of the model output variables, which can be treated statistically as if they were an experimentally or empirical observed set of data, instead of obtaining a single number for model outputs as in a deterministic simulation (Frey et al., 2002).

Random samples of the number of vehicles, average speed and fleet composition are generated from the respective Probabilistic Density Functions (PDFs) of the inputs, and one random value for each input is entered into the model to arrive at one estimate of the model output. This process is repeated over more than 600 iterations to arrive at multiple estimates of the model output. The multiple estimates are sample values of the PDF of the model output that reflects the uncertainty or variability in the model inputs.

Application

Study area

The Porto Metropolitan Area (PMA) was selected in this study to quantify road traffic emissions of GHG and air toxics. It is the second largest population agglomeration in Portugal constituted by the 16 municipalities with a total area of 1 883.3 km^2. The resident population of PMA in 2007 is about 1 679 854 (around 16% of the national population). Within the study area, the road network was subdivided into 3 types: urban, interurban and highways with the total length of 440.3 km, 398.8 km and 309.3 km respectively (Figure 1). As a total, 316 automatic counting points distributed over the domain were considered to characterize traffic flow fluctuations.

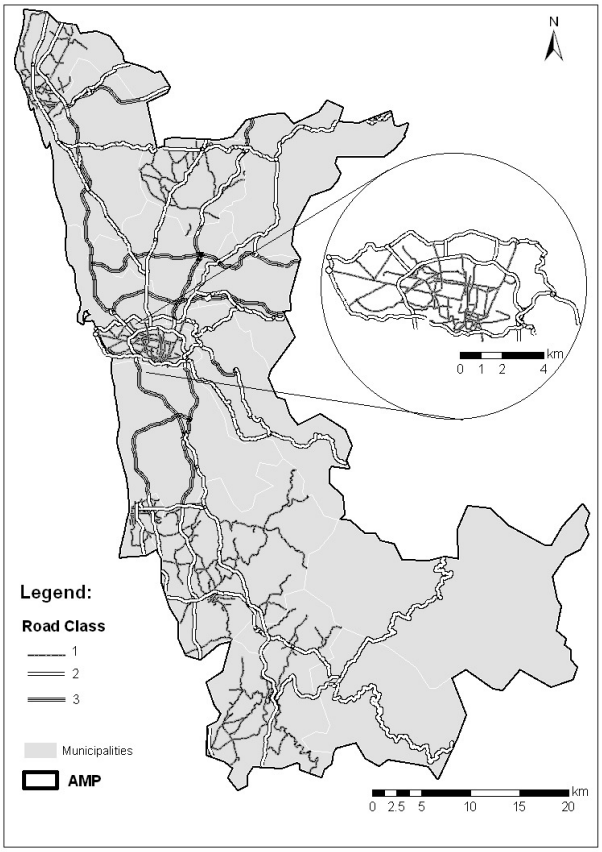

Figure 1: Administrative limits of the Porto Metropolitan Area and road network considered in the study.

Input Data

In order to characterize the fleet composition, traffic flow and vehicles speed of modelling domain, a set of random inputs is generated for each road. The PDF for vehicles classes is determined using the statistical information on vehicle registers and average number of kilometres travelled. For the traffic volume, data from the counting points attributed to each link were used, describing both temporal and spatial variations. Due to absence of vehicles speed measurements, this variable is estimated for each road segment considering the type of the road and taking into account the speed traffic behaviour from Joumard et al., (2006): urban (30±9.4 $km.h^{-1}$), interurban (70± 17.6$km.h^{-1}$) and highways (110±8.8 $km.h^{-1}$). A combination of random values generated by the Monte Carlo approach is used to create 625 independent inputs for each road segment to be used by TREM for the emission estimations.

Results

The results obtained from the multiple iterations of TREM using inputs generated with Monte Carlo approach are analysed in terms of the daily emissions aggregated by type of roads by distance unit, and by the total emission values for each road type. Table 1 includes the statistical parameters (average, standard deviation, percentiles 5 and 95) estimated for GHG and air toxic pollutants considering different vehicle technology mix and velocity fluctuations.

Globally, the results demonstrated that the range of the uncertainty produced in the model application depends on model inputs uncertainty range. Overall, the higher uncertainties are observed for urban roads (type 1), showing a wide range of distribution due to vehicles speed in congesting traffic and also the influence of vehicle technology mix. Moreover, the largest uncertainty associated to this type of road is obtained for the air toxic pollutants, especially for benzene.

Table 1: Statistical parameters of the daily emission rates for the different types of roads in the modelling domain.

Pollutant	Road type	Average	Standard Deviation	5th Percentile	95th Percentile
Greenhouse Gases					
CO_2 [g.km^{-1}]	1	255.903	54.334	188.666	380.319
	2	175.131	22.098	162.874	208.046
	3	196.099	12.356	175.459	206.445
CH_4 [mg.km^{-1}]	1	14.295	0.225	13.950	14.656
	2	16.327	0.224	16.059	16.672
	3	14.009	0.209	13.718	14.346
N_2O [mg.km^{-1}]	1	2.151	0.046	2.089	2.242
	2	3.908	0.045	3.848	3.997
	3	3.094	0.043	3.035	3.177
Air Toxic Pollutants					
PM [mg.km^{-1}]	1	32.442	6.259	23.854	45.143
	2	36.731	4.898	33.112	46.923
	3	49.282	4.961	40.776	54.132
Acetaldehyde [mg.km^{-1}]	1	7.235	1.898	4.881	11.591
	2	3.429	0.735	2.731	4.680
	3	2.999	0.077	2.871	3.114
Acrolein [mg.km^{-1}]	1	2.794	0.682	1.956	4.360
	2	1.462	0.267	1.194	1.918
	3	1.328	0.024	1.288	1.364
Benzene [mg.km^{-1}]	1	38.308	11.360	23.270	63.177
	2	12.515	4.352	8.895	20.177
	3	9.769	0.756	8.506	10.692
1,3-Butadiene [mg.km^{-1}]	1	7.365	2.137	4.508	11.992
	2	2.467	0.852	1.768	3.968
	3	1.970	0.152	1.717	2.148
Formaldehyde [mg.km^{-1}]	1	17.116	4.579	11.271	27.382
	2	7.350	1.797	5.743	10.448
	3	6.349	0.235	5.961	6.656

As regards the contribution of GHG, the highest values of CO_2 emissions are obtained for urban roads and highways, as expected, since the vehicles speed is a determinant factor for this pollutant (see Table 1).

The results for the air toxic pollutants, with the exception of PM, present the lowest order of magnitude for the whole set of parameters. All follow the same distribution behaviour once these pollutants are estimated as a fraction of NMVOC emissions for different vehicle technology. In general, from the results presented in Table 1, it is possible to conclude that the urban roads are identified as those which clearly have the highest emissions, followed by interurban roads and finally by highways. Such results reflect the high influence of reduced vehicles speed in urban areas.

Although the previous analysis allows a first evaluation of the influence of input parameters uncertainty on final emissions, it is important to analyse the obtained results in terms of total emissions for the whole road network in order to assess the influence of traffic flow variations in the emissions uncertainties. Thus, Figure 2 displays the average, minimum, maximum, P5 and P95 of the total daily emissions for the entire study area for working days (Wdays) and weekend (Wend) considering emission factors and also traffic flow variations.

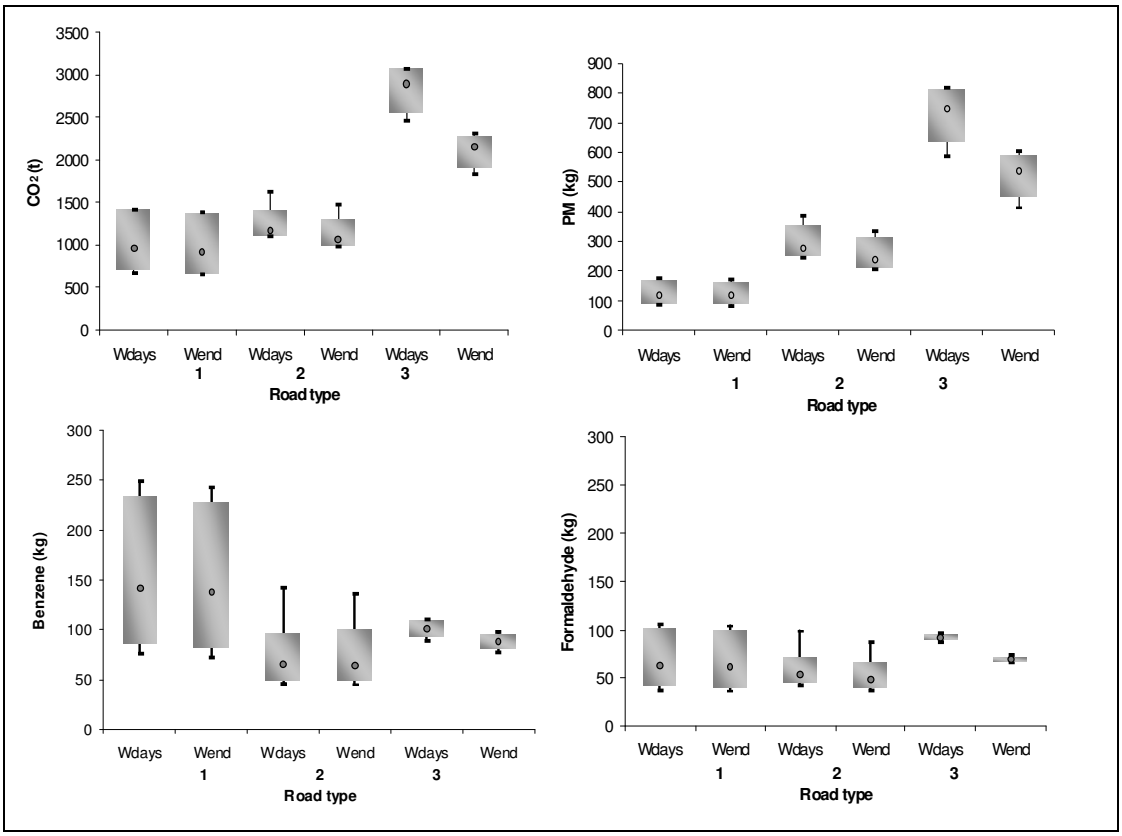

Figure 2. Statistical parameters for the total daily emissions of CO_2 , PM , Benzene and Formaldehyde for the different type of roads considering a working day and weekend.

According to Figure 2, only highways (type 3) show significant differences between weekday and weekend average emission rates. On the other hand, urban road (type 1) average emission rates do not vary significantly between weekdays and weekends. This second approach also shows that this road type presents a wide spread of values between percentiles 5 and 95, contributing to the overall uncertainty of emission estimations in urban areas. However, a different behaviour is observed for PM emissions. The higher values for the analyzed statistical parameters correspond to highways, followed by interurban roads. This distribution is associated to the high proportion of diesel vehicles on this road type.

Regarding the CO_2 emission rates, the highest values are obtained for the highways, instead of the urban roads. This is mainly due to the traffic flow variations being also considered in the second approach.

Due to the inherent differences in traffic characteristics, the analysis of emissions has also been performed for the municipalities. Thus, Porto urban roads exhibit the widest spread in the emission rate, 218.22 - 439.97 ton for CO_2 and 26.92 - 73.11kg for benzene considering 5%-95% range. In this way, Porto urban roads correspond to about 31% of total urban road emissions within the modelling domain.

Conclusions

Uncertainty quantification in emission data is useful in identifying problems and setting priorities for inventory improvement. The current work provides a description of the methodology and an application example to characterise a probability distribution of the emissions induced by road traffic in different types of roads considering vehicle technology mix, driving conditions and traffic volume fluctuations. Several statistical parameters were estimated, per distance unit, for GHG and air toxic pollutants only considering different vehicle technology mix and velocity fluctuations. The total daily emissions for the entire study area were presented considering emission factors and traffic flow variations. The resulting emissions, analysed in terms of cumulative distribution and uncertainty range, pointed out the largest uncertainties for urban

roads, mainly for the air toxics pollutants. Emissions calculated for highways are generally characterised by smaller uncertainty range in comparison with the other types of roads. Therefore, it should be noted the importance of uncertainty quantification on urban roads for inventory improvement, given the largest contribution of this type of roads in metropolitan areas.

Acknowledgments

The authors wish to thank the financial support of the Portuguese 'Ministério da Ciência, da Tecnologia e do Ensino Superior' for the PhD and Pos Doc grants SFRH/BD/22741/2005, SFRH/BD/47578/2008 and SFRH/BPD/40620/2007.

References

Abdel-Aziz, A., Frey, H.C. (2003), Quantification of Hourly Variability in NOx Emissions for Baseload Coal-Fired Power Plants, *J. Air & Waste Manage. Assoc.,* 53(11), 1401-1411.

Borrego C., Tchepel O., Barros N., Miranda A.I. (2000), Impact of road traffic emissions on air quality of the Lisbon region. *Atmospheric Environment*. 34, 4683-4690.

Borrego C., Tchepel O., Costa A.M., Amorim J.H., Miranda A.I. (2003), Emission and dispersion modelling of Lisbon air quality at local scale. *Atmospheric Environment*. 37, 5197-5205.

Borrego C., Tchepel O., Salmim L., Amorim J.H., Costa A.M., Janko J. (2004), Integrated modelling of road traffic emissions: application to Lisbon air quality management. *Cybernetics and Systems: An International journal*. 5-Jun, 35, 535-548

Boulter, P.G., McCrae, I.S., Barlow, T.J. (2007), A review of instantaneous emission models for road vehicles. PPR 267. Published Project Report. Transport research Laboratory.

EPA (1997), Guiding Principles for Monte Carlo Analysis; EPA/630R-97/001; U.S. Environmental Protection Agency: Washington, DC.

Frey H. C. Bammi S. (2002) Quantification of Variability and Uncertainty in Lawn and Garden Equipment NOx and Total Hydrocarbon Emission Factors. *J. Air & Waste Manage. Assoc*. 52:435-448.

Frey, H.C., Zheng, J. (2002a). Quantification of Variability and Uncertainty in Utility NOx Emission Inventories, *J. Air & Waste Manage. Assoc*, 52(9), 1083-1095.

Frey, H.C.; Zheng, J. (2002b) Probabilistic Analysis of Driving Cycle-Based Highway Vehicle Emission Factors; *Environ. Sci. Technol*. 36 (23),5184-5191.

Joumard, R., André, J-M., Aakko, P., Samaras, Z., Roujol, S., Zallinger, M., Kljun, N., Rapone, M., Markewitz, K., Weilenmann, M., André, M. (2006). Emission factor modelling and database for light vehicles. ARTEMIS deliverable 3. INRETS report LTE 0523. INRETS, Bron, France.

IPCC. 2000. Good Practice Guidance and Uncertainty Management in National Greenhouse Gas Inventories. National Greenhouse Gas Inventories Program, Intergovernmental Panel on Climate Change, Geneva

Sturm, P.J., Boulter, P., De Haan, P., Joumard, R., Hausberger, S., Hickmann, J., Keller, M., Niederle, W., Ntziachristos, L., Reiter, C., Samaras, Z., Schinagl, G., Schweizer, T., Pischinger, R., 1998. Instantaneous Emission Data and their Use in Estimating Passenger Car Emissions—VKM-THD Report, Vol. 74. Verlag der Techn. University of Graz, Austria, 42pp, ISBN 3-901351-24-8.

Winiwarter, W. and Rypdal K. (2001). Assessing the uncertainty associated with national greenhouse gas emission inventories: a case study for Austria. *Atmospheric Environment*, 35(22):5425-5440.

E-Motion: An Environmental Impact Assessment Modelling Framework

M. Vanhulsel, J. Vankerkom, L. Schrooten, I. De Vlieger, B. Degraeuwe, K. Dierckx, H. Michiels*

Vlaamse Instelling voor Technologisch Onderzoek (VITO), Boeretang 200, B-2400 Mol, Belgium, marlies.vanhulsel@vito.be

Research goal

The current research aims at assessing the impact of transport on the environment. To this end, a model is designed to map both the historic and future transport-related energy consumption and emissions. This model does not only estimate the emissions of road transport; it also calculates the emissions caused by off-road mobile machinery, rail traffic, inland navigation and maritime transport. Furthermore, E-Motion includes an external cost module valuing the human health effects of air pollution due to transport.

This research paper first outlines the general modelling framework of E-Motion, i.e. an Energy and emissions Model for Transport with geographical distribution. For illustration purposes, the energy and emission model for rail transport is described into more detail. Subsequently, the structure of the external cost module is elaborated on. Finally, some preliminary results of an environmental impact assessment for transport in Belgium are included.

Methodology

General approach to calculate energy consumption and emissions

To model energy consumption and emissions in Belgium, E-Motion comprises a modular framework. Each module within E-Motion corresponds to one travel mode, i.e. road, off-road mobile machinery, rail, inland navigation and maritime transport. In general, each of the modules start from detailed activity data and data concerning the composition of the fleet. The latter type of data source captures the distribution of the fleet according to characteristics believed to influence the energy consumption or/and emission factors, for instance the fuel type or age category. The activity data record the total mobility demand, such as the number of kilometres, tonne kilometres or hours, taking into account the fleet characteristics and travel profile. The historic calculations are based on inventory studies, whereas the estimations for future transport up to 2030 are founded on these historic input data and on a number of prognoses and expert judgements.

For each travel mode, the fleet and mobility data are combined with energy consumption factors and emission factors to estimate detailed energy consumption figures and emissions. For the calculation of emissions, European and national emission regulations and fuel specifications, for instance the directive defining the sulphur content of diesel, are consulted. Finally, the emissions calculated by E-Motion are geographically distributed per region or per road/rail/waterway segment, depending on the format in which input data on activities are supplied. The resulting energy consumptions and emissions within the proposed approach are determined at a disaggregated level. Consequently, the effect of changes in the distribution of the activities according to fuel type, technology, travel profile and other parameters influencing the energy consumption and emission figures, can easily be determined. Figure 1 shows this modelling framework for road transport.

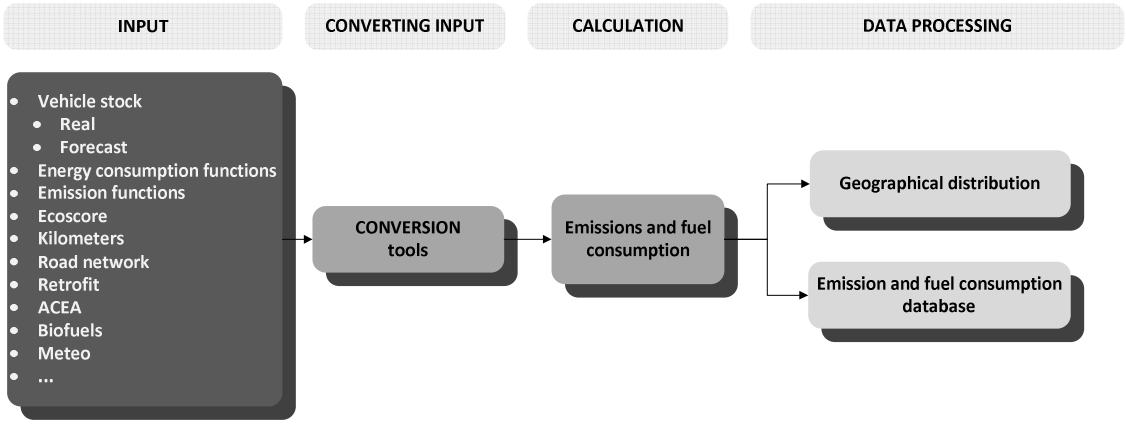

Figure 1: Modelling framework for road transport

Case study: railway

To illustrate this general process, the calculation of the energy consumption and emissions resulting from railway transport is considered here. This calculation framework is partly based on research efforts from the European project Ex-TREMIS (Chiffi et.al., 2007) and is visualized in Figure 2.

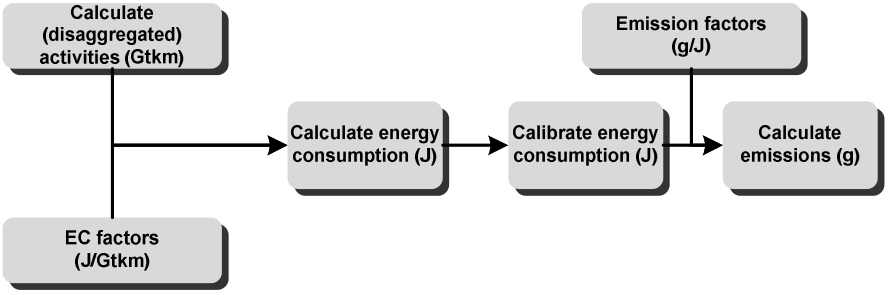

Figure 2: Energy consumption and emission calculation for railway transport

In the railway module, the yearly number of gross tonne kilometres (Gtkm), i.e. the number of tonne kilometres including the weight of the traction vehicle, constitute the basis of all calculations. Next to a division of the number of gross tonne kilometre with respect to the energy source (diesel or electric), this number is broken down according to a number of variables because of accuracy of the energy and emission estimations. The selected variables are assumed to influence either the energy consumption, or the emissions, or both. Examples of such variables are: the train company, the train type (goods or passengers), the type of traction vehicle (multiple unit or locomotive) and the service type - which determines the travel profile (freight train, local passenger train, intercity passenger train, high speed train, and other types). However, because data are not available in this desired level of detail, the first step of the process consists in deriving these detailed activity data from several data sources. Future activity data are based on the available, historic activity data and prognoses concerning growth/decline.

The outcome of this step is used to calculate the energy consumption by combining these activity data with energy consumption factors. The energy consumption factors are defined per energy source, train type and service type. Even though the energy consumption factors themselves do not change throughout the years, the railway model does allow taking into account changes in energy efficiency caused by improvements in load efficiency, by specifying a year dependent correction factor. An next step involves estimating the energy consumption for shunting activities, assuming a fixed energy supplement with respect to the productive freight activities.

Subsequently, for the train activities of the Belgian Railway Company (NMBS/SNCB), the calculated energy consumption is compared to the observed energy consumption reported on in

yearly statistics. This comparison enables calibrating the energy calculation. The resulting calibrated energy consumption figures form the basis for calculating the exhaust emissions. As PM2.5, VOC, CO and NO_x exhaust emissions are largely dependent on technology age classes, the current research distributes the energy consumptions along a number of technology age classes. The technology age classes ensue from the Rail Diesel Study (Halder and Löchter, 2005) and EC directives fixing the emission regulations of combustion engines installed in non-road mobile machinery (Directive 97/68/E; Directive 2004/26/EC).

Finally, both exhaust and non-exhaust emissions can be valued. On the one hand, the former emission calculations are based on the energy consumption, and are divided into technology-related (PM2.5, VOC, CO and NO_x) and fuel-related emissions (CH_4, CO_2, N_2O and SO_2). On the other hand, the non-exhaust emission calculations (PM2.5, PM10, TSP), mainly caused by abrasion of breaks, wheels, rails and overhead wires of trains, are founded on the number of train kilometres.

This modelling approach enables defining scenarios, which differ from one another on several aspects, such as the assumed activity growth rates, bio fuel blend percentage and distribution over technology age classes. Each scenario computation covers the energy consumption and the exhaust and non-exhaust emissions for the defined pollutants, specified per year, energy source, train company, train type, service type, traction vehicle type, technology age class.

External costs

In order to assess the human health effects of air pollution, noise and climate change caused by transport in Belgium, E-Motion incorporates an additional module evaluating the external costs. For the purpose of conciseness, this paper solely focuses on the external costs caused by the pollutants NO_x and PM2.5. This external cost model is designed according to the Impact Pathway Approach - developed within a series of European projects, commonly known as ExternE (Bickel and Friedrich, 2005) - and is extended with region specific dispersion modelling and population density information. The Impact Pathway Approach is a bottom up methodology, which calculates external costs based on emissions, as is illustrated here. Founded on the geographically distributed emissions for each transport mode, concentration maps are constructed by the atmospheric dispersion model BelEUROS (Deutsch et al., 2007; Deutsch et al., 2008). While determining air quality, BelEUROS considers thermodynamic criteria and meteorological conditions in its calculation of the chemical reactions.

The resulting concentration maps are linked to population maps to determine exposure. Figure 3 shows an example of such population density map with a 15x15 km resolution.

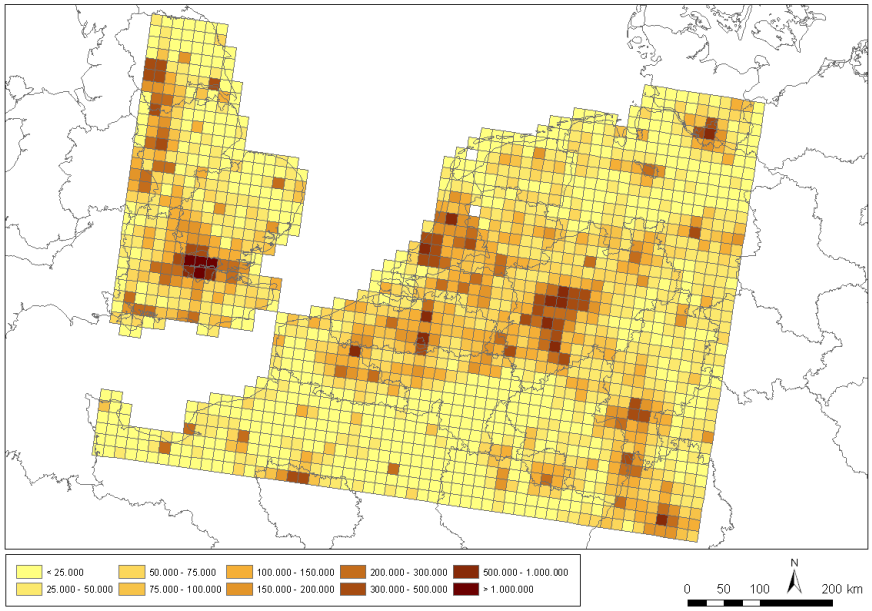

Figure 3: Population density per grid cell for study area in 2001

Subsequently, the DALY calculator (VMM, 2009) estimates the health effects of these concentrations based on concentration response functions from European research projects,

such as NEEDS (Torfs et al., 2007) and CAFE (Watkiss et.al., 2005), and values the corresponding monetary costs (de Hollander et.al., 1999; Murray and Lopez, 1996).

Results and discussion

The proposed modelling framework is implemented and fully operational for the modules concerning road transport, rail transport, off-road mobile machinery and external costs. Furthermore, scenario calculations for these modules can be executed as well. With respect to maritime transport and inland navigation, the implementation of the models was still on-going at the time of writing this paper.

Figure 4 visualizes preliminary results of the emission estimations. This figure shows CO_2 and NO_x emissions for the different transport modes, in the business-as-usual (BAU) scenario for the base year 2007 and for 2030. As the modelling efforts for maritime transport and inland navigation are still work in progress, the emissions of the modules are based on former modelling efforts (VMM, 2009). Even though the share of road transport decreases for the transport-related CO_2 and NO_x emissions, it remains the largest contribution compared to all other transport modes.

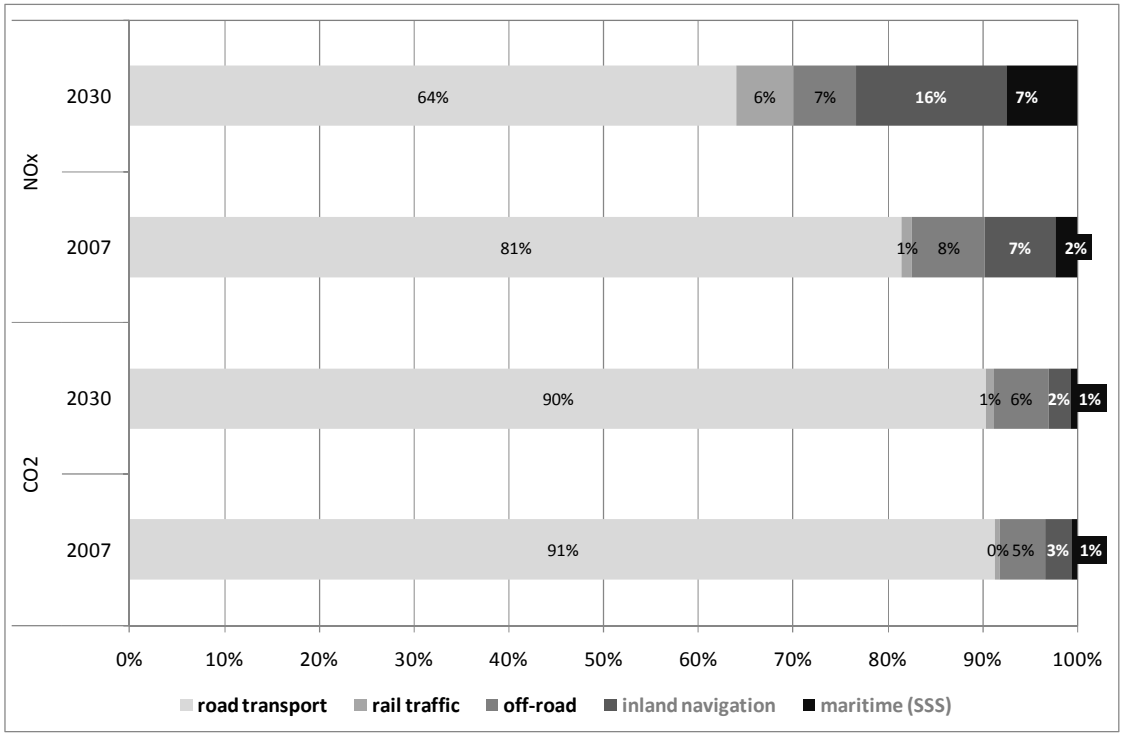

Figure 4: NO_x and CO_2 emissions per transport mode in Belgium (2007 & 2030)

Additionally, Table 1 presents preliminary emission factors for the Belgian fleet. The emission factors clearly show the impact of introducing Euro VI and 6, the new standard for heavy road transport and light road transport respectively, which largely affects NOx emissions. Regarding freight transportation by rail, the fleet emission factor for CO2 rises, as the effect of an increasing share of diesel engines compared to electric engines – mainly due to a rise in the number of gross tonne kilometres of international operators, deploying diesel engines - neutralizes the effect of reduced CO2 emissions caused by the use of bio-diesel. Conversely, the NOx emissions do not exhibit this trend, because of the replacement of pre-1990 vehicles within the fleet by new ones, which are required to meet more stringent emission standards. Additionally, compared to the fleet emission factors for freight transportation by rail, the corresponding factors for passenger transportation are considerably lower for both 2007 and 2030, as a result of the extreme electrification of the passenger rail transport (approximately 96% of the gross tonne kilometres of passenger transport are travelled by electric vehicles). Moreover, the fleet emission factors for passenger rail transport decline on the account of the introduction of biodiesel and fleet renewal. Concerning off-road mobile machinery, mainly the NO_x emission factors prove to drop considerably

Table 1 Fleet emission factors

BAU		Unit	NO_x		CO_2	
			2007	2030	2007	2030
Road	Car	kg/km	0.606	0.129	163.430	119.718
	LDV		1.036	0.248	227.968	163.349
	HDVr		4.998	0.423	577.580	524.925
	HDVa		7.338	0.608	760.390	667.604
Rail	Goods	kg/gross tkm	0.069	0.066	4.105	4.473
	Passenger		0.011	0.004	1.229	1.003
Off-road		kg/PJ	0.708	0.123	71.996	71.820

Next, to gain a better understanding of the external costs of transport in Belgium for a certain pollutant, the external cost module first estimates the total external costs, given the emission levels for the desired pollutant as determined within the BAU scenario. However, the resulting external costs also contain the costs caused by non-transport-related emissions. After all, the total amount of emissions needs to be accounted for in calculating the external costs due to interaction effects. Therefore, the next step consists of decreasing the transport-related emissions for the considered pollutant by 20%, all other things being equal. Thereafter, the external costs corresponding to this variant of the BAU scenario is computed as well. Subsequently, the outcome of these scenario calculations are compared and, as such, the marginal external costs of transport in Belgium can be obtained.

Figure 5 displays the external costs per tonne of PM2.5 and per tonne of NO_x emitted in Belgium. This figure shows that external costs due to NO_x emissions are lower than those caused by PM2.5 emissions. For 2030, the external cost of NO_x equals approximately 1,5kEUR/tonne, and for 2007, the external cost of NO_x is even negative. This has two main reasons. Firstly, of all pollutants considered in this study, primary PM2.5 causes the most adverse health effects. As this primary PM2.5 constitutes the largest component in the external costs of PM2.5, while it is inexistent in the external costs of NO_x, the external costs per tonne of PM2.5 exceed those of NO_x. Secondly, splitting up the external costs originating from NO_x emissions according to the underlying pollutants, i.e. ozone, nitrate aerosols, sulphate aerosols, other PM2.5 and PM10, reveals that the external costs of nitrate aerosols are positive, while the external costs of sulphate aerosols and ozone are negative. Within Belgium, where the VOC/NO_x ratio is low (Deutsch et.al., 2009), the degradation of ozone through its reaction with NO molecules is dominant over the NO_2-formation reaction, which normally founds the ozone formation. Consequently, increased NO_x emissions cause higher levels of ozone reduction. This effect declines in future scenarios, as the share of NO emissions in the total NO_x emissions continues to decrease in favour of NO_2. The external benefit of sulphate aerosols is largely due to the competition for ammonia groups, i.e. NH_4. In case more NO_x is emitted, more ammonium nitrates can be formed. Consequently, less ammonia groups are left available for the formation of sulphate aerosols, which thus causes an external benefit.

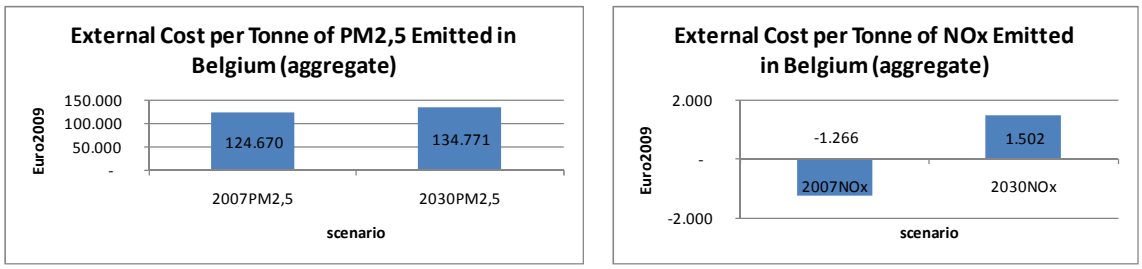

Figure 5: Aggregate external cost per tonne of PM2,5 and per tonne of NO_x emitted in Belgium

Conclusion

The results presented here suggest that the E-Motion modelling framework allows to clearly distinguish the share of the different transport modes in the total amount of transport-related

emissions. In establishing the E-Motion framework, considerable effort is put in aligning the different modules for the benefit of user friendliness. As a result, E-Motion is designed as such that it enables a straightforward, uncomplicated prediction of emissions for a number of different scenarios, providing as such an excellent basis to analyse the impact of transport-related policy decisions and technological changes on the environment.

References

Bickel, P. and Friedrich, R. (2005), ExternE - Externalities of Energy - Methodology 2005 Update, *Institut für Energiewirtschaft und Rationelle Energieanwendung – IER, Universität Stuttgart*, Germany. European Commission, Directorate-General for Research.

Chiffi, F., Schrooten, L. and De Vlieger, I. (2007), EX-TREMIS - Exploring non road Transport Emissions in Europe, Final Report for the *Institute for Prospective Technological Studies* (IPTS), DGJRC, Seville, Spain.

de Hollander E., Melse J., Lebret E. and Kramers P. (1999) An aggregate public health indicator to represent the impact of multiple environmental exposures, *Epidemiology*, 10, 606-617.

Deutsch F., Fierens F., Trimpeneers E., Janssen S., Veldeman N., Buekers J., Torfs R. and Vancraeynest L. (2009), Toekomstverkenning MIRA 2009: Wetenschappelijk rapport: Fotochemische Luchtverontreiniging, Report for the *Flemish Environment Agency* (VMM), http://www.milieurapport.be/Upload/main/WR_Fotochemie_v10_TW.pdf, Accessed on 23/03/2010, 68-72.

Deutsch F, Mensink C, Vankerkom J and Janssen L. (2007), Application and validation of a comprehensive model for PM10 and PM2.5 concentrations in Belgium and Europe, *Applied Mathematical Modelling*, 32, 1501-1510.

Deutsch, F., Vankerkom, F., Janssen, L., Janssen, S., Bencs, L., Van Grieken, R., Fierens, F., Dumont, G., and Mensink, C. (2008), Modelling concentrations of airborne primary and secondary PM10 and PM2.5 with the BelEUROS-model in Belgium, *Ecological Modelling*, 217, 3-4, 230-239.

Halder, M. and Löchter, A. (2005), Status and future development of the diesel fleet, Final report of *Rail Diesel Study*, WP 1.

Murray, C. and Lopez, A. (1996), The global burden of disease, Report for the *World Health Organisation and the World Bank*, Cambridge, MA Harvard School of Public Health.

Torfs R., Hurley F. and Rabl A. (2007) A set of concentration-response functions for NEEDS. Report for the *Integrated project NEEDS* (New Energy Externalities Developments for Sustainability), funded in the Sixth Framework Program.

VMM (2009), Milieurapport 2009: Milieuverkenning 2030, Report for the *Flemish Environment Agency* (VMM), http://www.milieurapport.be/upload/main/MIRA_compleet_TW.pdf, Accessed on 23/03/2010, 228-230 and 243-244.

Watkiss P., Holland, M., Hunt, A., Hurley, F. and Navrud, S. (2005), Final Methodology Paper (Volume 1) for *Service Contract for carrying out cost-benefit analysis of air quality related issues*, in particular in the *Clean Air For Europe* (CAFE) programme.

New Zealand's Greenhouse Gas Transport Emissions and an International Comparison

Haobo Wang and Melanie Hutton*

New Zealand Ministry of Transport[1], PO Box 3175, Wellington 6140, New Zealand,
h.wang@transport.govt.nz

1 Introduction

New Zealand has a population of 4.3 million. It consists of two narrow and long landmasses (the North Island and the South Island) and some smaller islands, partitioned by numerous hills and mountain ranges. Domestic transport emissions are a significant proportion of New Zealand's national total greenhouse gas (GHG) emissions (nearly 20% in 2007) (NZ MfE, 2009; NZ MED, 2009). In addition, transport has long been the largest GHG emitter in the New Zealand energy sector (NZ MED, 2009). As a country which has ratified the Kyoto Protocol, New Zealand has committed to reducing its emissions of GHGs over 2008-2012 to 1990 level or take responsibility for any emissions above this level if it cannot meet this target. Reducing GHG emissions from the transport sector would play an important part in fulfilling this commitment.

The objectives of this paper are to study the trends of New Zealand domestic transport GHG emissions since 1990, and to compare its emissions with those in 17 other OECD countries: Australia, as our closest trading partner, and the remainder chosen based on their trade relationship with or similarity of population size to New Zealand (thus potentially similar policy settings).

2 Data Sources and Issues

2.1 New Zealand data

The New Zealand transport GHG emission data are from the Ministry of Economic Development, presented as carbon dioxide equivalent (CO_2-e) emissions from the direct GHGs: carbon dioxide (CO_2), methane (CH_4) and nitrous oxide (N_2O) (NZ MED, 2009). Only domestic transport emissions are considered in this paper as the Kyoto Protocol target does not cover GHG emissions from international aviation and shipping. The national total GHG emission data are from the Ministry for the Environment, excluding the removal of emissions from the land use, land-use change and forestry sectors (NZ MfE, 2009).

Road traffic activity data are from the Ministry of Transport. There is very limited availability of traffic activity data for other modes (aviation, shipping and rail) in New Zealand. Population and gross domestic product (GDP) data are from Statistics New Zealand.

2.2 International data

All the international data come from the Organisation for Economic Co-operation and Development (OECD) and the International Transport Forum (ITF). They obtain their data on transport carbon dioxide emissions, population and GDP from the International Energy Agency (IEA) and the data on countries' national total GHG emissions based on national reports to the United Nations Framework Convention on Climate Change (UNFCCC) (OECD/ITF, 2008a). Note that the IEA data cover CO_2 emissions from fuel combustion and do not include non-CO_2 emissions. Given that CO_2 largely dominates transport-sector GHG emissions, it serves as a good proxy for overall transport GHG emissions (OECD/ITF, 2008b).

2.3 Data issues

The GHG transport emissions in New Zealand were calculated as those from the transport industry plus those from petroleum fuels sold via resellers (e.g. service stations). This is likely to

[1] Disclaimer: The opinions expressed in this paper are those of the authors, and do not necessarily represent the views of the Ministry of Transport.

result in an over-estimate of emissions attributed to the transport sector[2] as resellers also on-sell petroleum fuels for non-transport uses (e.g. diesel sold for powering stationary farm machinery) (NZ MED, 2009; NZ MED, 2010).

3 New Zealand's Transport Emissions

3.1 GHG emissions per capita

Domestic transport GHG emissions in New Zealand have grown by 64% since 1990 although such growth has slowed in recent years. A total of 14.3 Mt CO_2-e of GHG transport emissions was recorded in 2008 compared to 8.7 Mt CO_2-e in 1990. The vast majority of the emissions came from road transport (over 85%). Transport emissions have grown faster than population growth, resulting in an increase in per capita transport emissions (of 29% in 2008 as compared to 1990, see Fig. 1). Note, however, that the per capita transport emissions appear to have levelled out since 2004 (as indicated by the vertical line placed in Fig. 1) and decreased in 2008.

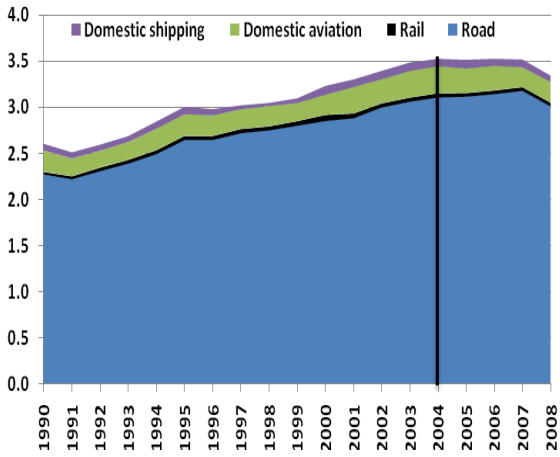

Fig. 1 Per capita domestic transport emissions, tonnes CO_2-e per capita per annum

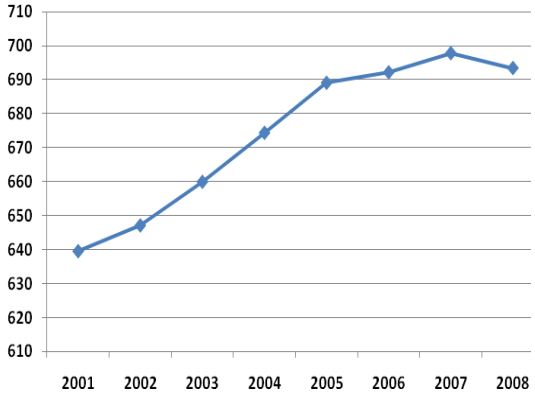

Fig. 3 Light duty vehicle ownership per 1000 inhabitants in New Zealand

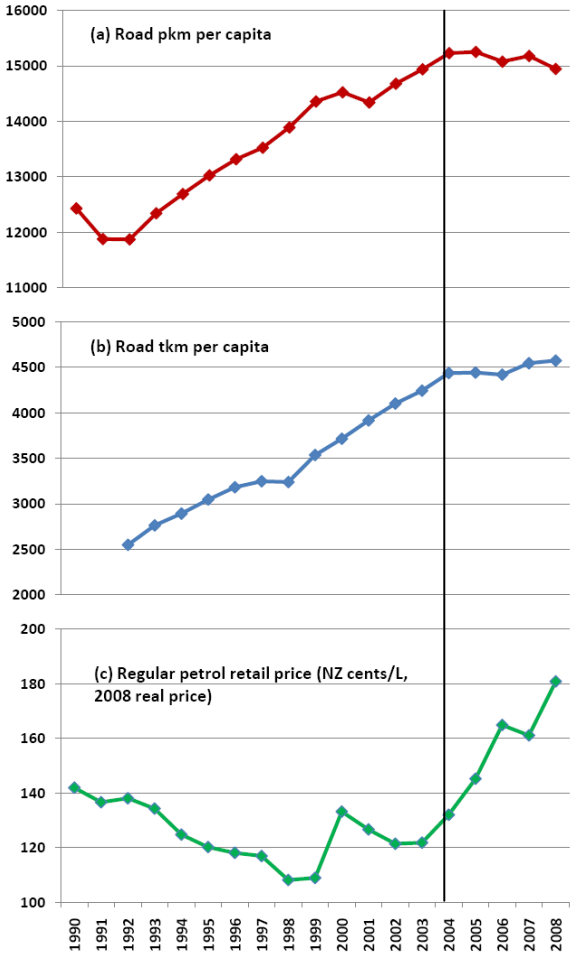

Fig. 2 Per capita transport tasks and petrol price (pkm: passenger kilometres travelled; tkm: freight tonne kilometres travelled). Note that no tkm data are available for 1990 and 1991

As shown in Fig. 2, both passenger (passenger kilometres travelled, pkm) and freight (tonne kilometres travelled, tkm) road transport activities per capita per annum have increased steadily over the last two decades. This may explain the large growth in per capita transport emissions discussed above. Further consideration of Fig. 2 has shown that road pkm per capita per

[2] New Zealand is required to report the information on total energy sector GHG emissions as part of the obligations under the UNFCCC and Kyoto Protocol. So transport share is not critical to the international obligation for reporting.

annum (Fig. 2a) have been rather stable since 2004 and that the growth in tkm per capita per annum (Fig. 2b) has slowed over the same period (as indicated by the vertical line placed in Fig. 2). The increase in ownership of light duty vehicles (LDVs including cars, vans, and sport utility vehicles) has also been much slower in recent years (Fig. 3). On the other hand, transport fuel prices have soared since 2004 (Fig. 2c). The sharp increase in fuel prices may have played an important role in the slowdown of road transport activities and LDV ownership. Note that LDV ownership rate in New Zealand is one of the highest in the world (as seen by comparing its data with those in Jacobs Consultancy (2006) and in UNECE (2005)).

It is found that domestic transport GHG emissions in New Zealand dropped significantly in 2008 to 14.3 Mt CO_2-e from 14.9 Mt CO_2-e in 2007 (NZ MED, 2009). This is most likely due to the very high transport fuel prices in 2008 and the beginning of the global economic recession.

3.2 GDP and GHG emissions

Fig. 4 shows the time series of GDP intensity of domestic transport GHG emissions in New Zealand. After being relatively stable for 13 years (between 0.115 and 0.120 Kg CO_2-e per NZ$ of GDP (1995/96 prices)), transport emissions per dollar of GDP have gradually decreased since 2004. This may present an early positive sign that the coupling between domestic transport GHG emissions and economic growth in New Zealand is getting weaker. However, it should be noted that economic growth in New Zealand is likely to remain weak in the next few years as it remains affected by the global economic recession. Thus, the downward trend in GDP intensity of transport emissions could be difficult to sustain over the short term.

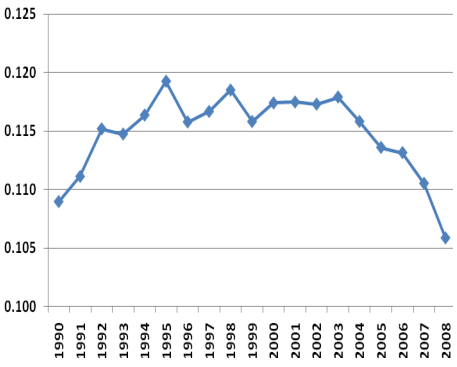

Fig. 4 GDP intensity of domestic transport GHG emissions (Kg CO_2-e per NZ$ of GDP (1995/96 prices))

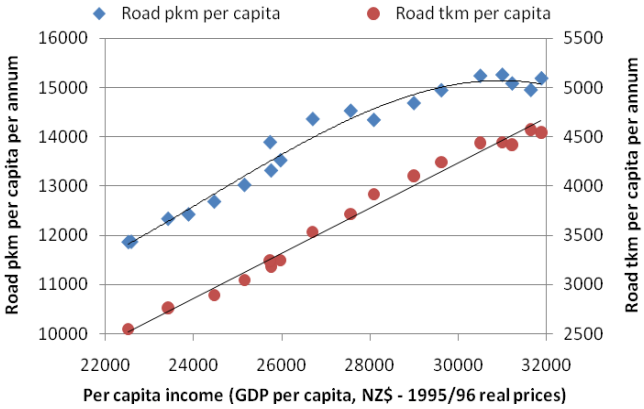

Fig. 5 Relationship of national per capita road transport tasks to per capita income, 1990 - 2008 (pkm: passenger kilometres travelled; tkm: freight tonne kilometres travelled). Note that no road tkm data are available for 1990 and 1991

Interestingly, it appears that there has been a saturating tendency for per capita road passenger kilometres travelled, as against per capita income growth, when per capita GDP is over NZ$30,000 (1995/96 real prices) (Fig. 5). A similar saturation has also been observed in Australia between per capita overall pkm (all modes) and per capita income (Cosgrove, 2008). As discussed above, the sharp increase in transport fuel prices in recent years may have contributed significantly to the levelling out of per capita pkm. A travel survey (NZ MoT, 2009) found that over the last 20 years New Zealand's daily travel time per capita has remained fairly stable, being consistent with the hypotheses of constant travel time budgets (Goodwin, 2005), but the shift of travel time towards driving from cycling and walking has greatly slowed in recent years. It might still be too early to tell whether or not this saturation of per capita road pkm can be sustained in the future. If it is, the future increase in road pkm in New Zealand will be likely to become more dependent on the population growth rate, and less dependent on the level of general economic prosperity (as measured by GDP).

In contrast, Fig. 5 suggests that growth in road freight tkm per capita in New Zealand will continue to increase alongside the growth of per capita income. Research (RPC, 2008) has forecast that New Zealand will experience a strong growth in freight transport demand over the next two decades (although this projection could be subject to future changes in the economic climate). It is therefore a reasonable argument that to increase freight transport efficiency will

be very important for New Zealand to reduce transport GHG emissions.

It is worth noting that the European Union has set an objective of reducing the link between economic growth and freight transport demand (decoupling), in order to achieve a low GHG emission transport system and that such decoupling has been observed in both the UK and Denmark (Jacobs Consultancy, 2006; McKinnon, 2007).

4 Comparison with Some OECD Countries

The latest transport emission, GDP, population and traffic data from other countries reported on the OECD website are from 2005 (with the CO_2 emission data being from the IEA). The following section thus provides a comparison of transport CO_2 emissions in New Zealand with those from selected OECD countries for that year. Note that the IEA estimates may differ from in-country reporting because the IEA may not have complete and accurate data for each country. To facilitate the international comparison, the New Zealand emission data used in this section are also from the IEA rather than from the NZ Ministry of Economic Development.

4.1 Carbon dioxide emissions per capita

Although New Zealand's total CO_2 emissions from domestic transport are relatively small compared to those of many other OECD countries, its per capita transport CO_2 emissions (3.4 tonnes CO_2 per capita in 2005) are high, being only under those of the US and Australia among the countries included in this paper (Fig. 6). It is noted that per capita domestic transport CO_2 emissions in New Zealand have levelled off since 2004. A few other OECD countries including Australia, Belgium, The Netherlands, Portugal and Switzerland have shown a similar trend. Nevertheless, most other OECD countries have still seen an increase in their per capita domestic transport CO_2 emissions (OECD/ITF, 2008a).

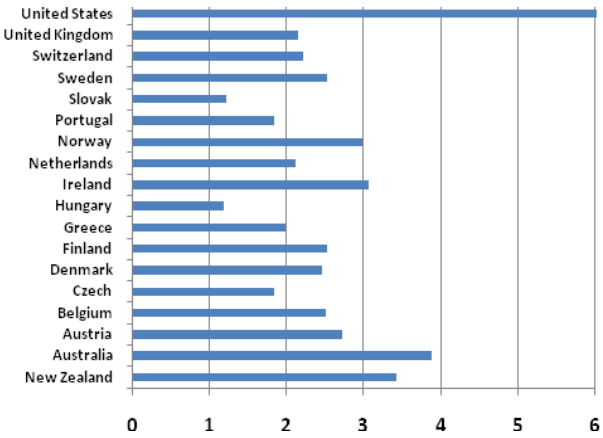

Fig. 6 Per capita domestic transport carbon dioxide emissions (tonnes CO_2 per capita per annum) in 2005

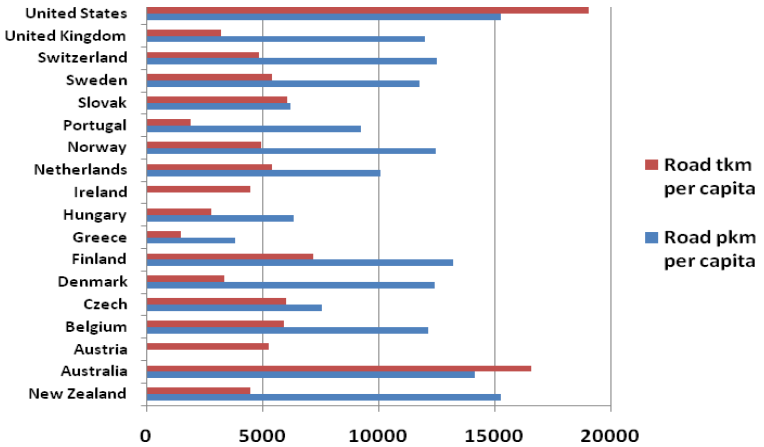

Fig. 7 Per capita road passenger and freight transport tasks in 2005 (pkm: passenger kilometres travelled; tkm: freight tonne kilometres travelled). Traffic data for other modes (rail, aviation and shipping) are scarce

It has been found that road transport emissions have determined the pattern of per capita overall transport emissions, with a share of about 90% for most countries. There are several reasons for New Zealand to have higher per capita CO_2 emissions from road transport: (a) as mentioned above, New Zealand has a higher ownership rate of LDVs; (b) New Zealand people, on average, travel longer distances than those of many other countries, partly due to a low population density over long landmasses (Fig. 7); and (c) New Zealand has many hilly and mountainous roads. Interestingly, although both per capita transport CO_2 emissions and per capita road passenger kilometres travelled are similar for New Zealand and Australia, per capita road freight tonne kilometres travelled are very different in the two countries (Fig. 7). This may warrant further research.

As shown in Fig. 8, per capita CO_2 emissions from domestic aviation in New Zealand are comparable to those in Australia and Norway, but much higher than those for many other OECD countries except the US. This could be explained by New Zealand's long landmasses and the fact that air travel is both the most convenient way to cross the strait between the two main islands and often the most cost effective due to a highly competitive domestic aviation market.

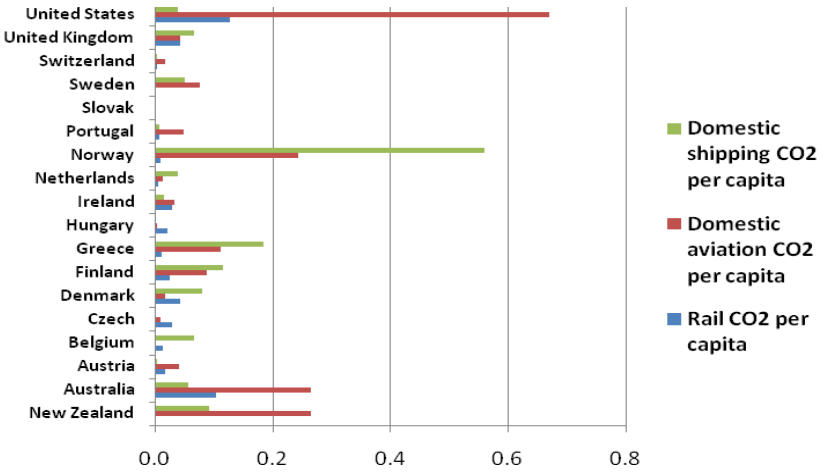

Fig. 8 Per capita carbon dioxide emissions (tonnes CO_2 per capita per annum) from domestic aviation, shipping and rail in 2005

4.2 GDP intensity of Carbon dioxide emissions

Fig. 9 shows that the GDP intensity of domestic transport CO_2 emissions in New Zealand in 2005 was just under that of the US but higher than that for any other OECD countries discussed in this paper. This may suggest that New Zealand has, on average, been using more transport energy to produce the same amount of GDP than its competitors, which makes New Zealand more vulnerable to fuel price increases and restrictions on supply.

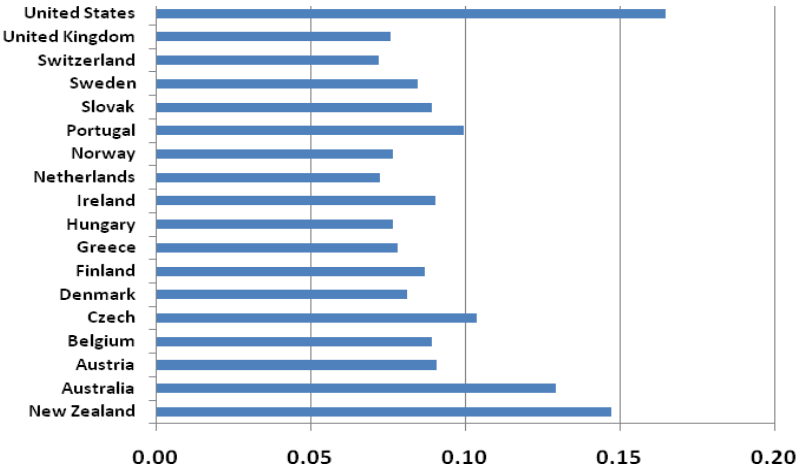

Fig. 9 GDP intensity of domestic transport carbon dioxide emissions (Kg CO_2 per US$ of GDP (Purchasing Power Parity, base year 2000)) in 2005

4.3 Relative importance of domestic transport emissions

Domestic transport contributed about 18% of national total GHG emissions in New Zealand in 2005, which is rather similar to the level for many other OECD countries. However, it must be borne in mind that New Zealand has a unique GHG emission profile among developed countries, in that nearly half of its total emissions in 2005 were produced by the agriculture sector. By comparison, emissions from agriculture typically make up about 10% of total GHG emissions in most other OECD countries (NZ MfE, 2009).

Domestic transport made up about 46% of the overall CO_2 emissions produced by fossil fuel combustion in New Zealand in 2005. This figure is just under that for Sweden but higher than those for any other OECD countries discussed in this paper, and well above the OECD average of 27%. One reason for this is that New Zealand's electricity generation system is dominated by renewable generation (producing around two thirds of New Zealand's electricity) (NZ MED, 2009).

5 Conclusions

The GDP intensity of domestic transport GHG emissions in New Zealand has gradually decreased and its per capita transport GHG emissions have levelled out since 2004. However, both are relatively high compared to those in many other OECD countries based on the 2005 transport CO_2 emission data.

Acknowledgements

The authors thank Mr. Philippe Crist at OECD, Mr. Ronald Mair at Statistics NZ and Ms. Sonia Petrie at the NZ Ministry for the Environment for their assistance. The authors also thank many colleagues at the Ministry of Transport for their assistance with data and their helpful comments.

References

Cosgrove D. (2008), Long-term emission trends for Australian transport, *The 31st Australasian Transport Research Forum*, Gold Coast, Queensland, Australia, October 2-3, 2008.

Goodwin P. (2005), The remarkable consistency of travel time, *Local Transport Today*, *LTT432 8 December*.

Jacobs Consultancy (2006), *European Best Practice, Draft Final Report (prepared for the UK Commission for Integrated Transport)*. Available: http://www.cfit.gov.uk/docs/2007/ebp/pdf/ebp-phase2.pdf.

McKinnon A. (2007), *CO_2 Emissions from Freight Transport in the UK (prepared for UK Commission for Integrated Transport)*. p. 20.

NZ MfE (New Zealand Ministry for the Environment, 2009), *New Zealand's Greenhouse Gas Inventory 1990-2007.* Wellington.

NZ MED (New Zealand Ministry of Economic Development, 2009), *New Zealand Energy Greenhouse Gas Emissions 2008 Calendar Year Edition.* Wellington, pp. 3–23.

NZ MED (New Zealand Ministry of Economic Development, 2010), Delivering the diesel – Liquid fuel deliveries in New Zealand 1990 – 2008.

NZ MoT (New Zealand Ministry of Transport, 2009), *How New Zealanders Travel – Trends in New Zealand household travel 1989 – 2008.* Wellington, pp. 4-5.

OECD/ITF (2008a). *Key Transport and Greenhouse Gas Indicators: Information by Country.* Available: http://www.internationaltransportforum.org/Topics/c02emissions.html.

OECD/ITF (2008b), *Greenhouse Gas Reduction Strategies in the Transport Sector – Preliminary Report.* 2008. Available: http://www.internationaltransportforum.org/Pub/pdf/08GHG.pdf.

RPC (Richard Paling Consulting, 2008), *National Freight Demands Study (prepared for the Ministries of Transport and Economic Development and the NZ Transport Agency).* Wellington, 2008, pp. 186-216.

UNECE (2005), *Trends in Europe and North America 2005*. Available: http://www.unece.org/stats/trends2005/Welcome.html.

Micro-Simulation of a Traffic Fleet to Predict the Impact of Traffic Management on Exhaust Emissions.

M. Madireddy[1], B. De Coensel[2], I. De Vlieger[1], D. Botteldooren[2], B. Beusen[1], B. Degraeuwe[1], G. Lenaers[1] , A, Can[2], A. Eijk[3]*

[1]Flemish Institute of Technological Research (VITO), NV, Boeretang, 2400 Mol, Belgium, madhava.madireddy@vito.be
[2] Ghent University, Sint-Pietersnieuwstraat 25, B-9000 Gent, Belgium
[3]TNO, Shoemakerstraat 97, P.O Box 6030, 2600 AJ Delft, Netherlands

Abstract

Despite the stringent air quality standards, urban traffic has been a major source of atmospheric pollution. It is therefore useful to investigate the potential effect of traffic management on emissions. Micro-simulation traffic models shall aid in developing traffic management systems and in urban planning practice. This study presents one such traffic model known as Paramics that can simulate a given traffic scenario based on the composition of the fleet and the characteristics of the roads, and outputs the speeds and the positions of each of the vehicles in the fleet. The output of Paramics was served as an input to Versit+, an emissions prediction model which can predict for each vehicle class, the temporal and spatial concentrations of the exhaust emissions. Before employing Versit+ for this study, the model was validated using the instantaneous emissions collected by VITO's On-Board Emissions and Energy Measurement (VOEM) system. Paramics and Versit+ were jointly used to examine two traffic management schemes in Nieuw Zurenborg, part of the 19th century city belt of Antwerp, Belgium. First, the effect of reduced speed limit in this network on per kilometre emissions is investigated. When the speed-limits for all the roads in this network were reduced, the model predicted that the emissions will be lower for CO_2, NOx and PM. Secondly, the effect of a green-wave (synchronization of traffic signal lights) along the N180, in this network was investigated. The two scenarios, with and without the green-wave were compared for emissions. The results showed that the presence of green-wave reduces the emissions by about 10%.

Introduction

Road transport is one of the major sources of atmospheric emissions and noise. The exhaust emissions are predominantly the byproducts of hydrocarbon fuel combustion which include oxides of nitrogen (NOx), particulate matter (PM), un-burnt hydrocarbons (HC), carbon monoxide (CO) and carbon dioxide (CO_2). Due to the increasing stringency of emissions standards by the European Environment Agency (EEA) over the past two decades, there has been a significant reduction in the road transport emissions. Despite this reduction, road transport activities still contribute significantly to environmental pollution, especially in areas with heavy traffic. Since increased demand for vehicles is increasing traffic on the roads, smooth traffic flow was key objective for traffic management authorities. But smooth traffic flow does not necessarily mean the emissions are minimized. Hence appropriate traffic management systems which also take into account the air quality effects are the need of the hour; accurate estimates are needed of concentrations and spatial distribution of air pollutants from the vehicles for such locations. This study presents a micro-simulation traffic model known as Paramics, an emissions prediction model known as Versit+, and their coupling. While earlier studies focus on the emissions at single intersection (De Coensel et al., 2007; Pandian et al., 2009), this study focuses on the overall emissions in the whole network.

Paramics: The Micro-simulation Traffic Model

Majority of the traffic management decisions are most often based on average flows on main arterial roads. However, small-scale changes in infrastructure and changes in driving behavior can have a large influence on traffic flows. For this purpose, microscopic simulation models are being increasingly used in the study of urban mobility problems.

Microscopic traffic simulation models aim to represent how vehicles circulate on the network, within an (urban) environment that is modelled in great detail (locations of curbs and stop lines, exact size of intersections etc.). Their outputs are the position, speed and acceleration of each vehicle on the network, at each time step. The model used for this study, Paramics, is based on behavioral rules, such as when to change lanes, when to overtake or how much distance to keep to the vehicle in front, form the core of the model. Its time step is 0.5s. When coupled with emission models for individual vehicles, microscopic traffic simulation models estimates the impact of detailed traffic management measures on emissions, taking into account the influence of braking and accelerating.

In this study, a micro-simulation network was constructed for the area of Nieuw Zurenborg, part of the 19th century city belt of Antwerp, Belgium. The road map of this network is shown in Figure-1 (left). The network was coded on the basis of Geographic Information Systems (GIS) data which comprises of roads, buildings, and aerial photographs, and traffic light timing data, supplied by the Antwerp police department. Further, traffic counts, supplied by the Flemish Department of Mobility and Public Works, were used to calibrate the traffic flows during morning rush hour. Figure-1 (right) shows a screenshot of the model. These traffic flows were inputted into Paramics by defining 'zones', from which traffic flows in and out to another zone.

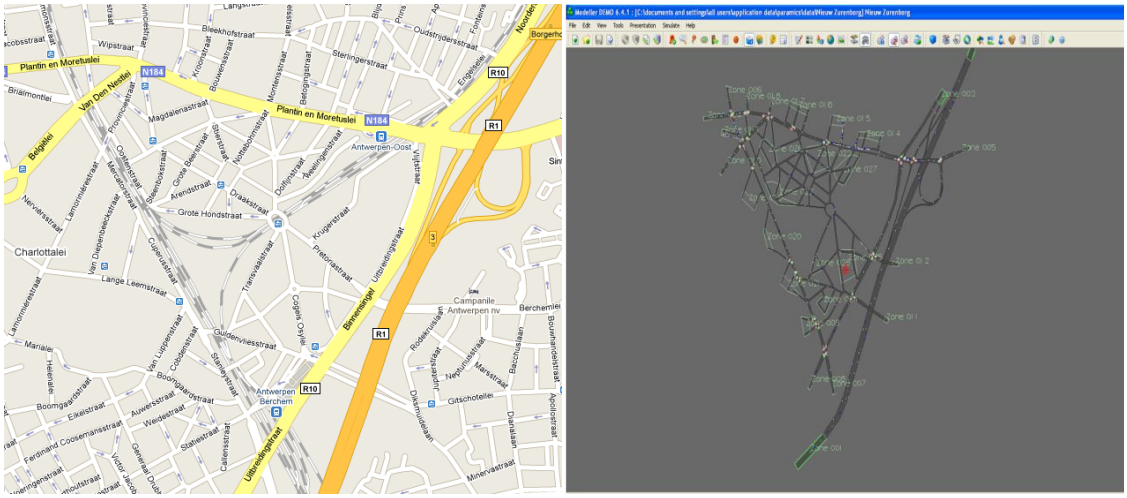

Figure 1: Map of the Nieuw Zurenborg (left) and representation of this area in Paramics (right).

Versit+: The Vehicle Emissions Model

Versit+ (Smit et al, 2007; Ligterink and De Lange, 2009), was developed by Dutch Organization of Applied Scientific Reserarch (TNO), in Delft, the Netherlands. The model consists of a set of statistical models for detailed vehicle categories that have been constructed using multiple linear regression analysis. The model is based on a very large database (12 000 tests on 153 speed profiles) with data for every vehicle class (heavy-duty, light diesel, medium-heavy duty, etc). However, the current version of Versit+ does not allow the user to choose among the Euro classes, fuel types, use of advanced emissions reduction technologies, etc. Hence, the model generates emissions for each vehicle class which represents an average or a typical vehicle. The inputs for the model are vehicle category, vehicle positions and speed for all vehicles in the network. These data can be obtained from measurements or from a microscopic traffic simulation model such as Paramics.

Versit+ defines a dynamic variable, which is a linear combination of velocity and acceleration and for a given driving cycle. Ten different regions were defined in the speed-acceleration map. These regions define the driving behavior of the vehicle such as idling, accelerating, aggressive highway driving, etc. Different emissions functions based on speed and acceleration were developed for each of these regions and the output of these emission functions is afterwards corrected for cold start, ageing and high emitters. Thus, the model is capable of relating emissions to driving behavior.

Validation of Versit+

Before Versit+ was used in this study for emissions prediction, a validation study was conducted on the model using the data obtained by VITO's On Road Emissions and Energy Measurement (VOEM) system. A better description of VOEM system was provided elsewhere (De Vlieger, 1997). This data were collected from the tests conducted on four diesel vehicles and a gasoline vehicle. The diesel vehicles tested were Citroen Berlingo, Citroen C4, Nissan Patrol and Opel Vivaro, while Volkswagen Golf is the only gasoline vehicle tested. The drive cycle used to collect this VOEM data was MOL_30, a 30 minute cycle which is a combination of ten minutes of city driving, ten minutes of suburban driving and ten minutes of highway driving. This cycle was chosen because it is more representative of the real-world driving than NEDC (New European Drive Cycle). The speed profiles of each of these vehicle tests were inputted into the Versit+, which gave the spatial continuous emissions predictions for CO_2, NOx and PM. The spatial emissions were then converted into temporal emissions based on instantaneous vehicle speed data. Then for every test, the results from the VOEM measurements were compared with those predicted by Versit+. Figure-3 presents the results predicted by Versit+ for a test conducted on the Citroen Berlingo, a diesel van tested on MOL_30 drive cycle. The correlations of each of the emissions were given in the title of the sub-plot (of figure-3) along with the type of emissions. It should be noted that Versit+ is able to predict the peaks of emissions quite well for both CO_2 and NOx although the true values of instantaneous emissions were over-estimated in most cases. Also, while the correlation of CO_2 is the highest (at about 0.90), the correlation of NOx is reasonable (0.80) and that for the PM was the lowest at 0.53.

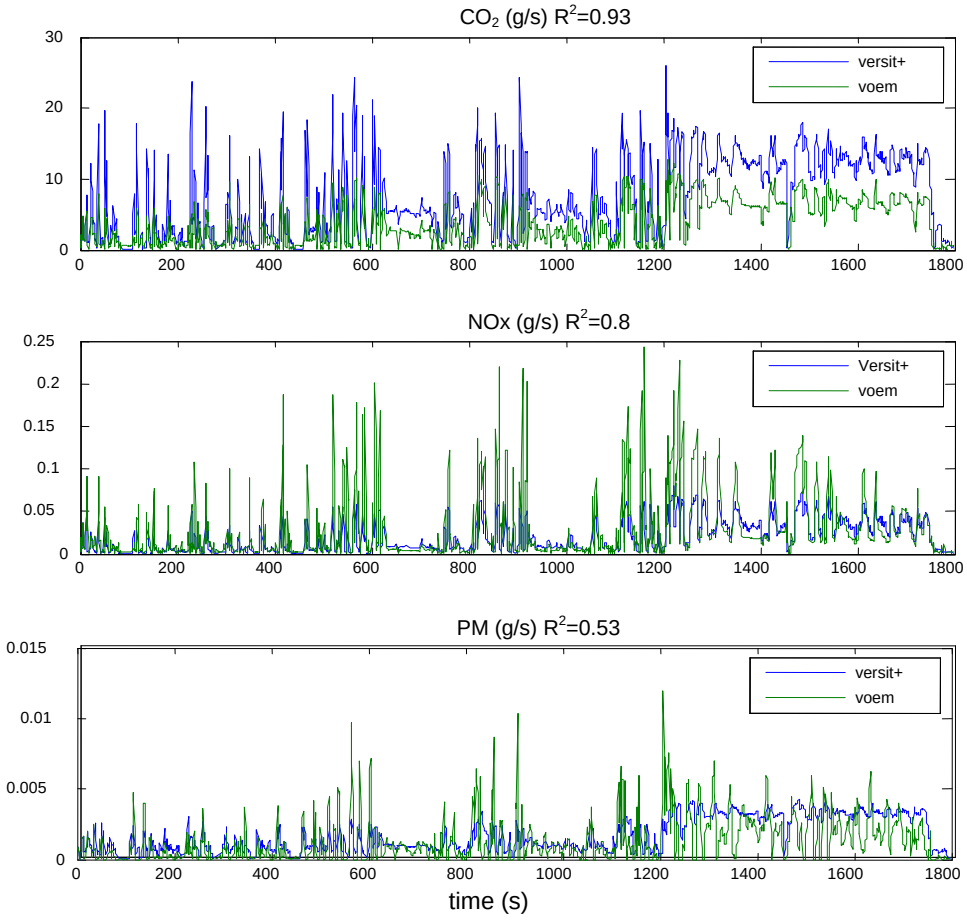

Figure 2: Comparison of the instantaneous data obtained from Versit+ with that of the measured data from VOEM for Citroen Berlingo on Mol_30 driving cycle. The correlations of the predicted and measured emissions are given in the title next to each pollutant.

The other tests conducted on Citroen Berlingo and other vehicles gave similar results with good predictions of CO_2 (average R^2 of 0.80). This indicates that the energy usage or fuel consumption was predicted well by the model. However, the predictions of NOx (average R^2 of 0.66) and PM (Average R^2 of 0.24) were not very good. The poor prediction of these emissions can be attributed to the fact that the model does not distinguish the emissions of gasoline vehicle from that of diesel vehicle and NOx and PM are predominantly a byproduct of diesel combustion. Also, the use of diesel particulate filters in some of the cars was not accounted for. In other words, the representation of 'average' car was not the same diesel car used for validation. But even with the poor predictions of NOx and PM for individual vehicles, Versit+ was chosen since the study focuses on total fleet composition in the network and this can be represented well by the database on which the model was based.

Investigation of Traffic Management Schemes

For this study, two different traffic management schemes were investigated: The effect of reduced road speed limit -and the effect of removing the synchronization of traffic lights along one of roads in the network.

Scheme-1: Effect of reduced road speed limit

To understand the effect of traffic speed limit on emissions, two scenarios are created using Paramics network file. The network in NewZurenborg is analyzed with original traffic at regular speed limits and a new scenario is created in the same network with speed limits reduced. The speed limit on the freeway was reduced from 100 kmph to 70 kmph, for the major roads the speed limits were reduced from 70 to 50 kmph, while for the minor roads the speeds were dropped from 50 to 30 kmph. From the results shown in Table-1, there was a significant reduction in all the emissions for both the vehicle classes. The CO_2 emissions dropped about 23% for cars and by about 41 % for HD vehicles.. HD vehicles showed about 32% reduction in both NOx and PM, while cars showed a reduction of 45% in NOx and 27% in PM emissions. This indicates that at reduced speeds in this network, there is a possibility of emissions reduction.

Table 1: Effect of reduced speed limit on network emissions

	Original Scenario		Reduced Speed	
Vehicle Class	Cars	HD	Cars	HD
CO_2 (g/km)	248.3	1241	191.9	736.5
NOx (g/km)	0.79	9.76	0.43	6.55
PM10 (g/km)	0.055	0.42	0.04	0.29

Scheme-2: Effect of green-wave on emissions

To understand the significance of synchronization of traffic lights along a road, the following scenarios were examined on N184 road or Plantijn & Moretuslei. The original scenario is the one with the green-wave, where all the traffic signals are co-ordinated. A second scenario was created by removing the synchronization or 'killing' the green-wave. The corresponding emissions in both the scenarios were compared. All the emissions were measured in g/km for both the vehicle classes (cars and medium-heavy duty vehicles) separately.

The CO_2 emissions increased by 10.3 percent for cars and 9.2 percent for medium-HD vehicles. Also the NOx emissions were increased by 9.9 percent and 9.2 percent, and PM10 emissions by 9.1 percent and 9.8 percent for cars and medium HD vehicles respectively. This indicates that the green-wave plays a significant role in emissions management since if the traffic flow is smoothened, there will be less acceleration and deceleration phases.

Table 2: Effect of green-wave along Plantijn & Moretuslei on emissions

	Original Scenario		Without Green-wave	
Vehicle Class	Cars	HD	Cars	HD
CO_2 (g/km)	328.3	1360	362.1	1486
NOx (g/km)	0.82	11.98	0.90	13.08
PM10 (g/km)	0.055	0.493	0.06	0.54

Conclusion and Discussion

This paper presented an emissions prediction model, Versit+. The model was validated using the real-time measurements and the model predictions were reasonable. Also, a micro-simulation traffic model known as Paramics was used to represent road-traffic in a selected network in Antwerp, Belgium. This network was then fed into Versit+ which generated the spatial and temporal distribution of each of the air pollutants, CO_2, NOx and PM.

The combination of these two models was used to investigate two traffic management schemes. The emissions model predicted that when the network speed-limit is reduced, the per kilometre emissions of CO_2, and thereby the fuel consumption can be reduced by about 25% for a typical fleet. This means that the vehicles are originally driving at a higher speed than is optimum for reduced emissions. In other words, there is originally significant acceleration and deceleration within the network. Reducing the speed-limit in this network could encourage driving at constant speeds and thereby promote eco-friendly driving. Also, if the 'green wave' on Plantijn & Moretuslei was removed, the emissions went up by about 10 percent.

References

B. De Coensel, D. Botteldooren, F. Vanhove, S. Logghe (2007), Microsimulation based corrections on the road traffic noise emission near intersections, *Acta Acustica united with Acustica* 93(2):241-252.

I De Vlieger , (1997), On-Board Emission And Fuel Consumption Measurement Campaign on Petrol-Driven Passenger Cars. *Atmos. Environ*, 31, 3753-3761.

N. E. Ligterink and R. De Lange, Refined Vehicle and Driving-behaviour Dependencies in the VERSIT+ Emission Model (2009), *In Proceedings of the Joint 17th Transport and Air Pollution Symposium and 3rd Environment and Transport Symposium (ETTAP)*, Toulouse, France.

Quadstone, Paramics: Micro-Simulation Traffic Model, http://www.paramics-online.com.

R. Smit., R. Smokers., E. Rabé (2007), A New Modelling Approach for Road Traffic Emissions: VERSIT+, *Transportation Research* Part D 12(6):414-422.

S. Pandian, S. Gokhale, A. K. Ghoshal (2009), Evaluating effects of traffic and vehicle characteristics on vehicular emissions near traffic intersections, *Transportation Research Part D* 14(3):180-196.

A monitoring system to control effects and effectiveness of traffic measures in urban areas

V. Diegmann[1], L. Neunhäuserer[1] and G. Gässler[1]*

[1] IVU Umwelt GmbH, 79110 Freiburg, Germany, volker.diegmann@ivu-umwelt.de

Introduction

Within a project on environmental traffic management in Braunschweig, Germany, ("UVM Umweltorientiertes Verkehrsmanagement Braunschweig") a monitoring system has been installed as part of an environmental traffic management system (ETMS). This paper describes the layout, the application and the validation of the monitoring system.

The effectiveness of implemented traffic measures for a selected hotspot as well as the side effects were assessed by comparing modelling results based on identical input data but using traffic data without any measures in one case and with reduced traffic in the other case. The results emphasise the importance of a monitoring system that offers the possibility to assess and control the consequences of traffic measures within the entire road network.

During the project, differences between results of the monitoring system and measurements were observed. It will be shown that these may be attributed to some degree to the emission factors of HBEFA 2.1 (INFRAS, 2004) which was used as the basis for emission modeling.

Motivation

European air quality limit values for PM10 and NO_2 are still exceeded in a number of cities in Germany and Europe. Vehicle emissions have been identified to play an important role in these limit value exceedances. Thus, clean air plans are usually focusing on traffic measures to improve air quality. Typical measures are low emission zones, traffic bans for heavy duty vehicles, speed limits or road traffic reduction, with the spatial extent ranging from a single street section up to the entire city center. These measures may be installed either permanently or temporarily.

In the context of quality assurance the effectiveness of the implemented traffic measures with respect to air quality improvement needs to be monitored. Additionally, it is important to control side effects on other street sections of the road network to prevent the emergence of new hot spots. In the case of an environmental traffic management system (ETMS), reliable traffic and air quality data are continuously needed as well (Diegmann and Gässler, 2009).

However, measured air quality data is usually not detailed enough for these purposes due to the limited number of measurement stations available along the considered road network. Instead, a monitoring system based on a modelling system that provides concentrations within all relevant street canyons may be used to gain the necessary information on air quality along the road network.

Monitoring system

The environmental monitoring system installed in Braunschweig is an implementation of IMMIS^{mt}. The core of IMMIS^{mt} consists of three models, forming a modeling chain to calculate traffic-induced emissions, urban and local dispersion. The data flow between the models is coordinated by software components controlling the temporal sequence of the overall system, which includes data supply, start of the models, data transmission to the archive and data export of the results to further clients (e. g. map clients).

All input and output data is passed through adjustable interfaces that are capable of controlling various data transmission techniques like SOAP, ASCII, or HTTP. The internal data storage structure is realized with a local or a client-server database (e. g. Oracle). The database stores all static data (e. g. road and canyon geometries, emission cadastre data) as well as all dynamic data for the current modeling interval. The system's archive is based on a client/server database and stores the total input and output data of all computations. With the simulator module, the

stored computations can be repeated - if desired with changed conditions. This allows for the analysis of scenarios, e. g. for planning traffic control measures.

Data requirement: The system is mainly driven by traffic data. Each street segment is characterized by a default traffic situation. This information can be updated for each time step in which the current situation can be derived from velocity profiles of the detected traffic data. The dispersion models use meteorological data such as temperature, wind data and stability class. Available data from air quality monitoring stations are used to derive background concentrations. To account for the variation of urban background concentration, emissions of main sources like industry, shipping, rail traffic, off-road traffic and domestic combustion, usually available from an emission cadastre, are used for the urban dispersion model. The modeling approach on the micro scale requires a parameterization of the major roads. All street segments with adjacent buildings, called sections, are described by their width, height and porosity.

Modeling control: The modeling process calculating the total concentration at a hot spot in a street canyon needs to account for the regional background caused by long range transport, the urban background caused by the urban emission sources and the additional pollutant load caused by the road traffic in the street canyon itself.

Based on incoming traffic data, emissions of the major roads are determined with the emission model IMMIS^{em} (IVU Umwelt, 2008). Together with emissions of other urban sources, the citywide spatial distribution of air pollutants is calculated using the urban dispersion model IMMIS^{net} (IVU Umwelt, 2008b). This provides the urban background concentration for each section and for the locations of air quality monitoring stations. The regional background can then be determined as difference between the observed concentration at the background station and the urban concentration modeled for the station. Finally, the micro scale model IMMIS^{cpb} (Yamartino and Wiegand, 1986) is applied to assess the additional concentration due to traffic within each street canyon with the Canyon Plume Box approach using meteorological and local emission data. To derive NO_2 values from the calculated NO_X concentrations, IMMIS^{mt} provides different methods ranging from simple statistical techniques based on measurements to photochemical models.

Application

The monitoring system was installed in street sections throughout the Braunschweig city center. Street sections of the northern and eastern inner ring road have already been identified in the Braunschweig clean air plan (Braunschweig 2007) to have a high traffic and pollutant load. These findings were confirmed by recalculation with a screening model (Figure 1).

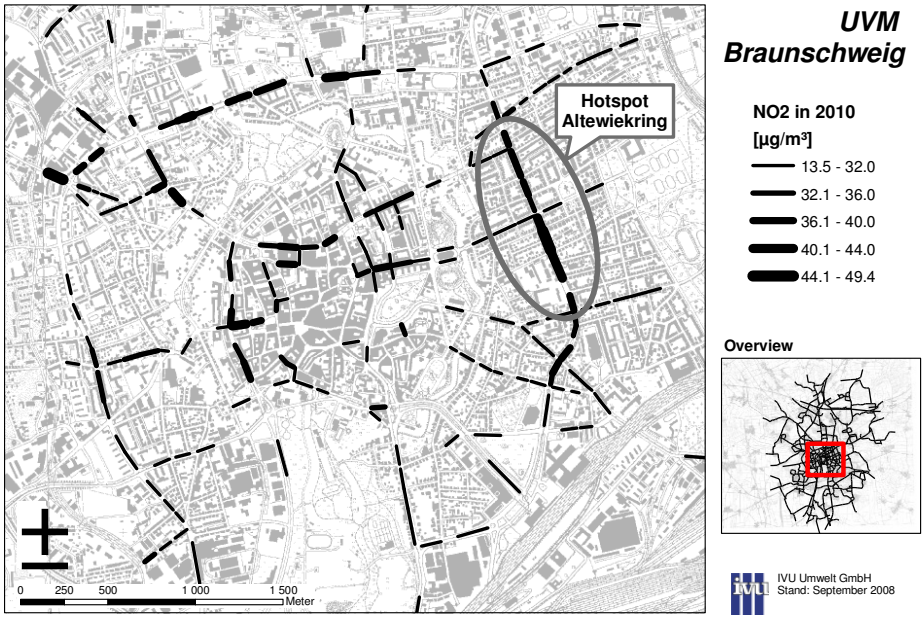

Figure 1: Recalculation of the NO_2 annual mean values for street sections in the city center of Braunschweig based on the Braunschweig clean air plan (Braunschweig 2007).

The Altewiekring, a part of the eastern inner ring road, was chosen as the hot spot to which traffic measures were applied. A monitoring station was installed there to provide air quality data for validation purposes. The traffic intensity in this part of the Altewiekring is about 38000 veh/day on weekdays, with hourly maximum values of 2200 veh/h. The annual mean values of the hot spot measurements in 2009 were 23 µg/m³ for PM10 and 52 µg/m³ for NO_2. The recalculation with a screening model based on the Braunschweig clean air plan predicted annual mean values of 30 µg/m³ for PM10 and 44 µg/m³ for NO_2 in 2010.

After implementing the system, monitoring was performed for several month in 2009, including a time period without any traffic measures and two time periods with traffic measures, in the following referred to as test phase 1 and 2. Hourly pollutant concentrations were calculated with IMMIS^{mt} for the Braunschweig road network, based on online traffic data, emissions from sources other than traffic (e. g. domestic combustion, industry), background concentrations and meteorological data.

Validation

Modelling results from IMMIS^{mt} were validated with the measured data from the monitoring station at the hot spot in Altewiekring. The modeled time series of PM10 daily mean values are in overall good agreement with measured values (Figure 2, top). The corresponding coefficient of determination calculates to very good 91 % (Figure 3, left). It should be kept in mind that the PM10 concentration measured and modelled at the hot spot is mainly influenced by the regional background concentration which is not part of the modeling procedure.

The modeled time series of NO_X hourly values agree very well with measured values in some parts (Figure 2, bottom). Maximum concentrations e.g. on 4 April 2009 or 19 May 2009 are well modeled. The overall characteristics of the measured time series is met by the model as well. However, the model often underestimates maximum concentration values. The coefficient of determination is 60 % (Figure 3, right) which is low compared to the PM10 result. This may be explained by the larger fraction of urban background und additional pollutant load due to traffic, both part of the modeling procedure. The averaging period which is a day for PM10 and an hour for NO_X may play a role as well because there is less variability associated with longer averaging periods.

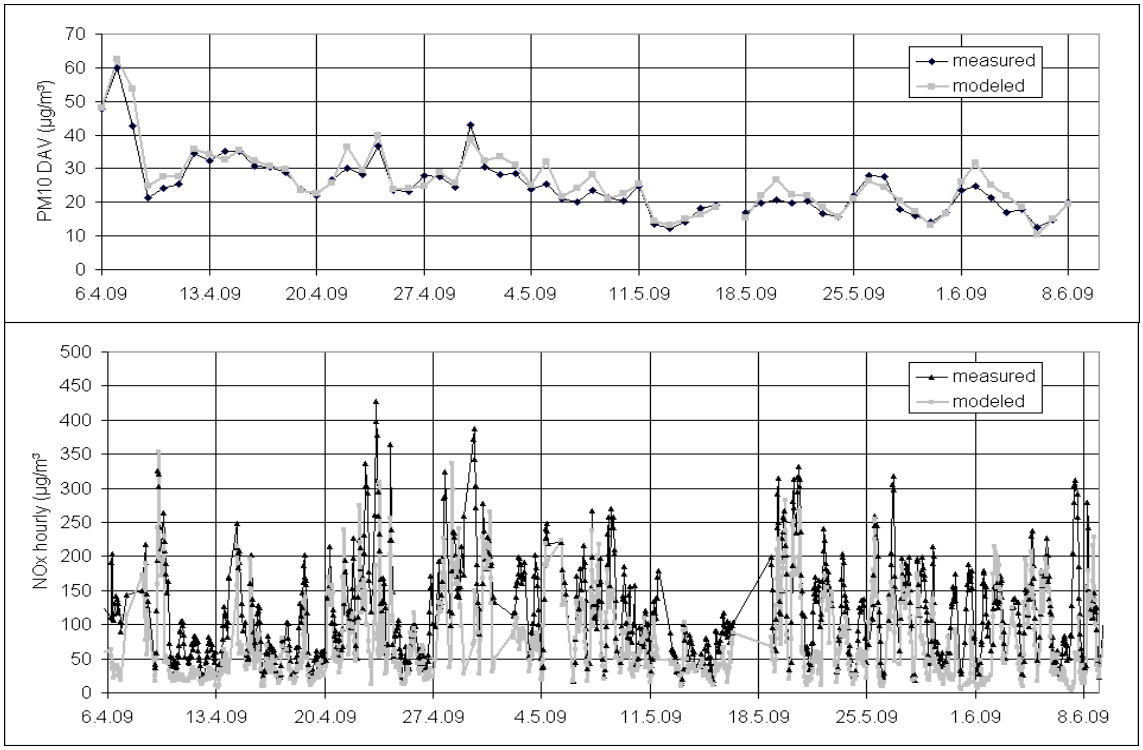

Figure 2: Time series of modeled and measured PM10 daily mean values (top) and NO_X hourly values (bottom).

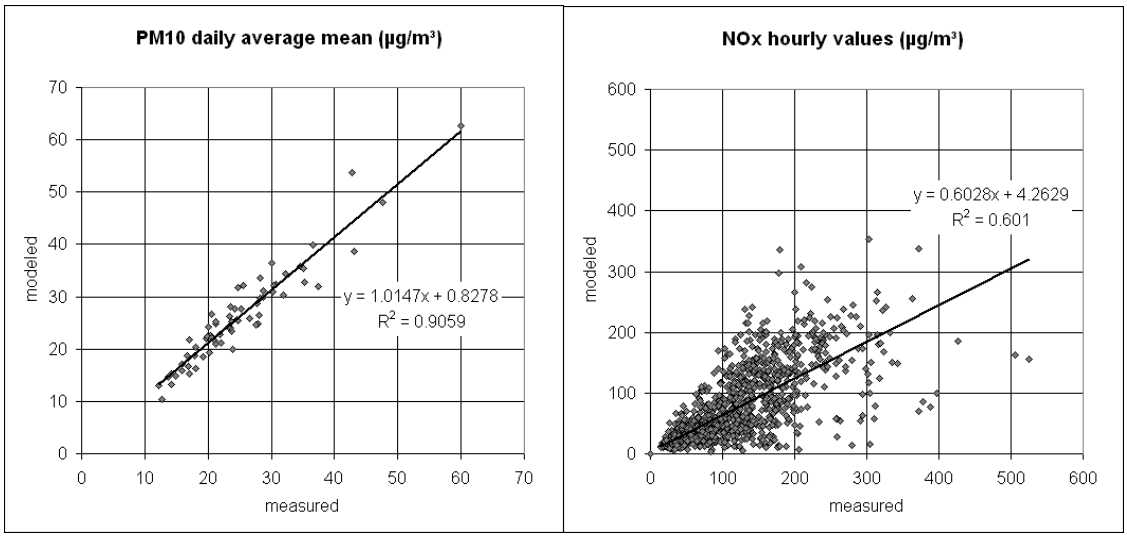

Figure 3: Scatterplot and regression analysis of modeled vs. measured data for PM10 daily mean and NO_X hourly values.

Table 1 shows measured and modelled PM10 and NO_X concentrations, averaged separately over the time period of each test phase and over both time periods. While measured PM10 concentrations are overestimated slightly by 5 % to 7 %, NO_X concentrations are underestimated significantly by 34 % to 35 %. Thus, NO_X model results just missed the data quality objectives for ambient air quality assessment required by the EU directive 2008/50/EC (EU, 2008) which allow a deviation of 30 % for the NO_X annual average.

It is widely accepted that the NO_X emission factors of HBEFA 2.1 (INFRAS, 2004) are in parts significantly too low. Current calculations based on the just published HBEFA 3.1 (INFRAS 2010) show NO_X emissions increasing up to 30 %. Hence, the NO_X underestimation of the modeled data may be attributed to a large degree to the emission factors of HBEFA 2.1 which was used as the basis for emission modelling in this study. The concurrent increase of HBEFA 3.1 PM10 emissions indicates the necessity to revise the currently used approach for modeling non-exhaust emissions according to Düring and Lohmeyer (2004).

Table 1: Comparison of average values for measured and modeled PM10 and NO_X

Substance	Period	ID	Measurement (µg/m³)	Model result (µg/m³)	Deviation (Mod-Meas)/Meas
PM10	06.04. - 10.05.	test phase 1	29.3	31.2	6.6 %
	11.05. - 09.06.	test phase 2	18.7	19.7	5.4 %
	01.04. - 09.06.	test phase 1+2	24.7	26.1	5.6 %
NO_X	06.04. - 10.05.	test phase 1	117.9	77.2	-34.5 %
	11.05. - 09.06.	test phase 2	117.1	76.3	-34.9 %
	01.04. - 09.06.	test phase 1+2	117.2	76.1	-35.1 %

Results

As described above, the simulator module of IMMIS^{mt} offers the possibility to repeat stored calculations using the same input data but replacing the traffic data. This allows to determine the effects of traffic measures on the pollutant load while keeping all other conditions constant. In the following, the paper will focus on the results for test phase 2.

Figure 4 shows the effects of the traffic measures implemented for Altewiekring at the hot spot site. Vehicle intensity was reduced by 14 %. Traffic-induced emissions decreased even more, they were reduced by 17 %. The disproportionate decrease of traffic emissions compared to vehicle intensity is due to improved traffic flow with less stop&go-situations. In combination with the meteorological conditions prevailing during test phase 2, reduction of the additional pollutant

load due to traffic was calculated to 13 % (PM10) and 12 % (NO_X). This results in a decrease of total concentrations by 4 % (PM10) and 10 % (NOX).

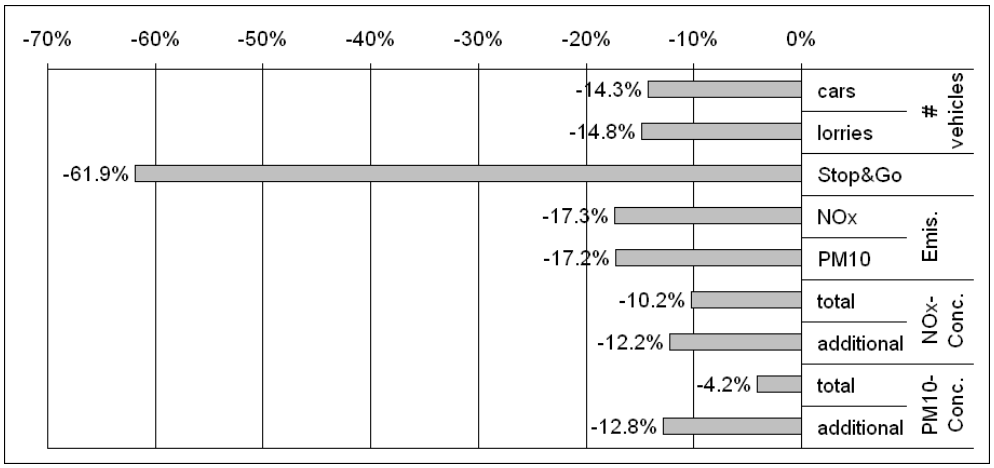

Figure 4: Effects of implemented measures on traffic load, traffic-induced emissions and pollutant load.

Figure 5 shows the differences of NO_X total concentration in the monitored street sections which result from implementing traffic measures for the hot spot site Altewiekring. The differences are calculated from modeling results for test phase 2 and from results for modeling test phase 2 with the traffic data replaced with data for the same period in the previous year when no traffic measures were applied. NO_X total concentration decreases by up to 14.4 µg/m³ and increases by up to 1.5 µg/m³. Relative differences between NO_X total concentration with and without traffic measures implemented vary between a reduction of 16 % and an increase of 6 %.

PM10 total concentration decreases by up to 2.2 µg/m³ and increases by up to 0.3 µg/m³. The relative differences of PM10 additional pollutant load due to traffic decrease by up to 16 % and increase by up to 20 %. The maximum increase of the additional pollutant load occurs in the street section representing Hamburger Straße. Due to the low fraction of the pollutant load with respect to the total concentration the relative differences of PM10 total concentration vary only between a reduction of 8.5 % and an increase of 1.9 %.

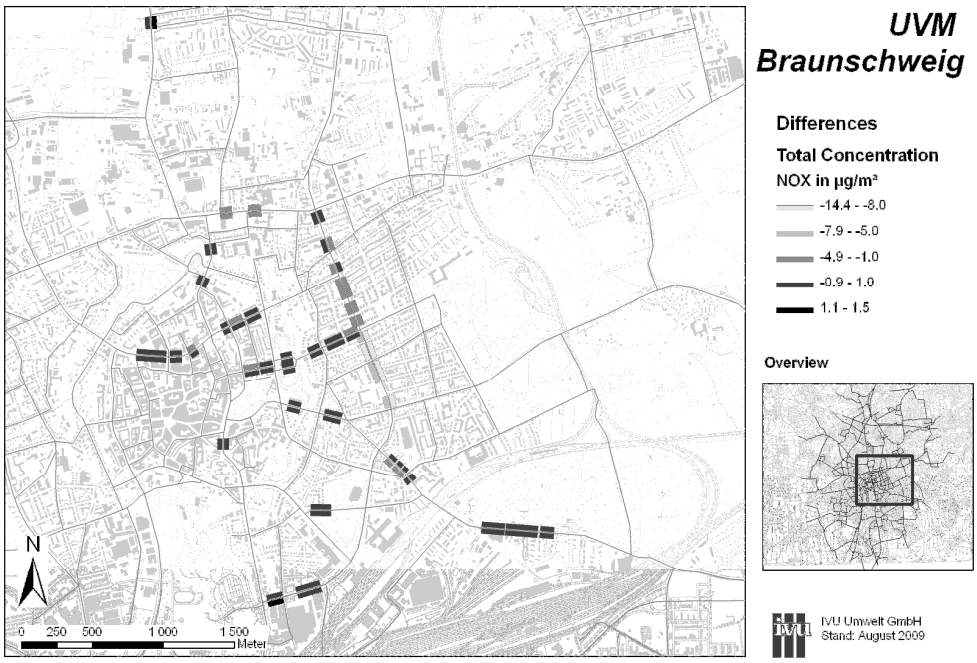

Figure 5: Effects of implemented measures on NO_X total concentration in street sections.

Conclusions

A model and data base supported monitoring system continuously controls the current traffic and air pollutant load. Hence, it allows to investigate the effects and effectiveness of traffic measures on air quality in urban areas while being much more cost-effective than measurements. Additionally, it offers the possibility to validate the implemented models and their input data.

Within the project "UVM Braunschweig", the implemented traffic measures reduced traffic at the hot spot site Altewiekring by 14 %. This induced a decrease of the calculated additional pollution load due to traffic by up to 13 % (PM10) and 12 % (NO_X). Considering the polluter fractions, this results in a decrease of total concentrations by 4 % (PM10) and 10 % (NOX). Side effects within the monitored street sections are mostly positive or neutral. However, impairment of air quality in a few street sections highlights the necessity of monitoring the pollutant situation within the relevant road network.

Validation of the model part of the monitoring system shows a significant underestimation of NO_X total concentration. This was attributed to the NO_X emissions factors of HBEFA 2.1 which had been the basis for emission modeling. Comparison with emission factors of HBEFA 3.1 for a mean traffic situation at the hot spot site showed an increase of NO_X emissions by 30 %.

Acknowledgements

This paper is an outcome of the joint project "UVM Umweltorientiertes Verkehrsmanagement Braunschweig". Project partners are BELLIS GmbH (Braunschweig), BLIC GmbH (Braunschweig), IVU Umwelt GmbH (Freiburg) and VMZ Berlin Betreibergesellschaft mbH. The project was founded by the German Federal Ministry of Transport, Building and Urban Development and supported by the Federal State of Lower Saxony and the City of Braunschweig.

References

Braunschweig (2007), Luftreinhalte- und Aktionsplan Braunschweig. Stadt Braunschweig. Erarbeitet durch das Niedersächsische Umweltministerium.

Diegmann, V., G. Gäßler (2009), Air Quality Management - From Traffic Management to Environmental Traffic Management. Abstracts of the 7th International Conference on Air Quality - Science and Application, March 24-27, 2009 in Istanbul, Turkey.

Düring I., A. Lohmeyer (2004), Modellierung nicht motorbedingter PM10-Emissionen von Straßen, in: Kommission Reinhaltung der Luft im VDI und DIN – Normenausschuss KRdL (eds): KRdL-Expertenforum Staub und Staubinhaltsstoffe, *KRdL-Schriftenreihe Band 33*, Düsseldorf.

EU (2008), *Directive 2008/50/EC of the European Parliament and of the Council of 21 May 2008 on Ambient Air Quality and Cleaner Air for Europe*, Official Journal of the European Union L 152.

INFRAS (2004), *Handbuch Emissionsfaktoren des Straßenverkehrs, HBEFA Version 2.1*, INFRAS, Bern, on behalf of UBA Berlin / BUWAL Bern / UBA Wien.

INFRAS (2010), *Handbuch Emissionsfaktoren des Straßenverkehrs. HBEFA Version 3.1.* Documentation in preparation, INFRAS, Bern.

IVU Umwelt (2008), *IMMIS$^{em/luft/lärm}$ Version 4.0 User's Guide*, IVU Umwelt GmbH.

IVU Umwelt. (2008b), *IMMIS^{net} – Handbook, Version 3.3*; IVU Umwelt GmbH; Freiburg, 2008 http://www.ivu-umwelt.de/upload/download/handbuecher/immisnet_arcgis_3.3_en.pdf).

Yamartino, R. J., G. Wiegand (1986), Development and Evaluation of Simple Models for the Flow, Turbulence and Pollutant Concentration Fields within an Urban Street Canyon, *Atmospheric Environment* Vol.20, No.11, pp 2137-2156

Impact of an Environmental Zone on Transport Emissions in the City of Graz

M. Rexeis[1], G. Röschel[2], S. Hausberger[1]*

[1] IVT, Institute for Internal Combustion Engines and Thermodynamics, Graz University of Technology, A-8010 Graz, Austria, rexeis@ivt.tugraz.at
[2] Sammer & Partner Consulting ltd. Graz, Vienna - Austria

Introduction

Due to frequent exceeding of the air quality limits for PM_{10} in the Greater area of Graz different measures for a reduction of PM_{10} emissions have been investigated and intensively discussed. One of the measures in the focus of politics is the implementation of an "Environmental zone" (EZ), which is an area with an all-season driving ban for vehicles with high specific emission levels. In Germany EZs have already been introduced in several cities.

In a study (Rexeis et al., 2009) for the Federal Government of Styria the impact of an environmental zone on transport emissions in the City of Graz was investigated by the Institute for Internal Combustion Engines and Thermodynamics, Graz University of Technology ("IVT") in collaboration with Sammer & Partner Consulting ltd. Graz ("ZIS+P"). Results from this study are presented in this paper.

Definition of the investigated measure

For the investigations the size and the location of the EZ have been provided by the Federal Government of Styria. In the study the affected area covers a portion of about 20% (26km²) of the Graz urban area in the south and west of the city centre and about 37% (95 000 people) of the Graz inhabitants.

The provisions for the restriction of access for the different vehicle technologies have been taken over from the according German legislation, which is already in force in cities like Berlin or Hannover since the year 2008. For the Graz case the final stage of the restrictions in the environmental zone was assumed to come into force in 2012 with the banishment of Diesel vehicles up to the emission standard Euro-3/III (years of construction approx. up to 2005) without PM-aftertreatment. Table 1 shows the definition of vehicle groups affected by driving bans inside the environmental zone in the different years.

Table 1: Vehicle groups affected by driving bans inside the environmental zone

2011	**from 2012 on**
gasoline without controlled 3-way catalyst diesel up to Euro-2 / II without PM aftertreatment	
	diesel Euro-2 / II with PM aftertreatment diesel Euro-3 / III without PM aftertreatment

Modelling approach

In the study in first step reference scenarios for traffic volumes and transport emissions without introduction of an EZ for the years 2011 and 2012 - in the following labelled as "Business As Usual" (BAU) scenarios – have been compiled. For the assessment of traffic volumes a traffic model for the Greater Graz area generated in VISUM software has been applied by ZIS+P. In particular for the depiction of the impact of the EZ regulation in the traffic model the transport demand was split into different kinds of traffic relations: "trips with source or target inside the EZ", "other trips within the Greater Graz area" and "transit traffic". These three types of traffic relations have been further classified into the groups "vehicles affected by driving bans" and "vehicles not affected by driving bans" as well as into "vehicles ≤ 3.5tons" and "vehicles > 3.5tons". So in total 12 subdivisions of traffic demand have been depicted in the traffic model.

The results of the traffic model were then used for the calculation of transport emissions with the model NEMO (Network Emission Model). This model has been developed at IVT with special focus on flexible and user friendly calculation of vehicle emissions in road networks. NEMO combines a detailed calculation of fleet composition and emission simulation, e.g. (Rexeis et al., 2008) and (Rexeis et al., 2005).

Share on vehicle stock affected by the driving ban

Figure 1 shows the shares on the vehicle stock according to the fleet-mix in the BAU scenario, which would be affected by the driving ban in 2011 and 2012. As information on the fleet-mix for the particular Graz case was not available from statistical data, NEMO results for the Austrian average fleet development were applied for the assessment of these numbers. In the year 2012 about one fourth of all passenger cars have been calculated to be affected by driving bans inside the zone. The majority of these vehicles would be diesel cars certified to the emission standards Euro-2 and Euro-3. In commercial transport the shares of banned vehicles would be even higher than for passenger cars due to the higher proportion of diesel vehicles. In 2012 approximately 40% of light commercial vehicles and nearly 50% of all HDV operated in local traffic would not be allowed to enter the EZ.

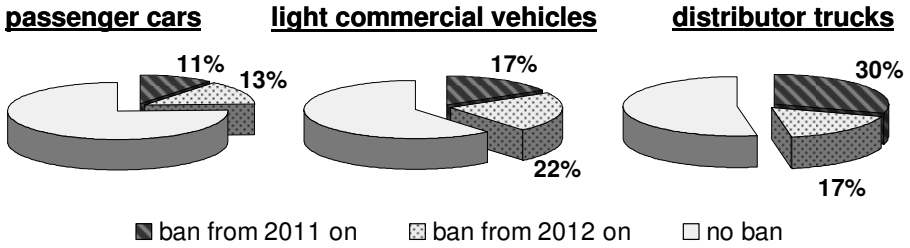

Figure 1: Shares of vehicle stock (according to the BAU scenario) affected by driving bans inside the EZ

In absolute numbers approximately 36 500 passenger cars would be directly affected by the EZ regulations, thereof about 15 000 cars owned by inhabitants of the EZ. For commercial vehicles (including busses) the total number of affected vehicles was assessed to be in the order of 5 000. In the above mentioned numbers potential grants of exception permissions to enter the EZ with a non-compliant vehicle (e.g. for socially disadvantaged people or for emergency vehicles) have not been considered.

Scenarios for reactions of affected vehicle owners

The introduction of a spatially limited EZ allows for a variety of possible reactions of the affected vehicle owners. Within the current study time and resources for a representative assessment of behaviour patterns based on opinion polls were not available. Hence in the study the scope of possible reactions has been depicted by different scenarios in order to reflect the range of uncertainties in the calculated effects. In the definitions of the scenarios it was distinguished between:

I. Scenarios for reactions related to choice of means of transport (e.g. purchase of a vehicle not restricted in the environmental zone, changeover to public transport, choice of alternative destinations outside the zone ….)

II. Scenarios for choice of vehicle technologies, which are purchased as a consequence of the environmental zone

As reference values for the parameterisation of these scenarios mainly data from Berlin have been analysed and transferred to Graz conditions. In Table 2 exemplarily the definitions of the scenarios for reactions related to choice of means of transport (owners of affected vehicles ≤ 3.5tons) differentiated by type of traffic relation are shown. Scenario A depicts a high number of changed or retrofitted vehicles in combination with a low number of granted exception permissions to enter the EZ with a non-compliant vehicle. Scenario B represents more disadvantageous assumtions regarding purchase of new or lower emitting vehicle technologies. In scenario A it is assumed that 62% of all trips with source or target inside the EZ, which are

performed with a non-compliant vehicle in the BAU scenario, are in case of an EZ performed with new purchased or retroffited vehicles. For 12% of the trips originally affected by the driving ban exeption permissions are estimated. The remaining shares of trips with non-compliant vehicles are allocated to reactions like change of transport mode (e.g. use of public transport) or choice of alternative destination ouside the EZ. However, also other trips within the Greater Graz area (with neither source or origin inside the EZ) are affected by the changed fleet composition due to the measure. It can be expected that also many vehicle owners, which only sometimes have to enter the EZ, will also change or retrofit their vehicle. As a consequence also the fleet composition outside the EZ can be expected to significantly differ to the BAU scenario. The number of trips ouside the EZ performed by changed vehicles compared to BAU was assumed to be higher in scenario A (50%) compared to scenario B (25%). The behaviour of the transit traffic was assumed to be not affected by the local EZ regulations.

Table 2: Scenarios for reactions of owners of affected vehicles ≤ 3.5tons differentiated by type of traffic relation

	trips with source or target inside the EZ		other trips within the Greater Graz area		transit traffic
	scenario A	scenario B	scenario A	scenario B	scenarios A and B
change of vehicle (including retrofit, if possible)	**62%**	**32%**	**50%**	**25%**	0%
obtains a exception permission to enter the EZ with a non-compliant vehicle	**12%**	**20%**	0%	0%	0%
no change compared to BAU	0%	0%	**50%**	**75%**	**100%**
change of transport mode at EZ border (non-compliant vehicle as far as the EZ border)	**9%**	**16%**	0%	0%	0%
change of transport mode	**9%**	**16%**	0%	0%	0%
change of destination to outside of the EZ	**9%**	**16%**	0%	0%	0%
sum of reactions	*100%*	*100%*	*100%*	*100%*	*100%*

Based on the assessment for changed travel demand and modal split the traffic model was applied to calculate the changed distribution of traffic volumes in the city road network in the different scenarios.

The results of the traffic model were then used for the calculation of transport emissions with NEMO. In the emission calculation then additionally the scenarios for purchased or retrofitted vehicle technology (according to scenario type II. on page 2) have been considered. In general retrofitting of PM aftertreatment systems gives a comparable small emission benefit, because such vehicles still show PM levels significantly higher than vehicles equipped with an OEM wall-flow particle filter or than gasoline vehicles. Furthermore the acquisition of new gasoline vehicles is more advantageous than the purchase of new diesel vehicles in terms of NO_x emission levels.

Results

The effects of the EZ in the two investigated years 2011 and 2012 have been determined by the difference of traffic volume and emissions in the BAU scenarios compared to the corresponding model results for the EZ scenarios. The total potential bandwidth in the effects originates from the combination of the margins in the different scenarios. The “most probable effect” of the EZ measure was assessed based on the average of the entire margin.

Figure 2 shows the calculated results for vehicle mileage. For the road network inside the EZ a slight decrease of driven vehicle kilometres was assessed (approx. -2% in 2011, -4% in 2012). This reduction can mainly be attributed to the omission of mileage of non-compliant vehicles, which are neither replaced nor obtain an exception permission. Outside the EZ a slight increase of mileage (approx. +0.5% in 2011, +1% in 2012) was calculated by the traffic model due to

bypass and relocation effects. The sum of mileage driven in the entire Greater Graz area (sum of “inside EZ” and “outside EZ”) was assessed to be nearly constant.

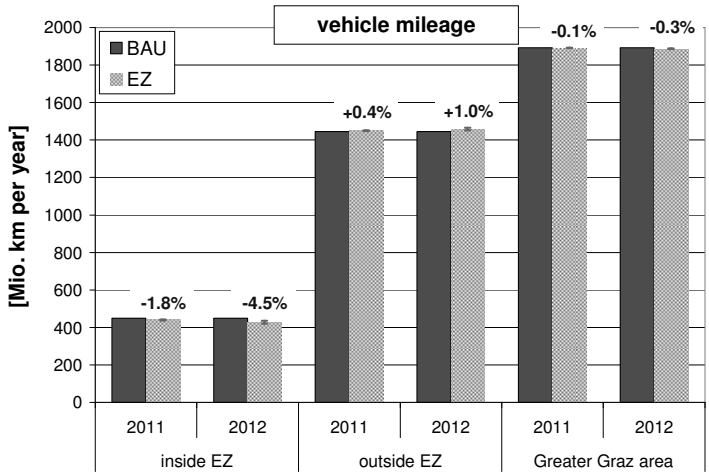

Figure 2: Calculated effects of the environmental zone (EZ) on vehicle mileage.

In Figure 3 the calculation results for particle emissions (PM_{10}) from vehicle exhaust are given. Inside the EZ for the first stage of the regulations in 2011 a reduction of approx. 25% was assessed. For 2012 a PM_{10} exhaust reduction of nearly 40% was simulated for the area inside the EZ. This improvement mainly results from the replacement of high emitting vehicles with new(er) vehicle technology and (to a less extend) from the reduction of mileage. The associated uncertainty in the results for the area inside the EZ is relatively small. Also for the road network outside the EZ a reduction of PM_{10} emissions from vehicle exhaust can be expected (the average reduction in the scenarios for 2012 is 8%). Here the positive effect of the lower emission levels overbalances the slight increase in vehicle mileage. However, the associated margin in the model results (for the year 2012: PM_{10} exhaust reductions between 2% and 16%) due to the uncertainties in the reactions of the affected vehicle owner has to be considered. For the entire area of Greater Graz the introduction of the EZ calculation was assessed to result in a PM_{10} exhaust reduction of about 11% in 2011 and 15% in 2012. This effect of the EZ in 2012 corresponds to a natural fleet renewal (without any measure) of 1.5 to 2 years.

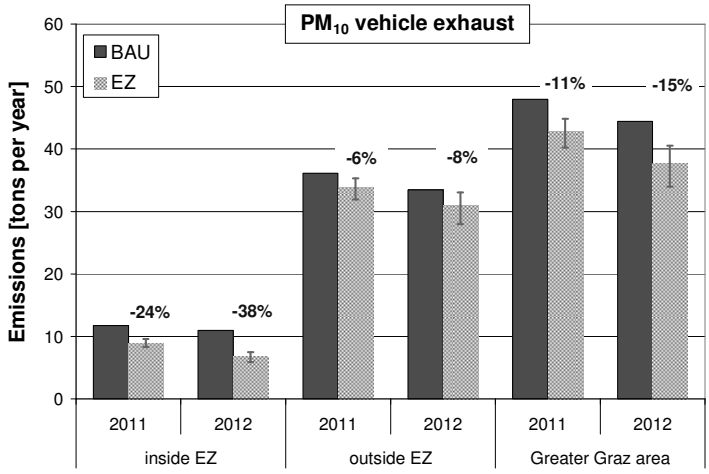

Figure 3: Calculated effects of the environmental zone (EZ) on PM_{10} from vehicle exhaust.

Figure 4 shows the assessment for total PM_{10} emissions from road traffic. This quantity is composed of particle emissions from vehicle exhaust and particles from abrasion and re-suspension processes (“non-exhaust”). The vehicle specific emissions levels related to PM non-exhaust can be regarded as independent from vehicle technology (old or new vehicle, gasoline or diesel engine) and hence can hardly be influenced by the EZ regulations. In the current study PM_{10} non-exhaust emission factors from (Düring et al., 2004) have been applied in the NEMO calculations. In the BAU scenarios the non-exhaust PM_{10} emissions have a share of about 75%

on the entire PM_{10} emissions from road traffic. Hence the effects of the EZ on total PM_{10} are significantly smaller than for PM from vehicle exhaust.

For the area inside the EZ a reduction of 8% (2011) and 14% (2012) for total PM_{10} emission from road traffic was calculated. Outside the EZ in both investigated years a slight reduction of total PM_{10} of about 1% can be expected. For the entire area of Greater Graz the assessment showed a reduction potential of 3% (2011) and 4% (2012). However, in the interpretation of model results for the road network outside the EZ and for the Greater Graz area the comparable large uncertainties in the assessment have to be kept in mind.

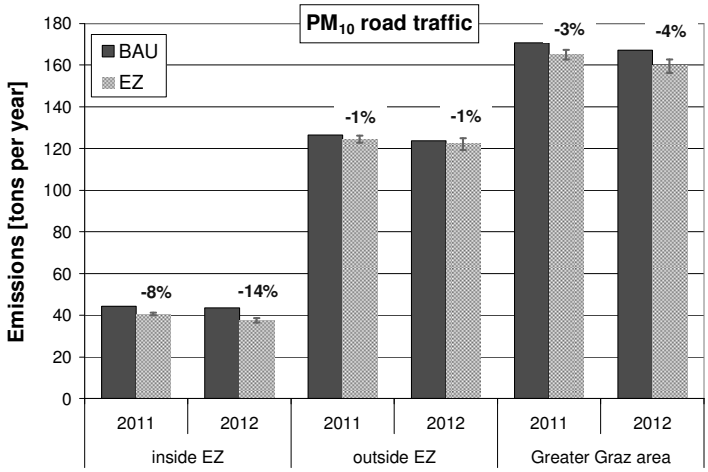

Figure 4: Calculated effects of the environmental zone (EZ) on total particle emissions from road traffic (PM_{10}).

In Figure 5 the calculated effects on NO_x emissions from road traffic are depicted. For NO_x it has to be considered, that especially for diesel passenger cars and light commercial vehicles the applied technological measures for a reduction of PM_{10} exhaust emissions bring only a small or no reduction of NO_x emissions. Only the replacement of diesel vehicles by gasoline propulsion results in a significant reduction of NO_x output. As a consequence, the effect of the EZ regulation on NO_x output are much smaller compared to PM_{10} exhaust. Inside the EZ a decrease of NO_x emissions by about 11% (2011) and 16% (2012) can be expected. Outside of the EZ area only a very small improvement was assessed (reduction of 3% in 2011 and of 1% in 2012). For the entire Greater area of Graz the implementation of the EZ was assessed to effect in a 5% reduction of NO_x from road traffic in both considered years.

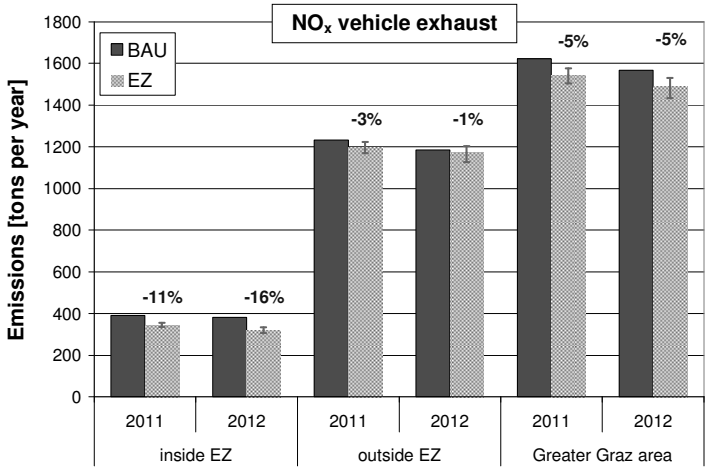

Figure 5: Calculated effects of the environmental zone (EZ) on NO_x emissions from road traffic.

Figure 6 shows the model results for tailpipe NO_2 emissions. Due to the known fact that current particle filter technology increases the share of NO_2 in the exhaust gas, the effects of the EZ on tailpipe NO_2 emissions are smaller compared to NO_x. Inside the EZ a small decrease in tailpipe

NO_2 was assessed (2% in 2011, 8% in 2012). Outside the EZ possibly even a small increase (+3% in 2012) has to be expected. Significant uncertainties in this context add the application of retrofit PM aftertreatment for heavy duty vehicles. Such systems can result in NO_2/NO_x shares between 10% and 60% (without any aftertreatment: approximately 7% NO_2/NO_x). As a consequence the impact of the EZ regulations on tailpipe NO_2 strongly depends on the definition of permitted retrofit filter systems.

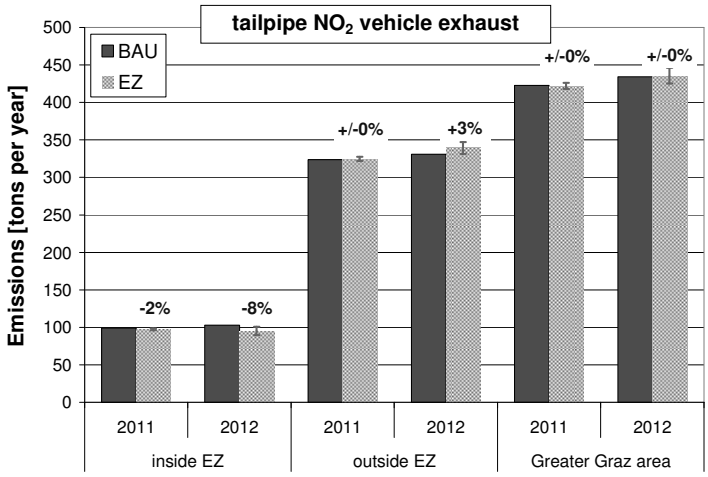

Figure 6: Calculated effects of the environmental zone (EZ) on tailpipe NO_2 emissions from road traffic.

Provided that the EZ regulations are not further tightened after the year 2012, the effects of the measure as defined in this study gradually decrease after 2012. In the mid of the next decade with or without measure nearly similar conditions for traffic volumes and emissions of road traffic can be expected due to the natural fleet renewal. If the positive effects of the analysed proposed EZ regulations in the city of Graz give a reasonable commensurability in relation to the burden for population and economy has to be judged by politics.

References

Düring I. et al. (2004). Berechnung der Kfz-bedingten Feinstaubemissionen infolge Aufwirbelung und Abrieb für den Emissionskataster Sachsen, Endbericht

Rexeis M., G. Röschel , S. Hausberger (2009), Auswirkung der Umweltzone „Variante 3“ auf Verkehrsaufkommen und KFZ-Emissionen im Sanierungsgebiet Großraum Graz, Bericht Nr. I-19/09/Rex Em 23/09/679

Rexeis M., S. Hausberger (2005), Calculation of Vehicle Emissions in Road Networks with the model “NEMO”; *Proceedings of the Transport&Airpollution Conference 2005*, 118-127, ISBN: 3-902465-16-6

Rexeis, M., S. Hausberger (2008), Trend of vehicle emission levels until 2020 – Prognosis based on current vehicle measurements and future emission legislation, Atmospheric Environment (2008), doi:10.1016/j.atmosenv.2008.09.034

Estimating the effect of on-road vehicle emission controls on future air quality in Paris, France

Y. Roustan[1], M. Pausader[1] and C. Seigneur[1]*

[1] CEREA, Joint Laboratory Ecole des Ponts ParisTech - EDF R&D, Université Paris-Est, 6-8 avenue Blaise Pascal, Cité Descartes Champs-sur-Marne 77455, France, roustan@cerea.enpc.fr

Introduction

The contribution of road traffic to air pollution in the Paris region, France, has been estimated to be significant (Zmirou et al., 2004; AIRPARIF, 2004; DRIRE, 2006; Nedellec et al., 2010). NO_x concentrations have decreased by about half from 1994 to 2008 whereas NO_2 concentrations have remained about constant. O_3 concentrations are variable from year to year but are fairly stationary since 2001 (36 $\pm$ 2 µg/m^3). Concentrations of $PM_{2.5}$ do not show a significant decrease from 2000 to 2007 with ambient concentrations remaining at 14 µg/m^3 in 2007 (AIRPARIF, 2010).

It is, therefore, of interest to understand how the implementation of planned emission control technology for on-road vehicles will affect the concentrations of air pollutants in future years. In particular, it is essential to understand whether the use of diesel particle filters (DPF) will have any adverse effects on the concentrations of NO_2 and other pollutants. Previous studies have shown that NO_2 concentrations in several European urban areas did not decrease although NO_x emissions had decreased (e.g., Carslaw, 2005). One proposed reason is that the NO_2 fraction in NO_x emissions is greater with the installation of a diesel particle filter because the catalytic device that oxidizes the organic compounds also oxidizes nitrogen compounds and some of the NO is converted to NO_2. As a result, NO_2 emissions from vehicles equipped with the early diesel particle filters are about 50% of NO_x emissions, whereas the NO_2 fraction of NO_x emissions from standard diesel or gasoline vehicles are on the order of 11% and 3-4%, respectively (e.g., Shorter et al., 2005; Kousoulidou et al., 2008). Another possible reason is that a decrease in NO_x emissions in an urban area, where ozone formation may be VOC-sensitive, may lead to an increase or little change in ozone concentrations (Pun et al., 2003; Sillman et al., 2003; Zhang et al., 2005). Since secondary NO_2 is formed by reaction of NO with ozone, the amount of NO_2 formed will be limited by ozone concentrations in areas where NO concentrations are greater than O_3 concentrations, and stationary O_3 concentrations will lead to stationary secondary NO_2 concentrations. Furthermore, changes in NO_x concentrations are likely to affect particulate nitrate concentrations directly (via a change in the precursors NO_x species) and indirectly (via a change in the oxidant levels). The effect on $PM_{2.5}$ concentrations of the decrease in primary PM emissions due to the installation of particle filters in new vehicles will not be proportional because of lower or little change in the secondary fraction of PM. Finally, future vehicle emission controls will lead to changes in VOC emissions. Decreases in VOC emissions are anticipated to lead to decreases in ozone concentrations, but a joint decrease in NO_x emissions may lead to a compensating effect and, as a result, little change in ozone concentrations. Clearly, such changes in vehicle emissions will have variable effects on air pollutant concentrations depending on the meteorology and chemical regime of the ambient atmosphere. Consequently, it is essential to investigate such effects over a wide variety of atmospheric conditions (e.g., an entire year).

We present here a modeling study of the effect of the future evolution of traffic emissions on air quality in the Paris region. We first describe the base model simulation and the method used to generate future emission scenarios. Next, we discuss the results of future year simulations. We address in particular NO_2, O_3 and $PM_{2.5}$ concentrations.

Methodology

The model simulations were conducted with POLAIR3D, an Eulerian tridimensional chemical-transport model (CTM) of the POLYPHEMUS modeling platform (Mallet et al., 2007) for the year 2005. The chemical mechanism RACM (Stockwell et al., 1997) is used to represent the chemical reactions between gaseous species with photolysis rates computed by the preprocessors FAST-JX (Wild et al. 2000). These models are used jointly with the SIREAM model (Debry et al., 2007) to represent the aerosol size distribution.

The simulations were conducted using two nested grids: the outer grid covers Europe with a horizontal grid spacing of 0.5° (i.e., anout 50 km) and five levels from the ground up to about 3 km; the inner grid covers the Paris region with a grid spacing of 0.05° (i.e., about 5 km) and 10 levels from the ground up to about 3 km (see Figure 1). The nesting is one-way. The boundary conditions of the continental simulation are derived from simulation results for the year 2005 of the LMDz-INCA global model (Guibert et al., 2005). The meteorology for the European domain was obtained from the European Centre for Medium-range Weather Forecasting (ECMWF, 0.36°, 60 vertical levels, time step of 3 hours). For the Paris region, the meteorology was simulated with the mesoscale meteorological model MM5 (Grell et al., 1994) using analysis nudging (4 km^2, 29 levels, time step of 3 hours).

The emission inventory for the European domain and the outer part of the regional domain was obtained from EMEP for 2005 (Vestreng et al., 2007) with an approximative horizontal resolution of 50 km^2. The emission inventory for the Paris region was obtained from the Paris air quality agency for 2000 for the traffic sector (AIRPARIF, 2004) and 2005 for other sectors with an approximative horizontal resolution of 1 km^2. All emissions databases are organised following the Selected Nomenclature for Air Pollution (SNAP). The traffic sector is disaggregated to the SNAP level 3 in the 2000 inventory, but not in the 2005 one, which was mandatory for this study. Temporal (GENEMIS project; Airparif) and vertical (Simpson et al., 2003; Airparif) distributions are applied by activity sectors to reach a one hour resolution and split the emissions among the different simulation levels. Natural biogenic (Simpson et al., 1999) and sea-salt emissions (Monahan et al., 1986) are also considered when relevant.

Emission scenarios

Since we focus here on the effect of vehicle emissions in the Paris region on future air quality in that area, all other emissions, boundary conditions and meteorology were kept constant in the model simulations. The development of a future emission inventory for on-road vehicles requires extrapolating both the vehicle fleet and the emission factors of the components of that fleet to a future year. It takes several years for the fleet to be renewed. To estimate the fleet in a given year, one can use the license plate registration database from previous years and estimate the fraction for each registration year and each vehicle class that is still in operation. The methodology of Lacour and Joumard (2002) was used here to estimate the evolution of the vehicle fleet and project it to 2005, 2010 and 2020. The evolution of the number of vehicle registrations in the Paris region is presented in Figure 1, the fraction of diesel vehicles has clearly increased from 1980 to 2008.

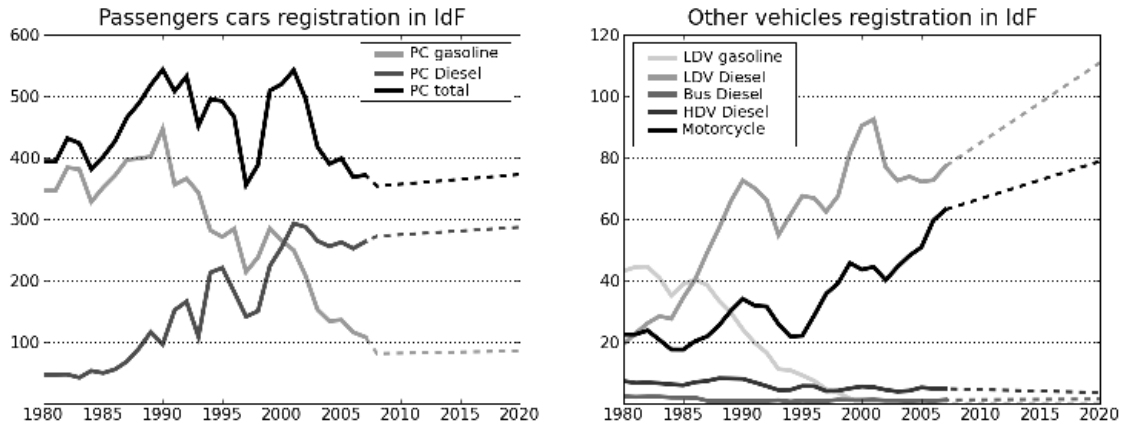

Figure 1: Temporal evolution of vehicle registration in the Paris region - source CGDD - SOeS (plain) and projection (dashed).

The emission factors are defined by vehicle class and we used the evolution of the vehicle fleet to estimate the overall evolution of the on-road vehicle emission inventory. Emission factors aggregated by class for France (Hugrel and Joumard, 2006) were used for NO_x, CO, NMVOC, PM, NH_3 and SO_x emissions. We assumed that no change occurred in the traffic patterns of a given class of vehicles. Therefore, the only changes governing the evolution of the emission inventory were the evolution of the fleet (and the use of class-specific emission factors) and the increase in the number of operating vehicles. At the European scale, the disaggregation of the

emissions of the inventory species among the CTM species is made following Passant (2002) for VOC and Simpson et al. (2003) for NO_x, PM and SO_x. At regional scale the disaggregation is made for NO_x and NMVOC following, respectively, Kousoulidou et al. (2008) and the GENEMIS project.

Figure 2 shows the evolution of NO_x and NO_2 emissions from 2000 to 2020 by vehicle category as well as for the total fleet. It appears clearly that NO_2 emissions for light-duty diesel trucks and private diesel vehicles increase until about 2010 as the first generation of diesel particle filters leads to greater NO_2 emissions, and decrease thereafter once the technology introduced in 2010 and 2015, which decreases NO_x emissions sufficiently due to the Euro 5 and 6 emission standards, starts to penetrate the overall diesel fleet. A first sensitivity scenario, in which we consider a constant NO_2/NO_x ratio, is introduced to study the impact of the evolution of the NO_x speciation.

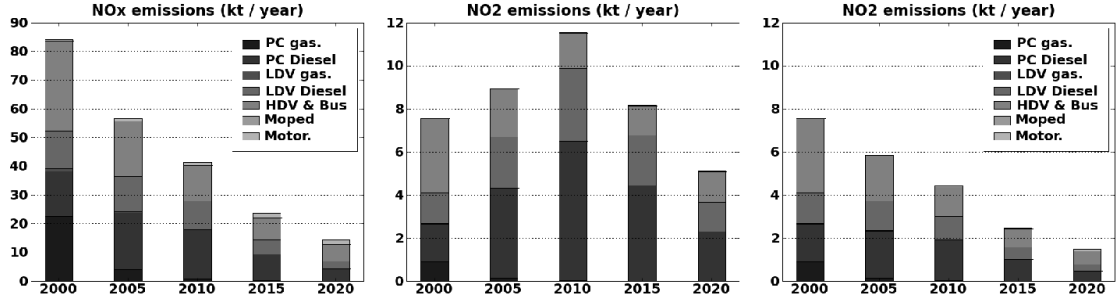

Figure 2: Temporal evolution of NO_x emissions from the traffic sector (left), NO_2 emissions for the reference scenario (center) and for the first sensitivity scenario (right).

Figure 3 shows the evolution of PM and NMVOC emissions over the same period. The implementation of diesel particle filters on private vehicles leads to a constant decrease in PM emissions as the new vehicles penetrate the diesel fleet. Overall, PM emissions decrease by nearly 90% from 2005 to 2020. The evolution of VOC emissions shown in Figure 4 shows decreasing trends for nearly all vehicle classes except passenger diesel vehicles which show a slight increase in the first ten years and motorcycles which show a slight increase in the last ten years. VOC emissions from diesel vehicles remain small compared to those from gasoline vehicles and the overall decrease in VOC emissions from 2005 to 2020 is significant (>30%). A second sensitivity scenario, in which we consider a constant NMVOC aggregated emission factor from 2005 to 2020 is introduced to study the impact of the decrease of the NMVOC emissions.

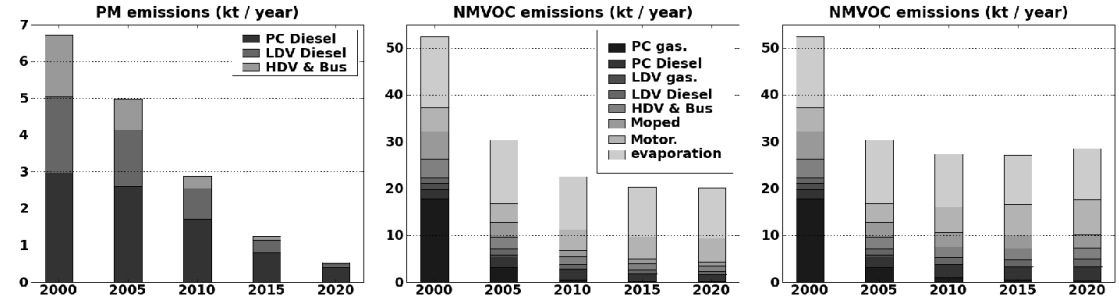

Figure 3: Temporal evolution of PM emissions (left), NMVOC emissions for the reference scenario (center) and for the second sensitivity scenario (right) for the traffic sector.

When considering other emission categories (industrial emissions, residential sources, biogenic sources, other mobile sources), there is still a significant decrease in NO_x (38%) and $PM_{2.5}$ (32%) emissions between 2005 and 2020. The decrease is relatively modest for NMVOC (7%).

Results

Model performance over the European domain was evaluated with ambient concentration data from the EMEP monitoring network. Model performance over the Paris region was evaluated here using data from the French air quality database (“Base de données de qualité de l’air”, BDQA, http://www.atmonet.org/). Model performance results are presented in Table 1 for O_3,

NO_2, PM_{10} and $PM_{2.5}$. Model performance is satisfactory compared to previous studies (e.g., Russell and Dennis, 2000; Seigneur et al., 2000; van Loon et al., 2007; Russell, 2008).

Table 1: Statistics over the whole year of comparison of simulation results at European and regional scales to the observations from the EMEP and BDQA networks: number of stations used to compute the statistics (N_s), observed mean (µg/m³), modeled mean (µg/m³), root mean square error (µg/m³) and temporal correlation (%).

	European domain					Regional domain				
Species	Ns	Obs.	Mod.	RMSE	Corr.	Ns	Obs.	Mod.	RMSE	Corr.
O_3 (hourly)	*78*	63.7	59.0	23.6	61.8	*40*	44.4	48.9	21.4	75.1
NO_2 (hourly)	*20*	8.1	5.8	9.0	29.1	*41*	32.1	24.4	18.9	53.7
PM_{10} (daily)	*23*	18.2	21.1	15.0	42.6	*23*	18.8	22.8	9.8	50.1
$PM_{2.5}$ (daily)	*17*	11.8	16.1	11.3	45.8	*6*	13.3	20.3	10.0	61.2

Model simulation results are presented in Figure 4 for the ozone season (April to September). For ozone, we present the average over that period of the daily maximum 8-hour average O_3 concentrations. Ozone concentrations increase from 2005 to 2020 in downtown Paris but start to decrease in the suburban areas. The increase in the central part of the region is due to the fact that the decrease in NO emissions (which leads to less titration of ozone) has a stronger effect than the decrease in VOC emissions. However, the decrease in VOC emissions is effective outside the central part of the domain, in suburban areas where the highest ozone concentrations are simulated.The consideration of the sensitivity scenarii for the year 2010 shows that the increase of ozone concentrations in downtown Paris would be less if the speciation of NO_x emissions would not change between 2010 and 2005. In this situation, the titration of ozone by NO would be more important. On the opposite, a lower decrease of the NMVOC emissions would lead to a larger increase of O_3 concentrations.

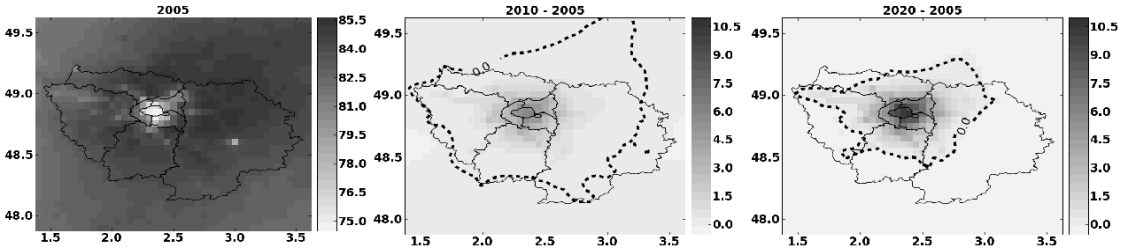

Figure 4: Daily maximum 8-hour average O_3 concentrations (in µg/m³) for 2005 (left) and absolute difference between 2010 and 2005 (center) and between 2020 and 2005 (right).

Results for NO_2 are presented in Figure 5; they correspond to the average over 2005 of the daily maximum 1-hour average NO_2 concentrations. NO_2 concentrations increase in downtown Paris beetween 2005 and 2010 but decrease in the suburban areas. They decrease everywhere in the simulation domain between 2005 and 2020. In 2010 the increase is due to the increase of emissions and then of primary NO_2 concentrations. The decrease in the suburb is due to the overall decrease of NO_x emissions, which leads to a decrease in secondary NO_2 formation. In 2020 both primary and secondary NO_2 concentrations decrease in the whole domain due to the strong decrease of NO_x emissions.

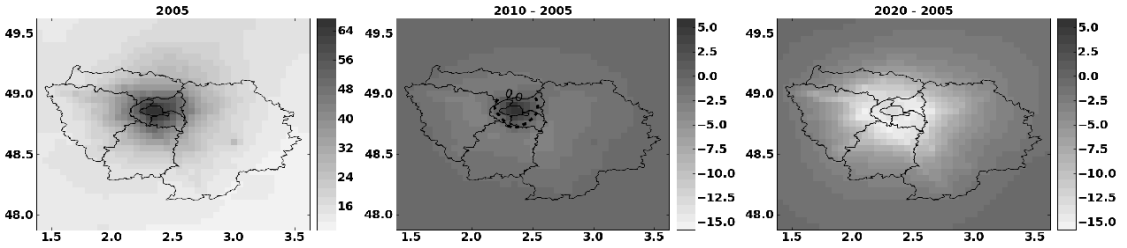

Figure 5: Daily maximum NO_2 concentrations (in µg/m³) for 2005 (left) and absolute difference between 2010 and 2005 (center) and between 2020 and 2005 (right).

The scenario on the speciation of NO_x emissions shows that the increase of NO_2 concentrations in downtown Paris does not occur in the case of a constant NO_2/NO_x ratio from 2005 to 2010.

Results for $PM_{2.5}$ are presented in Figure 6. $PM_{2.5}$ and PM_{10} concentrations decrease but the decrease is less than that of the PM emissions. The two main contributing factors to this less-than-proportional decrease in PM concentrations are (1) the effect of the boundary conditions and (2) the effect of secondary PM. In the absence of precipitation, fine particles have an atmospheric lifetime of several days and the boundary conditions have, therefore, a significant

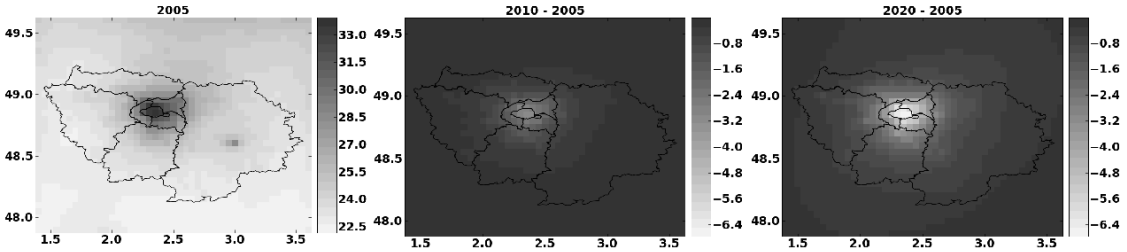

effect on PM concentrations within the inner domain of the Paris region.

Figure 6: Daily maximum $PM_{2.5}$ concentrations (in µg/m³) for 2005 (left) and absolute difference between 2010 and 2005 (center) and between 2020 and 2005 (right).

Conclusion

This modeling study of the impact of on-road vehicle emissions controls on future air quality in the Paris region addresses O_3, NO_2 and PM. The simulation results show different behaviours for these pollutants. For O_3, due to a stronger overall decrease of NO_x emissions than NMVOC emissions, we expect an increase of concentrations in dense urban area and a small decrease in suburban and rural areas. The increase in Paris downtown would be less in the case of a constant NO_2/NO_x ratio of the traffic emissions. For NO_2, the increase of emissions in downtown Paris leads to an increase of concentrations in this area in 2010. The overall decrease of NO_x emissions, however, leads to a decrease of NO_2 concentrations in the suburbs. This situation extends to the whole domain in 2020. The reduction of PM emissions leads to a non-proportionnal decrease of PM concentrations. The study results rely on several assumptions and include uncertainties concerning the projection of the traffic emission inventory (as for instance the ratio of Diesel passenger cars or the speciation of NO_x emissions in the future year). It would be interresting to complete this study with a sensitivity analysis concerning these assumptions. Moreover, in this study, we focused on the effect of the evolution of on-road vehicle emissions, a complete prospective study should include consideration of the evolution of emissions of the other activity sectors.

References

AIRPARIF (2004), Évaluation de la qualité de l'air en Île-de-France à l'échéance 2010 et impact du Plan de Protection de l'Atmosphère, AIRPARIF, Paris, France, http://www.airparif.asso.fr/airparif/pdf/Rppa.pdf.

AIRPARIF (2010), La qualité de l'air en Île-de-France en 2009, AIRPARIF, Paris, France, http://www.airparif.asso.fr/airparif/pdf/bilan_2009_100218.pdf.

Carslaw D. (2005), Evidence of an increasing NO_2/NO_X emissions ratio from road traffic emissions, *Atmospheric Environment*, 39, 4793-4802.

Debry E., K. Fahey, K. Sartelet, B. Sportisse, M. Tombette (2007), Technical Note: A new SIze REsolved Aerosol Model (SIREAM), *Atmosperic Chemistry and Physics*, 7, 1537-1547.

DRIRE, 2006. Plan de Protection de l'Atmosphère, rapport final, Direction régionale de l'industrie, de la recherche et de l'environnement de l'Île-de-France, Paris, France, http://www.ile-de-france.drire.gouv.fr/.

Grell G.A., J. Dudhia, D.R. Stauffer (1994), A description of the fifth generation Penn State/NCAR mesoscale model (MM5), NCAR Technical Note NCAR/TN-398 + STR, National Center for Atmospheric Research, Boulder, CO.

Guibert S., V. Matthias, Schulz M., Bosenberg J., Eixmann R., Mattis I., Pappalardo G., Perrone M.R., Spinelli N., Vaughan G. (2005), The vertical distribution of aerosol over Europe—synthesis of one year of EARLINET aerosol lidar measurements and aerosol transport modeling with LMDzT-INCA, *Atmospheric Environment*, 39, 2933–2943.

Hugrel C., R. Joumard (2006), Directives et facteurs agrégés d'émission des véhicules routiers en France de 1970 à 2025, INRETS, LTE - report 0611.

Kousoulidou M., L. Ntziachristos, G. Mellios, Z. Samaras (2008), Road-transport emissions projections to 2020 in European urban environments, *Atmospheric Environment*, 42, 7465-7475.

Lacour S., R. Joumard (2002), Parc, usage et émissions des véhicules routiers en france de 1970 à 2020, INRETS, LTE - report 0208.

van Loon M., R. Vautard, M. Schaap, R. Bergström, B. Bessagnet, J. Brandt, P.J.H. Builtjes, J.H. Christensen, C. Cuvelier, A. Graff, J.E. Jonson, M. Krol, J. Langner, P. Roberts, L. Rouil, R. Stern, L. Tarrason, P. Thunis, E. Vignati, L. White, P. Wind (2007), Evaluation of long-term ozone simulations from seven regional air quality models and their ensemble, *Atmospheric Environment*, 41, 2083-2097.

Mallet V., D. Quélo, B. Sportisse, M. Ahmed de Biasi, E. Debry, I. Korsakissok, L. Wu, Y. Roustan, K. Sartelet, M. Tombette, H. Foudhil (2007), Technical note : The air qulaity modeling system Polyphemus, *Atmospheric Chem istry and Physics*, 7, 5479-5487.

Monahan E., D. Spiel, K. Davidson (1986), A model of marine aerosol generation via whitecaps and wave disruption, *Oceanic Whitecaps*, D. Reidel, Dordrecht, 167-174.

Nedellec V., R. Lagache, B. Guillaume, C. Liousse, N. Jeannée, L. Mosqueron, H. Desqueyrous (2010), Effets des normes EURO IV et V sur la réductioin des impacts sanitaires du trafic routier urbain en France, *Environnement Risques & Santé*, 9, 39-50.

Passant N. (2002), Speciation of UK emissions of NMVOC, AEA Technology, AEAT/ENV/0545.

Pun B.K., C. Seigneur and W. White (2003), Day-of-the-week behavior of atmospheric ozone in three United States cities, *Journal of the Air & Waste Management Association*, 53, 789-801.

Russell A.G., R. Dennis (2000), NARSTO critical review of photochemical models and modeling, *Atmosperic Environment*, 34, 2283-2324.

Russell, A.G. (2008), EPA Supersites Program-related emissions-based particulate matter modeling: Initial applications and advances, *Journal of the Air & Waste Management Association*, 58, 289-302.

Seigneur C., B. Pun, P. Pai, J. F. Louis, P. Solomon, C. Emery, R. Morris, M. Zahniser, D. Worsnop, P. Koutrakis, W. White and I. Tombach (2000), Guidance for the performance evaluation of three-dimensional air quality modeling systems for particulate matter and visibility, *Journal of the Air & Waste Management Association*, 50, 588-599.

Seinfeld J.H., S.N. Pandis (1998), *Atmospheric Chemistry and Physics, Wiley-interscience*.

Shorter J.H., S. Herndon, M.S. Zahniser, D.D. Nelson, J. Wormhoudt, K.L. Demerjian, C.E. Kolb (2005), Real-time measurements of nitrogen oxide emissions from in-use New York City Transit buses using a chase vehicle, *Environmental Science & Technology*, 39, 7991-8000.

Sillman S., R. Vautard, L. Menut, D. Kley (2003), O3-NOx-VOC sensitivity and NOx-VOC indicators in Paris: Results from models and atmospheric pollution over the Paris area (ESQUIF) measurement, *Journal of Geophysical Research*, 108, doi:10.1029/2002JD001561.

Simpson D., W. Winiwarter, G. Brjesson, S. Cinderby, A. Ferreiro, A. Guenther, C. Hewitt, R. Janson, M. Khalil, S. Owen, T. Pierce, H. Puxbaum, M. Shearer, U. Skiba, R. Steinbrecher, L. Tarrason, M. Oquist (1999), Inventorying emissions from nature in Europe, *Journal of Geophysical Research*, 104, 8113-8152.

Simpson, D., H. Fagerli, J.E. Jonson, S. Tsyro, P. Wind, J.P. Tuovinen (2003), Transboundary Acidification, Eutrophication and Ground Level Ozone in Europe, *Part I. Unified EMEP Model Description,* EMEP/MSC-W Status report 1/2003.

Stockwell W., F. Kirchner, M. Kuhn, S. Seefeld (1997), A new mechanism for regional atmospheric chemistry modeling, *Journal of Geophysical. Research*., 102, 25847-25879.

Vestreng V., K. Mareckova, S. Kakareka, A. Malchykhina, T. Kukharchyk (2007), Inventory Report 2007, Emission data reported to LRTAP Convention and NEC Directive.

Wild O., X. Zhu, M.J. Prather (2000), Fast-J: Accurate Simulation of In- and Below-Cloud Photolysis in Tropospheric Chemical Models, *Journal of Atmospheric Chemistry*, 37, 245-282.

Zhang Y., K. Vijayaraghavan, C. Seigneur (2005), Evaluation of three probing techniques in a three-dimensional air quality model, *Journal of Geophysical Research*, 110, doi:10.1029/2004JD005248.

Zmirou D., S. Gauvin, I. Pin, I. Momas, F. Sahraoui, J. Just, Y. Le Moullec, F. Brémont, S. Cassadou, P. Reungoat, M. Albertini, N. Lauvergne, M. Chiron, A. Labbé (2004), Traffic related air pollution and incidence of childhood asthma: results of the Vesta case-control study, *Journal of Epidemiology & Community Health*, 58, 18-23.

Analysis of the Impacts of an Environmental Traffic Management System on Vehicle Emissions and Air Quality

L. Neunhäuserer[1] and V. Diegmann[1]*

[1] IVU Umwelt GmbH, 79110 Freiburg, Germany, lina.neunhaeuserer@ivu-umwelt.de

Introduction

Environmental traffic management systems (ETMS) are implemented to improve air quality in urban streets. They allow for a situation-related control of light signal systems to optimise road capacities and enhance traffic flow in street sections. Therefore, they are equipped with mitigation strategies and continuously provided with traffic and air quality data. In this context, it is usually presumed that improving the traffic flow results in lower vehicle emissions and thus in lower pollutant concentrations, provided that the vehicle intensity does not change.

In order to verify this assumption and to quantify potential effects, a test case has been set up in Cologne, Germany. The Cologne clean air plan 2006 reports NO_2 limit value exceedances at several monitoring stations and pollutant concentrations close to the limit values throughout the inner city. A low emission zone has been established for Cologne on January 1st, 2008, as a first step to improve air quality. Additionally, it is planned to install an ETMS for two heavily trafficked areas of Cologne. One of the two areas was chosen as a test case for which modelling was carried out in advance to assess the impacts of the ETMS on traffic-induced emissions and air quality. This paper describes the modelling procedure and discusses the outcome.

The test case

The test case was set up for Clevischer Ring in Cologne-Mülheim, 4 km north east of the Cologne Main Station. An air quality monitoring station is located in this part of Clevischer Ring, in a typical street canyon with buildings on both sides. Four traffic scenarios were modelled, a base scenario and three ETMS scenarios:

1) Base Scenario: typical hour with maximum traffic load, based on measured traffic data

2) Scenario 1: improved, traffic-dependent control and coordination of light signal systems

3) Scenario 2: scenario 1 plus gatekeeping at the southern, northern and western inlet

4) Scenario 3: scenario 2 plus restriction of existing public transport priority

The impact of the different scenarios on air quality was analysed for meteorological conditions under which the pollutant load resulting from vehicles was expected to be high and therefore potentially harmful. Considered pollutants were NO_X/NO_2 and PM10. In the following, this paper will focus on the NO_X/NO_2 results for the Base Scenario and Scenario 2 for the street section where the monitoring station Clevischer Ring is located.

Modelling

Modelling was carried out in four steps. First, the traffic data for the four scenarios was calculated. Then, the corresponding emissions for the hour with maximum traffic load were determined. Next, dispersion of the pollutants was modelled, based on the calculated emission data and on meteorological data for which the maximum additional pollutant load from traffic was to be expected. Finally, the decrease of the NO_2 annual mean concentration at the monitoring station Clevischer Ring was assessed based on the modelling results. In each step, the impact of the ETMS scenarios was analysed.

Traffic data for the four scenarios was modelled by project partner SIEMENS with VISSIM, a highly detailed microscopic simulation program for multi-modal traffic flow modelling. Figure 1 shows the considered road network which was divided into 11 street sections. Each street

section was defined to be located between two light signals. To capture the dynamics within the street sections, three cross sections were assigned to each of them for which traffic data was to be calculated.

VISSIM simulations were then run for each scenario for the hour with maximum traffic load. As the result, VISSIM provided for each direction of traffic time series of fleet composition, vehicle intensity, mean velocity and mean acceleration for each cross section as well as congestion data. The temporal resolution of all time series was 60 s.

Finally, for each street section the VISSIM traffic data of the respective cross sections was evaluated statistically to gain mean hourly values of fleet composition and velocity as well as the standard deviation of velocity.

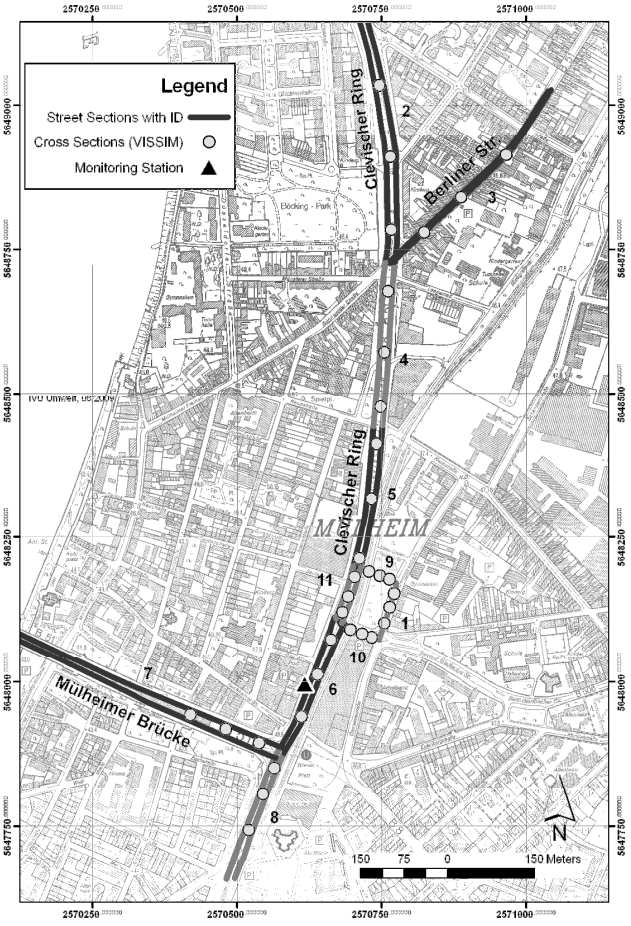

Figure 1: Modelled road network Clevischer Ring with street sections and cross sections.

Table 1 gives exemplarily the traffic data derived from VISSIM results for the Base Scenario and Scenario 2 for street section 6 where the air quality monitoring station is located. For the Base Scenario, the mean velocity of the northbound traffic is only half the mean velocity of the southbound traffic while the standard deviation is nearly twice as much. Applying Scenario 2 obviously improves the traffic flow, as the vehicle intensity increases in both directions compared to the Base Scenario. The mean velocity increases significantly for the northbound traffic and slightly for the southbound traffic while the standard deviation decreases. Scenario 1 and 3 are not shown here as traffic data results differ only slightly from Scenario 2.

The corresponding histograms of mean velocity in Figure 2 show graphically the findings given above. The histogram of northbound Base Scenario street section 6 exhibits a significantly broader and flatter distribution with its center at lower velocities than the southbound histogram. Scenario 2 shifts the distribution of both directions, but mainly of direction North, to higher velocities.

Other street sections, but not all, show a similar behaviour, as will be discussed for the emission data results (Figure 3).

Table 1: Traffic data evaluated statistically from VISSIM results, hour with maximum traffic load for street section 6, Base Scenario and Scenario 2

		Vehicles	Fractions		Velocity (km/h)		
	ID	(veh/h)	HDV	LDV	Bus	Mean	Std. Dev.
Base Scenario	6North	1804	5.0 %	5.5 %	0.2 %	23.7	2.0
	6South	1745	5.0 %	5.5 %	0.1 %	44.2	1.2
Scenario 2	6North	1820	5.2 %	5.3 %	0.2 %	41.9	1.1
	6South	1828	5.1 %	5.3 %	0.2 %	46.0	0.3

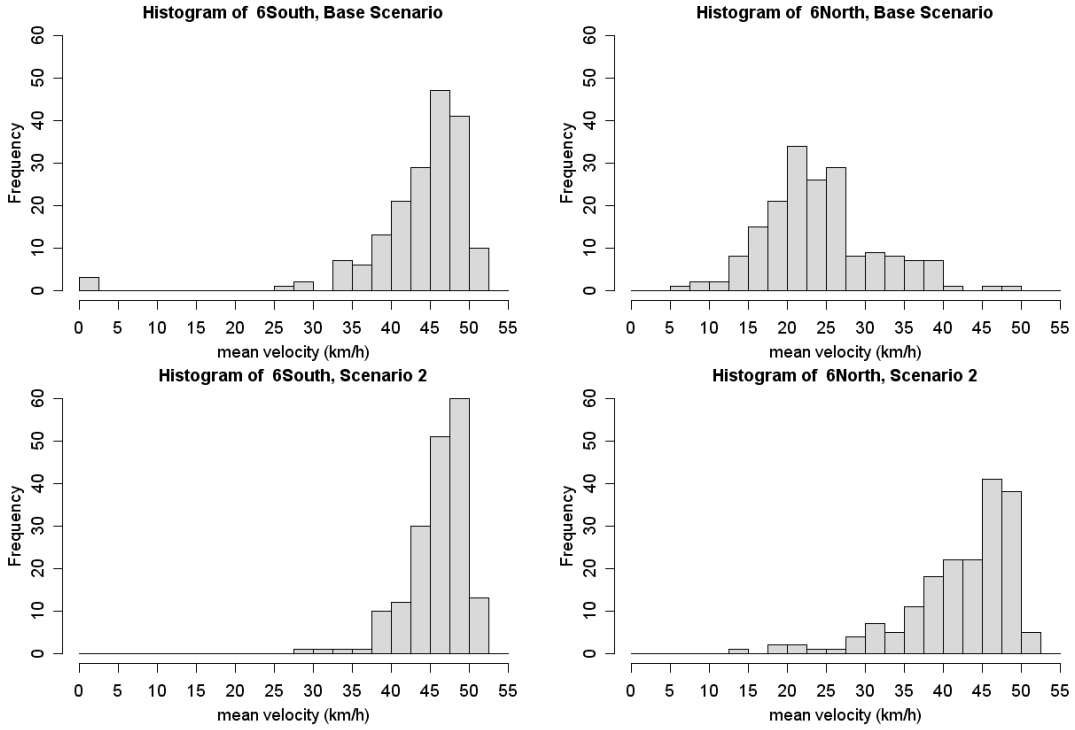

Figure 2: Histograms of mean velocity for street section 6 at air quality station, Base Scenario (top) and Scenario 2 (bottom).

Emission data for the hour with maximum traffic load was calculated for each street section in each scenario with IMMIS$^{em/micro}$ which is a special version of IMMIS^{em} (IVU Umwelt, 2008). Non-exhaust PM10 from abrasion and resuspension processes were determined using the approach by Düring and Lohmeyer (2004). IMMIS$^{em/micro}$ uses a linear combination of driving patterns defined in HBEFA 2.1 (Handbook of Emission Factors for Road Traffic, INFRAS, 2004) to derive traffic situations and emission factors for the traffic data described above. For each street section, the two driving patterns whose mean velocities enclose the mean velocity derived from the VISSIM data are combined such that the weighting factors sum up to unity. Additionally, the fraction of congestion is determined from the VISSIM congestion data. The corresponding emission factor is then calculated from the weighted emission factors of the chosen driving patterns, scaled with the fraction of fluent traffic flow, and the stop&go emission factor, scaled with the fraction of congestion.

Figure 3 shows the absolute values and the relative differences of the calculated NO_X emissions of Scenario 1 – 3 compared to the Base Scenario for each street section. Emissions depend on the chosen driving patterns and stop&go-fraction, on the vehicle intensity and on the fractions of HDV, LDV and busses as given exemplarily in Table 1.

The NO_X emissions of Scenario 1 – 3 decrease significantly for the street sections 5North, 5South, 6North, 8North and 11North at the centre of the considered road network. Lower emissions are also found for 2South, 4South and 9West. Street Section 7East emissions decrease for Scenario 1 and increase for Scenario 2 and 3. This is due to the gatekeeping function of 7East in the latter scenarios which leads to larger stop&go fractions, lower mean

velocities and less advantageous driving patterns. Increased emissions are also observed for 7West, 8South, 10East and 11South and to a small degree for 2North, 3West and 4North. Generally, NO_X emissions increase by at most 18 % while they decrease by up to 45 %.

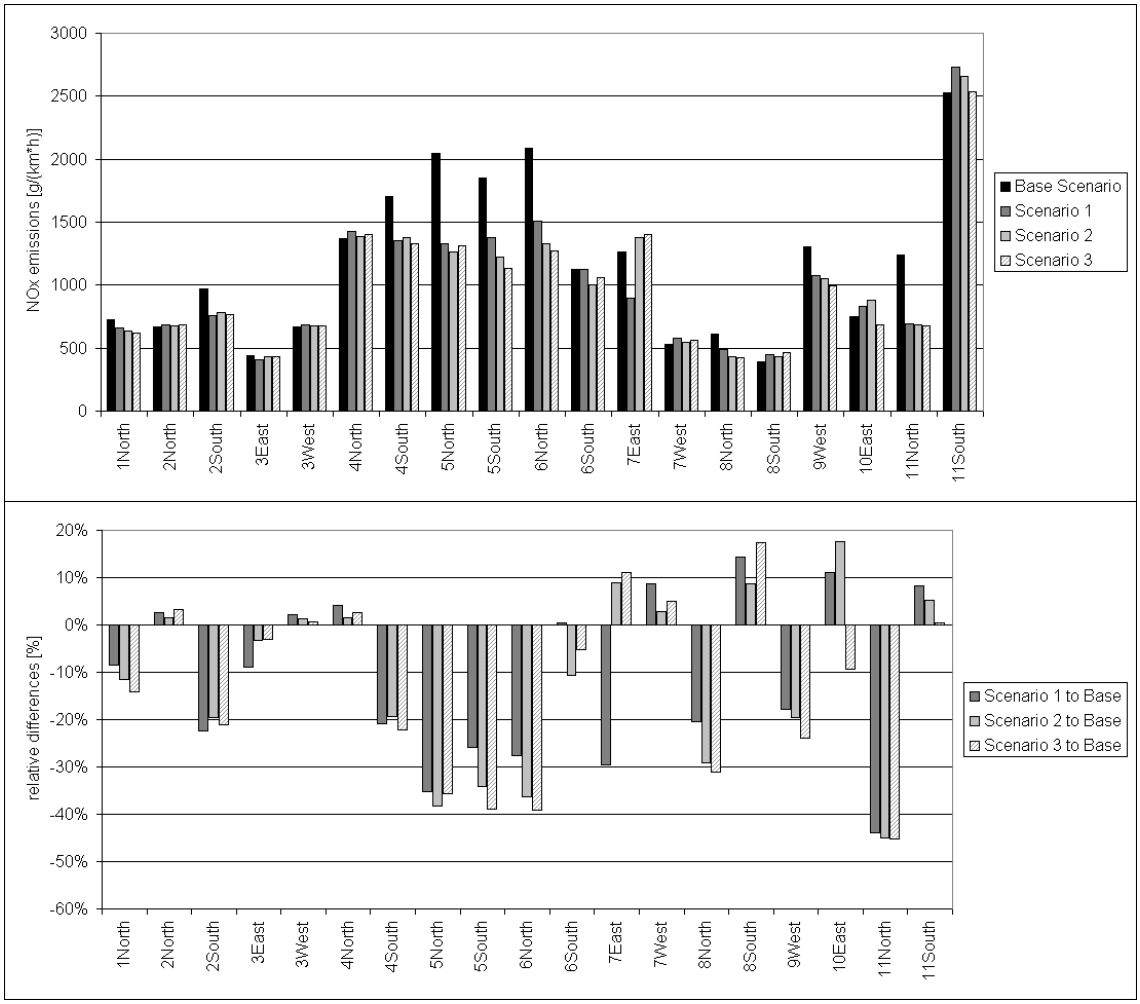

Figure 3: Absolute values (top) and relative differences (bottom) of NOX emissions of Scenarios 1 - 3 compared to the Base Scenario for all considered street sections.

Dispersion modelling was carried out with the three-dimensional microscale model MISKAM 5.02 (Eichhorn, 2008). MISKAM consists of a prognostic, non-hydrostatic wind field model and a Eulerian dispersion model. Buildings are considered in the form of rectangular block structures. The investigation area for the test case has a size of 200 m x 350 m with a horizontal resolution of 1 m. It contains the location of the air quality monitoring station and several street sections of Clevischer Ring (Figure 4). Building data for this area was provided by the Cologne city authorities.

Modelling was performed based on the IMMIS$^{em/micro}$ emission data described above and for meteorological conditions for which the maximum additional pollutant load from traffic was to be expected. Meteorological data and background concentrations were available for 2008 from the Cologne background station Chorweiler. First, the hours of maximum additional pollutant load were identified by analysing the differences of the measured concentration values between the air quality stations Clevischer Ring and Chorweiler. The concentration differences of the identified hours were then correlated with the respective wind directions. Finally, the critical wind direction was defined to be the wind direction for which large concentration differences, i. e. a high additional pollutant load, occured with high frequency. This was the case for a wind direction of 270°. The wind velocity was set to 2.3 m/s which was the annual mean value at Chorweiler in 2008.

Figure 4 shows exemplarily some of the modelling results within the investigation area for the level 1.3 m – 2.0 m above ground. For the Base Scenario, the NO_X additional pollutant load due

to traffic reaches its maximum close to the location of the air quality station (Figure 4, left). The respective street section 6 (Table 1) exhibits a canyon-like character and has a large vehicle intensity. North of the building block, concentrations on street section 6 decrease despite of constant emissions as the ventilation improves. Comparing the NO_X additional pollutant load of Scenario 2 with the Base Scenario, relative differences show a drop of concentrations of up to 40 % for street section 6 within the street-canyon area (Figure 4, right). Slight increases up to 5 % are observed for street section 11South in the northern part of the investigation area, for 10East and for 7East. For these street sections, emissions are larger in Scenario 2 than in the Base Scenario (Figure 3).

Figure 4: Left: NO_X additional pollutant load due to traffic emissions under critical wind direction 270° for Clevischer Ring at level 1.3 m – 2.0 m, Base Scenario. Right: Relative differences of NO_X additional pollutant load, Scenario 2 to Base Scenario.

The results described above are valid for an hour with maximum emissions under unfavourable meteorological conditions. Following the approach of Diegmann and Wiegand (2007), the impact of Scenario 2 on the NO_2 annual mean concentration in 2008 compared to the Base Scenario was assessed by assuming that Scenario 2 was implemented as a temporary measure under these conditions:

1) the measure was active only between 5 a.m. and 10 p.m.

2) the measure was activated as soon as the measured NO_2 hourly mean concentration at the monitoring station Clevischer Ring reached A: 60 µg/m³, B: 70 µg/m³, C: 80 µg/m³

3) when activated, the additional pollutant load due to traffic was reduced by 23.7 % compared to the Base Scenario, with 23.7 % being the reduction derived from the MISKAM modelling results for Scenario 2 and the Base Scenario at the location of the monitoring station.

The hourly NO_2 time series 2008 measured at Clevischer Ring was modified according to these parameters and the annual mean value was calculated. The results as well as the fraction of hours in a year for which the measure was to be activated are given in Table 2.

Table 2: Results for Scenario 2 implemented as a temporary measure

Case	A: 60 µg/m³	B: 70 µg/m³	C: 80 µg/m³
fraction of time with activated measure	45 %	36 %	26 %
potential reduction of NO_2 annual average	9.0 %	7.8 %	6.1 %

Conclusions

Modelling the four scenarios and analysing the results led to the following conclusions:

Modelling confirmed that under meteorologically unfavourable conditions the maximum additional pollutant load due to traffic occures close to the location of the monitoring station Clevischer Ring.

Enhancing the traffic flow results in a significant decrease of traffic emissions at the hot spot Clevischer Ring (street section 6) as well as for the considered street sections in total. At the same time, vehicle intensity increases slightly for most street sections (Scenario 1: up to 10 %, Scenarios 2 and 3: up to 5 %).

Scenario 1 leads to a significant decrease of the additional pollutant load within the investigation area and thus improves the air quality situation. Scenario 2 improves the situation further, mainly close to the monitoring station Clevischer Ring. For Scenario 3, concentrations decrease only in some parts of the investigation area compared with Scenario 2, mainly in the northern part. In the southern part and at the monitoring station concentrations increase slightly.

The significantly improved air quality situation at the monitoring station Clevischer Ring for Scenarios 1 to 3 compared to the Base Scenario goes along with minor increases of the additional pollutant load in non-critical areas.

Based on the modelling results for meteorologically unfavourable conditions and a theoretical approach, the potential of Scenario 2 to reduce the NO_2 annual mean concentration at the monitoring station Clevischer Ring was assessed to be 6 % to 9 % for 2008, depending on the parameters of the mitigation strategy.

The results presented here indicate that ETMS may be a worthwhile measure to improve the air quality in heavily trafficked areas. It may be noted that emission modelling was based on HBEFA 2.1 which was in effect at the time of the investigation and which preceeds HBEFA 3.1 now available since February 2010. So far it appears that emission calculations based on HBEFA 3.1 will increase the traffic-induced fraction of the pollutant load. Thus, the ETMS scenarios studied here may be even more effective. In any case, the effect on the surrounding road network should be considered carefully to avoid inducing new hot spots by eliminating existing ones.

Acknowledgements

This paper is an outcome of the joint project “Umweltsensitives Verkehrsmanagement Stadt Köln”. Project partners are IVU Umwelt GmbH, SIEMENS AG and Stadt Köln.

References

Diegmann V., G. Wiegand (2007), Potenzial dynamischer Verkehrslenkungsmaßnahmen als Instrument der Luftreinhaltung, *Gefahrstoffe – Reinhaltung der Luft*, 67, Nr. 4, 155-161.

Düring I., A. Lohmeyer (2004), Modellierung nicht motorbedingter PM10-Emissionen von Straßen, in: Kommission Reinhaltung der Luft im VDI und DIN – Normenausschuss KRdL (eds): KRdL-Expertenforum Staub und Staubinhaltsstoffe, KRdL-Schriftenreihe Band 33, Düsseldorf.

Eichhorn J. (2008), *MISKAM – Handbuch zu Version 5*, giese-eichhorn umweltmeteorologische software.

INFRAS (2004), *Handbuch Emissionsfaktoren des Straßenverkehrs, HBEFA Version 2.1*, INFRAS, Bern, on behalf of UBA Berlin / BUWAL Bern / UBA Wien.

IVU Umwelt (2008), *IMMIS$^{em/luft/lärm}$ Version 4.0 User’s Guide*, IVU Umwelt GmbH, Freiburg.

Biodistillate Transportation Fuels: Life Cycle Impacts

A. Broch[1], S.K. Hoekman[1],A. Gertler [1], C. Robbins[1],and M. Nataranjan [2]

1 Desert Research Institute, 2215 Raggio Blvd. Reno, NV 89512, amber.broch@dri.edu
2 Marathon Petroleum Company, LLC. Findlay, OH 45840

Introduction

Global climate change and concerns about greenhouse gases (GHG), dwindling supplies of fossil fuels and national energy security are driving growth in production and use of biofuels. Both in the US and EU, along with many other countries, alternative fuels use is becoming increasingly regulated through policy and mandates (US. Congress, 2007; Schwarzeneggar, 2007, EU Directive, 2003; UK RTFO, 2005). A goal of these policies is to decrease GHG emissions through the use of lower emitting alternative fuels. Life cycle assessments (LCA) are increasingly relied on in these policies as a way to ensure that the fuels are in fact meeting the GHG reduction targets. The LCA of a fuel provides the complete well-to-wheels (WTW) GHG emissions of a fuel through its production, storage and use, as illustrated in Figure 1. The WTW assessment can be broken down into two parts: well-to-tank (WTT) and tank-to-wheels (TTW). The combination of the two parts represents the complete well-to-wheels (WTW), or cradle-to-grave, life-cycle for a transportation fuel. The GHG emissions are usually provided in terms of CO_2 equivalents [$CO_{2,eq}$], or carbon intensity (CI). The global warming potential (GWP) by which each pollutant is converted to $CO_{2,eq}$ means that each gas has varying degree of impact on the total carbon intensity. For example, the GWP values for CO_2, CH_4 and N_2O are 1, 21, and 310, respectively. So, small differences in N_2O production can have large impacts of the final CI. Common LCA practice for biofuels is to use the "carbon neutral principal," since the carbon being emitted is the same carbon that was recently absorbed by the plant during its growth through photosynthesis (Russi, 2008) Therefore, there is minimal net contribution to GHG emissions from combustion of biofuels (though NOx and other minor pollutants do contribute to a small degree), so WTT results are generally similar to the complete WTW results.

Definition of boundaries and transparency of data and assumptions is of critical importance as small changes can have dramatic effects on the final results. For example, different allocation methods for contributing GHG emissions to various co-products produced along with the final biofuel can significantly impact the final GHG emissions attributed to the biofuel itself. Other influential factors include crop yields, fertilizer use, and nitrogen to N_2O conversion factors, farming energy and chemical requirements, and production scale (Wang, 2008). Additionally, the topic of indirect land use changes (ILUC) and how they are included (or not included) has become a growing area of concern since recent publications (Searchinger et al., 2008; Fargione et al., 2008), and may swing the final GHG benefits of a biofuel from positive to negative.

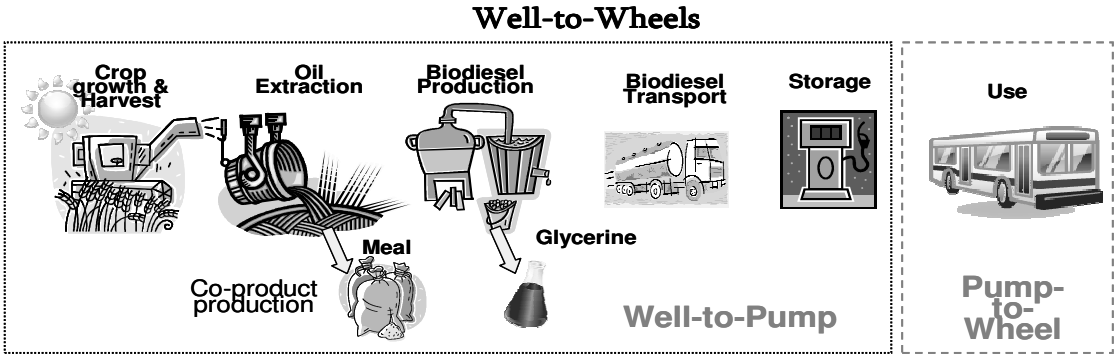

Figure 1: Well-to-Wheels pathway schematic for biodiesel.

As part of a study sponsored by the Coordinating Research Council (CRC) to assess the state-of-knowledge regarding plant- and animal- derived biofuels as blending materials for ultra-low sulfur diesel (ULSD) fuel in transportation applications, a literature survey of LCA studies on biodistillate fuels was completed in an effort to highlight the differences in assumptions and how they affect the final results (Hoekman et. al 2009). Besides a review of life-cycle assessments, the study

reviews policy drivers, feedstocks, fuel production technologies, emissions impacts, fuel properties and specifications, and in-use handling and performance. The term 'biodistillates' includes both traditionally-produced biodiesel (by transesterification) and second generation renewable diesel (produced through hydroprocessing). Over 50 studies on biodistillate LCA were reviewed (a full list of literature items with detailed summaries of results can be found in the CRC final report). The studies showed that most fuels lead to a 45-85% carbon intensity benefit relative to conventional diesel. However, the most influential assumptions are those with the greatest amount of uncertainty: the co-product allocation methods, N_2O conversion factors, and land use changes. In fact, the inclusion of indirect land use changes can swing the final results from a net benefit to a negative impact, which would influence its use in alternative fuel policies.

Carbon Intensity of Biodistillate Fuels

The literature search focused only on articles which discussed LCA of biodiesel or renewable diesel fuels (ethanol was excluded). Over 50 articles were obtained, covering a broad range of feedstocks and methods of production. Some studies compared biodiesel to conventional diesel while others considered only a single fuel, but investigated differences in assumptions, processes, or life-cycle scenarios. The most common feedstocks were rapeseed (frequent in many EU studies) and soybeans (used in many U.S. studies). Most studies considered biodiesel production via transesterification with methanol, though a few also investigated renewable diesel produced via catalytic hydroprocessing. Only those articles that included determined a carbon intensity for the biodistillate fuel, or compared the carbon intensity to a reference fuel (such as petroleum diesel) are discussed herein. Table 1 provides the list of references, listed by a study number. The study number provided can be cross referenced to Figures 2-4. Note the study numbers are not sequential: some studies included in the literature survey are not discussed herein if they did not include carbon intensity, so are excluded from the list (other studies including energy assessments were also included in the literature review). The data column in Table 1 refers to the Figure in which the study is included: a study included an assessment of carbon intensity is noted with a "G" and is included in Figure 1; a study that provides a percent benefit relative to a reference fuel is noted with an "R", and is included in Figure 2; a study including both is noted with a "GR", and is included in both Figures 1 and 2.

Of the studies included in the literature review, 26 of them reporting a carbon intensity value for a biodistillate fuel, which are included in Figure 2. Direct comparison among studies is not straight forward, since each study varies in its assumptions and pathways. Nevertheless, Fig. 2 shows a relatively tight range of CI results, with most values falling between 10 and 60 grams of $CO_{2,eq}$. per MJ of fuel produced. The range of conventional diesel CI values reported in these studies is from 22 to 240 grams of $CO_{2,eq}$. per MJ of fuel; this range is not shown in Fig. 2. CARB has adopted a value of 95 gm/ $CO_{2,eq}$ per MJ fuel for its reference fuel by which to measure CI reductions (Prahbu et al., 2009).

The relative CI difference between biofuel and conventional fuel reported in each study is illustrated in Fig. 3. (Figs. 2 and 3 consist of slightly different sets of studies due to differences in reporting: many studies only reported a percent increase or decrease, while some reported GWP for biodiesel but not for petroleum diesel). When possible, the complete WTW GHG emissions of the biodistillate and reference diesel are compared. The relative impacts of the biofuels varied widely among different studies: several showed a 90% or greater decrease in GHG emissions, while others showed less than 10% benefit. One study to note is No. 38 (Delucchi, 2006), which results in nearly a 50% increase in CI relative to petroleum diesel. This study highlights the potentially severe impacts of N_2O emissions due slight increase in N_2O conversion rations from N fertilizer use.

Figures 2 and 3 also illustrate the large variability in LCA results, even when considering similar feedstocks in similar locations. For example, soybean oil was examined biodiesel production in 13 studies in Fig. 2. The results of these studies ranged from 5.7 to 140 g $CO_{2,eq}$. When comparing these values to the reported CI for petroleum diesel (Fig. 3), the variability is even more pronounced. Although the CI for biodiesel in Study No. 1 [NREL] was quite high relative to the other soybean LCA cases, it also showed a large benefit relative to petroleum diesel (~ 80% benefit). Study No. 46 [Huo, et. al] also showed significant benefits for soy biodiesel at the upper end of its predicted range. The CI in study No. 14 [Hill] is comparable to Study No. 1, but results

in only a 43% benefit. Similarly, Study No. 30 [Kreider] and Study No. 28 [Kalnes] predicted comparable CI values, but No. 30 resulted in less than 25% reduction in GWP with respect to its reference fuel, while No. 28 showed a 75% decrease.

Table 1: Reference list for figures

Study Number	Data	Citation
1	**GR**	Sheehan J, Camobreco V, Duffield J, Graboski MS, and Shapouri H: A life cycle inventory of biodiesel and petroleum diesel for use in an urban bus. NREL/SR-580-24089(1998).
8	**GR**	Bernesson S, Nilsson D, and Hansson P-A: A limited LCA comparing large- and small-scale production of rape methyl ester (RME) under Swedish conditions. *Biomass & Bioenergy,* 26545-559 (2004).
9	**GR**	Carraretto C, Macor A, Mirandola A, Stoppato A, and Tonon S: Biodiesel as alternative fuel: Experimental analysis and energetic evaluations. Energy, 29(12-15), 2195-2211 (2004).
13	**GR**	Gartner SO, Helms H, Reinhardt G, and Rettenmaier N: An Assessment of Energy and Greenhouse Gases of NExBTL. 1-25 (2006).
14	**GR**	Hill J, Nelson E, Tilman D, Polasky S, and Tiffany D: Environmental, economic, and energetic costs and benefits of biodiesel and ethanol biofuels. Proceed.Nat.Acad.Sci., 103(30), 11206-11210 (2006).
15	**GR**	cycle assessment of biodiesel from tallow and used vegetable oil. Feedstocks for the Future: Renewables for the Production of Chemicals and Materials, 921239-252 (2006).
18	**R**	Koyama A, Iki H, Iguchi Y, Tsurutani K, Hayashi K, and Misawa S: Vegetable Oil Hydrogenating Process for Automotive Fuel. SAE Paper 2007-01-20301871-1876 (2007).
19	**GR**	Barber A, Campbell A, and Hennessy W: Primary energy and net greenhouse gas emissions from biodiesel made from New Zealand tallow - CRL Energy Report 06-11547b. CRL Energy Limited Report No 06-11547b1-41 (2007).
21	**R**	Cunningham J: Greener than green - Analysis of the lifecycle of biodiesel from farmer's field to pump reveals a startling reduction in overall carbon emissions compared to regular fuel. *Professional Engineering,* 20(11), 42-42 (2007).
22	**GR**	Edwards R, Larive JF, Mahieu V, and Rouveirolles P: Well-to-Wheels analysis of Future Automotive Fuels and Powertrains in the European Context. Version 2b(2006).
23	**R**	Greenhouse Gas Impacts of Expanded Renewable and Alternative Fuels Use. U.S.Environmental Protection Agency, (2007). http://www.epa.gov/oms/renewablefuels/420f07035.pdf
26	**GR**	organic farms - Evaluation of systems based on fuels produced in industrial-scale plants. Agricultural Systems, 94704-714 (2007).
27	**G**	Harding KG, Dennis JS, von Blottnitz H, and Harrison STL: A life-cycle comparison between inorganic and biological catalysis for the production of biodiesel. Journal of Cleaner Production, 16(13), 1368-1378 (2008).
28	**GR**	Kalnes T, Marker T, and Shonnard DR: Green diesel: A second generation biofuel. *International Journal of Chemical Reactor Engineering,* 5(2007).
29	**R**	Kaufman J: Renewable Diesel. (2007).
30	**GR**	Kreider JF and Curtiss PS: Comprehensive Evaluation of Impacts From Potential Future Automotive Fuel Replacements. Energy Sustainability, ES2007-362341-12 (2007).
31	**R**	Kuronen M, Mikkonen S, Aakko P, and Murtonen T: Hydrotreated Vegetable Oil as Fuel for Heavy Duty Diesel Engines. SAE International, 2007-01-4031(2007).
38	**GR**	Delucchi MA: Lifecycle Analyses of Biofuels. UCD-ITS-RR-06-081-78 (2006).
41	**G**	Panichelli L, Dauriat A, and Gnansounou E: Life Cycle Assessment of Soybean-Based Biodiesel in Argentina for Export. *Int.J.of LCA,* 14144-159 (2009).
42	**GR**	Proposal for Greenhouse Gases and Energy Savings Accounting in the French Context. *SAE World Congress & Exhibition Technical Papers,* 2008-01-0673(2008).
43	**GR**	Russi D: An integrated assessment of a large-scale biodiesel production in Italy: Killing several birds with one stone? *Energy Policy,* 36(3), 1169-1180 (2008).
44	**GR**	S&T2 Consultants Inc., Cheminfo Services Inc., MacLean H, and Fugacity Technology: Sensitivity Analysis of Biodiesel LCA Models to Determine Assumptions With the Greatest Influence on Outputs. (2008).
45	**GR**	Kalnes T, Marker T, Shonnard D, and Koers K: Green diesel production by hydrorefining renewable feedstocks. Biofuels-Q4(2008). www.biofuels-tech.com
46	**GR**	Huo H, Wang M, Bloyd C, and Putsche V: Life-Cycle Assessment of Energy and Greenhouse Gas Effects of Soybean-Derived Biodiesel and Renewable Fuels. ANL/ESD/08-2(2008).
47	**GR**	Hu Z, Tan P, Yan X, and Lou D: Life cycle energy, environment and economic assessment of soybean based biodiesel as an alternative automotive fuel in China. *Energy,* 33(11), 1654-1658 (2009).
49	**ER**	Whitaker M and Heath G: Life Cycle Assessment of the Use of Jatropha Biodiesel in Indian Locomotives. Technical Report NREL/TP-6A2-44428(2009).
50	**GR**	Jin H and Nelson R: Life Cycle Assessment of Tallow-Based Renewable Diesel Fuel. #542a(2008).
51	**G**	Nikander S: Greenhouse Gas and Energy Intensity Assessment of Product Chain Case Transport Biofuel. M.S. Thesis(Department of Civil and Environmental Engineering, Helsinki University of Technology), 1-88 (2008).
52	**GR**	Prabhu ACPAG and J.Duffy: Detailed California-Modified GREET Pathway for Biodiesel (Esterified Soyoil) from Midwest Soybeans. Draft V.2.1 CARB(2009).
53	**GR**	Prabhu A, Pham C, Glabe A, and J.Duffy: Detailed California-Modified GREET Pathway for Renewable Diesel from Midwest Soybeans. Draft V.2.1 CARB(2009).
54	**GR**	Kalnes T, Koers KP, Marker T, and Shonnard DR: A technoeconomic and environmental life cycle comparison of green diesel to biodiesel and syndiesel. *Environmental Progress & Sustainable Energy,* 28(1), 111-120 (2009).
55	**G**	Su C-L and Lee Y.-M.: Development status and life cycle inventory analysis of biofuels in Taiwan. *Energy Policy,* 37(2), 754-758 (2009).

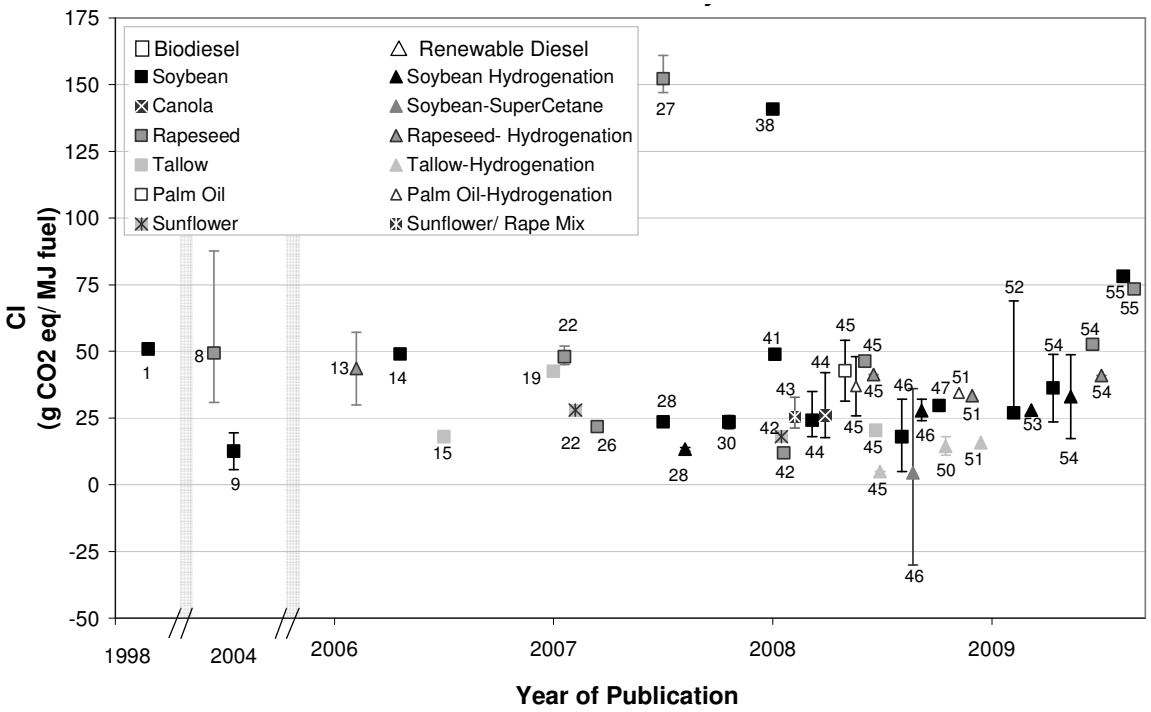

Figure 2: Carbon Intensity in grams of $CO_{2,eq}$ for 26 studies from 1998-2009. Numbering refers to study number in Table 1. Note the two breaks in the x-axis indicating gaps in publication dates. Also note that squares indicate biodiesel fuel, and triangles represent renewable diesel, and different feedstocks are represented by different shades. The bars represent a range of CI.

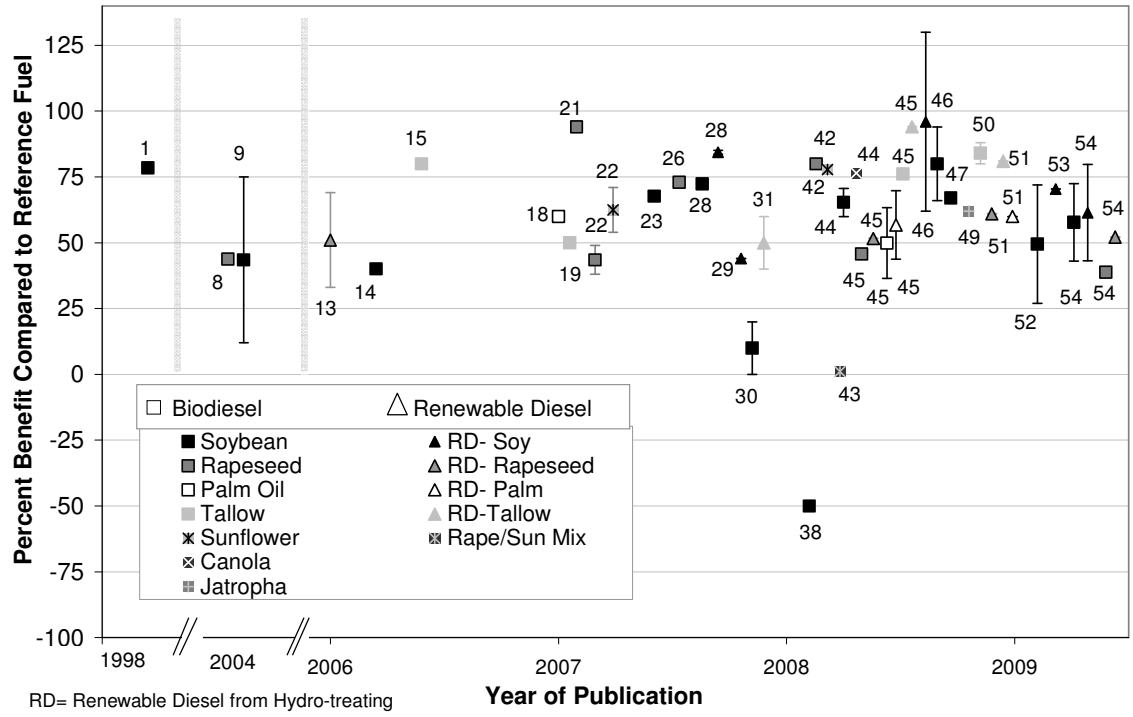

Figure 3: Global warming benefit relative to reference fuel (petroleum) for 31 studies from 1998-2009

To illustrate the how variability in assumptions affects the final results, several studies were selected which provided a breakdown of CI contribution from each stage of production

(agriculture, crushing and oil recovery, conversion, transport, combustion, and offsets from allocation or CO_2 uptake.) The contributions from each of the selected studies are shown in Figure 4. Studies for biodiesel from soybean oil (Study Nos. 1, 38, 44, and 52), and rapeseed oil (Study Nos. 8,22, and 45) are shown, along with studies about renewable diesel (Study Nos. 13, 45, and 53). Reference diesel fuel values presented in each study, shown as a black circle, are also shown in Fig. 4 for comparison.

Figure 4 illustrates significant variations in contributions from study to study, particularly in the area of agriculture (which includes assumptions about nitrogen use and N_2O conversion ratios), and in offsets (which includes either co-product allocation offsets, or offsets from assuming the carbon-neutral principal). In some studies, the carbon neutral principal is applied, so combustion emissions are not included even though there may be some offset from co-product allocation.

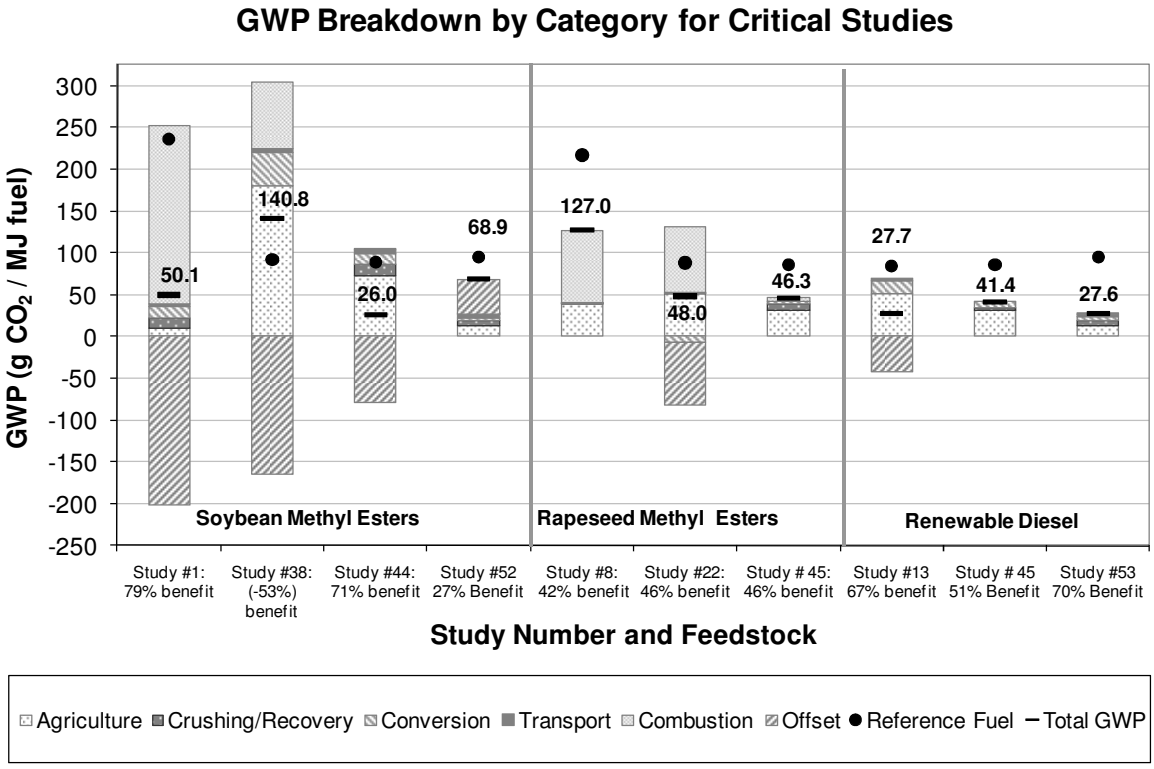

Figure 4: Contribution of individual life-cycle stages to overall GWP.

Figure 4 highlights the significance in variations in agricultural modeling, which have been under scrutiny since a recent publications (Crutzen, 2008). In Study No. 38, Delucchi assumes high N_2O conversion ratios, which attribute to high CI, resulting in a dis-benefit for biodiesel relative to fossil diesel. Also note that in Study No. 1 [NREL] emissions from agricultural practices are quite small. This is due to the fact that the study only includes CO_2 emissions, and neglects CH_4 and N_2O, which are the main emissions produced during agricultural phases, and contribute highly to $CO_{2,eq}$ emissions (CH_4 is worth 21 $CO_{2,eq}$ and N_2O is worth 310 $CO_{2,eq}$ [IPCC, 2006]).

Assumptions about offsets also cause large variation in the final results. In Study No. 1 [NREL], the offsets are due to assuming the carbon neutral principal, so the emissions from combustion are nearly offset. In Study No. 52 [Prahbu], the 'offsets' illustrated are actually due to the inclusion of indirect land use change effects. When included indirect ILUC, the benefits are changed from nearly a 75% benefit to only about a 25% benefit relative to conventional fuel. Although the NREL study (Study No. 1) included analysis of GHG emissions, the total inventory was not converted to a $CO_{2,eq}$. basis, so the reported GWP depicted in Fig. 4 is based strictly on CO_2 itself, and does not include contributions for N_2O or CH_4. Contributions from the agricultural phase were quite low in this study, but would be higher if N_2O and CH_4 emissions had been included.

Conclusions

Life-cycle assessments (LCA) of "well-to-wheels" energy inputs and GHG emissions are now recognized as important tools for understanding the relative benefits of biodistillate fuels compared to conventional fuels, and are becoming more frequently used in alternative fuel policies. However, LCA models are very data intensive, and require numerous inputs having high uncertainty. Some of the most critical inputs are in areas that are most uncertain – such as assumed agricultural practices and their emissions, impacts attributed to co-products, and land use changes (LUC). Variations in LCA model assumptions have drastic effects on the final results, especially for emissions, and small tweaks can me made to influence the final impact of the fuel. Consequently, it is difficult to directly compare LCA results from different studies. Comparison of relative effects between biofuel and conventional fuel scenarios conducted within the same study is often more informative.

The GHG emissions results for LCAs are usually expressed in terms of relative CI (g $CO_{2,eq}$ per MJ fuel). In almost every published LCA study, biodistillate scenarios resulted in lower CI compared to conventional diesel. In approximately 30 studies investigated here, the CI benefits of the biodistillate fuels ranged from 10% to 90%, with an overall average value of about 60%. However, several studies highlighted how small changes can drastically affect the final results, and in some cases, result in a dis-benefit for biodiesel. Some of the significant variations include indirect land use changes (ILUC), N_2O conversion rations, and co-product allocation. Inclusion of ILUC is growing, especially for policy applications, although at the time of this literature review, only one study included ILUC (Prabhu, 2009).

References

Crutzen PJ, Mosier AR, Smith KA, and Winiwarter W: N2O release from agro-biofuel production negates global warming reduction by replacing fossil fuels. Atmospheric Chemistry and Physics, 8(2), 389-395 (2008).

European Union: Directive 2003/30/EC of the European Parliament and of the Council of 8 May 2003 on the promotion of the use of biofuels or other renewable fuels for transport. *Official Journal of the European Union,* (17.5.2003), L 123/42-L 123/46 (2003).

Fargione J, Hill J, Tilman D, Polasky S, and Hawthorne P: Land clearing and the biofuel carbon debt. Science, 3191235-1237 (2008).

Hoekman, S. K., Gertler, A., Broch, A., and Robbins, C., "Investigation of Biodistillates as Potential Blendstocks for Transportation Fuels," CRC AVFL-17, Final Report June, http://www.crcao.com/reports/recentstudies2009/AVFL-17/CRC%20Report%20No%20AVFL-17%20June%202009_f.pdf, 2009.

IPCC, "IPCC Guidelines for National Greenhouse Gas Inventories. Vol. 4: Agriculture, Forestry, and Other Land Use," 2006.

Prabhu A, Pham C, Glabe A, and J.Duffy: Detailed California-Modified GREET Pathway for Renewable Diesel from Midwest Soybeans. Draft V.2.1 CARB(2009).

Russi D: An integrated assessment of a large-scale biodiesel production in Italy: Killing several birds with one stone? Energy Policy, 36(3), 1169-1180 (2008).

Schwarzenegger A: California Executive Order S-01-07 (California Low Carbon Fuel Standard). (2007). http://gov.ca.gov/executive-order/5172/

Searchinger T, Heimlich R, Houghton RA, Dong F, Elobeid A, Fabiosa J, Tokgoz S, Hayes D, and Yu TH: Use of U.S. croplands for biofuels increases greenhouse gases through emissions from land-use change. Science, 3191238-1240 (2008).

UK Department of Transport: UK Policy, Renewable Transport Fuel Obligation. (2005). http://www.dft.gov.uk/pgr/roads/environment/rtfo/

U.S.Congress: H.R. 6: Energy Independence and Security Act of 2007. P.L. 110-140(2007). http://www.govtrack.us/congress/bill.xpd?bill=h110-6

Wang M: Life cycle analysis practicality. (2008).

GHG balance for light vehicles fuelled with different biofuel blends

D. Pillot, R. Vidon, P. Tassel and P. Perret*

Lab. Transports et Environnement, INRETS, Case 24, 69675 Bron, France - email : didier.pillot@inrets.fr

Summary

The methodology and results of three relevant and extensive studies of the global warming potential of various biomass-based fuels are discussed and plotted together, along with the conventional fossil fuels (both gasoline and diesel). These "well-to-tank" GHG emission assessments are based on the assumption of unchanged land use. In this respect, relatively good homogeneity of results is observed for the plant-based ethanols. Global warming potential of biomass-based esters is subject to more contrasted estimations, due to many possible assumptions regarding the substituted products, including fossil transport fuels, as well as animal feed and electricity. On the tank-to-wheel side, CO_2 emission variations obtained with different biofuel blends tested at INRETS on current passenger cars are compared with the emission models proposed by the ADEME working group and the JEC one dealing with LCA analyses. Small but significant CO_2 reductions are observed over realistic driving cycles with blends containing as little as 5 to 10% biofuel by volume. These reductions are underestimated by emission models used in JEC and EMPA tank-to-wheel analyses.

Context

Concern over climate changes is growing as the facts and figures give reality to the blackest predictions. In addition, oil availability could fail rapidly to reach an ever-growing global fuel demand. Alternatives and renewable fuels are thus seen as a partial but quick response to the transport energy demand and for reducing greenhouse gas (GHG) emissions. Alternative fuels could bridge the transition to low-carbon road transport as electric cars remain a long-term solution or simply become one of the renewable energy sources. But careful energy and environmental balance assessments are required to check that investments and public financial support for every biofuel production are worth the benefits. Through the case study of light vehicles fuelled with different biofuel blends, we propose to assess their GHG balance with different methodologies of Life Cycle Assessment (LCA).

Methodology

To date, several methodologies have been proposed to conduct biofuels Life Cycle Analyses. The French Agency for Environment and Energy Management (ADEME) published in 2008 a methodology for the calculation of the energy and GHG balance dedicated to the first-generation of biofuels produced in France (also named agro-fuels). The JRC-EUCAR-CONCAWE (JEC) working group provides as well comprehensive and regularly revised energy and GHG emissions data, from well to tank (WTT) and from tank to wheel (TTW), for any fuel used in road vehicles (Edwards et al., 2008). A third main reference taken into consideration is the global and thorough GHG analyses proposed by EMPA/ENERS for many Swiss-made biofuels and other ones from abroad (Zah et al., 2007). Some aspects such as GHG emissions from direct and indirect land use changes or the emission of N_2O resulting from the fertilizers are still in debate. These highly sensitive factors towards the GHG emissions of the biofuel pathways are not clearly analysed in the above mentioned LCAs. GHG emissions from biofuel production are also strongly influenced by the feedstock production stage and those emissions vary considerably from one feedstock to another. Careful analysis of each pathway allow for precise fossil energy consumed and GHG emissions per unit of biofuel energy produced. It does not address other relevant impact indicators, namely, acidification potential, eutrophication potential, ozone depletion potential and various toxicity potentials. Other environmental concerns associated with energetic crops such as carbon stock decreases, water depletion and pollution, and biodiversity loss, are not discussed as well.

A crucial point of the GHG balance is the choice of the appropriate allocation method to share the consumptions and emissions of the production process between products and by-products. Indeed, cereals or oilseeds cultivation and transformation processes do not generate solely

biofuels. Each pathway generates in addition by-products in large quantities, 2 tons per ton of fuel produced as an average. These by-products are valued in animal feed, fertiliser, energy or in industry. There are various methods of allocation to distribute the environmental loads between products and by-products, and the choice of the method strongly influences the results of LCA. However, at the present time, there is no consensus on the rules of allocation most adapted to the context of the biofuels, in spite of the recommendation of the Renewable Energy Directive (RED) to use the allocation of the impacts between different by-products according to energy pro rata.
The committee in charge of the ADEME LCA methodology has adopted a differentiated approach according to the nature of the by-product: in the reference scenarios, by-products being spread (fertiliser) or valued in fuels are treated by substitution (on the basis of their weight or their economic value), the others by-products (feed, industrial products, e.g. glycerin) being treated on an energy prorate basis.

For the JEC group, substitution of conventional fuels by alternatives is only plausible at a limited level, i.e. between 5 and 15% at the maximum, at the 2010-2020 horizon. Therefore, “the true impact of the change can only be properly assessed by looking at the incremental sources of energy that will provide alternative fuels, and the incremental savings that can be achieved by reducing supply of conventional fuels”. This incremental approach considers allocation of the environmental costs by extending the system boundaries.

The Swiss LCA from EMPA uses database of the Ecoinvent® Life Cycle Inventory. Consistent allocation rules are mainly based on economic thinking.

With respect to global warming potential, most LCA studies only take into account the contribution of CO_2, N_2O and CH_4 (Menichetti and Otto, 2009) and calculate the CO_2-equivalent impact of these gases over a 100-year period. Common factors of equivalence are taken by the 3 LCA selected, following the IPCC recommendation (third assessment report). Methane is given with a GWP 23 times higher than CO_2 and 1kg of N_2O is equivalent to 296 kg of CO_2 emissions. The IPCC method for calculating global warming potential actually includes a list of over 60 gases. In their Life Cycle Analysis of the HVO production, Arvidsson et al. (2010) account for the CO and HC GWPs, giving respectively to these gases an impact factor of 2 and 3 times compared to CO_2.

Comparative results of GHG balance for different biofuel pathways

The well-to-tank (WTT) studies relate emissions with respect to a megajoule (MJ) of fuel produced (g CO_2eq/MJ), but in order to compare fossil and alternative fuels, they also include the direct CO_2 emissions of gasoline or diesel during combustion phase in the engine (“fossil” CO_2). Authors of the ADEME study express as well global warming potential of different biofuel pathways in g CO_2 eq./MJ of biofuel, but they integrate the fact that biofuels are usually used as blends in vehicle and they attribute an additional credit of CO_2 for each MJ of biofuel produced if reductions of CO_2 emissions are measured during the blend combustion phase, compared to the neat fossil fuel. No data on these CO_2 savings during the blends use are given in the synthesis of LCA results published by ADEME (2009) so that it is not possible to estimate the order of magnitude of this “secondary” fossil CO_2 credit. It might reach several percents in comparison with a “neutral” combustion as it is assumed in the EMPA assessment. ADEME proposed LCA results for different crops-based biofuels produced and used as E10 or B10 in Euro 4 and Euro 5 vehicles. GHG emissions are expressed as g CO_2eq/MJ of biofuel, which are relevant to well-to-wheel analysis.

Comparisons are given for a number of first-generation biofuel pathways analysed in the 4 studies mentioned above, considering different feedstock for biofuel production. Biodiesels and ethanols are the main fuels considered but additional LCAs are compared as regards hydrotreated vegetable oil (HVO), in agreement with the list of biofuels tested in our laboratory. The comparisons are detailed with reference to the petroleum fuels, free of biofuel (specific fuels currently used for the vehicle certification).

All studies show that the most important steps in the production chain of biofuels are the agriculture and the production of the biofuels. The GHG emissions are dominated by the plant production step, mostly through N_2O emissions. This is largely due to the fact that plants, and particularly rapeseed, require a lot of nitrogen fertiliser. A large uncertainty remains in the N_2O emissions assessment from soil and fertilizers: nitrous oxide emissions from soil are difficult to

estimate. The values used in the model of HVO from rape in the Swedish study (Arvidsson et al., 2010) are about twice as high per kg of oil as the values used in the JEC study (Edwards et al., 2007) for rapeseed biodiesel. The 3 main studies selected have adopted the conversion factor recommended by the IPCC experts. Only low direct emissions of CH_4 and N_2O are assumed for conversion plant in the JEC study, because of data gaps. This reduces the greenhouse gas emissions by about 10-20% according to Jungbluth et al. (2008).

The "transformation" stage results in fossil energy credits through the by-products including the residue from pressing the oil seeds and the glycerine produced by the esterification process. Several ways are offered to value these by-products: the residue after pressing (or cake) is a protein-rich animal feed used usually in substitution of otherwise imported soy meal. But the cake and glycerine as well can be fermented to produce biogas and fuel the process; this way allows for a much more favourable energy and GHG balance for the seed oil methyl ester (ME) production. However, as it gives the farmer a higher income to sell glycerine as a chemical and the cake as animal feed, this scenario is the most common and the one selected among the different pathways analysed by the JEC for the comparisons presented on figure 1.

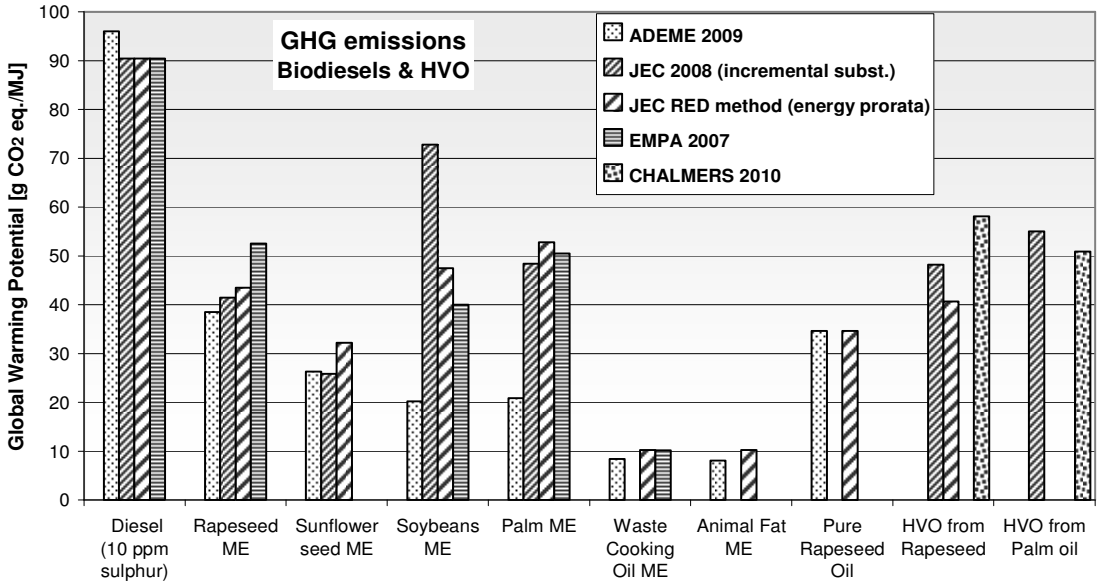

Figure 1: Well-to-tank Global Warming Potential of different vegetable and waste-oil based biofuel pathways according to the selected studies. For comparison, assessments of the conventional diesel fuel cycle GHG emissions are also shown.

The most environmental-friendly alternative fuels are by far, the ones based on waste organic material such as used cooking oil and animal fat. There is of course no production phase, but only a transformation one. As a consequence, there is little uncertainty as regards the GWP assessment and studies agree on values around 10 g CO_2 eq/MJ. On the contrary, the highest variability among results is found for the soybeans ME: the main reasons which explain such differences are the agricultural yields and the assumptions made on allocation of impacts and the fate of glycerine. This co-product always found with methyl ester production can be used to substitute animal feed or as a chemical. A third factor which influences the results is the type of energy system used in the transformation process, and particularly the existence of modern natural gas-fired cogeneration plants.

Generally, any changes in agricultural practices and technology improvement in the fertilizer industry can lead to a significant reduction of overall GHG emissions balance of 1st generation biofuels.

Palm oil-based diesel compares favourably to conventional diesel, in terms of GHG emissions. However, if previously non cultivated lands are converted for palm oil production, the net resulting balance can be dramatically negative.

As far as land use change is concerned, regional differences in agricultural production are more important than differences due to transports: burning of residues and CO_2 emissions due to land

transformation can double the overall GWP, e.g. when the reference land use is unfertilised grassland compared to wheat cultivation (Börjesson and Tufvesson, 2010).

On figure 2, the results for ethanol from various plants present a relatively good homogeneity, except for the case of corn ethanol: several factors can affect the GHG balance, e.g. the type of technology used in the milling plant, the process fuel used (natural gas, coal or renewables), the use of co-generation or not, and the fate of distiller grains and solubles (DDGS). In the best cases, the use of fossil fuels in the process can be largely limited, due to the conversion of by-products to heat and possibly electricity (cogeneration); for example, using bagasse to fuel the sugar cane ethanol manufacturing plant is a well established practice.
Interesting comparisons are given by ADEME as regards ETBE production: this perfect additive for the gasoline fuel from the point of view of petrol refineries has long been the only way of introducing ethanol in the conventional fuel; but its overall GWP balance is hardly positive compared to gasoline and new directives to impose E10 had to be implemented to force the use of ethanol instead of ETBE on the fuel market.

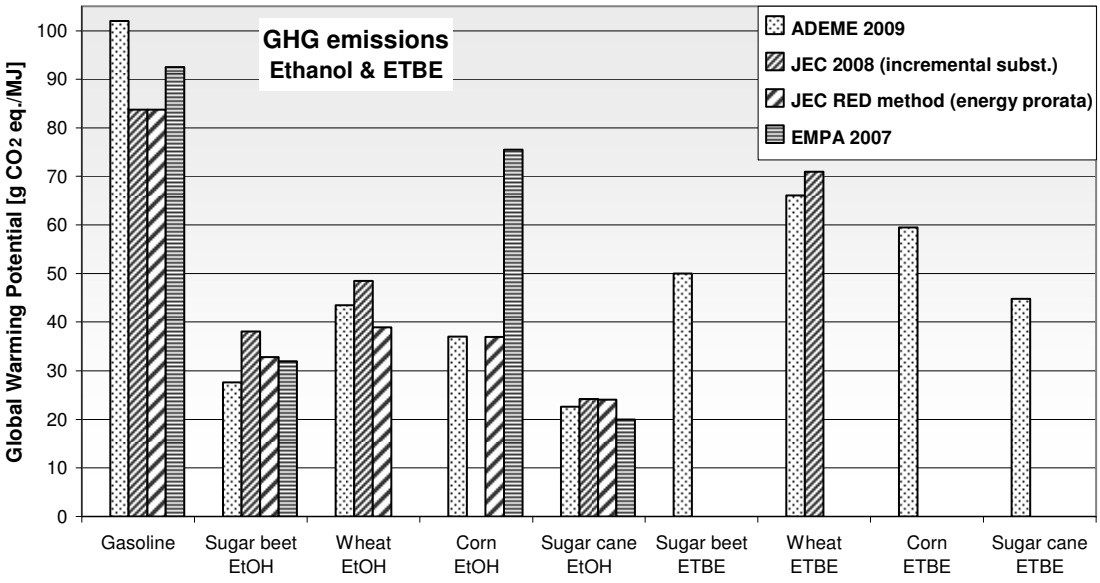

Figure 2: Well-to-tank Global Warming Potential of different ethanol and ETBE pathways from crops, according to the selected studies. For comparison, assessments of the conventional gasoline fuel cycle GHG emissions are also shown.

Results of well to wheels analyses

The well-to-wheel (WTW) studies express results per kilometre (km), calculated as the sum of the tank-to-wheel (TTW) "fossil" emissions (g CO_2 eq/km) plus the indirect emissions calculated as the product of the WTT emissions (g CO_2 eq/MJ) and the TTW energy consumed by the vehicle per unit of distance covered (MJ/km), referring to a specific driving cycle.

The ADEME analysis uses data of tank-to-wheel CO_2 emissions measured directly with some blends that are relevant to Europe in 2010 and beyond, i.e. E10, E85, B10 and B30. The functional unit is 1 km driven with a "standard" passenger car, whereas the Swedish results initially refer to 1 kWh energy out from the engine of a heavy-duty truck. Corrections were made to calculate equivalent results for passenger cars. The JEC analysis derived emissions along the NEDC cycle from a common, "virtual" vehicle, representing a typical European compact size 5-seater sedan. Simulations were made for the current engine types of 2010, i.e. a gasoline engine with port injection, a gasoline one with direct injection and 2 diesel direct-injection equipped vehicles, with and without particulate filter. All 2010 simulated vehicles comply with Euro IV. The functional unit of the EMPA study is expressed as 1 person transported over a distance of 1km. Passenger cars fulfilling the EURO 3 emission standards are the basis for the comparison.

As regards the agro-fuels selected for our tests, no information was available about the crops used as feedstock. But INRETS measurements give precise tank-to-wheel CO_2 emission factors

for different biofuel blends (g CO_2/km). The tailpipe emissions of eight light vehicles were measured according to the CVS standard method and analyzed to assess the regulated pollutants and CO_2 (Pillot et al., 2009). Two Euro-4 gasoline vehicles were tested with the reference gasoline fuel and E10 (10% ethanol by volume) and 6 diesel ones were measured with B0, B5, B30 and a neat hydrotreated vegetable oil (HVO). We used "real-world" driving cycles such as the ARTEMIS set to represent realistic and various traffic conditions and regulatory cycles (NEDC, FTP) as well.

Table 1: CO_2 emission variations measured (g/km) on 8 passenger cars with different biofuel blends relatively to fossil fuels (ARTEMIS cycles, means of 3 subcycle results)

Euro 4 vehicles	B5 / Diesel	B30 / Diesel	neat HVO / Diesel
* DDI 78 kW	– 2.1%	– 1.5%	– 6.4%
* DDI 81 kW	– 1.1%	+ 0.5%	– 4.7%
** DPF 81 kW	+ 2.4%	+ 1.8%	– 3.6%
** DPF 95 kW	– 1.2%	+ 0.1%	– 4.5%

	E10 / Gasoline
° GII 82 kW	– 2.4%
°° GDI 103 kW	– 3.2%

* Diesel vehicle with Direct Injection
** Diesel DI with particulate filter
° Gasoline vehicle with Indirect Injection
°° Gasoline vehicle with Direct Injection

Emissions variations over the NEDC and FTP cycles are not presented but they are weaker than the ones obtained on the ARTEMIS cycles, except for the neat HVO which gives quite similar variations. Significant CO_2 reductions are observed with the neat HVO, from 3.6 to 6.4 % and to a lesser extent, with E10 compared to the respective petroleum-based fuel. CO_2 variations are smaller with the B5 but still significant and little savings are possible for 3 vehicles out of 4. Surprisingly, the B30 blend gives the opposite trend. Adapted engine tuning could perhaps avoid possible CO_2 penalties with the B30 blend.

JEC emissions over the NEDC cycle show a small trend towards CO_2 increase when using B5 compared to diesel fuel and a reduction of 3.4 % with a synthetic diesel. The case of E5 is also taken as an example, and this blend gives no real variation of CO_2 emissions over the NEDC cycle according to the JEC database. The EMPA models assume no change in the CO_2 emissions for blends with low percentages of ethanol or ester.

When current or plausible blends are considered, global CO_2 emissions per km are easily compared to the conventional fossil fuel pathways and more meaningful. Figures 3a and 3b compare the global CO_2 emissions per km from 4 fuel blends with vehicles of different technologies (Euro 3 et 4). Emissions reductions obtained with B10 and E10 (ADEME) are much higher than the ones presented by JEC with B5 and E5, not only because of the higher content of biofuel and the reduced GWP attributed to the biofuel pathways over the production phase: they also take into account the real CO_2 abatement measured on vehicles in use.

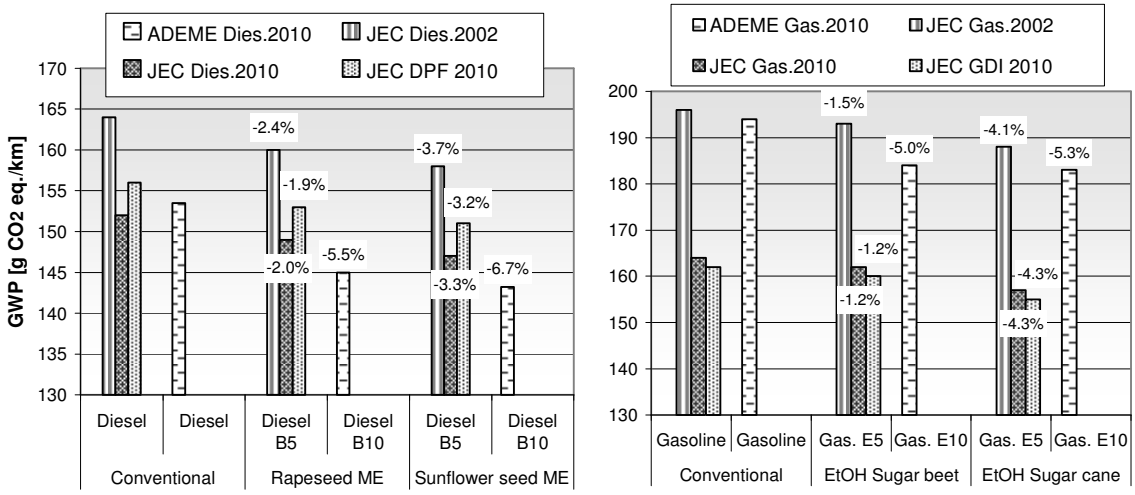

Figure 3a & 3b: Well-to-wheel Global Warming Potential of different fuel blends with plants based biofuel (E5, E10, B5 and B10).

Conclusion

The present analysis identifies GHG emission results for selected biofuel pathways relative to conventional fuels. As a matter of fact, creating first-generation biofuels such as sugar beet ethanol or rapeseed biodiesel is an energy-consuming process and a source of GHG emissions. The stages involved with growing crops on an industrial scale imply farm equipment, fertilizer, harvesting, transporting the feedstock to the biorefinery, converting the feedstock into fuel, and further transporting the biofuel to a petroleum refinery or service station. With these first-generation biofuels, the processes result in higher amounts of GHG emissions than for the conventional petroleum fuels, for both the production and transformation steps. The "well-to-tank" analyses reviewed offer a wide range of global warming potential, depending on many factors such as the principle on which, parts of the emissions are allocated to the by-products (mass or energy or economic basis for the animal food or industrial products substituted). The global GHG balance from well to wheel remains generally in favour of biofuels, so far as the crop field does not replace a forest or uncultivated land. On the "tank-to-wheel" side, the CO_2 emitted by the vehicles using biofuel is just not accounted for (or deducted in proportion to the energetic content of biofuel when using blend). But CO_2 emission reductions obtained with different biofuel blends tested at INRETS on current passenger cars highlight the role of biofuels in the engine efficiency. Small but significant CO_2 reductions are observed over realistic driving cycles with blends containing as little as 5 to 10% biofuel by volume. These reductions are underestimated by emission models used in JEC and EMPA tank-to-wheel analyses.

References

ADEME, MEEDDAT, MAP, IFP and ONIGC (2008), Elaboration d'un référentiel méthodologique pour la réalisation d'Analyses de Cycle de Vie appliquées aux biocarburants de première génération en France - Rapport final, BIO Intelligence Service, *ADEME pub.* France.

Arvidsson R., S. Persson, M. Fröling and M. Svanström (2010), Life cycle assessment of hydrotreated vegetable oil from rape, oil palm and Jatropha, *J. Clean Prod.*, doi:10.1016/j.jclepro.2010.02.008

BIO Intelligence Service (2009), Analyses de Cycle de Vie appliquées aux biocarburants de première génération consommés en France, Synthèse, *ADEME pub.* France

Börjesson P., L.M. Tufvesson (2010), Agricultural crop-based biofuels – resource efficiency and environmental performance including direct land use changes, *J Clean Prod*, doi:10.1016/j.jclepro. 2010.01.001

Edwards R., J.-F. Larivé, V. Mahieu and P. Rouveirolles (2007), Well-to-wheel analysis of future automotive fuels and powertrains in the European context, Well-to-wheels report, Version 2c, Report from Concawe, EUcar and Joint Research Centre of the European Commission (IES).

Edwards R., J.-F. Larivé, V. Mahieu and P. Rouveirolles (2008), Well-to-wheel analysis of future automotive fuels and powertrains in the European context, Well-to-Tank report, V3.0, Appendix 2, Report from Concawe, EUcar and Joint Research Centre of the European Commission (IES).

Jungbluth N., S. Büsser, R. Frischknecht and M. Tuchschmid (2008), Life Cycle Assessment of Biomass-to-Liquid Fuels, Final Report, *ESU-services GmbH*, Uster, Switzerland.

Menichetti E., M. Otto (2009), Energy balance and greenhouse gas emissions of biofuels from a life-cycle perspective, in: *R.W. Howarth and S. Bringezu (eds)*, Biofuels: Environmental Consequences and Interactions with Changing Land Use. Proc. of the Scientific Committee on Problems of the Environment (SCOPE) International Biofuels Project Rapid Assessment, 22–25 September 2008, Gummersbach, Germany, Cornell University, NY, USA (2009), 81–109.

Pillot D., J.-L. Besombes, F. Cazier, B. Hanoune, E. Combet, E. Delbende, H. Nouali, R. Vidon, P. Tassel and P. Perret (2009), Exhaust emissions from light vehicles fuelled with different biofuels, *Proc. 17th Int. Symp.* "Transport and air pollution", ETTAP 2009, Toulouse, France

Zah R., H. Böni, M. Gauch, R. Hischier, M. Lehmann and P. Wäger (2007), Ökobilanz von Energie produkten: Ökologische Bewertung von Biotreibstoffen, Schlussbericht, Abteilung Technologie und Gesellschaft, EMPA im Auftrag des Bundesamtes für Energie, des Bundesamtes für Umwelt und des Bundesamtes für Landwirtschaft, Bern, Switzerland.